A multi-temporal approach to using multispectral remote sensing for the prospection of clandestine mass graves in temperate environments

Emily Anne Norton

A thesis submitted in partial fulfilment of the requirements of Bournemouth University for the degree of Doctor of Philosophy

Bournemouth University

November 2019

Dedicated to Lesley

"*Only an aunt can give hugs like a mother, keep secrets like a sister and share love like a friend*"

Unknown

A multi-temporal approach to using multispectral remote sensing for the prospection of clandestine mass graves in temperate environments

Emily Anne Norton

Abstract

Recent years have seen mass graves resulting from human rights abuses and violations become a stimulant for criminal proceedings and investigations. As a consequence the prospection for clandestine mass graves is at the forefront of international forensics and is considered of ever increasing importance. This study investigates the utility of archive orbital multispectral imagery for the detection of clandestine mass graves specifically in temperate environments, using spatial variations in vegetation stress as indicators of disturbance, indicative of the presence of a mass grave.

Three studies were undertaken. The first monitored vegetation stress at the surface of two small-scale controlled mass graves, one containing mammalian remains (pigs) and the other empty, using a hand held field spectrometer for the first 121 days post burial. It was found that vegetation stress was not influenced by the presence of mammalian remains over this short time frame, however, the disturbance caused by creating the grave was detectable. Meteorological factors including temperature and dew point were found to affect the NDVI recorded more than other meteorological variables such as precipitation. Geophysical surveys were also undertaken, using temporal electrical imaging and electromagnetic profiling, to provide a spatial measure of the state of decomposition within the grave and to indicate the detectability of both a full and an empty grave throughout the study. By undertaking regular geophysical surveys it was found that both graves were able to be detected using both techniques up to 121 days post burial. The percentage difference in geophysical response from both techniques, between the pig and empty grave compared to the undisturbed ground peaked at 70 days post burial. This peak corresponded to the period where climatic events were recorded, including increased precipitation and decreasing ambient temperatures. Therefore, it is clear that the results obtained from the geophysical surveys were influenced heavily by climatic factors and in the case of this study, enabled the graves to be more readily detected.

The second study was a long term decadal investigation of variations in NDVI of a large-scale, mass grave site resulting from the 2001 Foot and Mouth epidemic. This provided a pre-operational proof-of-concept for clandestine human mass grave detection using multi-

temporal (18 day repeat period or multiple thereof), multi-spectral (visible to infra-red – 0.45-12.5µm), medium and fine spatial resolution (30m and 5m ground sample distance) orbital remote sensing of a known burial location. A dense time-series of archive satellite images was used to study variations in NDVI of the vegetation directly above the grave, compared to the undisturbed vegetation surrounding it. By calculating NDVI using fine spatial resolution imagery from RapidEye (5m), the time frame within which significance was detected between the grave surfaces and the undisturbed ground, was able to be extended to 9 years, 11 months post burial.

The third study concerned the active prospection of clandestine human mass graves in Bosnia where differences in vegetation stress, on a small spatial (~15m) but large temporal scales (exceeding a decade post burial), were examined for a number of known mass burial locations. In turn, graves were prospected for on the basis of appropriate spatial and temporal variations in vegetative stress and health. It was found that medium spatial resolution imagery (30m) was not useful in locating human mass graves on Cancari Road, however fine spatial resolution imagery (5m) was successful in detecting the disturbance caused by the exhumation of Cancari Road Grave 1 (CR01) in 2009.

To conclude, variations in vegetation stress, derived through vegetation indices, can be used to locate areas of disturbance that may be indicative of a mass grave and other man made changes over time. However, it is important to consider the spatial resolution of the orbital platform and its appropriateness in relation to the extent of the target.

Acknowledgments

This thesis would not have been possible without the Bournemouth University's Vice Chancellor's Scholarship and the match funders, the Inforce Foundation. I have benefitted greatly from the extensive knowledge and experience of my supervisors, Professor Timothy Darvill, Andrew Ford and previously, Paul Cheetham and Dr Karina Gerdau-Radonic. Thank you for being a part of this journey. Thanks are also extended to the Faculty of Science and Technology and Department of Archaeology, Anthropology and Forensic Science for their support. Special thanks go to Pippa Gillingham, Shaun Bendall, Harry Manley, Damian Evans, Dean Burnard, Naomi Bailey and last but not least, Louise Pearson. Thanks also to my examiners Dr Alistair Ruffell and Professor Kate Welham, whose comments greatly improved this thesis.

I would like to thank the following external organisations for their invaluable support, advice and in many cases for providing access to data, without which this research would not have been possible. Natural Environment Research Council's Airborne Research Survey Facility and Field Spectroscopy Facility; DMC International Imaging; Airbus Defence and Space Ltd; BlackBridge Ltd; Getmapping PLC; Environment Agency Geoinfomatics Team; Analytical Spectral Devices Inc. and the European Space Agency. For the support shown by the remote sensing community, particularly the members of the Remote Sensing and Photogrammetry Society I am thankful and humbled.

Data collection would not have been possible without Will Bond, Arjan Gosal, Heather Papworth, Catie Gutmann Roberts, Adrian Blake, Danny Sheath and Hannah Haydock – thank you all. To the brilliant and inspiring PhD students that I have had the pleasure of working alongside, we have shared times of elation and stress; your unrelenting support throughout has been amazing. Through undertaking this PhD I have made some lifelong friends, for the coffees, pizza, quiz nights and banger racing – thank you. Lara, your support during the crucial last few months has been amazing.

My family have been incredible throughout this challenging time, keeping me grounded, encouraging me, reassuring me in times of doubt and supporting me unconditionally. Thanks to my Mum, for understanding me always. To Dad, for being there no matter what. To Chris, for always making me smile. To Lydia, for reminding me that life is for living. To Nan, for being my sounding board and always being at the other end of the phone. I want to thank you all from the bottom of my heart. Finally a thank you to Guy - we made it! Thank you for believing in me, driving down to Bournemouth from East Yorkshire to remind me that there was light at the end of the tunnel and loving me always.

Table of Contents

List of Figures

List of Tables

Abbreviations

AOI	Area Of Interest
ASTER	Advanced Spaceborne Thermal Emission and Reflection Radiometer
ATCOR	Atmospheric CORrection
AVHRR	Advanced Very High Resolution Radiometer
AVHLA	Animal Health and Veterinary Laboratories Agency
AVIRIS	Airborne Visible/Infrared Imaging Spectrometer
BGL	Below ground level
BIL	Band-interleaved-by-line
BIP	Band-interleaved-by-pixel
BSQ	Band Sequential
BCAL	Boise Center Aerospace Laboratory
CASI	Compact Airborne Spectrographic Imager
CCD	Charge Coupled Devices
CHRIS	Compact High-Resolution Imaging Spectrometer
DAIS	Digital Airborne Imaging Spectrometer
DEFRA	Department for Environment, Food & Rural Affairs
DEM	Digital Elevation Model
dGPS	Differential Global Positioning System
DMC	Disaster Monitoring Constellation
DN	Digital Numbers
DOS	Dark Object Subtraction
DSM	Digital Surface Model
DTM	Digital Terrain Model
EA	Environment Agency
EM	Electromagnetic
EOS	End Of Season
EO-1	Earth Observing One
EROS	Earth Resources Observation and Science
ESA	European Space Agency
ESPA	EROS Science Processing Architecture
EVI	Enhanced Vegetation Index
FCIR	False Colour Infrared
FLAASH	Fast Line-of-sight Atmospheric Analysis of Hypercubes
FOV	Field of View
GCP	Ground Control Point
GIMMS	Global Inventory Modelling and Mapping Studies
GIS	Geographical Information System
GPR	Ground Penetrating Radar
GSD	Ground Sample Distance
HANTS	Harmonic Analysis of Time Series
HMM	Histogram Minimum Method
ICC	International Criminal Court
ICESat	Ice, Cloud and Land Elevation Satellite
ICJ	International Court of Justice
ICMP	International Commission for Missing Persons
ICTY	International Criminal Tribunal for the Former Yugoslavia

IFOV	Instantaneous Field of View
JPL	Jet Propulsion Laboratory
LAI	Leaf Area Index
LEDAPS	Landsat Ecosystem Disturbance Adaptive Processing System
LiDAR	Light Detection and Ranging
MERIS	Medium Resolution Imaging Spectrometer
MGRS	Military Grid Reference System
MODIS	Moderate Resolution Imaging Spectroradiometer
MODTRAN	MODerate Resolution Atmospheric TRANsmission
MRENDVI	Modified Red Edge Normalised Difference Vegetation Index
MSG	Meteosat Second Generation
MVS	Multi-View Stereo
NASA	National Aeronautics and Space Administration
NOAA	National Oceanic and Atmospheric Administration
NBGs	Natural Burial Grounds
NDVI	Normalised Difference Vegetation Index
NIR	Near Infrared
OLI	Operational Land Imager
PCA	Permanent Court of Arbitration
PIS	Primary Inhumation Site
POES	Polar Operational Environmental Satellite
PVI	Perpendicular Vegetation Index
QUAC	QUick Atmospheric Correction
RENDVI	Red Edge Normalised Difference Vegetation Index
Res	Resistivity
RTC	Radiative Transfer Code
RVI	Ratio Vegetation Index
SAR	Synthetic Aperture Radar
SfM	Structure From Motion
SIS	Secondary Inhumation Site
SOS	Start of Season
SPIRITS	Software for the Processing and Interpretation of Remotely sensed Image Time Series
SRTM	Shuttle Radar Topography Mission
SWIR	Short Wave Infrared
TINDVI	Time Integrated Normalised Difference Vegetation Index
TIR	Thermal Infrared
USGS	United States Geological Survey
UTM	Universal Transverse Mercator
VI	Vegetation Index
Vis	Visible
VMD	Vertical Magnetic Dipole
VNIR	Visible-Near Infrared
WGS	World Geodetic System

Authors Declaration

I confirm that all of the work presented in this thesis is my own.

1 Introduction

Mass graves can occur as a result of mass disasters, epidemics, human rights abuses, war and conflict. They are worldwide, societal, political and humanitarian issues. Mass graves exist in many forms, shapes and sizes and are considered complex structures which offer geographical challenges to those responsible for their investigation (Kalacska et al. 2009). Clandestine mass graves are the principle source of physical evidence for criminal proceedings and therefore are of significant forensic importance. Legal proceedings relating to human rights abuses are becoming increasingly common internationally; the ability therefore, to detect and locate mass grave sites accurately is critical. The International Commission for Missing Persons (ICMP) report an estimated 10,000 people are still missing following conflict in the Former Yugoslavia in the early 1990s, the remains of whom are presumed to be interred in clandestine mass graves (ICMP, personal communication, 20 August 2013). The humanitarian importance of detecting such sites is currently at the forefront of international forensics and, following the establishment of the International Criminal Court (ICC), atrocities including war crimes and genocide will not, without a level of international scrutiny, be tolerated. The first standard operating procedures for the scientific detection and investigation of mass graves were published by Cox et al. (2008b).

When searching for mass graves it is imperative that methodologies and techniques employed are carefully considered and adapted and, that those selected, should be of high scientific standing, for evidence to be accepted for future judicial proceedings (Hunter et al. 2001). Cox et al. (2008a) suggest that non-invasive techniques (i.e. airborne/ orbital remote sensing and/or geophysics) should be employed prior to invasive techniques (i.e. probing or test trenching) to maintain the integrity of the scene and to preserve evidence. Anderson et al. (2008) state that a non-destructive approach is key during the initial stages of detecting mass grave sites and added that this process should aim to identify a relatively small area to undergo further investigation whilst eliminating false positives.

Published scientific knowledge detailing appropriate techniques for the detection of mass graves is limited and scarce with "…no widely acknowledged and accepted…standards and protocols…" (Cheetham et al. 2008, p.185). Case reports and grey literature constitute the majority of the published literature (e.g. Owsley et al. 1996; Garrido-Varas and Leiva 2012; Fernandez-Alvarez et al. 2016; Rubio-Melendi et al. 2018), many of which identify eye witness testimony as the most common and successful way of locating a mass grave (McGray 2001; Schmitt 2002; Ruwanpura et al. 2006; Tuller 2012). Other methods (excluding eye witness testimony) utilised during the prospection of mass graves are often

based on poor scientific principles and have no proven repeatability and reliability. In addition, these techniques are often used on an ad hoc basis with the chosen methods being dependent on the resources and finances available rather than being the most scientifically appropriate. Consequently, there is no real understanding of the parameters involved in the detection of mass graves, therefore, it is not currently possible to formulate any well founded scientific protocols for their accurate detection.

In prospecting for clandestine mass graves, the international forensic community is increasingly considering the application of remote sensing techniques (particularly orbital remote sensing). Imagery obtained remotely, provides accurate and detailed information regarding specific geographical locations in a timely, systematic and scientifically rigorous manner. Remote sensing is an established and well-studied science and some of the principles, particularly those relating to the detection of disturbed soil and vegetation, could potentially be used to locate and detect mass graves. Consequently, mass graves could in turn, be remotely detected over large areas independent of physical and political boundaries. An additional consideration would be that the dangers associated with conducting forensic operations in-country could be avoided, allowing for site detection to be carried out remotely in a safe environment (Kalacska and Bell 2006).

Without locating and excavating clandestine human mass graves, international criminal tribunals and proceedings would not have scientific, admissible forensic evidence on which to build a robust criminal case. Furthermore, the families of the missing and the disappeared remain waiting for justice and closure.

This document begins with a review of the published literature relating to the search and detection of clandestine mass graves including traditional and more novel methodologies. A technical review relating to the principles of remote sensing will be presented prior to introducing vegetation indices, including the Normalised Difference Vegetation Index (NDVI), and how this could be utilised to identify anomalies that may be indicative of clandestine mass graves. The literature review will contextualise the research and provide a robust scientific basis from which the aim and research questions of the study are derived.

2 Literature Review

2.1 Definition of a Mass Grave

A grave is defined by the Oxford English Dictionary (2018) as "an excavation in the earth for the reception of a corpse" and is synonymous with burial. There is no consensus in forensic literature as to the exact definition of a mass grave or burial. Mass graves created as a result of crimes against humanity and/or genocide are perceived to be "complex products of large scale crime" (Skinner and Sterenberg 2005, p. 221) and are a multifaceted matrix of human remains and associated artefacts (Tuller and Duric 2006).

Mass graves are often defined by the number of individuals buried within them. Mant (1987) stated that a grave containing two or more bodies in contact with each another could be considered a mass grave. Whereas Skinner (1987), suggested a mass grave should contain at least six individuals, in direct contact, that have been indiscriminately placed.

In 1991, the United Nations introduced a variety of categories to classify burials including: individual (one person, buried alone); commingled (two or more persons buried at the same time or over a period of time); primary (where the individual is first buried); secondary (where remains have been removed from a primary grave and reburied); disturbed (altered by human intervention) or undisturbed. The classification of graves using these terms allows for each grave site to be documented with ease.

In 2001 and 2008 Komar furthered the categorisation of burial sites by suggesting three distinct categories including: single, multiple and mass graves. The values assigned to each category were based on the overall scale of the graves being studied, therefore, in 2001 multiple graves were deemed to be those which contained between two and five individuals; with mass graves containing in excess of six. In Komar's 2008 study, the number of individuals present within the graves ranged from one to nine and then from twenty-eight through to a maximum of four-hundred and sixty in others. This difference in scale prompted a revision in the definition of multiple graves, which were deemed to be those containing between two and nine individuals, with mass graves being redefined to those containing in excess of ten. In the case of Komar (2001; 2008) the definition of a mass grave was situation and case specific, reiterating the need for definitions to be flexible and adaptable. The term multiple burials is also used by Vanezis (1999) to describe clandestine graves resulting from human rights abuses, however, no reference to the number of interred individuals was made. Jessee and Skinner (2005, p.55) state, mass graves are "archaeological features with humanitarian and forensic importance" and suggest several types of mass graves where the

definitions are based on the grave's distinct archaeological characteristics. For example, a primary inhumation site (PIS) and/or a primary mass grave contain multiple remains that share a similar cause and manner of death. Whereas, secondary inhumation sites (SIS) and/or a secondary mass graves are characterised by the movement of remains from a primary mass grave to another location; with the interred remains being "…severely disarticulated and commingled…" (Jessee and Skinner 2005, p. 58).

The United Nations Special Rapporteur (United Nations 1991) stated that a mass grave can be a burial, in any location, where three or more victims of extra judicial, summary or arbitrary executions are buried. For this definition to apply, the individuals cannot have died in combat or armed confrontation. This was the first definition to state that a mass grave can be located anywhere, including natural features such as caves. In contrast, a surface deposition can also be considered a mass grave (Harrington 1999; Simmons 2002), however, there must be an element of concealment for this definition to apply. This definition was adopted by the International Criminal Tribunal for the Former Yugoslavia (ICTY) in 1996, as the graves associated with the political unrest were discovered in a variety of locations including caves, mines as well as surface deposits.

Schmitt (2002) added to the preceding definitions by acknowledging that, victims within mass graves often share a common trait that is connected with the cause and manner of their deaths and felt this should be represented in the definition. In the same year, Haglund (2002) alluded to the fact that the definition of a mass grave is often tailored to fit the interests and aims of the investigating organisations; as a result, definitions often incorporate details which pertain to specific cases i.e. location, nature of death and the number of individuals buried.

A more simplistic, flexible definition was offered by Ruwanpura et al. (2006) who suggested that it is reasonable to assume that a burial site containing a number of dead individuals (i.e. more than one) can be deemed a mass grave. In many cases, this is the basis on which mass graves are defined, with details relating to the number of individuals buried stated within reports. Cox et al. (2008a: p10) added that a mass grave can be considered as "a demonstrable place of deliberate disposal of multiple dead within the same grave structure".

It is evident that the definition of mass graves has been adapted in recent years to reflect their context and the number of individuals they contain (Table 1 for a summary of definitions). Interestingly, the size or extent of mass graves is not included in any of the published definitions reviewed above; perhaps alluding to their complexity and variability. The extent or size of a mass grave is an important factor to consider when using satellite remote sensing as each sensor has limitations; these will be introduced and discussed further in this review.

For the purposes of this research, the definition of a mass grave is a demonstrable place of deliberate disposal that contains two or more individuals (including mammalian remains), that are buried below ground level (BGL). This definition is crucial to contextualise this research.

Table 1 - Definitions of a mass graves and related sites within literature.

Reference	Category	No. Individuals	Characteristics
Mant (1987)	Mass grave	≥2	In contact
Skinner (1987)	Mass grave	≥6	In direct contact and indiscriminately placed
United Nations (1991)	Individual burial	1	Buried alone
	Commingled burial	>2	Buried at the same time or over a period of time
	Mass grave	>3	Any location. Victims of extra judicial, summary or arbitrary executions.
	Primary burial	Not specified	Where individual/s are first buried
	Secondary burial	Not specified	Where remains have been removed from a primary grave and reinterred
Komar 2001	Multiple graves	2-5	
	Mass grave	>6	
Schmitt (2002)	Mass graves	Not specified	Indiv. Share a common trait that is connected to their cause and manner of death
Jessee and Skinner (2005 p.58)	Primary mass grave (Primary inhumation site – PIS)	Multiple	Share similar cause and manner of death
	Secondary mass grave (Secondary inhumation site – SIS)	Multiple	Remains are "…severely disarticulated and commingled…"
Ruwanpura et al. (2006)	Mass grave	>1	
Slaus et al. (2007)	Mass grave	>3	
Cox et al. (2008a p.10)	Mass grave	Multiple	"…place of deliberate disposal…in the same grave structure"
Komar 2008	Multiple graves	2-9	
	Mass grave	>10	

2.2 Forensic Archaeology – The Vehicle for Mass Grave Investigation

Forensic archaeology is a stand-alone discipline that "…involves the transference of theory and underlying principles to an unusual context…" (Hunter and Cox 2005, p. 3). Skinner and Sterenberg (2005) state that the mapping and excavation skills of traditionally trained archaeologists, are able to be applied to recent death scenes or sites where bodies have been disposed. This was first reported by Morse et al. (1976) who detailed the introduction of traditionally trained archaeologists as advisors for investigations in the United States; focused around the search and location of buried human remains.

Forensic archaeology has most recently been defined by Groen et al. (2015a, pIi) as "…a forensic discipline that uses archaeological theories, methods and techniques in a legal context". Traditionally trained archaeologists undertaking forensic casework are required to operate under a legal remit, whereby, all evidence is collected, regardless of its perceived importance, to recreate and "…reconstruct the specifics of a single event" (Connor and Scott 2001: p3).

Forensic archaeology does not solely relate to the search and detection of mass graves; it is routinely employed in the search and recovery of individual buried human remains and associated evidence (e.g. Morse et al. 1976; Congram 2008). Mass graves and their investigation have increasingly been cause for publication within scientific literature, predominantly in the form of case studies and reports with the emphasis placed on the identification of the interred individuals (forensic anthropology), rather than detailing the search and location process (Owsley et al. 1996; Brkic et al. 1997; Brkic et al. 2000; Haglund et al. 2001; Stover and Ryan 2001; Stover et al. 2003; Jankauskas et al. 2005; Baraybar and Gasior 2006; Ruwanpura et al. 2006; Djuric et al. 2007; Slaus et al. 2007; Garrido-Varas and Leiva 2012; Bevernage and Colaert 2014; Szleszkowski et al. 2014; Nunez et al. 2015). In response to the increasing international interest and profile of mass grave investigation, Cox et al. (2008b) published the first comprehensive set of standard operating procedures and methods specifically for the scientific investigation of mass graves.

The process of searching, detecting and locating clandestine mass graves, is the area of expertise of the forensic archaeologist and is often conducted during the Site Assessment Phase (Anderson et al. 2008). Traditionally, eye witness testimony alongside geophysics (Bevan 1991; France et al. 1996; Nobes 2000; Powell 2004; Pringle and Jervis 2010; Molina et al. 2016; Fernandez-Alvarez et al. 2016; Schuldenrein et al. 2017), landform observations and remote sensing techniques (including terrestrial, airborne and orbital observations) can

be used during site assessment (Grip et al. 2000; Davenport 2001; Ruffell 2002; Kalacska and Bell 2006; Kalacska et al. 2009; Wang et al. 2013; Leblanc et al. 2014). Archaeologists are able to recognise landform changes (e.g. depressions) and are able therefore to identify potential anomalies within an undisturbed environment. From these anomalies, interpretations regarding the context of the grave can be deduced and corroborated with intelligence, including eye-witness testimony. The aim of which is to reduce the spatial extent of potential search areas and focus the investigation. In Bosnia and Herzegovina, following conflict in the early 1990s, on the occasions where eye witness statements were not corroborated by physical evidence or other witness accounts, they were deemed unreliable and consequently excluded from further investigation (Komar 2008). This emphasises the need for a multidisciplinary approach, where a variety of evidence from multiple sources is collated and considered, to provide a solid scientific basis for a legal case. Although this study will ultimately focus on the remote sensing of vegetation, and subsequent vegetation stress at the surface of mass graves, it is intended that this will be utilised alongside existing techniques, including geophysics, and will corroborate or refute eye witness testimony and other documentary evidence.

2.3 Creation of Graves in the Context of Human Rights Abuses, Genocide and Armed Conflict

When creating a grave, natural existing ground sediments are removed either manually or mechanically (Ellis and Wright 2016). As a consequence, the sediment horizons become mixed, resulting in a disturbed soil matrix, where the natural topsoil may be placed at the base of the grave and in turn, lower sub-sediment may be deposited towards the grave surface (Bevan 2001; Figure 1). Disturbance is the"…physical disruption associated with the burial process" (France et al. 1992 p. 1447) and it has been suggested that the changes in sediment composition could last indefinitely (Bevan 2001). The grave surface is an important feature that can be used to indicate the presence of a clandestine burial. Over time, the soil within the grave column compacts and shallow regular depressions can become visible on the ground (Bevan 1991). Primary depressions occur when the mixed matrix sediment begins to settle and compress through the grave column, this is followed by secondary depressions, which are a result of the decomposition process (e.g. the collapse of the abdominal region) (Hochrein 2002).

Leblanc et al. (2014) add that the process of creating a grave changes the ground mineralogy. In the early stages of decomposition, sediment in direct contact with human remains has increased alkalinity; although it is unknown how long such changes in sediment chemistry persist (Owsley 1995). The disturbance of the natural sediment and the interment of human remains can cause air pockets to form, where, as decomposition progresses, in excess of four hundred decomposition compounds are released into the grave matrix; with forty being detectable at the ground surface, regardless of depth and age of burial (Dent et al. 2004; Vass et al. 2004; Carter et al. 2007; Vass et al. 2008; Dekeirsschieter et al. 2009; Vass et al. 2010; Vass 2012; Dalva et al. 2015; Forbes et al. 2016).

Mass graves can be prepared in advance of the killing, just prior to interment, or at the time of interment (Komar 2008). Graves can be used as a control mechanism of the target victim population, whereby, the perpetrators want the grave to be clearly visible to the local community (Schmitt 2002). Therefore, it is possible that the grave would be created in close proximity to the settlement where the target population reside. However, if the killings are planned and are politically sensitive, graves may be prepared at the time of the killings or shortly thereafter; as a consequence of needing to dispose of a large number of human remains discreetly.

Schmitt (2002) states that in some cases, perpetrators do not need to disguise the killings by burying the individuals; in these scenarios, mass graves have been known to have been created by others (including family members and survivors) who have had no part in the killings. With the introduction of international criminal investigations, perpetrators have been reported to have revisited mass grave sites post-interment to exhume and move the human remains entirely and deposit them in secondary graves; in some cases tertiary graves to avoid detection (Schmitt 2002; Brown 2006). Mass graves can also be a political tool to intimidate survivors and can be used as a form of propaganda (Cheetham et al. 2008). Komar (2008) expands on this and introduces the concept of 'agents of burial'. By considering the way individuals are interred it could indicate who (in generic group terms), may have been responsible for their burial. In cases where the same ethnic group, relatives or associated army bury the dead, these are considered "self" burials. These are noted as being "considerate interments", where individuals are placed into the graves with care (Komar 2008). In contrast, burials created by different ethnic groups or opposing armed forces are known as "other" or enemy burials, and can often be characterised by "erratic commingling", where bodies are deposited en masse with visible disrespect and violation (Komar 2008).

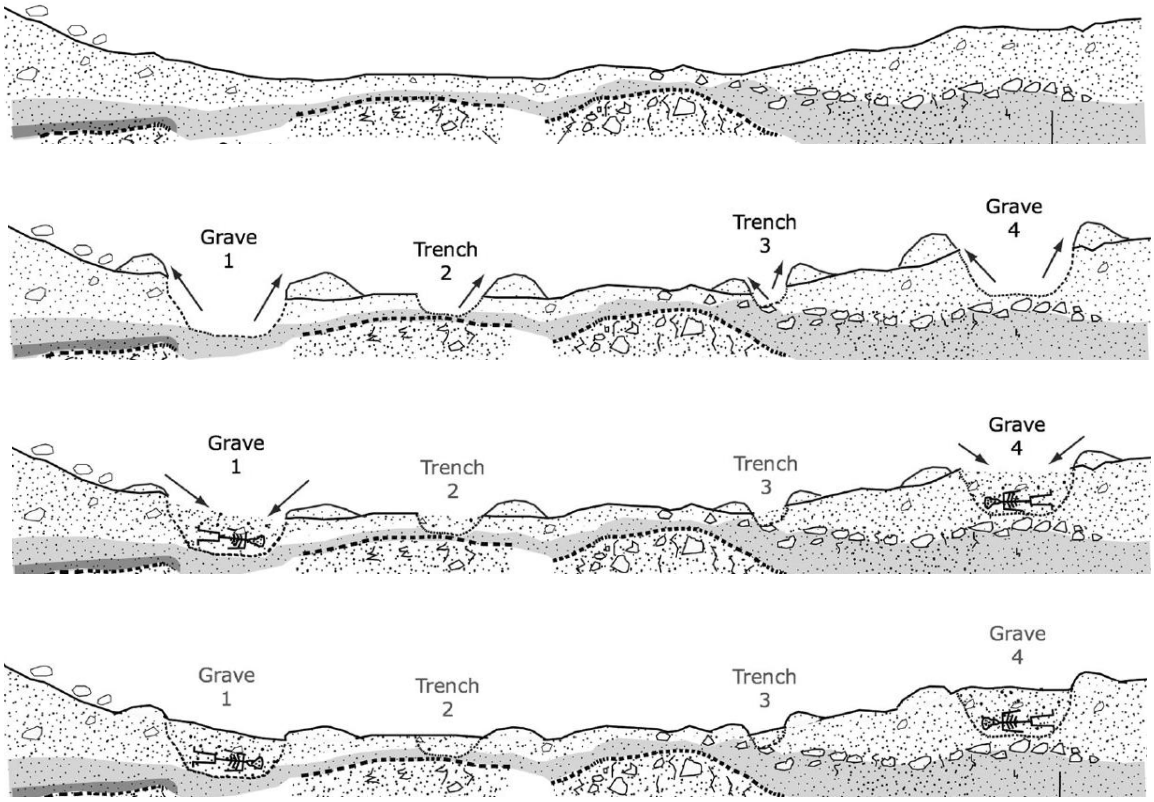

Figure 1 - Schematic demonstrating undisturbed ground with natural stratigraphy versus the mixed stratigraphy and change in surface topography that can occur when a grave or trench is created. Source: Adapted from Schuldenrein et al. 2017, p. 154.

2.4 The Search for Clandestine Mass Graves

The process of searching, detecting and locating clandestine graves/ burials is a "...labour-intensive, time-consuming, and often frustrating task" for many investigators (Doolittle and Bellantoni 2010, p. 941); nevertheless this process is crucial for the judicial process. Cheetham et al. (2008, p.189) state that "the successful location of such sites will always depend on using a combination of structured phases..." if this advice is adhered to, the forensic investigation is likely to be more focussed in its efforts – allowing for resources to be utilised efficiently. It is recommended that a visual inspection of any potential mass grave site should be conducted, recording the vegetation present and any obvious areas of disturbance (Cox et al. 2008b). These observations can be useful when trying to focus and reduce the search area, so that further investigations can go on to confirm or eliminate suspected areas. Pringle et al. (2012) state that current best practice includes the investigators creating a "conceptual target" of the suspected burial site with geological maps, imagery and

intelligence being analysed prior to the commencement of any fieldwork; this approach was also advocated by Cox et al. (2008b).

Traditional archaeological methods and techniques have been utilised in the search and location of clandestine burials, including geophysical and remote sensing techniques, with varying success. Skinner and Sterenberg (2005) and Tuller and Duric (2006 p. 192) state that traditional archaeological searching strategies and techniques employed for individual clandestine burials, have in many cases simply been scaled-up to deal with mass graves, which are deemed to be a "…relatively new phenomenon". This is further emphasised by the notable lack of published scientific literature relating to appropriate techniques and methodologies. Cheetham et al. (2008, p. 185) further this point by stating that there are "no widely acknowledged and accepted…standards and protocols" for mass grave detection; consequently, the techniques utilised in the search for mass graves are often ad hoc and dependent on available resources and finances, rather than on the basis of their scientific reputation. Techniques often employed for the prospection of clandestine burials include eye witness testimony, scent-detection dogs/ cadaver dogs, aerial photography, T-bar probes or augers, geophysical techniques, forensic botany, forensic entomology, scavenging patterns, field techniques as well as more recently, remote sensing techniques (including ground based, airborne and orbital); the latter of which will be reviewed in the following sections (Bevan 1991; France et al. 1992; Owsley 1995; Miller 1996; Nobes 2000; Haglund et al. 2001; Watters and Hunter 2004; Cheetham 2005; Coyle et al. 2005; Kalacska and Bell 2006; Schultz and Dupras 2008; Kalacska et al. 2009; Pringle et al. 2012; Leblanc et al. 2014; Molina et al. 2015; Molina et al. 2016).

Schmitt (2002) states that strict time constraints and the fact that resources are usually limited often influence the choice of techniques utilised in the search for mass graves. This statement is perhaps now outdated in light of this research which, if successful, will allow for much of the planning and searching to be carried out remotely using satellite imagery, therefore, fewer resources may be required when conducting investigations in-country.

Cox et al. (2008b) attempted to standardise and outline appropriate scientific methods and procedures by developing a set of suggested protocols; including a section dedicated to the process of searching and locating mass graves. Prior to this, the only internationally recognised document that included advice on the archaeological recovery of evidence relating to large scale, human rights abuses was the 'Manual on the Effective Prevention and Investigation of Extra-legal, Arbitrary and Summary Executions' by the UN (1991). Cheetham et al. (2008) recognise this as being dated in its approach, having now been updated by Cox et al. (2008b). The manual published by the UN (1991) was the first of its

kind and for a considerable number of years it was the only available guidance for international forensic investigators; it contained specific advice relating to the disinterment and analysis of skeletal remains. The document was created by a large number of established criminal and forensic investigators who recognised the need for standardisation in specific cases i.e. executions. There is no tangible evidence identifying the groups that have used the protocols detailed within either the UN (1991) manual or the scientific investigation of mass grave guidelines (Cox et al. 2008b) and how influential these protocols have been on international forensic investigations; as its use has not yet been reported within literature. Additionally, questions remain as to how these suggested standards have been tested, whether they are able to be applied internationally and also whether they will be disseminated to active forensic teams globally. In light of the above it is clear that the success relating to the choices of techniques used to detect mass graves is not present within literature. Cox et al's. (2008b) text is now outdated due to advancements in technology, allowing the remote sensing of vegetation and vegetation stress at the grave surface, to take a more central role in the search for mass graves.

2.5 Non-Invasive Techniques Traditionally Employed for the Detection of Clandestine Mass Graves

2.5.1 Eye Witness Testimony – The Cornerstone of Mass Grave Forensic Investigation

Much of the literature relating to the detection of mass graves exists in the form of case reports which state that the most common and successful way of locating mass graves is through eye witness testimony (Hunter et al. 2001; McGray 2001; Schmitt 2002; Cheetham et al. 2008; Steele 2008). Eye witness testimony can be vital in both area and site location and is stated as being "...the initial information that informs a broader search strategy" (Cheetham et al. 2008, p. 192). This is further emphasised by Schmitt (2002, p. 280) who describes eye witness testimony as being "the cornerstone of mass grave forensic investigation". Mass graves and their locations are rarely a secret in local society, witnesses who provide potential locations of graves via written or oral testimony can be survivors, family members of the missing or the perpetrators who took part in the killings or burials (Schmitt 2002). These testimonies have often led investigators to the exact location of the grave, as well as adding context and an indication as to the potential motivation behind the killings. Eye witness testimony is recognised as playing such a significant role in the location

of graves, that in many investigations "the corroboration of such testimony becomes the goal of the exhumation" (Schmitt 2002, p. 280). The accuracy of eye witness testimony has been tested using archaeological techniques in discrete phases; firstly by determining whether a mass grave exists in the suggested location, by probing the site, carrying out geophysical surveys or using cadaver dogs (Schmitt 2002). Once the site is confirmed, the excavation, collection and documentation can be undertaken, followed by analysis before leading to the reporting phase, the output of which be used later in judicial proceedings (Schmitt 2002).

Eye witness testimony proved to be particularly useful in the location of the mass graves resulting from the Spanish Civil War (1936-1939). Interviews were conducted with surviving family members, who were able to tell investigators the location of grave sites, provide an estimated number of the missing and also provide evidence that may contribute to the process of identification (Rios et al. 2010; Rios et al. 2012). Brkic et al. (1997; Brkic et al. 2000) document how individuals who helped load or bury bodies in mass graves in Croatia provided accurate locations through oral testimony. However, in the case of a Chilean mass grave, eye witnesses and their evidence proved to be less useful with inquiries resulting in "…ambiguities or unreliable information" (Garrido-Varas and Leiva 2012, p. 20). Gupta (2013) states that misleading testimony can be provided by witnesses due to social or political motivations and in some cases repression. This is further demonstrated by Ruwanpura et al. (2006) where a number of approximate locations of mass grave sites in Sri Lanka were identified by prisoners who undertook the executions. However, when these were later investigated, using intrusive techniques, it was found that only six out of the twenty five locations identified contained human remains; demonstrating that an element of caution must be taken when relying on eye witness testimony to identify the location of mass graves. In light of this, a multidisciplinary approach utilising complimentary techniques and methodologies is recommended to assess the validity of provided intelligence (France et al. 1992; Schmitt 2002). There may also be cases where eye witness testimony does not exist, evidence including media reports can be used alongside techniques including orbital remote sensing to narrow down search areas and provide a location for further scrutiny.

2.5.2 Geophysical Survey

Geophysical techniques are often utilised during the search for burial sites due to their ability to detect anomalies indicative of disturbance that persist long after the initial disturbance has occurred. They have been extensively used in archaeology and are a well-established discipline particularly for the search of single clandestine burials, as well as for the prospection of other sub-surface artefacts (Miller 1996; Hunter et al. 2001; Buck 2003;

Powell 2004; Cheetham 2005; Pringle et al. 2008; Pringle and Jervis 2010; Pringle et al. 2012; Hansen et al. 2014; Molina et al. 2015; Pringle et al. 2015; Molina et al. 2016). However, limited forensic research has been carried out to ascertain optimal geophysical methodologies and associated parameters required specifically for the detection of mass graves, with much of the published literature existing in the form of case reports rather than scientific studies (Juerges et al. 2010; Hansen et al. 2014; Fernandez-Alvarez et al. 2016; Schuldenrein et al. 2017; Rubio-Melendi et al 2018.). The use of geophysical techniques, which measure the Earth's physical, electrical and chemical properties, are often advocated within literature due to the fact that they are non-invasive and therefore, do not compromise the integrity of potential grave sites (Owsley 1995); it is suggested that such techniques should be used to focus the investigation (Buck 2003). This approach is often adopted in the search for individual clandestine graves and/ or missing person's cases, rather than for international mass grave investigations, where geophysics is considered later during the site location phase, once the investigative team are in-country.

2.5.2.1 Ground Penetrating Radar (GPR)

Ground penetrating radar (GPR) has proven useful for the detection of both modern and historical burials and is recognised as an important tool (Bevan 1991; France et al. 1992; Owsley 1995; Davis et al. 2000; Hammon et al. 2000; Nobes 2000; Davenport 2001; Buck et al. 2003; Conyers 2006; Schultz et al. 2006; Schultz 2007; Ruffell et al. 2009; Dalan et al. 2010; Pringle et al. 2012; Hansen et al. 2014; Fernandez-Alvarez et al. 2016; Schuldenrein et al. 2017; Rubio-Melendi et al. 2018). In forensic contexts, GPR is reported as the most commonly utilised geophysical technique and is often the geophysical tool of choice due to its published detection success (Schultz 2007; Hansen et al. 2014). GPR operates using two antennae, one of which pulses electromagnetic waves (microwaves) into the ground whilst the other, measures the waves that are reflected off sub-surface features (i.e. burials or archaeological structures) (Buck 2003). It is by observing the strength of the returning waves and also the time it takes for the waves to return to the instrument, that the presence of an artefact and also its depth, can be determined (Cheetham 2005, p. 86). GPR "…creates approximate soil profiles" and can therefore be used to detect variations in soil moisture or density; which can be indicative of a burial (Bevan 1991, p. 1311). Limited geophysical surveys have been carried out on mass graves, therefore, there are currently no specifically tailored protocols (Cheetham et al. 2008); therefore, resulting in traditional archaeological methods and parameters being employed during the search for mass graves. A recent study that utilised and tested GPR in a clandestine grave scenario, monitored both simulated and

human clandestine graves in Colombia, South America (Molina et al. 2016). Anomalies corresponding with the locations of the graves were detected, however the amplitude decreased over time. It was therefore concluded that GPR was primarily detecting the disturbed grave fill rather than the target itself i.e. the buried human remains. Additional research in Colombia, on simulated burials containing buried pigs, found that GPR was able to obtain 'good' GPR time slices up to nineteen weeks post burial, however, post nineteen weeks the time slices deteriorated (Molina et al. 2015). An advantage of GPR over other geophysical techniques was demonstrated by France et al. (1992) who reported that GPR offered the most information, in real time, when a skilled and experienced operator was used when compared to magnetic and electromagnetic techniques. However, France et al. (1992) compared only GPR, magnetic and electromagnetic techniques and did not take into account resistivity surveys. As demonstrated, GPR is often stated as being the preferred geophysical technique, however, Ruffell et al. (2009) reported a case study, focused around locating a burial of a missing person in Northern Ireland, where GPR was employed alongside cadaver dogs and witness testimony as part of a multidisciplinary approach. Both the GPR and cadaver dogs indicated a possible grave, however, once intrusive investigation was undertaken no human remains were discovered. As a result Ruffell et al. (2009) state that this should be a cautionary tale. In addition, GPR is known to produce unreliable results in wet, clay-rich or saline soils, due to the instrument having difficulty delineating features such as graves; it is recommended in such cases that other techniques are employed (Ruffell and McKinley 2005).

GPR has also been noted as being useful in the search for buried items including illegally buried waste, allowing for the 'informed positioning' of other geophysical techniques that offer more detailed information, in this case, electrical resistivity imaging (ERI) (Ruffell and Kulessa 2009). GPR was found to be a rapid technique and by combining both GPR and ERI, cross validation of results and enhanced data interpretation was achieved (Ruffell and Kulessa 2009). Orlando and Marchesi (2001) employed GPR in the detection and characterisation of historical waste sites in Italy. GPR successfully located the dump site and also enabled the spatial extent of the sites to be ascertained; due to the buried matter producing "...diffraction and non-continuous reflections..." thus causing an anomaly (Orlando and Marchesi 2001, p. 163). To truth the site, intrusive techniques were used; this being the equivalent of using a probe or augur in forensic cases.

Therefore, it can be seen that GPR has its limitations. Although not mentioned above, it is important to note that GPR surveys are relatively time consuming and cannot be used easily over large areas or uneven surfaces. In contrast, remote sensing can be used to investigate large areas, regardless of their topography and could therefore be used as a starter point for

investigations, where informed decisions can then be made as to the most appropriate geophysical technique.

2.5.2.2 Earth Resistivity

Using earth resistivity or resistivity mapping, is increasingly being investigated for the detection of burials (Buck 2003; Pringle and Jervis 2010). Scott and Hunter (2004, p. 33) state that resistivity "involves passing an electrical current into the ground between two remote electrodes and measuring the electrical potential between two or more electrodes" to determine the electrical properties of the subsurface (Cheetham 2005). Subsurface anomalies are detected by recording a series of measurements along a constructed grid following which the resistivity values are plotted and compared (Buck 2003). The ground measured by the resistivity array is rarely completely uniform and consequently, the resistivity measured is actually "apparent resistivity" (Scott and Hunter 2004, p. 34). Pringle and Jervis (2010) suggest that bulk ground resistivity surveys are underutilised within forensic surveys and intimate that a reason for this may be due to the perceived poor resolution of the technique, when compared to GPR; as well as there being a general lack of literature detailing previous successes. Resistivity is sensitive to a wide variety of changes in the ground that may be attributable to a grave being present. However, care should be taken, as in order to detect the anomaly, the response from the grave has to be above that of the background variation; if this is not the case the site may remain undetected (Scott and Hunter 2004). Scott and Hunter (2004) suggest that in the case of mass graves, the response from the anomaly (i.e. the mass of buried human remains) may be much larger; therefore hypothetically, resistivity may be a more useful technique.

Recent research on simulated burials containing mammalian remains revealed that resistivity can be utilised for the detection of naked and wrapped burials (Cheetham 2005; Pringle et al. 2008; Jervis et al. 2009; Pringle et al. 2012). However, there are variables which have been shown to affect the techniques detection success including, soil type, time of interment and burial environment (Pringle et al. 2010). The major difficulty when utilising resistivity is the fact that there is not a 'typical burial anomaly', in fact, the act of burying a body/bodies and disturbing the ground has the potential to either increase or decrease the measured, apparent resistivity (Scott and Hunter 2004). Therefore, ground truthing any detected anomalies is vital, by using T-bar probes or augers, prior to full scale excavations being undertaken (Owsley 1995; Haglund et al. 2001).

Juerges et al. (2010) carried out a study which directly compared electrical resistivity and magnetic geophysical techniques on simulated burials (0.25-1 year old) in four contrasting environments. Varying levels of success were reported for the use of magnetic surveys, whereas, electrical resistivity located anomalies that corresponded directly to the locations of the simulated burials. Grave fluid was collected from the graves, it was found to contain an elevated concentration of iron which was suggested to have caused the observed magnetic anomalies (Jurges et al. 2010). The production and increased volume of decomposition fluid was suggested to have caused the low resistivity anomalies observed (Jurges et al. 2010). Therefore, it was concluded that resistivity was more successful in locating anomalies when compared to magnetic techniques; if a magnetic survey is to be carried out, that it should be used alongside a complimentary technique (Jurges et al. 2010).

More recently GPR and bulk ground resistivity were compared for detecting unmarked single burials, specifically in graveyards (Hansen et al. 2014). Soil type was demonstrated to have greatly affected the successful detection of unmarked burials. GPR was found to be optimal for detection of burials in coarse soils, whereas resistivity surveys were found to be optimal in clay rich soils; with both techniques noted as successful in sandy and black earth soils (Hansen et al. 2014).

Within the literature resistivity surveys are the only geophysical technique to have been successful in detecting human mass graves. In 2002 the ICMP conducted resistivity surveys on a suspected mass grave site in Batajnica, Serbia and Montenegro. It was found that the mass grave had high apparent resistivity when compared to the surrounding geology (ICMP 2004). Following this, the ICMP along with a number of forensic specialists carried out an interdisciplinary project in Bosnia and Herzegovina in 2005 which investigated the application of resistivity surveys (both mapping and imaging) for detecting mass graves; among other techniques. It was found that resistivity mapping was able to successfully locate four out of the five graves surveyed (ICMP 2005). However, it was noted that the resistivity values, of the graves, were a mixture of either low or high readings and consequently, caution should be taken when applying the technique; with areas of both low and high apparent resistivity being investigated.

Although resistivity surveys have demonstrable success in locating human mass graves in Bosnia and Herzegovina, this remains a rarity in published literature with many of the studies being carried out on simulated single graves. Conducting resistivity surveys on anomalies identified through the analysis of remote sensing imagery may be a promising avenue for further research.

2.5.2.3 Electromagnetic Systems

The final geophysical technique that will be discussed in this review is electromagnetics (EM); these systems measure the bulk conductivity of a volume of soil and can be used to detect subsurface ferrous and non-ferrous metallics (France et al. 1992; Pringle et al. 2008). Bevan (1991) states that electromagnetic instruments provide a fast measurement of the electro-conductivity of the Earth that can be used in either a horizontal or a vertical orientation depending on whether the survey is prospecting for shallow, near surface features or deep features (Pringle et al. 2008). An anomaly is detected when the response from the sub-surface target is much higher or lower than the relative measurements obtained around it. Consequently, for an anomaly to be detected the sensitivity of the detector needs to be exceeded by the response from the buried object, as well as the response from the natural background variation (Nobes 2000). It should be noted that unlike many geophysical techniques, EM systems only need to pass near the target to retrieve a response; as electromagnetic responses are received from a larger area of the sub-surface (Nobes 2000). In a study conducted by Nobes (2000) an EM system as well as GPR was employed in the search for a clandestine burial, however, resistivity was not utilised. It was reported that the EM system identified an anomaly that coincided with the location of the buried body whereas, the GPR did not. It was suggested that this may have been due to the presence of sandy sediment, which may have masked any grave-like features.

Similar to GPR, there is no published literature that details electromagnetic surveys being carried out on human mass graves. Although there are a number of papers including Nobes (2000) who utilise this technique to locate anomalies, synonymous with single burials, there is no real understanding of this techniques appropriateness or suitability for locating mass graves.

2.5.3 Documentary Evidence

Documentary evidence has also been proven useful in the search and location of mass graves. Cheetham et al. (2008) state that on the ground photographic documentation is becoming increasingly useful. Evidence can be collected by the media, civilians via mobile phones which are now common worldwide. An example of this is the Petrovic video of the Kravica warehouse massacre, which was used as evidence in the trials for the International Criminal Tribunal for the Former Yugoslavia (ICTY) (Cheetham et al. 2008).

2.5.4 Aerial Photography

Aerial photography is widely acknowledged as being one of the earliest forms of remote sensing (Brilis et al. 2000). Aerial photography archives are large and established, dating back to the Second World War, which are largely underutilised in a forensic context. However, in recent years a shift has occurred which has seen aerial imagery being utilised during the search and location of clandestine graves, in both domestic and international casework (Cox et al. 2008b). Aerial photography is suggested as a useful resource that can be considered for use during the search, detection and location of mass graves (Anderson et al. 2008).

The first known aerial photographs were collected in 1858 using a camera attached to a balloon in France by Gaspard-Feliz Tounachon (Campbell and Wynne 2011). Aerial photographs were later used in the early 1900s for military purposes including, aerial reconnaissance during World War I. Developments continued to be made through the early 1900s and by 1930 it is noted by Campbell and Wynne (2011) that aerial photography and photogrammetry "...the science...of obtaining spatial measurements and other geometrically reliable derived products from photographs" (Lillesand et al. 2008, p. 146), had begun to be utilised.

A scene is recorded by a camera onto photographic film, when electromagnetic radiation passes through the lens and is focussed on a recording medium or film, resulting in an aerial photograph (Gibson 2000). Gibson (2000) emphasises that the characteristics of the film chosen, as well as the lens and the filters used, determine the signal that is recorded and therefore, the photograph produced. There are many benefits to using aerial photography, Lillesand et al. (2008, p. 50) state that "…aerial photography offers a simple, reliable, flexible and inexpensive means of acquiring…" imagery of specific areas of interest. Stereo imagery can also be acquired (i.e. where a target on the Earth's surface is imaged at least twice, which ideally has an overlap of 60%), this imagery can be used to measure the geometric properties of a surface, hence the term photogrammetry.

Aerial photography collects imagery of areas on a local scale, this can be useful in a forensic context when the investigation area is relatively small. During the conflict in Bosnia and Herzegovina in the 1990s, air photos were obtained by the United States Authorities for the purposes of locating areas of ground disturbance or exposed soil. The air photos were used by investigators and experts to aid in the location of mass grave sites and were later used as evidence in the ICTY criminal trials (Manning 2003).

However, the ability to capture aerial imagery relies on access to aircraft and resulting photographs record a single moment in time. Imagery is rarely collected with a temporal study in mind and is often collected during periods of conflict. In the case of mass graves, following the re-colonisation of exposed soil, the evidential value of this data may be significantly reduced. In addition, there are further issues relating to airspace and permissions that may hamper the ability to collect such imagery in the first place. More recently, research by Baier and Rando (2016) explored the utility of using photogrammetry, specifically Structure-from-Motion, to aid in mass grave recording; using this technique, a mass grave was simulated and recorded in three dimensions.

Neither aerial photography nor photogrammetry will be used within this research, as orbital remote sensing is collected routinely with a known repeat cycle, therefore enabling a large scale, temporal study to be conducted encompassing large spatial extents.

2.5.5 Remote Sensing as a Tool for Detecting Disturbance indicative of the Presence of Mass Graves

Davenport (2001) reported that remote sensing methods are increasingly utilised by forensic investigators, to prospect for clandestine human mass graves and to locate physical evidence related to human rights abuses and/or violations. The very nature of remote sensing, particularly satellite imagery, is advantageous for documenting human rights abuses and prospecting for mass graves, as it offers the unique opportunity to collect real-time evidence, as well as evidence both pre- and post-event.

Remote sensing is defined by Lillesand et al. (2008, p. 1) as the "science and art of obtaining information about an object, area or phenomenon through the analysis of data acquired by a device that is not in contact with the object, area or phenomenon". It is an established field of science and is widely used for the "study of the Earth's atmosphere as well as its surface" (Rees 1990, p. 1). This includes utilising sensors on airborne and orbital platforms for multiple applications including: oil and mineral prospection, earth resource and environmental monitoring (Sabins 1997) as well as military and intelligence applications (Wang et al. 2013).

Wang et al. (2013) state that the major benefit of satellite imagery over other detection techniques is that it can provide accurate and detailed information, regarding a specific geographical area of interest in a relatively short period of time, independent of political or physical boundaries. However, using satellite imagery as documentary evidence in a court of

law to document and demonstrate human rights abuses and violations is under researched and ill-defined (Wang et al. 2013). Without employing standard operating procedures and considering the ethics involved, meaningful evidence that would usually be admissible in court is unable to be heard. However, satellite imagery and aerial imagery has already been admitted as evidence in cases at the International Criminal Court (ICC), International Court of Justice (ICJ), ICTY and the Permanent Court of Arbitration (PCA) at The Hague (Wang et al. 2013). In these cases the satellite and aerial imagery was overwhelming and damning, clearly showing mass graves being constructed, as well as piles of bodies waiting to be buried.

Raymond (2012), during an interview with CBC Radio, outlined three postures that can be used by investigators that enable human rights abuses and violations to be monitored using orbital imagery. The first, known as the 'detection posture' is where satellite imagery is used prior to an atrocity occurring; with analysts monitoring potential build-ups of forces and infrastructure. The second, the 'deterrence posture', is adopted during the early stages of alleged atrocities, where observations from the imagery can be communicated to civilians, providing a warning. 'The documentation posture' is employed following an atrocity, where evidence is collected retrospectively. These postures, or approaches as defined by Raymond (2012), outline how remote sensing, specifically, in this instance orbital imagery, can be used for the efficient detection and documentation of human rights abuses and violations across the globe.

Cox et al. (2008b) suggest that remote sensing, specifically airborne and orbital satellite imagery is utilised in the later planning stages, whereas, aerial photography can is advised to be used in the early stages, to advise operations in-country. It is stated by Davenport (2001) that remote sensing, when used appropriately, can be an incredibly useful tool for forensic investigators as it can save time, lives, resources and money.

The American Association for the Advancement of Science, specifically the Scientific Responsibility, Human Rights and Law Program (SRHRL), advocate the use of geospatial information, including remotely sensed imagery, for human rights litigation (Harris et al. 2018) and have recently published a document outlining technical and legal considerations. It is emphasised that remotely sensed data can offer solutions to some of the most difficult human rights documentation challenges including, destruction, military movements or disturbance; by providing access to otherwise inaccessible areas (Harris et al. 2018). Not only can they observe these events, they can pinpoint the date, time and location and provide a chronology to aid any investigations. Such imagery can be considered alongside witness testimony and digital evidence to either corroborate or refute it; as was the case in the ICTY

where satellite and aerial imagery alongside witness testimony were provided as evidence for the prosecution (Harris et al. 2018). Within the paper by Harris et al. (2018) the creation of false-colour composite images and the use of multispectral imaging capable of revealing information including vegetation stress is noted. However, limitations of such technology are also outlined and include coverage and resolution; government restrictions; ethical considerations and cost (Harris et al. 2018).

2.5.5.1 Previous Research using Remote Sensing for the Detection of Clandestine Graves

To detect grave sites accurately it is imperative to understand the effect that disturbance directly attributable to the creation of the grave, as well as, the presence of buried organic remains, has on the surrounding ground and vegetation. Research undertaken to date investigating the use of remote sensing methods for grave detection can be split into three approaches:

1. Remote sensing for the detection of vegetation stress
2. Remote sensing for the detection of differences in spectral characteristics of disturbed versus undisturbed soil
3. Remote sensing where elevation change i.e. loss or gain, is used as a proxy for detecting disturbed soil

Previous research has demonstrated that the presence of buried organic remains, essentially a contaminant in the soil matrix, alters the vegetation and soil surrounding and directly above mass burials, resulting in areas of either positively or negatively stressed vegetation (Kalacska and Bell 2006; Kalacska et al. 2009). The lack of knowledge regarding the relationship between organic decomposition by-products and the effect of this on the reflectance of vegetation, above mass graves, is a limiting factor.

Kalacska and Bell (2006) were some of the first researchers to suggest remote sensing, using a combination of field spectroscopy, airborne and satellite imagery; as a potential new means of detecting mass graves. Kalacska et al. (2009) went on to conduct research in the Costa Rican tropics, where both airborne hyperspectral imagery (collected using a HyMap II sensor on board a WB57 aircraft) and field reflectance spectroscopy (using an ASD FieldSpec FR spectroradiometer with a spectral range of 350-2500nm) were used as complimentary techniques to monitor a simulated mass grave site, over a period of sixteen months. Two identical, relatively small mass graves were created, one containing cattle and the other

empty, containing backfilled soil (control grave). Kalacska et al. (2009) reported at two hours post burial, there were no significant spectral differences between the surfaces of the two graves which were dominated by disturbed soil. After five months, vegetation had begun to colonise the control grave; at this point reflectance spectra of soil and vegetation were being directly compared, resulting in inevitable spectral differences being observed. At sixteen months, the final monitoring phase, it was reported that both graves had become colonised with vegetation. However, it was found that the grave containing the cattle had been colonised to a lesser extent when visually compared to the control grave (Kalacska et al. 2009). The reflectance spectra of the colonising vegetation from above the cattle grave revealed that, the Red Edge was less steep than that of the control grave (Figure 2). The Red Edge is "…the sharp change in leaf reflectance between 680 and 750nm" indicative of vegetation chlorophyll status and vegetation stress (Horler et al. 1983).

Following on from Kalacska et al. (2009), Norton (2010) conducted research to assess the application of field reflectance spectroscopy for locating graves in temperate environments. An ASD LabSpec spectrometer, in combination with a high intensity contact probe, was used during a pilot study and also during field studies on human burials at Natural Burial Grounds (NBG's) to measure soil reflectance. During the pilot laboratory study, simulated mini mass graves containing organic minced beef (Figure 3) were created and monitored over four consecutive weeks with reflectance spectra collected from grave and non-grave areas of soil at the beginning and end of each week. After carrying out principle component analysis, it was found that grave soil was able to be distinguished from non-grave soil regardless of the age of burial or changes in soil moisture (Figure 4).

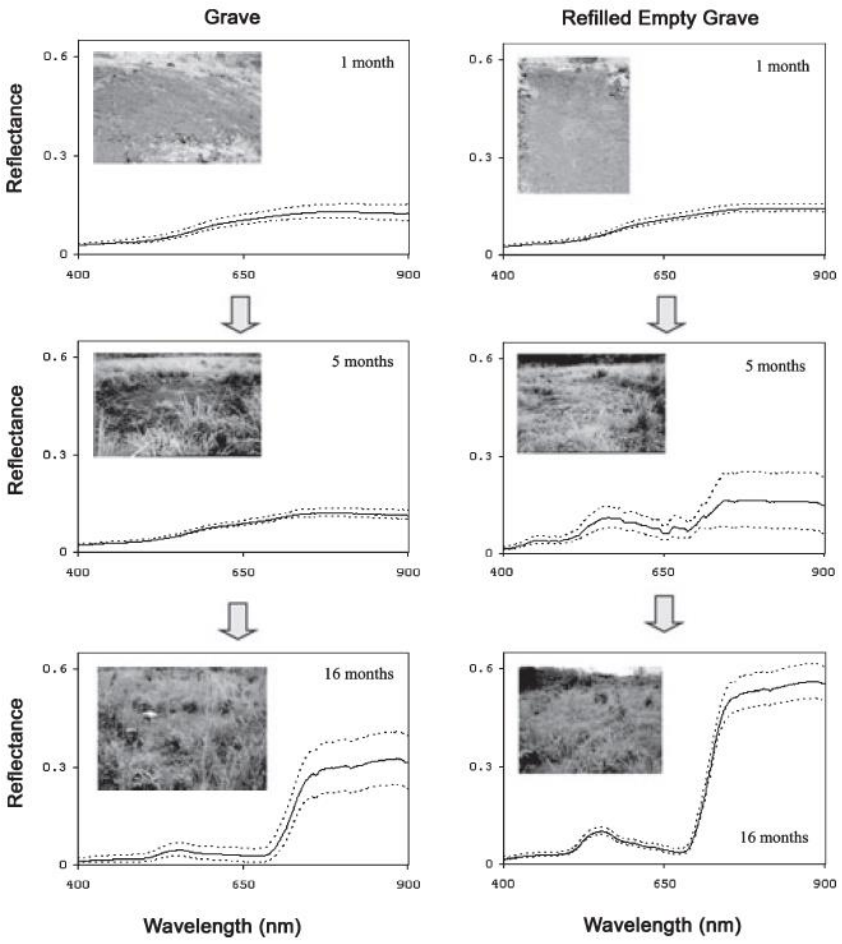

Figure 2 - Progression of the spectral signatures of the experimental mass grave and the control grave over 16 months derived from the in situ hand-held measurements. Mean (solid line), standard deviation (dotted lines). (Kalacska et al. 2009).

Figure 3 - Images relating to the collection of soil reflectance spectra from simulated mass graves during the control, laboratory experiment. Source: Norton 2010.

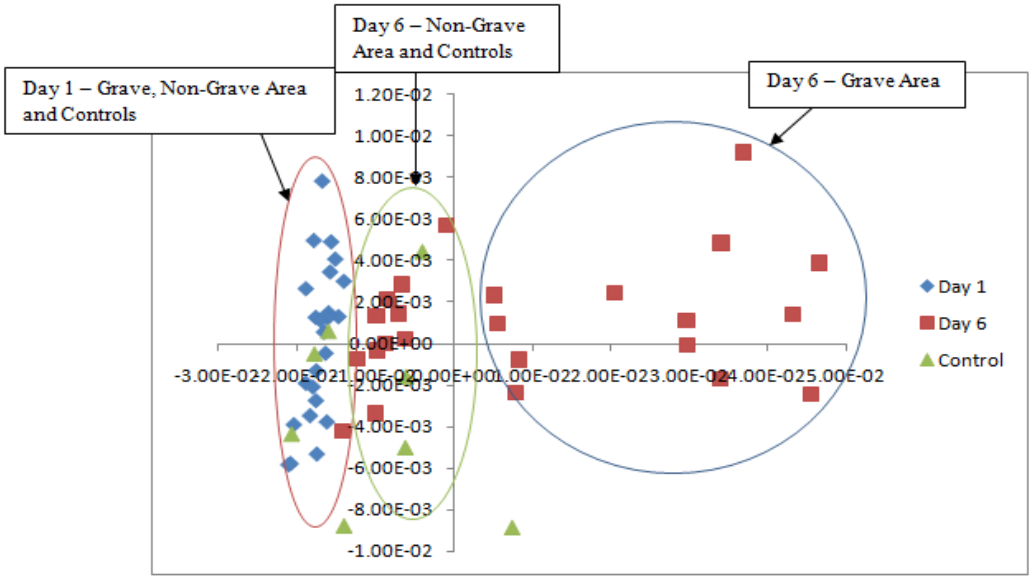

Figure 4 - Principle component similarity map showing three components, spectra collected on day one, spectra collected on day six for the non-grave areas and controls and spectra collected on day six over the grave. Source: Norton, 2010.

The second strand to this research was the collection of soil reflectance spectra from human burials at NBG's (Figure 5). Through undertaking Principle Component Analysis it was found that 75% of the similarity maps produced, demonstrated that grave soil and non-grave soil could be differentiated (Figure 6 for an example similarity map).

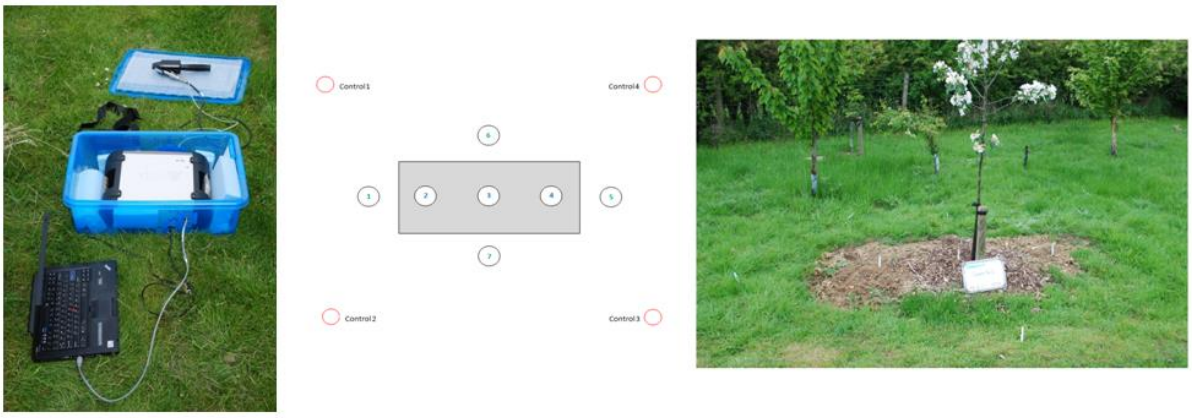

Figure 5 - Photographs of sample collection from an example grave at one of the Natural Burial Grounds. The ASD LabSpec (far left), schematic diagram of measurement points for each grave (centre) and an example grave from which spectral measurements of the soil were taken (far right). Source: Norton, 2010.

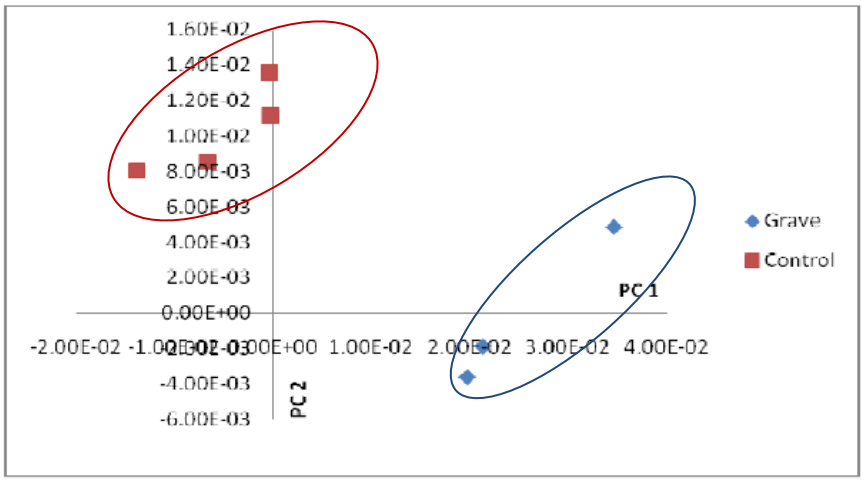

Figure 6 - Example of a principle component similarity map for one of the human burials at a natural burial site, showing two distinct groupings – one for the grave (circled in blue) and one for a control area i.e. non-burial (circled in red). Source: Norton, 2010.

Recent research by Leblanc et al. (2014) focused on the use of airborne hyperspectral imaging for the detection of single graves, rather than mass graves, in the semi-urban outskirts of Ottawa, Canada. It was stated that, due to the smaller size/ quantity of the remains, and the extent of the grave, the probability of detection was lower, hence why fine spatial and spectral resolution imagery was selected. During this study there were two targets, one grave containing at least one buried pig and an empty grave. Two hyperspectral sensors (CASI and SASI), with a spectral range of 208-2524nm, were flown on two occasions (20th July and 5th August 2011) at an altitude of 643m; resulting in a ground spatial resolution of 0.75m and 0.69m for the CASI and SASI respectively (Leblanc et al. 2014). During the overflight there was simultaneous ground data campaign where spectral measurements were collected from various targets using a hand held ASD FieldSpec 3. This data was used to calibrate and atmospherically correct the airborne imagery. Following the acquisition of the imagery and pre-processing, including atmospheric correction using Fast Line-of-sight Atmospheric Analysis of Hypercubes – FLAASH, narrow band vegetation indices were calculated. The study was designed to observe the relative difference between vegetation. Therefore, the search aimed to locate small scale anomalies (maximum size of 4m^2) with a spectral signature indicative of disturbed soil. Two of the targets were located within 10m of the true burial location. Further work was recommended to determine the applicability of the method in varying climes, landscapes and other land cover types (Leblanc et al. 2014). Leblanc et al. (2014) suggest, for future studies, where the spectral bands of interest are not well defined, hyperspectral imagery could be more useful than multispectral imagery, as it provides increased spectral information. However, in studies

where airborne hyperspectral imagery is collected, temporal resolution is often poor, with only a handful of observations; from which generalised comments and conclusions are drawn. Furthermore, airborne imagery is expensive to obtain and opportunistic, whereas, orbital imagery is repeatable, has relatively fine temporal (platform dependent) and spatial resolution, which will improve rapidly with advancements in technology.

Orbital remote sensing (Landsat 5 TM imagery) was used in Iraq, after receiving eye witness testimonies regarding the location of mass graves from both Bedouin's and other locals, to identify areas of extensive disturbance including features, trench outlines and spoil piles (Schuldenrein et al. 2017, p. 135). The areas identified underwent both surface and sub-surface surveys including geophysics and excavations, which verified the presence of human remains and therefore, the existence of the mass graves (Schuldenrein et al. 2017). In total ten graves, approximately 3.5m in width, were located using this multidisciplinary approach. This approach is similar to that of the US military during the unrest in the Former Yugoslavia in the 1990's, where U-2 aerial photography was captured of suspected execution and mass grave sites, where disturbance including excavated pits/ trenches, spoil piles and piles of executed bodies were able to be observed. This imagery was subsequently submitted as evidence during the criminal trials of the ICTY.

Research by Corcoran et al. (2018) investigating the use of terrestrial Light Detection and Ranging (LiDAR) to detect elevation change associated with unmarked graves, demonstrated that immediately post creation elevation loss was observed and persisted until 108 days post burial. However, no further elevation changes were measured post 108 days up until 643 days after burial creation. This was the case for all simulated graves including, a single grave, a grave containing three individuals and a grave containing six individuals. The same observation was made for a control grave, containing only backfilled soil. The research was undertaken with the aim "…to support the narrowing down of possible unmarked grave locations" (Corcoran et al. 2018). However, several scans were undertaken to generate the required data due to large trees and other obstructions causing significant gaps in the point cloud data. Due to this method being terrestrial, this requires a significant amount of evidence to be in hand prior to this method being employed i.e. an area of interest must already be established. This method would be impractical and inefficient when used over large spatial extents and rendered useless in areas inaccessible due to political tensions or difficult terrain. In addition, as multiple data collections are required of the same area over relatively protracted time periods this method would be inappropriate for high profile investigations with significant time pressures. Elevation change will not be considered further within this research, as the results obtained by Corcoran et al. (2018) were inconclusive when detecting changes in elevation in excess of 108 days post burial.

Evers et al. (2018) investigated the applicability of low altitude, near infrared aerial photography collected using an unmanned aerial vehicle (UAV) to aid in the detection of clandestine burials. This research was inspired by the use of near infrared photography for the detection of archaeological anomalies. Evers et al. (2018) focussed on the detection of grave edges i.e. the junction between disturbed and undisturbed soil at a Natural Burial Ground containing 138 individuals who had been interred between 2000 and 2017. It was noted that the grave edges could be successfully delineated however, weather conditions, cloud cover, sun position and the age of the grave were limiting factors due to the influence of each of these on the appearance of the graves in both the visible and near infrared regions. Consequently, variations in the images were observed following the application of the edge detection algorithms. It is clear that although using UAVs enables data from larger spatial extents to be collected when compared to terrestrial methods (Corcoran et al. 2018), this pales into insignificance when compared to the potential data collection available from orbital platforms. The use of UAVs is also limited by the factors listed above and can therefore only be employed in a limited set of circumstances, particularly if spectral information is to be derived from the data and interrogated.

The potential for remote sensing to be used on a number of platforms, airborne or terrestrial, for the detection of graves has been demonstrated by Kalacska et al. (2009), Norton (2010), Leblanc et al. (2014), Corcoran et al. (2017) and Evers et al. (2018). However, it is clear that additional research is needed in temperate environments, where analogues representative of humans and their decomposition are used, the effect of different grave surfaces are explored and where the site is frequently monitored to deduce the variables responsible for spectral differences in vegetation above graves. Imagery from various platforms including the use of fine temporal, freely available, medium spatial resolution orbital imagery will be considered with vegetation stress above mass graves monitored over extended time periods. This research aims to produce a viable method using orbital remote sensing that enables investigations to be undertaken at relatively large spatial scales therefore, being more applicable and practical in the context of searching for clandestine mass graves.

To determine the applicability of remote sensing in the detection of mass graves it is key to consider vegetation physiology and understand how disturbance can be quantified through observing vegetation stress; often via vegetation indices.

2.5.6 Vegetation Physiology

The pigments contained within leaves, such as chlorophyll, are related directly to the physiological function of vegetation; chlorophyll absorbs electromagnetic radiation in the red and blue regions, this energy then contributes to the photosynthetic process (Sims and Gamon 2002). Consequently, pigments within leaves can be used as a proxy to indicate the physiological state of vegetation, chlorophyll often being the pigment of choice as it reduces more readily than other pigments, when the plant is under stress or during senescence (Sims and Gamon 2002).

In recent years, trends in vegetation phenology "...the study of the timing of recurrent biological events..." (Richardson et al. 2013, p. 156), both localised and worldwide, have gained scientific interest due to the fact phenological responses of vegetation can be used as an indicator of factors including climate change. Studies into these are carried out through large area vegetation monitoring using either ground based techniques, and imagery from airborne or orbital platforms (Eastman et al. 2013; Richardson et al. 2013). Zwiggelaar (1998) states that variations in vegetation physiology, occurring within during the growing season, are caused by a number of factors including: change in cellular size, chemical composition, water concentration, in addition, to other plant stress factors; all of which can be affected by climatic and anthropogenic activities. Consequently, due to these irregular and uncharacteristic changes in vegetation over seasons, events such as, climate change, deforestation and disturbances relating to the creation of graves can be detected. In tropical ecosystems vegetation phenology may be less affected by temperature and also the availability of sunlight but may be more sensitive to seasonal shifts in precipitation i.e. dry and rainy seasons, which are very different to temperate climes (Cleland et al. 2007). Furthermore, the orbital phenological investigation and monitoring of vegetation in the tropics is often hampered by the presence of cloud and/or haze, meaning that cloud free observations can be a rarity.

Central to the investigation of phenology are vegetation indices, where spectral data is utilised by scientists worldwide to infer and investigate natural, as well as man-made phenomena. Bannari et al. (1995) published a comprehensive review of vegetation indices that have been developed for a variety of applications, with more than forty having been developed prior to 1995. The spectral characteristics of vegetation are directly related to their chemical composition and also the physical properties of plants, as well as the spectral properties of the illumination source, which in most cases is the Sun (Zwiggelaar 1998). Vegetation indices are formed by combining several spectral values that are either added, divided or multiplied; alternatively, indices can be created by forming linear combinations of

spectral band data to create a single value (Jackson and Huete 1991). Through the calculation, the vegetation signal is enhanced whilst other factors which are known to affect their values are dampened. The successful use of vegetation indices requires considerable knowledge of the variables inputted and also recognition of the factors that can affect the calculated value i.e. the structure of the vegetation canopy and influences of the external environment (Jackson and Huete 1991). Vegetation indices were primarily created to allow plant signals to be extracted from spectral data. Factors including, soil background, moisture, solar zenith angles and also the instrument view angles, as well as, the atmospheric column can have a major impact on the calculated values (Jackson and Huete 1991). Jackson and Huete (1991) state that until the soil is fully colonised by vegetation, the soil will continue to influence the indices. In addition, the solar angle is known to have a notable impact on vegetation indices, due to vegetation being non-lambertian, a non-perfect reflector; causing solar radiation to be scattered in many different directions. Therefore, differences in solar angle can cause different spectral values to be obtained, even from the same surface (Jackson and Huete 1991).

High vegetation index values often indicate pixels, or areas, that contain healthy vegetation whereas, low values can either indicate that the pixel contains small quantities of vegetation or vegetation that is stressed (Campbell and Wynne 2011). Therefore, low vegetation index values observed following an event can be indicative of disturbance; this is due to the sudden presence of large quantities of soil relative to vegetation. If low values persist over time, with very little recovery in the index value observed, this could be interpreted as an area containing stressed vegetation.

Caution must be taken when calculating vegetation indices from imagery, derived from different platforms and instruments, over the same area of interest. Jackson and Huete (1991) state that the indices calculated may not be the comparable due to differences in the detector, the filter characteristics of the instrument as well as, the differences in the band-response functions.

2.5.6.1 Vegetation Indices

There are two classes of vegetation indices (VI), ratios and linear combinations. A ratio VI is commonly a ratio of two spectral bands, examples of which are, the Ratio Vegetation Index (RVI) and the Normalised Difference Vegetation Index (NDVI). Whereas, linear combination VIs are an orthogonal set of a number of linear equations that are calculated from a number of spectral bands, an example of which are the tasselled cap transformation

(Kauth-Thomas transformation) and the Perpendicular Vegetation Index (PVI) (Jackson and Huete 1991). Campbell and Wynne (2011) state that applying ratio VI's, including NDVI, to living vegetation is an established science and is often used due to the inverse relationship that exists between vegetation brightness in the red and infrared regions. The absorption of red light by the chlorophyll present, in combination with, the strong reflection of infrared light by the internal plant structure, means that the values for each of these electromagnetic regions will be different. Therefore, the values will be higher during the active growing period of the vegetation.

Vegetation indices can also be split into two categories, broadband and narrowband greenness. Broadband greenness is one of the simplest calculations which enables investigators to measure the quantity and health of green vegetation; providing a measure of the amount and quality of the chlorophyll content present within vegetation (EXELIS 2015d). These indices directly compare reflectance measurements from the NIR to those in the red regions; they are widely applied and are often successful due to the features examined being spectrally broad. Broadband greenness is used for applications including: vegetation phenology studies, land-use casework, climate change monitoring and also crop health studies. Examples of indices that fall under this category are Enhanced Vegetation Index (EVI) and the Normalised Vegetation Difference Index (NDVI) among others.

Narrowband greenness has very similar principles to broadband greenness, as they measure the quantity and health of green vegetation, the primary difference being that they utilise reflectance measurements in the red and NIR to sample the red edge portion (690-740nm) of the reflectance curve (EXELIS 2015e). Consequently, narrowband VIs are more sensitive to smaller, subtle changes in vegetation health and are able to be used in dense vegetation environments where broadband indices tend to saturate (EXELIS 2015e).

2.5.6.1.1 Normalised Difference Vegetation Index (NDVI)

The most well-known and established vegetation index is the NDVI, introduced by Deering in 1978 and Tucker in 1979 (Brown et al. 2006 - Equation 1). NDVI is often used to monitor vegetation health and dynamics; this index allows for relatively simple temporal and spatial comparisons to be made (Brown et al. 2006). NDVI is a ratio which uses the NIR and red bands (from the visible part of the electromagnetic spectrum) to monitor green vegetation. The index is the ratio of the difference between the NIR and red band divided by their sum, as can be seen below (Brown et al. 2006; Morawitz et al. 2006). This calculation results in an image as seen in Figure 7.

Equation 1 - NDVI Equation

$$NDVI = \frac{(NIR - R)}{(NIR + R)}$$

NDVI is monitored globally by the Global Inventory Modelling and Mapping Studies (GIMMS) group at NASA's Goddard Space Flight Centre, using the Advanced Very High Resolution Radiometer sensor onboard the National Oceanic and Atmospheric Administration satellite (NOAA). Global NDVI timeseries have been collected and archived since 1981, with a bi-weekly temporal resolution (Eastman et al. 2013). This imagery has coarse spatial resolution (1-8km) and is therefore, not suitable to be used to detect small scale changes, rather large scale issues such as climate change/ deforestation. Typically data from channels 1 (visible band, 0.50-0.68μm) and 2 (near infrared band, 0.725-1μm) of the AVHRR are used to calculate vegetation indices; namely NDVI and also the Simple Vegetation Index (VI) (Lillesand et al. 2008). In literature, NDVI is stated as being preferential when compared to other vegetation indices, as it compensates for factors including varying illumination, slope of surface and aspect (Lillesand et al. 2008), making it widely applicable and flexible. Due to its relatively simple, robust and repeatable nature, NDVI is of considerable value when used as an indicator of environmental change (Eastman et al. 2013). Within this research, NDVI will be assessed for use in mass grave detection, to ascertain its success in detecting areas of stressed vegetation across relatively large spatial scales, using archive multispectral imagery.

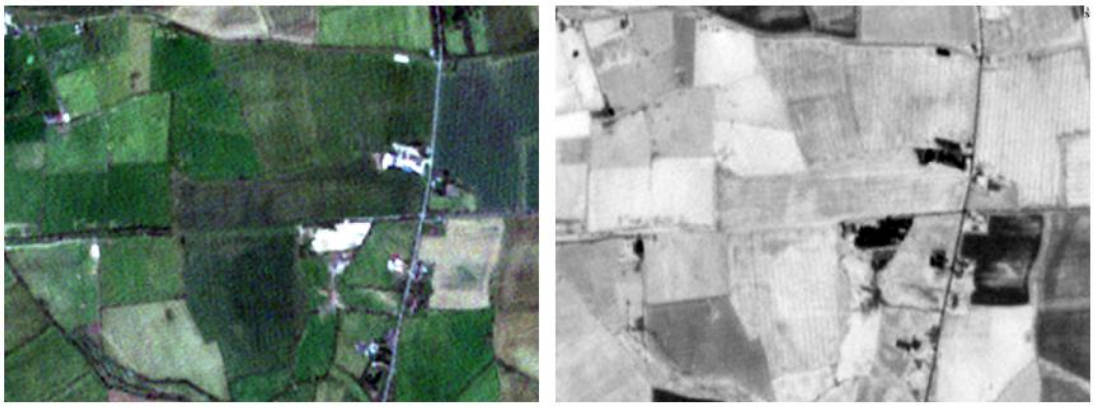

Figure 7 - Example of an atmospherically corrected true colour composite, prior to NDVI calculation (left) and a NDVI image (right), both from April 2010 in the same location. Images produced by the author.

2.5.6.1.2 Enhanced Vegetation Index (EVI)

The enhanced vegetation index (EVI) was proposed by the MODIS Land Discipline Group and was developed to correct for the distortions in reflectance caused by particles in the atmosphere, as well as soil beneath vegetation canopy. EVI and NDVI are considered global based vegetation indices that provide continuous information, both spatial and temporal, regarding global vegetation dynamics (Matsushita et al. 2007). Similar to the NDVI, EVI is a ratio between the red and NIR values, with the primary differences being the inclusion of a soil adjustment factor, coefficients for atmospheric resistance and values derived from the blue portion of the electromagnetic spectrum (Lie and Huete, 1995; Equation 2). The inclusion of which results in background noise, atmospheric noise as well as saturation in many cases being reduced (USGS 2017). Nevertheless, EVI is often referred to as a modified version of the NDVI, with an increased sensitivity in high biomass regions resulting in the improved monitoring of vegetation (Matsushita et al. 2007). However, the inclusion of the soil adjustment factor results in EVI being more sensitive to topographic conditions, when compared to other indices i.e. NDVI; therefore, Matsushita et al (2007) recommend removal of the topographic effect from the reflectance data prior to the calculation of EVI when data is collected from areas of rough terrain.

Equation 2 - EVI Equation

$$EVI = 2.5 \frac{(NIR - RED)}{(NIR + 6 \text{ x } RED - 7.5 \text{ x } BLUE + 1)}$$

2.5.6.1.3 Normalised Difference Moisture Index (NDMI)

The normalised difference moisture index (NDMI) is calculated as a ratio between the NIR and the short wave infrared (SWIR) (USGS 2017; Equation 3). The NDMI is also referred to in literature as the normalised difference water index (NDWI). This index is primarily utilised to indicate plant water stress as it is closely related to plant water content and has been successfully applied in forest change detection studies, to track changes in plant biomass and water stress (Wilson and Sader 2002; Jin and Sader 2005). The combination of the NIR and SWIR enables variations in reflectance caused by leaf internal structure and dry content to be removed therefore, enhancing the accuracy in retrieving water content.

Equation 3 - NDMI Equation

$$NDMI = \frac{(NIR - SWIR)}{(NIR + SWIR)}$$

2.5.6.1.4 Soil Adjusted Vegetation Index (SAVI)

The soil adjusted vegetation index (SAVI) is a ratio between the red and NIR bands (USGS 2017) and is a modified version of the NDVI. It has been demonstrated that soil background has considerable influence on the reflectance spectra obtained, particularly in the case of partial vegetation canopies, with dark soils resulting in higher vegetation index values (Huete 1988). Due to NDVI being sensitive to soil optical properties, the SAVI was developed, which with the addition of the soil adjustment factor (L), minimises "…the secondary backscattering effect of canopy-transmitted soil background reflected radiation" (Huete 1988, p. 107). Therefore, reducing the impact that the soil has on the vegetation reflectance spectra obtained. By including a constant (L), SAVI models "the first order of soil-vegetation interactions and significantly reduces soil background effects across a wide range of vegetation conditions" (Qi et al 1994, p. 121). It has been demonstrated by Huete (1988) that an L value of 0.5 accommodates most land cover types; this is used by the USGS (2017) to calculate SAVI for the bulk processing of Landsat products. However, an L value of 1 or 0.25 can be used if there is low vegetation density or for the latter, higher densities (Huete 1988). If the L value is 0, the SAVI is equal to the NDVI (Bannari et al. 1995).

Equation 4 - SAVI Equation

$$SAVI = \frac{(NIR - R)}{(NIR + R + L)}\ (1 + L)$$

2.5.6.1.5 Modified Soil Adjusted Vegetation Index (MSAVI)

The modified soil adjusted vegetation index (MSAVI) is developed from the SAVI and is a ratio between the Red and NIR with a self-adjusting L function; this maximises the reduction of soil effects on vegetation reflectance spectra (USGS 2017). The MSAVI increases the dynamic range of the signal whilst minimising the influence of the soil therefore, increasing the "vegetation signal to soil noise ratio" (Qi et al. 1994, p. 119). When applying MSAVI, no prior knowledge is required regarding the quantity of vegetation cover as the L value is self-

adjusting; this is in contrast to SAVI where typically a *L* value of 0.5 is used, as this was found to reduce soil noise considerably over most land cover types (Qi et al. 1994).

Equation 5 - MSAVI Equation

$$MSAVI = \frac{(2\mathrm{NIR} + 1 - \sqrt{(2NIR + 1)^2 - 8(\mathrm{NIR} - \mathrm{R})})}{2}$$

2.5.6.2 Satellite Instruments operating in the Red - Near Infra-Red (NIR)

The potential for using vegetation indices, for the prospection of clandestine human mass graves is clear. Therefore, it is important to identify the satellite instruments that operate in the red to NIR, from which indices including NDVI, EVI, SAVI and MSAVI can be derived.

With the increased interest in monitoring the Earth's surface using remote sensing techniques, satellite technology has diversified and there are a number of operation satellites that carry vegetation specific sensors. Cleland et al. (2007) state that satellite observations are increasingly important for studies of phenological and environmental changes, due to the fact that they are able to image vast areas on the Earth's surface and collect regular observations; a feature unique to orbital remote sensing.

AVHRR is a broadband scanner, onboard the NOAA satellite, that senses in the visible, near-infrared and also the thermal infrared wavelengths. The first AVHRR was launched in 1978 with the AVHRR/3 launched in 1998 (NOAA SIS 2013). This sensor has an outstanding temporal resolution, with the same area on the Earth's surface being imaged twice a day. Two different sets of imagery are collected, local-area coverage (LAC) and also global-area coverage (GAC), with a spatial resolution of ~1.1km and ~4km respectively. Consequently, AVHRR is regularly used for monitoring global green vegetation dynamics, on a daily basis, as opposed to monitoring small scale, subtle vegetation changes (Holben 1986). Unfortunately, due to the coarse spatial resolution of the imagery acquired, by AVHRR, this data is not suitable for forensic applications.

Satellite Pour L'Observation de la Terre (SPOT) is a vegetation programme developed by France, the European Commission, Belgium, Italy and Sweden, with SPOT1 launched in 1986 (Zwiggelaar 1998). Since 1986 there have been several SPOT sensors launched, with the latest SPOT 7 operational since June 2014. SPOT 1, 2 and 3 collect imagery in a single panchromatic band (10m spatial resolution) and three multispectral bands (20m spatial

resolution). Both SPOT 4 and 5 were enhanced to collect imagery in the short wave infrared (20m spatial resolution), as well as, extra panchromatic bands, allowing for the generation of finer spatial resolution products of 2.5m and 5m respectively (SPOT Image 2010). This is also true for SPOT 6 and 7, which both have five spectral bands (spectral range - 0.45-0.890 µm), with a spatial resolution of 1.5m. The revisit period is one day as both missions operate at the same time; the revisit period can increase to 1-3 days when only one sensor is in operation (ASTRIUM 2015). Both SPOT 4 and SPOT 5 include a VEGETATION instrument that collects imagery in four spectral bands (spectral range - 0.45-1.75µm), with a spatial resolution of 1km and a revisit period of one day (SPOT Image 2010). The imagery obtained from these platforms are used to produce a number of products, including daily and ten-day composites, as well as global coverage.

The VEGETATION images are processed, archived and distributed by the Belgian Research Institute (VITO); with imagery older than three months freely available from http://free.vgt.vito.be. VGT products have coarse spatial resolution of 1km, therefore, this data would be inappropriate for use in small scale vegetation studies or for forensic applications.

MODIS on-board the TERRA (EO AM; launched 1999) and AQUA satellites (EO PM; launched 2002) also have vegetation specific bands. Operating in a complimentary way, TERRA and AQUA have a revisit period of one to two days and acquire imagery in 36 spectral bands (spectral range: 620nm – 14.385µm). The spatial resolution ranges from 250m in bands 1-2, 500m in bands 3-7 and 1km in bands 8-36 (NASA 2015). These sensors are primarily tasked with measuring biological and physical processes on a global basis, providing a series of long term observations to enable global change on both the Earth's surface, as well as atmospheric change, to be observed and quantified (Zwiggelaar 1998). Two vegetation indices (EVI and NDVI) are calculated globally at a spatial resolution of 1km, 500m and 250m at 16 day intervals (Didan 2014). MODIS produces images/ composites that are of too coarse spatial resolution to be used for applications including the detection of small scale disturbances i.e. mass graves. Consequently, this research will utilise multispectral imagery from satellites with relatively fine spatial (>1km) and temporal resolution, that acquire imagery in the visible to near-infrared wavelengths; from which vegetation indices can be derived. Therefore, imagery will be sought from Landsat (5TM – 8 OLI), SPOT, Disaster Monitoring Constellation (DMC) and RapidEye.

2.5.6.3 Quantifying Disturbance through Vegetation Response

Detecting disturbance by using vegetation response as a proxy requires vegetation to be monitored and imaged at multiple scales from terrestrial observations through to orbital images. To extract this information, vegetation indices can be calculated for whole scenes (pixel by pixel), following which the scenes can be stacked and analysed as a time series. This allows for the vegetation and it's response to be studied over time, therefore, providing a temporal perspective. There are multiple methods of analysing time series including the Harmonic Analysis of Time Series (HANTS), which allows vegetation phenology to be studied and changes within the seasonal response to be quantified. Alternatively, time series can be analysed to detect change or disturbance via breakpoints, using methods such as Breaks for Additive Season and Trend (BFAST). Both approaches are used for a number of applications including ecological studies, climatology and agriculture.

In many cases, cloud contaminates scenes causing the temporal continuity, consistency and reliability of datasets to be less than optimal (Zhou et al. 2012); with temporal continuity referring to how regularly imagery is acquired for a particular area on the Earth's surface. Consequently, time series data is often irregularly spaced through time, the only exception being the NDVI and EVI multi-day composites recorded by MODIS. To remedy this, HANTS was developed by W. Verhoef of the National Aerospace Laboratory of the Netherlands (NLR). Zhou et al. (2013) state that HANTS is one of the most widely used time series reconstruction methods, with many studies having demonstrated it successful application. The software is able to process irregularly spaced observations through time. However, to investigate phenology, irregular observations have to be fitted onto a smooth phenology curve, HANTS achieves this by performing two tasks. The first is to screen the data and remove cloud affected observations, this is based on operator input parameters and the second, is to reconstruct the time series (Zhou et al. 2013). During the first stage, cloud contaminated data is flagged as invalid during the iteration process; the algorithm only considers the most significant frequencies within the data and applies a least squares curve fitting procedure that is based on harmonic components (Roerink and Menenti 2000; Zhou et al. 2013). After the recalculation of the values, on the basis of the remaining valid points, the iterations are repeated until the maximum error is deemed acceptable and/or the number of remaining points has reached its threshold (Roerink and Menenti 2000). The iterations are controlled by five parameters and are inputted by the investigator including: the number of frequencies (NOF); the Degree of Over-Determinedness (DOD); Fit Error Tolerance (FET); Delta (damping factor) and the Scaling factor. Both the FET and DOD are illustrated in Figure 8. Once the iteration process is complete, the time series is reconstructed based on the remaining data (Zhou et al. 2013), resulting in a smooth curve being produced. HANTS

produces a number of outputs, one being the harmonic analysis of the time series, this is a mathematical expression that is representative of the NDVI trend and from this, it is possible to extract phenological metrics including the SOS and EOS (De Jong et al. 2009; Figure 9).

HANTS is recognised as a flexible analysis tool within literature, however, a major disadvantage is that there are no objective rules to determine the curve fitting parameters to be inputted (Roerink and Menenti 2000; De Jong et al. 2011). Rather the process is an iterative one, that requires the user to be experienced user of the software and only after running a large number of combinations of parameters, is the curve fitting successful (Roerink and Menenti 2000; De Jong et al. 2011).

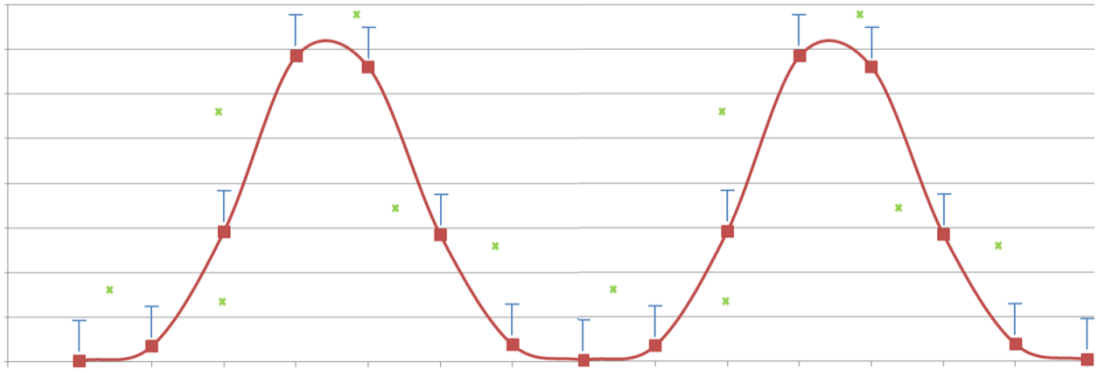

Figure 8 - Schematic the HANTs curve fitting procedure – specifically FET and DOD. FET is represented by the blue bars therefore the observations represented by the green cross will be removed during the next iteration. The DOD observations, the minimum number of observations that must remain, are represented by red squares.

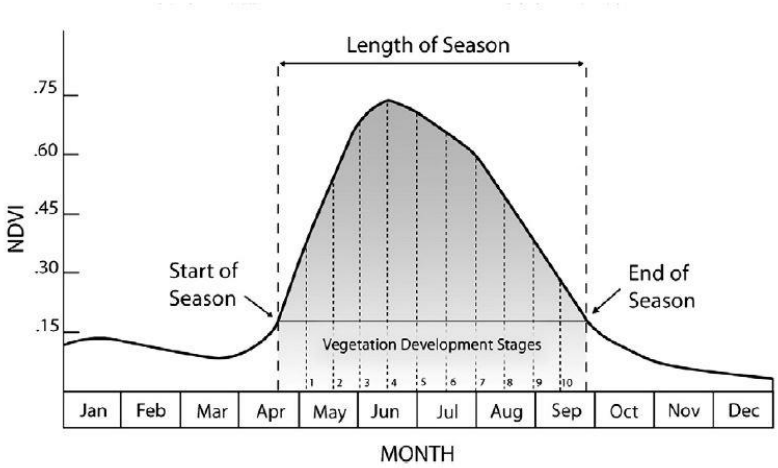

Figure 9 - Example of a single growing season and related phenological metrics. Start of Season (SOS), End of Season (EOS) and the shaded area underneath the curve is the Time Integrated NDVI (De Jong et al. 2011, p. 696).

An alternative method to HANTS is Breaks for Additive Seasonal and Trend (BFAST) developed by Verbesselt et al. (2010), it is focussed on the detection of abrupt changes or disturbances. BFAST is a generic change detection method which centres around the decomposition of time series into three components; trend, seasonal and noise (or remainder). The code required to process time series using the bfast package is open source and available from http://bfast.R-Forge.R-project.org/, with the processing being carried out in R.

BFAST is primarily used to detect abrupt changes in the seasonal and trend components of time series, whilst simultaneously identifying the time, magnitude and direction of change; all without the need to select a reference period, threshold or define a trajectory (Verbesselt et al. 2010). Similar to HANTS, BFAST is able to process irregular time series; a benefit, particularly in temperate regions where cloud cover is likely or when using data derived from a medium temporal resolution satellites i.e. Landsat. The bfast package developed by Verbesselt et al. (2010) accepts zipped data files, in the format tar.gz. These are available to be ordered from the USGS Earth Resources Observation and Science (EROS) Center – Science Processing Architecture (ESPA) On Demand Interface. Using this interface, Landsat products can be bulk ordered and downloaded with the option also to order spectral indices including; NDVI, EVI, SAVI, MSAVI, NDMI among others. Landsat imagery has been successfully used within BFAST to detect changes at 30m spatial resolution, however, a limitation is the temporal resolution of the platform being 16 days for Landsat 4, 5 TM, 7 ETM+ and 8 OLI.

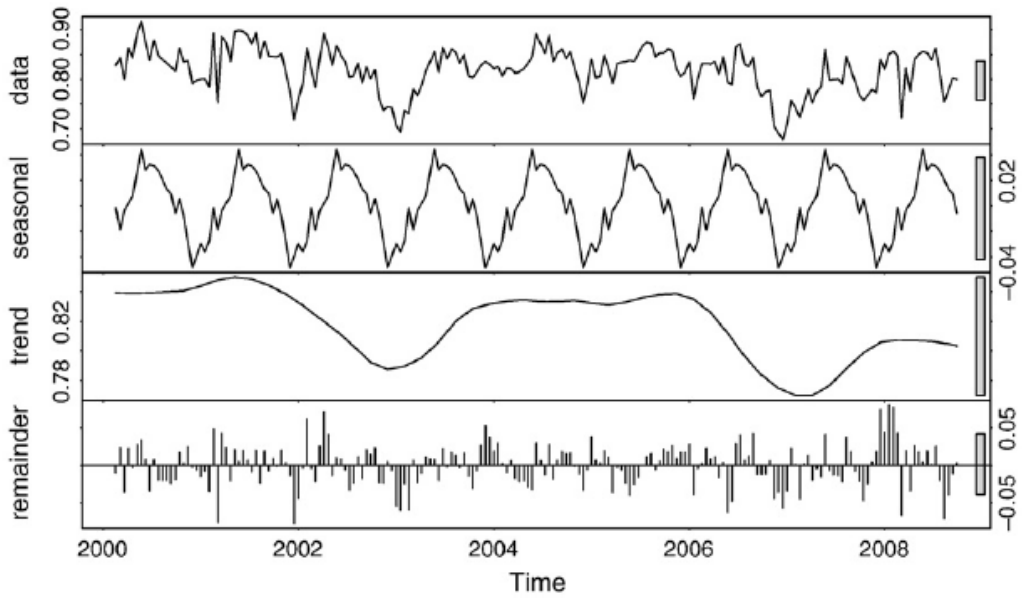

Figure 10 - Decomposition of a 16-day NDVI time series into seasonal, trend and remainder components using BFAST. Source: Verbesselt et al. 2010

The bfast package has a number of processing routines including bfastmonitor, which enables the monitoring of disturbances in near-real time (Verbesselt et al. 2012). Within the bfastmonitor routine, disturbances are detected within time series data by automatically identifying a stable history period, from which the season-trend variation is modelled and disturbances are be identified (Verbesselt et al. 2012). It is imperative that the stable history period, either selected or imputed by the user, is free of disturbances (Verbesselt et al. 2012). Once the history period is defined, a regression model (default is linear trend) is fitted to the data, prior to a monitoring period being utilised to determine whether the observations conform to the stable regression model or whether a disturbance is detected (Verbesselt et al. 2010; Figure 11).

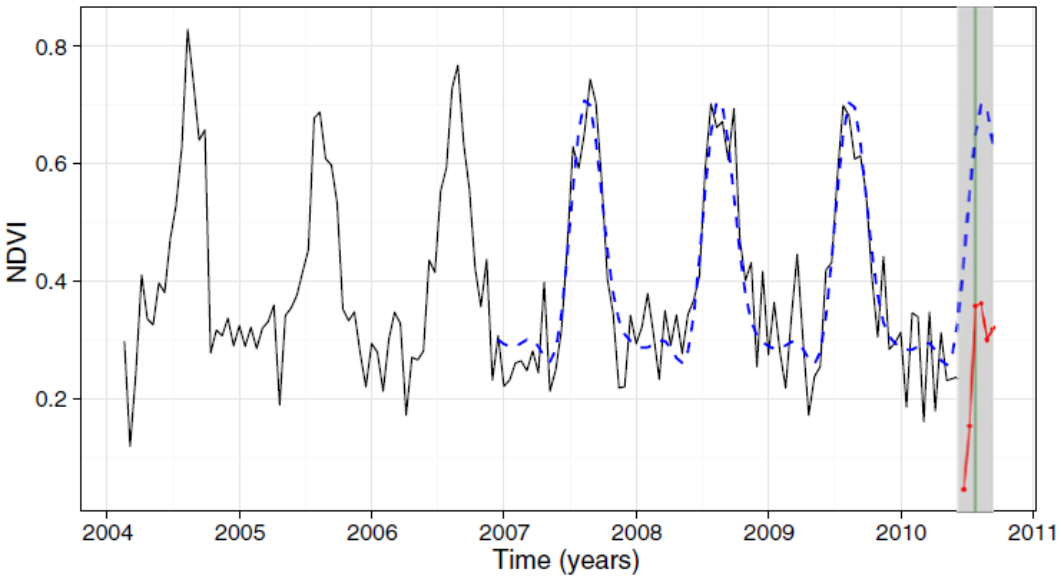

Figure 11 - NDVI time series analysed using bfastmonitor. From 2004 until mid-2010 is considered the history period with the monitoring period indicated by the grey background. A stable history is identified within the history period (i.e. 2007 until mid-2010) and used to model and predict the normal seasonal pattern (blue dashed line). Source: Verbesselt et al. 2012.

2.6. Conclusions

Through a detailed review of relevant literature, it has been demonstrated that there is potential for orbital remote sensing to contribute to the detection of clandestine mass graves, alongside other established methods; enabling the scale of search areas to be reduced and false positives to be eliminated.

Research published to date has been conducted in tropical climes where airborne hyperspectral imaging and field spectroscopy campaigns were undertaken. It was found that

the presence of buried organic remains affected the rate of vegetation re-colonisation and vegetation stress during the first 16 months post burial. However, multispectral orbital imagery has not been evaluated for use; the data for which exists in established archived and has relatively fine spatial resolution.

Therefore, this research will evaluate, multispectral orbital imagery (monitoring in the red to NIR regions) and derived vegetation indices to detect disturbance indicative of the presence of a mass grave.

If successful, this would allow detection of mass graves over large spatial and temporal scales, providing forensic investigators with an invaluable tool. The use of archive remote sensing imagery, particularly from multispectral orbital platforms, provides investigators with a unique opportunity to observe an area of interest, both pre and post burial; current methods used for grave detection do not allow this.

The techniques currently utilised in the detection of clandestine mass graves are presented in Table 2, highlighting the phases when each can be employed.

To successfully employ remote sensing in the detection of mass graves it is imperative that forensic investigators consider the principles of remote sensing, including the resolution of the system (i.e. spatial, spectral, temporal and radiometric) and that this forms a significant part of the decision making process when selecting a platform.

Table 2 - Summary of Possible Techniques that could be utilised to Locate Clandestine Mass Graves in Temperate Environments

Technique	Pre-Interment	Co-Interment	Post-Interment
Eye Witness Testimony			X
Geophysics			X
Geospatial Techniques (GIS)			X
Archive Aerial Photography	X	X	X
Archive Airborne Imagery (Multispectral & Hyperspectral)	X	X	X
Archive ALS	X	X	X
Archive Satellite Imagery (Multispectral & Hyperspectral)	X	X	X
Contemporary Airborne Imagery (Multispectral & Hyperspectral)			X

2.7 Technical Literature Review

Having discussed the potential for imagery from orbital platforms for the quantification of vegetation stress, specifically for forensic applications, it is important to conduct a technical review. When forensic investigators are selecting a satellite and imagery that is most appropriate for their case, it is imperative that the principles, advantages and limitations of the chosen sensor are considered and understood. Therefore, the following sections will present remote sensing fundamentals and principals that should be considered during this process.

2.8 Remote Sensing for Earth Observation

The observation of the Earth from orbital platforms has become increasingly common over the last forty years, allowing for a wide range of geophysical and biological phenomena to be observed globally (Committee on Scientific Accomplishments of Earth Observation from Space 2008, p. 8). Data can be acquired from satellite platforms (typically >700km above ground level), from high or low altitudes (>300km and <50m above ground level respectively), from airborne platforms or via ground based, terrestrial methods.

The data acquired from each of altitude can be used alone, or as part of a data collection campaign with a multi-scale approach i.e. with data from varying altitudes being compared (Lillesand et al. 2008). When adopting this approach it is possible to obtain detailed spectral information of a specific area, whilst also utilising ground observation data for calibration purposes and quantification of the atmospheric column.

2.8.1 Resolution in Remote Sensing - Basic Principles

The varying types of resolution should be considered carefully prior to employing remotely sensed imagery in a forensic context. The consideration of the four types of resolution: spatial, spectral, temporal and radiometric, should play a major part in the decision making process when selecting a platform. If an unsuitable platform is employed, it could potentially prevent the detection of the target.

2.8.1.1 Spatial Resolution

All sensors have a limit as to the size of the smallest area on the Earth's surface that can be 'viewed'; this is defined as the spatial resolution. Alternatively, spatial resolution can be described as the smallest resolvable detail. Spatial resolution determines the fineness of the image produced, i.e. the spatial detail of the imagery (Campbell and Wynne 2011).

The energy sensed by an instrument, or any imaging element, at any given point in time, is known as the Instantaneous Field of View (IFOV). The IFOV is the '...core angle within which the incident energy is focussed on the detector' (Lillesand et al. 2008, p. 355) and is expressed as the angle β in Figure 10. Campbell and Wynne (2011) state that the choice of sensor and the altitude, the data is acquired, can influence the ability to record spatial data.

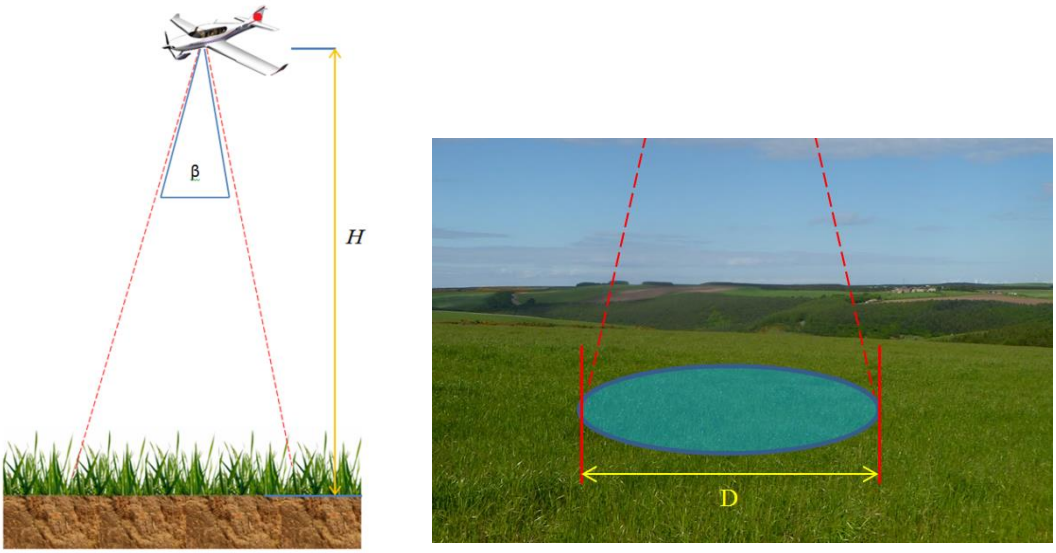

Figure 12 - Schematic showing Instantaneous Field of View (IFOV) and Footprint. H = altitude, β = IFOV, D = Diameter of the Ground Sample Distance (GSD).

Figure 12 illustrates the area of the ground surface (D) that is observed by the sensor when the IFOV is viewing the ground from directly above (i.e. nadir). This area is essentially the footprint and is often referred to as the sensor's spatial resolution. This area is primarily a function of the sensor IFOV, platform altitude (H in Figure 10) and local relief of the ground.

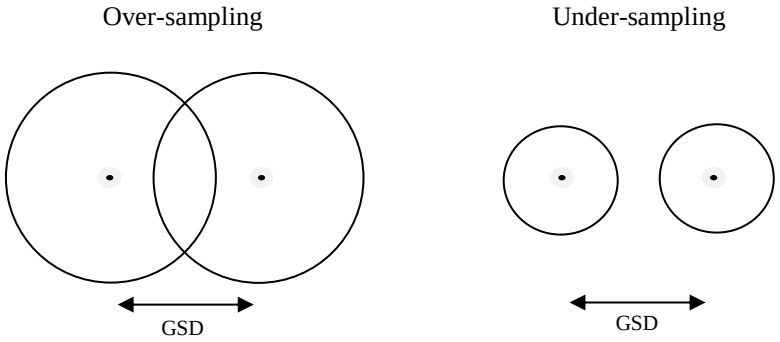

Figure 13 - Figure demonstrating how varying footprint size can result in over-sampling and under-sampling whilst the GSD remains constant.

It is important to note that the Ground Sample Distance (units of distance) is not equal to the IFOV (units of angle) of the sensor (Shaw and Burke 2003). It is possible that two systems can have the same GSD, but image a larger or smaller footprint; this can lead to over or

under sampling (Figure 13). If an area is over sampled, the area within the footprint is influencing two pixels, therefore, resulting in a mixed pixel. However, if the area is under sampled there is a significant gap between the pixels, leaving areas that are not imaged. This can affect the accuracy of the data, particularly if the digital numbers of specific pixels are being interrogated to identify and quantify relative differences in the imagery to detect anomalies. When the sensor is not at nadir (for instance, at the edge of a "swath"), the size of the footprint increases laterally in equal proportions. In other words, the footprint is larger toward the edge of an image rather than when it is close to its centre or nadir. Consequently, scale distortions occur, which should be accounted for during the pre-processing stage (Lillesand et al. 2008). The complicating factors of varying altitude, relief and viewing angles means that resolution is often better referred to as either "nominal GSD" or "nominal spatial resolution".

Satellites that have fine spatial resolution include: QuickBird (panchromatic 0.61m, multispectral 2.44m), IKONOS (panchromatic 0.82m, multispectral 3.2m) and SPOT-5 (panchromatic 5m, multispectral 10m and SWIR 20m). Those with medium spatial resolution include Landsat TM+, ETM+ and OLI TIRS, with a spatial resolution in the multispectral of 30m. Coarse spatial resolution satellites include the Moderate Resolution Imaging Spectrometer (MODIS) and the AVHRR sensor; on-board the NOAA Geostationary Operational Environmental Satellites (GOES). These instruments are tasked with monitoring global change frequently, i.e. acquiring data of the whole Earth's surface every one to two days, and depending on the spectral bands, the spatial resolution varies from 250-1100m. Archive imagery from both medium and coarse spatial resolution satellites have in recent years become freely available and are being increasingly used for a vast number of Earth observation applications including climate change studies and vegetation dynamics. Fine spatial resolution imagery is often commercially available rather than freely accessible via archives.

2.8.1.2 Spectral Resolution

Spectral resolution should be considered carefully when selecting a sensor for use in a forensic context. If the sensor does not acquire imagery in the spectral bands relating to vegetation, it is unlikely to be able to be used for studies relating to the monitoring of vegetation.

Campbell and Wynne (2011) state that remote sensing as an application, is dependent on observed spectral differences in electromagnetic energy which are reflected, transmitted or

emitted from features on the Earth's surface. Energy is radiated in waves of differing lengths from the µm to m, some of which are visible (~0.4-0.7µm or 400-700nm); this is illustrated in Figure 14. The optical portion of the electromagnetic spectrum includes the near infrared (NIR).

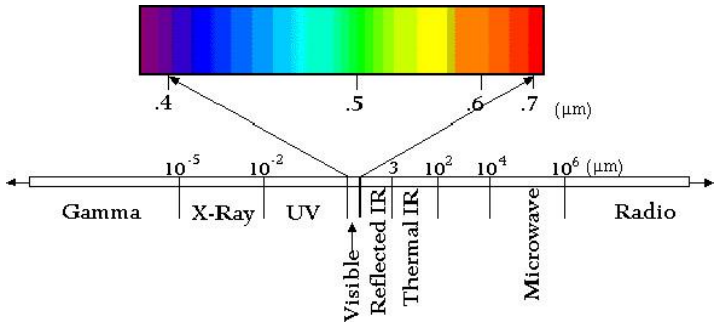

Figure 14 - The electromagnetic spectrum. Source: http://landsat.usgs.gov/images/Spectral_Bands.jpg [Accessed 09/08/15].

Electromagnetic energy originates from the Sun, once it arrives at the Earth's surface, where the majority is reflected, it is often referred to as upwelling energy.

The energy emitted from the Sun and the Earth is illustrated in Figure 15. At a temperature of 6000K the Sun emits a large proportion of energy in the ultraviolet, visible and infrared, whereas at longer wavelengths the energy emitted reduces. In contrast, the Earth emits energy in the longer wavelength, beginning at ~8µm (or 800nm) at a temperature of 300K.

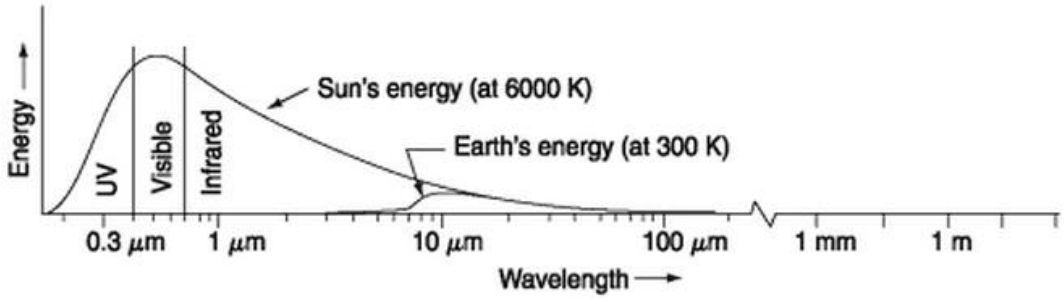

Figure 15 - Spectral characteristics of the Sun and Earth's energy. Source: Lillesand et al. 2008, p. 11.

To observe narrow portions of the electromagnetic spectrum, radiometers or charged coupled devices (CCDs) are used. Figure 16 shows a number of satellite platforms and the bandwidths that are used for the observation of the Earth's surface. It can be seen that all

sensors in Figure 16 collect imagery in the same portions (i.e. blue, green and red), however, the band positioning and width varies from instrument to instrument; in line with each satellites mission.

Therefore, spectral resolution can be defined as 'the spectral bandwidth within which data is collected' in the electromagnetic spectrum Joseph (2005, p. 7). Put simply, spectral resolution refers directly to the width of the spectral bands in a remote sensing system (Mather 2004, p. 31). Consequently, the spectral resolution of a system, describes how successfully a sensor is able to define fine wavelength intervals; where, the finer the spectral resolution, the narrower the wavelength range for a particular band.

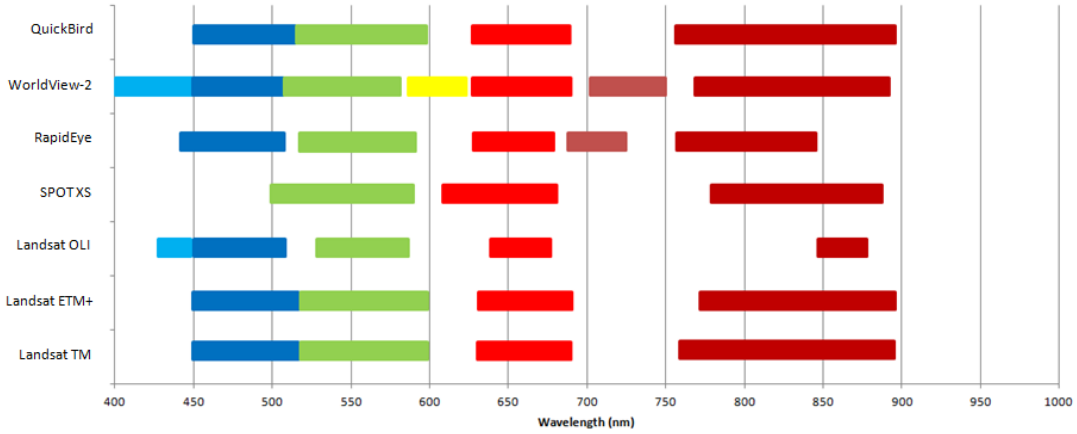

Figure 16 - Comparison of spectral band positioning and bandwidth for a selection of multispectral satellites.

Within each spectral band the sensitivity varies and can be represented as a bell curve (Figure 17), where there is greater sensitivity at the centre of the curve (Campbell and Wynne 2011). Consequently, the spectral bands, or bandwidth for each system, are defined using the full width, half maximum value (FWHM). This is the value when the instrument response is at one half of its maximum value and is presented as a range or bandwidth (e.g. Landsat TM Band 1's FWHM is 0.45-0.52µm) (Campbell and Wynne 2011).

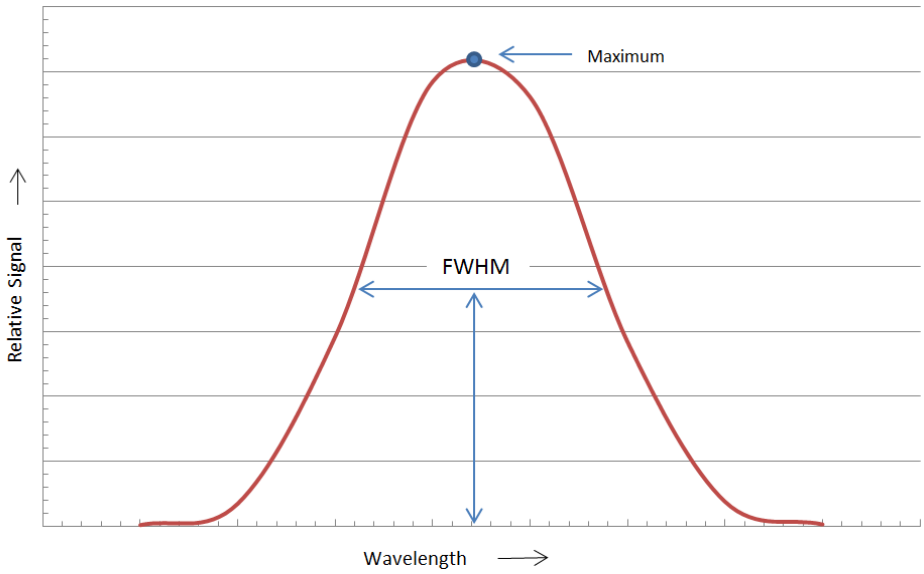

Figure 17 - Full width, half maximum (FWHM).

Sensors collecting remotely sensed imagery can be classed as either multispectral or hyperspectral. Multispectral sensors collect energy over several, commonly 4 or more, individual wavelength ranges and at various spectral resolutions, that are usually relatively coarse. Hyperspectral sensors have large quantities of narrowly defined spectral bands (200 or more) and therefore have fine spectral resolution in comparison. An example of which is the Airborne Visible Infrared Imaging Spectrometer (AVIRIS), this instrument measures in 224 spectral bands from 400 to 2500nm, as illustrated in Figure 18 (Campbell and Wynne 2011). Hyperspectral sensors, as implied by the prefix 'hyper', have an excess of bands across the electromagnetic spectrum where measurements are made. Due to this, imagery is captured in wavelengths that are greatly affected by the atmosphere; with useable data being collected in the atmospheric windows (Figure 20). However, as hyperspectral sensors have fine spectral resolution, they are often considered to be better for detecting and discriminating between targets based on their individual spectral response (Campbell and Wynne 2011).

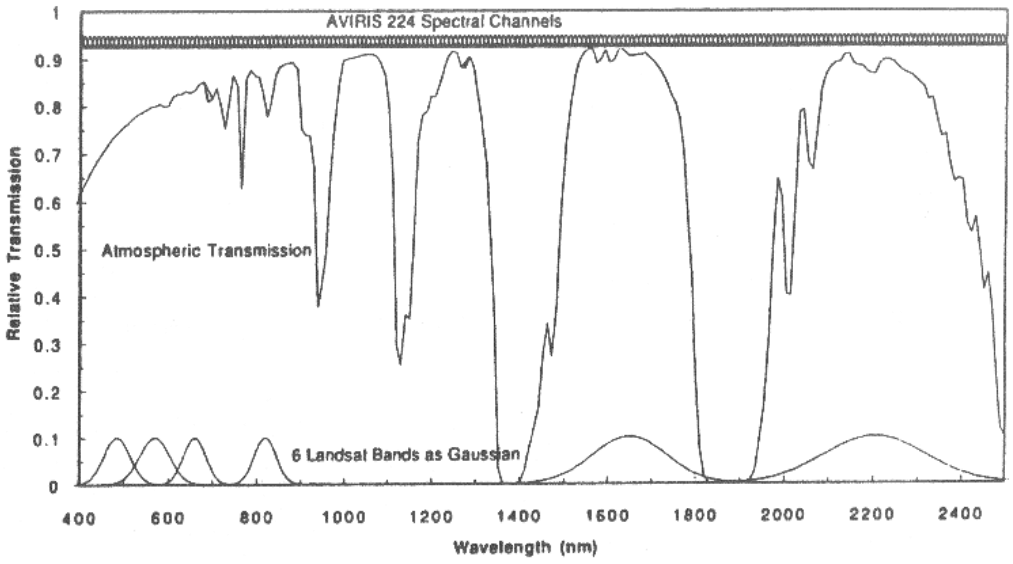

Figure 18 - Comparison of the AVIRIS 224 spectral bands compared to Landsat TM 6 bands (not including the thermal infrared band), alongside the atmospheric transmission where the atmospheric windows can be clearly identified. Source: http://www.ece.rice.edu/~erzsebet/esann99/esann99-em19.gif [Accessed 09/08/2015]

Hyperspectral sensors/ instruments are often airborne rather than spaceborne, consequently, they do not collect imagery regularly and are therefore not suitable for temporal studies that require regular repeat observations. The exception to this is the Hyperion instrument aboard NASA's EO1 satellite, this was originally an experimental mission launched in late 2000, however, due to high demand for its data, the mission has continued.

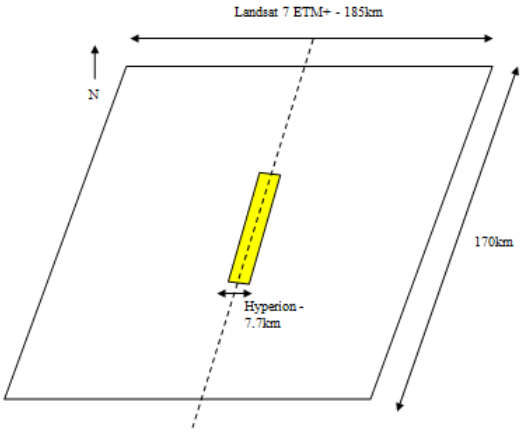

Figure 19 - Comparison between the footprint of Landsat 7 ETM+ and the Hyperion sensor.

The footprint of Landsat 7 ETM+ when compared to the footprint of the Hyperion sensor is much larger, with a swath width of 185km versus 7.7km (Figure 19). This is one of the major limitations of orbital hyperspectral systems, due to the excess quantity of bands used to image the Earth's surface, the quantity of data increases exponentially. Thus, there is a trade off in the systems footprint, potentially leaving areas not imaged. This is less of an issue with airborne systems, as the area of interest will be able to be imaged completely. However, for many applications, several bands derived from multispectral sensors, are sufficient for the scientific mission being undertaken, with hyperspectral instruments producing too much imagery in comparison. The processing of hyperspectral imagery is time consuming, complex to interpret and can result in data storage issues. Consequently, this research will use imagery derived from multispectral sensors that collect spectral data in a small number of spectral bands, allowing for quicker, easier analysis and less data storage issues. This data will be accessed through archives dating back to the 1970's.

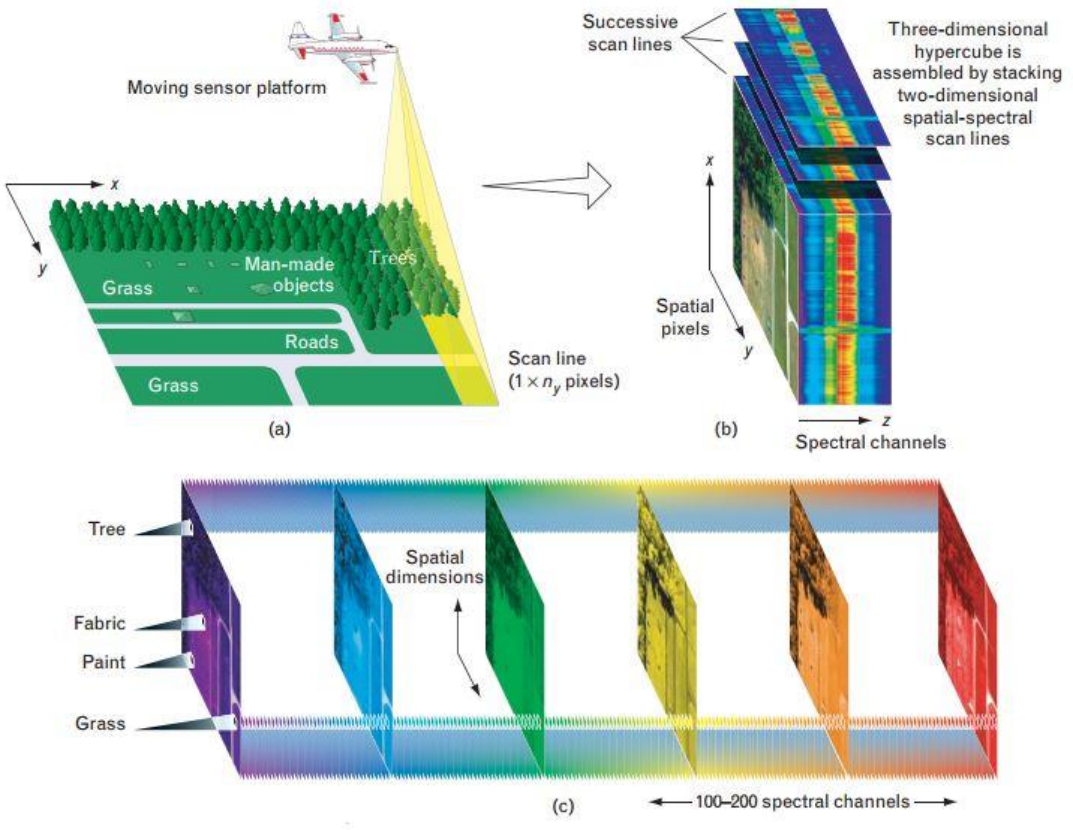

Figure 20 - a) Example of hyperspectral data acquisition b) Example of hypercube, where the acquired pixels have been stacked across all bands to produce a 3D data cube, with the spectral channels visible along the z axis c) Diagram showing the hyperspectral data collected over 100-200 spectral channels. (Amended from Shaw and Burke 2003, p. 7).

2.8.1.3 Temporal Resolution

Temporal resolution is the capability to view the same target, under similar conditions repeatedly (Joseph 2005). Often, researchers are interested in monitoring the Earth's surface to measure change over time to enable future events to be modelled, as opposed to using the imagery retrospectively. One of the major advantages of satellite remote sensing is that data can be collected from a specific area of interest, at regular intervals through time, in a repeatable manner (Joseph 2005 – Table 3 for examples of revisit periods). The development of orbital remote sensing has allowed the true potential of temporal resolution to be realised. Currently, there are established archives containing images of the Earth's surface spanning the past forty years, enabling temporal studies to be carried out to observe and quantify change over time. However, orbital imaging is evolving and developing rapidly each year, allowing data acquisitions of a specific area of interest to be requested at increasingly finer spatial resolutions and in near-real time.

Table 3 - Example of common satellites and their respective revisit periods.

Satellite	Instruments	Repeat/ Revisit Period
Earth Observing System (EOS AM)/ TERRA	MODIS ASTER	1-2 days
WorldView-2	WorldView-2	1.7 days
QuickBird	BGIS 2000	3 days
Landsat series	MSS TM+ ETM+ OLI TIRS	16-18 days
SPOT	SPOT P (Panchromatic) SPOT XS (Multispectral)	26 days

For orbital remote sensing, the temporal resolution of the sensor is inherently linked to the orbit into which the satellite is placed. It is unlikely that the orbit of a satellite will significantly influence the decision making process, however, it should be considered alongside the temporal resolution.

There are different orbits into which satellites can be placed, depending on their function and application (Figure 21 shows examples of each).

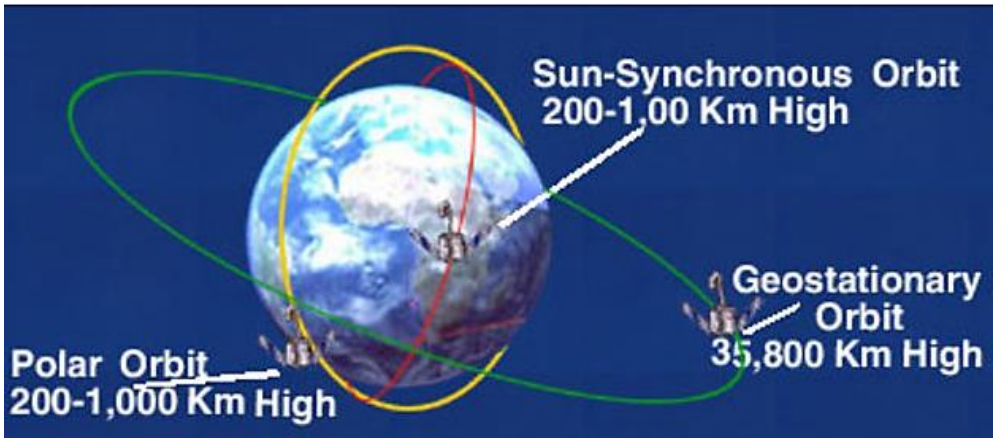

Figure 21 - Diagram demonstrating the different satellite orbits (Source: ESA).

Geosynchronous orbits are where the orbital period is synchronised with the rotational period of the Earth (Joseph 2005), that is, the angular velocity of the platform's orbit is the same as the Earth's angular velocity. Geostationary orbits are noted by Joseph (2005) as being a unique type of geosynchronous orbit, often used for communication satellites; with the satellite positioned in the equatorial plane, at an altitude of around 36,000km. Satellites in these orbits in effect remain stationary, in respect to the Earth's surface (Campbell and Wynne 2011). An advantage of geostationary orbits is remote sensing persistence and their ability to rapidly, consistently and repeatedly image the same target on the Earth's surface. In the case of geostationary meteorological satellites they can image the same target as frequently as every fifteen minutes e.g. Meteosat Second Generation (MSG). The disadvantages of such orbits are firstly, the position of the sun appears to change in relation to the target, causing inconsistencies in the angle of illumination for each successive image and secondly, the extreme altitude (35,000km) means that for any given IFOV, as long as all other factors are equal, the nominal spatial resolution is relatively low.

The illumination conditions, at the time when a remotely sensed image is collected, are important. Ideally all images, with the exception of geostationary platforms (as discussed above), would be collected under uniform illumination conditions; however, this is not often the case. With this in mind, sun-synchronous orbits were developed; they move westward, following the suns progress and therefore, inherently reduce variations in illumination (Joseph 2005). Observations collected by satellites in sun-synchronous orbits (i.e. Landsat - Figure 22) vary in illumination throughout seasons but repeat on a yearly basis (Campbell and Wynne 2011). As a result of this, these satellites are often used, and best suited, to monitoring annual changes in land cover (Lillesand et al. 2008). Satellites placed in a sun-synchronous orbit are near-polar orbiting (passing up and over the North Pole and down and

under the South Pole), whilst maintaining an altitude between 200-1000km and can therefore, be considered as low level satellites (Barrett 1999). It is noted by Joseph (2005) that satellites placed in a sun synchronous orbit are necessary to investigate and study changing phenomena, such as vegetation growth and snow melt off. Therefore, satellites operating in these orbits are more suited for use in a forensic context.

Polar orbits are considered sun-synchronous due to the fact that they pass the Equator at the same local time each day however, true polar orbits are those which have an inclination of 90^{o} to the Equator. Satellites in these orbits are commonly earth observing and include Terra and Aqua which carry the MODIS instrument.

The revisit time is dependent on the orbit within which the satellite is placed; this can vary from minutes to days, e.g. the Landsat series has a revisit time of sixteen days. Revisit times are also dependent on factors including latitude, the sensors field of view (FOV) and cloud cover; which may prevent useable, cloud-free imagery from being collected.

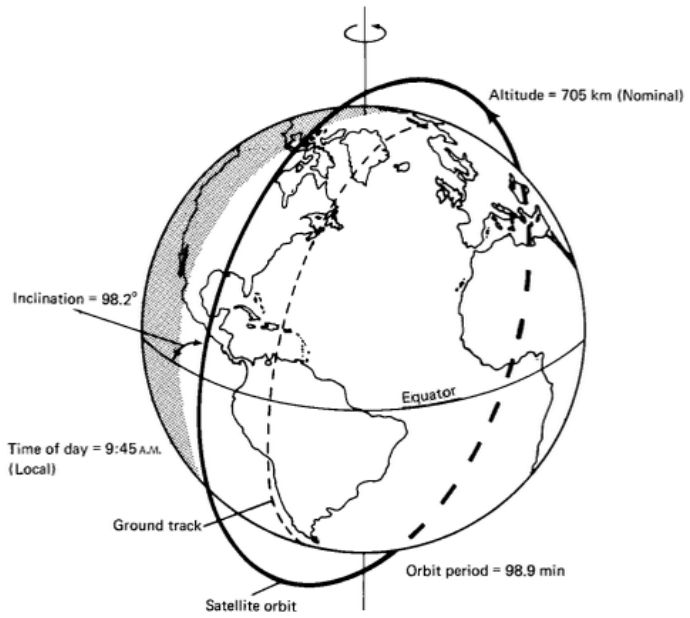

Figure 22 - Sun-synchronous orbit of Landsat-4 TM and 5 TM (Lillesand et al. 2008, p. 395 – adapted from NASA diagram).

In a forensic context, the ability to observe events prior to, during and after a criminal act is invaluable, consequently, the temporal resolution of individual satellites should be one of the factors considered when deciding upon a suitable platform and derived imagery.

2.8.1.4 Radiometric Resolution and BIT Depth

Radiometric resolution is defined by Campbell and Wynne (2011, p. 286) "...as the ability of an imaging system to record many levels of brightness...". Imaging systems that have coarse radiometric resolution observe scenes using a limited number of brightness levels, whereas, if the system has fine radiometric resolution, many more levels of brightness would be employed (Campbell and Wynne 2011). Mather (2004) states that radiometric resolution can be considered to be the system's radiometric sensitivity i.e. relating to the number of digital quantisation levels used to express the data collected by the sensor. Quantisation from an analogue signal to a digital number is carried out by an Analogue to Digital Converter (ADC). If the system converts the analogue voltage into very few digital numbers, the resulting image will be a degraded version, with much of the detail originally detected, unable to be resolved when the image is created. Conversely, if the ADC quantises the signal into many different levels, the detail will be able to be resolved and the resulting image will appear visually detailed. The quantisation process is key for the image to be stored as a series of digital numbers, either in byte, integer or floating point format; each having different BIT depths.

This process can cause a loss of resolution whereby, if an image has been quantised using many levels, the converted wide range of brightness may then be stored as a 4 BIT data, meaning that the detail first recorded has been degraded during the storage process. This can occur due to a number of reasons, one being that the smaller the BIT depth, the less the storage space is required. However, this is a comprise, in that some of the radiometric resolution and detail is lost, to enable more data to be collected overall. Figure 23 below details examples of the numbers of grey scales increasing as the bit depth increases.

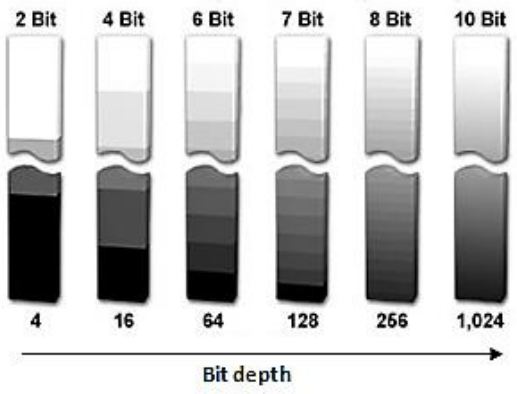

Figure 23 - Bit depth in digital images. Adapted from: http://zeiss-campus.magnet.fsu.edu/articles/basics/digitalimaging.html [Accessed: 11/08/15].

2.7.2 Factors Affecting the Spectral Response Detected by Sensors

Factors known to affect the quantity of energy entering a remote sensing instrument are summarised in Figure 26.

Electromagnetic radiation passes through the atmosphere twice, causing interactions (scattering and/ or absorption) to occur between the radiation and the atmospheric particulates and gases. These interactions result in light rays being deflected and/ or absorbed, reducing the amount of radiation that is returned to the sensor; this is observed as haziness or blurring in the resulting image (Mather 2004). Atmospheric gases, particularly oxygen, nitrogen and the ozone, are stated as being the primary cause of scattering. However, particulates and water vapour are also known to contribute to this process (Campbell and Wynne 2011). There are two types of scattering detailed within the literature, selective scattering and non-selective scattering. Selective scattering (i.e. Rayleigh scattering) affects specific wavelengths of electromagnetic radiation, whereas, non-selective scattering is wavelength dependent and is predominantly caused by particulates that exceed 10µm (i.e. water droplets will produce scattering in all visible wavelengths) (Mather 2004). Rayleigh scattering is caused by very small particles (smaller in size than the wavelength of the radiation); shorter wavelengths are more affected by this form of scattering than longer wavelengths (Figure 24). The reason why the sky appears blue is due to Rayleigh scattering, with the blue portion of the electromagnetic spectrum being more heavily scattered than other visible wavelengths (Mather 2004; Campbell and Wynne 2011).

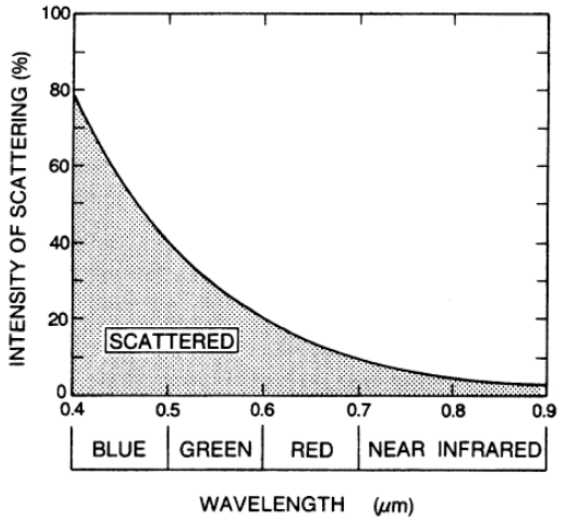

Figure 24 - Rayleigh scattering in the Earth's atmosphere (Campbell and Wynne 2011, p. 41).

Absorption converts the energy present in electromagnetic radiation into the internal energy of the absorbing molecule; gases including water vapour, carbon dioxide and the ozone are known to be primarily responsible for this process (Mather 2004). These gases absorb radiation in specific regions of the spectrum, known as absorption bands (Mather 2004). Campbell and Wynne (2011) state that in two regions (several bands between 5.5 and 7.0µm and above 27.0µm) absorption can exceed 80% if the atmosphere contains large amounts of water vapour.

The effect of scattering and absorption varies in different areas of the spectrum (Campbell and Wynne 2011). Remote sensing cannot be carried out in areas of the spectrum that are seriously affected by scattering and absorption, as this effectively causes the atmosphere to appear opaque to incoming or outgoing radiation (Mather 2004). Atmospheric windows are regions of the spectrum that are relatively, but not completely, free from the effects of scattering and absorption (Figure 25). Through these windows, radiation is able to travel through the atmosphere more freely, with less scattering and absorption interactions (Mather 2004).

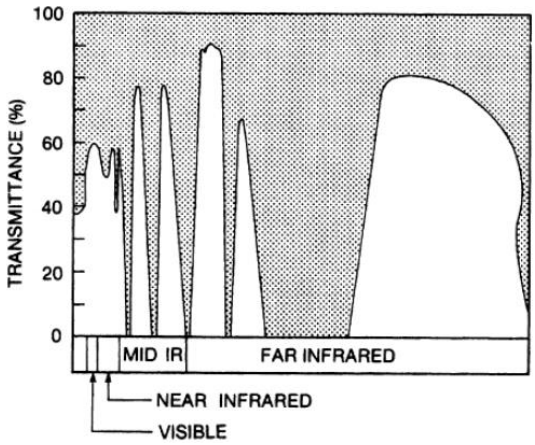

Figure 25 - Atmospheric windows, the shaded region represents absorption of radiation (Campbell and Wynne 2011, p. 45).

The distance between the target and the instrument is the path length and contains the atmospheric column. The length of the path and depth of the column do not need to be equal. The depth of the column can vary, as the Earth's atmosphere expands and contracts, according to conditions including solar and magnetic conditions. For atmospheric effects to be eliminated during pre-processing routines, it is crucial that the atmosphere can be quantified (Shaw and Burke 2003). As the solar illumination angle changes throughout the

day, the atmospheric path length increases, therefore, resulting in the scattering of the solar radiation also being increased; the look angle is affected similarly. Therefore, an accurate record detailing when and where imagery was acquired is crucial for the successful implementation of atmospheric correction procedures. This information can be located within the imagery's metadata and is often inputted manually into atmospheric correction software. Clouds, ground cover and trees may also cause the target to become shrouded in shadow, or cause additional reflection and/ or scattering onto the target (Figure 26; Shaw and Burke 2003); altering the illumination and therefore, the reflectance spectra recorded.

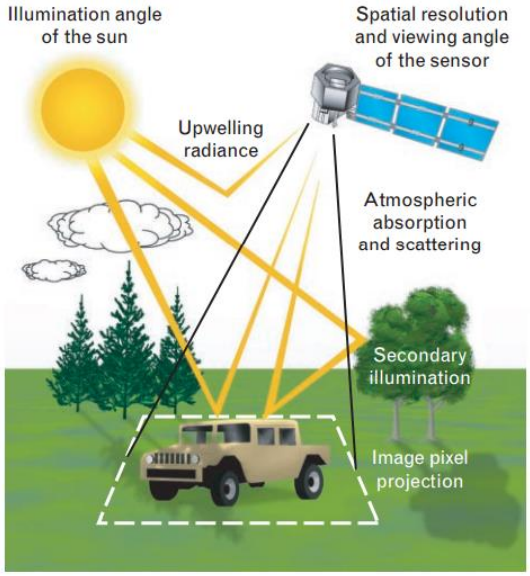

Figure 26 - Factors known to affect energy entering the sensor (Shaw and Burke 2003, p. 8).

2.7.3 Atmospheric Correction

To correct and account for some of the factors detailed in the previous section, it is necessary and in some cases vital, to pre-process imagery particularly when analysing surface reflectance. This process "...minimises or removes the atmospheric influences...to extract more accurate information" (Tyagi and Bhosle 2011, p. 564). It also allows for all available spectral information within the pixels to be examined. To carry out accurate atmospheric correction, a number of properties must be known, including the quantity of water vapour in the atmospheric column, the distribution of aerosols and scene visibility. As there are often no direct measurements of these properties, they are calculated from the image pixels (EXELIS 2015a).

Pre-processing tools used for atmospheric correction include 'Image Based Atmospheric Correction', Radiative Transfer Models (RTM) and radiative transfer code (RTC). Image Based Atmospheric correction examines the spectra within the scene and identifies a very dark object or feature; the values from which are then subtracted from the digital values of all pixels (Campbell and Wynne 2011, p. 306). This process is also referred to as Dark Object Subtraction (DOS). The advantages of such methods are their simplicity, they require no accompanying information to be inputted and therefore have almost universal applicability (Campbell and Wynne 2011, p. 306). Modules employing the RTC, model the physical behaviour of solar radiation as it passes through the atmosphere and requires additional information to be inputted; it is not an automated process (Campbell and Wynne 2011, p. 306). However, RTMs, although complex, have notable advantages when considering scientific rigor, accuracy and applicability to a variety of environments. Examples of RTC include: MODerate Resolution Atmospheric TRANsmission (MODTRAN) and 6S (Second Simulation of the Satellite Signal in the Solar Spectrum). These are quoted as being some of the most widely used atmospheric correction codes in remote sensing (Campbell and Wynne 2011, p. 311).

There are a number of software packages, many accessible through paid licences, that contain atmospheric correction packages, examples include: ENVI (licensed through Harris Geospatial) and ERDAS Imagine (licensed through Hexagon Geospatial), among others. Both software packages have add-ons that contain atmospheric correction modules. ENVI contains two atmospheric modelling tools, the first being the Fast Line-of-sight Atmospheric Analysis of Hypercubes (FLAASH) and the second, QUick Atmospheric Correction (QUAC) (both developed by Spectra Sciences Inc.). QUAC is faster than most other atmospheric correction tools and is able to atmospherically correct from the visible (VIS) through to the short wave infrared wavelengths (SWIR). No additional information is required as the process determines the correction parameters from pixels within the image itself (EXELIS 2015b). It uses the principle of Dark Object Subtraction (DOS) and is most effective and accurate when the image is comprised of, a range of different land cover types and contains sufficiently dark pixels to carry out the subtraction. FLAASH is a more complex tool that corrects wavelengths in the VIS through to the SWIR regions and is a first principles tool incorporating the MODTRAN RTC (developed by Spectral Sciences Inc and the US Air Force Research Laboratory) (EXELIS 2015c; MODTRAN5 2015). The inclusion of MODTRAN within FLAASH allows for a unique MODTRAN solution to be calculated for each image; this is dependent on the user selecting the most applicable standard MODTRAN model atmospheres and aerosol types, to represent the scene (EXELIS 2015c). MODTRAN has been "...extensively validated and serves as the community standard

atmospheric band model" (MODTRAN5 2015). FLAASH has the added benefit of being able to atmospherically correct both multispectral and hyperspectral imagery (Anderson et al.1999). The ATmospheric CORrection (ATCOR) module (developed by DLR, German Aerospace Centre and integrated into IMAGINE by GEOSYSTEMS GmbH) within the ERDAS Imagine software also employs the MODTRAN code.

The correction of the atmospheric column and associated artefacts, is a key component of pre-processing that, is required in instances where spectral and reflectance information is being interrogated. This is also true for applications including mass grave detection, where the targets are relatively small and the presence of artefacts within the atmosphere, could adversely affect any derivatives or indices calculated; either by masking them entirely or creating false positives. Therefore, performing such corrections is crucial for this research and any applications where satellite imagery is being used to quantify spectral responses.

2.8.4 Remote Sensing Systems 1 - Active

It is important to briefly introduce the two types of remote sensing systems, active and passive systems. Active systems are instruments that generate their own source of electromagnetic radiation, this radiation is then directed at the Earth's surface and the energy scattered back is detected by the instrument (Gibson 2000). As active sensors generate their own electromagnetic radiation they are "…independent of solar and terrestrial radiation" (Campbell and Wynne 2011, p. 55). The most common active remote sensing instruments are Synthetic Aperture Radar (SAR) and Light Detection and Ranging (LiDAR). The major advantage of these sensors is that they can operate during the night, cloudy and adverse weather conditions, as they are not affected by illumination (Campbell and Wynne 2011).

2.8.4.1 Synthetic Aperture Radar (SAR)

SAR is a sensor that "…allows compact radar systems to acquire imagery of fine spatial resolutions at any altitude" (Campbell and Wynne 2011, p. 205). They are unique in the fact that they are able to acquire images in darkness, through cloud cover and also during adverse weather conditions and are used for both Earth Observation, as well as military applications. SAR is included in the category imaging radar and can be either airborne or space borne; in both cases, the antenna transmitting the electromagnetic energy (microwaves – 3-25cm) is fixed below the platform and pointed to the side. These systems produce uninterrupted strips of imagery, over large areas, that run parallel to the platform's flight line hence the term side

looking radar systems (Lillesand et al. 2008; Figure 27). These systems operate through microwaves being transmitted in a series of pulses (over milliseconds), that move in a narrow beam towards the Earth's surface; once a wave comes into contact with a surface or object, a return wave is reflected back to the detector (Lillesand et al. 2008). By recording the time that the return wave arrives at the detector, a measure of distance can be calculated between the object and the detector; different objects produce different strengths of return waves i.e. a building would produce a stronger wave than reflection off of a grass covered football pitch (Lillesand et al. 2008). The wavelengths utilised in imaging radar are illustrated in Table 4, Mather (2004, p. 12) states that the wavelength "…determines the observed roughness of the surface…"; the radar image will appear smooth where the surface has a roughness with a frequency less than that of the radiation.

Table 4 - Radar wavelengths (Mather 2004, p. 11).

Band Designation	Frequency (MHz)	Wavelength (cm)
P	300-1000	30-100
L	1000-2000	15-30
S	2000-4000	7.5-15
C	4000-8000	3.75-7.5
X	8000-12000	2.5-3.75
K_u	12000-18000	1.667-2.5
K	18000-27000	1.111-1.667
K_a	27000-40000	0.75-1.111

Therefore, SAR has the capability to be an incredibly powerful remote sensing tool, as areas on the Earth's surface that would not usually be accessible, due to remoteness or atmospheric conditions are observable i.e. the tropics that are persistently cloud covered (Campbell and Wynne 2011). However, it must be mentioned that SAR does not replace multispectral or hyperspectral imaging systems, as these allow for spectral information outside the microwave portion of the electromagnetic spectrum to be recorded. The first orbital SAR launched was NASA's Seasat in 1978, that used a wavelength of 23.5cm (known as L-band) (Gibson 2000). The purpose of this instrument was to monitor global oceanographic

phenomena, as well as to test various parameters that would later be used in the design and specification of further ocean and terrestrial remote sensing systems. Examples of SAR's include: ENVISAT, TerraSAR-X, the COSMO-SkyMed constellation and Sentinel-1. When considering the use of SAR for locating mass graves it is important to note that no spectral information can be acquired using this sensor, therefore, once the initial disturbance, associated with the burial, has settled the grave would be undetectable. Additionally, SAR imagery is not freely available therefore restricting the method from being used readily.

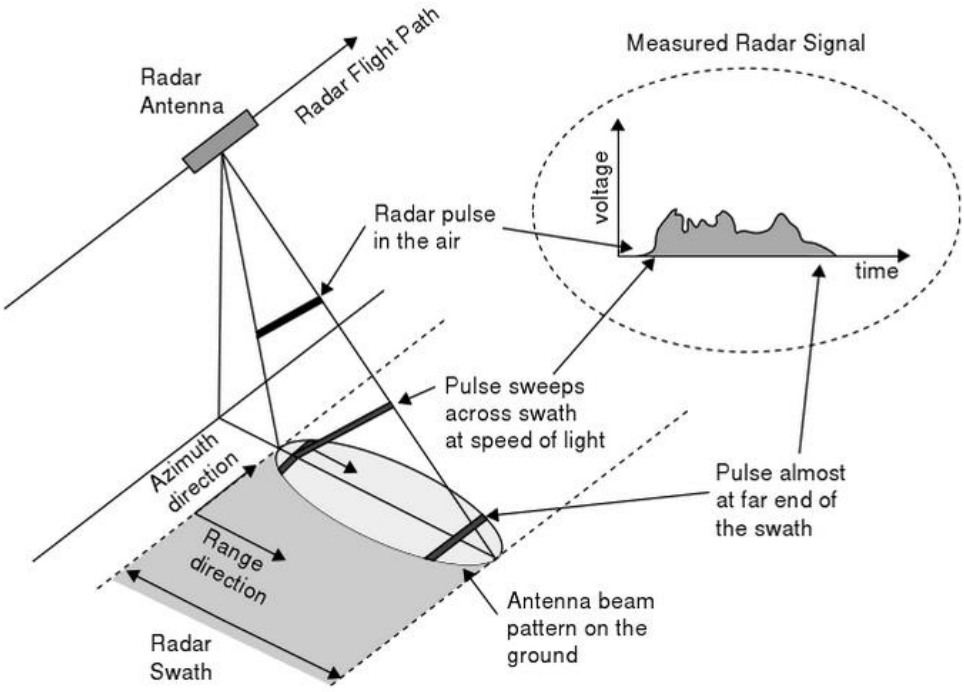

Figure 27 - Imaging geometry for a side-looking radar system (Van Zyl and Kim 2011, p. 4).

2.8.4.2 Airborne Laser Scanning (ALS)

Lasers are the illumination source for LiDAR and operate at much shorter wavelengths (0.5 – 1.5µm) when compared to those used by SAR (Gibson 2000). LiDAR provides detailed data of high spatial accuracy and precision (Campbell and Wynne 2011; Aktaruzzaman et al. 2011). LiDAR has a unique capability when compared to other remote sensing instruments, namely due to its ability to reliably separate land cover from the Earth's surface to reveal otherwise invisible features (Campbell and Wynne 2011). Gibson (2000) states that LiDAR can obtain highly accurate topographic measurements, where the data collected allow elevation changes to be monitored. LiDAR data is used for many applications including:

urban planning (Gonzalez-Aguilera et al. 2013), floodplain mapping (Aktaruzzaman et al. 2011), environmental monitoring and also for the study of forest canopies (Whitehurst et al. 2013), among others. Most LiDAR are scanning instruments on airborne platforms, with the exception of the orbital ICESat (Ice, Cloud and Land Elevation Satellite), hence it is often referred to as Airborne Laser Scanning (ALS). ALS is capable of collecting sufficient point measurements of surface elevations to enable the production of DEM with spatial resolutions typically in the range of 25cm to 2m, with uncertainties in elevation of approximately ±15cm. Laser scanning can also be carried out terrestrially, however, this will not be considered in the review as it has not been documented as a potential technique in the context of mass graves.

SAR and LiDAR are active sensors and are powerful instruments that enable a wide range of studies to be carried out, for a variety of applications. However, in a forensic context, specifically the detection of mass graves, both techniques being predominantly airborne, do not offer sufficient temporal resolution i.e. they collect data sporadically, and therefore, cannot be used for temporal studies. Unlike multispectral orbital sensors, both instruments could only be utilised in the search for disturbance rather than for vegetation studies. However, if a dataset existed or could be obtained over a suspected mass grave, it could be used in conjunction with multispectral orbital imagery and other pre-existing techniques to detect disturbance post grave creation and prior to the grave settling.

2.8.5 Remote Sensing Systems 2: Passive

Passive remote systems use the sun as a source of electromagnetic radiation. The sun's rays interact with the Earth's surface, and the detectors on board quantify the energy that is reflected back to the sensor (Gibson 2000). Put simply, "… a passive system senses naturally available energy" (Lillesand et al. 2008, p. 9). There are many types of passive remote sensors including aerial photography using panchromatic, colour and false colour infrared film, as well as multispectral and hyperspectral scanners.

2.8.6 Remote Sensing Scanning Systems

There are two main types of passive remote sensing scanning systems, used for the collection of both multispectral and hyperspectral digital data. Whiskbroom (across-track or transverse) and pushbroom (along-track) scanners. Whiskbroom scanners (across-track or transverse) (Figure 28 (b)) use a rotating or oscillating mirror to scan the Earth's surface along scan lines

that are approximately at 90^{o} to the platform's direction of movement (also known as the flight line or track) (Lillesand et al. 2008). Lines of imagery are collected using an across-track scanning mechanism, whilst the image itself is produced through the forward movement of the platform (either airborne or orbital) (Schaepan 2009). As the platform travels forward, a series of "…narrow strips of observation i.e. two dimensional images of rows and columns are produced" (Lillesand et al. 2008, p. 103).

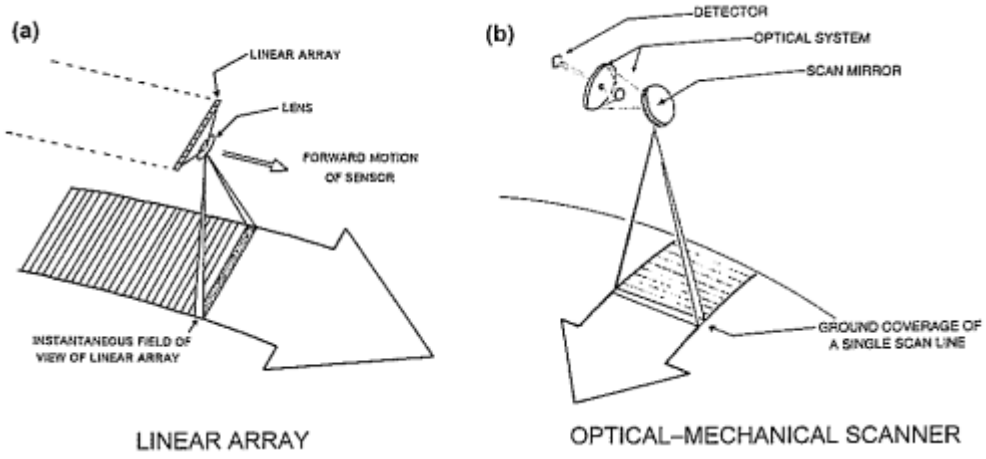

Figure 28 - Diagram of (a) Pushbroom scanner (b) Whiskbroom scanner. (Campbell and Wynne 2008, p. 103).

Incoming energy from the Earth's surface is reflected off the oscillating mirrors onto a dichronic grating, from which the light is directed through a prism or alternatively, a diffraction grating causing the light to be plit into the portions of the EM spectrum that are detectable (Lillesand et al. 2008). The light is detected independently by the electro-optical detector array which is comprised of radiometers or charged coupled devices (CCD) (Lillesand et al. 2008). Schaepan (2009) states that the principle advantage of a whiskbroom scanner is its high spectral uniformity, which is due to the detector array being fixed. Examples of passive remote sensing systems that utilise the whiskbroom, or across-track scanner, are Landsat TM, Landsat ETM+, the hyperspectral Airborne Infrared Imaging Spectrometer (AVIRIS - mounted onto NASA's ER-2 research aircraft), DAIS (Digital Airborne Imaging Spectrometer), HyMap and MODIS (Moderate Resolution Imaging Spectroradiometer, onboard NASA's earth observing systems, TERRA and AQUA).

Pushbroom systems differ to whiskbroom scanners as they do not rely on rotating/oscillating mirrors to direct energy to a detector, but instead, use a linear array of CCDs (Gibson 2000,

see Figure 28 (a)). Pushroom scanners are designed to be compact and can contain over 1,000 individual CCD's; with each spectral band requiring dedicated linear arrays (Lillesand et al. 2008). The forward motion of the platform allows for the image to be constructed. Schaepan (2009, p. 170) notes that a pushbroom system "…acquires a series of one dimensional samples that are orthogonal to the platforms line of flight". The principle advantage of this scanner is its solid state construction (i.e. the lack of moving parts), therefore, it is considered more reliable and to have a longer life expectancy (Gibson 2000; Lillesand et al. 2008). However, a disadvantage is the complexity of the linear array which requires detailed calibration (Lillesand et al. 2008).

An example of an airborne system that operates a pushbroom scanning system is the Compact Airborne Spectrographic Imager (CASI), noted by Lillesand et al. (2008) as the "…first commercially developed, programmable airborne hyperspectral scanner". Orbital systems utilising a pushbroom scanner include: Landsat 8 OLI TIRS, SPOT, QuickBird, IKONOS, Medium Resolution Imaging Spectrometer (MERIS) and Hyperion, which is onboard NASA's Earth Observing-1 (EO-1) satellite.

It should be noted that although the scanning system of a sensor would not form a part of the decision making process when selecting a platform, it is integral to how each system operates. As such, when choosing a platform it is more likely that the resolution of the system (i.e. spatial/ spectral/ temporal or radiometric) would play a more substantial role in the decision/ selection process.

2.8.7 Summary

This chapter has considered and reviewed existing literature detailing methods traditionally employed in the detection of mass graves. It has also demonstrated the potential for remote sensing, specifically orbital imagery and derived vegetation indices, such as NDVI, to be added to the suite of existing techniques for the search for mass graves in temperate environments. Additionally, the scientific background and principles underpinning remote sensing and sensors have been addressed within the technical literature review.

3 Aim and Research Questions

3.1 Aim

This research aims to evaluate the utility of archive multispectral satellite imagery to monitor temporal changes in vegetation stress, via NDVI, as a means to detect clandestine human mass graves in temperate environments.

3.2 Research Questions

The research questions below are outlined by chapter and are based on the gaps in knowledge identified through conducting the literature review.

Chapter 5 - Field Spectroscopy, Derived Vegetation Indices and Geophysics for Monitoring Differences in Vegetation on a Small-Scale, Controlled Mass Grave Containing Mammalian Remains

1. What is the relationship between decomposition and NDVI?
2. What is the relationship between grave surface and NDVI?
3. What is the relationship between the thickness of the pig material and NDVI?
4. What is the relationship between the thickness of the overburden and NDVI?
5. What is the relationship between grave depth and NDVI?
6. What is the relationship between meteorological variables and NDVI?

Chapter 6 - A Multi-Platform, Multi-Temporal Investigation of Differences in NDVI and Surface Elevation Changes of a Large-Scale, Proxy Mass Grave (Foot and Mouth) over Decadal Time Scales to Provide a Pre-Operational Proof-of-Concept for Clandestine Human Mass Grave Prospection

1. Is NDVI influenced by the presence of mass graves and if so, how long for?
2. Are both full and empty mass graves detectable, using NDVI, up to 10 years post burial?
3. What is the relationship between NDVI and the presence of a decadal mass grave?

Chapter 7 - The Detection of Clandestine Human Mass Graves in Bosnia and Herzegovina - A Multi-Platform Approach

1. Can NDVI derived from medium spatial resolution imagery, be used to detect disturbance associated with the creation, interment or exhumation of human mass graves?
2. Can NDVI derived from fine spatial resolution imagery, be used to detect disturbance associated with the creation, interment or exhumation of human mass graves?
3. Can vegetation stress be used to locate both primary and secondary mass graves?

4 General Methods and Study Sites

It is important to outline the rationale for the methods undertaken and how they varied for each chapter. This research focuses on three study sites, the first of which is a small scale, controlled simulated mammalian mass grave. Secondly, a large scale proxy mass grave containing mammalian remains from the Foot and Mouth epidemic 2001 and lastly, an investigation into how the relative health of vegetation (over time), via the calculation of vegetation indices, above human mass graves can be used to locate clandestine human mass graves in Bosnia and Herzegovina. For the three study sites, NDVI was calculated for all archive satellite imagery scenes to assess whether changes in NDVI over time can be used to detect human mass graves in temperate environments.

4.1 Site Selection

Before investigating whether variations in temporal NDVI derived from orbital remote sensing could be used to detect actual human mass graves in places such as Bosnia and Herzegovina, it was imperative to conduct smaller scale experiments as a proof-of-concept. For this purpose, two sites within the UK were located: East Holme, Dorset and the Former RAF Pershore airfield, Worcestershire.

4.1.1 East Holme Experimental Site

The first site needed to be local to Bournemouth University (within one hour's drive) to allow spectral data collection when the weather was optimal. A suitable site was located on private land near East Holme, Dorset. The land had been used for forensic experiments previously, however the area where the simulated mass grave was created avoided these sections. As pig remains were to be buried at the site, the appropriate licences and permissions were applied for via Department for Environment, Food & Rural Affairs / Animal Health and Veterinary Laboratories Agency (DEFRA/ AVHLA) and the Environment Agency (EA). These were subsequently granted by summer 2013 (Animal By-Products Registration Reference: U1143934), allowing the creation of the grave and experiment to commence. Following grave creation and the interment of the pigs in August 2013, the peak of the growing season had already passed and was progressing towards

winter. Spectral data was collected via a hand held instrument (GER1500) on loan from the Natural Environment Research Council Field Spectroscopy Facility (NERC FSF). The study carried out at East Holme was designed to be short term with a maximum potential experimental period of two years; this was later reduced to focus on the first four months post burial. This allowed investigations into how the disturbance of the soil, as well as the presence of the pig remains, affected the vegetation and soil on the surface of a mass grave during the first four months. The spectra collected by the GER1500 was pre-processed and convolved to be equivalent to Landsat, from which NDVI was calculated (using protocols detailed in Chapter 5). To understand whether the presence or absence of a mass of decomposing pig remains had an effect on the vegetation and surface of the graves, investigations into the relationships between NDVI and grave depth, thickness of pig material, and thickness of overburden, as well as meteorological variables were undertaken.

4.1.2 Former RAF Pershore airfield

During 2001 a Foot and Mouth Epidemic occurred in the UK. As a result of the enforced culling of livestock, a number of emergency mass burial sites were created. It was found that the carcasses were burned at a majority of burial sites, the exception being the Former RAF Pershore airfield near Throckmorton, Worcestershire. This site was used for the burial of upwards of ~139,000 animal carcasses in purpose built burial cells, over a very short period of time commencing in May 2001. Due to the site being a disused airfield, the runways provided a reference not only to help the alignment of the satellite imagery but also to identify whether the vegetation indices calculated were correct (i.e. low values should be observed over the runways due to a lack of vegetation present). Furthermore, the site is surrounded by arable fields and areas of undisturbed native vegetation. These were used for comparison with the vegetation on the grave surfaces. The site is privately owned and the area containing the mass graves is fenced off and has restricted access. The graves themselves have not been managed and the vegetation has not been mown. The only activity at the site has been the routine extraction of leachate from the graves through pipes installed at the time of grave creation. Further details relating to the structure of the burial cells and the site as a whole are detailed in Chapter 6.

4.1.3 Cancari Road, Bosnia and Herzegovina

In 1995, during the conflict in the Former Yugoslavia, 13 human secondary mass graves were created along Cancari Road in Bosnia and Herzegovina. The search that resulted in the selection of the Cancari Road mass graves was extensive and included consideration of hundreds of known mass grave sites across Bosnia and Herzegovina. Grey literature, tribunal reports and exhumation records were interrogated to establish as much information as possible for each site prior to reducing the potential graves to a select few. The Cancari Road mass graves were chosen for this study as they were located within a small geographical area (within 6km) and, consequently, within a single scene of imagery during each acquisition, regardless of sensor. Consequently, it is assumed that any errors within the imagery would affect the scene in its entirety. In addition, the graves were subject to much scrutiny by the ICTY in an effort to link human remains from the Cancari Road to primary mass grave locations. Consequently, a significant amount of documentary evidence was available for use, including aerial photographs acquired around the time of burial which helped located the exact locations of the mass graves in the first instance. From these locations NDVI values over almost a 20-year time scale were extracted and variations in temporal NDVI were used to ascertain whether NDVI derived from both fine and medium spatial resolution archive imagery could be utilised for the detection of mass graves.

4.1.4 Summary of research approach

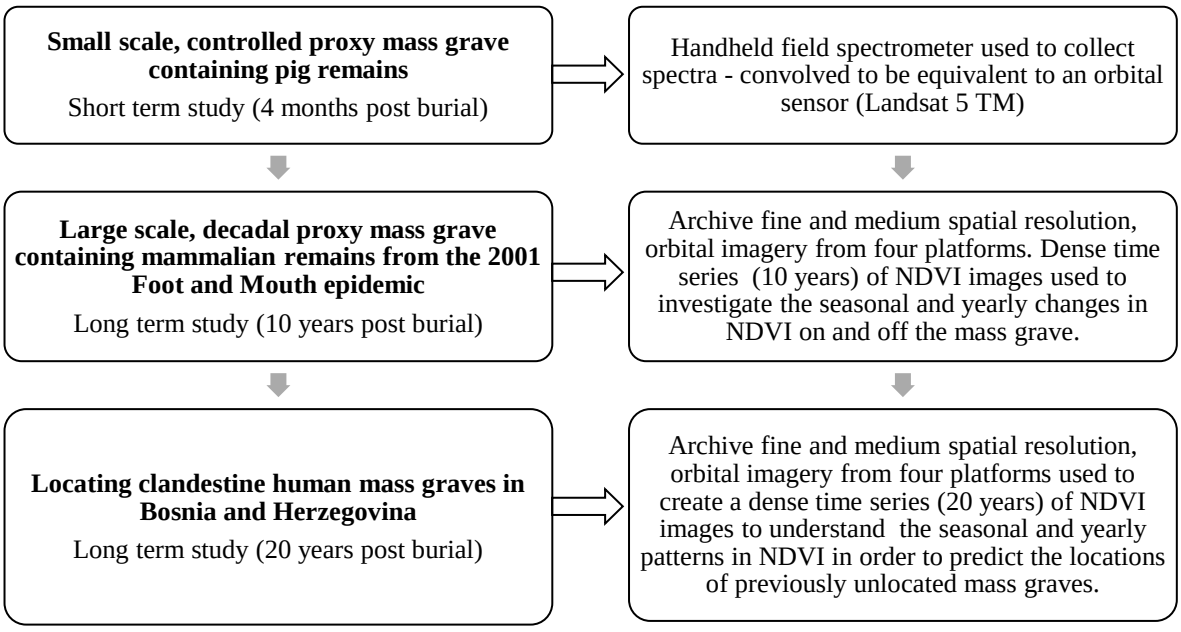

Figure 29 – Summary flow chart of the research method.

4.2 Rationale for the use of multispectral imagery

Multispectral imagery was chosen over hyperspectral imagery because both sites, Former RAF Pershore airfield and Cancari Road, Bosnia and Herzegovina, required a dense time series of imagery to investigate subtle changes in vegetation stress over large temporal scales (in excess of 10 and 20 years respectively). Hyperspectral imagery, although useful due to its large spectral range, often has coarse temporal resolution due to it being acquired via an airborne platform and therefore would not provide the dense time series required for this study. Furthermore, relatively large archives for multispectral imagery exist which have worldwide coverage every ~16 days with medium resolution (e.g. 30 m) starting in 1972 with the launch of Landsat 1. The Landsat archive is freely accessible to search and if registered as a user, imagery can be downloaded without charge via the USGS's multiple interfaces. Therefore, if successful, forensic mass grave detection using multispectral imagery could be employed without significant financial burden.

4.3 Rationale for the multispectral orbital platforms and sensors chosen

Vegetation has been shown to be affected by the presence of a mass grave, this has been measured through variations in vegetation stress over varying timescales (Kalacska and Bell 2006; Kalacska et al. 2009; Norton 2010; Leblanc et al. 2014). Vegetation stress and health can be monitored through the calculation of vegetation indices such as NDVI. NDVI has been chosen as the vegetation index for this research as it is established and well-known.

There are numerous factors that need to be considered when selecting appropriate platforms including spectral, spatial and temporal resolution. To calculate NDVI, data from both the red and NIR bands are required therefore, it is imperative that the multispectral orbital platform/s selected image within these spectral bands. Furthermore, spatial resolution is vitally important. Many of the sensors used to calculate vegetation indices, derive information regarding global phenology or climate change have coarse spatial resolution (i.e. 1km from AVHRR). Such spatial resolutions are too coarse for the detection of relatively small features like mass graves (~15m - length) and were therefore deemed unsuitable for use within this research. To conduct studies investigating variations in NDVI over time, a dense time series was required. To have relatively fine spatial resolution and a regular repeat period (fine temporal resolutions), platforms including Landsat, were deemed to be most

appropriate, as it has a spatial resolution of 30m and a repeat period of 16 days. Subject to cloud cover, this meant imagery was potentially available every 16 days. Furthermore, Landsat, having been launched in 1972, had the largest archive that was freely available for download with worldwide coverage.

Cloud free imagery was sought for both the Former RAF Pershore airfield site and Cancari Road in Bosnia and Herzegovina, however, it was found that there were gaps in the time series where no imagery was available. The gaps in the data between 2004 and 2008 were due to the scan line corrector failing on Landsat 7 ETM. Therefore, additional imagery was obtained for the Former RAF Pershore airfield and the Cancari Road in Bosnia and Herzegovina. Archive imagery from the Disaster Monitoring Constellation (DMC) was gifted by DMCii Ltd, with the 2004-2009 imagery acquired by UK-DMC with a 32 metre ground sample distance and the 2010-2011 images acquired by UK-DMC2, with a 22 metre ground sample distance. Both sensors were design to mimic Landsat and are calibrated within +/- 1% Landsat 7 ETM+. However, data gaps still existed within the imagery, therefore an ESA data grant was written (and subsequently granted) which gave access to additional Landsat, SPOT and RapidEye imagery resulting in a dense time series. Imagery from Landsat, SPOT and RapidEye were also used for Cancari Road, however no DMC imagery was available for this site. Following the launch of the USGS Earth resources observation and science (EROS) center science processing architecture (ESPA) interface, additional Landsat scenes were acquired to enhance the density of the time series. The imagery obtained from USGS EROS ESPA were terrain corrected (L1T), radiometrically and atmospherically pre-processed.

4.3.1 Compatibility of sensors

To the author's knowledge, this research is the first time the sensors detailed above have been combined into a single time series to study variations in NDVI in the context of mass graves. Therefore, it was important to consider the compatibility of the sensors and the impact that this would have on the results obtained (technical specifications for each of the platforms and sensors are located in Appendix 1). It was noted that when NDVI was calculated for each scene, the values within the produced map would be correct relative to the different surface types, with areas known to be non-graves or undisturbed ground used as a baseline measurement. This was the case for both study sites. In light of the above, the spectral range of the red and NIR bands were compared for each sensor as seen in Figure 30. In addition, the time of image acquisition for each sensor was also compared as well as the spatial resolution of each sensor.

4.3.1.1 Comparison of the spectral range for the red and NIR spectral bands

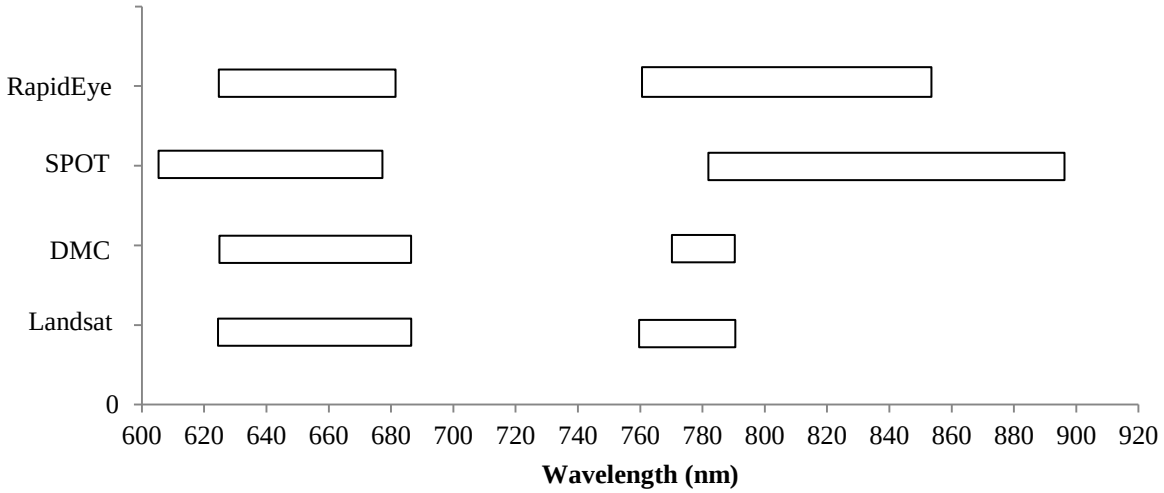

Figure 30 - Comparison between the red (left) and NIR (right) spectral bands for each sensor

It can be seen from Figure 30 that broadly speaking, the red and NIR spectral bands for each sensor overlap, with SPOT varying the most, only overlapping slightly with the NIR wavelengths recorded by Landsat, the primary sensor. As NDVI is a ratio between the red and the NIR, values the sensors were deemed suitable for use within this research.

4.3.1.2 Comparison of the time of image acquisition

Depending on where the AOI is located within a scene (Appendix 1), if the imagery is collected at solar noon then there is less chance of shadow; this is known to influence spectral measurements and consequently, NDVI. As can be seen from Table 5, the time of imagery acquisition for the Former RAF Pershore airfield ranged from 9.30am for DMC through to 11:50am for RapidEye. The effects of this are likely to be most obvious in the winter with dark mornings compared to those in summer. Within this research summer images were predominantly used and therefore, the influence of the time of image acquisition is likely to be minimal. In contrast, the time of image acquisition for the Cancari Road mass graves (Table 6) ranged from 8:50am for Landsat 5 TM through to 10:21am for RapidEye; therefore imagery is collected in a shorter period of time however, it is collected earlier than images for the Pershore site. As with the Pershore imagery, the effect of this is likely to be greater in winter. However, imagery from the spring through to autumn was

predominantly used. Therefore, the effect of this on the spectra obtained is likely to be minimal.

Table 5 - Comparison between times of image acquisition for all sensors for the Former RAF Pershore.

Platform	Time of Imagery Acquisition (am)
Landsat 5 TM	10:33
Landsat 7 ETM+	10:47
DMC	9:30
SPOT	11:46
RapidEye	11:50

Table 6 - Comparison between times of image acquisition for all sensors for the Cancari Road mass graves.

Platform	Time of Imagery Acquisition (am)
Landsat 5 TM	8:50
Landsat 7 ETM+	9:20
Landsat 8 OLI	9:27
SPOT	9:52
RapidEye	10:21

The spatial resolution of the sensors varied from medium (30m for Landsat) to fine spatial resolution (5m for RapidEye) (**Table 7**). As stated previously this was due to the fact that there were significant data gaps in the Landsat imagery therefore, imagery from multiple sensors was acquired. All imagery was processed with the original spatial resolution, rather than resizing the pixels to match the Landsat imagery, as this would have resulted in a loss of spectral data.

Table 7 - Spatial resolution of the sensors.

Platform	Spatial Resolution (m)
Landsat 5 TM	30
Landsat 7 ETM+	30
Landsat 8 OLI	30
DMC / DMC-2	32 or 22
SPOT	20
RapidEye	5

4.3.2 Pre-processing methods

All satellite multispectral imagery, with the exception of those obtained from USGS EROS ESPA, underwent pre-processing including radiometric calibration and atmospheric correction, prior to the calculation of NDVI in ENVI version 5.3 (Harris Geospatial Solutions). The specific pre-processing stages undertaken for each imagery type is outlined within Chapters 6 and 7. Screenshots of each pre-processing stages are located in Appendix 1.

5 Field Spectroscopy, Derived Vegetation Indices and Geophysics for Monitoring Differences in Vegetation on a Small-Scale, Controlled Mass Grave Containing Mammalian Remains

NDVI has been utilised extensively in numerous disciplines however it has not yet been proven to be effective for the detection of buried organic remains. Consequently, this chapter will detail investigations into whether changes in NDVI during the first four months post burial on the surface of small-scale mass graves, one containing disarticulated porcine remains and the other empty; can be used as a detection tool. In situ below ground temperature measurements were undertaken to monitor decomposition throughout the study. Additionally, geophysics was undertaken to provide a spatial measure of the state of decomposition. The results will be presented before providing a discussion and conclusion commenting on the effectiveness and utility of using variations in NDVI and geophysical survey techniques to detect mass graves in temperate environments.

5.1 Method

5.1.1 Field Site and Proxy Mass Graves

The field site is located on a private estate close to East Holme, Wareham, Dorset, UK ($50^{o}39'54.43^{o}$N $2^{o}7'52.84^{o}$W - Figure 31) and was an existing Department for Environment, Food & Rural Affairs (DEFRA)/ Animal Health and Veterinary Laboratories Agency (AHVLA) certified experimental area (Animal By-Products Registration Reference: U1143934). The field site and surrounding area is predominantly pasture and grassland. The field was previously used as an experimental area whereby proxy graves were created for a number of Bournemouth University research projects. The area where the proxy mass graves were created for this study avoided any areas that had undergone prior disturbance.

Figure 31 - Location of the field site (red rectangle) and weather station IDORSETW15 (green circle) overlaid on 1:50,000 Ordnance Survey topographic map (© Crown copyright and database right 2018 Ordnance Survey).

The two graves were created on the 6th August 2013 once certification to use the site for scientific research was granted by DEFRA/AVHLA, the Environment Agency (EA) and the land owner. To satisfy conditions stipulated by the EA, a hardwearing fence was erected around the site to ensure that animals were not able to access the graves and graze on the grave surface (Figure 33). The presence of the fence enabled the vegetation at the grave sites and control area to colonise and undergo seasonal changes without disturbance from large mammals (especially foxes and grazing cattle).

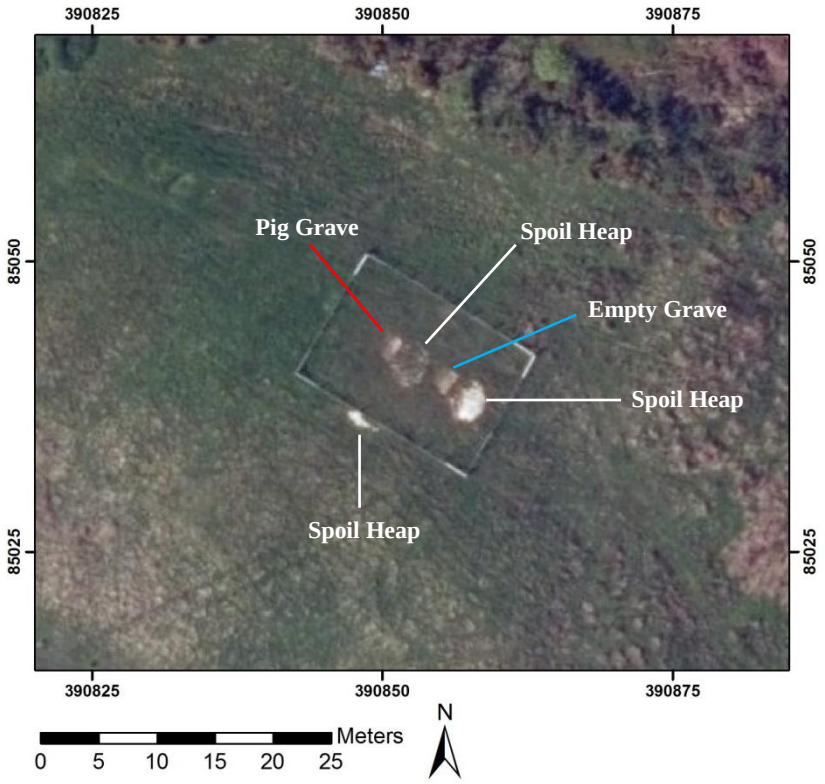

Figure 32 - Field site shown in an orthophoto from 2014. Experimental area is located within the rectangular fence.

An experimental area was created (Figure 32 and Figure 33) which contained two simulated mass graves (dimensions L: 2m x W: 1.6m x D: ranging from 0.5m- ~1.2m) replicating the ramped graves seen in Bosnia and Herzegovina. One grave contained ~350kg of disarticulated pig remains (including pig head, bones, skin, offal and trotters) whilst the other was a control containing only backfilled soil, thus simulating disturbed ground or an empty grave. Pig remains were chosen to be used as a proxy for human remains due to their reported similarities to human tissue composition as well as the skin to bone ratio (Matuszewski et al. 2019). They are also an accepted proxy for human remains in forensic studies (Cunningham et al. 2011). Disarticulated remains were chosen as an alternative to whole carcasses due to budgetary constraints, and also as the length of the study was relatively short it was important that the decomposition process was promoted wherever possible. The two graves were created using a small 360^{o} excavator and were designed to replicate mass graves in countries such as Bosnia and Herzegovina that were created using heavy excavation machinery.

Figure 33 - Image of experimental site, prior to interment of pig remains

At the northern end of both the pig and empty grave the depth was relatively shallow (~0.5m) with a gradual slope towards the southern wall where the grave reached a maximum depth of 1.2m (Figure 34 and Figure 35). Therefore, the depth and density of mammalian remains were greater at the southern end of the grave as opposed to the northern end. This enabled investigations into whether differences in the depth and quantity of organic mass has an effect on vegetation stress at the grave surface. The thickness of the topsoil was kept constant across the length of the grave and within both the pig and control grave. Ideally a suite of graves with differing variables including grave size, topsoil depth would have been created, but under the constraints of both time and resources this was not possible. Both the pig and control grave had two surface types, with half of the grave re-turfed with the original grass and the other half left as bare soil (Figure 36). This was to ensure that the site yielded as much data as possible and allowed for comparisons to be made between the stress of existing vegetation vs. re-colonising species. In addition the site contained an area of grass (of comparable size to the experimental graves) that remained undisturbed throughout the study, from which background reflectance spectra of native vegetation were collected. The

background spectra were used as a baseline signature and allowed for comparisons to be made between the spectral responses of the vegetation above the two experimental graves.

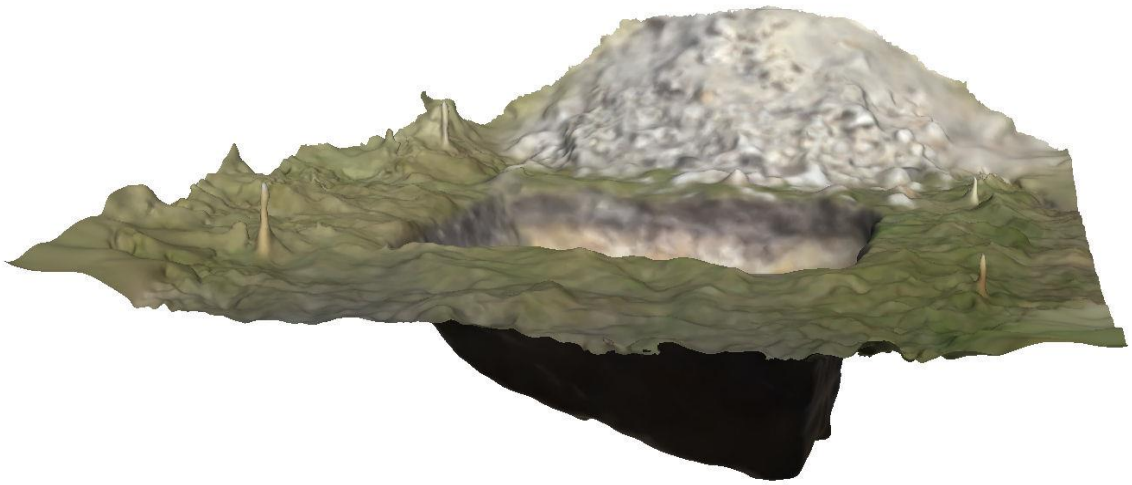

Figure 34 - 3D perspective view of a DEM of the experimental grave prior to interment of pig remains at East Holme, draped with RGB values, created using Structure from Motion (SfM) (AgiSoft PhotoScan).

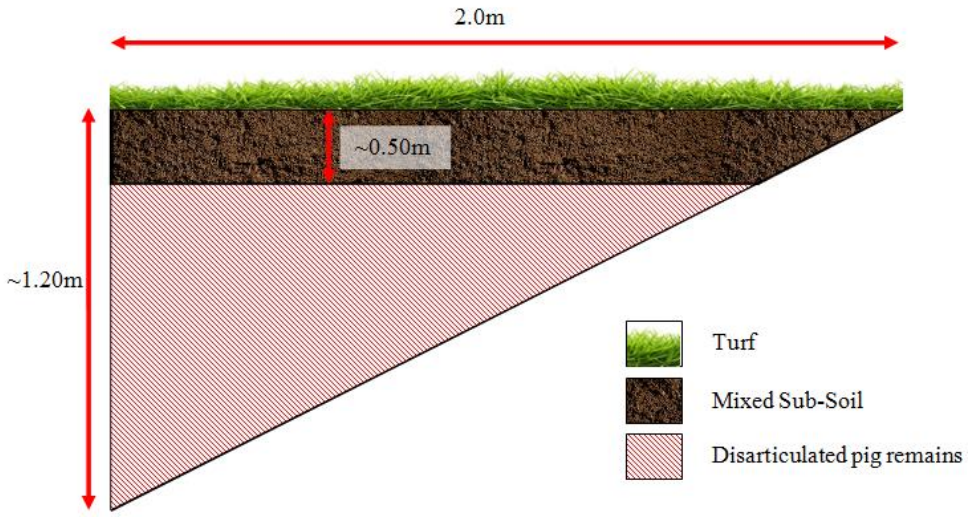

Figure 35 - Schematic showing the cross section of the pig grave (not to scale).

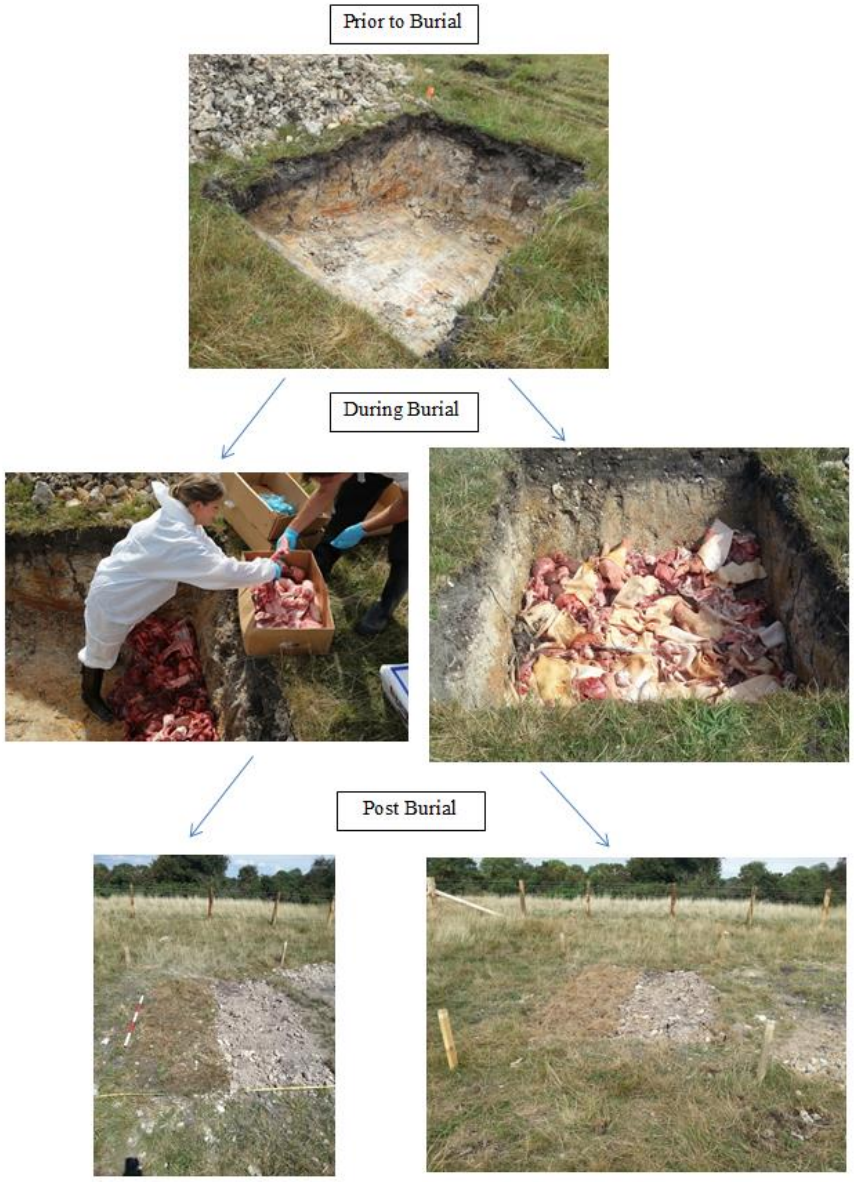

Figure 36 - Photographs of the experimental graves taken prior to, during and post burial on 6th August 2013.

5.1.2 Temperature monitoring

From the time of interment in-situ temperature measurements were taken with two TinyTag data loggers each with two temperature probes attached. In both the pig and the empty grave, a probe was on top of and in direct contact with the pig remains at approx. 50cm, with the second probe placed at 30cm below ground level (BGL); the probes were also positioned in the empty grave at the same depths (Figure 37). Temperature data was collected once every four hours; with this being used to investigate the temperature gradient within the graves over time. It was anticipated that the temperature gradient calculated would indicate the state

of decomposition of the buried remains over time and that this could then be further validated through regular geophysical surveys using a multiplex six probe resistance metre (courtesy of Bournemouth University). The geophysical techniques implemented are discussed further in Section 5.1.6. Unfortunately during 21st September 2013 (approximately one month post burial) the probe wires attached to the data logger in the control grave were damaged; a decision was made not to recover the probe so as not to disturb the grave. Consequently, no temperature data exists for the control grave beyond one month post burial.

Figure 37 - Photograph showing the locations of the TinyTag data loggers in the pig grave at 50cm (left) and 30cm BGL (right).

5.1.3 Weather Station

To study the influence of meteorological variables on NDVI, the ambient air temperature, relative humidity, air pressure, precipitation and wind speed were measured and recorded every thirty minutes by a weather station (installed 18th September 2013). However, on two occasions the data logger failed, therefore, there were significant time periods where no meteorological data was recorded (March 2014 – June 2014 and December 2014 – March 2015).

Consequently, a local weather station IDORSETW15 was selected as a replacement. The weather station was located in Wareham, 2.20 miles north east of the research site (Figure 31). This station was a similar specification (Maplin USB Weather Forecaster) to the station installed at the research site (Maplin USB Wireless Weather Forecaster) and was the only station located within a five mile radius that had continuous archive data (every ten minutes) from summer 2013 through to summer 2015. To establish whether the weather data from the IDORSETW15 station was comparable to the research site station, the data from both were

plotted and compared for the mean monthly temperature and humidity. It was found that there was a 2^{o}C maximum difference between the mean daily temperatures of the two weather stations (Figure 38). The replacement station recorded higher temperatures than at the experimental site; this may be due to the IDORSETW15 station being located in a residential area and consequently, temperatures are likely to be higher when compared to those recorded in a rural area. When mean daily humidity was considered it was found that there was a 5% maximum difference between the two stations mean daily recordings (Figure 39). The IDORSETW15 station was therefore deemed a suitable replacement and was subsequently used to assess the strength of the relationships between meteorological variables and vegetation stress (observed using spectral measurements from handheld field spectroscopy instrumentation).

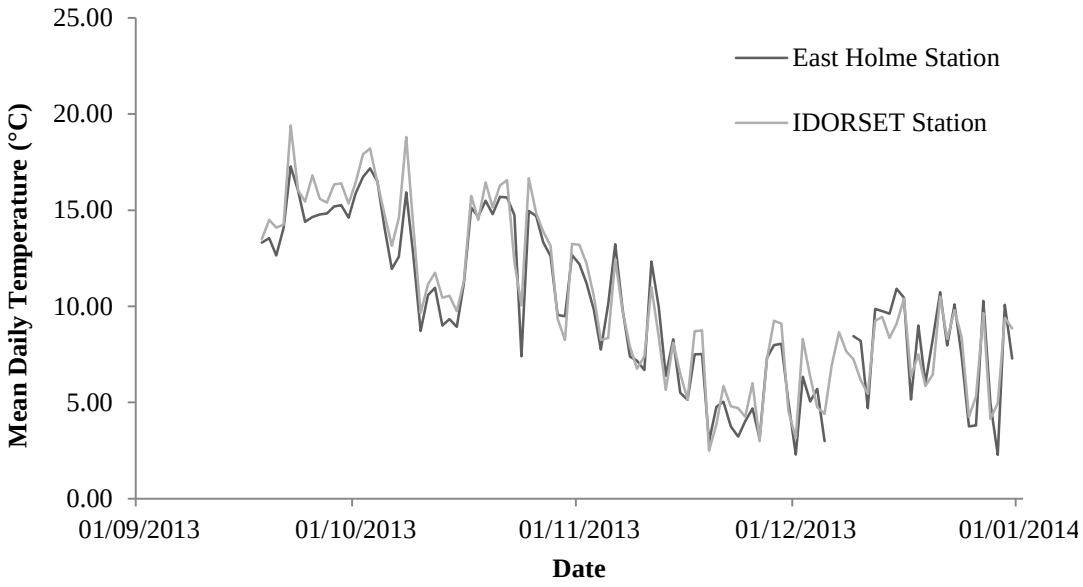

Figure 38 - Comparison of the mean daily ambient temperature measurements for the two weather stations.

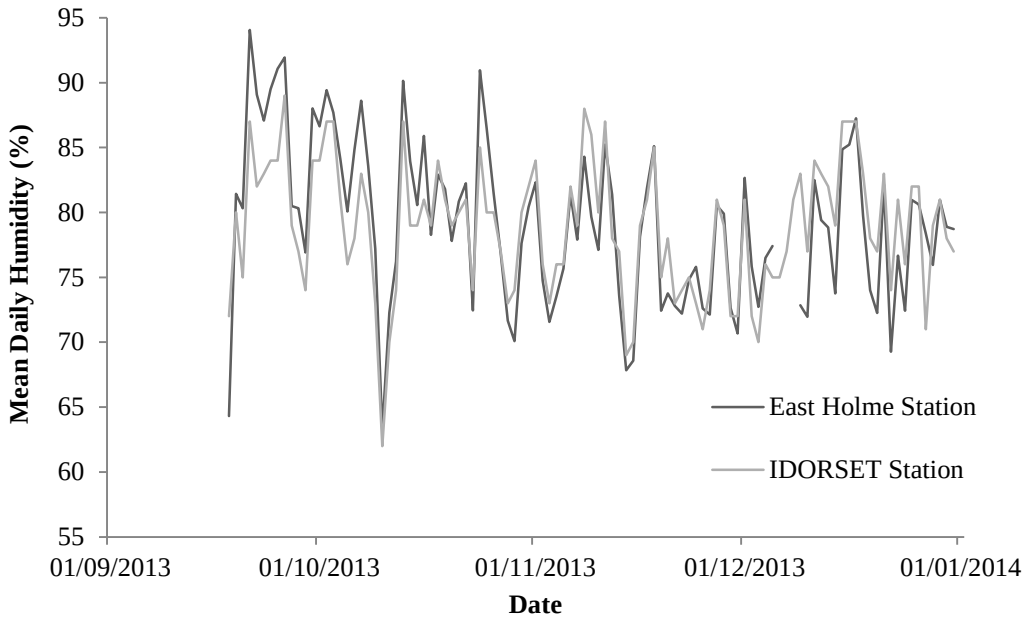

Figure 39 - Comparison of the mean daily humidity measurements for the two weather stations.

Monthly weather history records for the IDORSETW15 station were downloaded from the Weather Underground website[1] including; ambient temperature, dew point, humidity, wind speed, precipitation accumulation and pressure. The data was downloaded in monthly blocks and included daily low, high and mean readings for each variable listed above.

5.1.4 Field Reflectance Spectroscopy – supported by the Natural Environment Research Council's Field Spectroscopy Facility

Reflectance spectra were collected four times during the first four months post burial using a GER1500[2] at optimal times around solar noon (+/-2 hours). Training was provided by Natural Environment Research Council's (NERC) Field Spectroscopy Facility (FSF). Reflectance spectra were collected from sample points on the grave containing pig remains, the control grave as well as the undisturbed area of grass (Figure 40). A calibrated reflectance panel (Ref: SRT #033 97A15E-1520) - supplied by NERC FSF) was used in between each measurement to ensure that any changes in solar illumination between the collection of each reflectance spectra could be quantified. The sample points were allocated via random stratified sampling using ArcMap and the random shapes tool. A Leica VIVA

[1] http://www.wunderground.com/personal-weather-station/dashboard?ID=IDORSETW15#history/s20150701/e20150723/mcustom [Accessed October 2015]

[2] Instrument provided by NERC FSF through grants: 664.1112 and 688.1113.

differential global positioning system (dGPS) was used to find the location of the sample points at the site using the stakeout function, once located, numbered plastic pegs were placed into the ground to mark the sample point locations (Figure 41 and Figure 42).

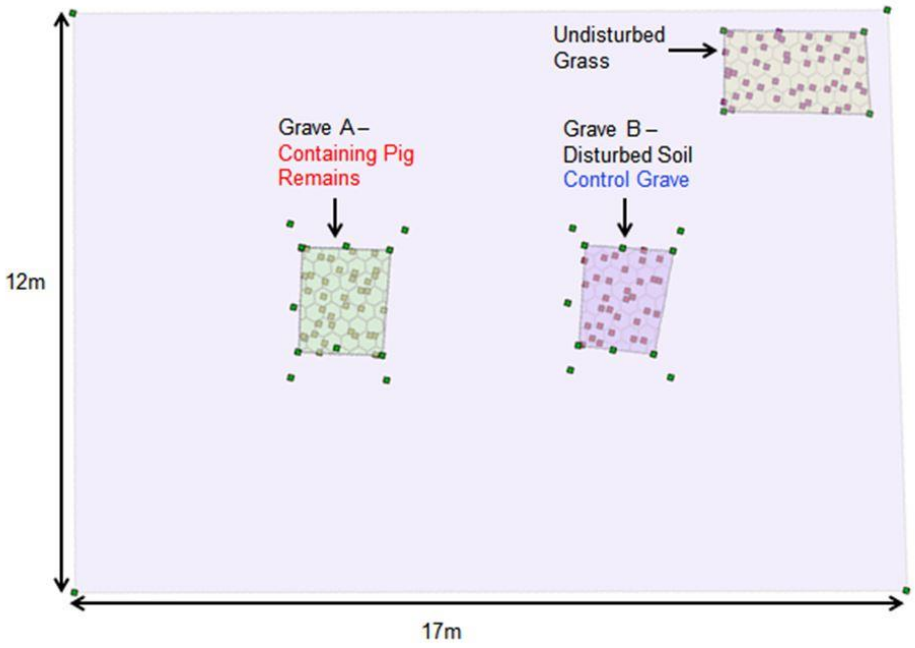

Figure 40 - Schematic layout of the experimental site including the control grass area and the defined sample points where reflectance spectra were collected.

Figure 41 - Reflectance spectra sampling points.

Figure 42 - GER1500 in use at the East Holme experimental site.

5.1.4.1 Processing of the GER1500 Reflectance Spectra

The spectra collected using the GER1500 were processed using guidance contained within the FSF document (MacLellan 2006). The FSF toolbox was used for the post processing of all GER1500 spectra collected, the steps used are summarised in Figure 43; please refer to Appendix 2 for full details and the MATLAB code used. All spectra collected by the GER1500 (manufactured by Spectra Vista Corporation – SVC) are stored in a signature text file format and have the extension .sig. Each .sig file contains header information followed by two columns of spectra, one for the target and the second for the corresponding reference spectra.

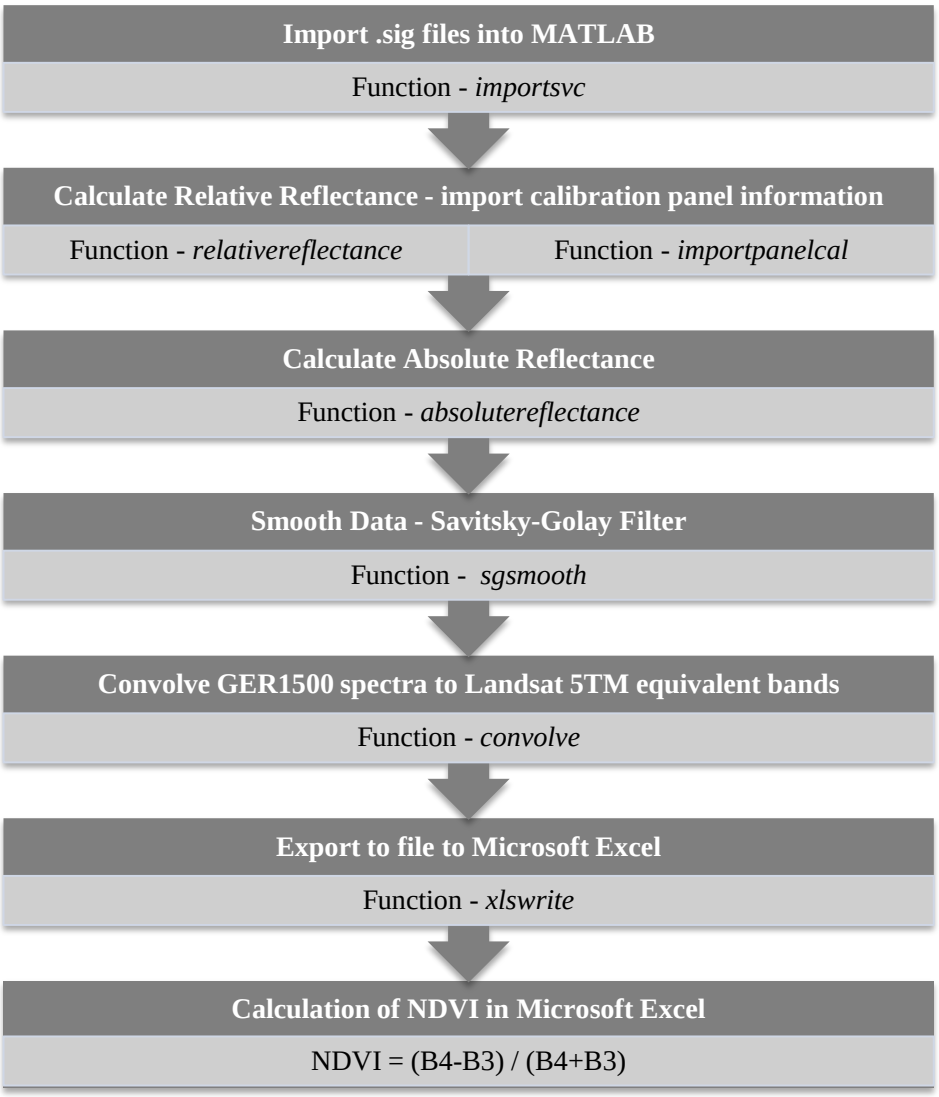

Figure 43 - Summary flow chart outlining the post processing steps conducted in MATLAB and Microsoft Excel to process the GER1500 spectra.

Equation 6 - NDVI Equation

$$NDVI = \frac{(NIR - R)}{(NIR + R)}$$

The NDVI (Equation 6) was calculated for each sample (1-115). A .csv file was then created for each 'surface type' demonstrating where GER1500 spectral measurements were collected during each visit to the site (Table 8).

Table 8 - Table detailing the surface types at the East Holme experimental area and the number of spectral samples collected on each.

Surface Type	Number of spectral samples collected
Pig Grave - Turf	19
Pig Grave - Soil	18
Empty Grave - Turf	13
Empty Grave - Soil	18
Undisturbed Grass	47

5.1.4.1.1 Interrogation of the convolved GER1500 spectral data

Easting and northing coordinates were generated when the sample points were created therefore, the data could be plotted in a GIS (ArcMap version 10.3.1) such that the NDVI across the grave surfaces could be examined through time.

The NDVI calculated using the convolved GER1500 spectra were comparable to the NDVI calculated using Landsat 5 TM bands. The main difference between the two sets of data was the path length, with the GER1500 being approximately 1m versus Landsat's orbital path length. By changing the symbology, (i.e. by introducing a colour ramp and an equal interval classification containing five classes) the NDVI values across each sample area (i.e. pig grave, empty grave and the undisturbed grass) were able to be visually compared.

5.1.5 Creation of Orthophotos and DSMs for determining the relationship between NDVI and the pig grave

Photographs of the grave were taken using a digital camera phone at three successive intervals:

1) When the grave was empty
2) When the grave contained pig remains
3) When the grave was back-filled

Multi-View Stereo Structure-from-Motion (MVS-SfM) photogrammetry (using Agisoft's Photoscan) was used to create Digital Surface Models (DSM) with 1cm resolution in the British National Grid projection. These were required to ascertain the relationships between the thickness of the pig remains, overburden and depth of the grave, using the following calculations:.

Thickness of pig material = Pig filled grave – empty grave

Thickness of overburden = Full grave – pig filled grave

Depth of grave = Full grave – empty grave

The resulting thickness and depths were then extracted for the location of each field spectroscopy observation in ArcMap using the tool 'extract values to points'.

5.1.6 Geophysical Survey

Temporal electrical imaging and electromagnetic profiling was acquired in three dimensions across the site with readings taken at 0.5m intervals along traverses with a 0.5m traverse interval (Figure 45 and Figure 44). The surveys commenced in the southernmost corner of the site. The site was surveyed four times within the first four months post burial (up to 121 days post burial), to provide a spatial measure of the state of decomposition within the grave (principally based on conductivity) and to ascertain whether the disturbance caused by creating the grave could be detected. The survey grid included an area of undisturbed ground (a control) which was used to ascertain a background value for the site, this was located in between the two graves and is highlighted in green in Figure 46.

Figure 44 - Photographs of geophysical surveys being carried out at the East Holme experimental site. Left to right: Multiplexed earth resistance (Geoscan Research RM15) and electromagnetic (Geonics – EM38B).

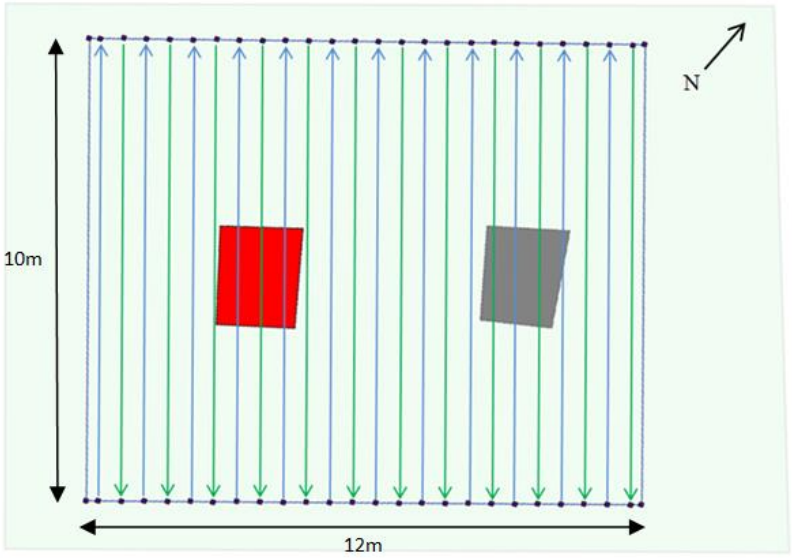

Figure 45 - Schematic diagram of experimental site, demonstrating the 10m x 12m geophysical survey grid with a 50cm traverse interval.

5.1.6.1 Post-processing of Geophysical Survey Data

5.1.6.1.1 Post-processing of the Electromagnetic Vertical Magnetic Dipole (VMD) Quadrature Response Survey Data

The electromagnetic survey data was initially opened in notepad, where the header information was deleted and the file was saved as a .txt file. After which the data was separated out into two worksheets, one for the quadrature (a measure of conductivity) and one for the inphase (a measure of magnetic susceptibility). Dummy readings (2047.5 – as defined by Geoplot) were inputted to complete the second grid. A new input grid template was set up within Geoplot containing the details in Table 9.

The first stage of post processing the electromagnetic survey data was to zigzag correct the survey data using the 'invert traverse mode' tool where the direction was changed to horizontal. The two grids were then combined into one using the mastergrid tool, saving first as .plm and then as a .cmp file; for both the inphase and quadrature.

Table 9 - Details inputted into Geoplot for creating a new input grid template for the EM data.

New input grid template	EM38i10
Walked (Direction)	North
Length	10m
Reading Interval	0.5m
Width	10m
Traverse	0.5m
Instrument	EM38
Unit	ppt - parts per thousand

The same areas that were used to extract the pig and empty grave (control) and also the undisturbed ground for the resistance data were used for the extraction of EM values (Figure 46). Similarly, the mean, maximum and minimum quadrature response values were calculated and then compared to the background response in terms of percentage difference.

5.1.6.1.2 Post-processing of Resistance Survey Data

The resistance survey data was processed using Geoplot 3.0 (Geoscan Research). As the survey grid was 10m x 12m, two grids of 10m x 10m were combined to create a mastergrid (10m x 20m), the second grid contained only two lines of geophysical data, the remainder contained dummy readings. A mastergrid was created and saved as a .pml file, from which a composite (.cmp) file was created; both files were saved with filenames relating to the date the data was collected. This process was carried out for each electrode separation (0.5m, 1.0m and 1.5m). The data was despiked twice, to remove spurious readings, and interpolated twice in both the x and y directions, to smooth the image. After each processing stage, the data was saved as a new .cmp file to maintain best practice.

The mean, maximum and minimum resistance values were calculated for each area and for each depth. The percentage difference between the resistance values for both the pig and empty grave were calculated relative to those obtained from the control area.

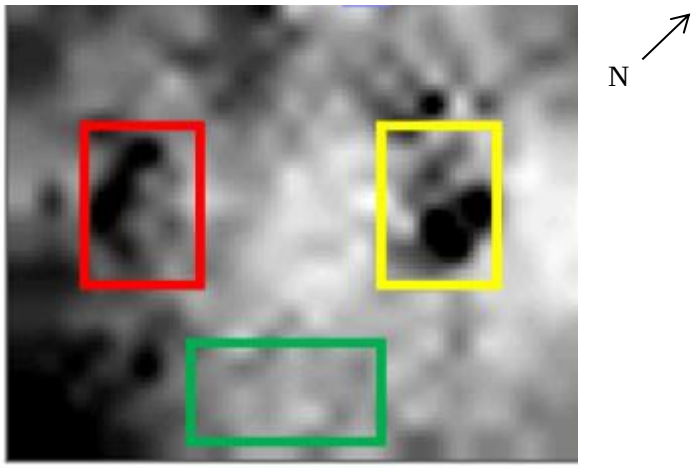

Figure 46 - Example resistance survey result indicating the areas where resistance values were extracted for the pig grave (red), empty grave (yellow) and the undisturbed ground (green). Image cropped to the survey grid 10m x 12m.

5.2 Results

5.2.1 Detecting disturbance through geophysical survey

To assess whether disturbance caused by creating the graves and to investigate the relationship between decomposition and NDVI for both the pig and empty grave, four geophysical surveys were carried out during 2013. The electromagnetic and resistance results corresponding to each of these dates are presented, before summarising the overall findings.

5.2.1.1 Electromagnetic results up to and including 121 days post interment

Within each electromagnetic vertical magnetic dipole (VMD) quadrature response plot, the anomaly representing the pig grave is outlined in red with the anomaly representing the empty grave (control) outlined in yellow (Figure 47). The thick black outline visible on the left and right side of the plot are high conductivity readings and correspond to the metal fence surrounding the site. At the end of each survey line, the instrument was in close proximity to the fence and therefore, its effect is observed in the plots. The mean, minimum and maximum conductivity measured in milliSiemens per metre (mS/m) were calculated for the pig and empty grave and the undisturbed ground for each survey conducted (Table 10). The black and dark grey areas of the plot represent high conductivity, whereas the light grey through to white areas, represent low conductivity.

At 14 days post interment the pig grave has a higher mean conductivity than the empty grave and the area of undisturbed ground (Table 10). The only difference between the empty grave and the pig grave is the presence of organic remains; therefore it is likely that the observed difference in conductivity is due to the presence of the disarticulated pig remains. The layer of disarticulated remains may have prevented water from draining away from the grave causing pooling at the grave base. High conductivity is likely observed due to the remains having higher moisture content when compared to the surrounding soil; regardless of the remains not yet being in an advanced stage of decomposition. The empty grave exhibited higher maximum conductivity when compared to the area of undisturbed ground, this may be indicative of the differences in soil compaction due to the recent creation of the grave; causing a difference in soil moisture when compared to the relatively compact, undisturbed soil surrounding the graves (Table 10). The ground surrounding the empty grave provided a noisy signal, and is visible in both plots (Figure 47). Taking into account meteorological variables, from day of interment to the 20th August 2013, there was a total recorded rainfall of 0.86mm; therefore, it can be stated that the soil across the site was generally dry. When ambient air temperature is considered, the mean temperature (taking into account the temperature over 24 hours) was 18.0^{o}C, with a maximum and a minimum of 19.7 ^{o}C and 15.9 ^{o}C respectively; the air temperature was neither excessively hot nor cold.

At 43 days post interment, the pig grave is clearly visible as an area of high conductivity compared to the rest of the site (Figure 47). The empty grave is not visible or discernible due to the contrast parameters used. The pig grave has higher mean and maximum conductivity values when compared to the empty grave and the undisturbed ground (Table 10). The backfill in both the pig and empty grave are likely to be equally uncompact, the only difference being the presence of the pig remains, which appear to be highly conductive. The empty grave was found to have lower average conductivity than the undisturbed ground, with the maximum being 5.13mS/m in contrast with the undisturbed ground maximum which was 10.13mS/m. The meteorological data for the two weeks preceding the survey, showed that rainfall was recorded almost every day, bar four, resulting in a total rainfall of 3.4mm. Through the act of creating the graves and the resulting disturbance, the backfill in the empty grave is likely to be less compact than the undisturbed ground, known to be compact clay, and therefore enabled drainage of moisture resulting from the rainfall.

At 70 days post interment the pig grave is observable as an area of high conductivity compared to the rest of the site (Figure 47). The empty grave is not clear in either plot due to the contrast parameters used. The values for the empty grave were extracted and are detailed in Table 10. As previously observed, the pig grave has higher average and maximum

conductivity when compared to the values for the empty grave and also the undisturbed ground. Similar to the observations at 43 days post interment, at 70 days the empty grave has lower mean and maximum conductivity values when compared to the pig grave and also the undisturbed ground, which exhibits higher conductivity values. It is important to consider the difference between the empty grave and the undisturbed ground to ascertain why the undisturbed ground has higher conductivity. The difference is the disturbance that the empty grave has undergone, leading to a difference in soil compaction and porosity. Consequently, the empty grave is less compact and is free draining, whereas, the undisturbed ground is comprised of compact clay which is likely to retain water; resulting in high conductivity readings.

At 121 days post interment the pig grave is again clearly visible in the plots as an area of high conductivity compared to the rest of the site (Figure 47). The empty grave is indistinguishable from the general background variation and is unclear on the quadrature and profile plot. The quadrature responses recorded for all of the areas of the site are presented within Table 10. The pig grave has higher mean and maximum conductivity (peaking at 19.89 mS/m) when compared to the empty grave and undisturbed ground. The empty grave has a lower maximum conductivity value when compared to the equivalent values for the pig grave and also the undisturbed ground, which are exhibiting higher conductivity values. However, the mean conductivity for the empty grave, as well as the minimum, has increased to exceed that of the undisturbed ground. The increase in conductivity could be due to water pooling at the base of the empty grave. Alternatively, the observed increase may be due to the gradual compaction and settling of the grave, although this will not be as compact as the undisturbed ground. When considering the meteorological data a month prior to the survey date it was found that the preceding month saw rainfall almost every day resulting in an excess of moisture that could not drain away from the grave causing pooling at the base of the empty grave. This along with the presence of the conductive pig remains would also account for the increase in mean and maximum conductivity.

In summary, the pig grave remained consistently visible in the electromagnetic quadrature plots due its high conductivity values compared to the rest of the site (empty grave and control undisturbed) throughout the survey period; up to and including 121 days post burial. The highest absolute conductivities for the pig grave were recorded at 121 days post burial.

To further investigate the differences between the surveys, conducted at irregular intervals, the percentage differences were calculated between the undisturbed ground, the pig and empty grave; using the values for mean conductivity. For the purposes of calculating the percentage difference between the two graves and the undisturbed ground, it is assumed that,

the undisturbed ground is the control with the variable being either the pig or the empty grave respectively.

20th August 2013 – 14 days post interment

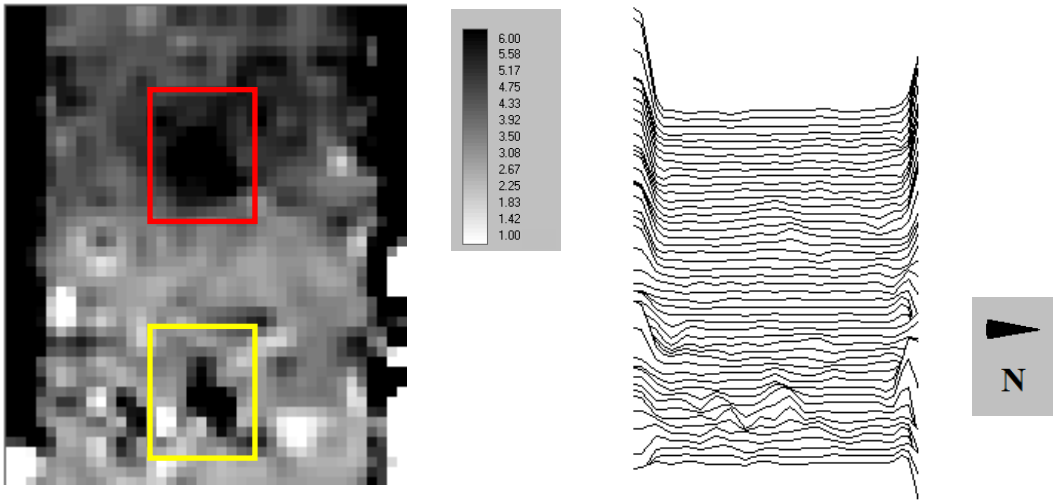

18th September 2013 – 43 days post interment

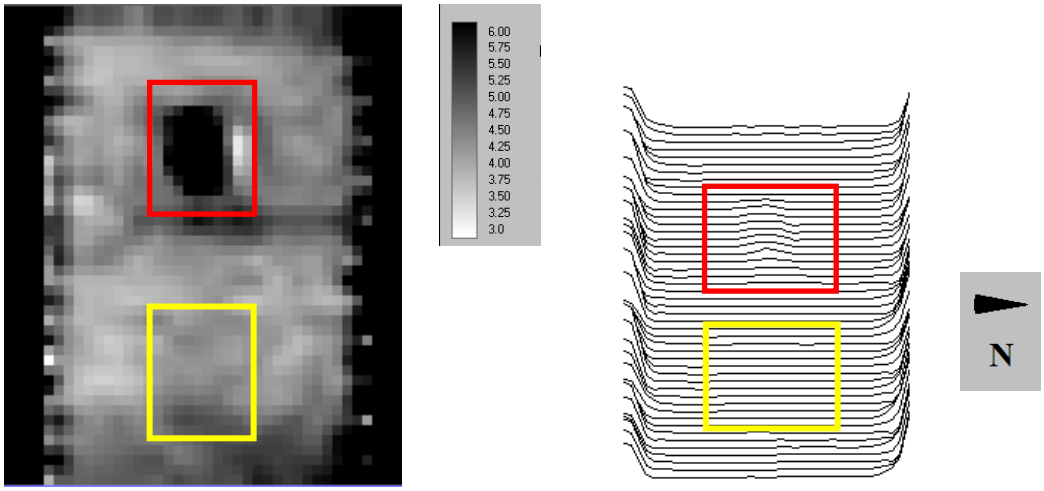

15th October 2013 – 70 days post interment

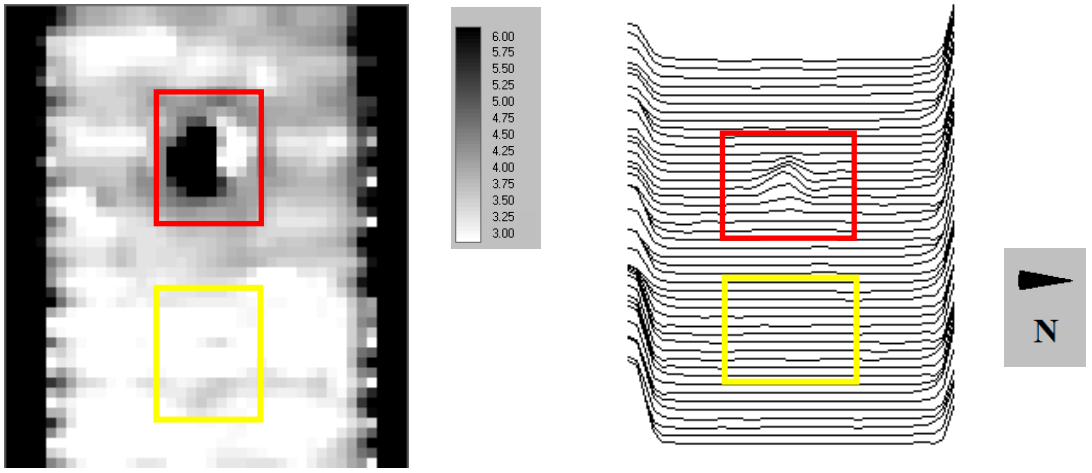

5th December 2013 – 121 days post interment

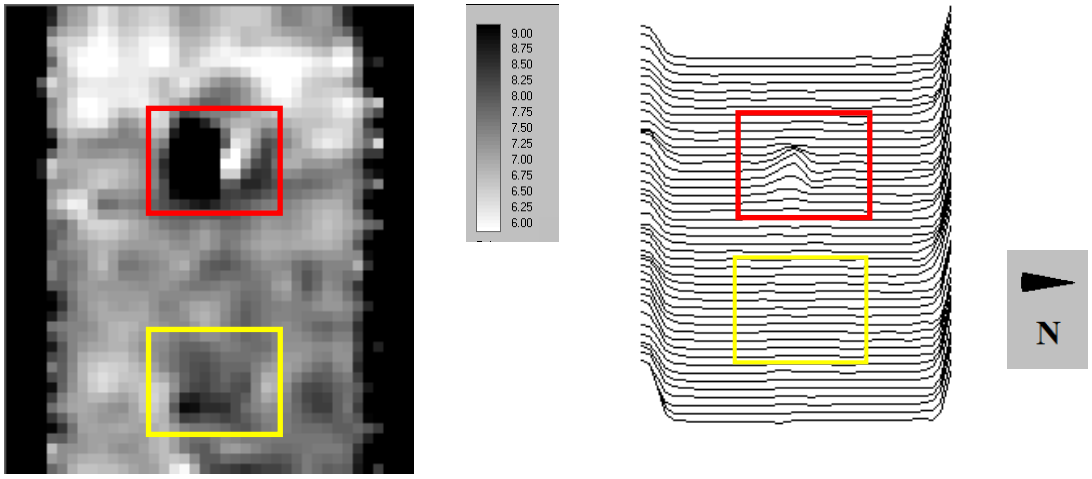

Figure 47 - Electromagnetic quadrature results up to and including 121 days post interment (pig grave is outlined in red and the empty grave is outlined in yellow). Scale in mS/m.

Table 10 - Mean, minimum and maximum conductivity for the experimental site up to 121 days post interment.

	Pig Grave			Empty Grave			Undisturbed Ground		
	Mean. (mS/m)	Max. (mS/m)	Min. (mS/m)	Mean. (mS/m)	Max. (mS/m)	Min. (mS/m)	Mean. (mS/m)	Max. (mS/m)	Min. (mS/m)
20/08/13	6.31	8.10	2.05	4.97	9.24	2.05	4.08	6.39	2.29
18/09/13	6.60	12.48	3.28	4.67	5.13	4.26	6.01	10.13	3.47
15/10/13	7.01	15.59	2.47	3.22	3.63	2.89	4.66	9.65	2.28
05/12/13	11.06	19.89	5.96	8.05	8.91	7.51	7.98	9.95	6.22

5.2.1.2 Percentage difference between the mean quadrature response of the pig grave and undisturbed ground up to 121 days post interment

It can be seen in Table 11, at 14 days post burial there was a percentage difference of +54.66% between the mean quadrature response of the pig grave and the undisturbed ground. This then dropped to +9.82% at 43 days post burial. At 70 days post burial there was a percentage difference between the two areas of +50.43% which then reduced to +38.60% by 121 days. The general trend is that the percentage difference between the mean conductivities of the pig grave and the undisturbed ground decreases over time; with the exception being at 43 days post burial, when the quadrature response of the undisturbed ground is similar to that of the pig grave (Table 11 and Figure 48). This is could be indicative of two events, firstly, a climatic event occurring one week prior to the survey, where an increase in precipitation was recorded and therefore, increased ground moisture levels were observed. Alternatively, the increased conductivity observed could be due to a decomposition event.

It is important to note that the pig grave exhibited higher conductivities compared to the area of undisturbed ground (ranging between +9.82 and 54.66% difference). The mean conductivity of the pig grave increased with each survey and peaks at 11.06 (mS/m) at 121 days post burial. This would suggest that there was decomposing soft tissue present within the grave throughout the study period. However, it is clear that climatic factors, including precipitation, affect the conductivity of both the undisturbed ground and to some extent the pig grave. Therefore, it cannot be stated that decomposition was the only factor causing high conductivity readings.

Table 11 - Percentage difference between the mean quadrature response of the pig grave and the undisturbed ground up to 121 days post interment.

Survey Date	Days Post Burial	Mean. Undisturbed Ground (mS/m)	Mean. Pig Grave (mS/m)	% Difference
20/08/13	14	4.08	6.31	+54.66
18/09/13	43	6.01	6.60	+9.82
15/10/13	70	4.66	7.01	+50.43
05/12/13	121	7.98	11.06	+38.60

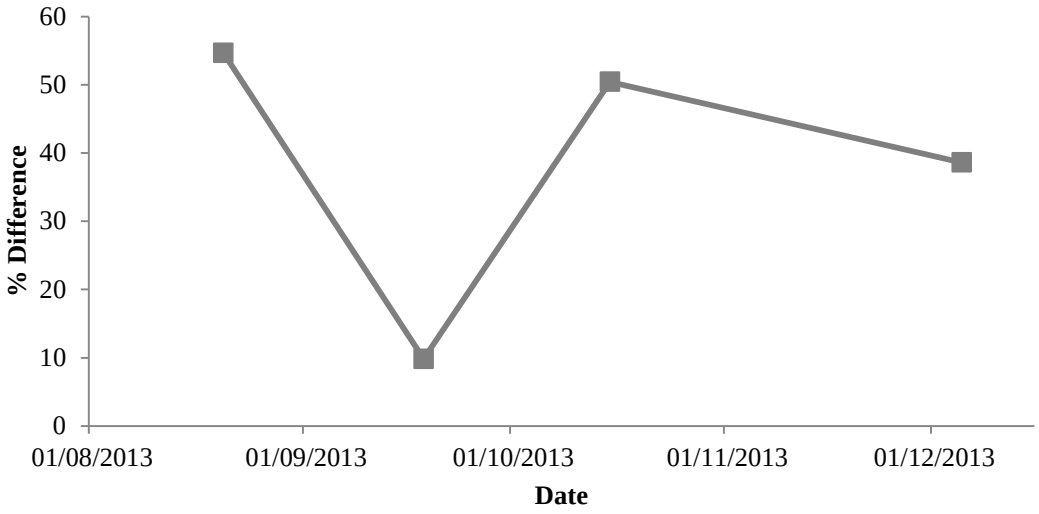

Figure 48 - Line graph showing the percentage difference in conductivity between the pig grave and the undisturbed ground up to 121 days post interment.

5.2.1.3 Percentage Difference between the mean quadrature response of the empty grave and the undisturbed ground up to 121 days post interment

The percentage difference between the mean conductivity values recorded for the undisturbed ground and the empty grave over time are presented in Table 12. It can be seen that at 14 days post burial the mean quadrature response of the empty grave was +21.81% higher than the undisturbed ground. However, at 43 days post burial the difference in conductivity of the empty grave decreased to -22.30% when compared to the undisturbed ground readings. This was also found to be the case at 70 days post burial, where the values dropped to -30.90%. In contrast, at 121 days, the empty grave was +0.88% higher than the undisturbed ground.

Table 12 - Percentage difference between the quadrature response of the empty grave and the undisturbed ground up to 121 days post interment.

Survey Date	Days Post Burial	Mean. Undisturbed Ground (mS/m)	Mean. Empty Grave (mS/m)	% Difference
20/08/13	14	4.08	4.97	+21.81
18/09/13	43	6.01	4.67	-22.30
15/10/13	70	4.66	3.22	-30.90
05/12/13	121	7.98	8.05	+0.88

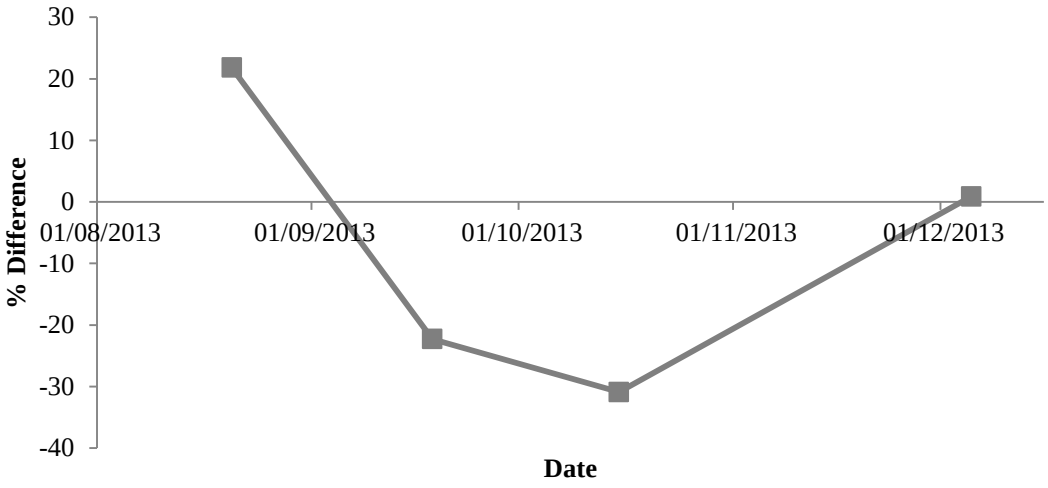

Figure 49 - Line graph showing the percentage difference in conductivity between the empty grave and the undisturbed ground up to 121 days post interment.

Mean conductivity of the empty grave decreased over time supporting the suggestion that the fill was uncompact and therefore, precipitation/ moisture was able to drain freely. In contrast, at 121 days post burial, the mean conductivity peaked, this was likely due to the subsequent compaction of the grave fill and as a consequence, more moisture was retained. At this point the mean conductivity of the empty grave and undisturbed ground were similar (-0.88% difference). This was likely to have been caused by soil compaction within the empty grave including the collapse of any voids present, resulting in similar moisture levels.

The conductivity of the undisturbed ground appeared to be heavily influenced by climatic variables, including ambient temperature and precipitation. The mean conductivity of the undisturbed ground increased steadily over time with the exception being at 70 days post burial where it decreased to 4.66 mS/m. In the weeks prior to the survey on the 18/09/13 (43 days post burial) an increased quantity of precipitation was recorded, which caused the undisturbed ground to exhibit higher mean conductivity than was observed previously. Whereas, at 70 days post burial the ground exhibited lower conductivity; appearing to be dryer in comparison. The higher levels of precipitation in the lead up to the survey at 121 days post burial resulted in increased conductivity being observed.

In evaluating the use of electromagnetic survey in the detection of burials up to 121 days post burial it was found that, empty graves appear to be less easily distinguishable from the surrounding undisturbed ground and can exhibit a signal that can be lost in the background response, relatively soon post burial (~43 days). Even after prolonged periods of time (up to 121 days post burial) the empty grave has been shown to have a maximum difference of

+0.88% to the ground surrounding it. Therefore, it is unrealistic to state that an empty grave could be accurately located using this technique in similar environments after 121 days. However, it is important to note that the empty grave is detectable for the first three months post burial. Further research is required to investigate the detectability of mass graves following the first three months post burial.

5.2.1.4 Percentage difference between the mean quadrature response of the empty grave and the pig grave up to 121 days post interment

To ascertain whether the pig and empty grave can be differentiated from one another using electromagnetic survey, the mean quadrature responses up to 121 days post interment were compared. As the difference between the pig and empty grave is the presence of pig material, it is possible to determine the contribution of the pig remains and how this affects the quadrature response by calculating the percentage difference over time; for this purpose, the empty grave is considered the control. The percentage difference between the mean values recorded for the empty and pig grave during the first 121 days post burial are detailed in Table 13.

Table 13 - Percentage difference between the quadrature response of the empty grave and the pig grave up to 121 days post interment.

Survey Date	Days Post Burial	Mean. Empty Grave (mS/m)	Mean. Pig Grave (mS/m)	% Difference
20/08/13	14	4.97	6.31	+27.00
18/09/13	43	4.67	6.60	+41.33
15/10/13	70	3.22	7.01	+117.7
05/12/13	121	8.05	11.06	+37.39

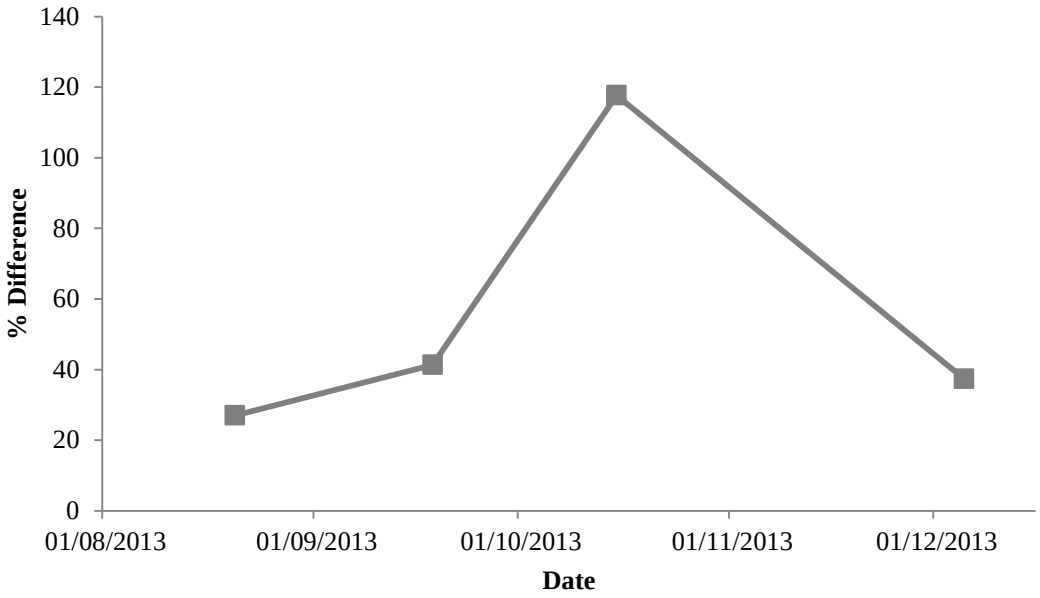

Figure 50 - Line graph showing the percentage difference in conductivity between the empty grave and the pig grave up to 121 days post interment.

At 14 days post burial the conductivity values from the pig grave were 27.00% higher than the empty grave, this percentage difference increased to 41.33% by 43 days post burial. At 70 days post burial the percentage difference peaked, with the mean quadrature response from the pig grave being over 100% higher than the empty grave (Figure 50). Although the percentage difference decreased to 37.39% at 121 days post burial; the mean conductivity of the pig grave was consistently higher than that of the empty grave throughout the study period.

When considering the fluctuations in mean conductivity of the graves over the 121 day study period, it was found that the values related to the empty grave decreased until the last observation, where conductivity peaked at 8.05mS/m and became comparable to the values obtained from the undisturbed ground. The initial low conductivity is indicative of loose grave fill, allowing moisture to drain freely. However, over time, the grave fill settles and becomes more compact therefore enabling the retention of moisture; resulting in higher conductivity readings.

In contrast, the conductivity of the pig grave increases over time, with the highest readings recorded at 121 days post burial (11.06 mS/m). The grave containing the pig remains has an equally uncompact fill to the empty grave immediately post burial but also contains the pig remains which are highly conductive in comparison to a grave fill that only contains soil. Due to the pig remains being disarticulated, as opposed to whole body systems, it is likely

that this creates a layer that is relatively non-permeable to moisture, whereby moisture is absorbed by the remains rather than reaching the base of the grave. The consistent rise in conductivity, which appears to peak at 121 days post burial, is also indicative of decomposition occurring within the pig grave. Therefore, on the basis of the above, it was observed that decomposition was occurring over the whole study period, however at 121 days post burial it appears that the low ambient air temperature may have caused the cessation of decomposition, hence the reduced percentage difference between the pig and empty grave. To confirm this, the temperatures recorded by the TinyTag in the pig grave, at both 30 and 50cm BGL, were compared with each other and also that of the IDORSET weather station, the results of which are presented in Section 5.2.1.9.

5.2.1.5 Resistance results up to and including 121 days post interment

Four twin electrode resistance surveys of the experimental site were carried out during the first 121 days post interment. The data was despiked and interpolated in the x and y for the electrode separations of 0.5m, 1.0m and 1.5m (0.43m, 0.87m and 1.3m – nominal depths, calculated by 0.867*the separation).

The first survey was undertaken on the 20th August 2013. The plots resulting from the three electrode separations are presented in Figure 51. Table 14 shows the mean, maximum and minimum resistance values calculated from readings over the graves, whilst the control ground (background) mean, maximum and minimum values were calculated from the area directly between the two graves (refer to Figure 46).

At 14 days post burial, the pig and control grave are distinguishable from the background as high resistance features at all electrode separations however, as the electrode separation increases the graves become less clear (Figure 51). At 0.5m separation the graves are clearly distinguishable as areas of high resistance surrounded by a noisy background in both plots. As this survey was carried out soon after grave creation, it is likely that the high resistance observed was due to the act of disturbance and therefore, related to the fact that the fill is uncompact. At 1.0m separation, both graves exhibit similar resistance values as the background and as a result are barely discernible. However, there is an area of high resistance in the empty grave which is likely to be due to a void in the grave fill. At 1.5m separation the graves are not able to be differentiated from the natural background variation at the site, the exception being the void identified at 1.0m separation in the empty grave which remains as a high resistance anomaly.

Within literature graves have been described as low resistance features (Jervis et al. 2009; Juerges et al. 2010; Pringle et al. 2012) whereas, this survey has demonstrated that at 14 days post burial both graves, pig and empty, are high resistance features at 0.5m electrode separation and although resistance decreases as the electrode separation increases, they cannot be visually differentiated from the background variation. This could be due to the fact that little, if any, decomposition had occurred since burial, and that the grave fill was loose and dry due to it being exposed whilst the graves were created. These findings are consistent with those reported by Bray 1996 (cited in Cheetham 2005) where the recent, looser and less compact back fill was interpreted as being dryer; resulting in higher resistance values recorded. Consequently, it can be suggested that the high resistance anomalies observed at 0.5m separation and to an extent 1.0m, were artefacts of disturbance i.e. a combination of loose grave fill and surface disruption.

The mean, minimum and maximum apparent resistance values (ohm) were calculated for the pig grave, empty grave and the undisturbed ground for each electrode separation (Table 14). In each case the undisturbed ground is considered as being representative of the background variation.

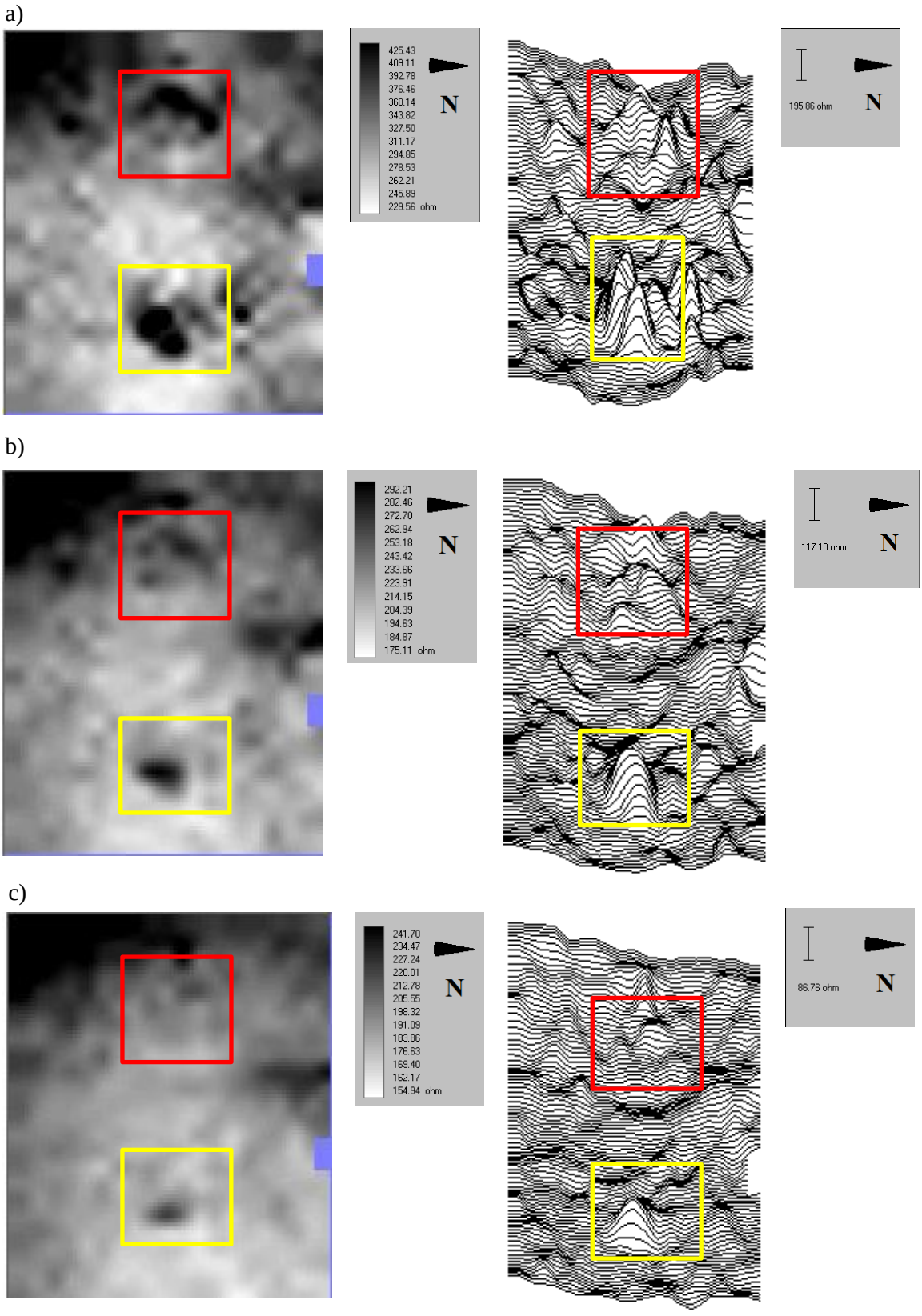

Figure 51 - Resistance survey result for 20th August 2013 at: a) 0.5m electrode separation, b) 1.0m electrode separation c) 1.5m electrode separation – 14 days post interment (pig grave is outlined in red and the empty grave in yellow).

Table 14 - Mean, minimum and maximum apparent resistance at three electrode separations on 20th August 2013 (Undis. Ground – undisturbed ground).

Electrode separation	Mean. Pig Grave (ohm/%)	Max. Pig Grave (ohm)	Min. Pig Grave (ohm)	Mean. Empty Grave (ohm/%)	Max. Empty Grave (ohm)	Min. Empty Grave (ohm)	Mean. Undis. Ground (ohm)	Max. Undis. Ground (ohm)	Min. Undis. Ground (ohm)
0.5m	314.5 +5%	362.0	266.5	364.7 +21%	478.0	268.5	301.3	333.5	275.0
1.0m	224.5 -1%	260.0	205.5	222.2 -2%	290.0	188.0	227.5	244.0	212.0
1.5m	189.8 -5%	198.5	179.5	183.7 -8%	220.5	167.5	198.7	214.0	191.0

It can be seen, in Table 14, that the highest resistance contrasts are recorded at 0.5m electrode separation for both graves, with the empty grave exhibiting a higher resistance when compared to the pig grave and the undisturbed ground. Therefore, suggesting that the pig grave is more conductive and is of lower resistance than the empty grave. As electrode separation increases, the resistance also changes. To enable comparisons to be made, percentage change was calculated and compared to the undisturbed ground for the two graves. This was calculated from the difference between the resistance and the undisturbed ground. It was found that the shallowest electrode separation resulted in a higher resistance values for the empty grave when compared to the pig grave. When considering results from 1.0m electrode separation the values obtained from both graves were very similar to the undisturbed ground, with -1% and -2% difference respectively. The pig grave however, exhibited a marginally higher apparent resistance. Similarly, at 1.5m separation the pig grave had a marginally higher mean apparent resistance compared to the empty grave. Table 14 confirms that the near surface disruption has caused higher resistance, however, as the electrode separation increases the graves appear as low resistance features.

Therefore, unlike the conductivity survey, carried out using an EM38, resistivity surveys allow for differentiation by depth, to an extent, whereby a grave is likely to be detectable due to the presence of a high resistivity anomaly at narrow electrode separations whilst exhibiting lower overall resistance at wider separations. This confirms the proposition that on first appearance the plots are dominated by the high resistance near-surface disruption however, the graves themselves remain as low resistance features.

The second resistance survey was carried out 43 days post interment. At 43 days post burial the pig and empty grave are visible in the resistance plot at 0.5m whereas, at 1.0m electrode separation the pig grave is less visible (Figure 52). In contrast to the results obtained from

the first survey, at 14 days post burial, the pig grave was found to be a low rather than high resistance anomaly whereas, the empty grave persists as a high resistance feature. The presence of a low resistance anomaly for the pig grave may be due to the increased presence of decomposition fluid and increased moisture within the grave structure, which is indicative of pooling near the surface, particularly for the 0.5m separation. The site is predominantly clay therefore there may be limited leaching of fluid from the remains into the surrounding undisturbed soil. Furthermore, the layer of disarticulated pig remains could be acting as an impermeable barrier resulting in pooling directly above the remains. The empty grave is dominated by an area of high resistance, potentially indicative of a void in the grave fill; it was present in the previous survey and is therefore considered an artefact of disturbance/ creation of the grave. The uncompact fill in the empty grave would allow moisture to drain freely to the base of the grave. At 1.0m electrode separation the pig grave is visible once more as a low resistance feature and is observable within the profile plot (Figure 52). The empty grave exhibits similar resistances to the plot from the 0.5m separation, with an area of high resistance visible.

The highest resistance contrasts are recorded at 0.5m separation for both graves; this is to be expected as this depth relates to the level where the pig remains are in direct contact with the overburden of soil and where water pooling could occur (Table 15). The empty grave has less apparent resistance contrast than the undisturbed ground surrounding it. As suggested above, this may be due to the act of creating a grave, where through the disturbance of the soil matrix there is a change in the compaction and thus soil moisture. At 0.5m electrode separation, the undisturbed ground has higher resistance than both the pig and empty grave. As suggested above, this is likely due to the empty grave containing a void and also as the grave fill is uncompact the soil is relatively free draining. At 1.0m separation, the empty grave's resistance is marginally higher than the pig grave. It is interesting that the percentage contrast between the two graves is identical even though the ranges (maximum and minimum) are different. Thus, indicating that the mass of mammalian matter is exhibiting approximately the same resistance as the damp soil in the empty grave at both 1.0m and 1.5m electrode separations. At 1.5m electrode separation the pig grave has higher resistance when compared to the empty grave, but is lower than the undisturbed ground; in this case the pig grave is producing resistances that are very similar to the undisturbed ground and therefore, may not be easily differentiated from background variation.

a)

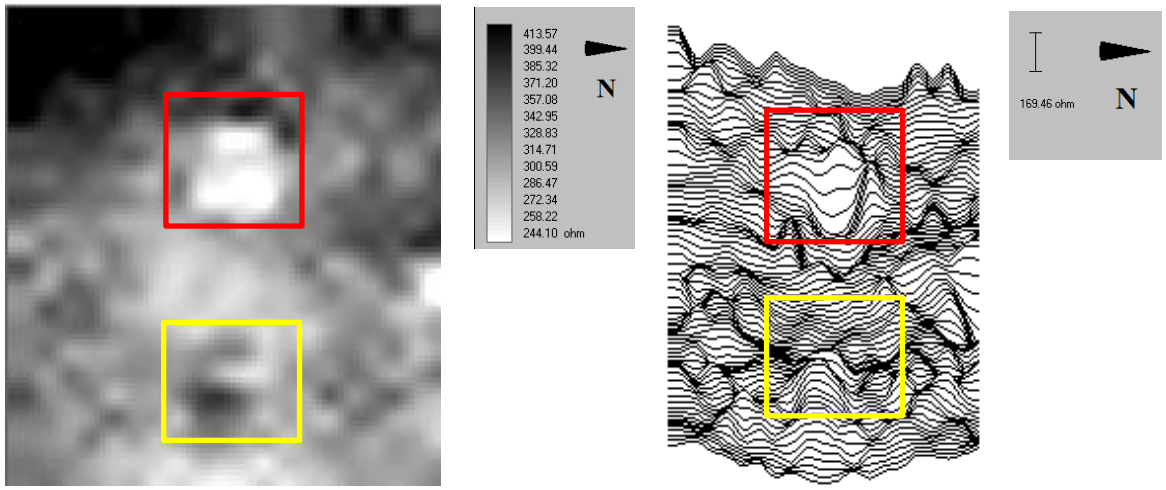

b)

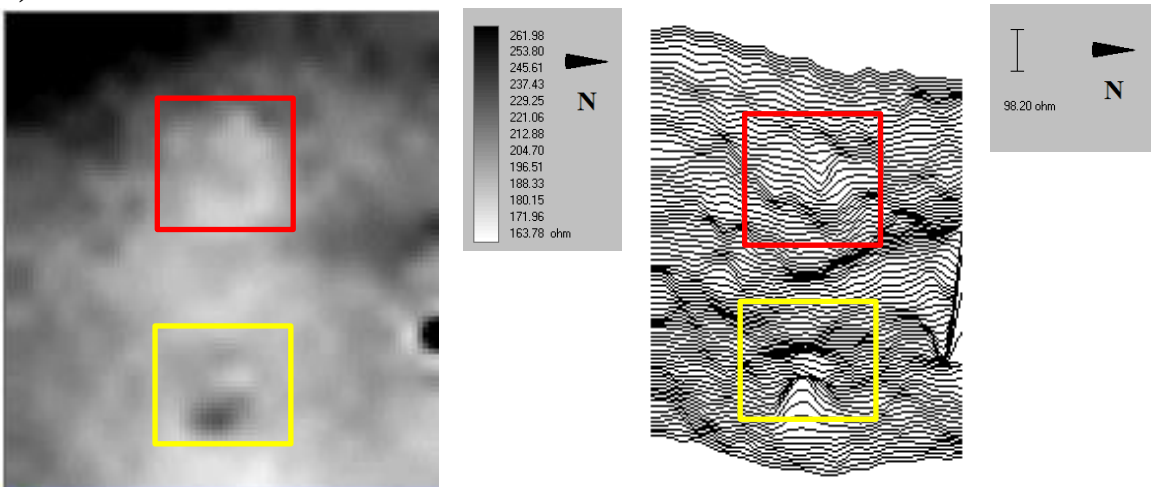

c)

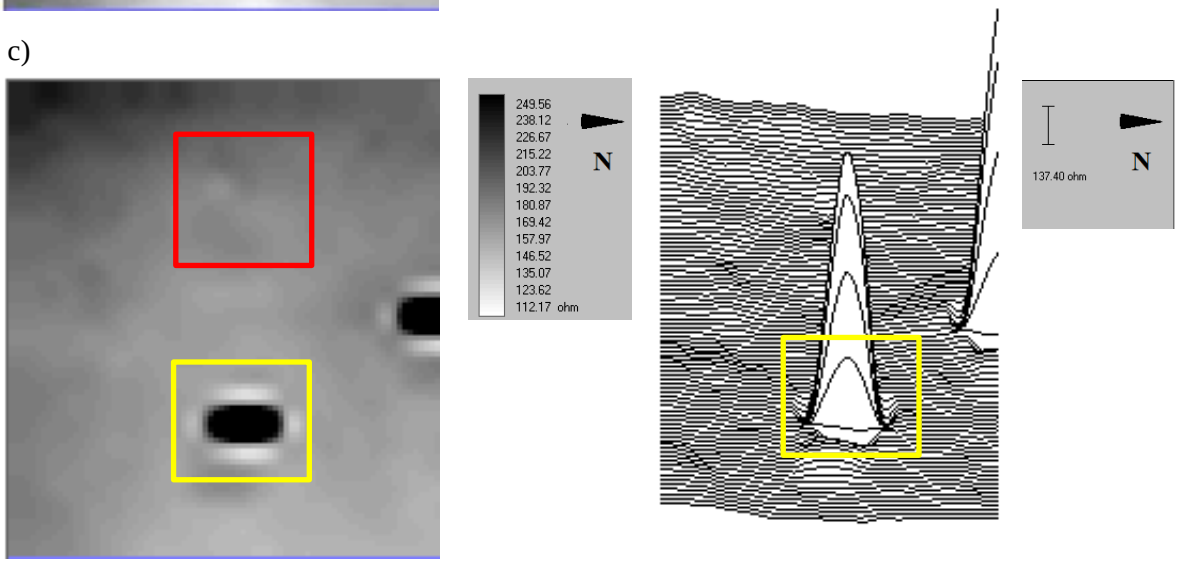

Figure 52 - Resistance survey result for 18th September 2013 at: a) 0.5m electrode separation b) 1.0m electrode separation c) 1.5m electrode separation – 43 days post interment (pig grave is outlined in red and the empty grave in yellow). Please note: there is a reading spike over the empty grave that is due to a bad electrode contact – this was omitted from the final results.

Table 15 - Mean, minimum and maximum apparent resistance at three electrode separations on 18th September 2013. (Undis. Ground – undisturbed ground).

Electrode separation	Mean. Pig Grave (ohm/ %)	Max. Pig Grave (ohm)	Min. Pig Grave (ohm)	Mean. Empty Grave (ohm/ %)	Max. Empty Grave (ohm)	Min. Empty Grave (ohm)	Mean. Undis. Ground (ohm)	Max. Undis. Ground (ohm)	Min. Undis. Ground (ohm)
0.5m	256.0 -21%	297.0	227.5	303.7 -7%	343.0	253.0	326.0	401.0	298.5
1.0m	189.8 -11%	203.5	181.0	190.0 -11%	229.0	171.0	213.2	235.5	203.0
1.5m	173.8 -2%	179.0	168.0	158.9 -11%	175.0	149.0	178.2	185.5	170.0

The third resistance survey was carried out 70 days post interment and the effect of disturbance is visible again, particularly in the empty grave. At 0.5m separation the pig grave exhibited low resistance whereas, the empty grave cannot be visually distinguished from the background variation. During the week prior to the survey, 11.9mm of rainfall was recorded; therefore, this could be contributing to the pooling above the pig remains, reducing the resistance. At 1.0m electrode separation neither of the graves can be seen clearly in the plots, with the void in the empty grave persisting as a high resistance feature, confirming that the grave, at 70 days post interment, had not compacted fully.

Within Table 16, it can be seen that at 0.5m electrode separation both the pig and empty grave have lower apparent resistance than the area of undisturbed ground, with the empty grave exhibiting higher apparent resistance than the pig grave. When 1.0m electrode separation is considered it was found that the pig grave and the empty grave have a lower resistance than the undisturbed ground, with the empty grave having a marginally lower apparent resistance than the pig grave. Notably the pig and empty grave have similar resistance readings at this electrode separation, this is reflected in the plot where the graves cannot be differentiated. At 1.5m electrode separation the pig grave has a marginally higher resistance than the empty grave but a lower resistance compared to the undisturbed ground. On consideration of the mean apparent resistance values of the empty grave for each of the separations it is clear that the control grave has stabilised, this is evidenced by the percentage change which ranges from -12 to -13% across all separations. In contrast, the pig grave has not stabilised by 70 days post burial.

a)

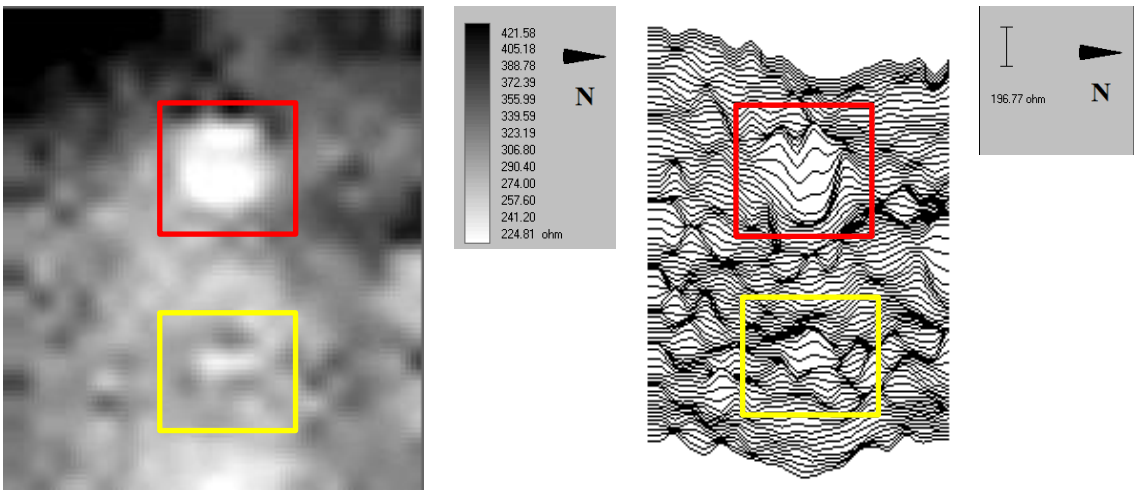

b)

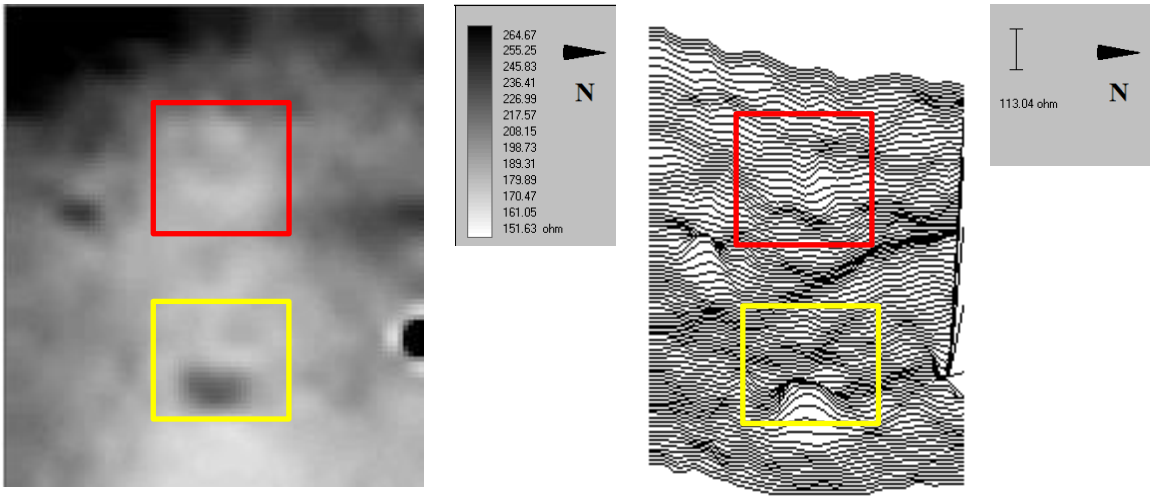

c)

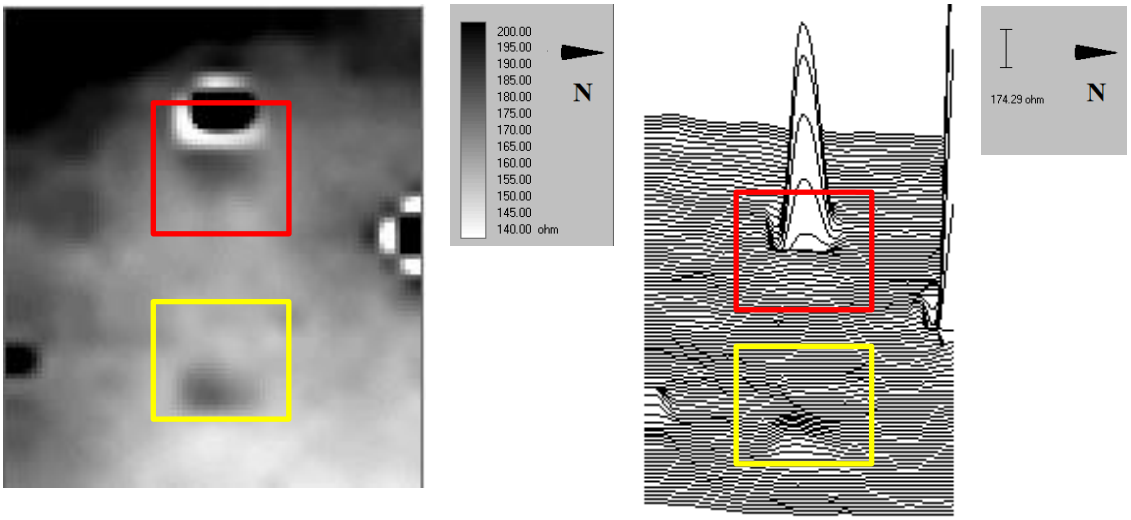

Figure 53 - Resistance survey result for 15th October 2013 at: a) 0.5m electrode separation b) 1.0m electrode separation c) 1.5m electrode separation – 70 days post interment (pig grave is outlined in red and the empty grave in yellow). There is a reading spike over the pig grave that is due to a bad electrode contact – this was omitted from the final results.

Table 16 - Mean, minimum and maximum apparent resistance at three electrode separations on 15th October 2013 (Undis. Ground – undisturbed ground).

Electrode separation	Mean. Pig Grave (ohm/%)	Max. Pig Grave (ohm)	Min. Pig Grave (ohm)	Mean. Empty Grave (ohm/%)	Max. Empty Grave (ohm)	Min. Empty Grave (ohm)	Mean. Undis. Ground (ohm)	Max. Undis. Ground (ohm)	Min. Undis. Ground (ohm)
0.5m	231.0 -27%	260.0	209.5	275.5 -13%	295.5	254.0	315.8	391.0	287.0
1.0m	186.2 -11%	199.0	178.0	182.4 -13%	220.0	165.5	209.2	238.5	192.0
1.5m	173.8 -2%	180.5	167.5	155.4 -12%	176.0	144.0	176.7	185.0	167.0

The final survey was carried out 121 days post interment. Both the pig and control grave were not easily differentiated at 121 days post burial, with similar apparent resistance values obtained across the site (Figure 54). There was little variation between the pig and empty graves and the undisturbed ground across the three electrode separations with the exception of 1.5m (Table 17). As expected, the resistance values decreased as depth increased. At 0.5m separation the pig grave has lower mean apparent resistance when compared to the empty grave; with both graves having lower resistance than the undisturbed ground. When considering the resistance at 1.0m separation, both the pig and empty grave had lower values than that of the undisturbed ground, with the pig grave exhibiting higher resistance than the empty grave. At 1.5m separation the resistance of the pig grave exceeds that of the empty grave and undisturbed ground by 1%. When considering the resistance response from the empty grave over the different separations, it can be seen that the percentage difference between the undisturbed ground and the grave remains the same when the electrode separations increase. Notably, this trend was observed in the previous survey at 70 days post burial. The undisturbed ground had the highest resistance values across all three separations, this being due to soil compaction and therefore, the soil may be dryer. Due to the survey being undertaken in December, it is unlikely that there was active decomposition, due to low ambient air temperature. Consequently, the response recorded by the resistance meter was more likely due to the moisture content of the soil rather than an increased quantity of decomposition fluid or leachate at the base of the pig grave. Overall, the effect observed could be due to the disturbance caused through the creation of the graves (i.e. loose grave fill); the presence of the disarticulated pig remains has caused pooling in the upper portion of the grave and therefore, moisture has been retained which is detectable as low resistance. This is further supported by the control grave exhibiting low resistance but was still affected by meteorological variables such as rainfall; without the presence of organic remains.

a)

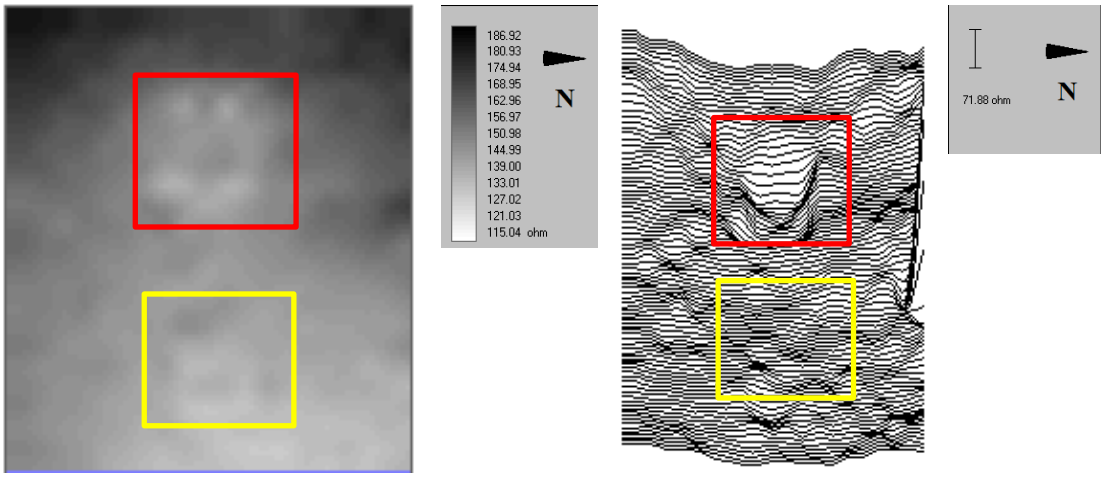

b)

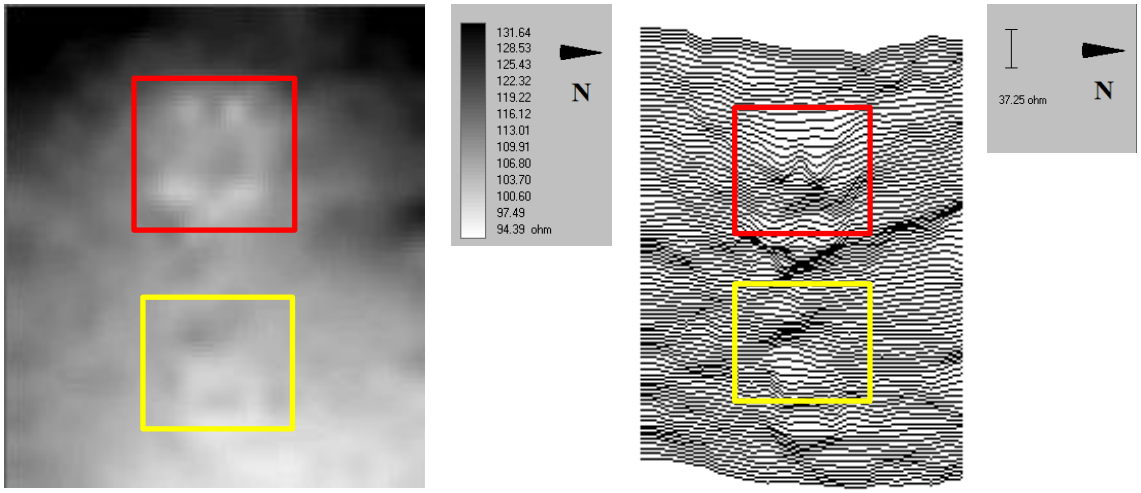

c)

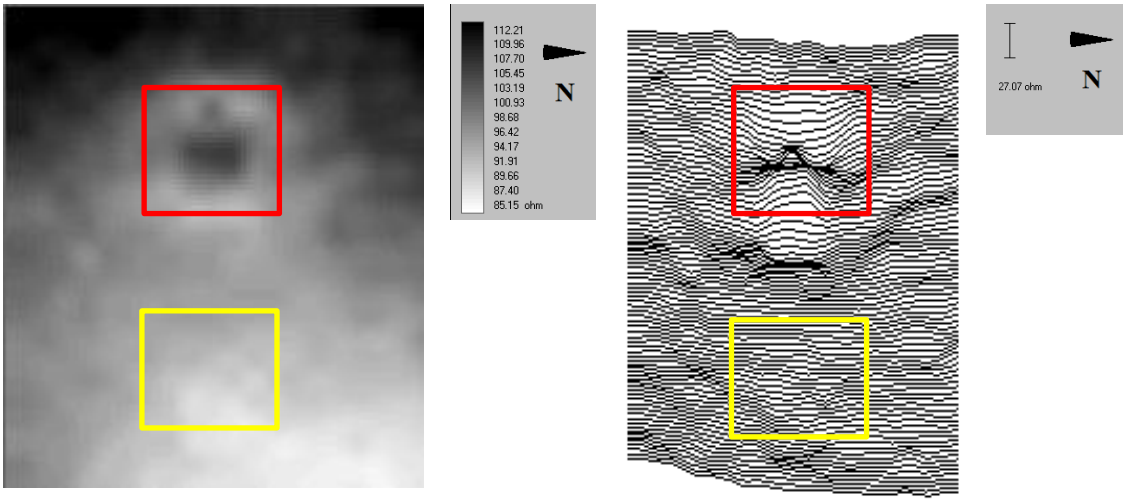

Figure 54 - Resistance survey result for 5th December 2013 at: a) 0.5m electrode separation b) 1.0 electrode separation c) 1.5m electrode separation – 121 days post interment (pig grave is outlined in red and the empty grave in yellow).

Table 17 - Mean, minimum and maximum apparent resistance at three electrode separations on 5th December 2013. (Undis. Ground – undisturbed ground).

Electrode separation	Mean. Pig Grave (ohm/%)	Max. Pig Grave (ohm)	Min. Pig Grave (ohm)	Mean. Empty Grave (ohm/%)	Max. Empty Grave (ohm)	Min. Empty Grave (ohm)	Mean. Undis. Ground (ohm)	Max. Undis. Ground (ohm)	Min. Undis. Ground (ohm)
0.5m	129.6 -14%	139.0	124.0	132.7 -12%	140.5	124.5	150.2	156.5	145.5
1.0m	107.3 -6%	112.0	103.0	100.1 -12%	103.0	98.0	114.3	115.5	112.5
1.5m	100.3 +1%	105.5	95.5	88.0 -12%	90.0	84.0	99.8	101.0	97.0

5.2.1.6 Investigation into the percentage difference in resistance between the pig grave and the undisturbed ground over time and electrode separation

To investigate the differences between the resistance surveys, which were conducted at irregular intervals through time, the percentage difference for the pig grave in relation to the undisturbed ground was calculated using the mean apparent resistance. The percentage difference between the mean values recorded for the undisturbed ground and pig grave, over time and at each electrode separation is presented in Figure 55. To comment on the percentage differences between the pig grave and the undisturbed ground, it is assumed that the control ground is representative of the surrounding area, leaving the pig grave as the variable.

At 0.5m electrode separation the mean apparent resistance of the pig grave was initially higher (+4.4%) than the undisturbed ground, however, after 43 days post burial, the mean resistance was lower than the undisturbed ground and remained so for the remainder of the study period (Table 14). At 14 days post burial the pig grave had a percentage difference in apparent resistance of +4.4% which increased to -21.5% at 43 days. The largest percentage difference at 0.5m electrode separation was observed at 70 days post burial (-26.9%), this value reduced to -13.7% by 121 days.

When comparing the pig grave and the undisturbed ground at 1.0m electrode separation it was found that the mean apparent resistance of the pig grave was consistently lower than the undisturbed ground. The percentage difference between the mean resistance values reduces at 121 days after peaking at 70 days post burial (Table 18). At 14 days post burial the percentage difference between the mean apparent resistance of the pig grave and the undisturbed ground was -4.5%, this decreased to -2.5% at 43 days, and further decreased to -

1.6% at 70 days post burial (Table 18). Similar to the results obtained for 0.5m and 1.0m electrode separation at 121 days post burial the percentage difference reduced, in this case to +0.5%.

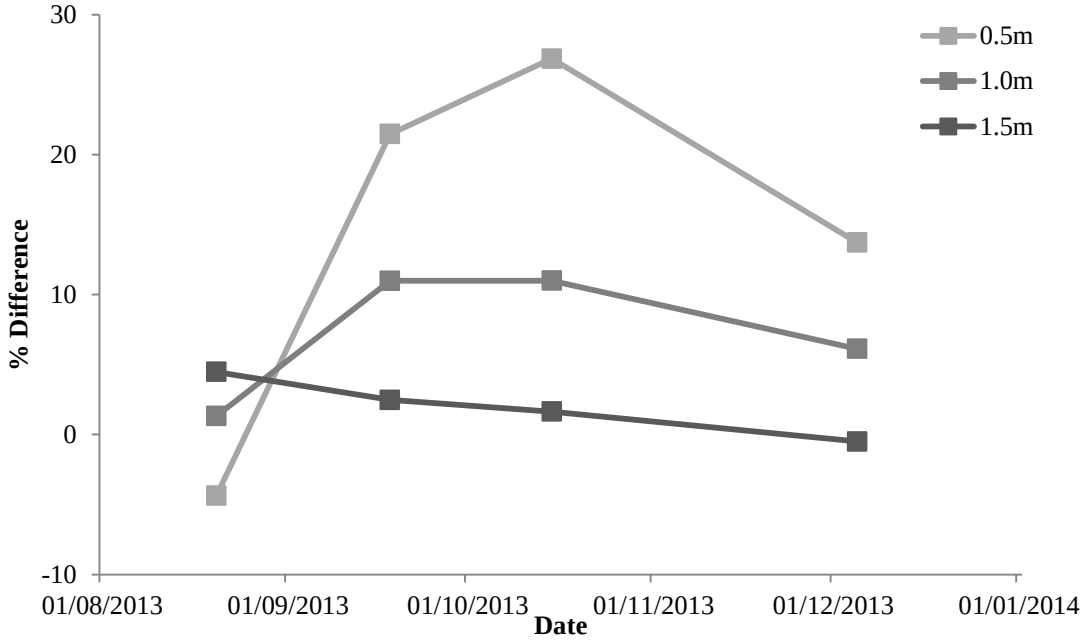

Figure 55 - Line plot showing the percentage difference in mean apparent resistance between the undisturbed ground and the pig grave for 0.5m, 1.0m and 1.5m electrode separations over time.

Figure 55 illustrates the changes in percentage difference between the undisturbed ground and the pig grave over time and electrode separation (the values were inverted to visualise the fluctuations in percentage difference). It can be seen that the largest percentage differences in mean apparent resistance between the two surfaces existed at 0.5m electrode separation; likely due to the disruption (i.e. variation in the compaction of the soil) in the upper portion of the pig grave (i.e. ~0.5m depth), when compared to the undisturbed ground. The percentage difference for the 1.0m electrode separation follows the same trend as the 0.5m, demonstrating that the mean resistance for the pig grave plateaus at 43 and 70 days respectively, before decreasing at 121 days post burial. This is indicative of the grave settling and the grave fill becoming more compact, and may also be indicative of the cessation of decomposition.

Table 18 - Percentage difference between the pig grave compared with undisturbed ground over time and electrode separation.

0.5m Electrode Separation			
Days Post Burial	Mean. Undisturbed Ground (ohm)	Mean. Pig Grave (ohm)	% Difference
14	301.3	314.5	+4.4
43	326.0	256.0	-21.5
70	315.8	231.0	-26.9
121	150.2	129.6	-13.7
1.0m Electrode Separation			
Days Post Burial	Mean. Undisturbed Ground (ohm)	Mean. Pig Grave (ohm)	% Difference
14	227.5	224.5	-1.3
43	213.2	189.8	-11.0
70	209.2	186.2	-11.0
121	114.3	107.3	-6.1
1.5m Electrode Separation			
Days Post Burial	Mean. Undisturbed Ground (ohm)	Mean. Pig Grave (ohm)	% Difference
14	198.7	189.8	-4.5
43	178.2	173.8	-2.5
70	176.7	173.8	-1.6
121	99.8	100.3	+0.5

5.2.1.7 Investigation into the percentage difference in resistance between the empty grave and the undisturbed ground over time and electrode separation

At 14 days post burial the percentage difference in the mean apparent resistance of the empty grave was found to be 21% higher than the equivalent value for the undisturbed ground. However at 43, 70 and 121 days post burial the mean apparent resistance of the empty grave was lower than the undisturbed ground, resulting in percentage differences which peaked at 70 days with a value of -12.8% (Table 19).

At 1.0m electrode separation, for the four surveys conducted, it was found that the mean apparent resistance for the empty grave was consistently lower than that of the undisturbed ground. There was a steady increase in the percentage difference from 14 days through to 70 days where the difference peaked at -12.8% before reducing marginally to -12.4%. This is the same scenario for the pig grave at the equivalent separation where the percentage difference was found to peak at 70 days before reducing at 121 days post burial (Table 19).

As can be seen from Table 19, at 1.5m electrode separation, the empty grave has a consistently lower mean apparent resistance than the undisturbed ground at the site. A steady increase in the percentage difference is observable from 14 days through 70 days where the difference in resistance peaks (-12.1%) before reducing slightly at 121 days post burial (-11.8%).

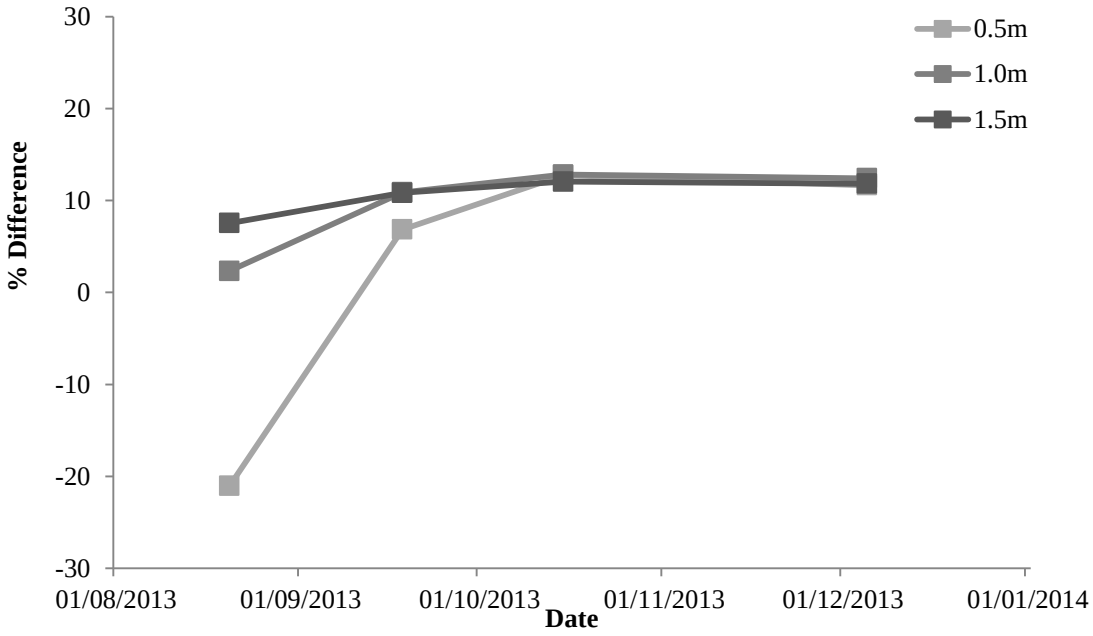

Figure 56 - Line plot showing the percentage difference in mean apparent resistance between the undisturbed ground and the empty grave for three electrode separations over time.

Figure 56 illustrates the change in percentage difference between the mean resistance of the undisturbed ground and empty grave over time and electrode separation (the values have been inverted). It can be seen that the largest percentage differences in mean apparent resistance exists between the two surfaces at 0.5m and 1.0m electrode separation. This is due to the disruption of the grave fill during creation of the grave, when compared to the undisturbed ground.

Table 19 - Percentage difference between the undisturbed ground and the empty grave over time and electrode separation.

0.5m Electrode Separation			
Days Post Burial	Mean. Undisturbed Ground (ohm)	Mean. Empty Grave (ohm)	% Difference
14	301.3	364.7	+21.0
43	326.0	303.7	-6.8
70	315.8	275.5	-12.8
121	150.2	132.7	-11.7
1.0m Electrode Separation			
Days Post Burial	Mean. Undisturbed Ground (ohm)	Mean. Empty Grave (ohm)	% Difference
14	227.5	222.2	-2.3
43	213.2	190.0	-10.9
70	209.2	182.4	-12.8
121	114.3	100.1	-12.4
1.5m Electrode Separation			
Days Post Burial	Mean. Undisturbed Ground (ohm)	Mean. Empty Grave (ohm)	% Difference
14	198.7	183.7	-7.6
43	178.2	158.9	-10.8
70	176.7	155.4	-12.1
121	99.8	88.0	-11.8

5.2.1.8 Investigation into the percentage difference in resistance between the empty grave and the pig grave over time and electrode separation

The percentage difference between the mean resistance values recorded for the empty and pig grave over time at each electrode separation can be seen in percentage difference between the two graves increases further to 14.00% (Table 20). When calculating percentage difference, it is assumed that the empty grave is normal in comparison to the pig grave thus taking into account the effect that the remains has on the resistance results.

At 0.5m electrode separation it was observed that the mean apparent resistance of the pig grave remained consistently lower than the empty grave over the study period; with a maximum percentage difference being present at 70 days post burial (-16.2%), before reducing to -2.3% at 121 days post burial (percentage difference between the two graves increases further to 14.00% (Table 20)).

When the percentage difference between the empty and the pig grave is considered at 1.0m electrode separation, it was found that at 14 days post burial the mean apparent resistance of the pig grave was marginally higher than the control grave. At 43 days post burial, the pig grave exhibited slightly lower mean resistance than the empty grave. However, from 70 through to 121 days, the mean resistance of the pig grave was higher than the empty grave, with the maximum difference observed at 121 days post burial (+7.19%) (Table 20). At 1.5m electrode separation the mean resistance of the pig grave was consistently higher than the empty grave throughout the study. However, at 121 days post burial the percentage difference between the two graves increased further to 14.00%.

Figure 57 and Figure 58 illustrate the percentage difference in mean resistance between the pig and empty grave over the study period (121 days) for each electrode separation; for context and comparison the percentage difference obtained during conductivity surveys by the EM38B was added to Figure 58. As can be seen, the trend is comparable between the findings of the resistance and conductivity surveys with increases in percentage difference up to 70 days post burial, after which, at 121 days post burial, the percentage difference decreases.

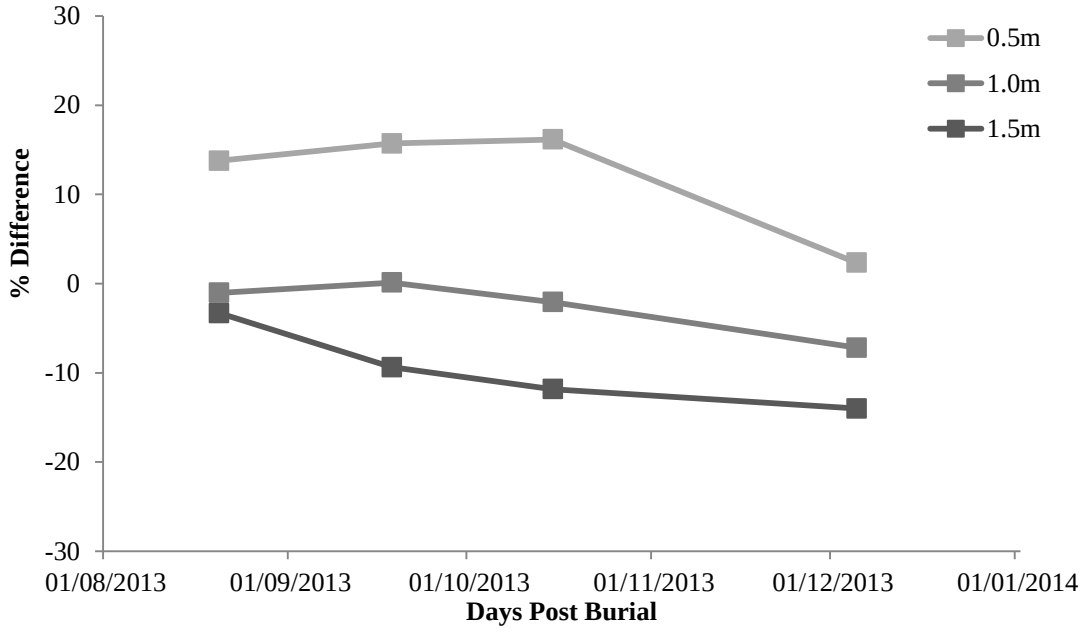

Figure 57 - Line plot showing the percentage difference in mean apparent resistance between the empty grave and the pig grave for three electrode separations (0.5m, 1.0m, 1.5m) over time.

Table 20 - Percentage difference between the pig grave when compared to the empty grave over time and electrode separation.

0.5m Electrode Separation			
Days Post Burial	Mean. Empty Grave (ohm)	Mean. Pig Grave (ohm)	% Difference
14	364.7	314.5	-13.8
43	303.7	256.0	-15.7
70	275.5	231.0	-16.2
121	132.7	129.6	-2.3
1.0m Electrode Separation			
Days Post Burial	Mean. Empty Grave (ohm)	Mean. Pig Grave (ohm)	% Difference
14	222.2	224.5	+1.04
43	190.0	189.8	-0.12
70	182.4	186.2	+2.08
121	100.1	107.3	+7.19
1.5m Electrode Separation			
Days Post Burial	Mean. Empty Grave (ohm)	Mean. Pig Grave (ohm)	% Difference
14	183.7	189.8	+3.32
43	158.9	173.8	+9.38
70	155.4	173.8	+11.84
121	88.0	100.3	+14.00

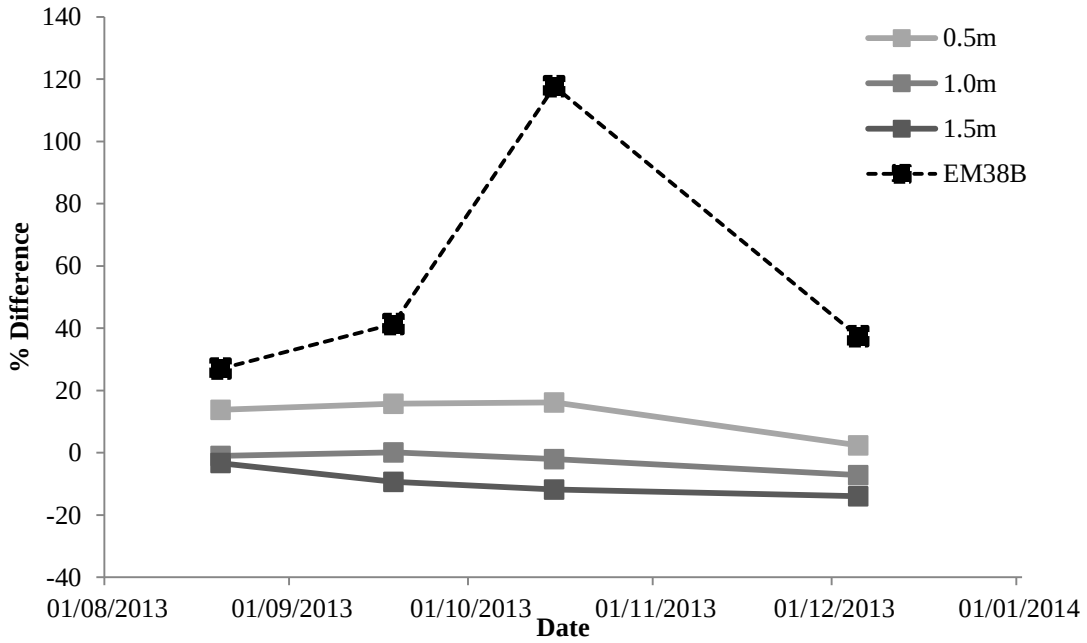

Figure 58 - Line plot showing the percentage difference in response between the empty and pig grave for the three electrode separations (0.5m, 1.0m, 1.5m) and the EM38 over time.

5.2.1.9 Using fluctuations in below ground temperature within the pig grave as an indicator of decomposition processes

Geophysical surveys were carried out to better understand whether decomposition was occurring within the pig grave during the first four months post burial. As has been demonstrated in the previous sections, it appears that much of the geophysical responses detected was due to the presence of disturbed ground or excess water through pooling; resulting in high conductivity and low resistance. As stated in Section 5.1.2, TinyTag data loggers were placed into both the pig and empty grave to measure the temperature at 50cm BGL (in direct contact with the pig remains) and 30cm BGL. Due to the probe in the empty grave being damaged, only one month of temperature data exists, but this allows for comparisons to be made between the two graves for the first month of data collection, whilst also taking into account ambient air temperature at the site.

Figure 59 shows the fluctuations in mean daily ambient temperature along with the two TinyTags in the pig and the empty grave. The red vertical lines indicate when geophysical surveys were conducted for context. Overall, ambient temperature is decreasing from between ~20-25^{o}C in August to less than 10^{o}C in December. On first glance the temperatures recorded by the TinyTags appear to be following this trend. However, on closer inspection, from date of interment until mid-September 2013, the pig grave temperature exceeds the mean ambient daily temperature and the temperature recorded in the control grave. It is logical that the probe at 30cm would be affected more readily by variations in ambient temperature due to its proximity to the surface compared to the probe at 50cm. The temperature at 50cm BGL should be more indicative of the temperature of the pig remains and should therefore be considered when trying to ascertain whether decomposition processes were occurring.

It can be seen that when the ambient temperature decreases the 30cm probe responds almost immediately, whereas, the 50cm probe takes longer to respond, as is expected (Figure 56). However, when the temperature increases there is, in some instances, a lag in the temperature increase for the 50cm probe e.g. at ~06/09/13 and 05/10/13. When the temperature recorded by the probe at 50cm exceeds that of the 30cm probe it is possible that decomposition is occurring within the grave. This is more clearly illustrated when a running mean, with an interval of 7, is calculated for all of the temperature readings and plotted over time (Figure 60).

Increased precipitation was recorded from mid-September 2013 through to mid-November. Throughout this period the BGL temperature at 50cm was regularly higher than the

temperature at 30cm within the pig grave (Figure 59) even whilst the ambient temperature was decreasing; thus indicating a period of decomposition. All of the factors above including decomposition within the grave, increased precipitation and decreasing ambient temperature heavily influenced the geophysical results observed. The increased moisture within the grave resulted in the grave being detectable as a highly conductive and low resistance feature in comparison to the undisturbed ground surrounding it. This was observed most clearly during the October 2013 survey.

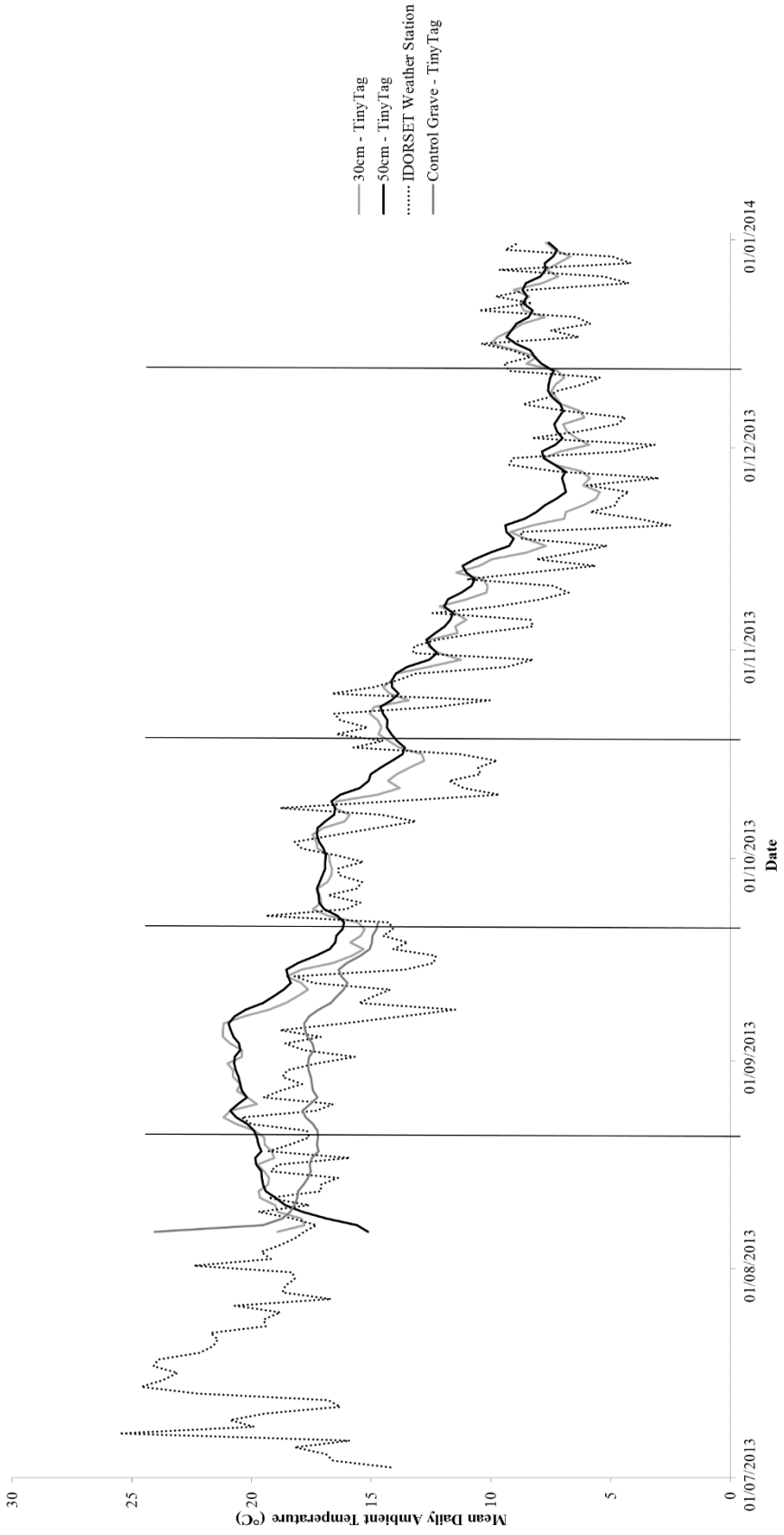

Figure 59 - Line plot showing ambient temperature and the TinyTag BGL temperatures over the study period. Red vertical lines correspond with the dates of geophysical surveys.

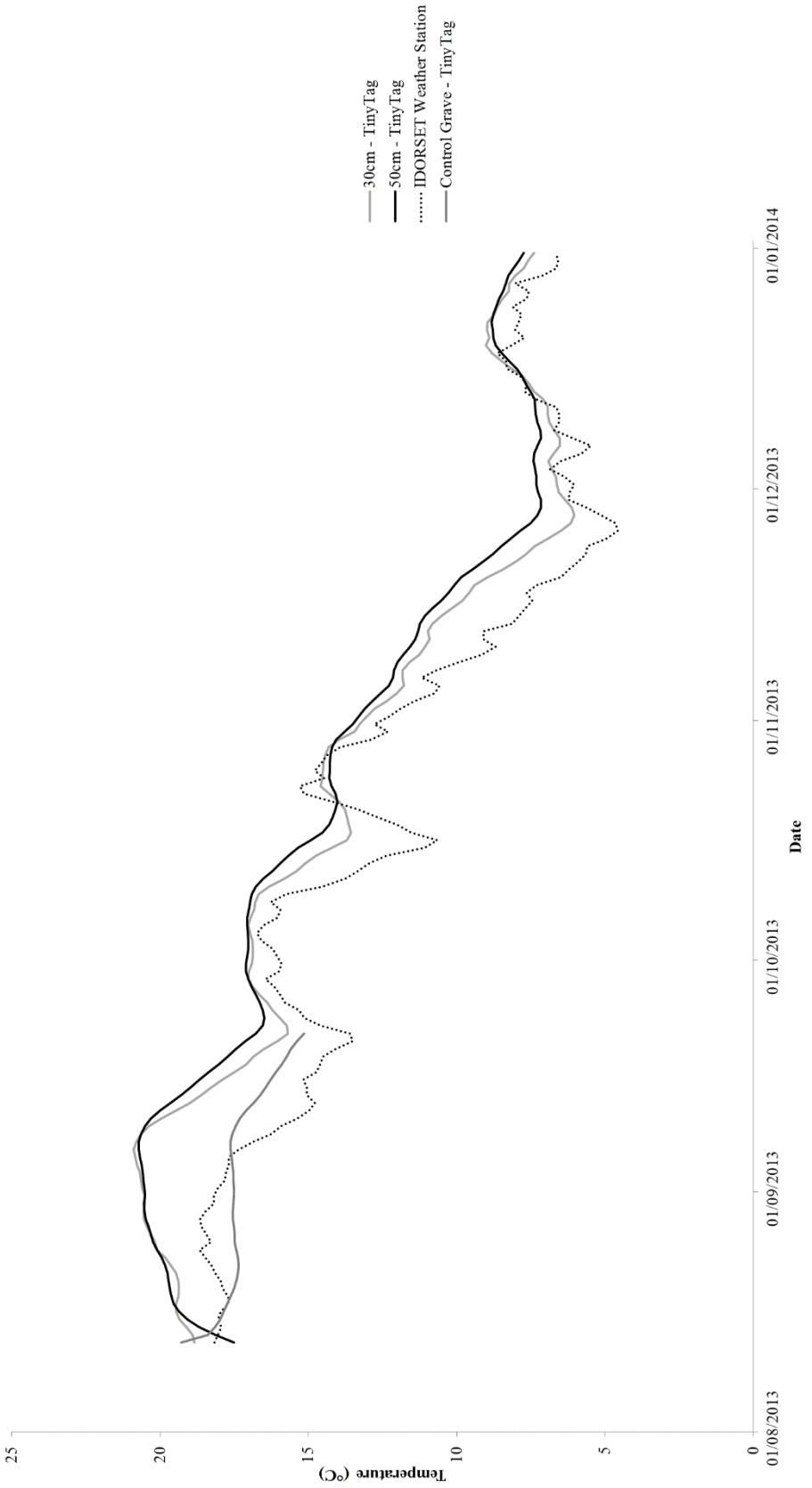

Figure 60 - Line plot showing a running mean (interval of 7) of ambient temperature and the TinyTag BGL temperatures over the study period.

5.2.2 The relationship between grave surface and NDVI

To understand the relationship between grave surface and NDVI, it was important to visualise how NDVI varied across the different grave surfaces over time and how this compared to the area of undisturbed grass. Consequently, the NDVI values for each sample point were interpolated in ArcMap using Inverse Distance Weighted (IDW) and maps were created for each data collection. IDW was selected as opposed to other interpolation techniques, as it assumes that the characteristics of surrounding points are driven by local variation; in this instance the presence of disturbed ground and/or buried mammalian remains. Furthermore, the principles of IDW assume that sample points that are close to one another are more alike compared to those that are further away. In the context of the experimental graves, the sample points located on the turfed portions, and the derived NDVI, were likely to be more similar when compared to those on the soil half of the graves. A red to green colour ramp was applied to each sample point, where red is indicative of low NDVI and green being high NDVI. For context, an aerial photograph of the site with a spatial resolution of 12.5cm (provided by Getmapping Plc, image from May 2014) was placed behind each map.

The first spectral data was collected on the 19th August 2013, 13 days post burial (dpb). The boundary between the turf and soil on both the empty and the pig grave was observable, with the soil halves of both graves exhibiting low NDVI, ranging between 0.1 and 0.2 (represented by the red dot markers) (Figure 61). The turfed areas of the graves had higher NDVI values of between 0.3 and 0.4. However, both the empty and pig grave exhibited lower NDVI values compared to the area of undisturbed grass, which had NDVI values of 0.5 and above (Figure 61). These results were expected as the turf had begun to dry out due to the warm ambient temperature whilst the graves were created, and were therefore exhibiting lower NDVI than the undisturbed area. If the graves had not been re-turfed following their creation, it is expected that both of the grave areas would have exhibited low NDVI values. The map created through the interpolation of the NDVI values, when directly compared to photographs taken of the graves on the 16th August 2013 (three days prior to the data collection), can be seen to be representative with the turf appearing dry and brown on both graves (Figure 62).

Following the second spectral data collection on the 22nd August 2013 (16 dpb), the boundary between the turf and soil halves of the graves was clearer in the pig grave compared to the empty grave (Figure 63). The NDVI obtained from the turf half of the pig grave is higher than the equivalent area on the empty grave and therefore, the vegetation appears to be less stressed. In contrast, the empty grave is uniformly stressed across the two

surfaces (turf and soil). The undisturbed grass, compared to the two graves, had higher NDVI values ranging from 0.5-0.8. However, three anomalous sample points were recorded, in the north western and south eastern corners, which have low NDVI. Photographs were taken of the site on 16th August 2013 and can be seen in Figure 62.

Following data collection on 10th October 2013 (65 dpb), the turf half of the pig grave was clearly distinguishable from the soil half, with NDVI values ranging from 0.2-0.4 (Figure 65). As the turf half of the empty grave exhibited low NDVI, it was less distinguishable from the soil half and therefore appears to be stressed across the whole surface. In contrast, the area of undisturbed grass exhibited high NDVI. Thus, it appears that the turf above the pig grave is less stressed compared to the empty grave. When this is compared to the photographs taken on the 13th October 2013 (3 days post data collection – Figure 64), the turf on the full grave looks less dry and has new vegetation growth. However, the equivalent area on the empty grave does not have any new vegetation.

After collecting spectral data on the 5th December 2013 (121 dpb), the turf half of the pig grave appears to have higher NDVI than the equivalent side on the empty grave, which still has some low NDVI values present (Figure 67). However, both the empty and pig grave, specifically the turf half, appears to have higher NDVI compared to the previous three maps. The soil half of the pig grave continues to exhibit low NDVI values through a lack of colonising vegetation present. In contrast, the soil half of the empty grave has some areas that have colonised. The baseline NDVI values for the site are represented by the undisturbed grass which exhibits NDVI ranging from 0.4-0.8. The observed changes in NDVI of the undisturbed grass are expected with NDVI steadily decreasing, this is usual at the start of the winter season when vegetation enters senescence. Photographs taken on the 5th December 2013 (the day of data collection – Figure 66) show that the full grave (turf half) is less dry and weeds are present. In contrast, the empty grave appears dry and has very little new vegetation growth.

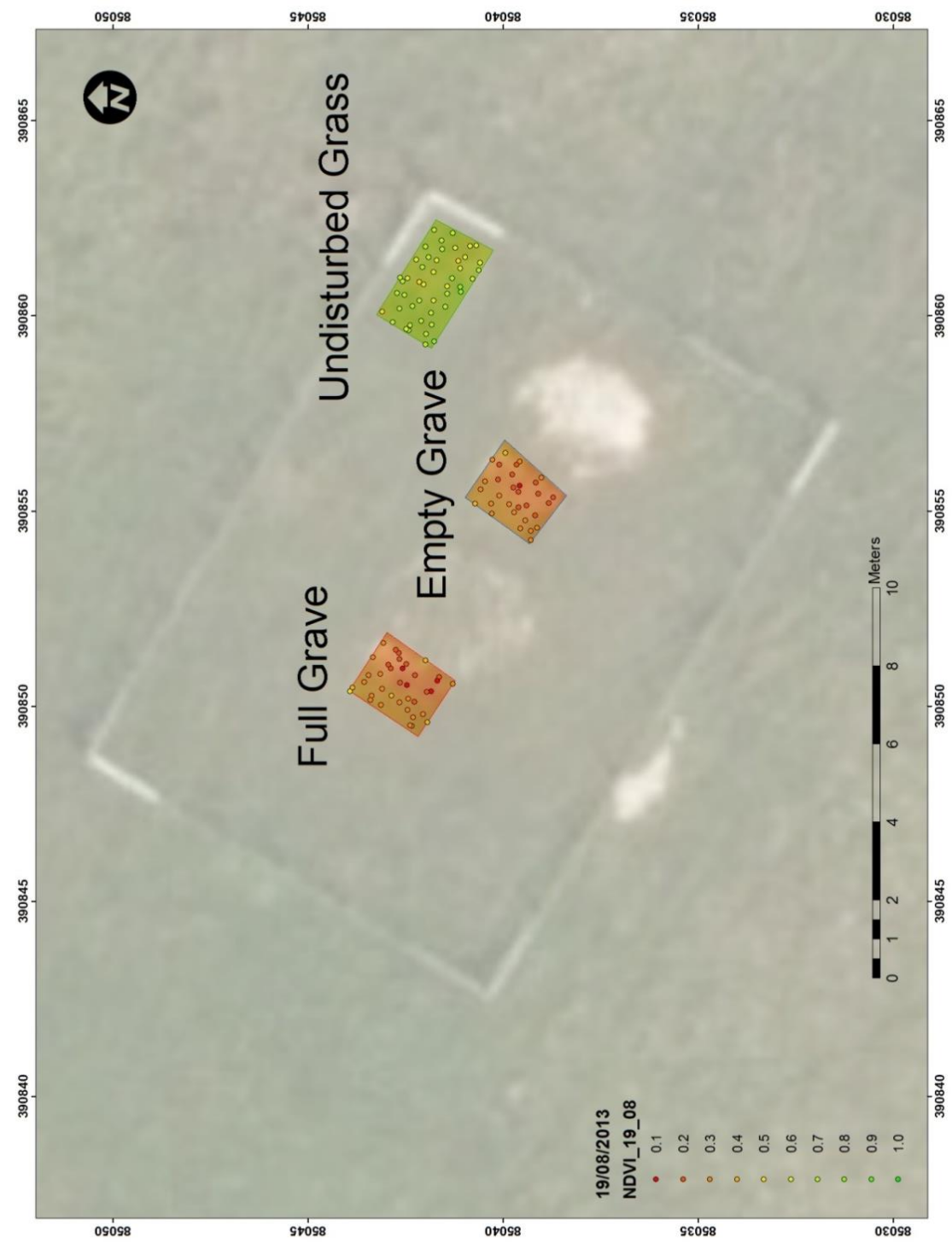

Figure 61 - Convolved and interpolated (IDW) NDVI for the pig and empty grave and the area of undisturbed grass on 19th August 2013. The white rectangular outline represents the location of the fence whilst the white areas within are the areas where the soil was placed during grave creation.

Figure 62 - Photograph of the pig grave (top) and the empty grave (bottom) taken on 16th August 2013.

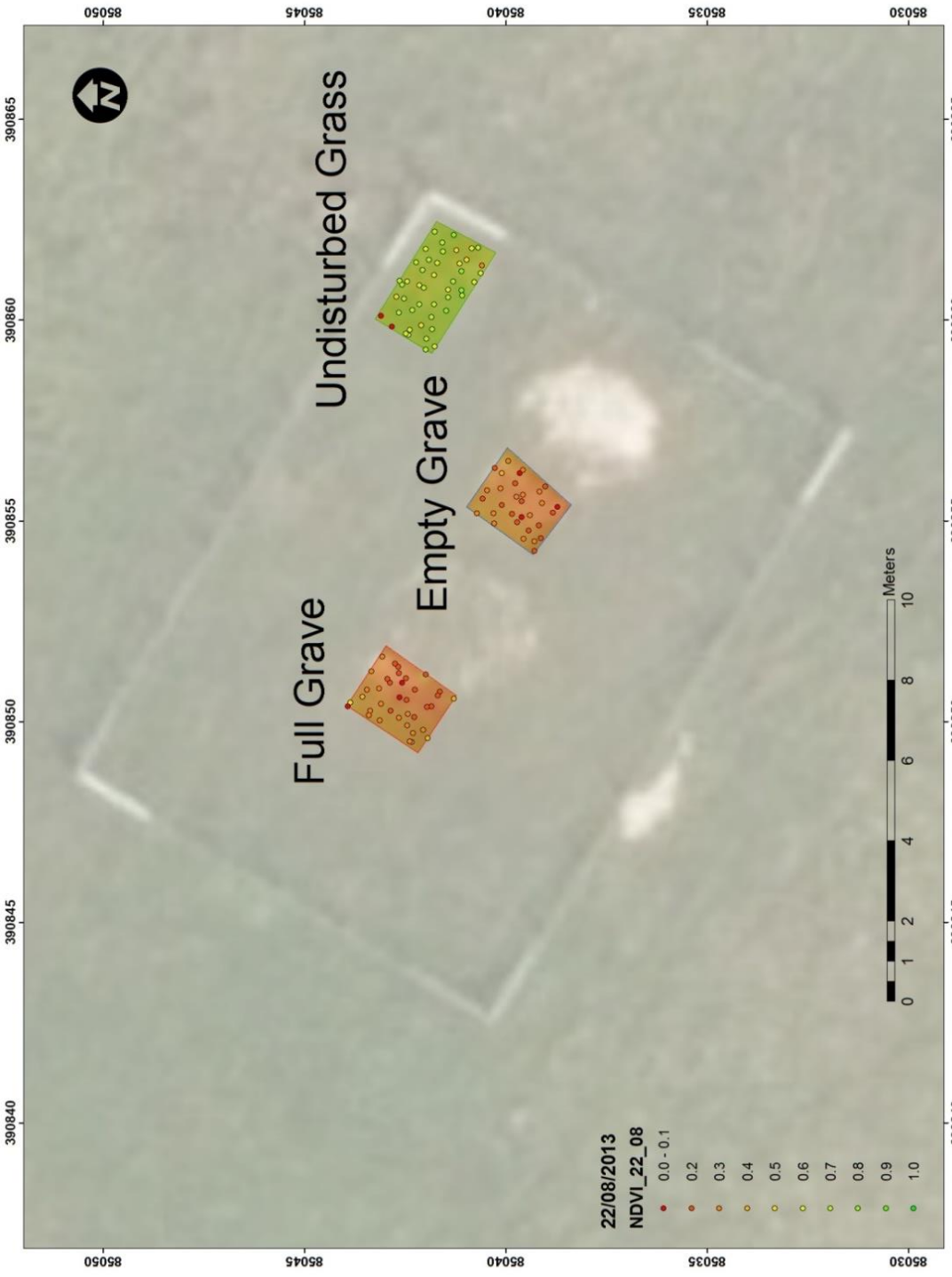

Figure 63 - Convolved and interpolated (IDW) NDVI for the pig and empty grave and the area of undisturbed grass on 22nd August 2013. The white rectangular outline represents the location of the fence whilst the white areas within are the areas where the soil was placed during grave creation.

Figure 64 - Photograph of the pig grave (top) and the empty grave (bottom) taken on 10th October 2013.

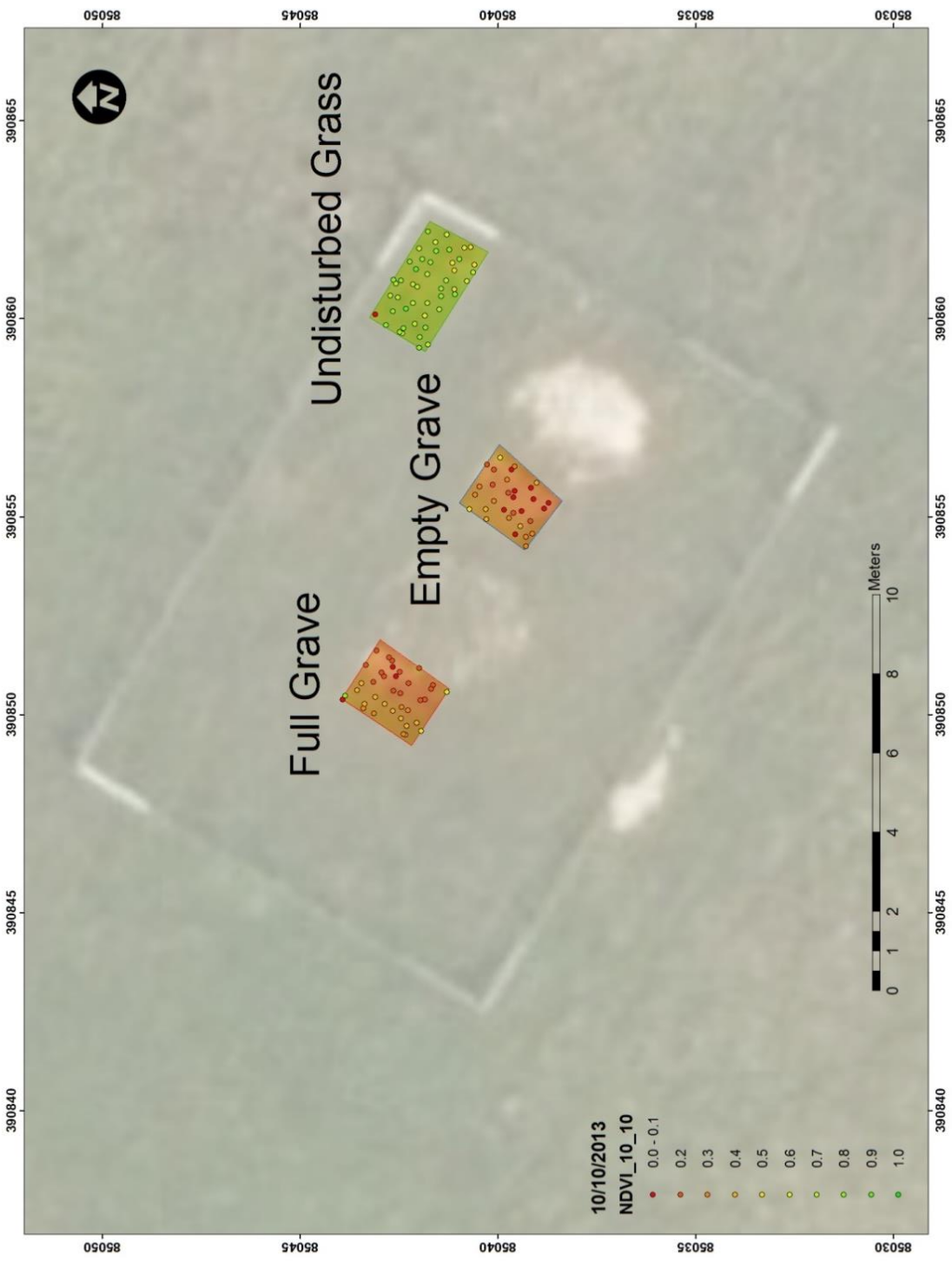

Figure 65 - Convolved and interpolated (IDW) NDVI for the pig and empty grave and the area of undisturbed grass on 22nd October 2013. The white rectangular outline represents the location of the fence whilst the white areas within are the areas where the soil was placed during grave creation.

Figure 66 - Photograph of the pig grave (top) and the empty grave (bottom) taken on 5th December 2013.

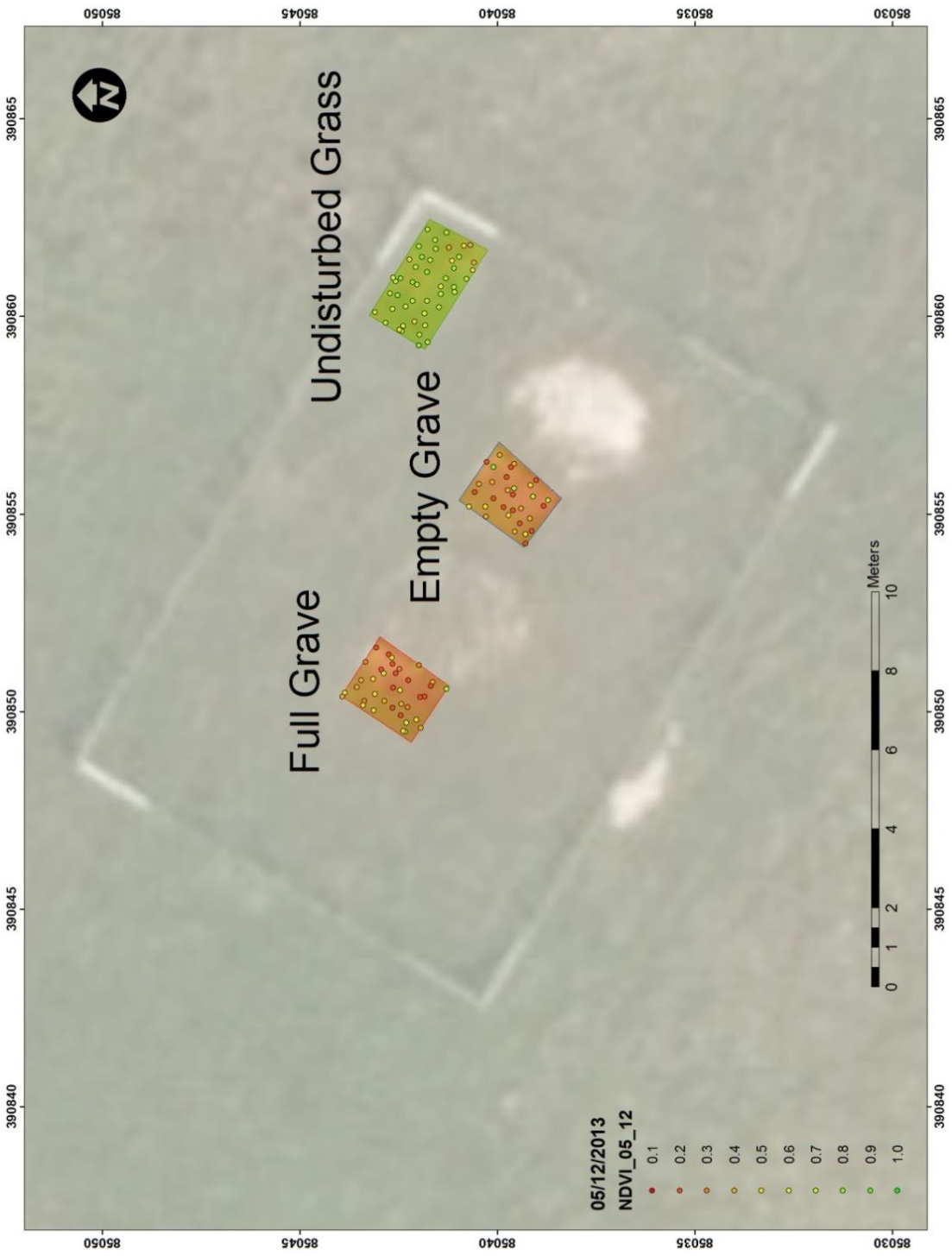

Figure 67 - Convolved and interpolated (IDW) NDVI for the pig (full) and empty grave and the area of undisturbed grass on 5th December 2013. The white rectangular outline represents the location of the fence whilst the white areas within are the areas where the soil was placed during grave creation.

5.2.2.1 Comparison of NDVI over time for each surface type

The NDVI values for the four surface types: pig grave – grass; pig grave – soil; empty grave – grass; empty grave – soil and the undisturbed vegetation NDVI values were compared. To understand the variance present within each data set, f-tests were conducted, prior to running t-tests, to ascertain whether significance existed between the NDVI of the surface types and the undisturbed vegetation (control).

At 13, 16, 65 and 121 dpb significance was observed (*** $p<0.001$) in NDVI for all surface types when compared to the control undisturbed vegetation (Figure 68, Figure 69, Figure 70 and Figure 71). Refer to Appendix 2 for f-test and t-test outputs. In contrast, throughout the study, no significance was observed between the turfed halves of the pig and empty grave, nor the soil halves ($p>0.05$).

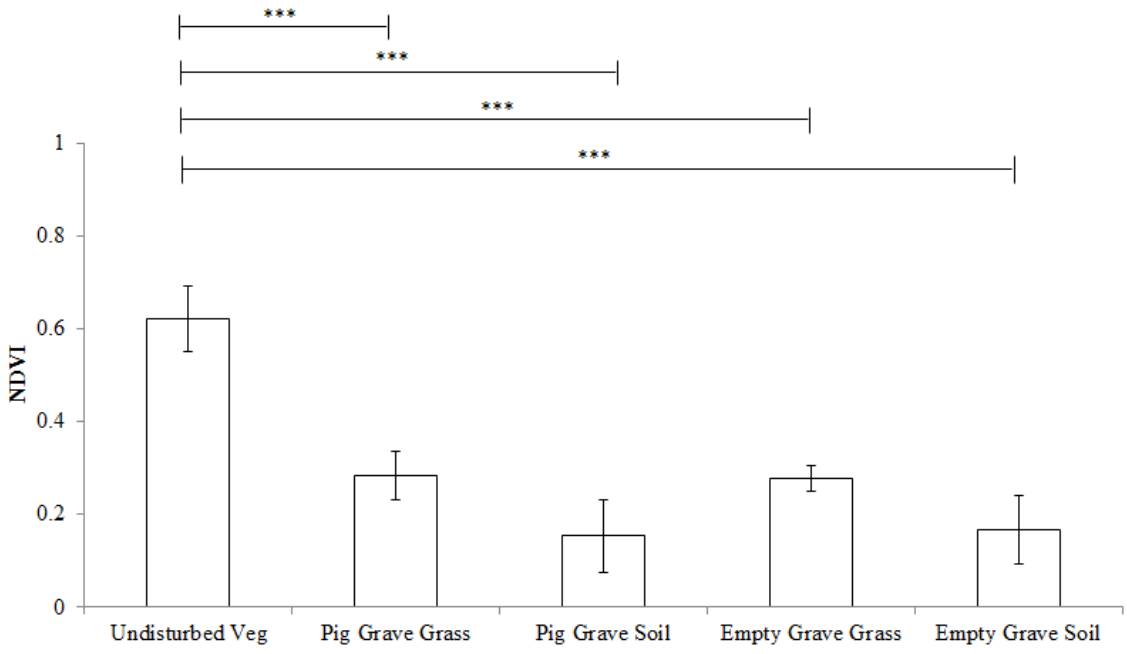

Figure 68 – NDVI calculated for each surface type on 19th August 2013. Sample variation represented as +/- SD, significance calculated using an F-test and Two-sample T-test, *** $p<0.001$.

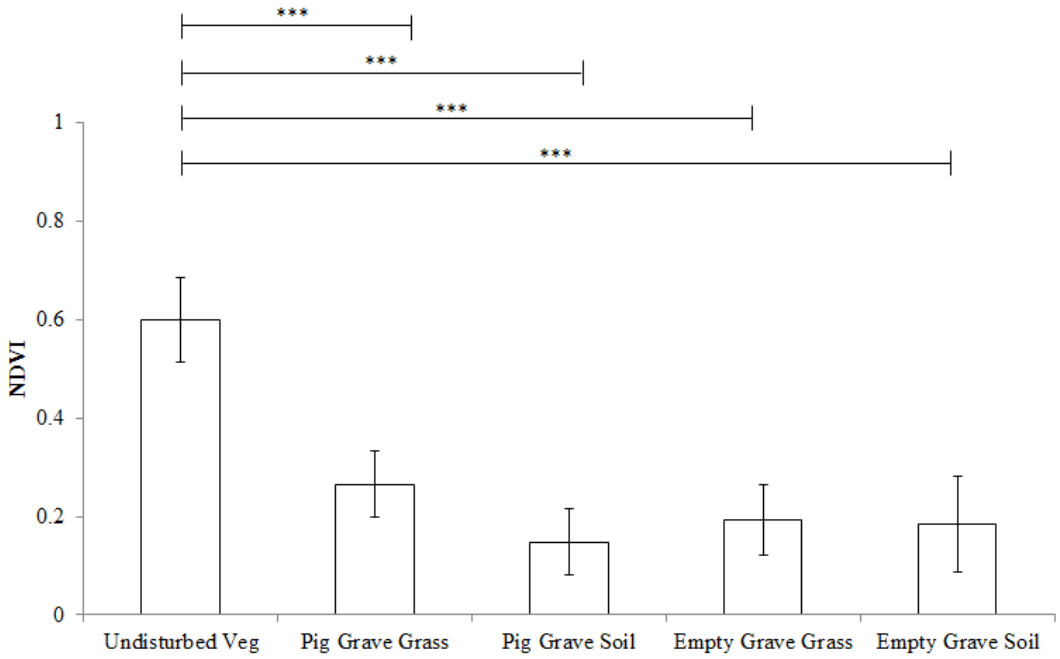

Figure 69 - NDVI calculated for each surface type on 22nd August 2013. Sample variation represented as +/- SD, significance calculated using an F-test and Two-sample T-test, * *p*<0.001.**

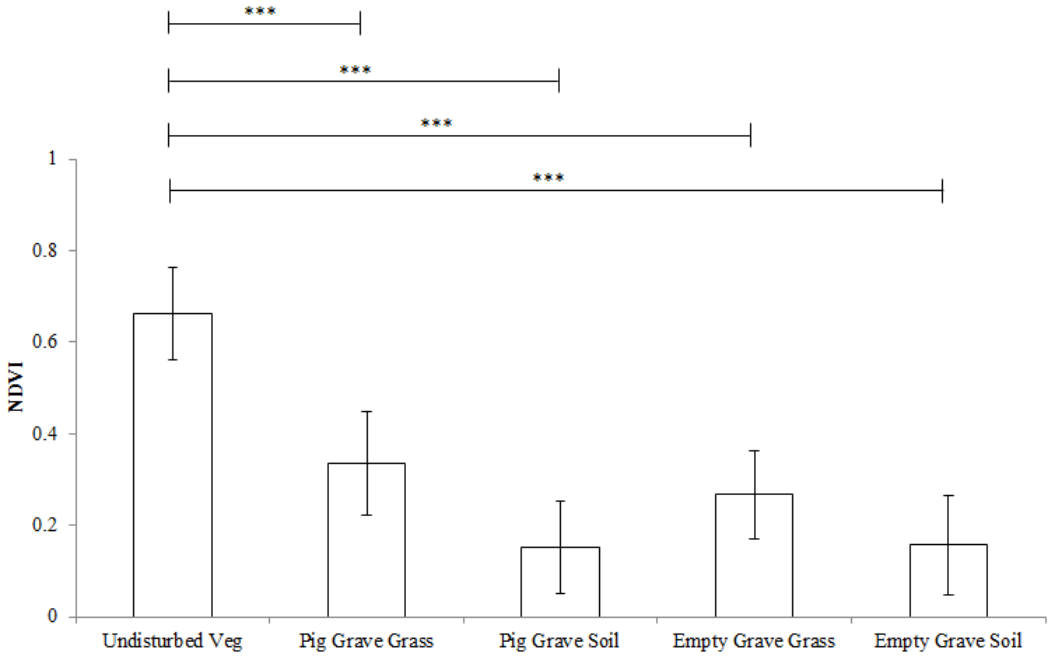

Figure 70 - NDVI calculated for each surface type on 10th October 2013. Sample variation represented as +/- SD, significance calculated using an F-test and Two-sample T-test, * *p*<0.001.**

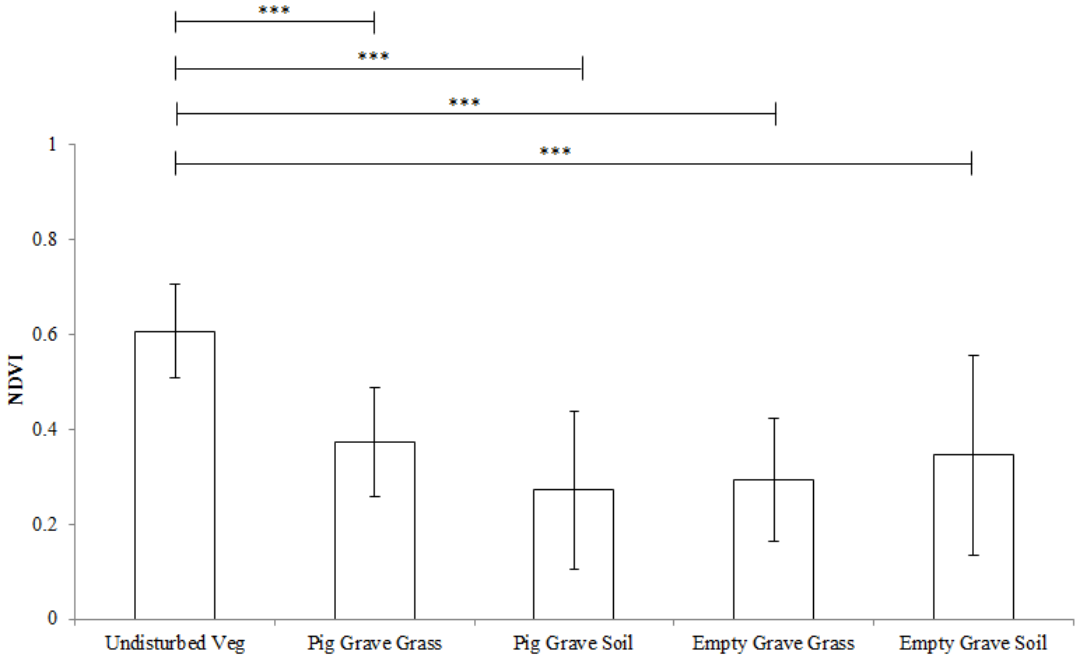

Figure 71 - NDVI calculated for each surface type on 5th December 2013. Sample variation represented as +/- SD, significance calculated using an F-test and Two-sample T-test, *** p<0.001.

Boxplots were created to assess how similar the convolved NDVI values were across each grave (pig or empty) and surface type (soil or grass) for each date (Figure 72). At 13 dpb (19th August 2013), the NDVI for soil and grass were very similar for both the pig and empty graves; with the grass halves having higher NDVI. From data collected on the 22nd August 2013, the NDVI values obtained for the pig grave were similar to those collected on the 19th August 2013. The empty grave exhibited a wider range of NDVI values, represented by the longer boxes present within the boxplots. NDVI calculated from spectra collected on the 10th October 2013 were similar to the previous two observations, with the grass half of the graves exhibiting higher NDVI than the soil. The final data collection at 121 dpb indicated that there were a wide range of NDVI values for each surface type however, they were not visually different and exhibited similar NDVI regardless of surface type. Therefore, NDVI appears to be affected by grave surface type, with differences in NDVI attributable to the presence of soil and grass rather than as a result of the grave contents. Consequently, it appears that up to 121 days post burial the contents of the grave does not have an effect on the NDVI obtained from the grave surface. However, the disturbance associated with creating a grave, whether full or empty, is detectable, even when the grave is re-turfed; with persistently low NDVI being observed compared to areas of undisturbed vegetation.

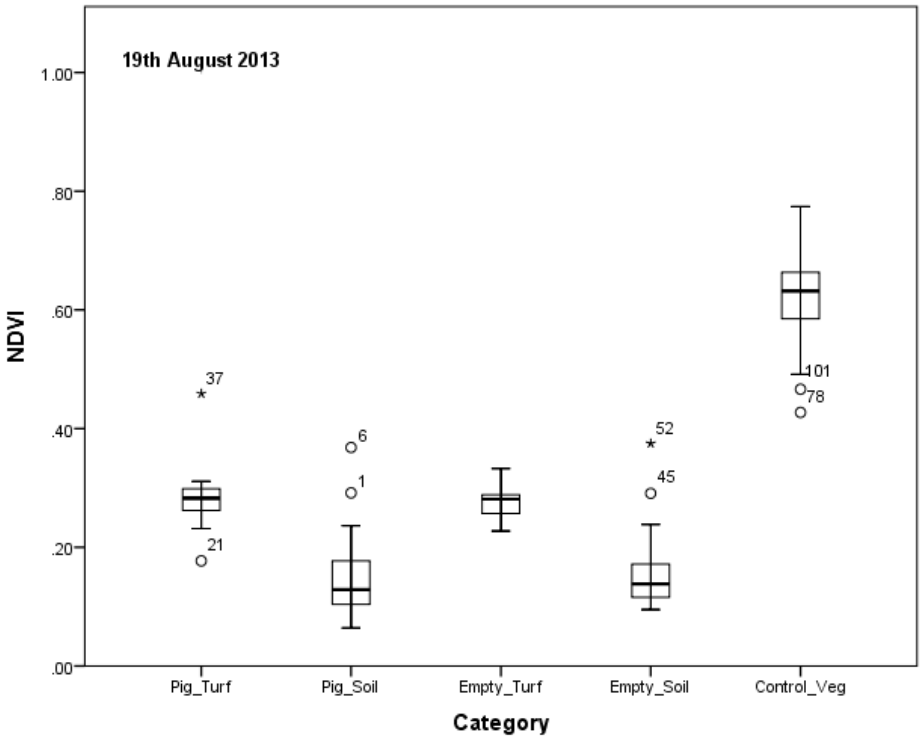
19th August 2013
NDVI
1.00
.80
.60
.40
.20
.00
37
6
1
21
52
45
101
78
Pig_Turf
Pig_Soil
Empty_Turf
Empty_Soil
Control_Veg
Category

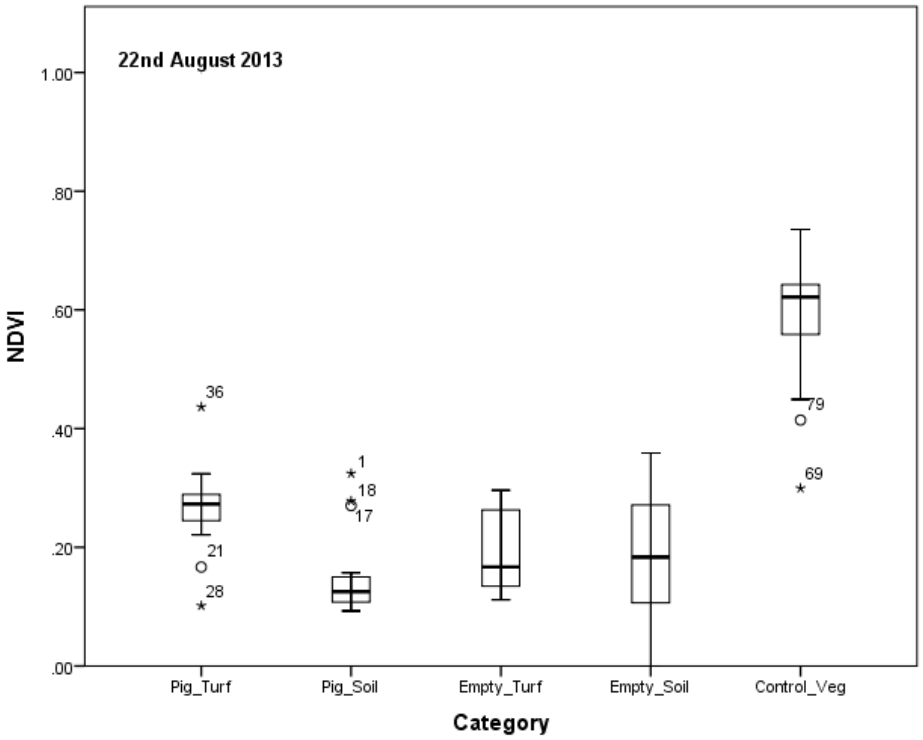
22nd August 2013
NDVI
1.00
.80
.60
.40
.20
.00
36
1
18
17
21
28
79
69
Pig_Turf
Pig_Soil
Empty_Turf
Empty_Soil
Control_Veg
Category

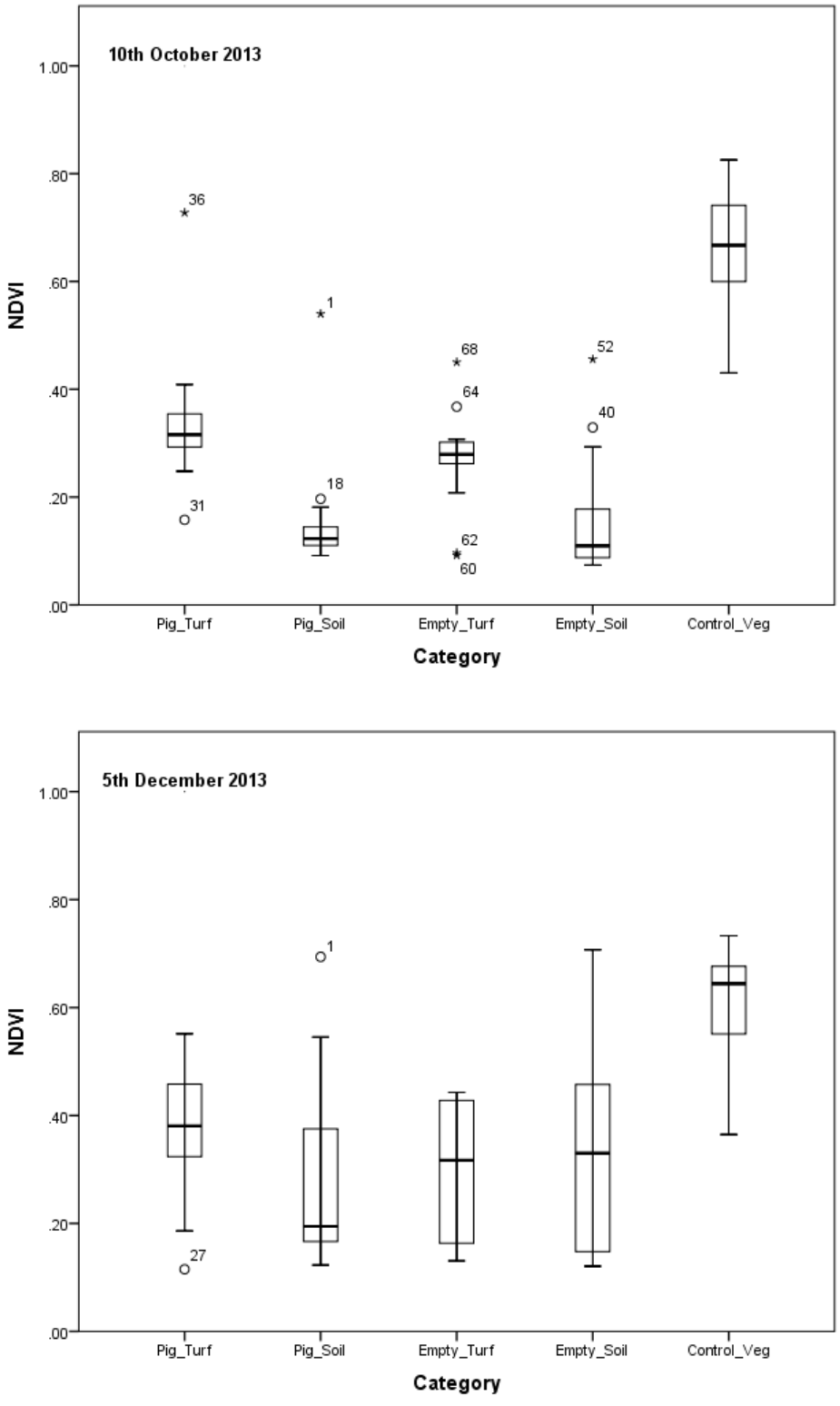

Figure 72 - NDVI for each surface type up to 121 days post burial. The red representing the pig grave, blue representing the empty grave and the green box representing the undisturbed vegetation (control area).

5.2.3 The relationship between the thickness of the disarticulated pig material and NDVI

The thickness of the disarticulated pig remains varied across the grave due to the ramped design; with the southern end deeper than the northern end. To study the relationship between the thickness of the pig remains and NDVI over time, the values for the thickness of the remains were extracted using the method outlined in Section 5.1.5. See Figure 73

Figure 73 for the orthophoto and DSM for thickness of pig material. These values were plotted against the NDVI, which were derived from convolving the GER1500 spectra into Landsat 5 TM equivalent NDVI values from the sample points. Figure 74 show the thickness of pig remains at each sample point and the corresponding NDVI values for the four observation dates.

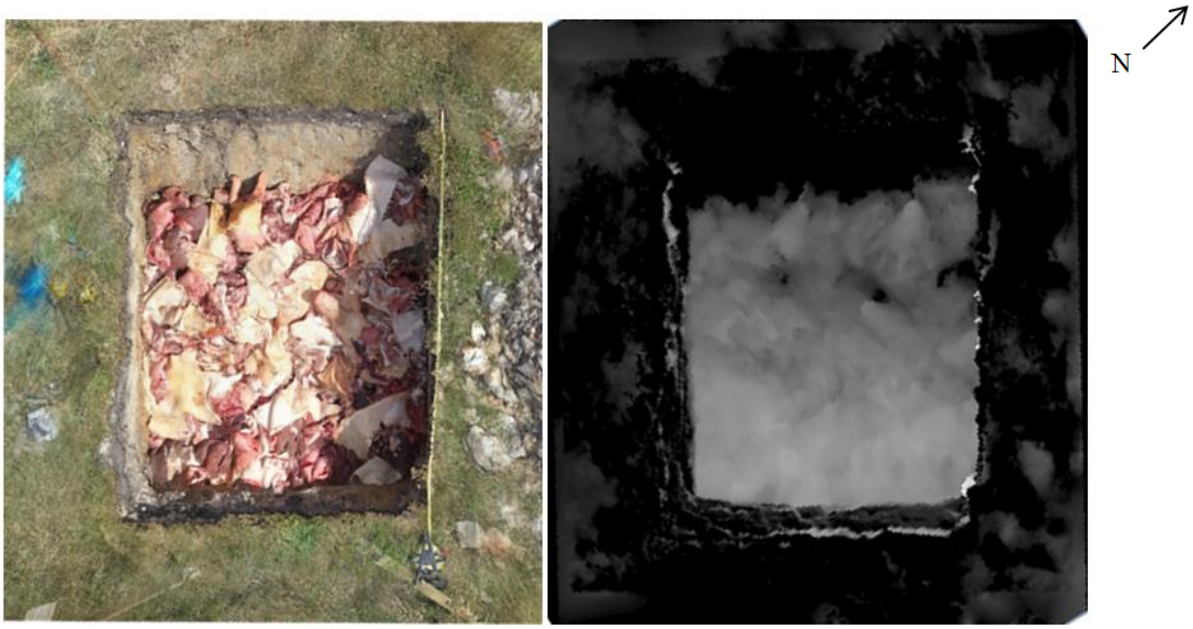

Figure 73 - Orthophoto of the pig material in the grave on 08/08/13 (left) and DSM of the pig grave used to extract the thickness of the pig material (right).

Some of the NDVI values were below zero, it was found these sample points were located on the grave edge. As these sample points did not overlay pig remains they were omitted from the dataset.

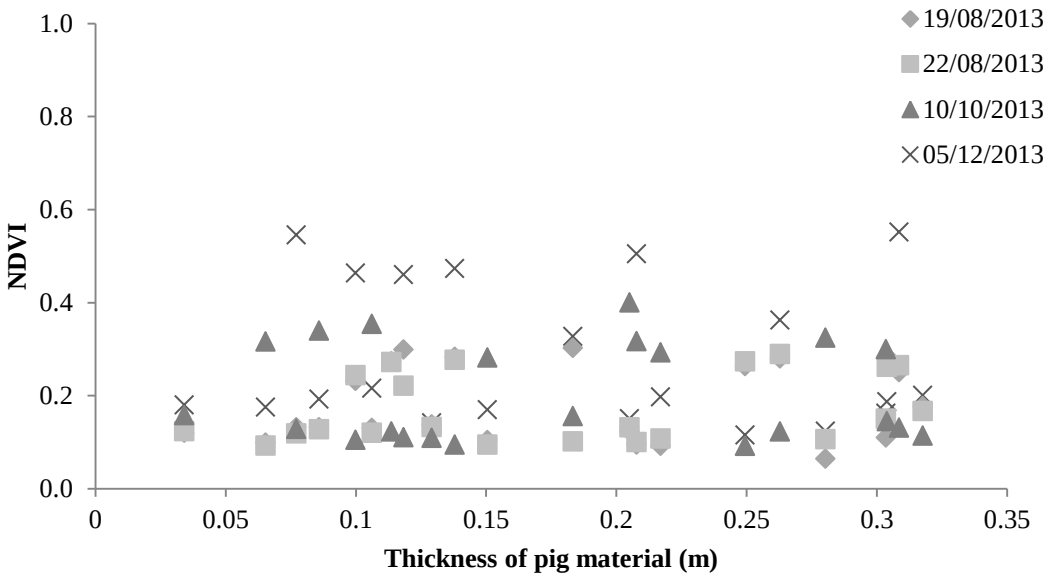

Figure 74 - Thickness of pig material and NDVI over time.

It can be seen in Figure 74 that NDVI remains relatively stable as the thickness of the pig remains increase, with the NDVI values between 0.0-0.6 with no distinct groupings. When the two grave surfaces were considered (i.e. soil and grass), NDVI increased across the graves throughout each of the four observations. It was observed that at 70 dpb (10th October 2013), that the turfed half had higher NDVI however, in December 2013 (at 121 dpb) some of the NDVI values had increased from the soil half of the grave (Figure 75).

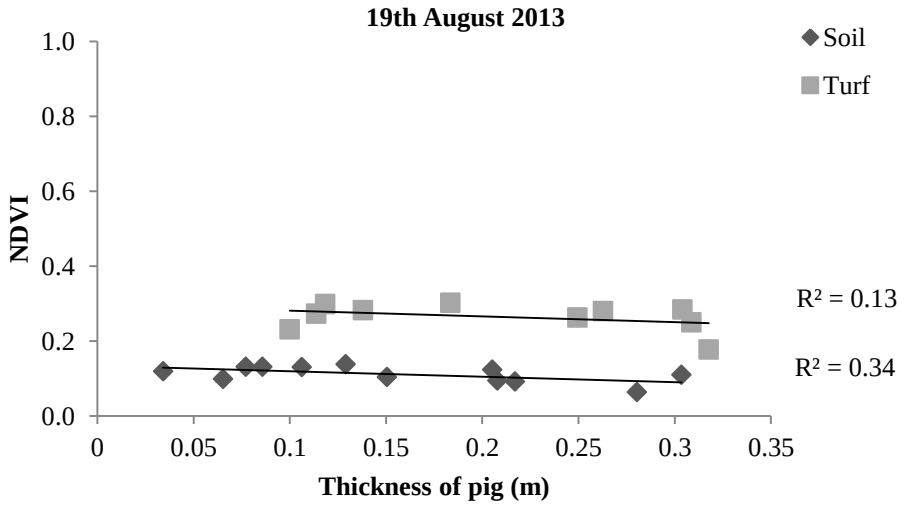

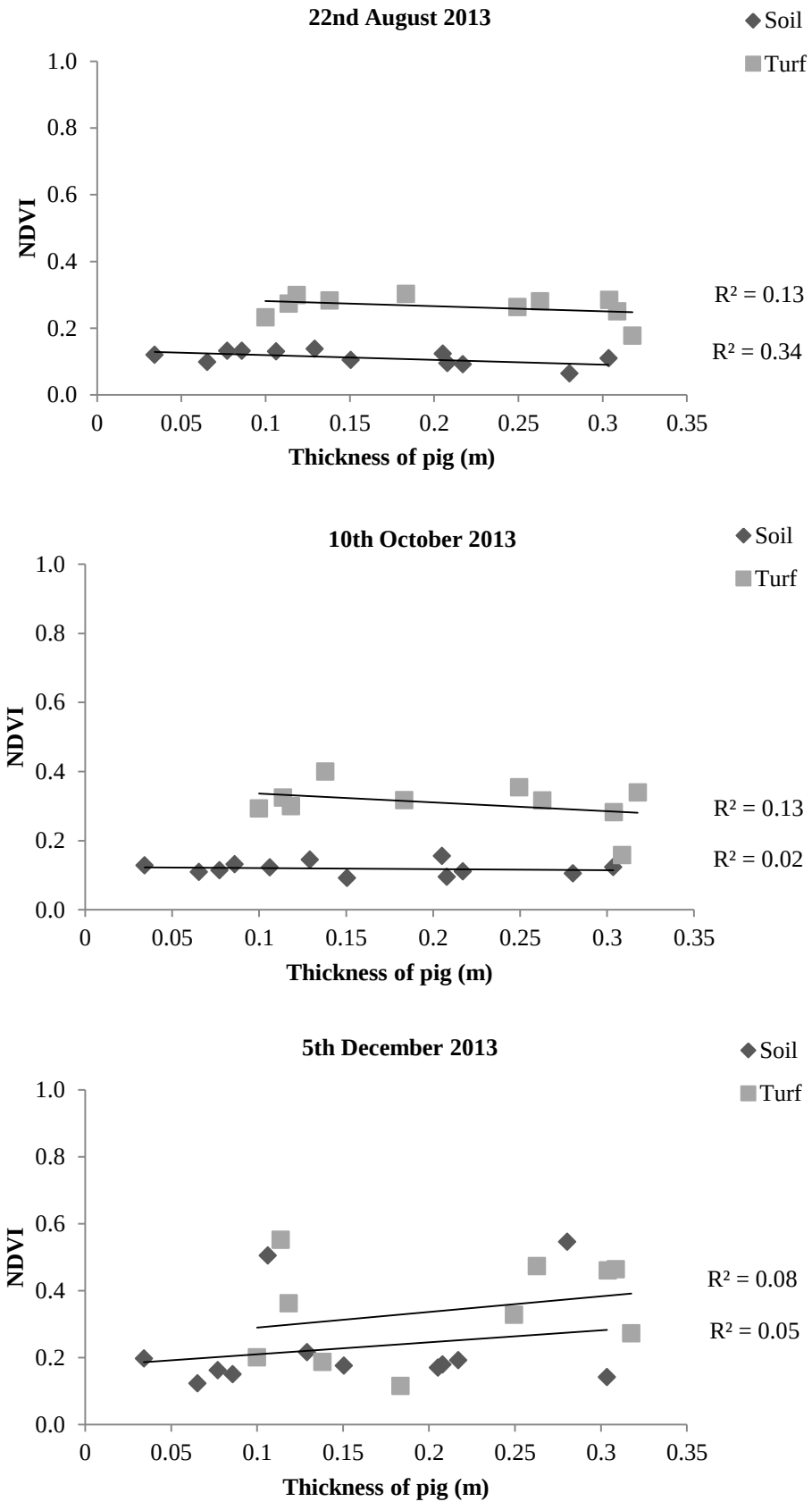

Figure 75 - Thickness of pig matter and NDVI for both soil and turf surface types, up to 121 days post burial.

It is expected that over a period of time, the thickness of the pig material would change due to both decomposition and compaction of the grave fill. Subsidence of the grave surface was considered as an indicator of change in the thickness of pig remains; however, changes in surface topography may be due to soil compaction and settling rather than being solely due to decomposition.

To assess the direction and strength of the relationship between NDVI and the thickness of the pig material over time the gradient of the linear regression line (Slope), correlation coefficient (r) and the coefficient of determination (r^2) were calculated for each surface type and each date (Table 21). The soil half of the grave had a slightly negative correlation at 13 and 121 dpb however, there was no correlation at 16 or 65 days. The same trend was observed from the turfed half of the grave. However, the negative correlations at 13 and 121 dpb were marginally higher than those observed from the soil half of the grave. Within the scatter plots for each of the individual dates it is clear that the data, rather than being diagonal, is horizontal therefore accounting for the low values obtained for slope (Figure 75). Where a negative value for slope was obtained, an equivalent negative correlation was observed through the correlation coefficient (r). The strength of the relationship between the two variables is weak for both surface types throughout the study period, ranging from -0.57 – +0.27 for the soil half of the grave versus -0.38 - +0.45 for the turf half. To determine the percentage of data represented by the linear relationship the r^2 values were calculated for both the soil and turf halves of the grave. It was found that the values were low across all dates regardless of surface type (Table 21). In conclusion, there does not appear to be a relationship between NDVI of the two surface types and the thickness of the pig material over the study period.

Table 21 – The relationship between NDVI and the thickness of pig material over time.

	Soil			
	19/08/2013 13 dpb	22/08/2013 16 dpb	10/10/2013 65 dbp	05/12/2013 121 dpb
Slope	-0.14	0.04	0.06	-0.27
Correlation Coefficient (r)	-0.58	0.18	0.27	-0.17
Coefficient of Determination (r^2)	0.34	0.03	0.07	0.03
	Turf			
	19/08/2013 13 dpb	22/08/2013 16 dpb	10/10/2013 65 dbp	05/12/2013 121 dpb
Slope	-0.16	0.00	0.32	-0.62
Correlation Coefficient (r)	-0.37	0.00	0.45	-0.38
Coefficient of Determination (r^2)	0.13	0.00	0.21	0.14

5.2.4 The relationship between the thickness of the overburden and NDVI

The thickness of the overburden was calculated using the method described within Section 5.1.5 and the NDVI values used were convolved from the GER1500 spectra to be equivalent to the spectral bands of Landsat 5 TM. Similar to the graphs relating to the thickness of the pig material, a number of values existing which were of zero or less thickness, indicating these were above ground level. On further inspection it was found that these sample points were located at the grave edge and were therefore omitted from the scatter plots. Figure 76 shows the generated orthophoto and DSM from which the thickness of the overburden was extracted. The grave depth for each sample point could not be calculated until the grave had been backfilled, therefore, the generated orthophoto and DSM were used.

The thickness of the overburden (the soil on top of the pig remains) ranged between 0.40-0.65m thick at the southern end of the grave. However, due to the ramped design the overburden at the northern end was shallower (ranging from between 0.10-0.30m). Consequently, the scatter plots have two clusters of values representing the differences in thickness of overburden across the grave (Figure 77). NDVI increased across the grave over time with the grass half having higher NDVI compared to the soil. This is observed until December (121 dpb), where the NDVI for the grass samples are more variable (Figure 78). The grave surface would have subsided over time, potentially decreasing the overburden in areas this being due to either decomposition of the pig remains and/ or the compaction of the soil.

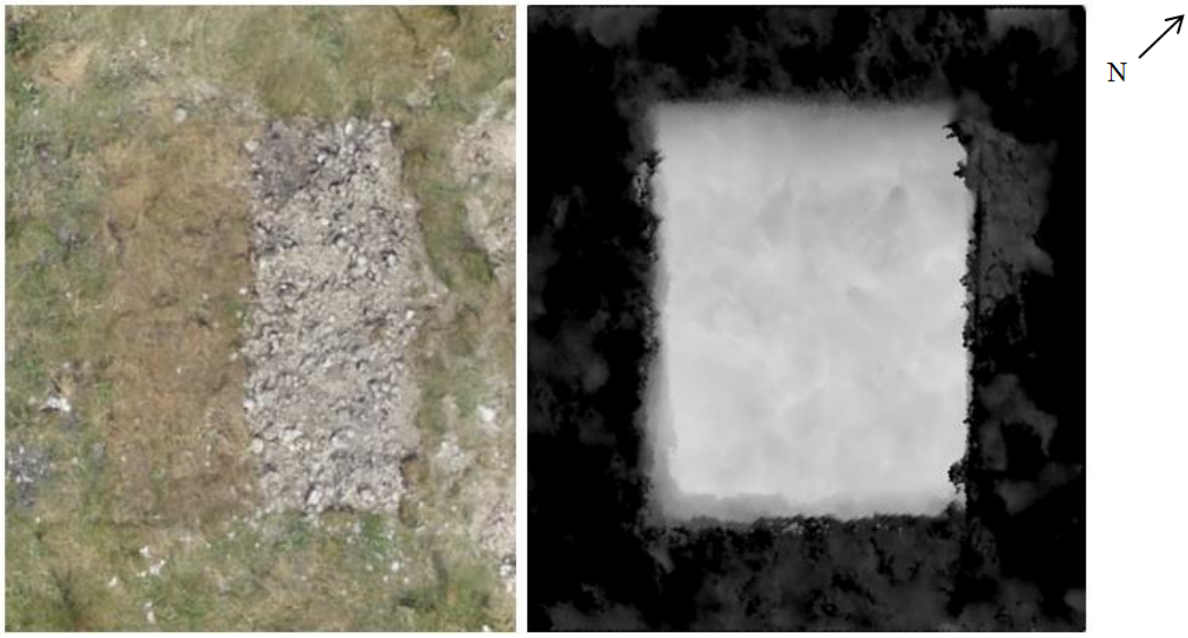

Figure 76 - Orthophoto showing the full pig grave on 06/08/13 (left) and a DSM, of the same date, used to extract the thickness of the overburden across the grave (right).

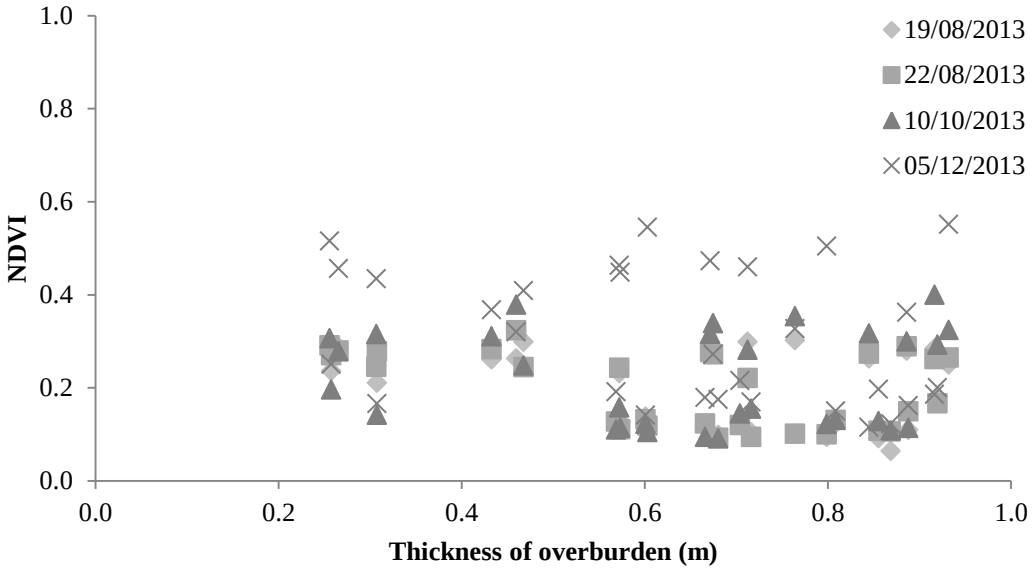

Figure 77 - Scatter plot showing thickness of the overburden and NDVI over time.

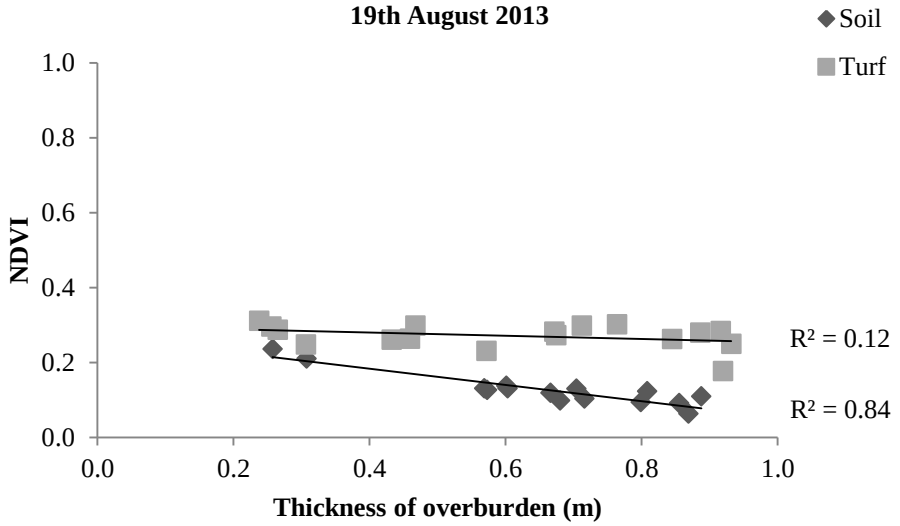

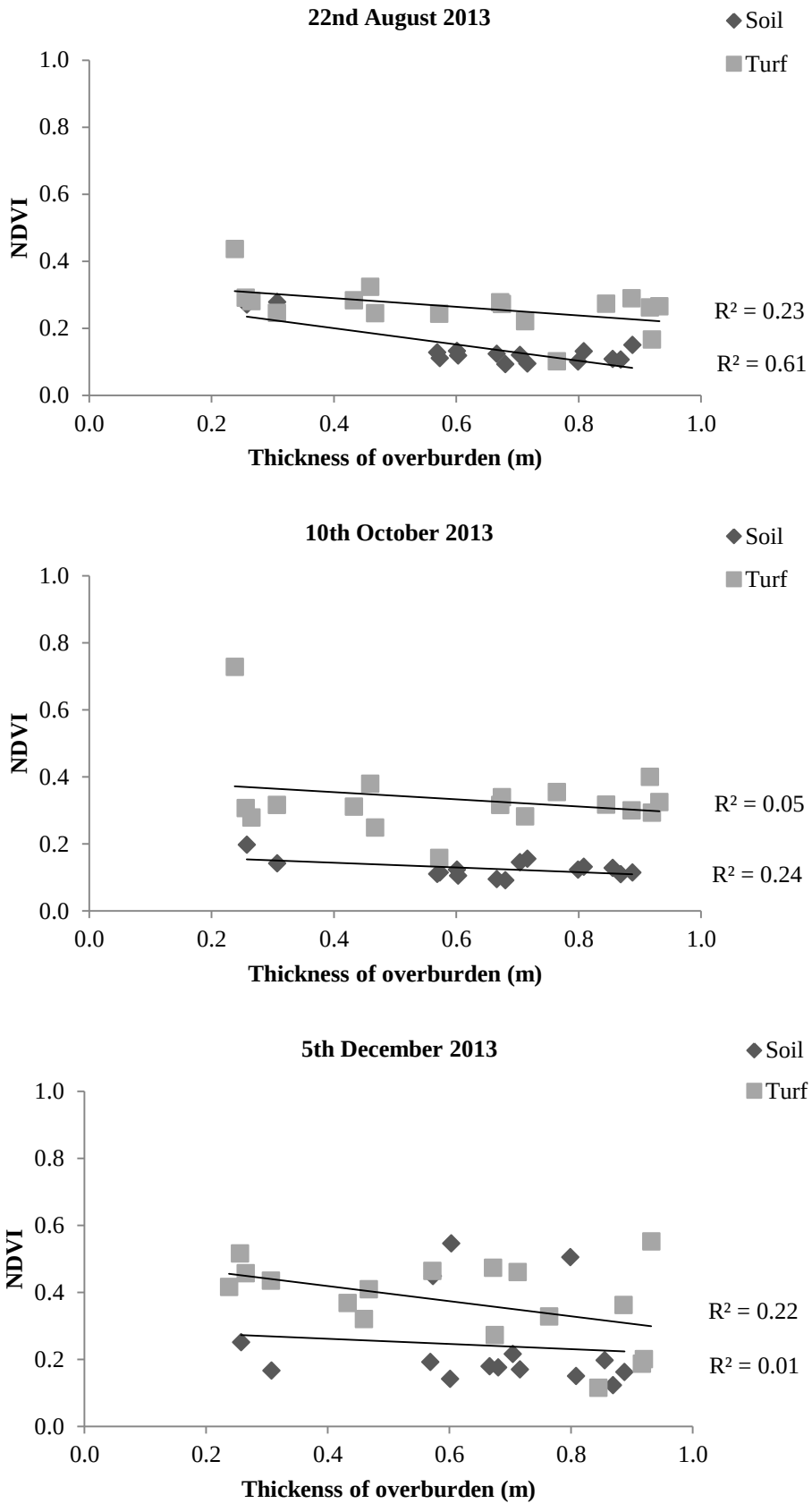

Figure 78 - The thickness of overburden and NDVI for both soil and turf surface types, up to 121 days post burial.

Unlike the relationship between thickness of pig remains and NDVI, the scatter plots in Figure 78 show a more obvious negative linear correlation. To quantify the relationship between NDVI and the thickness of the overburden, the slope of the linear regression line was calculated. For all study dates it was found that a negative linear relationship existed for both surface types (soil and grass – Table 22). The values for slope across both surface types are low and do not exceed -0.47. The strength and direction of this relationship was measured the correlation coefficient (r). It was found for the soil surface that, there was a negative linear relationship which was strongest at 13 dpb (-0.85) that decreased to -0.55 at 121 dpb; indicating that the relationship between the two variables weakens over time. This was also observed for the grass half with the relationship strongest at 13 dpb before decreasing at 65 dpb to -0.28, however, at 121 dpb the strength of the relationship increased to -0.37. Overall, the grass surface of the pig grave has a weaker negative linear relationship compared to the soil surface. The calculated r^2 values indicated that, at 13 dpb, the linear regression line accounted for 72% of the relationship for the soil half of the grave, after which the value decreased to 30% at 121 dpb. In contrast, the values for the grass half of the grave were lower, the highest being at 16 dpb ($r^2 = 0.22$ or 22%) before reducing to 8% at 65 dpb, after which it increased to 21% at 121 dpb. A moderately strong negative linear relationship existed between the NDVI derived from the soil half of the grave and the thickness of overburden, however this weakened over time. A complex relationship existed between the NDVI from the grass half of the grave and the thickness of overburden where a weak linear relationship was present that fluctuated in strength over time.

Table 22 - Quantifying the relationship between NDVI and the thickness of overburden up to 121 days post burial.

	Soil			
	19/08/2013	22/08/2013	10/10/2013	05/12/2013
	13 dpb	16 dpb	65 dbp	121 dpb
Slope	-0.24	-0.24	-0.40	-0.47
Correlation Coefficient (r)	-0.85	-0.78	-0.75	-0.55
Coefficient of Determination (r^2)	0.72	0.60	0.57	0.30
	Turf			
	19/08/2013	22/08/2013	10/10/2013	05/12/2013
	13 dpb	16 dpb	65 dbp	121 dpb
Slope	-0.20	-0.24	-0.23	-0.28
Correlation Coefficient (r)	-0.56	-0.47	-0.28	-0.37
Coefficient of Determination (r^2)	0.06	0.22	0.08	0.21

5.2.5 The relationship between grave depth and NDVI

To investigate the relationship between NDVI and the grave depth, the NDVI values were derived through convolving the GER1500 spectra. Unlike the thickness of pig material and overburden, the depth of the grave remained stable over time and thus can be considered a constant with the NDVI being the varying factor. Figure 79 shows the orthophoto and DSM that were created to enable the values for grave depth to be extracted. A scatter plot was produced to ascertain whether a relationship existed between grave depth and NDVI over the study period. It was found that some values were clustering around zero, as in previous sections, it was identified that these sample points were located around the grave edge and consequently were omitted from the final results (Figure 80).

Figure 79 - Orthophoto of the empty pig grave on 13/07/13 (left) and the DSM used to extract values for grave depth (right).

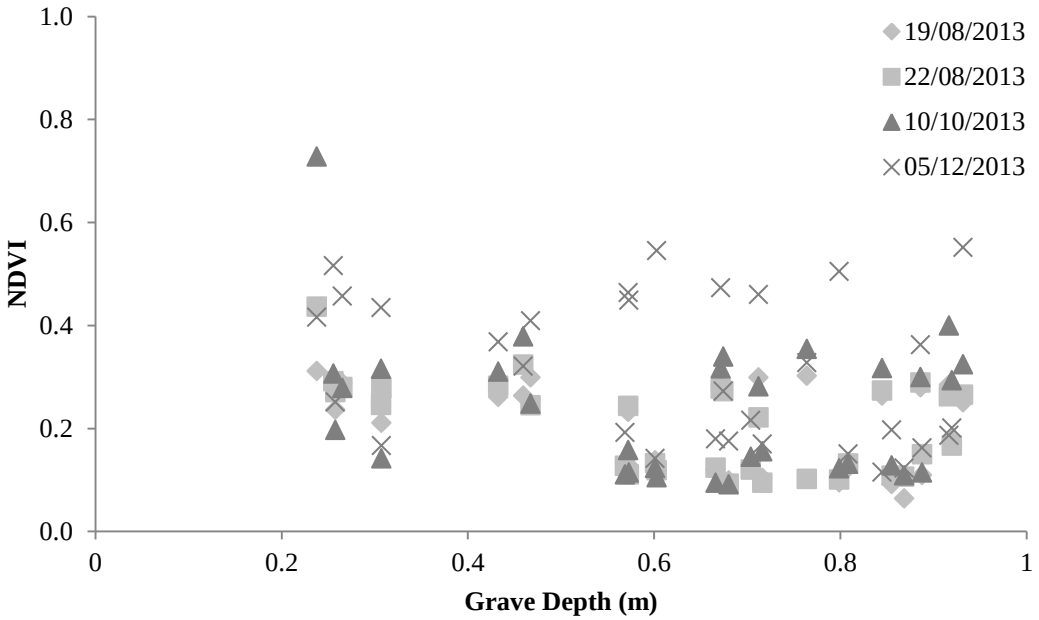

Figure 80 - Depth of the grave and NDVI over time.

It can be seen from Figure 80 that the NDVI values obtained on the 5th December 2013 are for the most part, higher than those obtained during the previous three data collections.

It is important to consider how NDVI varied across the two surface types i.e. the soil and grass and ascertain whether this is related to grave depth of the grave during the first 121 days post burial. Therefore, scatter plots were produced (Figure 81). The NDVI values obtained from data collection on the 19th and 22nd August 2013 are similar, particularly in relation to the noticeable separation of the spectral values obtained from the soil versus the re-turfed grass; which exhibited higher NDVI (Figure 81). Data collected on the 10th October 2013, showed a similar pattern as the August results however, there was a slight increase of NDVI values, specifically for the grass half of the grave; regardless of increasing grave depth. In contrast to the three earlier data collections, data from the 5th December 2013 showed that the NDVI of the grass had increased uniformly across the grave, seemingly regardless of the changing grave depth. The soil also exhibited higher NDVI values than previously observed.

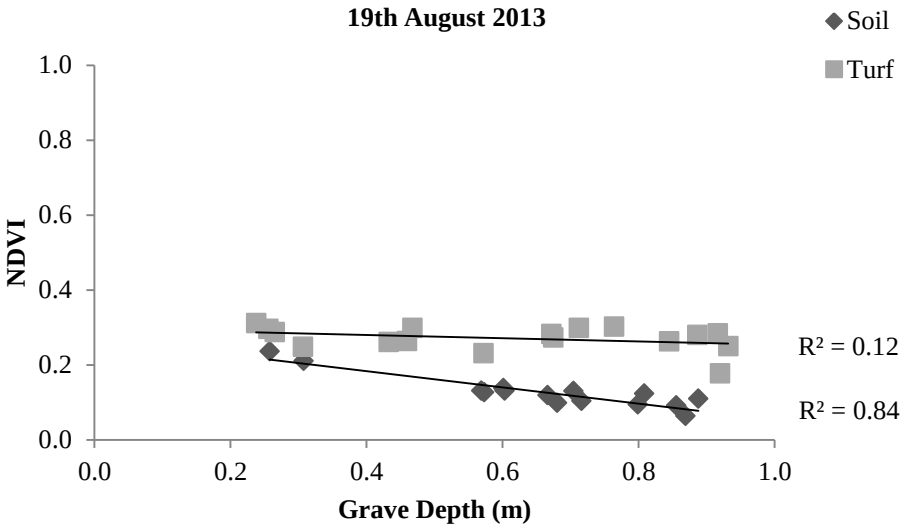
19th August 2013
Soil
Turf
NDVI
1.0
0.8
0.6
0.4
0.2
0.0
0.0
0.2
0.4
0.6
0.8
1.0
Grave Depth (m)
R² = 0.12
R² = 0.84

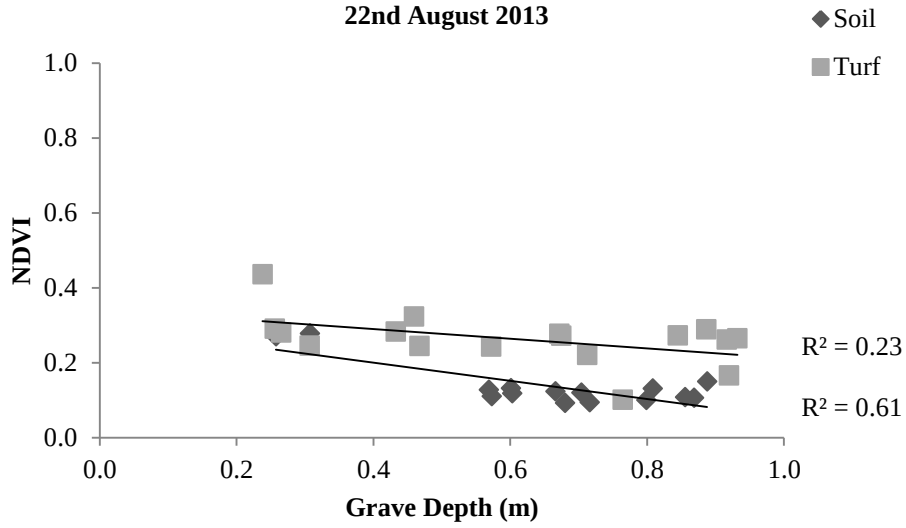
22nd August 2013
Soil
Turf
NDVI
1.0
0.8
0.6
0.4
0.2
0.0
0.0
0.2
0.4
0.6
0.8
1.0
Grave Depth (m)
R² = 0.23
R² = 0.61

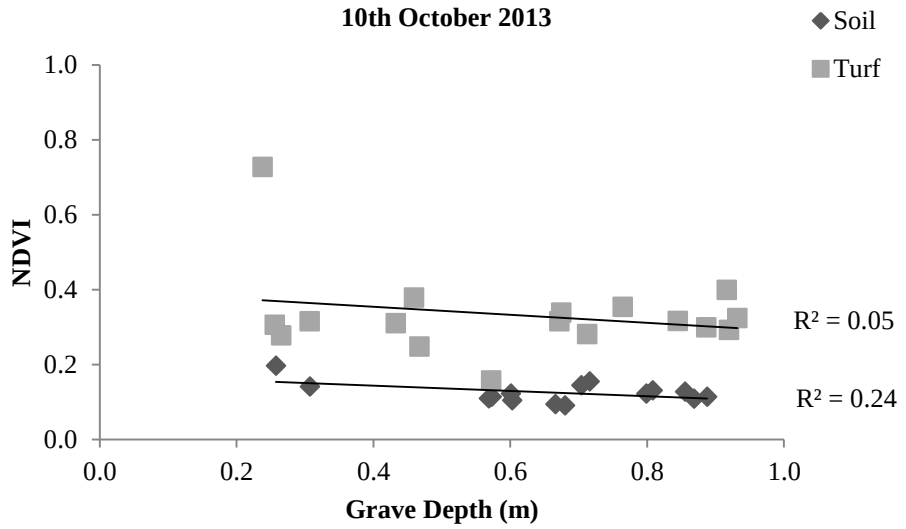
10th October 2013
Soil
Turf
NDVI
1.0
0.8
0.6
0.4
0.2
0.0
0.0
0.2
0.4
0.6
0.8
1.0
Grave Depth (m)
R² = 0.05
R² = 0.24

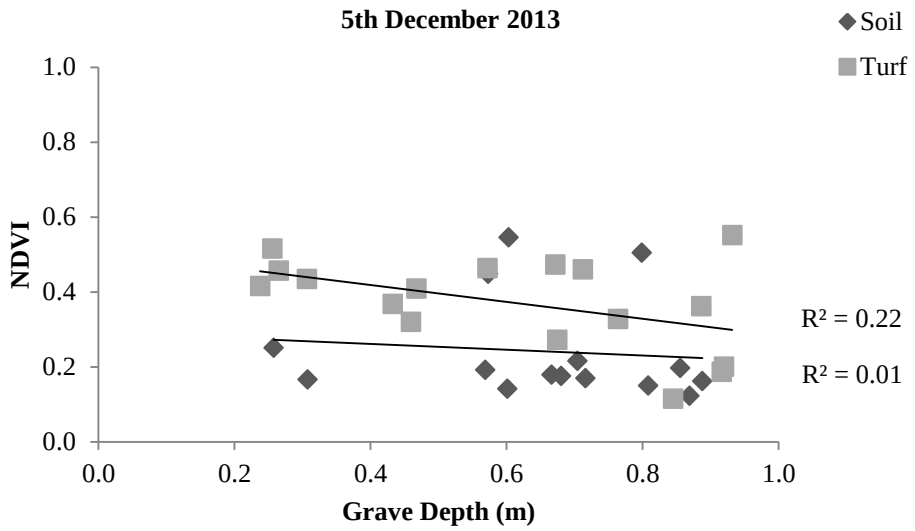

Figure 81 - The relationship between grave depth and NDVI for both soil and turf surface types, up to 121 days post burial.

The relationship between NDVI of the soil half of the grave and grave depth over time is negative and linear; this is indicated by the negative values for slope obtained (Table 23). The values are small indicating that the slope in each scatter plot is not steep (Figure 81). A negative linear relationship existed between the NDVI from the grass half of the grave however, the values are low, ranging from -0.09 to -0.14 indicating that the data is almost horizontal. The strength of the linear relationship between the two variables for the soil half of the grave is strong up until 121 dpb, when the value drops to -0.39 from a maximum of -0.88 (at 13 dpb); indicating the relationship weakens over time. Whereas, the strength of the relationship for the grass half is relatively strong at 13 dpb, with this becoming weaker, dropping to -0.28 at 65 dbp. At 121 dpb the relationship is stronger resulting in an r value of -0.37. The ability for the linear regression line to explain the relationship between NDVI from the soil half of the grave and depth decreases over time, ranging from 84% (at 13 dpb) to 1% (at 121 dpb). The r^2 values for the grass half of the grave follow the same pattern as the correlation coefficient, resulting in an increase at 121 dpb. However, the values from the grass half of the grave are lower than those from the soil half, indicating that a complex relationship exists between NDVI and grave depth. Overall, there is a relationship between NDVI, for both surface types and grave depth over time, which varies in strength depending on the surface type.

Table 23 - Quantifying the relationship between NDVI and grave depth up to 121 days post burial.

	Soil			
	19/08/2013	22/08/2013	10/10/2013	05/12/2013
	13 dpb	16 dpb	65 dbp	121 dpb
Slope	-0.23	-0.14	-0.18	-0.21
Correlation Coefficient (r)	-0.88	-0.63	-0.55	-0.39
Coefficient of Determination (r^2)	0.84	0.61	0.24	0.01
	Turf			
	19/08/2013	22/08/2013	10/10/2013	05/12/2013
	13 dpb	16 dpb	65 dbp	121 dpb
Slope	-0.09	-0.11	-0.11	-0.14
Correlation Coefficient (r)	-0.52	-0.48	-0.28	-0.37
Coefficient of Determination (r^2)	0.12	0.23	0.05	0.22

5.2.6 The relationship between NDVI and meteorological variables

Relationships between the meteorological variables and NDVI of the surface types for each of the graves were investigated and compared to the relationships exhibited by the area of undisturbed grass (control). This section considers weather events one week (7 days) prior to spectra collection. Please refer to Appendix 2 for data relating to meteorological variables occurring two weeks (14 days) and four weeks (28 days) prior to data collection. For each of the defined periods mean values for ambient air temperature, humidity, precipitation, dew point, wind speed and pressure were calculated. All areas of the site were considered including, the pig grave (turf and soil), empty grave (turf and soil) and the area of undisturbed vegetation (control). Scatter plots were produced for each meteorological variables and plotted against the mean NDVI (convolved GER1500 spectra) for each surface type (Figure 82). The gradient of the linear relationship, the correlation coefficient (r) and the coefficient of determination (r^2) were calculated for each surface type and time period, to determine the direction and strength of the relationship.

5.2.6.1 Relationship between NDVI and meteorological events occurring one week prior to spectral data collection – on the turf half of the graves

The slope of the linear regression line showed that the trend line for the turf half of the pig and empty grave was almost horizontal and in a negative direction. Whereas, the trend line for the undisturbed grass was horizontal in most cases, exhibiting two positive and one

negative trend (humidity, rainfall and wind speed respectively). The meteorological variables occurring one week prior to data collection have relationships with each surface and affect the resulting NDVI values. It can be seen from the r values in Table 24 that the pig grave (grass surface) has stronger positive linear correlations compared to the empty grave (grass surface) and the undisturbed grass, suggesting that as dew point (r = 1), wind speed (r =-0.92) and pressure (r = 0.83) increase NDVI also increases. The NDVI of the turfed half of the pig grave has weak positive relationships with cumulative rainfall (r = 0.37), strong negative relationships with ambient temperature (r = -0.89) and moderately negative relationship with humidity (r = -0.57). In contrast, the corresponding half of the empty grave has predominantly negative linear correlations, all of which are moderate, with the exception of humidity which is weak (r = -0.24). Whereas, for the area of undisturbed grass, the relationships are predominantly positive with rainfall having the strongest relationship, pressure and humidity moderate and temperature and dew point the weakest. The undisturbed grass has a weak negative correlation between NDVI and wind speed.

Therefore in summary, at one week prior to spectra collection the NDVI of the pig grave is most strongly affected by temperature, dew point, wind speed and pressure. The empty grave is affected by the same variables however, the correlation is weaker and negative in direction. In contrast, the NDVI of the undisturbed grass was most affected by rainfall, pressure and humidity followed by temperature, dew point and wind speed. The r^2 values calculated for each scatter plot indicate that the linear regression line explained the relationship between NDVI and wind speed, temperature and dew point best for the turf half of the pig grave (ranging between 77-95%) whereas, less of the data for the empty grave was explained. For the undisturbed grass, one relationship was explained, between NDVI and cumulative rainfall (r^2 – 0.88) (Table 24).

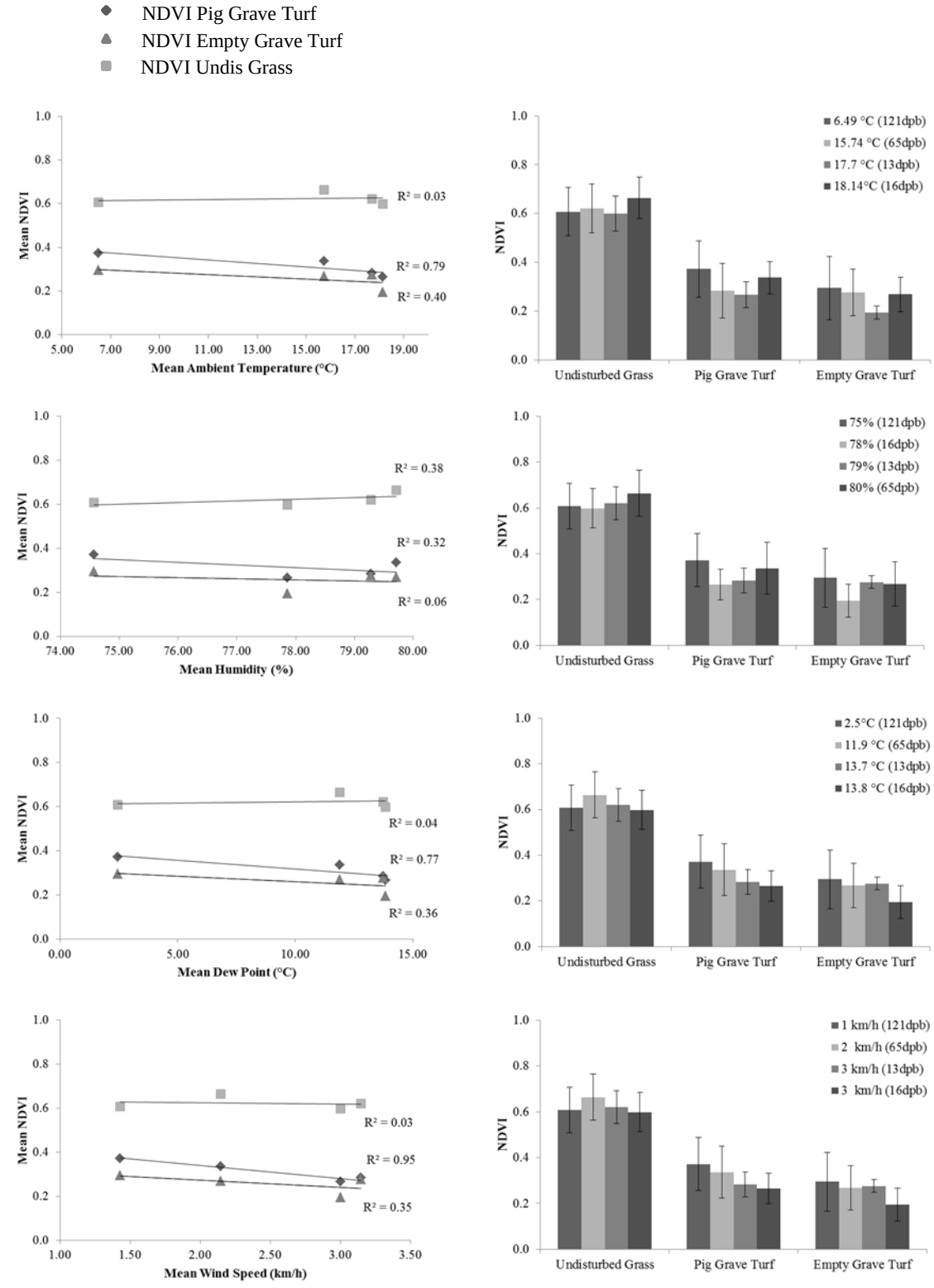
NDVI Pig Grave Turf
NDVI Empty Grave Turf
NDVI Undis Grass
Mean NDVI
Mean Ambient Temperature (°C)
R² = 0.03
R² = 0.79
R² = 0.40
NDVI
6.49 °C (121dpb)
15.74 °C (65dpb)
17.7 °C (13dpb)
18.14°C (16dpb)
Undisturbed Grass
Pig Grave Turf
Empty Grave Turf
Mean Humidity (%)
R² = 0.38
R² = 0.32
R² = 0.06
75% (121dpb)
78% (16dpb)
79% (13dpb)
80% (65dpb)
Mean Dew Point (°C)
R² = 0.04
R² = 0.77
R² = 0.36
2.5°C (121dpb)
11.9 °C (65dpb)
13.7 °C (13dpb)
13.8 °C (16dpb)
Mean Wind Speed (km/h)
R² = 0.03
R² = 0.95
R² = 0.35
1 km/h (121dpb)
2 km/h (65dpb)
3 km/h (13dpb)
3 km/h (16dpb)

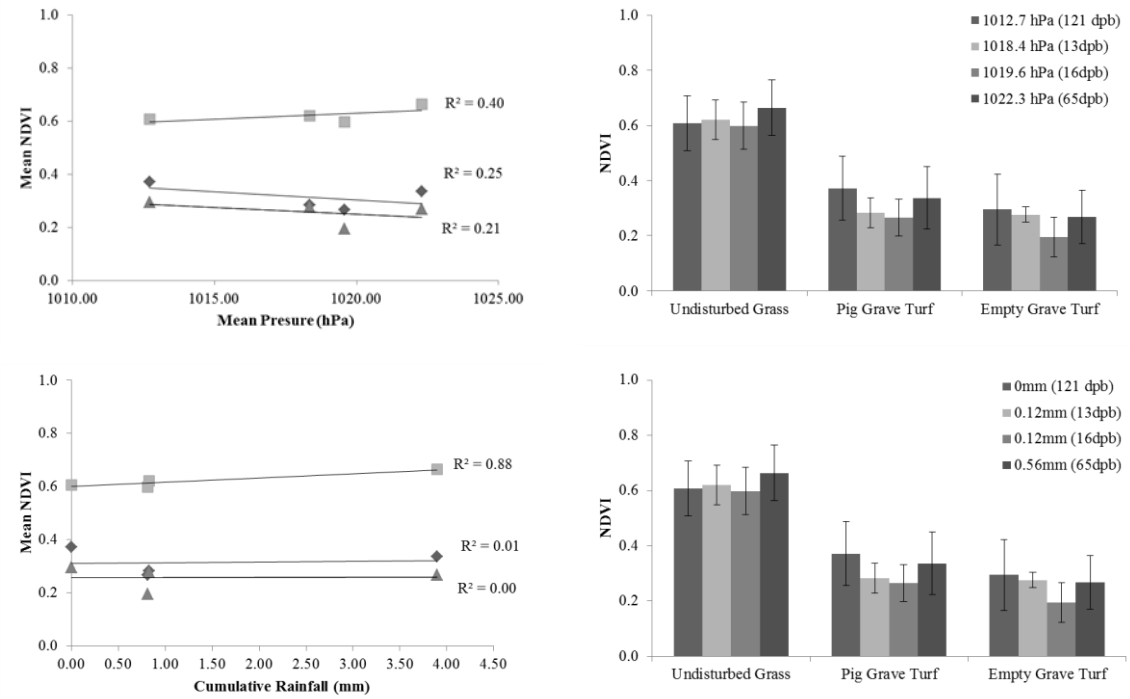

Figure 82 – The relationships existing between NDVI of the grass halves of the graves relative to the control (undisturbed grass) and meteorological variables, one week prior to spectra collection.

Table 24 – Description of the direction and strength of the linear relationship between NDVI calculated from convolved GER1500 data on the grass half of the experimental graves and meteorological variables (one week prior to data collection).

FUNCTION		Pig Grave Grass	Empty Grave Grass	Undisturbed Grass
SLOPE	NDVI vs Temp	-0.01	-0.01	0.00
	NDVI vs Humidity	-0.01	0.00	0.01
	NDVI vs Dew Point	-0.01	0.00	0.00
	NDVI vs Wind Speed	-0.06	-0.03	-0.01
	NDVI vs Pressure	-0.01	-0.01	0.00
	NDVI vs Cumul. Rainfall	0.00	0.00	0.02
CORREL (r)	NDVI vs Temp	-0.89	-0.63	0.18
	NDVI vs Humidity	-0.57	-0.24	0.62
	NDVI vs Dew Point	1.00	-0.60	0.21
	NDVI vs Wind Speed	0.92	-0.59	-0.16
	NDVI vs Pressure	0.83	-0.46	0.63
	NDVI vs Cumul. Rainfall	0.37	0.01	0.94
RSQ (r^2 or %)	NDVI vs Temp	0.79 79%	0.40 40%	0.03 3%
	NDVI vs Humidity	0.32 32%	0.06 6%	0.38 38%
	NDVI vs Dew Point	0.77 77%	0.36 36%	0.04 4%
	NDVI vs Wind Speed	0.95 95%	0.35 35%	0.03 3%
	NDVI vs Pressure	0.25 25%	0.21 21%	0.40 40%
	NDVI vs Cumul. Rainfall	0.01 1%	0.00 0%	0.88 88%

5.2.6.2 Relationship between NDVI and meteorological events occurring one week prior to spectral data collection – on the soil half of the graves

The slope of the linear regression line was calculated for each scatter plot and showed that the trend line for the soil half of both the pig and empty grave was almost horizontal and in a negative direction (Figure 83 and Table 25). In contrast, the trend line for the undisturbed grass was horizontal, exhibiting two positives and one negative trend (humidity, rainfall and wind speed respectively, as described previously). When the strength and direction of the relationships were considered for each surface type, via the correlation coefficient, it was found that the NDVI from the pig grave had a strong positive correlation with dew point, wind speed and pressure, in addition to a strong negative correlation with temperature and humidity. A weak positive relationship was found with cumulative rainfall. The empty grave exhibited strong negative linear correlations with all meteorological variables with the exception of cumulative rainfall, which had a negative correlation (Table 25). The correlation coefficient describing the relationships between the NDVI from the undisturbed grass and the meteorological variables has been presented in the previous section and will not be repeated in this section. The r^2 values for the linear regression lines for the pig grave explains a high percentage of the relationships apart from cumulative rain, where only 28% is explained. Similarly, the values for the empty grave (soil) explain a high percentage of the data with the exception of wind speed and cumulative rainfall, which have lower r^2 values (0.61 and 0.38 respectively - Table 25).

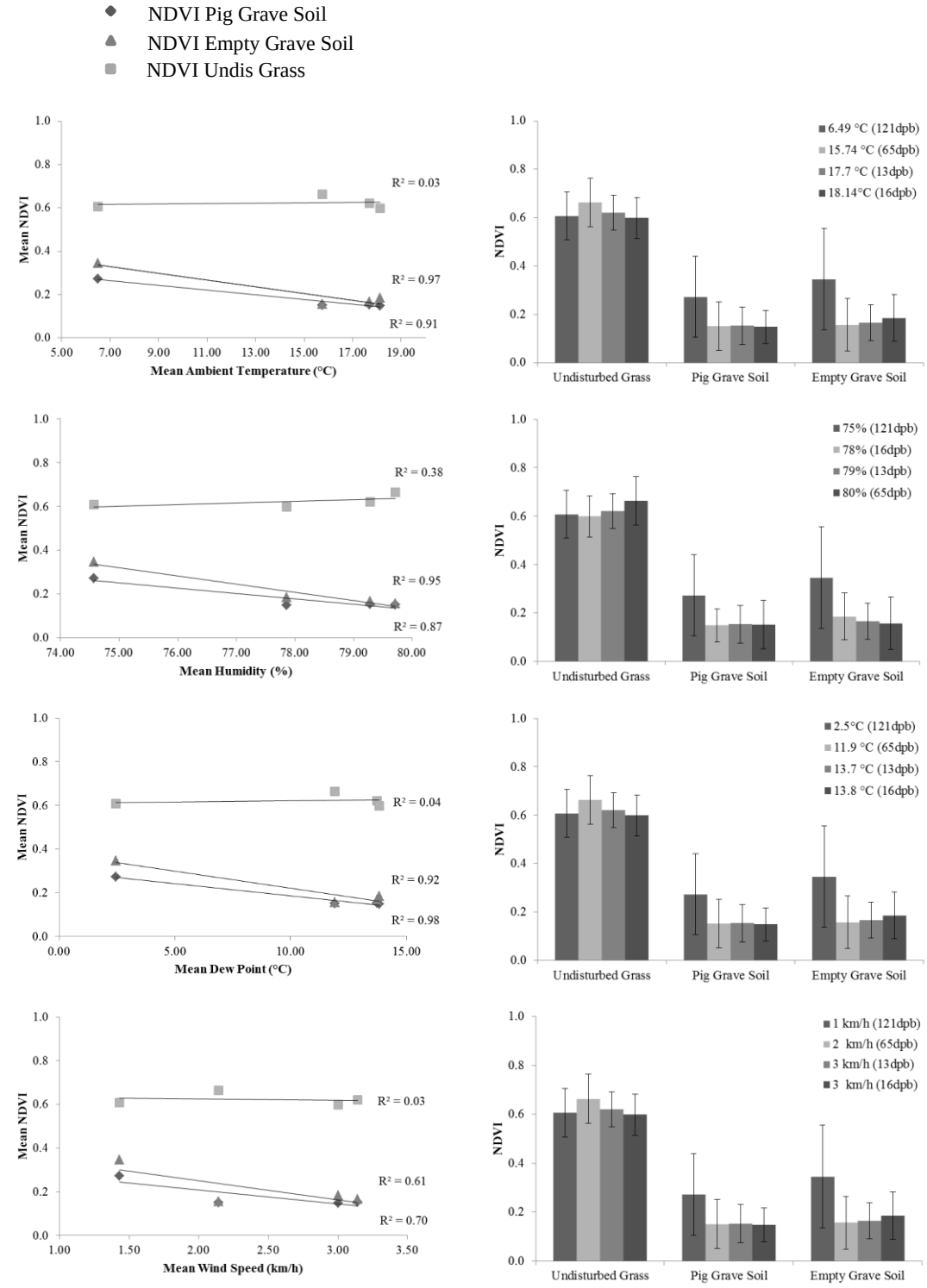
NDVI Pig Grave Soil
NDVI Empty Grave Soil
NDVI Undis Grass
Mean NDVI
Mean Ambient Temperature (°C)
R² = 0.03
R² = 0.97
R² = 0.91
NDVI
6.49 °C (121dpb)
15.74 °C (65dpb)
17.7 °C (13dpb)
18.14°C (16dpb)
Undisturbed Grass
Pig Grave Soil
Empty Grave Soil
Mean Humidity (%)
R² = 0.38
R² = 0.95
R² = 0.87
75% (121dpb)
78% (16dpb)
79% (13dpb)
80% (65dpb)
Mean Dew Point (°C)
R² = 0.04
R² = 0.92
R² = 0.98
2.5°C (121dpb)
11.9 °C (65dpb)
13.7 °C (13dpb)
13.8 °C (16dpb)
Mean Wind Speed (km/h)
R² = 0.03
R² = 0.61
R² = 0.70
1 km/h (121dpb)
2 km/h (65dpb)
3 km/h (13dpb)
3 km/h (16dpb)

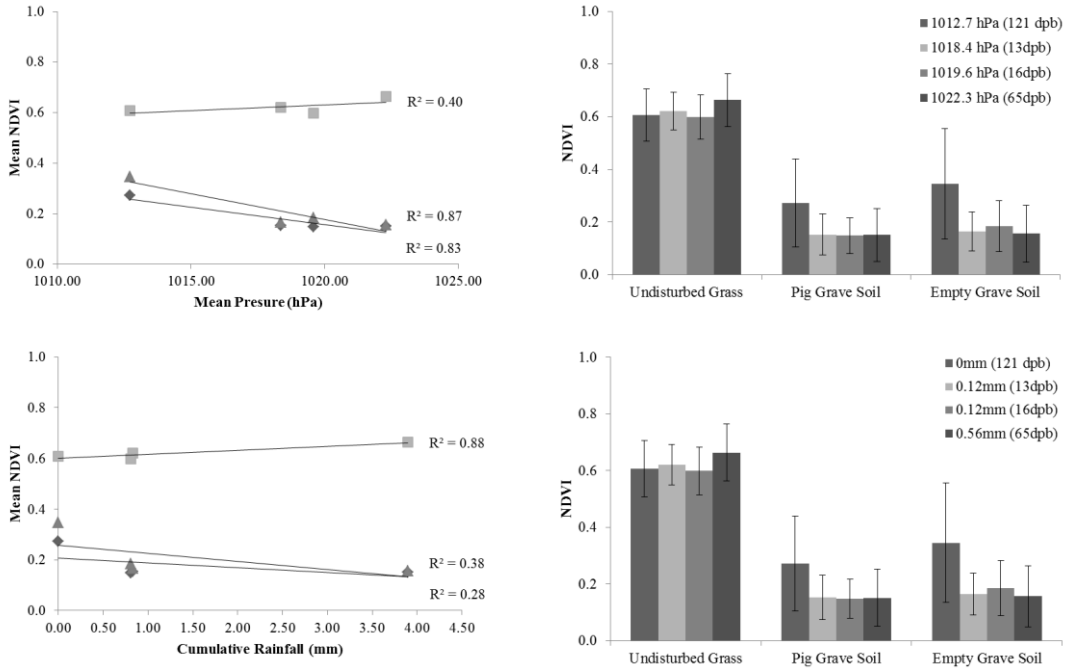

Figure 83 - The relationships existing between NDVI of the soil halves of the graves relative to the control (undisturbed grass) and meteorological variables, one week prior to spectra collection.

Table 25 - Description of the direction and strength of the linear relationship between NDVI calculated from convolved GER1500 data on the soil half of the experimental graves and meteorological variables (one week prior to data collection).

FUNCTION		Pig Grave Soil	Empty Grave Soil	Undisturbed Grass
SLOPE	NDVI vs Temp	-0.01	-0.02	0.00
	NDVI vs Humidity	-0.02	-0.04	0.01
	NDVI vs Dew Point	-0.01	-0.02	0.00
	NDVI vs Wind Speed	-0.06	-0.09	-0.01
	NDVI vs Pressure	-0.01	-0.02	0.00
	NDVI vs Cumul. Rainfall	-0.02	-0.03	0.02
CORREL (r)	NDVI vs Temp	-0.98	-0.95	0.18
	NDVI vs Humidity	-0.93	-0.98	0.62
	NDVI vs Dew Point	1.00	-0.96	0.21
	NDVI vs Wind Speed	0.92	-0.78	-0.16
	NDVI vs Pressure	0.83	-0.93	0.63
	NDVI vs Cumul. Rainfall	0.37	-0.61	0.94
RSQ (r^2 or %)	NDVI vs Temp	0.97 97%	0.91 91%	0.03 3%
	NDVI vs Humidity	0.87 87%	0.95 95%	0.38 38%
	NDVI vs Dew Point	0.98 98%	0.92 92%	0.04 4%
	NDVI vs Wind Speed	0.70 70%	0.61 61%	0.03 3%
	NDVI vs Pressure	0.83 83%	0.87 87%	0.40 40%
	NDVI vs Cumul. Rainfall	0.28 28%	0.38 38%	0.88 88%

5.2.6.3 Summary of results – relationships between NDVI and meteorological variables one week prior to spectra collection

Based on the investigation into the relationship between NDVI of the burial surfaces and meteorological variables one week prior to spectra collection, it was found that the linear relationships are the same for the pig grave regardless of surface type (i.e. turf or soil); the exception being for the soil surface where humidity had a stronger negative relationship than for the grass surface. The empty grave, for both surfaces, exhibited predominantly negative relationships, with the turf surface having one weak positive correlation; the correlation coefficients for the soil surface exhibited all negative correlations that are stronger than those of the grass surface. The relationship between NDVI and the varying surface types were also investigated for both two and four weeks prior to spectra collection, the results of which are located in Appendix 2.

5.3 Discussion

5.3.1 What is the relationship between decomposition and NDVI?

NDVI was not affected by decomposition up to 121 days post burial. This was observed through the lack of variation in NDVI across the surface types, throughout the study period. This may be due to the timing of the study, being undertaken from August through to December (summer – autumn – winter transition), where the browning of vegetation occurs and senescence commences, whereas, variations in NDVI are most visible during the growing season. Throughout this period, ambient temperature decreases. Consequently, it is probable that the rate of decomposition decreased throughout the study period and therefore, did not affect the NDVI of the surface vegetation.

The relationship between decomposition derived from geophysical survey responses and NDVI has not been previously investigated. Consequently, it is important to consider the variables that affect both geophysical survey responses and the rate of decomposition. Geophysical surveys are known to be affected by climatic and geological variables; with geophysical responses from forensic clandestine burials varying more than those from obtained from archaeological graves (Pringle et al. 2012). Therefore, it is imperative that meteorological variables are considered alongside the geophysical responses recorded (Jervis et al. 2009b).

Electromagnetic quadrature surveys conducted on both the pig and empty grave found that, the conductivity of the pig grave was consistently higher than the empty grave and also the undisturbed ground. The mean conductivity of the pig grave increased with each survey, peaking at 121 days post burial, suggesting that decomposing soft tissue was present within the grave throughout the duration of the study. However, the temperatures recorded by the data loggers within the pig grave, indicated that the decomposition process was slow during the first 121 days post burial; therefore limiting the decomposition fluid produced. This would have limited effect on the conductivity of the pig remains and of the grave. However, climatic factors, namely precipitation, were found to have affected the undisturbed ground, with higher conductivities recorded compared to the empty grave, and to some extent the pig grave. Consequently, fluctuations in soil moisture are directly related to precipitation events and would have contributed to the high conductance anomalies observed, rather than being solely due to the presence of decomposition fluid.

Throughout the study, the conductance of the empty grave was lower than both the pig grave and the control, undisturbed ground; this was due to differences in compaction. The fill of the empty grave was not compact, allowing moisture to permeate through the grave column with relative ease, resulting in the empty grave being dryer compared to both the pig grave and the undisturbed ground. In contrast, the undisturbed ground was comprised of clay and therefore, rather than moisture draining away it was retained resulting in high conductance being observed (Pringle et al. 2012). Although this response would be similar to that produced by a grave, the response observed would be greater and therefore, it is likely that this would be interpreted as waterlogged ground rather than a grave.

The resistance surveys carried out on the pig and empty grave found that initially the resistance of both graves was high, this being attributable to the backfill being loose, less compact and therefore dryer than the surrounding soil. This finding was consistent with those reported by Bray (1996 cited in Cheetham 2005) and Jervis and Pringle (2014). In contrast, at 43 days post burial, both the pig and empty graves were low resistance anomalies; the empty grave exhibiting higher resistance in comparison. The low resistance observed for the pig grave is an indicator of increased moisture, a mixture of rainfall and decomposition fluid that had pooled on top and surrounding the layer of disarticulated pig remains; in addition to the presence of the remaining flesh which was conductive. This was found in a study by Carter et al. (2010), who buried juvenile rats to understand how soil moisture influences the breakdown of cadavers following burial in sand and clay burial conditions. The availability of moisture was found to be controlled by soil texture, structure and the availability of moisture is determined by the forces with which water is held between

soil particles (matric potential) (Carter et al. 2010). It was found that grave fill moisture content modified the relationship between temperature and cadaver decomposition, whereby decomposition was more rapid in wetter grave fill. However, once the soil became too wet the rate of decomposition decreased, regardless of temperature (Carter et al. 2010). It was suggested that the slower decomposition rate could be attributed to a decrease in aerobic microbial metabolism (Carter et al. 2010). Thus, grave fill moisture content was found to be the dominant environmental variable affecting cadaver decomposition in soil, through the modification of the relationship between temperature and cadaver decomposition. It is possible that due to the climatic events throughout the duration of the study including increased precipitation and decreasing ambient temperatures, in addition to the soil type and compaction of the grave column, that decomposition of the pig remains was limited. Therefore, by reducing the rate of decomposition any potential impacts on the vegetation and soil present at the grave surface were also reduced and/ or restricted.

5.3.1.1 Detectability

The disturbance caused when creating the graves resulted in both the pig and empty graves being detected using electromagnetic and resistance surveys for the duration of the study. The disturbance caused the grave fills to be less compact, compared to the surrounding soil matrix. The empty grave had a loose grave fill that was free draining and also contained voids which caused low conductance and high resistance anomalies to be observed in the electromagnetic and resistance surveys respectively. The pig grave had an equally loose grave fill but had a layer of disarticulated pig material which contained moisture and also prevented fluid from draining away freely. The high conductance and low resistance anomalies observed were likely due to the decomposition fluids produced as well as the presence of remaining flesh within the grave. Although decomposition within the pig grave was slow, the decomposition processes will have somewhat contributed to the overall moisture content within the grave; this is suggested by the consistent rise in conductivity over the study period. The conductivity and resistance of the graves were also likely to have been influenced by meteorological variables including precipitation and the ambient air temperature.

As the ambient temperature decreased, the ground temperature also decreased (recorded by the data loggers within the pig grave). Therefore, the ground would not have dried as readily compared to when the ambient temperature was higher. The decrease in temperature was observed in the data at both 30cm and 50cm BGL; the temperature was more stable at the

lower depth. This decrease in ambient temperature may have slowed down the rate of decomposition and potentially caused it to cease over the winter (Rodriguez and Bass 1985). If the study had continued into Spring/ Summer 2014, it is likely that decomposition would have commenced again with increases in ambient temperature.

5.3.1.2 How long can graves be located using electromagnetic and resistivity surveys?

An empty grave could be located using electromagnetic quadrature surveys (using a vertical magnetic direction orientation) up to 70 days post burial, in similar environmental conditions (i.e. similar subsoils). However, this is dependent on the climatic events prior to the survey. Empty graves appear to be less easily detectable, as they exhibit a signal which can be lost in the background response relatively soon post burial. In this study, the undisturbed ground in both the electromagnetic and resistance surveys was affected by meteorological events, particularly precipitation, causing an increase in soil moisture and therefore, increased conductivity and decreased resistance. Soil particle size is integral to retention of water, as clay has a small particle size it retains water well compared to other soils i.e. sandy loams (Bethell and Carver 1987). The empty grave had lower conductivity than both the undisturbed ground and the pig grave, which was caused by the presence of uncompact soil which allowed water to drain freely through the grave column. Consequently, the grave fill was dryer than the surrounding soil matrix.

From this study it has been evidenced that a grave containing disarticulated pig remains, could be located at least up to 121 days post burial using electromagnetic quadrature surveys; in similar environmental conditions. The results obtained indicated that the pig grave could be detected throughout the duration of the study due to the contents of the grave remaining conductive. Climatic variables including increased levels of precipitation and decreasing ambient temperatures throughout the duration of the study increased the moisture content of the graves. At 70 days post burial there is a peak in the percentage difference between the grave and the undisturbed ground. During this study the graves were detectable between 14 – 70 days post burial at this site.

For resistance surveys, it was found that, as electrode separation increases, resistance decreases until at depth (~1.5m nominally) the pig grave is comparable to the undisturbed ground i.e. the percentage difference is small and the resistance is low. The decreasing resistance at wider electrode separations indicates the presence of pig remains. However, whether the pig graves would be successfully detected, or not, would be dependent on the

grave depth and the orientation of the geophysical equipment during the survey. From this research, it was found that using resistance surveys both the pig and empty grave were detectable up to a maximum of 121 days post burial. Similar to the results from the electromagnetic surveys, there is an increase in the percentage difference between the pig and empty grave, compared to the undisturbed ground up to 70 days post burial, after which the percentage difference decreases. Therefore, if a disturbance was present and a grave was suspected in similar environmental conditions, resistivity surveys are likely to locate the disturbance synonymous with a grave. Resistance plots, particularly at narrow electrode separations (i.e. 0.5m), are dominated by the signature caused by the disturbance from creating a grave. EM (vertical mode) provides one depth of analysis (bulk measurements to a nominal depth of 1.5m) and therefore, it is not possible to isolate or analyse the changes in conductivity occurring with depth. Furthermore, the orientation of the EM is not sensitive at the surface but at 30cm and falls off as depth increases.

The results obtained from both the electromagnetic quadrature and resistivity surveys found that the percentage difference between the pig and empty grave compared to the undisturbed ground peaked at 70 days post burial (October 2013). This peak corresponded to the period where increased precipitation and decreasing ambient temperatures were recorded, indicating that the geophysical survey results obtained were affected by climatic events; which in this case enabled the graves to be more easily detected. Further studies are required to ascertain the impact of climatic variables throughout seasons and for different soil types, to better understand how the deployment of such geophysical techniques will impact the success or failure to locate mass graves.

5.3.2 What is the relationship between grave surface and NDVI?

The relationship between grave surface type and NDVI has not been investigated previously. This research found that NDVI can differentiate between the grass and soil halves of both pig and empty graves, particularly at 13 and 65 days post burial; with the NDVI of the grass being higher than that of the soil. However, it was not possible to differentiate between a grave containing pig remains and an empty grave, using NDVI from 65 up to 121 days post burial. The reasons for this could be the length of the study, the time of the year that the study was undertaken and/or that decomposition appeared to have no impact on NDVI within this time frame. The study was undertaken from August through to December 2013. As has been mentioned, the limited decomposition which occurred within the pig grave was possibly due to environmental conditions i.e. low ambient temperature, increased

precipitation events and the presence of clay soil. The vegetation on the surface of both graves was affected by the decreasing ambient temperature and was likely entering senescence at the later stages of the study due to the approaching winter. In addition, the soil halves of both graves were not re-colonised over the duration of the study. Thus, making any attempt to analyse the stress of the colonising vegetation on the graves, and comparing this with the background and other vegetated halves of the graves, impossible.

Further work should be conducted to monitor vegetation colonisation on the grave surfaces, as part of a long term study and to record the stress of vegetation using the NDVI collected by field spectroscopy, with focus placed on the growing season. This was not achievable within the timeframe of this research at this site; however, the following chapter studies variations in NDVI on graves containing mammalian remains as well as empty graves, over a decadal time frame using archive multispectral orbital imagery.

5.3.3 What is the relationship between the thickness of the pig material and NDVI?

A relationship between the thickness of the pig material and NDVI was not observed for the duration of the study, for the soil nor the grass surface. This was initially unexpected, on the basis that the thicker the pig material the more decomposition would occur, the by-products of which would affect the vegetation at the grave surface. However, as has been mentioned, little decomposition appeared to have occurred within the pig grave; likely due to a combination of low ambient temperature, precipitation events and the soil particle size. If the graves been interred at the start of the year, during spring and allowed to proceed through the seasons, it is probable that with increases in ambient air temperature the rate of decomposition would have increased.

Caccianiga et al. (2012) found that when monitoring the vegetation dynamics and recovery above pig graves, the recovery was very slow for all graves throughout the summer and autumn, even when the graves were interred in May. Recovery was noted in November and was found to accelerate the following March (approximately ten months post burial). Furthermore, it was found that no difference existed between the pig and control graves, as a result it was concluded that decomposition played a non-critical role in vegetation recovery. Therefore, further research is required for an equivalent length of time and in the same environmental conditions as this study, but which commences in the spring, the results of which could be compared to the findings presented here, as well as a longer term study which could be compared to the findings of Caccianiga et al. (2012).

5.3.4 What is the relationship between the thickness of the overburden and NDVI?

A moderately strong linear relationship was found to exist between NDVI and the thickness of the overburden for the soil half of the pig grave, although this relationship weakened over time. Whereas, the relationship between NDVI and the grass half of the pig grave was found to be more complex, with a weak linear relationship. Caccianiga et al. (2012) conducted a similar study in Italy, where pig carcasses were buried and the grave surfaces monitored to assess the effect on vegetation structure and composition during colonisation and post recovery; the depth of the graves ranged between 80-90cm and had a 40cm overburden, which is equivalent to the overburden used within this research. It was suggested that the thickness of overburden could be one of the principle factors affecting the influence of the burial on surface vegetation; a 40cm overburden was suggested to have had little effect on the plant community that eventually colonised the graves. This supported findings from Van Belle et al. (2009) and also from France et al. (1992) who suggested that the presence of a decomposing pig carcass did not significantly affect plant growth. It is worth noting that this research was not focussed on plant growth per sae but more the monitoring of plant stress, through the calculation and comparison of NDVI. To investigate the relationship between NDVI and the thickness of the overburden, further studies are required which compare identical grave structures and contents with varying thicknesses of overburden over a longer study period.

5.3.5 What is the relationship between grave depth and NDVI?

A linear relationship existed between NDVI and depth of the pig grave that varied in strength over time depending on the surface type. This relationship was unexpected as although the grave depth varies across the grave, it does not change over time. The observed relationship is hard to explain, one interpretation is, that this is an apparent relationship resulting from only one variable (NDVI) changing over time with the other, grave depth, remaining constant.

5.3.6 What is the relationship between meteorological variables and NDVI?

The relationships between the two surface types were found to differ regardless of grave contents. The grass halves of the graves had the strongest relationships with, and therefore are most likely, to be affected by temperature, dew point and wind speed. The soil halves of both graves exhibited strong relationships with dew point, temperature and humidity. The strength of the relationships were found to differ with grave contents, with the pig grave having the strongest relationships. The relationships between NDVI from the empty grave and the meteorological variables were weaker compared to the pig grave. The relationships observed do not link directly to causality, hence they are reported with caution as the complexities are unexplained and it is unclear how the variables interact and influence each other. The undisturbed grass was most strongly correlated with rainfall, pressure and humidity followed by temperature; this is representative of the background vegetation at the site. There are no examples of published literature with which the results of this subsection can be compared, i.e. variations in NDVI over time for the graves, which is for all intensive purposes disturbed ground. Thus, to understand the impact of climatic variables on NDVI in general, it has been necessary to report the findings of Hou et al. (2015) who used the GIMMS NDVI dataset to investigate variations in NDVI and how these related to climate. It was found that the relationship between NDVI (of undisturbed ground) and temperature is positive and stronger than precipitation; thus, indicating that temperature was a limiting factor for the growth of vegetation in the Southwestern Karst Region of China (Hou et al. 2015). The climates between the region of China and the site at East Holme are clearly different however, due to the lack of relevant literature available; the results of the two studies will be compared. Areas of grassland were investigated and it was found that the resulting NDVI was correlated more strongly with temperature and precipitation whereas, at East Holme it was found that the relationship between precipitation and NDVI (from the area of undisturbed grass) was stronger ($r^2 = 0.875$) than that of temperature ($r^2 = 0.031$). Thus, the limiting factor influencing the NDVI was precipitation (taking into account the meteorological events one month prior to spectra collection). The differences reported in the relationships are likely due to geographical location and climate zone. To further investigate the relationship between NDVI on the grave surface and meteorological variables, it is important that the soil halves of the graves are allowed to colonise fully, as this will provide insights into the limiting factors for vegetation colonisation on disturbed ground which could then be used to understand these complex relationships further.

5.4 Conclusions

This study provided insights into whether disturbance resulting from the creation of small scale simulated mass graves, one empty and the other containing disarticulated porcine remains, could be detected up to 121 days post burial. This was investigated through two approaches, the first through the monitoring of NDVI from the surface of the mass graves using a hand held field spectrometer and the second, through regular geophysical surveys and monitoring of below ground temperature, to provide a spatial measure of the decomposition within the graves for the duration of the study.

It was found that the NDVI was unaffected by the presence of the buried mammalian remains up to 121 days post burial. This is thought to be due to the length of the study, which was relatively short and also the study being undertaken during the later summer – autumn – winter transition. During this period the ambient temperature was decreasing steadily, potentially inhibiting vegetation colonisation on the grave surface. It was found that the NDVI was affected by meteorological variables including temperature and dew point, with precipitation having a lesser impact in comparison.

However, although the study proved too short to fully understand the effect of the buried pig remains on NDVI, the disturbance resulting from the creation of the graves was observed up to 121 days post burial via both NDVI and geophysical surveys.

Through the results obtained via the geophysical surveys, both electromagnetic and resistance, it was found that artefacts of disturbance including loose grave fill and voids, in both the pig and empty grave were detected; allowing both graves to be differentiated from each other and also from the undisturbed, control area during the first 121 days post burial. The percentage difference in geophysical response from both techniques, between the pig and empty grave compared to the undisturbed ground peaked at 70 days post burial, during October 2013. This peak corresponded to the period where climatic events including increased precipitation and decreasing ambient temperatures were recorded. Therefore, it is clear that the results obtained from the geophysical surveys were influenced heavily by climatic factors and in the case of this study, enabled the graves to be more readily detected.

At 13, 16, 65 and 121 days post burial, significance was observed (*** $p<0.001$) in the NDVI values for all surface types compared to the control, undisturbed vegetation. However, no significance was found between the turfed halves or soil halves of the pig and empty graves. Therefore, suggesting that utilising NDVI would not aid in the differentiation between a full or empty grave, up to 121 days post burial. However, both graves were

detected and were able to be differentiated from areas of undisturbed vegetation. The graves were characterised by low NDVI, for all surface types; with the grass used to re-turf the surfaces exhibiting stress (via low NDVI), as a result of the disturbance. The soil halves of the grave consistently exhibited low NDVI, representative of soil with little to no vegetation recolonisation.

This research, in principal, has demonstrated that orbital remote sensing could be used to identify disturbance indicative of a mass grave; characterised by low NDVI that would persist over a period of time. Using a multispectral orbital platform such as Landsat, disturbance and/ or concealment could be detected, once located a targeted approach could be adopted employing geophysical surveys to identify the spatial extent of the mass grave. The deployment of a combination of methods and techniques has been advocated extensively within literature in the context of grave detection (France et al. 1992; Schmitt 2002).

This research suggests that in the event that a grave was turfed post creation or left as bare soil to naturally colonise, that this could be detected up to 121 days post burial. This research however has taken hand held measurements, close to the ground surface and then convolved the spectra to be equivalent to an orbital platform with a much greater distance between the ground and the instrument. Therefore, in this instance spatial resolution of the imagery and or pixel size was not an issue, however, when employing orbital platforms this should be given careful consideration. This will be investigated within the remainder of this research through the monitoring of large scale mammalian mass graves over a decadal time period and human mass graves in Bosnia and Herzegovina over in excess of 20 years.

6 A Multi-Platform, Multi-Temporal Investigation of Differences in NDVI and Surface Elevation Changes of a Large-Scale, Proxy Mass Grave (Foot and Mouth) over Decadal Time Scales to Provide a Pre-Operational Proof-of-Concept for Clandestine Human Mass Grave Prospection

This chapter aims to identify if NDVI can be used to detect large scale proxy mass graves containing mammalian remains, to provide a pre-operational proof-of-concept for clandestine human mass grave detection. Using archive multispectral imagery from orbital platforms prior to, during and post burial, variations in NDVI were observed over a decadal time period.

6.1 Location and Description of Field Site

The field site was the Former RAF Pershore airfield, near Throckmorton, Worcestershire, UK (Figure 84). The site is located on a natural plateau between the villages of Throckmorton, Lower Moor, and Upper Moor and ceased military operations in 1978. During the 2001 Foot and Mouth outbreak the site was used for the rapid mass burial of ~139,000 animal carcasses (sheep: 121,060, cattle; 12,295, pigs: 5,631 and deer: 400) between 4th April 2001 and 19th May 2001 (Det Norske Veritas 2003). The site was primarily chosen due to the presence of a Lias clay substrate, which was noted as a suitable material to contain burials due to its low permeability (Det Norske Veritas 2003). In 2001, nine burial cells (dimensions: L: 75m x W: 12.5m and L: 50m x W: 25m) were created to receive animal carcasses. Five cells, as well as half of a sixth were filled; the additional three remained empty and were backfilled with soil (both natural and contaminated). The land is currently leased from Qinetiq on a 25 year lease however, during the 2001 outbreak the land was owned by DEFRA (Worcestershire County Council 2011).

The site includes a unique combination of land cover types and areas of disturbance (Figure 85):

1. Foot and Mouth burial cells that were excavated, carcasses deposited, backfilled and then were allowed to colonise naturally. This is the area that has been used within this research as a proxy mass grave and will be referenced throughout this chapter as 'full burials'.
2. Foot and Mouth burial cells that were excavated, backfilled and grassed over, which are contemporaneous with the full burials. These cells contained no carcasses and will be referred to as 'empty burials'.
3. Archaeological sites identified at the time of the Foot and Mouth burial, that were excavated, backfilled and grassed over. These are considered contemporary disturbance containing no organic remains.
4. Landfill sites that were excavated, backfilled and grassed over, containing mixed organic and non-organic buried material.
5. Undisturbed, grass dominated areas. These were deemed control areas and will be referred to as 'undisturbed grass'.
6. Concrete runways and tracks.

A number of data sets exist for the site including, archive aerial photography, geophysical surveys and independent environmental reports (e.g. the Det Norske Veritas Environmental and Public Health Risk Assessment Report 2003). Although this experimental site is in close proximity to a landfill site and also areas of contemporary disturbance, neither of these will form a part of this thesis as they do not contain mammalian remains.

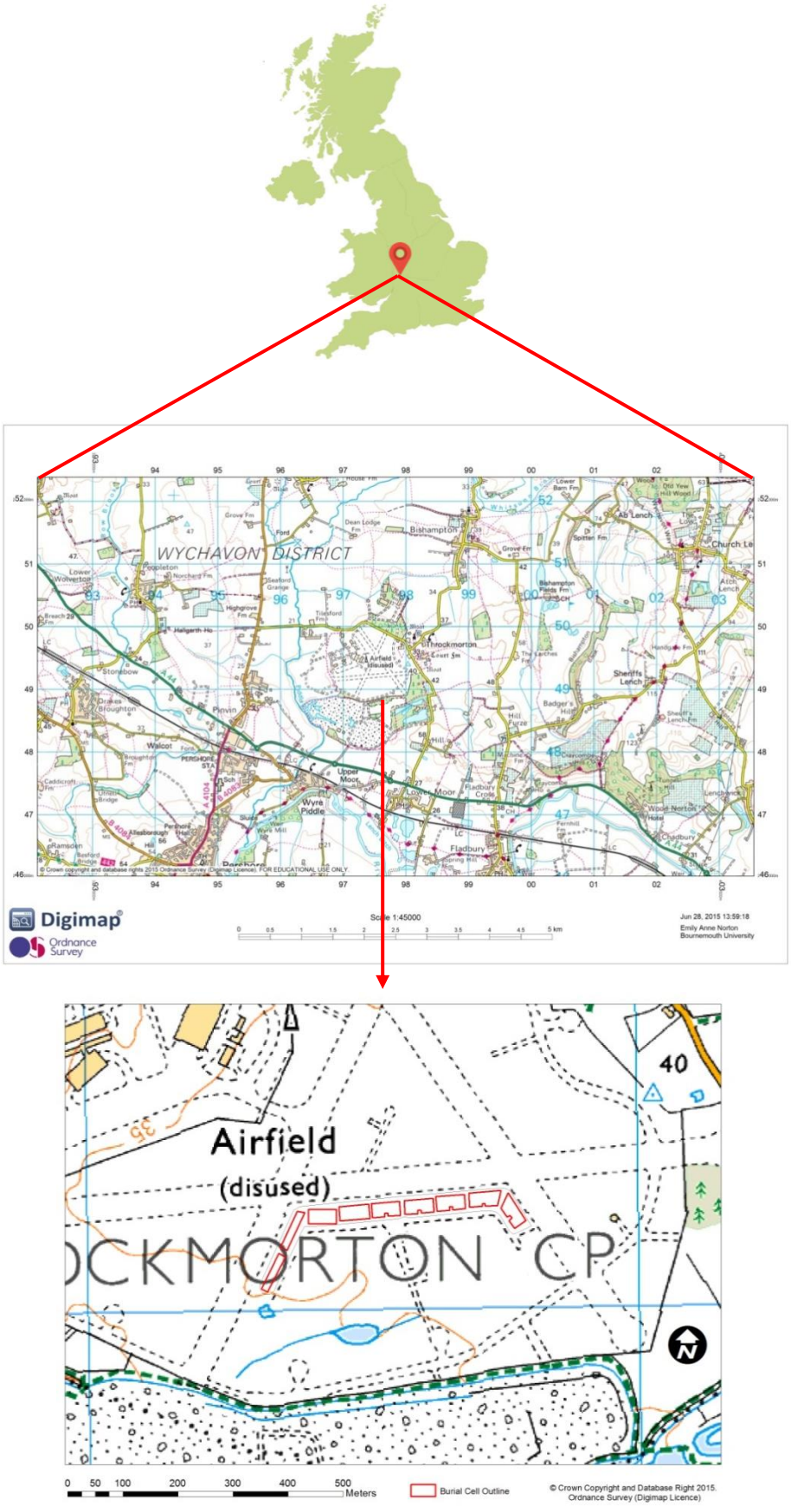

Figure 84 - The location of the Former RAF Pershore airfield in the context of the UK, the local area and the exact location of the burial cells (outlined in red).

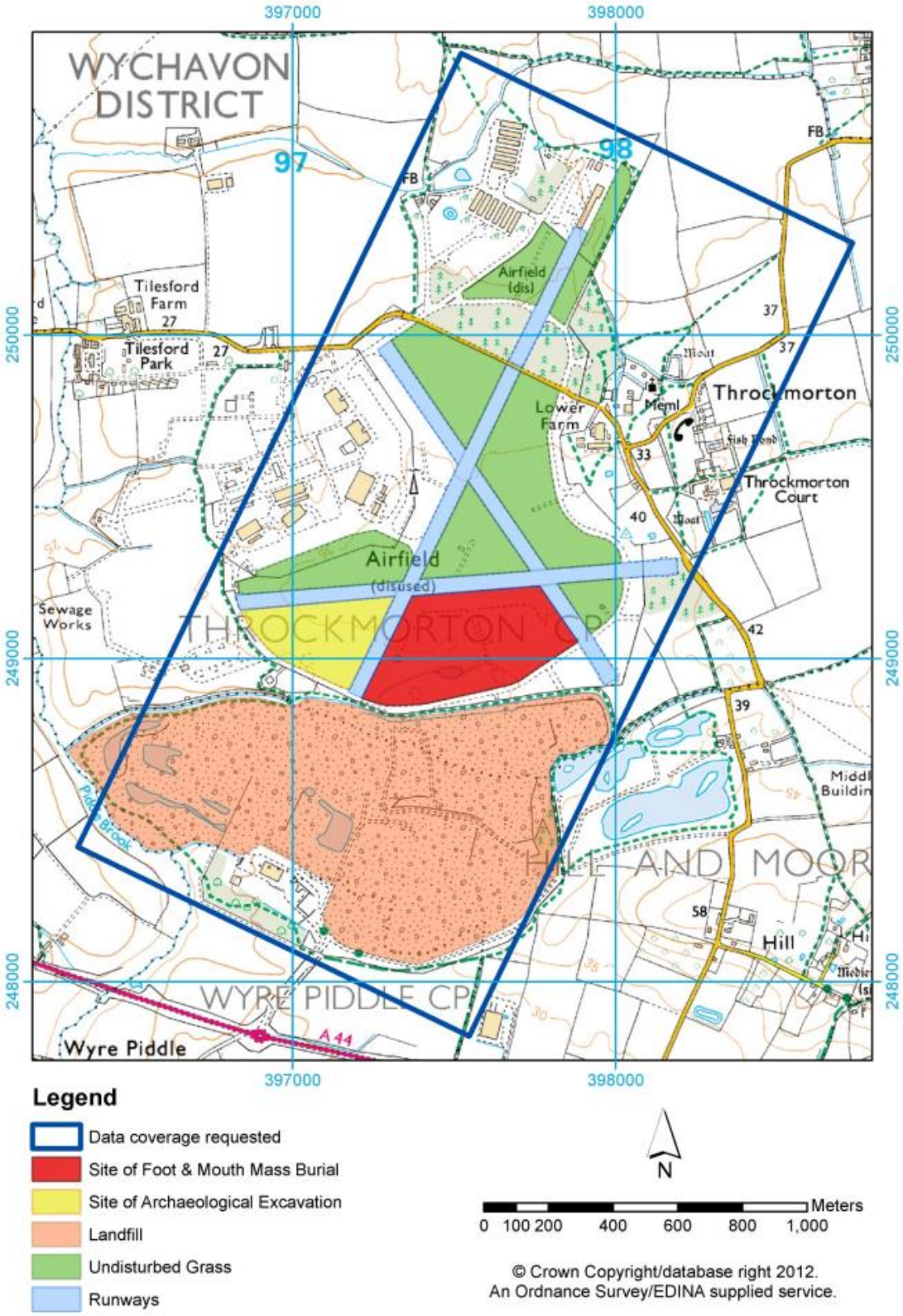

Figure 85 - Ordnance Survey map showing the research site and the variety of land cover types at the Former airfield at RAF Pershore.

6.2 The Foot and Mouth Burial Cells

The burial cells were designed and constructed to have minimal environmental impact, specifically on the surrounding land and nearby water courses (Figure 86: Det Norske Veritas 2003). The burial cells were not lined as they were surrounded by compact clay (Lias clay), with known low permeability. Det Norske Veritas' report (2003, Appendix II, p.20) notes that cells one to five contained carcasses and pieces of plastic sheeting; used to line the delivery vehicles. Cell six contained a large quantity of contaminated soil and remaining carcasses but was noted as being half filled. In contrast, cells seven through to nine contained soil and no mammalian remains (Figure 87). Cell six, will not be included within this research due to the fact that it is neither full nor empty. Following burial, the cells were intermediately capped with approximately one and a half metres of soil before being capped again after six months with an additional four to five metres of soil (a mixture of sub-soil and brown clay). This was then compacted with a 40 tonne vehicle (Det Norske Veritas 2003, p II.21), the area was not seeded and was allowed to colonise naturally.

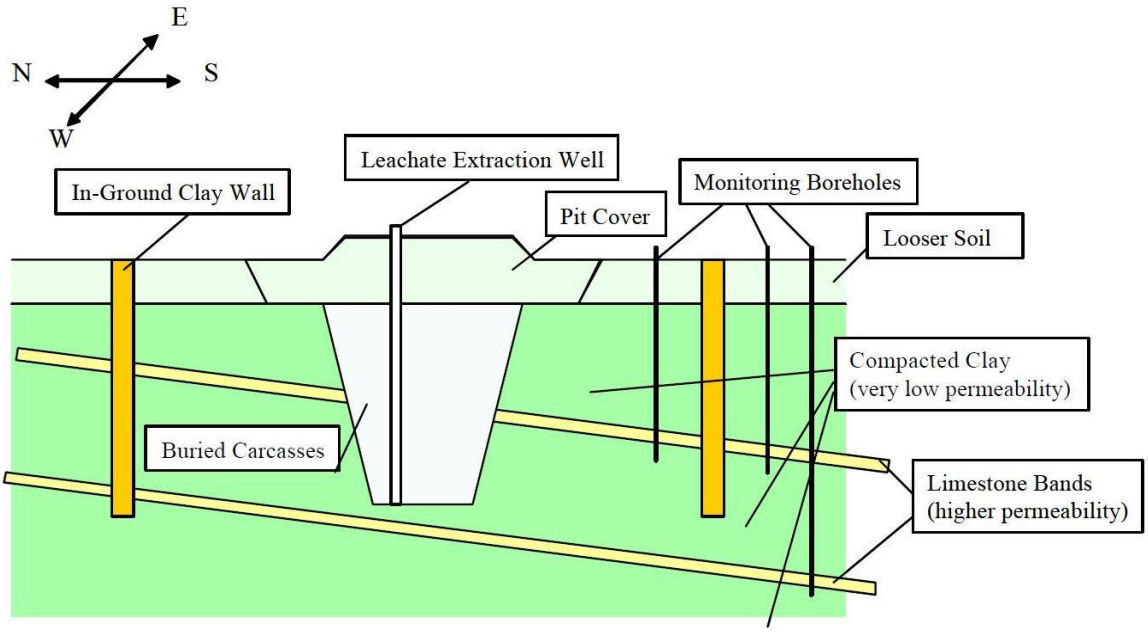

Figure 86 - Cross-section of the burial cell construction (Source: Det Norske Veritas 2003, p. V).

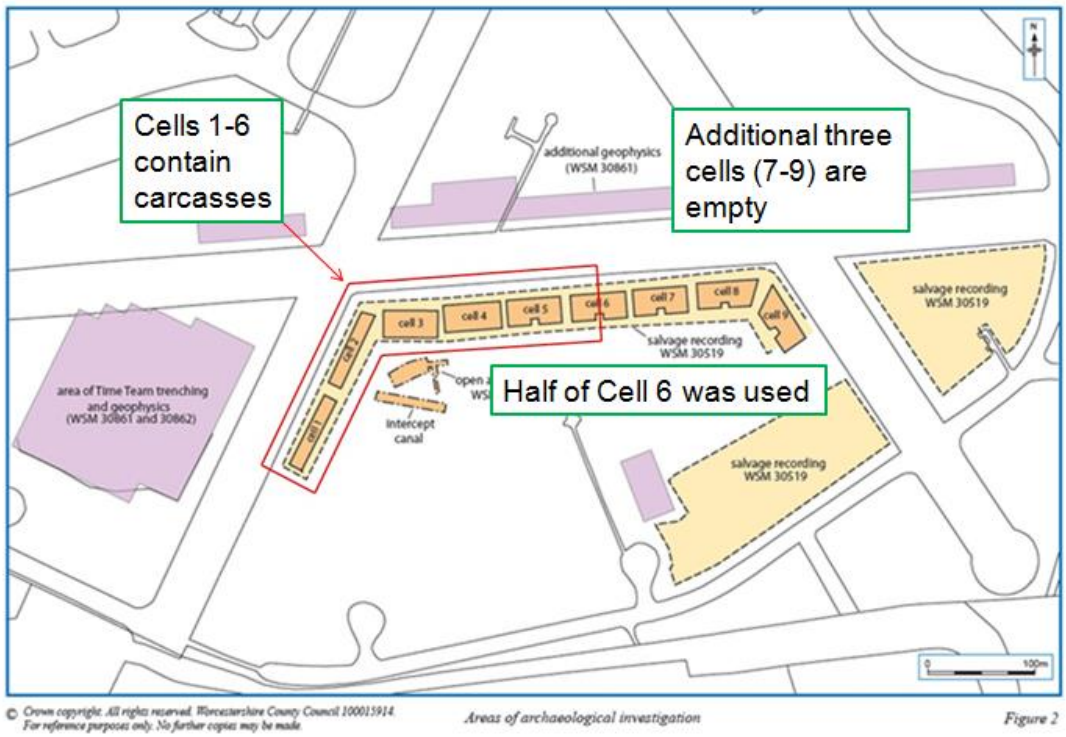

Figure 87 - Burial cell locations in the context of the site (Amended from: Worcestershire County Council 2011).

6.3 Archive Multispectral Satellite Imagery

In excess of 640 archive orthorectified (and georeferenced) images from four orbital platforms including Landsat, SPOT, DMC and RapidEye were located and acquired for the area around and including the Former RAF Pershore airfield, from 1990 through to 2011 (i.e. pre-, co- and post-interment). However, due to the presence of cloud, haze and misalignment in some of the images, only 172 of the images were used in the final analyses, the dates of which are presented in Figure 88.

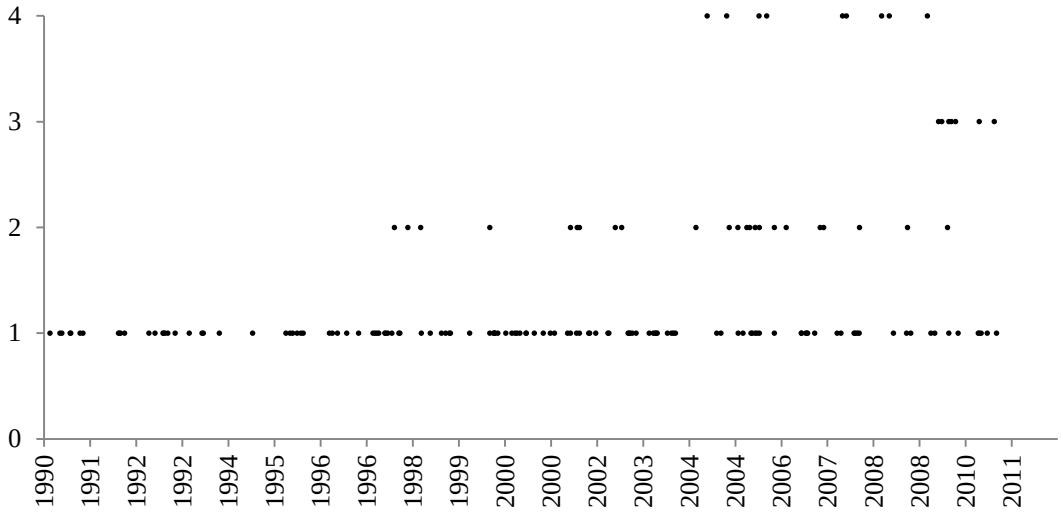

Figure 88 - The time series of 172 images from four orbital platforms used within this research (1 - Landsat; 2 - SPOT; 3 - DMC; 4 – RapidEye).

As mentioned in Chapter 4, the primary sensor was Landsat (both 5 TM and 7 ETM+). The imagery was obtained from the USGS EarthExplorer interface, USGS Earth Resources Observation and Science (EROS) Center Science Processing Architecture (ESPA) On Demand Interface (U.S. Geological Survey 2018) and also an ESA data grant[3]. The secondary sensor was DMC, the imagery was gifted by DMCii Ltd for use within this research. SPOT was the tertiary sensor and the quaternary sensor was RapidEye, both of which were obtained via an ESA data grant[3].

The majority (130) of the archive images used were Landsat images, obtained from either the USGS or ESA archives (Figure 89). All available 'cloud free' images were ordered for all sensors. However, on completion of the pre-processing routine, it was found that some images were hazy; potentially affecting the extracted NDVI values. Consequently, these images were omitted from the final NDVI time series. The number of images per year, from each platform, is presented in Figure 90.

[3] European Space Agency, Project ID: 26349

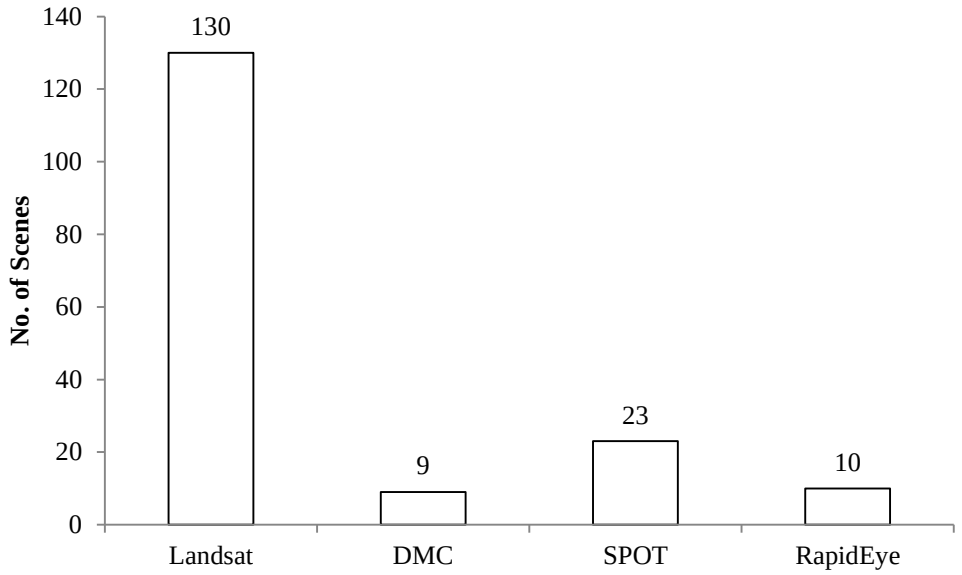

Figure 89 - The number of archive images used from each platform.

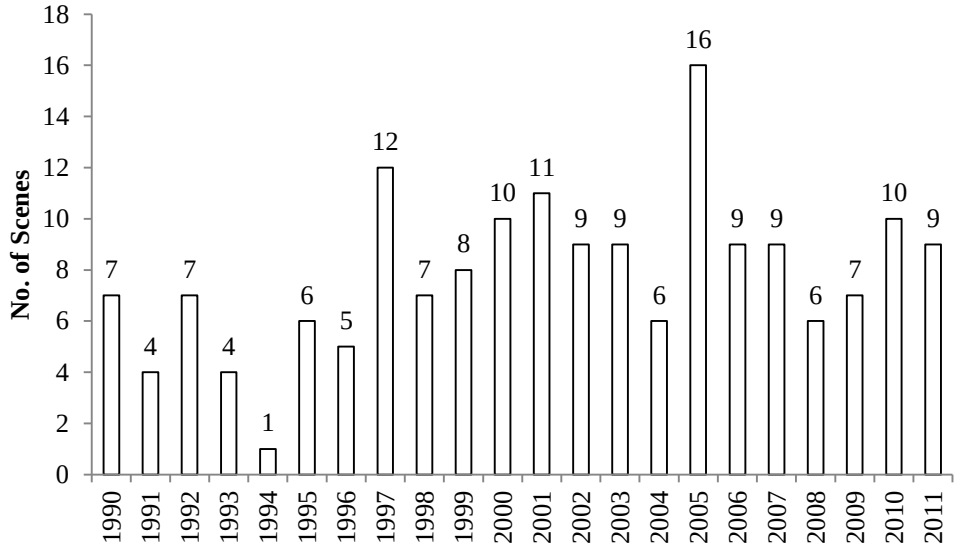

Figure 90 - The number of archive orbital images, from all four platforms, used in the final time series per year.

The rationale behind the choice of the platforms used has been discussed previously in Chapter 4. Therefore, the methods presented in the following section detailing the pre-processing routines, will be platform specific and relevant to this case study. Each scene was subject to atmospheric correction, fine registration and NDVI calculation, either in ENVI or at source (for example images of each processing stage see Figure 91). The scenes pre-processed at source were those obtained from the USGS's ESPA On Demand Interface and

will be discussed in detail in the sections below. Due to the imagery being acquired from various sources including, USGS EarthExplorer, USGS ESPA and ESA, the levels of pre-processing carried out by the imagery provider varied. For example Landsat 5 TM and Landsat 7 ETM+ were obtained from the USGS Earth Explorer interface and required significant levels of processing compared to RapidEye which required very little pre-processing. Having completed the necessary pre-processing, the scenes were spatially subset for ease of computing and exported into ArcMap (Version 10.1), where NDVI values were extracted for all land cover types using the sampling points. Within the following section, each pre-processing step is introduced in turn and includes variations specific to each platform.

6.3.1 Radiometric Calibration

All Landsat imagery, with the exception of those obtained from the USGS ESPA interface, was radiometrically calibrated using the Radiometic Correction tool within ENVI 5.3 (Harris Geospatial Solutions). The full extent of the scene and all spectral bands were inputted and FLAASH settings were applied, producing a radiance image that was in a band-interleaved-by-line (BIL) and floating band format; combining all bands into a single file.

Both the DMC and SPOT imagery did not require radiometric calibration as this had already been completed at source by the imagery provider. The RapidEye imagery, although radiometrically calibrated, was in band sequential format rather than BIL, therefore, it was necessary to carry out a conversion to enable atmospheric correction to be undertaken.

6.3.2 Atmospheric Correction

For the imagery obtained via the USGS's ESPA On Demand Interface, pre-processing was undertaken at source. All imagery obtained from the ESPA is generated by the Landsat Ecosystem Disturbance Adaptive Processing System (LEDAPS); originally developed by NASA. This routine applies MODIS atmospheric correction processes to Landsat imagery (5 TM and 7 ETM+); producing a reflectance product (USGS 2017).

6.3.2.1 Fast Line-of-sight Atmospheric Analysis of Hypercubes (FLAASH) Atmospheric Correction

FLAASH was used to atmospherically correct the Landsat and RapidEye imagery. Following the selection of the sensor type, the technical fields containing platform specific data, i.e. sensor altitude (km) automatically populated. To apply the correct atmospheric parameters for each scene, the details of the flight date and time (located within the scene's metadata file) were inputted; enabling an atmospheric model to be selected that took into account the AOI's location in terms of Latitude. The aerosol model chosen was consistently 'rural', as this best described the location of the Former RAF Pershore airfield. On advice of technical staff at BlackBridge (source of the RapidEye imagery), the aerosol retrieval tool was not used during the atmospheric correction process, as it required wavelengths that were not included within the RapidEye imagery. After the parameters above were set the FLAASH process was initialised.

6.3.2.2 QUick Atmospheric Correction (QUAC)

QUAC was chosen over FLAASH for the DMC and SPOT imagery, as ENVI (Version 5.3) did not have the multispectral pre-set parameters for these sensors. As both the DMC and SPOT imagery, were already in the BIL format, they were directly inputted into the QUAC tool. The sensor type was specified as being 'unknown' and the full extent of the image and all bands were considered during the correction process.

6.3.3 Fine Registration

Once the images obtained from USGS Earth Explorer were radiometrically calibrated and atmospherically corrected, each was geometrically registered using the Geometric Correction toolbox within ENVI 5.3. This ensured that when extracting the NDVI values in bulk from a data stack, values were extracted from the same pixels in each image. Therefore, the warp image was registered to a master image (Landsat 5TM - 30th April 2011). The master image was chosen as it geometrically matched a 1:25000 scale OS map of the airfield and surrounding area (downloaded from Digimap using Bournemouth University's Educational licence). Tie points were automatically generated using a general cross correlation matching method, before the generated tie points were filtered. As the red and near infrared bands were used for the calculation of the NDVI, it was decided that near infrared band in the warp

image, would be matched to the equivalent band in the master image. The number of tie points requested was set at 600, producing more than were required for the registration. The image registration process was then initialised, producing a registered warp image. Polynomial warping, the default setting, was carried, followed by cubic convolution resampling. The output pixel size was stated as being the same size as the imagery originally inputted (e.g. in the case of Landsat 30m x 30m). Prior to the image registration being completed it was necessary to run the warping process before exporting the resulting image and renaming it with a new filename.

6.3.4 NDVI Calculation

The spectral toolbox within ENVI was used to calculate the NDVI for the Landsat and SPOT scenes, obtained from USGS EarthExplorer and ESA respectively. Each radiometrically calibrated, atmospherically corrected, and geometrically registered image was inputted into the NDVI calculation tool and the full extent of each image was considered. For the calculation of the NDVI for Landsat images (TM and ETM+), the bands used were bands 3 and 4 (red and near infrared respectively) whereas, for the SPOT images, the bands used were bands 2 and 3 (red and near infrared respectively).

As ENVI did not have a pre-set option to automatically calculate NDVI for the DMC or RapidEye imagery, NDVI was calculated manually using the following equations in Band Math (Equation 7 and Equation 8). This took into account bands 2 and 1. for the DMC imagery and bands 3 and 5 for the RapidEye imagery, equating to the red and the near infrared bands respectively.

Equation 7 – Bandmath NDVI calculation for DMC Imagery

$$NDVI = \frac{(float(b1) - b2)}{(b1 + b2)}$$

Equation 8 – Bandmath NDVI Calculation for RapidEye Imagery

$$NDVI = \frac{(float(b5) - b3)}{(b5 + b3)}$$

6.3.5 Spatial Subsetting

All imagery was subset to the imagery with the smallest overall extent, in this instance this was RapidEye. Subsetting was primarily carried out for ease of computing.

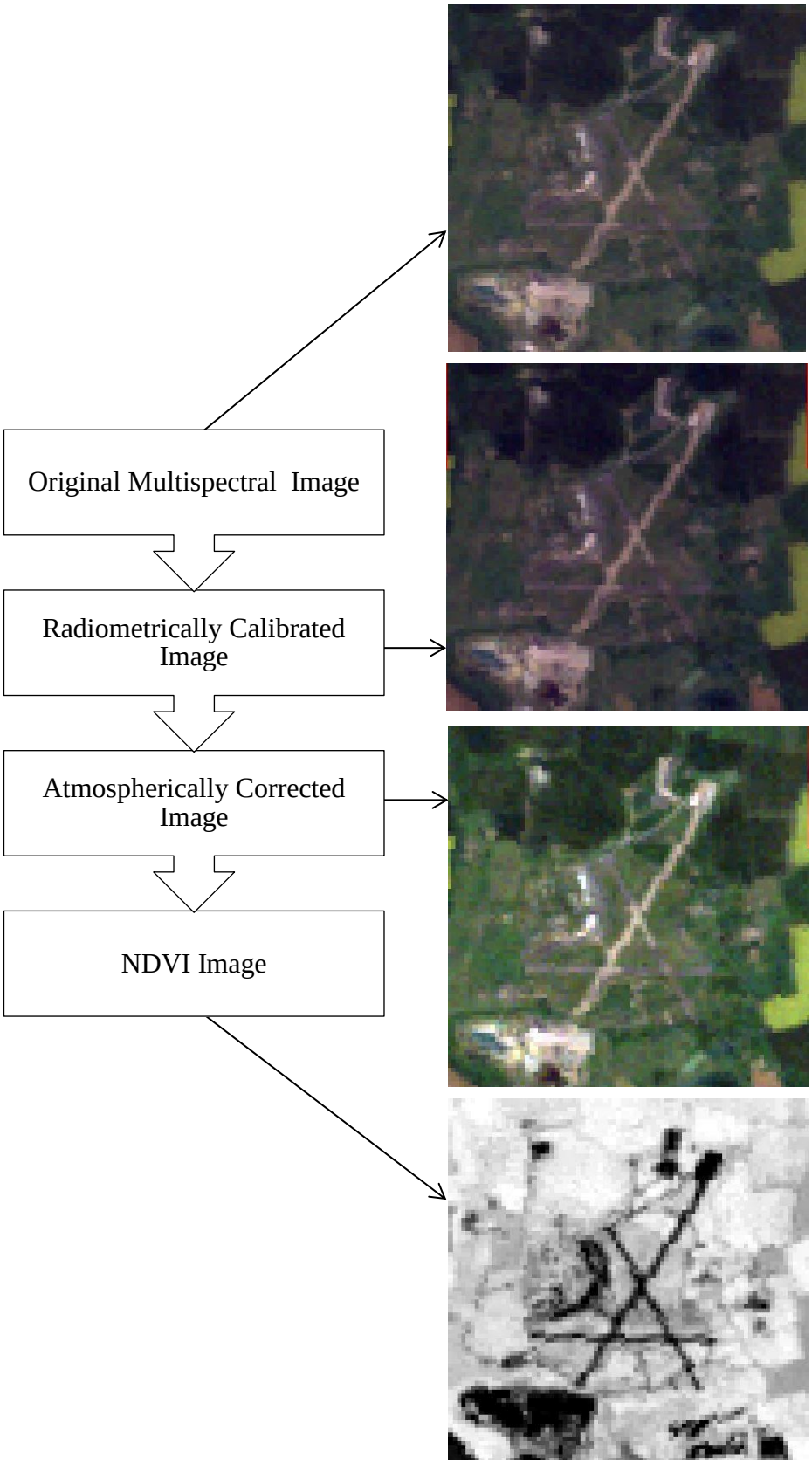

Figure 91 - Example images of the Former RAF Pershore airfield for each pre-processing stage using Landsat imagery. Images produced by the author.

6.3.6 Creation of Shapefiles / Sample Points in ArcMap

A 1:25000 OS map was downloaded from Digimap (using the Bournemouth University Licence), to georectify a map provided by Worcestershire Archaeology, which identified the areas of the site excavated during the creation of the burial cells. Shapefiles (i.e. polygons) were created in ArcMap for each burial cell, using the Worcestershire Archaeology map as a guide (Figure 87). Once the burial area was digitised, vegetated areas dominated by grass, were identified which remained stable for the duration of the study period; these are referred to as undisturbed vegetation throughout the chapter and are the control to which the NDVI values from the grave areas are compared. The control points were placed 40m away from any roads (thus taking into account the Landsat 30m pixel size and the potential error, ⅓ pixel) (Figure 92). Shapefiles (points) were also created for both the full and empty graves; a thirty by thirty metre fishnet was constructed and used to ensure that each point represented a single pixel (Figure 93). Overall, there were 15 points for the full burial, 10 points on the empty burials and 30 points for the undisturbed, control vegetation.

To visually assess whether the burial area, consisting of both the full and empty burial cells, could be located during their creation and how long differences in NDVI persisted; NDVI maps (13 in total) were created. Imagery collected between April to October, from 1999 through to 2011 (ten years post burial) was selected to enable investigations into variations in NDVI across the site, during both the growing season and peak of summer; prior to, during and post interment.

It was hypothesised that the creation of the burials would be initially detectable through a sudden reduction in NDVI, this being indicative of disturbance and of a surface predominantly comprised of soil. However, it was unclear how the NDVI values of the different surface types would respond to the disturbance and recover, compared to undisturbed areas, over a decadal timeframe. Furthermore, previous research such as Kalacska et al. (2009) has been conducted over relatively short timeframes i.e. 16 months.

The imagery used to produce the NDVI maps were kept in the original spatial resolution of the platform (Landsat – 30m; DMC – 32m; SPOT – 20m and RapidEye – 5m). A colour ramp, which ranged from red to green, was applied to each map with red representing low NDVI and green, high NDVI. For display purposes, cubic convolution interpolation was applied to each map, eliminating the pixelated effect and resulting in a clearer image. The 1:25000 OS map originally used for georectification of the site map, was retained beneath each NDVI map to provide context.

The Extract Multi Values to Points tool within ArcMap 10.3.1, was used to extract the NDVI values from each point within the images and across each surface type. The attribute table for each shapefile was saved as a .txt file and opened in Microsoft Excel where NDVI values were plotted for each surface. The data was formatted to enable processing within SPSS (IBM SPSS Statistics 24); from which boxplots were produced. Line plots were created for mean and median NDVI over time, including all observations, to visualise the trend in NDVI for the different surface types for the duration of the study period. Due to the noisy signal observed, a number of smoothing methods were trialled, including calculating a running average and exponential smoothing, the results of which are documented within Sections 6.4.3.1 and 6.4.3.2.

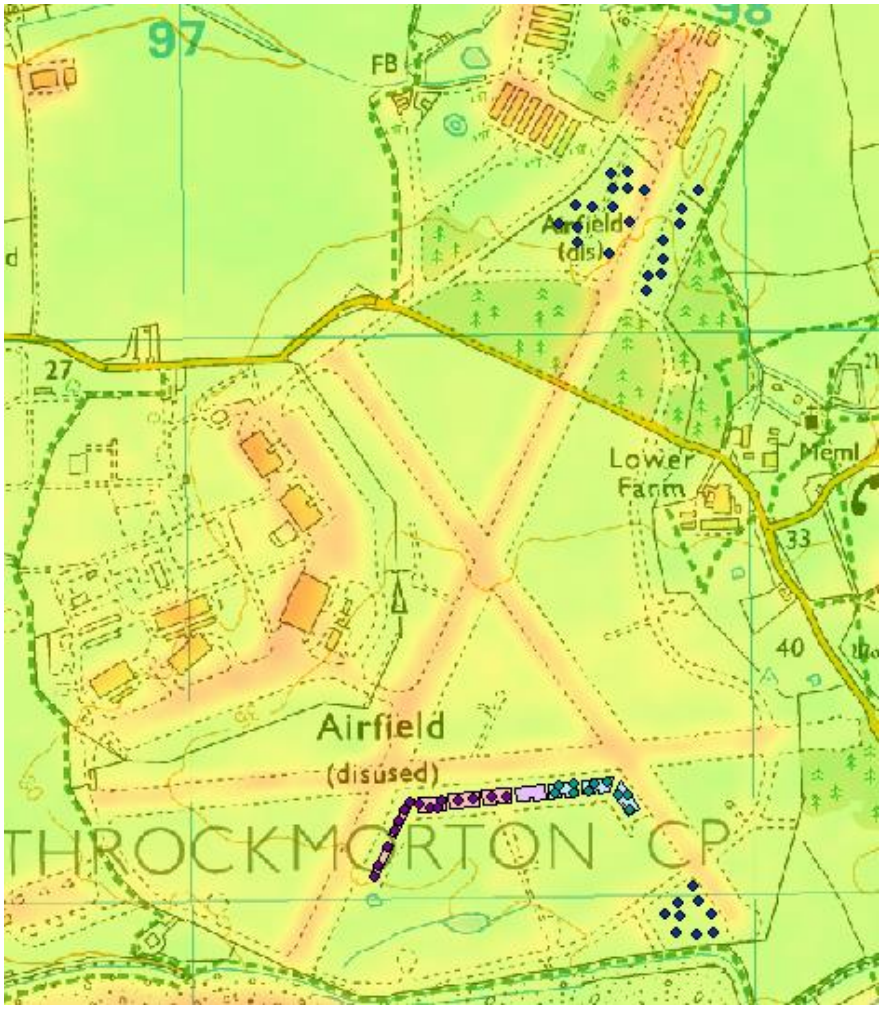

Figure 92 - NDVI map of Former RAF Pershore airfield illustrating the location of the sample points for full (red diamonds) and empty (green diamonds) burials along with those for the undisturbed, control vegetation (blue diamonds).

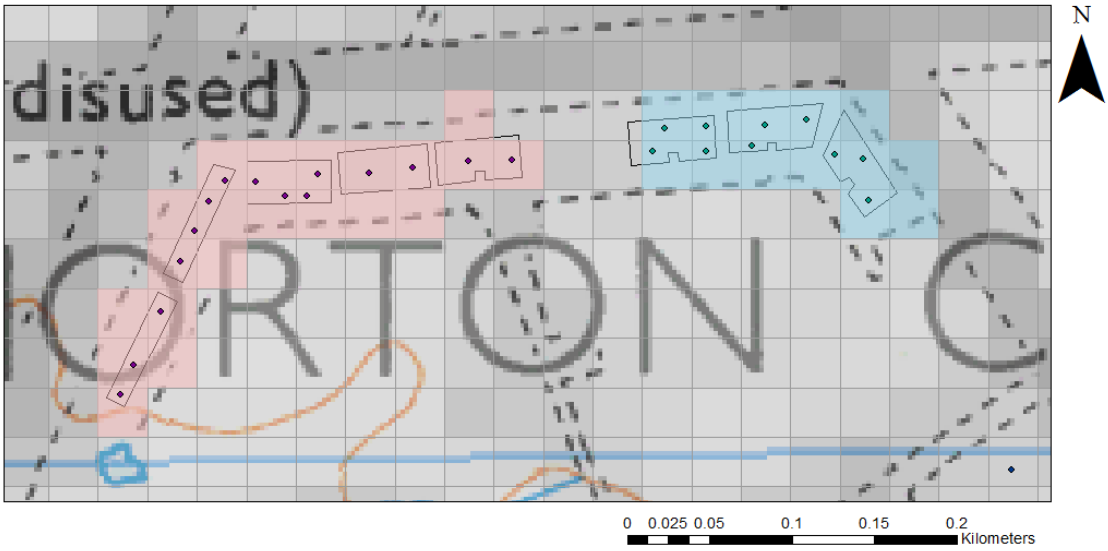

Figure 93 – Shapefile points for the full (pink) and empty (blue) burial cells, with one point created per pixel.

6.4 Results

6.4.1 NDVI maps and box plots of the full graves, empty graves and control vegetation at Former RAF Pershore airfield over the time scale of a decade post burial.

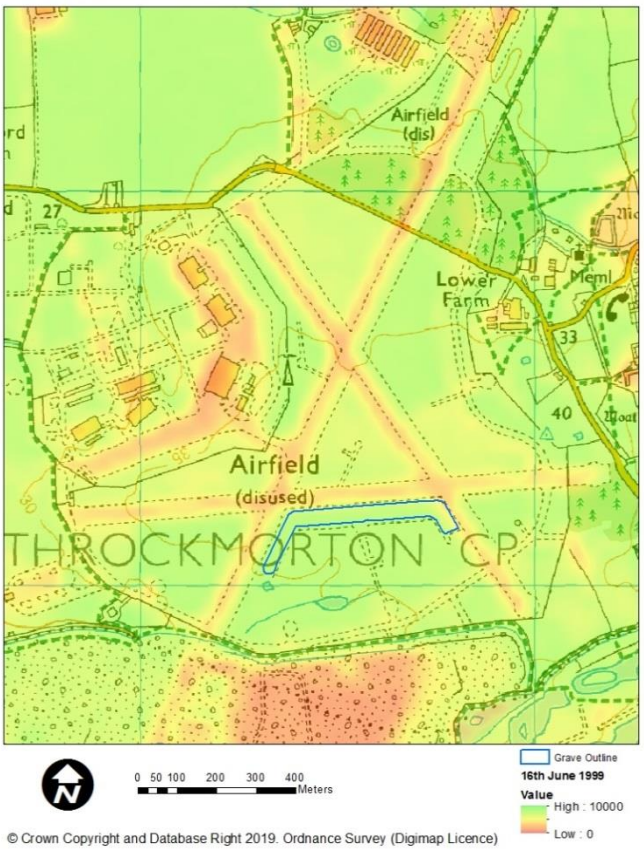

Figure 94 - NDVI map of the Former RAF Pershore airfield on 16th June 1999 – 11 months prior the creation of the burial site. Stable NDVI values are observed across the vegetated areas of the site.

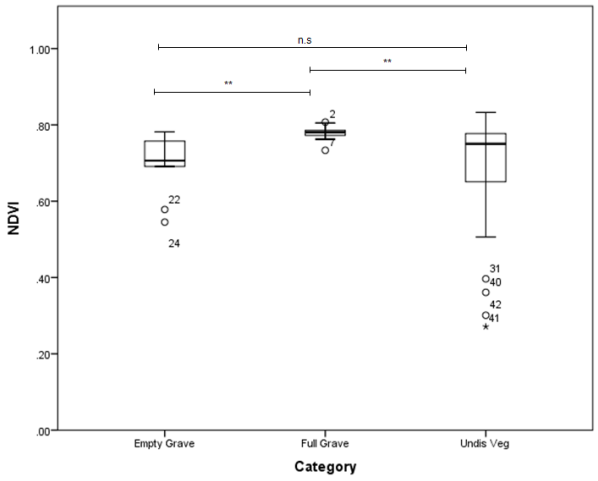

Figure 95 - NDVI across the three surface types on 16th June 1999. The NDVI values are similar across the site and are relatively high (* = p<0.001, ** = p<0.01, * = p<0.05, *n.s* = p>0.05).**

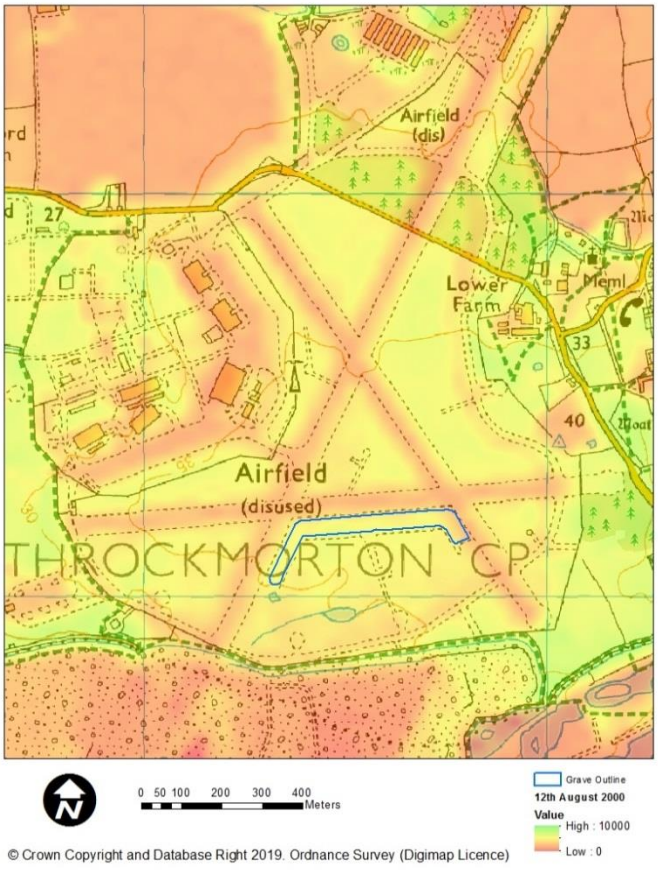

Figure 96 - NDVI map of the Former RAF Pershore airfield on 12th August 2000 – prior to grave creation. Low NDVI values are observed in the fields north of the site due to ploughing and south of the site, as this is a landfill site. However, stable NDVI values are observed across the vegetated areas of the site.

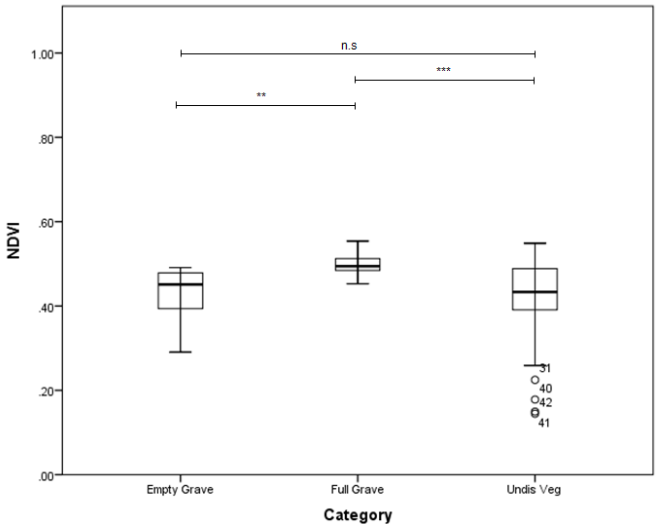

Figure 97 - NDVI across the three surface types on 12th August 2000. The NDVI values are similar across the site (* = p<0.001, ** = p<0.01, * = p<0.05, *n.s* = p>0.05).**

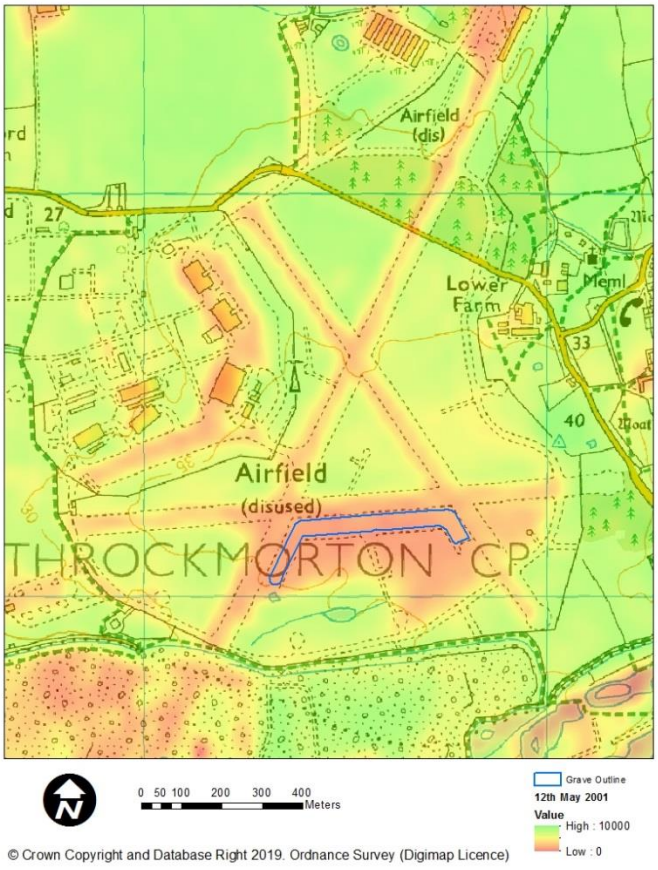

Figure 98 - NDVI map of the Former RAF Pershore airfield on 12th May 2001 – during the creation of the burial site. Low NDVI values are observed in the area where the graves were created.

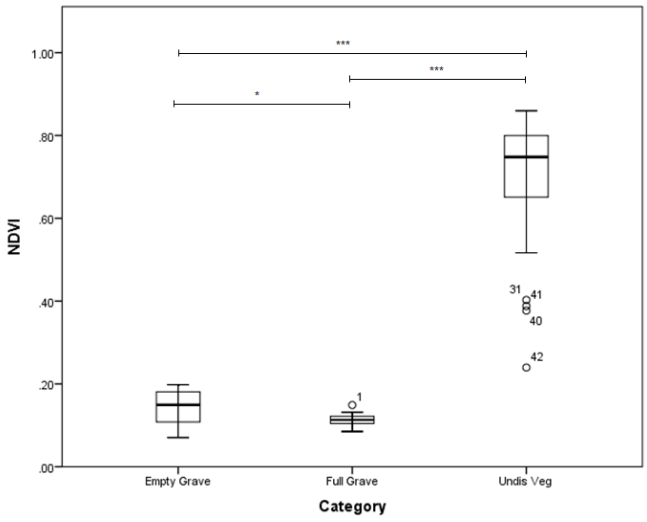

Figure 99 - NDVI across the three surface types on 12th May 2001. The NDVI values remain high for the undisturbed vegetation however, both the full and empty burials exhibit low NDVI, indicative of disturbance and the presence of soil. * significance is observed between the undisturbed vegetation and the two grave surfaces (*** = $p<0.001$, ** = $p<0.01$, * = $p<0.05$, *n.s* = $p>0.05$).**

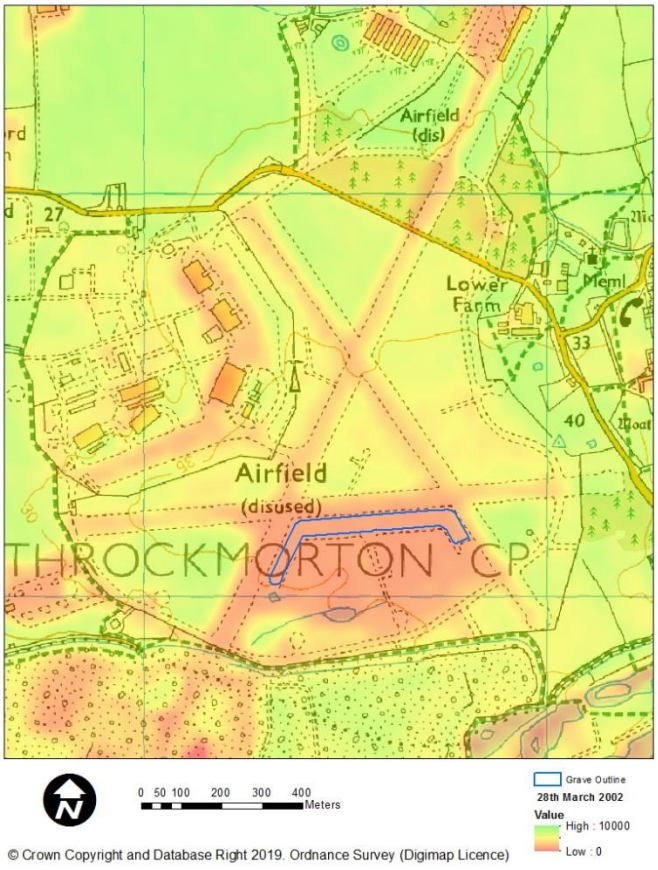

Figure 100 - NDVI map of the Former RAF Pershore airfield on 28th March 2002 – 8 months post burial. Low NDVI values persist in the area where the graves were created.

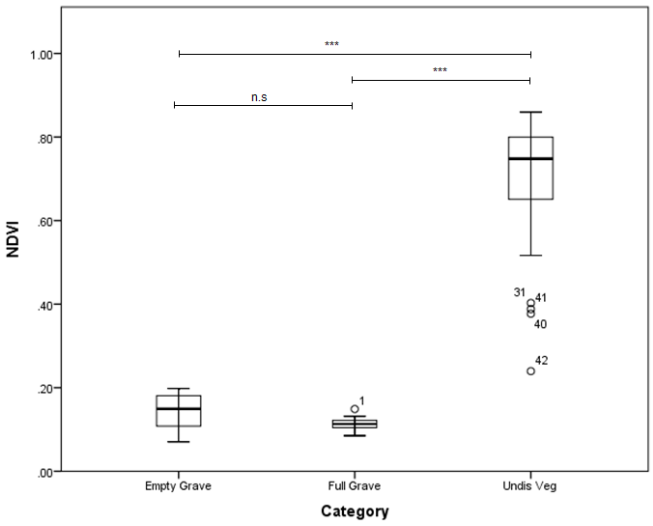

Figure 101 - NDVI across the three surface types on 28th March 2002. NDVI remains high for the undisturbed vegetation however, both the full and empty burials exhibit low NDVI at 8 months post burial. * significance is observed between the undisturbed vegetation and the two grave surfaces (*** = $p<0.001$, ** = $p<0.01$, * = $p<0.05$, *n.s* = $p>0.05$).**

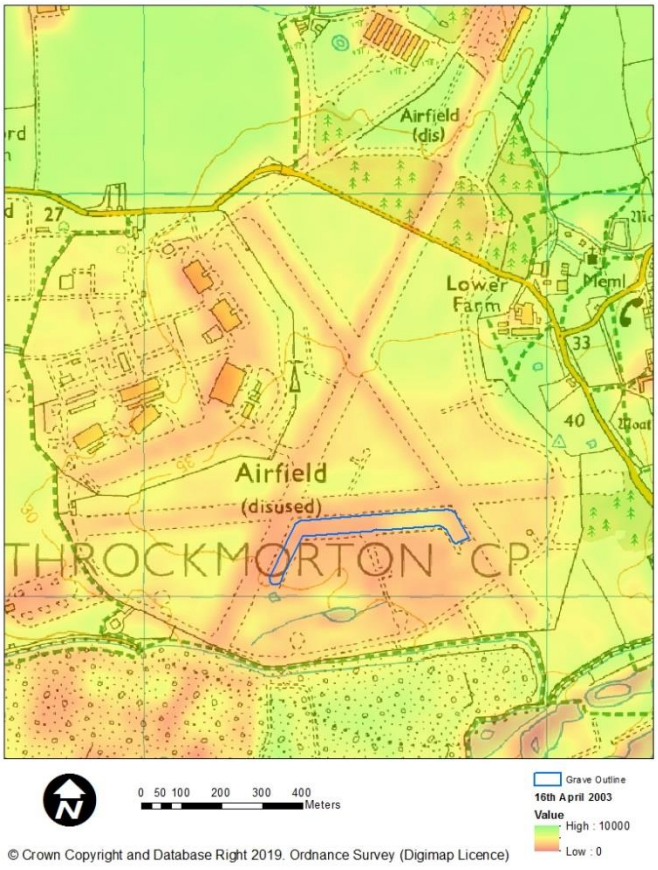

Figure 102 - NDVI map of the Former RAF Pershore airfield on 16th April 2003 – 1 year, 11 months post burial. Low NDVI values persist in the area where the graves were created compared to the other sections of the site. There appears to be a difference in the NDVI values above the full and empty graves.

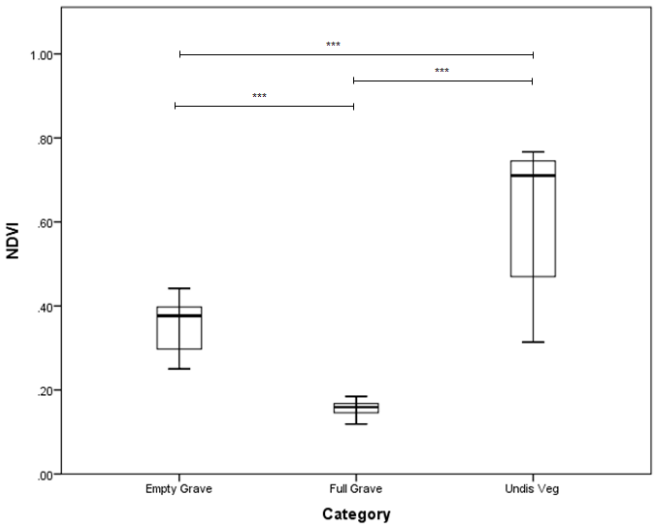

Figure 103 - NDVI across the three surface types on 16th April 2003. NDVI values are higher for the control vegetation with both the full and empty graves exhibiting lower NDVI values at 1 year, 11 months post burial. In addition, the NDVI of the empty graves is higher than the full graves. * significance is observed between the NDVI values of all surface types (*** = p<0.001, ** = p<0.01, * = p<0.05, *n.s* = p>0.05).**

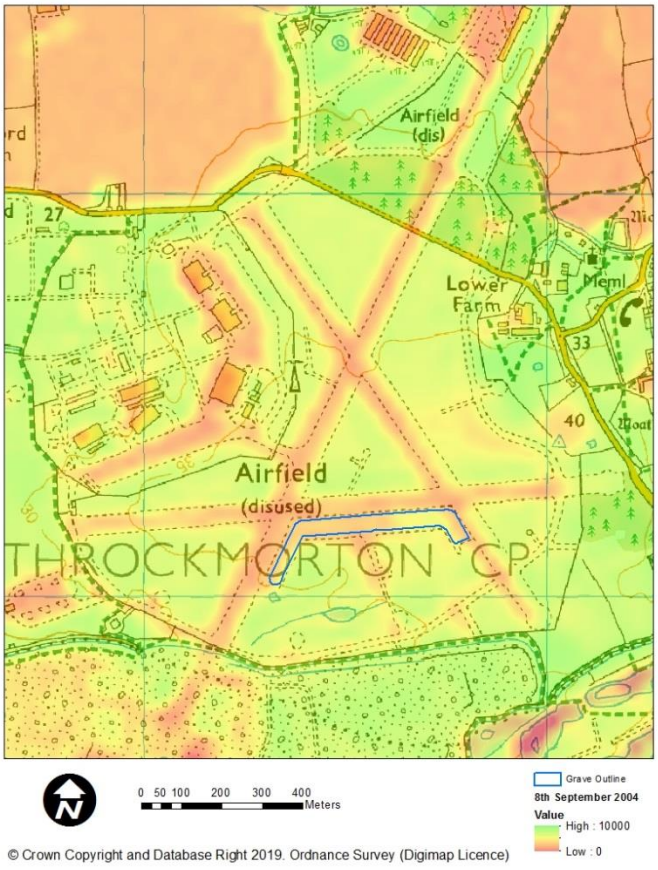

Figure 104 - NDVI map of the Former RAF Pershore airfield on 8th September 2004 – 3 years, 4 months post burial. Low NDVI values persist in the area where the graves were created with a visible difference in the NDVI of the vegetation above the full and empty graves.

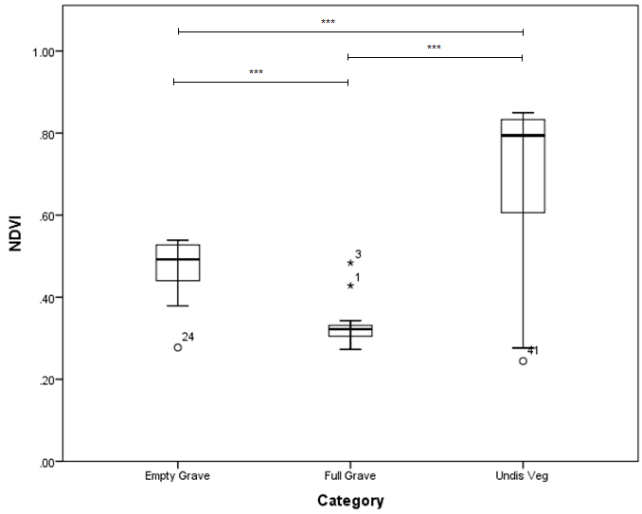

Figure 105 - NDVI across the three surface types on 8th September 2004. NDVI values are higher for the control vegetation with both the full and empty graves exhibiting lower NDVI values at 3 years, 4 months post burial. * significance is observed between the NDVI of all surface types (*** = p<0.001, ** = p<0.01, * = p<0.05, *n.s* = p>0.05).**

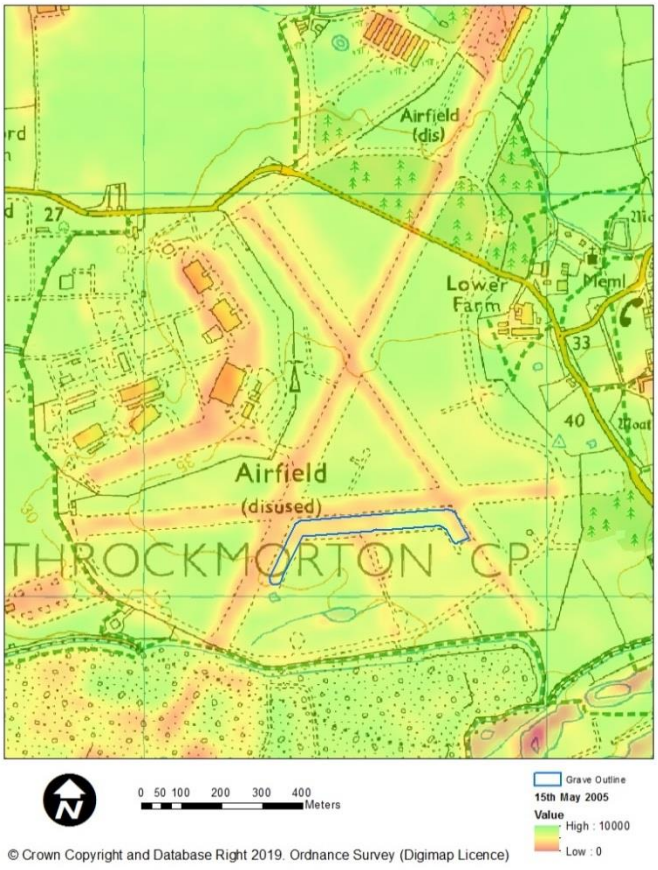

Figure 106 - NDVI map of the Former RAF Pershore airfield on 15th May 2005 – 4 years post burial. The NDVI values within the grave outline are slightly lower than the rest of the site. Differences in NDVI between the full and empty graves are visible.

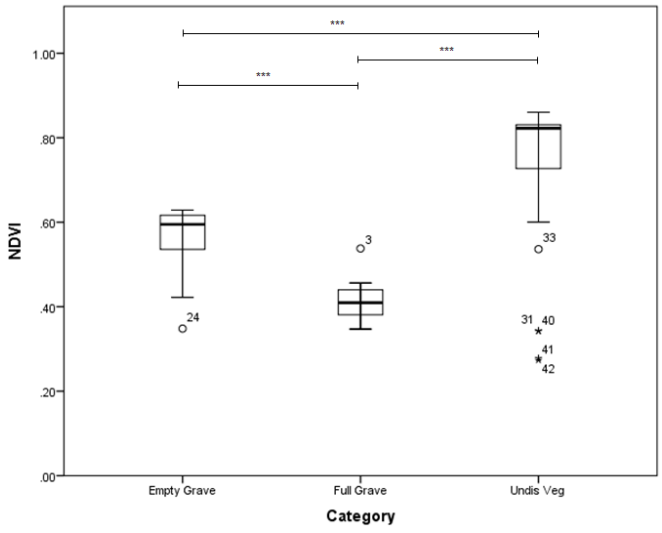

Figure 107 - NDVI across the three surface types on 15th May 2005. At 4 years post burial, the NDVI values are higher for the control vegetation than both the full and empty graves. The NDVI of the empty graves is higher compared to the full graves. * significance is observed between the NDVI of all surface types (*** = $p<0.001$, ** = $p<0.01$, * = $p<0.05$, *n.s* = $p>0.05$).**

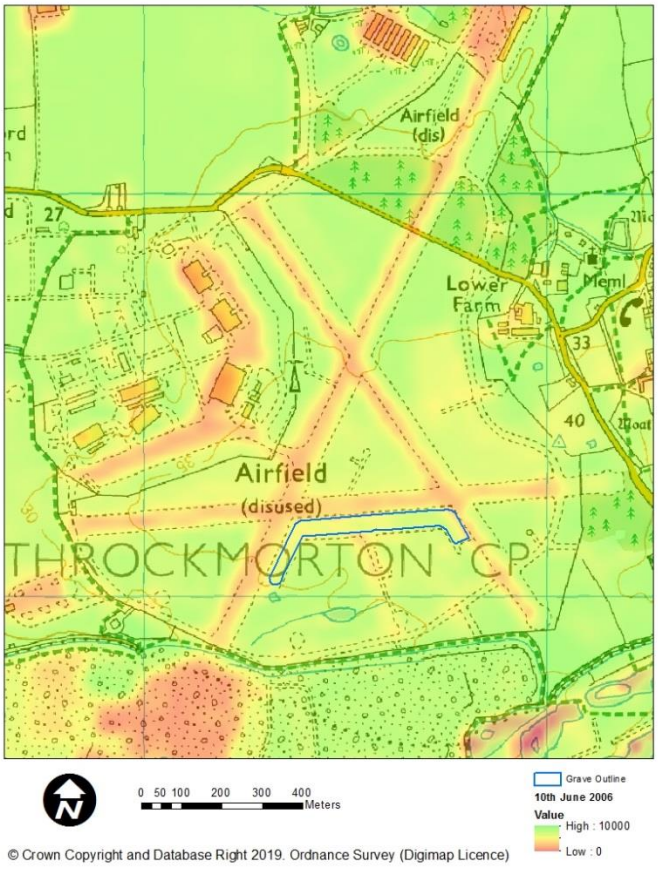

Figure 108 - NDVI map of the Former RAF Pershore airfield on 10th June 2006 – 5 years, 1 month post burial. The NDVI values within the grave outline are lower than the rest of the site, with a visible difference in NDVI between the full and empty graves.

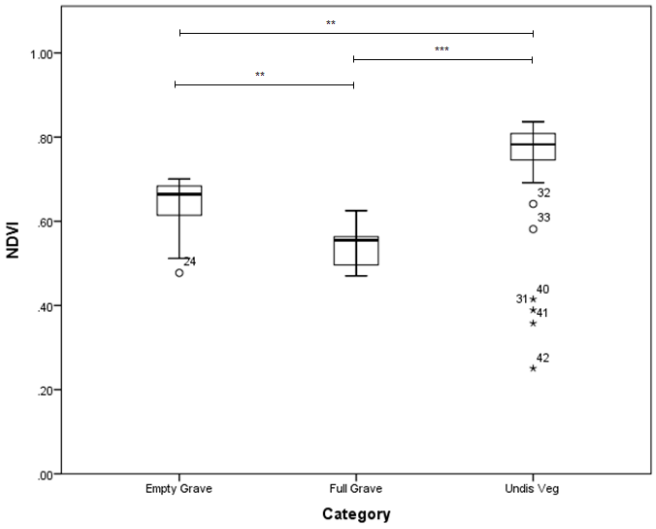

Figure 109 - NDVI across the three surface types on 10th June 2006. There remains to be a visible difference in the NDVI values of the undisturbed vegetation compared to the two grave surfaces at 5 years, 1 months post burial. ** significance was observed between the full and empty graves, with * significance between the control vegetation and the full grave (*** = $p<0.001$, ** = $p<0.01$, * = $p<0.05$, *n.s* = $p>0.05$).**

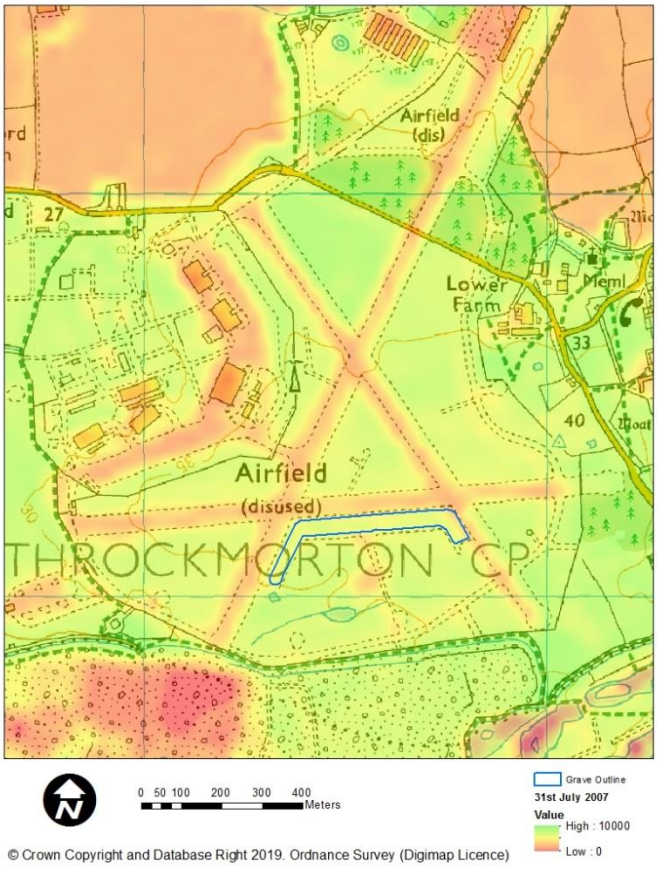

Figure 110 - NDVI map of the Former RAF Pershore airfield on 31st July 2007 – 6 years, 2 months post burial. The NDVI values within the grave outline are similar to the rest of the site, with no visible differences in NDVI between the full and empty graves.

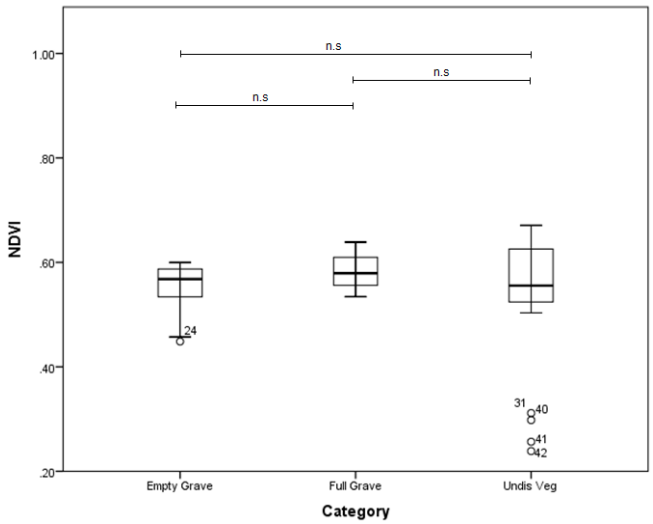

Figure 111 - NDVI across the three surface types on 31st July 2007. NDVI values for the undisturbed vegetation are similar to both grave surfaces; with no visible nor statistically significant difference (*p>0.05)* between the three surfaces at 6 years, 2 months post burial (* = *p*<0.001, ** = *p*<0.01, * = *p*<0.05, *n.s* = *p*>0.05).**

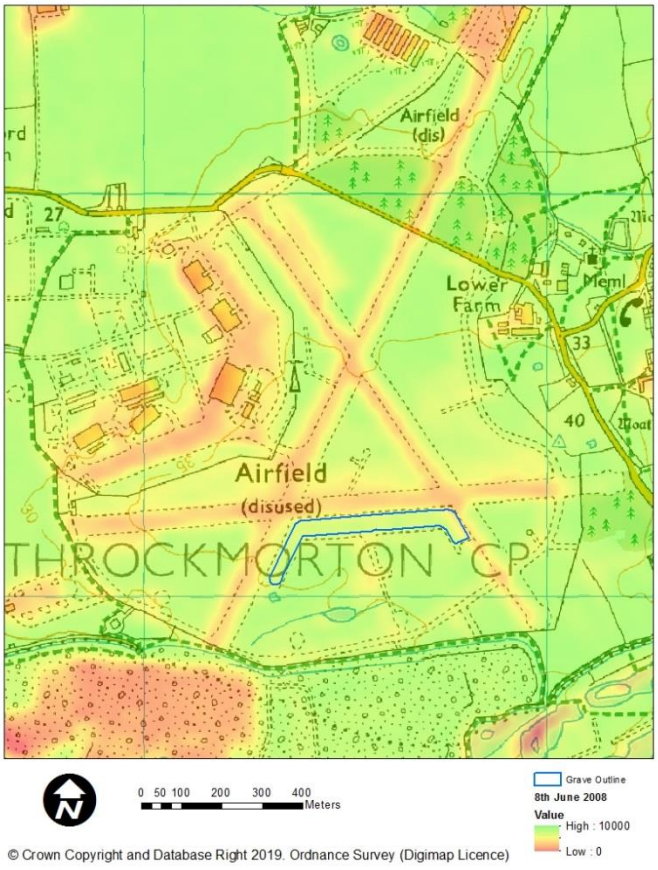

Figure 112 - NDVI map of the Former RAF Pershore airfield on 8th June 2008 – 7 years, 1 month post burial. The NDVI values within the grave outline are similar to the rest of the site; with no observable difference in NDVI between the full and empty graves.

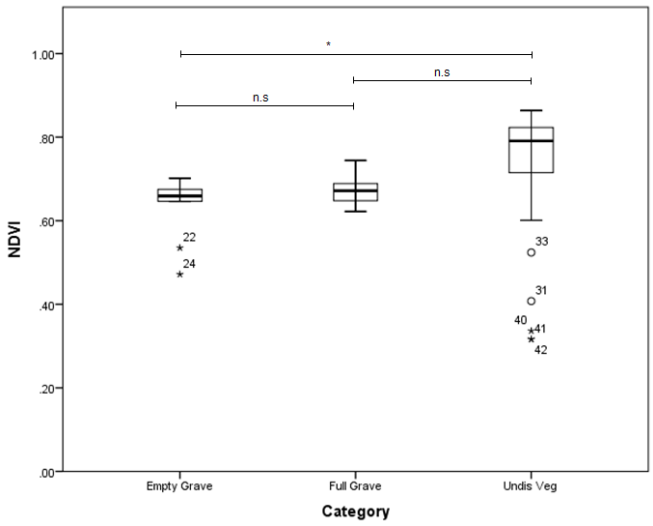

Figure 113 - NDVI across the three surface types on 8th June 2008. NDVI values for the undisturbed vegetation are higher than those of the empty and full grave at 7 years, 1 month post burial. * significance was found between the control vegetation and the empty grave however, there was no significance (*p>0.05)* between the NDVI of the two grave surfaces (* = *p*<0.001, ** = *p*<0.01, * = *p*<0.05, *n.s* = *p*>0.05).**

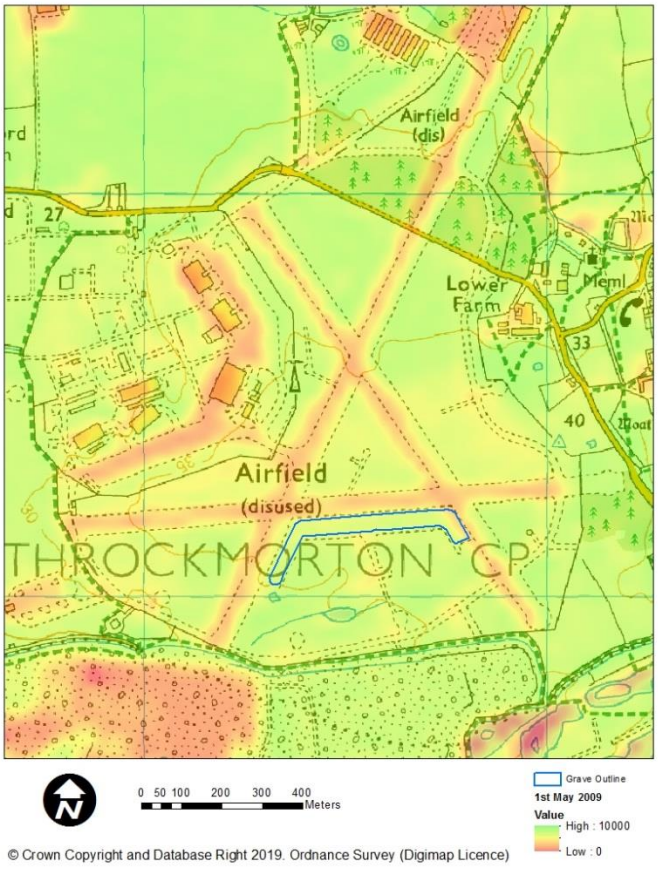

Figure 114 - NDVI map of the Former RAF Pershore airfield on 1st May 2009 – 8 years post burial. The NDVI values within the grave outline are similar to the rest of the vegetated areas of the site and there is no difference in NDVI between the full and empty graves.

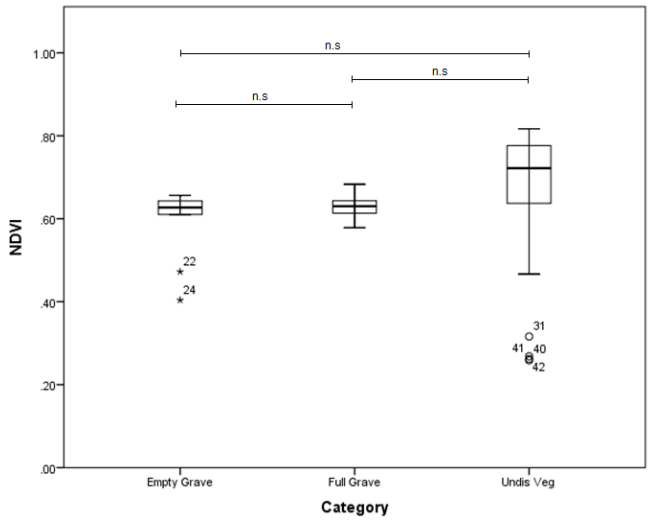

Figure 115 - NDVI across the three surface types on 1st May 2009. NDVI values for the undisturbed vegetation are similar to the empty and full graves at 8 years post. No significance (*p>0.05)* was observed between any of the surface types (* = *p*<0.001, ** = *p*<0.01, * = *p*<0.05, *n.s* = *p*>0.05*).***

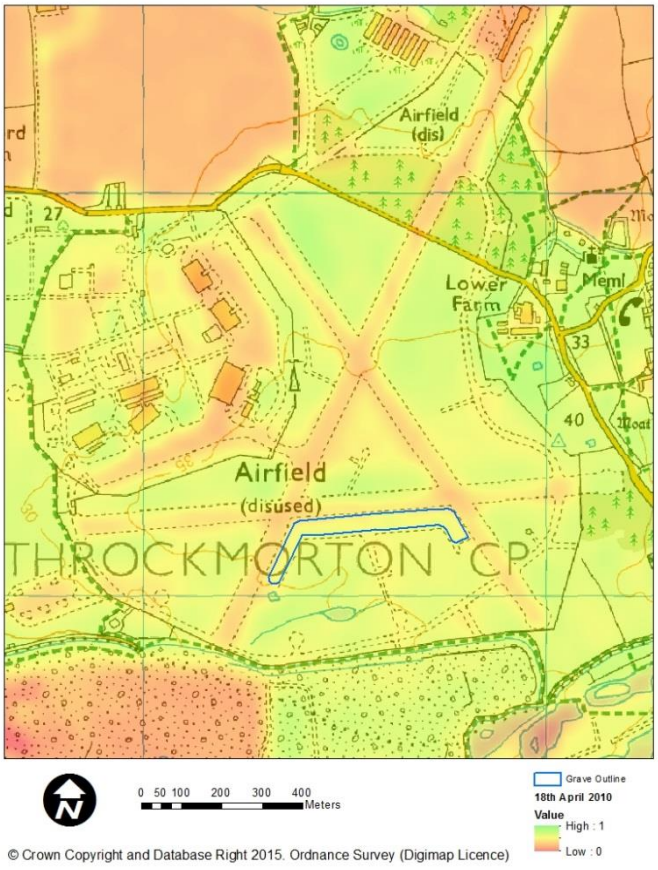

Figure 116 - NDVI map of the Former RAF Pershore airfield on 25th September 2010 – 9 years, 4 months post burial. The NDVI values within the grave outline are similar to the rest of the site; with no visible difference in NDVI between the full and empty graves.

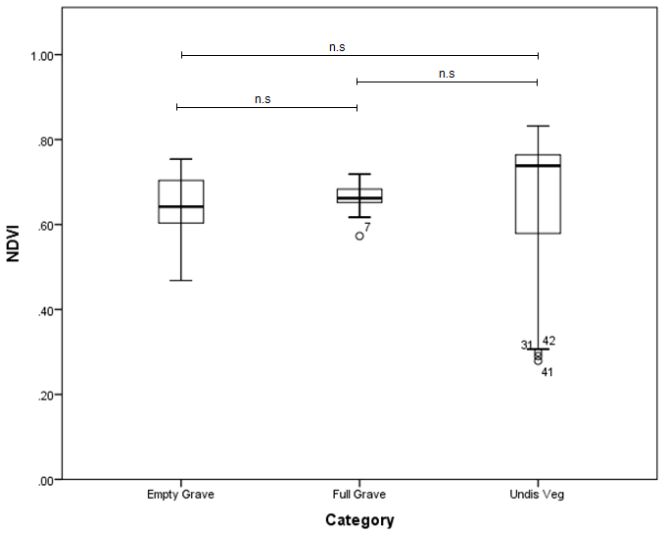

Figure 117 - NDVI across the three surface types on 25th September 2010. NDVI values for the control vegetation are comparable to those of the empty and full grave at 9 years, 4 months post burial. No significance (*p>0.05)* was observed between any of the surface types (* = *p*<0.001, ** = *p*<0.01, * = *p*<0.05, *n.s* = *p*>0.05).**

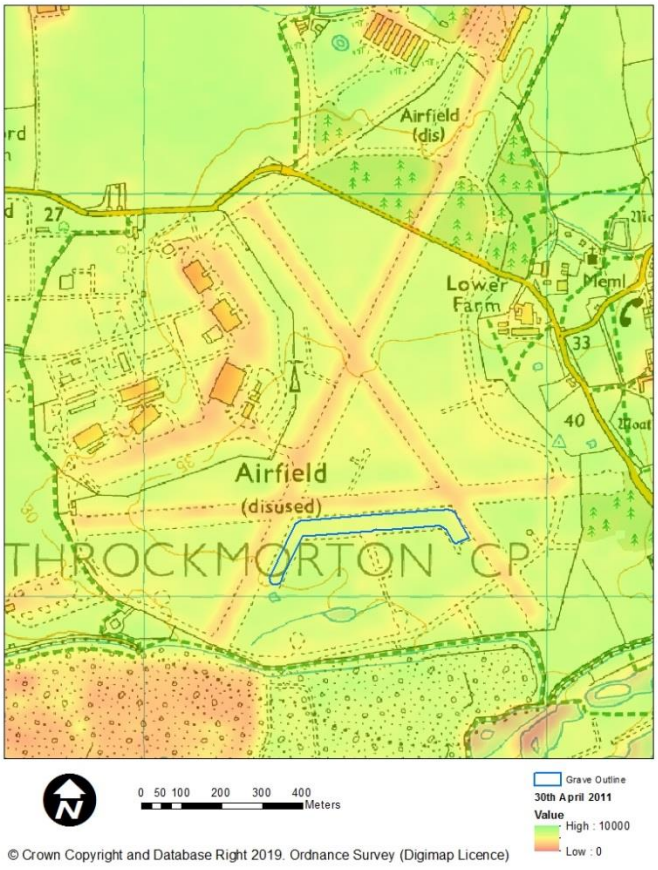

Figure 118 - NDVI map of the Former RAF Pershore airfield on 30th April 2011 – 9 years, 11 months post burial. The NDVI values within the grave outline are similar to the rest of the site; with no visible difference in NDVI between the full and empty graves.

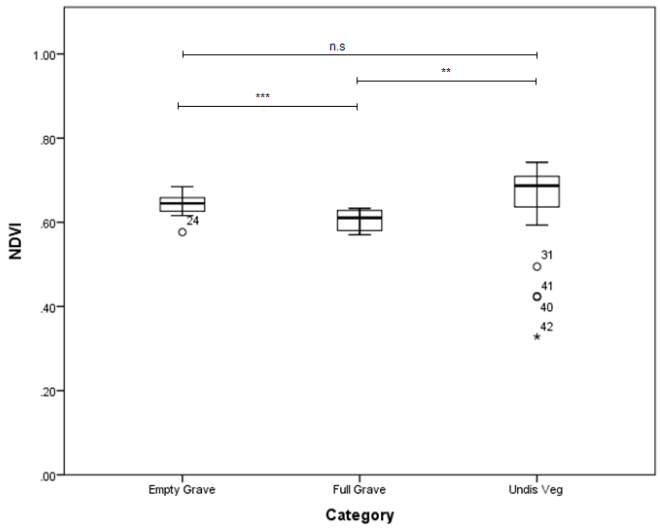

Figure 119 - NDVI across the three surface types on 30th April 2011. NDVI values for the undisturbed vegetation are comparable to the NDVI of the empty and full graves at 9 years, 11 months post burial. There is no visible difference between the NDVI values of the grave surfaces. However, there is significance between the NDVI of the full grave and the empty grave (***) as well as the undisturbed vegetation (**) (* = $p<0.001$, ** = $p<0.01$, * = $p<0.05$, *n.s* = $p>0.05$).**

6.4.2 Summary of Results for NDVI Time Slices at Former RAF Pershore.

NDVI maps were produced for the Former RAF Pershore airfield, from 13 archive Landsat multispectral images (both 5 TM and 7 ETM+) firstly, to assess whether the disturbance caused through the creation of mass graves was able to be observed using NDVI. Secondly, to ascertain how long a detectable difference in the NDVI signal would persist.

Prior to the mass graves being created (i.e. prior to May 2001) it was found that the vegetated areas of the site exhibited stable NDVI values. Throughout the study period, arable fields to the north of the airfield periodically exhibited low NDVI, which was indicative of ploughing; this was visible in multiple NDVI maps including August 2000, September 2004, July 2007 and September 2010.

During May 2001, the area containing the mass graves was dominated by low NDVI, contrasting with the remainder of the site, the NDVI of which remained stable and relatively high. This continued through 2002 until April 2003 when the NDVI of the full and empty graves were visibly different, with the vegetation above the empty grave exhibiting a higher NDVI compared to the full grave; this persisted until May 2005. In the NDVI map from June 2006, there was no visible difference between the NDVI of vegetation above the full and empty graves, however, the NDVI of both were still lower than the control vegetation. By July 2007 (6 years, 2 months post burial), the NDVI of vegetation within the grave areas appeared to have equalised and was similar to that of the control, undisturbed vegetation. However, in June 2008 (7 years and 1 month post burial), although the NDVI appeared to have recovered in 2006, there was a visible difference between the NDVI of the graves and the control vegetation. Post June 2008, it was found that NDVI fluctuated following the seasons across all surfaces. In many of the maps, the NDVI of the graves was often lower than the undisturbed vegetation. These results are represented within the boxplots in Figure 120.

Therefore, it appears that NDVI derived from archive multispectral orbital imagery with medium spatial resolution can be used to identify a disturbance indicative of the creation of a mass grave, whether empty or full, at the Former RAF Pershore airfield site. These NDVI values can also be used to locate a full or empty grave, and distinguish it from undisturbed ground, up to 5 years, 2 months post burial, with the potential to expand this time frame up to 7 years post burial.

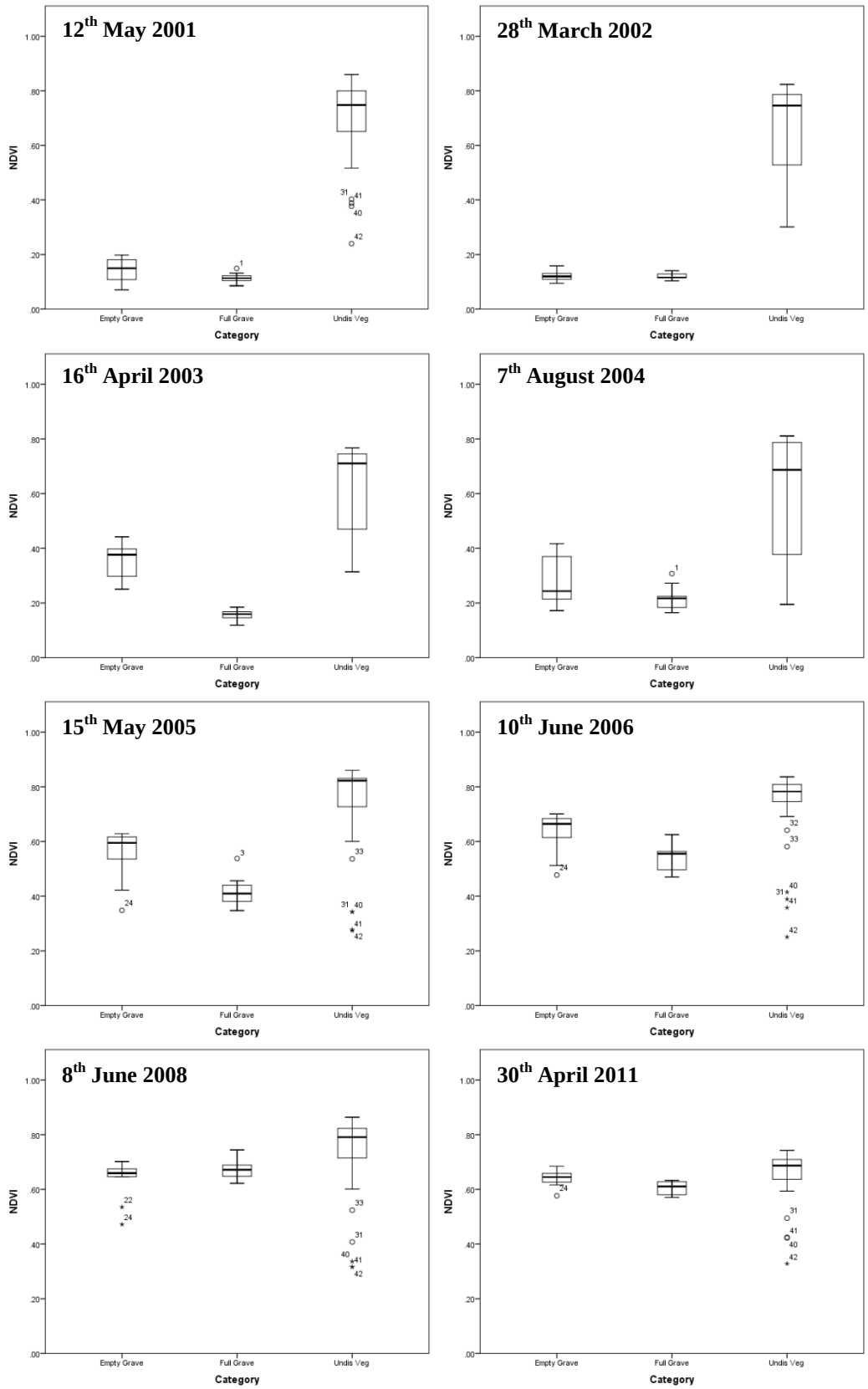

Figure 120 - Boxplots from NDVI maps focusing around April through to June 2001 - 2011, showing the recovery of the vegetation atop the full and empty grave compared to the undisturbed, control vegetation. Outliers are represented by the clear circles with extreme outliers represented by an asterix.

The NDVI values for the three surface types, undisturbed vegetation, full graves and empty graves were compared for 13 Landsat scenes from 1999-2011; up to ten years post burial. To understand the variance present within each data set, f-tests were conducted, prior to running t-tests, to ascertain whether significance existed between the NDVI of the surface types and the undisturbed vegetation (control) (for outputs of statistical tests, refer to Appendix 3).

Prior to grave creation (1999-2000), significance (** $p<0.01$) was observed between the NDVI values of the undisturbed vegetation and the area later used for burial. Although significance was observed, the NDVI values for all surface types were high (0.4-0.8) and therefore, the significance observed was likely due to natural fluctuations in the relative health of the vegetation as opposed to disturbance. Disturbance is characterised by a sudden decrease in NDVI (<0.2), representing a surface dominated by soil rather than vegetation.

In May 2001 during grave creation, significance (*** $p<0.001$) was observed between the undisturbed vegetation and both the full and empty graves. Unlike the significance observed in 1999 and 2000, this was accompanied by a sudden reduction in NDVI (between 0.0-0.2). Therefore, this is considered the point of disturbance, or breakpoint, within the data. Similar significance (*** $p<0.001$) was observed in 2002, however, no significance ($p>0.05$) was observed between the NDVI of the full and empty graves. This is indicative of disturbance having affected both the full and empty graves and suggests that vegetation has begun to colonise the grave surfaces. Significance (*** $p<0.001$) was observed between the NDVI values of all surface types in April 2003. This is the first instance, post burial, that significance was observed between the full and empty graves. This suggests that soil, or stressed vegetation, dominated the surface of the full graves, whereas, the higher NDVI on the surface of the empty graves may be indicative of vegetation starting to colonise the surface.

In September 2004, significance (*** $p<0.001$) existed between all surfaces. The NDVI had increased overall compared to 2003. However, the NDVI of the full graves remained lower than the empty graves, with a significance of *** ($p<0.001$). The same level of significance was observed in 2005, with the NDVI increasing steadily for all surface types compared to 2004.

Lower significances were found in 2006, namely between the undisturbed vegetation and the empty grave (** $p<0.01$) as well as the empty grave and the full grave (** $p<0.01$). Therefore, suggesting that the vegetation at the surface of the empty grave was recovering and becoming increasingly similar to the control, undisturbed vegetation. The differences in NDVI between the full and empty graves were less significant than previously observed,

suggesting that both surfaces were, at 5 years and 1 month post burial, colonised with vegetation and recovering. However, the previously observed significance (*** $p<0.001$) between the full grave and the undisturbed grave was maintained.

2007 was the first year where no significance ($p>0.05$) was observed between the undisturbed vegetation and the two grave surfaces. Therefore, suggesting that the surfaces of both the full and empty graves were colonised at 6 years, 2 months and that the vegetation was exhibiting comparable stress to the undisturbed areas of the site.

In June 2008, significance was observed only between the undisturbed vegetation and the empty grave (* $p<0.05$). There was no significance between the three surface types in 2009 and 2010. However, in 2011, significance was observed between the full and empty grave (*** $p<0.001$) as well as the full grave and undisturbed vegetation (** $p<0.01$).

Therefore, to ascertain whether the significance observed within the 2011 Landsat imagery was detectable in imagery of fine spatial resolution (RapidEye); boxplots were produced (Figure 121) and statistical analysis was undertaken.

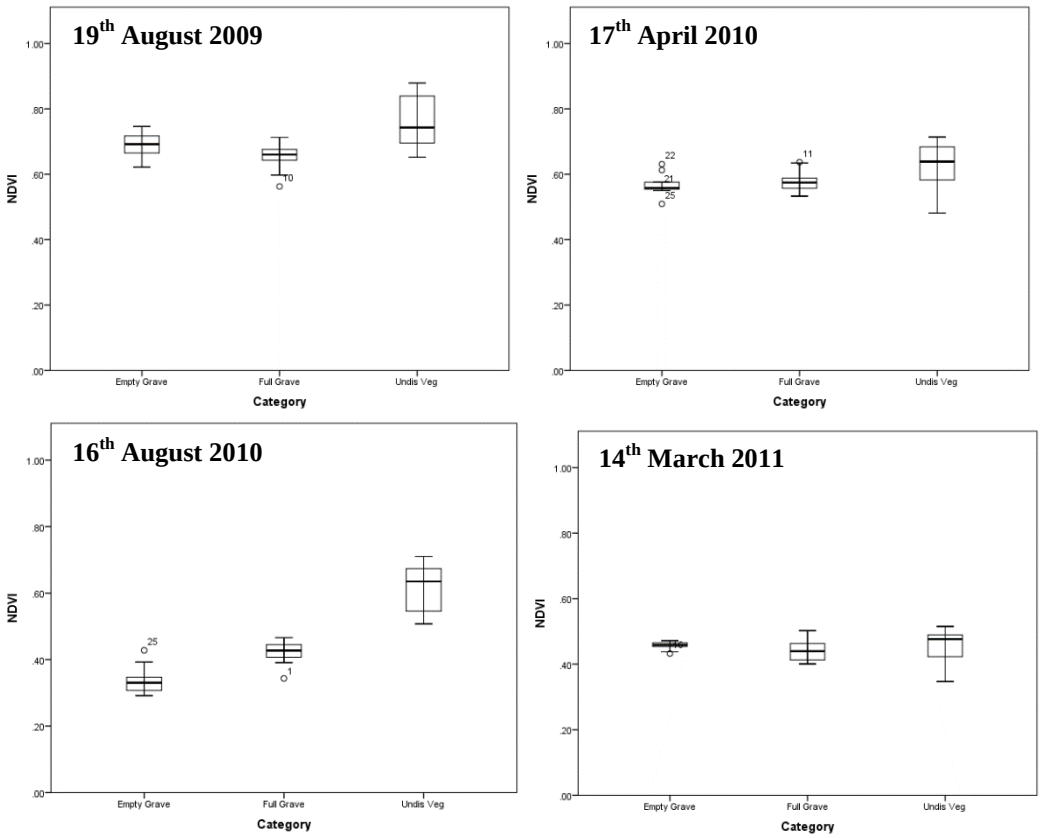

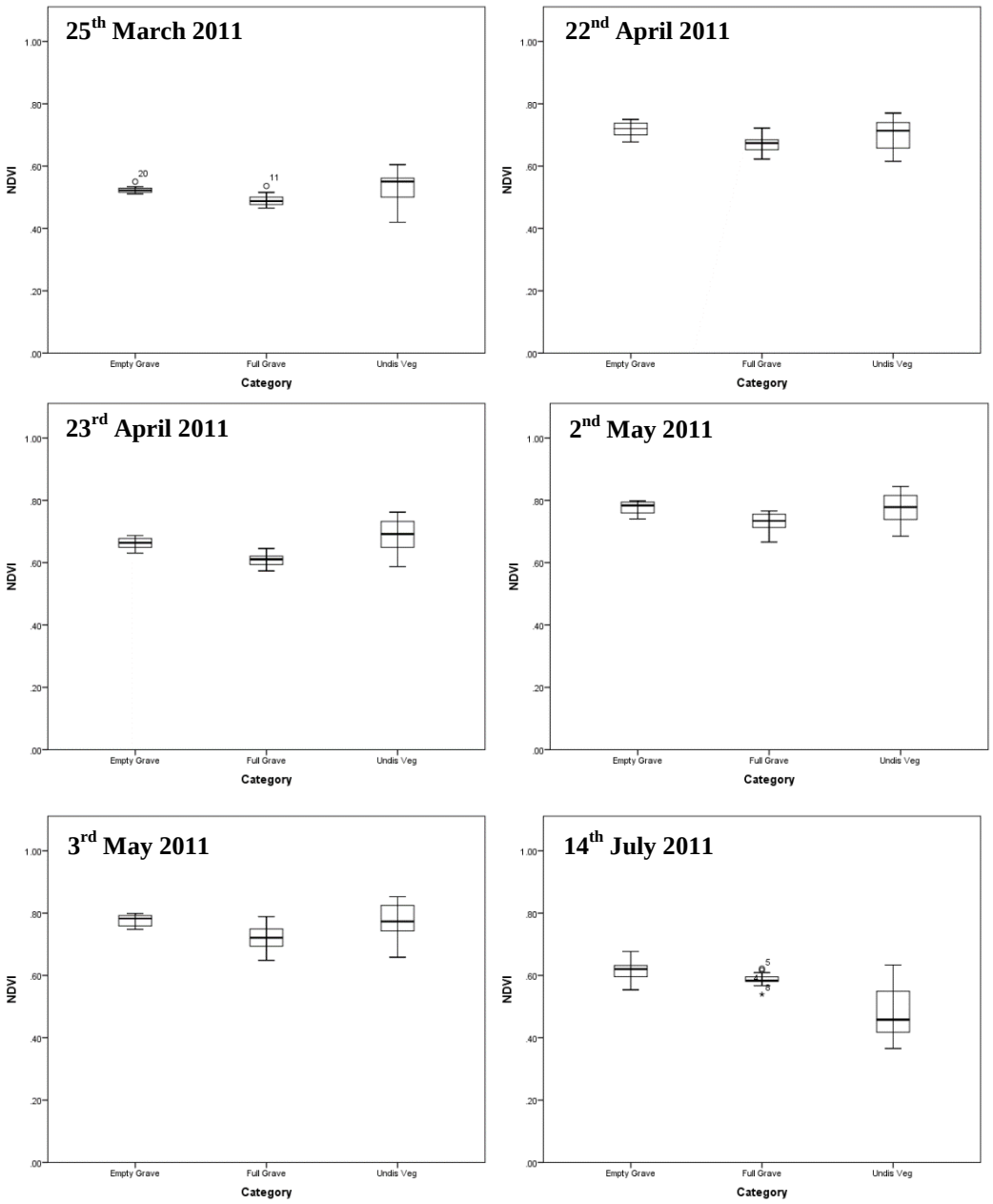

Figure 121 - Boxplots derived from the RapidEye NDVI maps, post 2009, for the full and empty grave compared to the undisturbed, control vegetation.

As observed within the Landsat boxplots, NDVI was relatively high and stable across the site by 2009. The NDVI values for each surface type appear visually similar within the RapidEye boxplots (Figure 121). However, significance was observed for each surface type during 2009, 2010 and 2011, with the exception of 14th March 2011 where no significance (n.s) was found (summarised in Table 26

Table 26). The lack of significance is likely due to the vegetation being in a period of senescence. Therefore, the results of the statistical tests undertaken, suggest that the surfaces had not recovered and equalised; with significance existing in all cases for the full grave compared to the undisturbed ground, excluding 14th March 2011. In contrast, the empty

graves appear to be more similar to the undisturbed vegetation, with lower levels of significance observed. Interestingly, the full and empty graves appear to be able to be differentiated statistically with *** (p<0.001) significance observed for seven out of the ten RapidEye observations.

Table 26 – Statistical significance of NDVI for the surface types, derived from RapidEye, calculated using an F-test and Two-Sample T-Test

Date	Undis Veg vs. Full Grave	Undis Veg vs. Empty Grave	Full Grave vs. Empty Grave
19/08/2009	*** (p<0.001)	*** (p<0.001)	* (p<0.05)
17/04/2010	*** (p<0.001)	*** (p<0.001)	n.s (p>0.05)
16/08/2010	*** (p<0.001)	*** (p<0.001)	*** (p<0.001)
14/03/2010	n.s (p>0.05)	n.s (p>0.05)	n.s (p>0.05)
25/03/2010	** (p<0.01)	n.s (p>0.05)	*** (p<0.001)
22/04/2010	** (p<0.01)	n.s (p>0.05)	*** (p<0.001)
23/04/2010	*** (p<0.001)	* (p<0.05)	*** (p<0.001)
02/05/2011	*** (p<0.001)	n.s (p>0.05)	*** (p<0.001)
03/05/2011	*** (p<0.001)	n.s (p>0.05)	*** (p<0.001)
14/07/2011	*** (p<0.001)	*** (p<0.001)	*** (p<0.001)

6.4.3 Smoothing of NDVI values over time to visualise the yearly and seasonal trends in NDVI over the different grave surfaces

To observe the trend of the full time series, including imagery from Landsat, DMC, SPOT and RapidEye, the mean NDVI for the undisturbed ground, the empty and full graves were plotted against time; for the full decadal study period (2001-2011). The values comprised of the mean for all points on each surface type, for each date (Appendix 3). Overall, the NDVI of the undisturbed vegetation was higher than that of the empty and full graves until the point of vegetation equalisation, due to the fact that immediately post creation and for some years after, the NDVI for the grave surfaces was dominated by soil rather than vegetation. In contrast, the area of undisturbed vegetation was unaffected by the creation of the graves and should therefore, be representative of the natural, seasonal and yearly fluctuations in NDVI; which can be influenced by variables including meteorological events. Relationships between NDVI at the site and meteorological variables have been investigated and are discussed in a later section.

The median NDVI values were also plotted for each surface type from 1997 through to 2011. It was found that the trend observed for mean NDVI values was maintained. To identify how similar or dissimilar the mean and median values were for each surface type over time, a plot

was produced (Figure 122). The difference between the mean and median NDVI values was small, with the majority of data varying by a maximum of 0.05. However, there were a number of peaks and troughs, notably in 1997, 2000 and 2009, which represented outliers. Therefore, median NDVI values will be used for the remainder of this chapter, as they are less affected by outliers when compared to mean values. The mean takes into account all of the values divided by the population of the sample and can therefore be skewed by outliers. However, the median is calculated by identifying the central value and as a consequence is less affected. The line and scatter plots for the mean NDVI over time including those where smoothing techniques were applied are located in Appendix 3.

On plotting the median NDVI of the full and empty graves compared to the undisturbed grass (Figure 123 to Figure 126) it was observed that the full and empty graves were behaving similarly, following the same trend throughout the study period. This is likely due to both types of grave being in the same locale and subject to the same meteorological conditions. However, it is also observed that there are measureable differences in the NDVI obtained from the surface of the full graves compared to the empty graves as well as the undisturbed vegetation. This has been illustrated previously in Section 6.4.1 and 6.4.2.

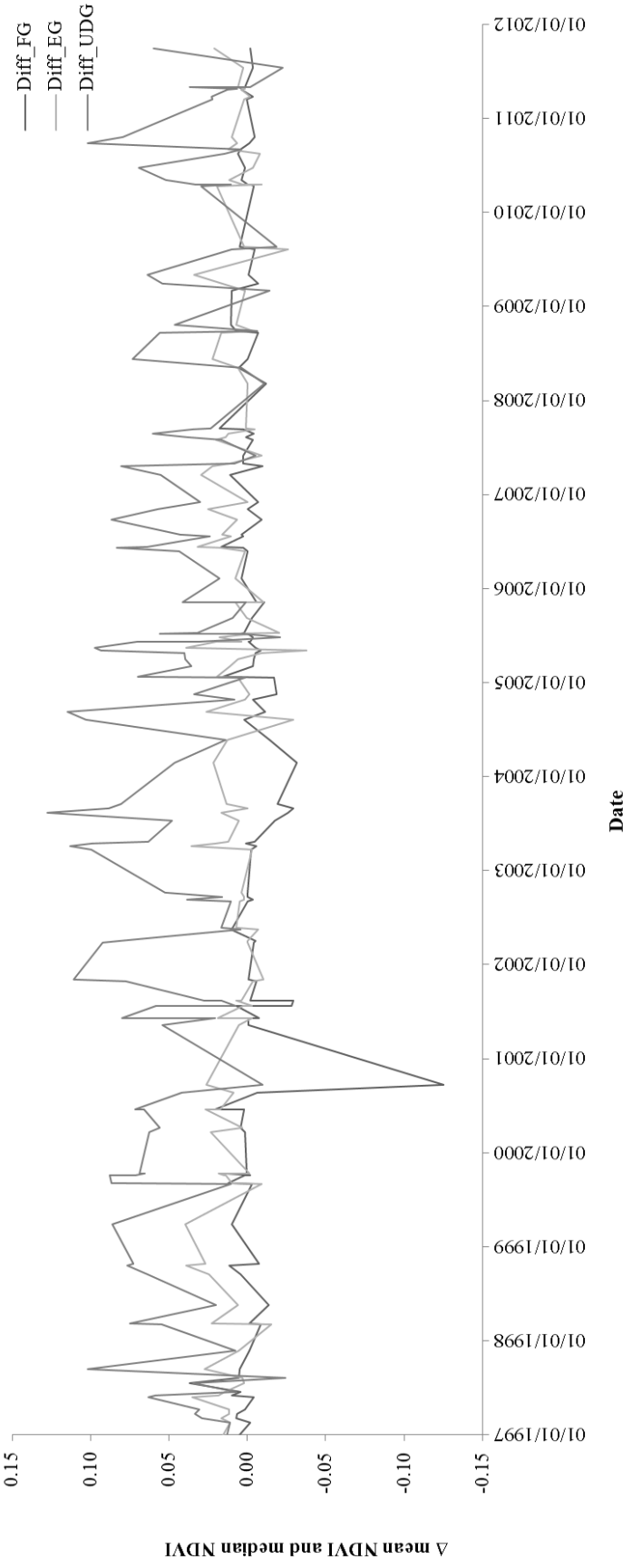

Figure 122 - Difference between the mean and median NDVI for all surface types over the study period.

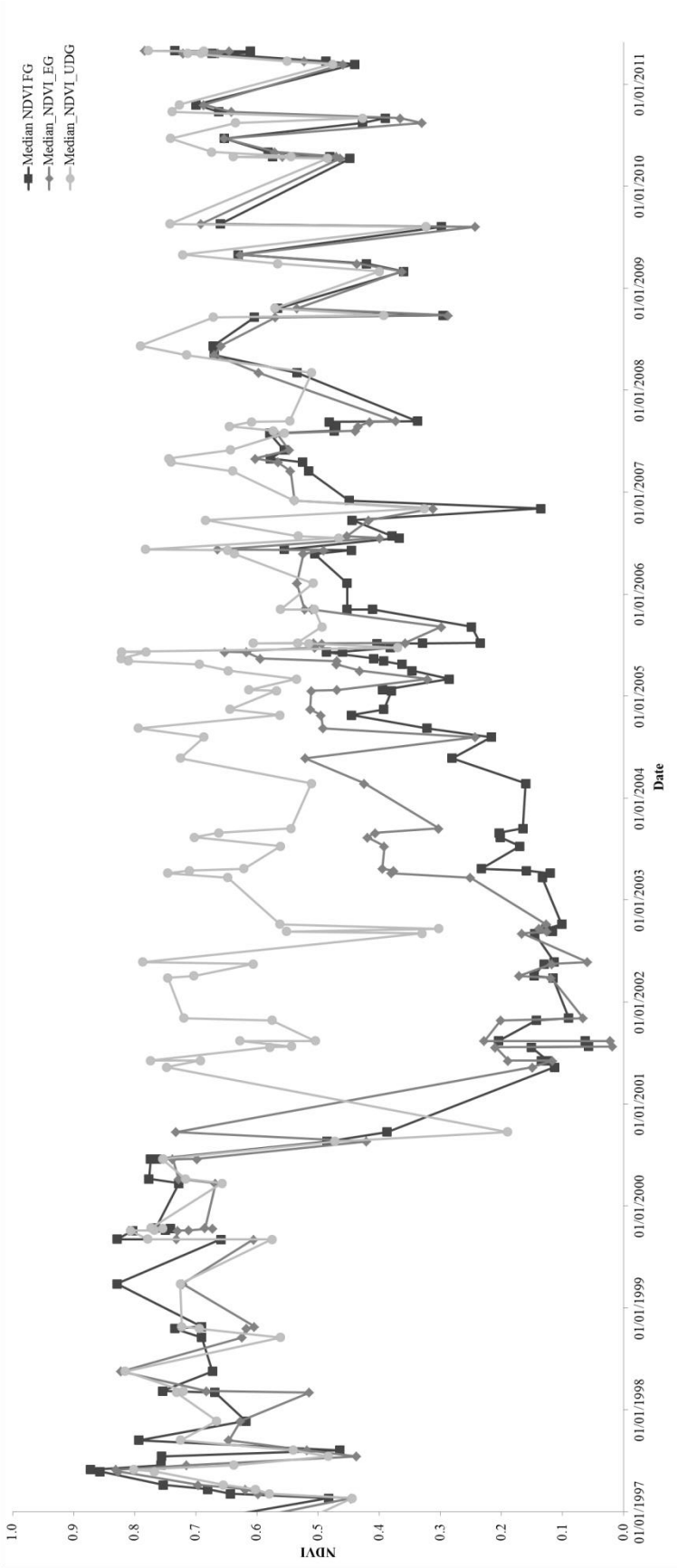

Figure 123 - Median NDVI of the Full (FG) and Empty Graves (EG) compared to the Undisturbed Grass (UDG) Over Time (1997-2011).

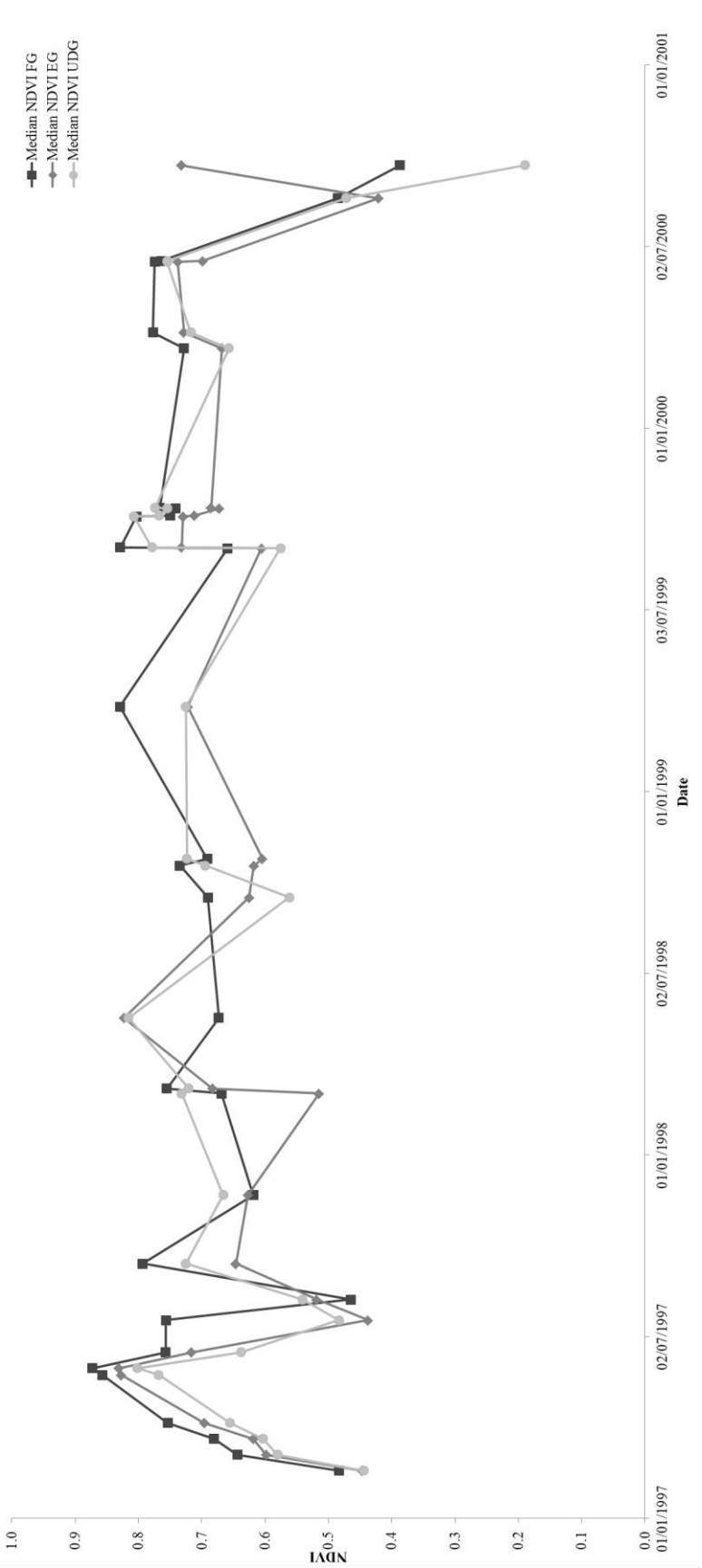

Figure 124 - Median NDVI of the Full (FG) and Empty Graves (EG) compared to the Undisturbed Grass (UDG) prior to grave creation (1997-2001).

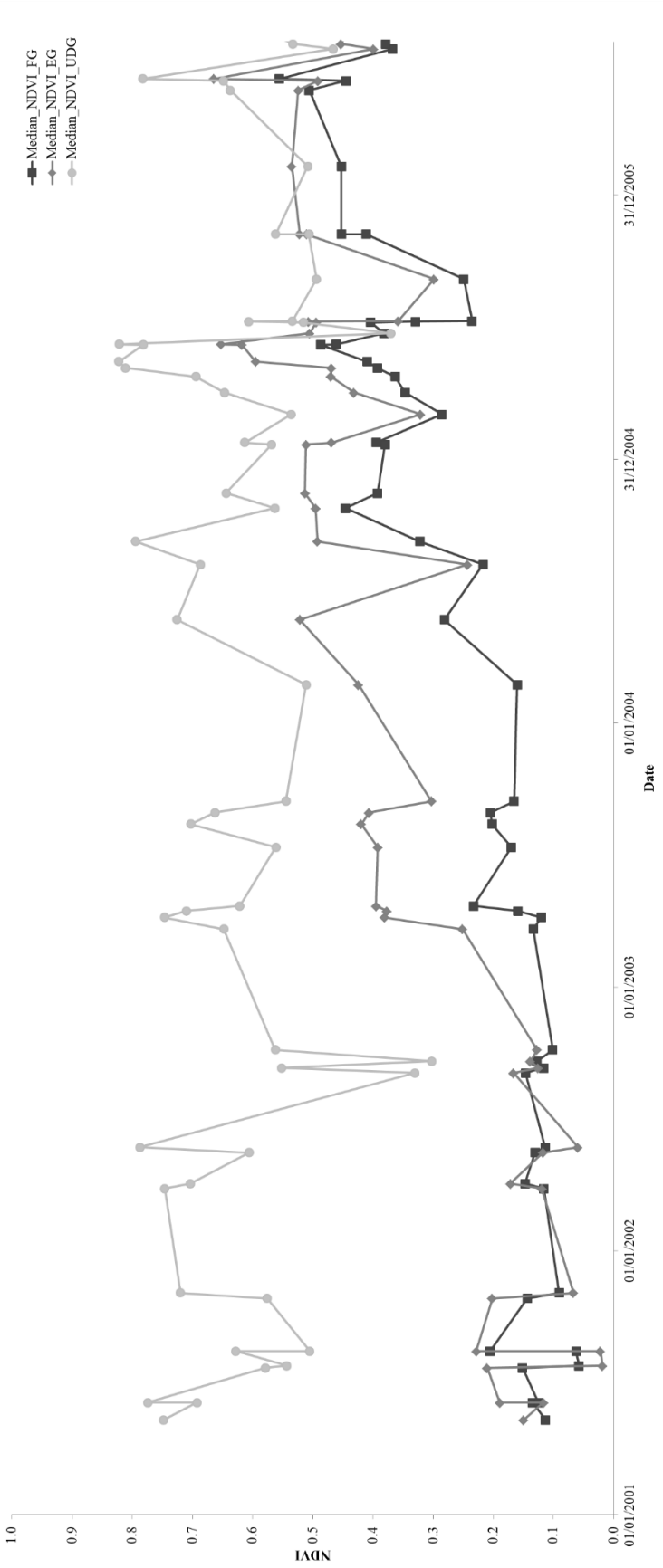

Figure 125 - Median NDVI of the Full (FG) and Empty Graves (EG) compared to the Undisturbed Grass (UDG) during the first 5 years post-burial (2001-2006).

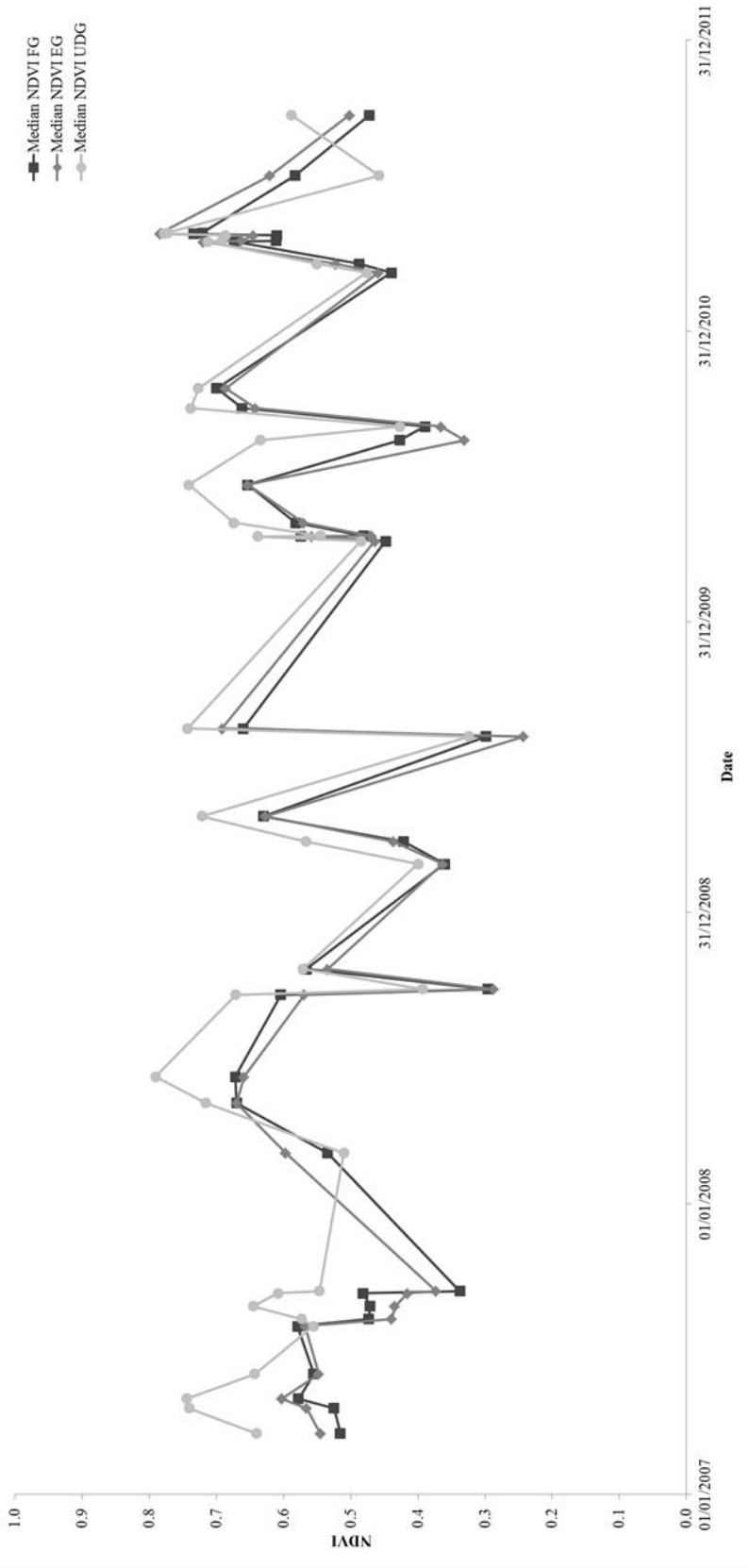

Figure 126 - Median NDVI of the Full (FG) and Empty Graves (EG) compared to the Undisturbed Grass (UDG) 6 years post-burial up to a decade (2007-2011).

6.4.3.1 Smoothing the time series using a running median

To reduce noise from cloud and haze, filtering was undertaken manually through the selection of cloud free images and fine registration (both automatic and manual). Images that initially appeared cloud free were reassessed and removed if haze was present following pre-processing. Any variations that remained were likely due to the use of a combination of sensors for the time series. However, within each individual image the NDVI values are comparable and relative to each other, regardless of their actual value. Therefore, there was little need to employ smoothing techniques that identify and remove outliers as this would have likely removed data points that were legitimately exhibiting high or low NDVI, the latter of which may represent grave creation. Consequently, smoothing methods including running median and exponential smoothing were applied, as they allow for a trend to be revealed whilst preserving the original data values.

A moving median, with varying intervals, was applied to the data resulting in Figure 127 to Figure 130; using Microsoft Excel 2010. Intervals of 5, 10, 15 and 20 were used to determine how the trend was affected and also to ascertain which interval was optimal. Modifying the intervals allowed for greater or less data values to be used to calculate the smoothed data, i.e. an interval of 5 used the previous five median values to create an average which then becomes the data point.

When an interval of 5 was used (Figure 127) the time series was somewhat smoothed, however, fluctuations could still be clearly visualised which detracted from the overall trend. Consequently, a dataset with an interval of 10 was calculated (Figure 128), the time series was much smoother when compared to using an interval of 5, with the trend for each surface type clearly visible. However, it should be noted that the whole time series was shifted to the right therefore, making it appear as though the graves were created later than they actually were. For the purpose of smoothing the time series, the data shift is not an issue as the trend through time is being examined rather than being used to ascertain the dates when the disturbance occurred.

An interval of 15 produced a smoothed time series that allowed each of the surface types and their trend over time to be clearly observed (Figure 129). A downward trend in NDVI for the area of undisturbed ground was observed; this was not as obvious in the previous iterations with an interval of 5 and 10. The shift in the data, as mentioned previously, is also clearly visible in this plot.

Applying an interval of 20 produced a very smooth time series, with no clear peaks and troughs (Figure 130). Intervals larger than 20 were not considered as this would have

encroached on the data from 2001, i.e. when the burial was created. After considering each of the intervals and the resulting plots, an interval of 10 was optimal as it enabled the trends to be visualised across the full time series, for each of the surface types, whilst smoothing the majority of the extreme peaks and troughs.

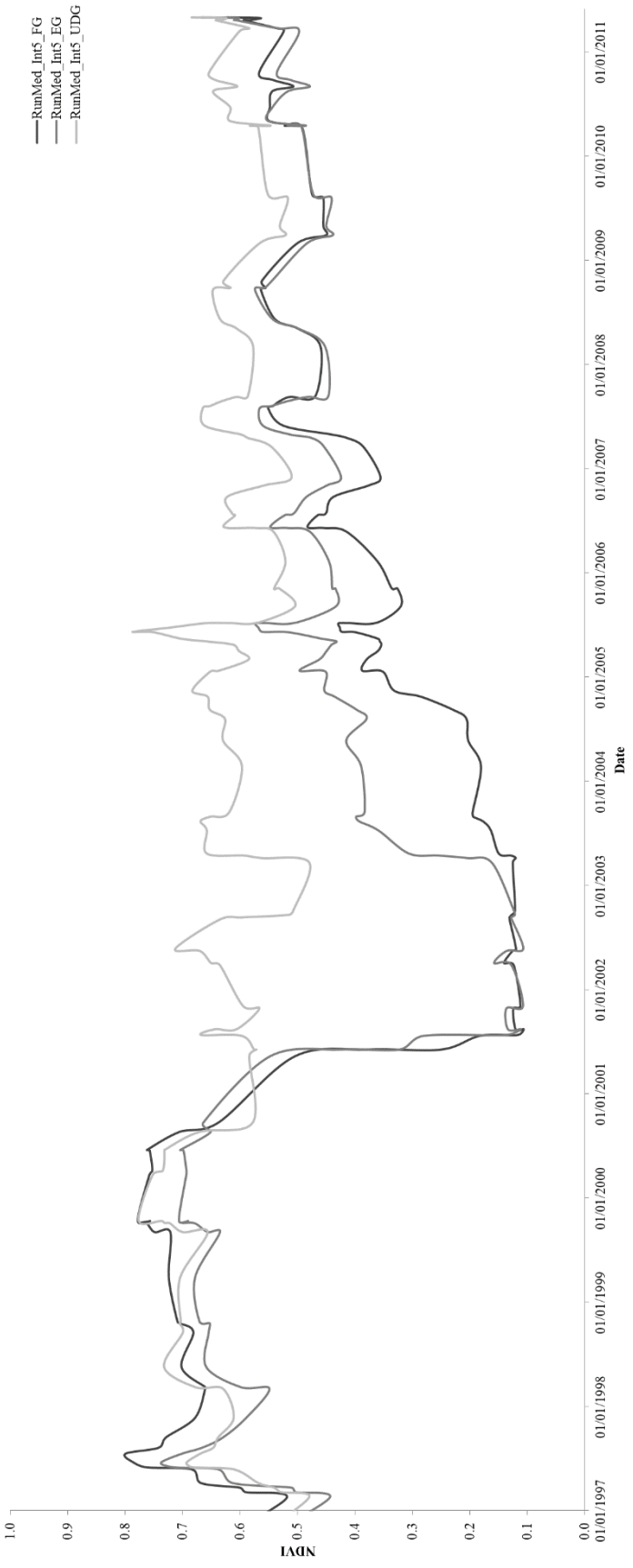

Figure 127 - Running median of the median NDVI 1997-2011 (Interval 5)

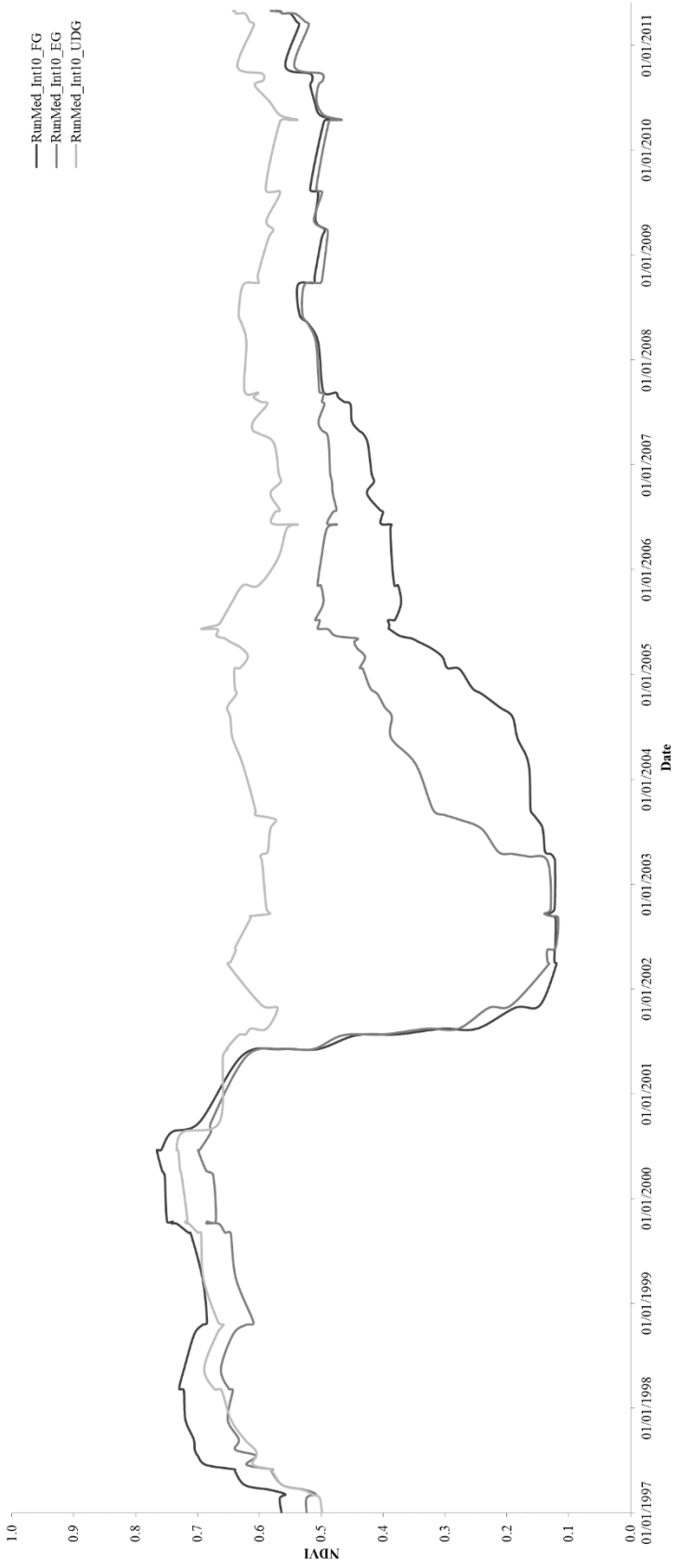

Figure 128 - Running median of the median NDVI 1997-2011 (Interval 10)

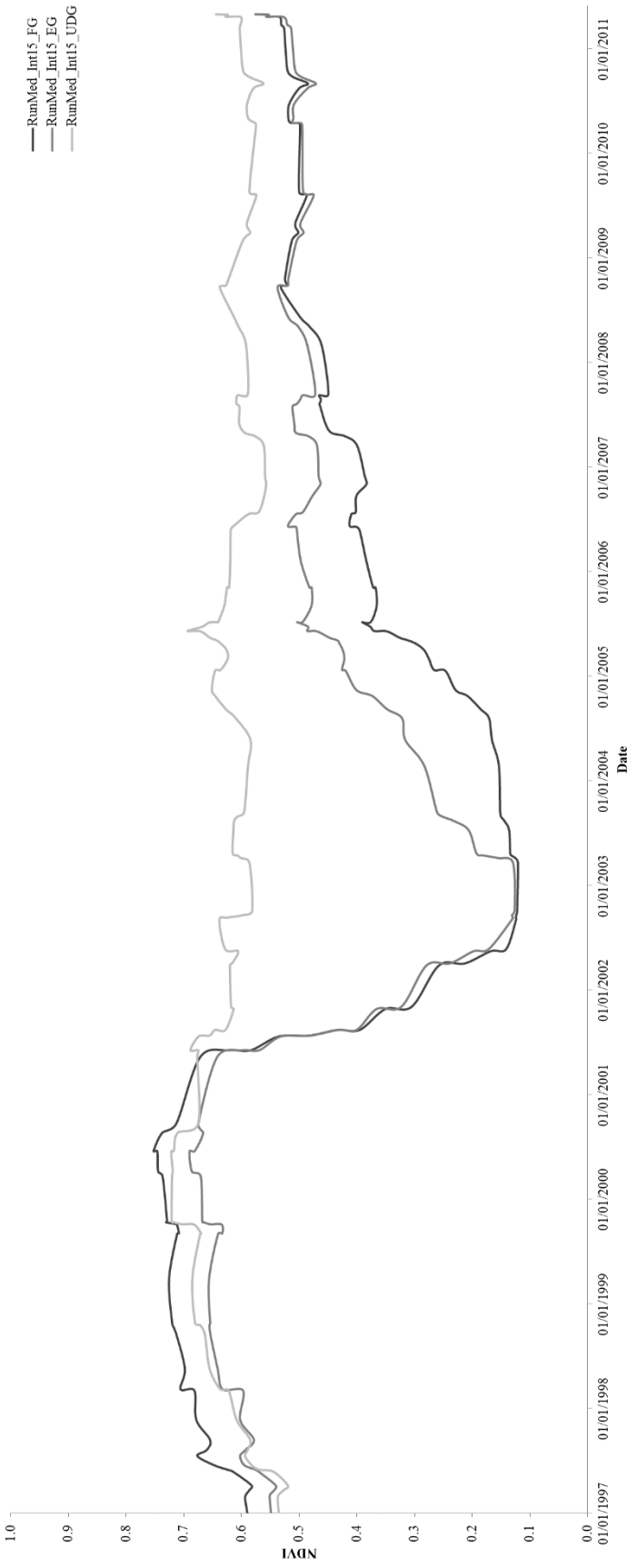

Figure 129 - Running median of the median NDVI 1997-2011 (Interval 15)

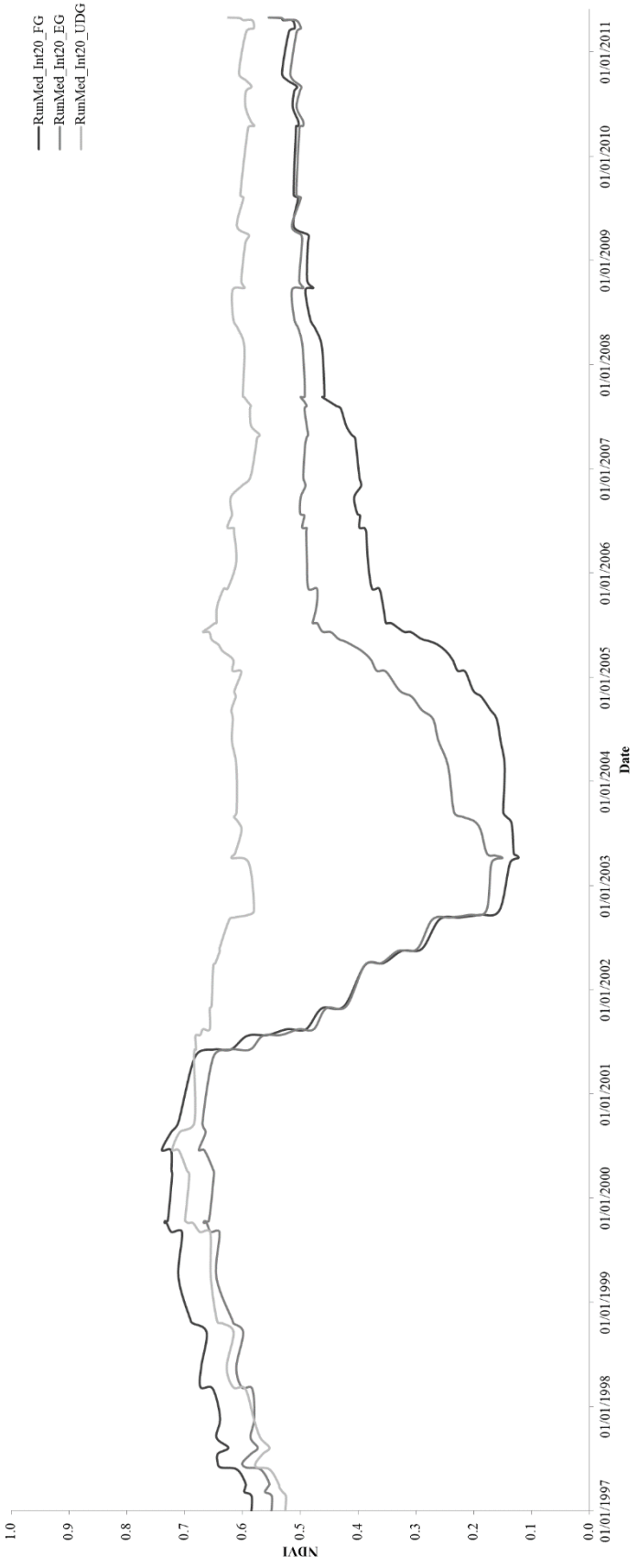

Figure 130 - Running median of the median NDVI 1997-2011 (Interval 20)

6.4.3.2 Smoothing the time series using exponential smoothing

In addition to the running median, exponential smoothing was also applied using three damping factors, to identify which would produce the most smoothed time series. This was carried out in Microsoft Excel 2010 using the data analysis toolkit add-in. Three damping factors (0.1, 0.5 and 0.9) were trialled on the median NDVI's for all surface types. Put simply, when the damping factor is set to 0.9, the data point prior to the current data point is given less weighting than the one that appears after it, which is given more weighting. The plots resulting from the exponential smoothing can be seen in Figure 131 through to Figure 133.

It was found that the higher the damping factor, the smoother the time series; with a damping factor of 0.5 having produced the most optimal smoothed time series for this dataset. The fluctuations in NDVI were smoothed significantly, but the overall trend of the data was preserved. Therefore, a plot was produced for the median NDVI that had already been smoothed using a running median (interval of 10) and then exponential smoothing with a damping factor of 0.5 was applied (Figure 134). This resulted in a graph where the data was not shifted and a sudden reduction in NDVI during 2001 was able to be observed; indicating the times of grave creation/ disturbance. Prior to grave creation, the NDVI of all surface types were stable fluctuating between 0.65 and 0.75. It was also observed that the vegetation on the empty grave surface recovered, in both quantity and stress, quicker than vegetation on the surface of the full grave. This appeared to continue until the end of 2008, when the NDVI for each surface type has a similar trend across the seasons and years. This is consistent with the findings from the previous section where the individual NDVI maps were used to visualise the changes in NDVI over time.

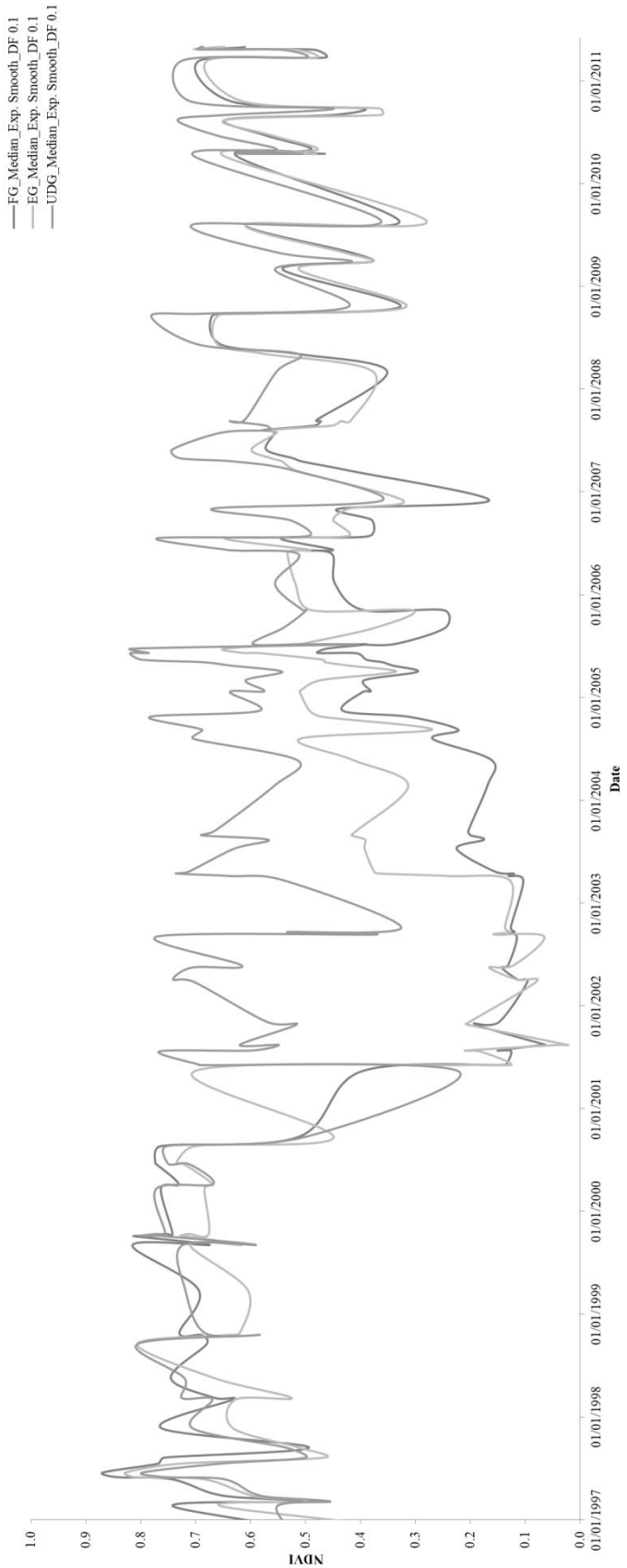

Figure 131 - Exponential Smoothing of median NDVI - 1997 to 2011 with a damping factor of 0.1.

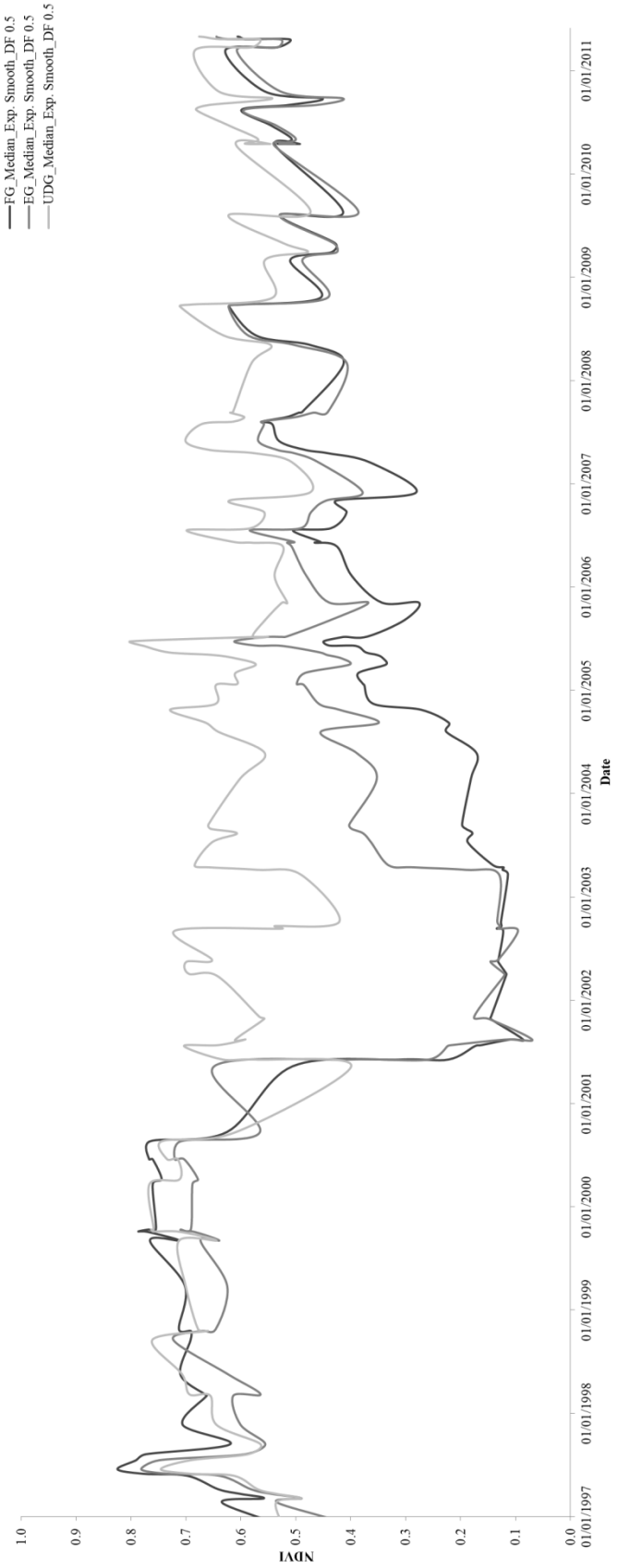

Figure 132 - Exponential Smoothing of median NDVI - 1997 to 2011 with a damping factor of 0.5.

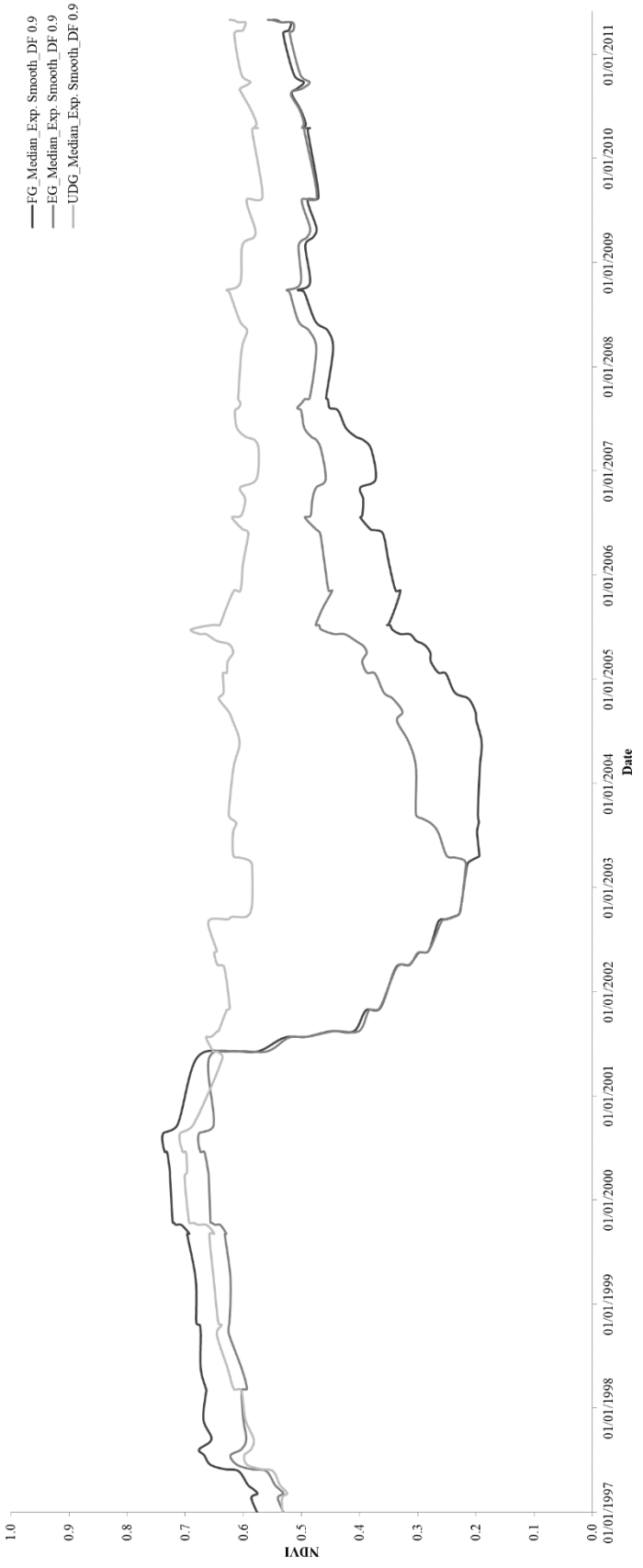

Figure 133 - Exponential Smoothing of median NDVI - 1997 to 2011 with a damping factor of 0.9.

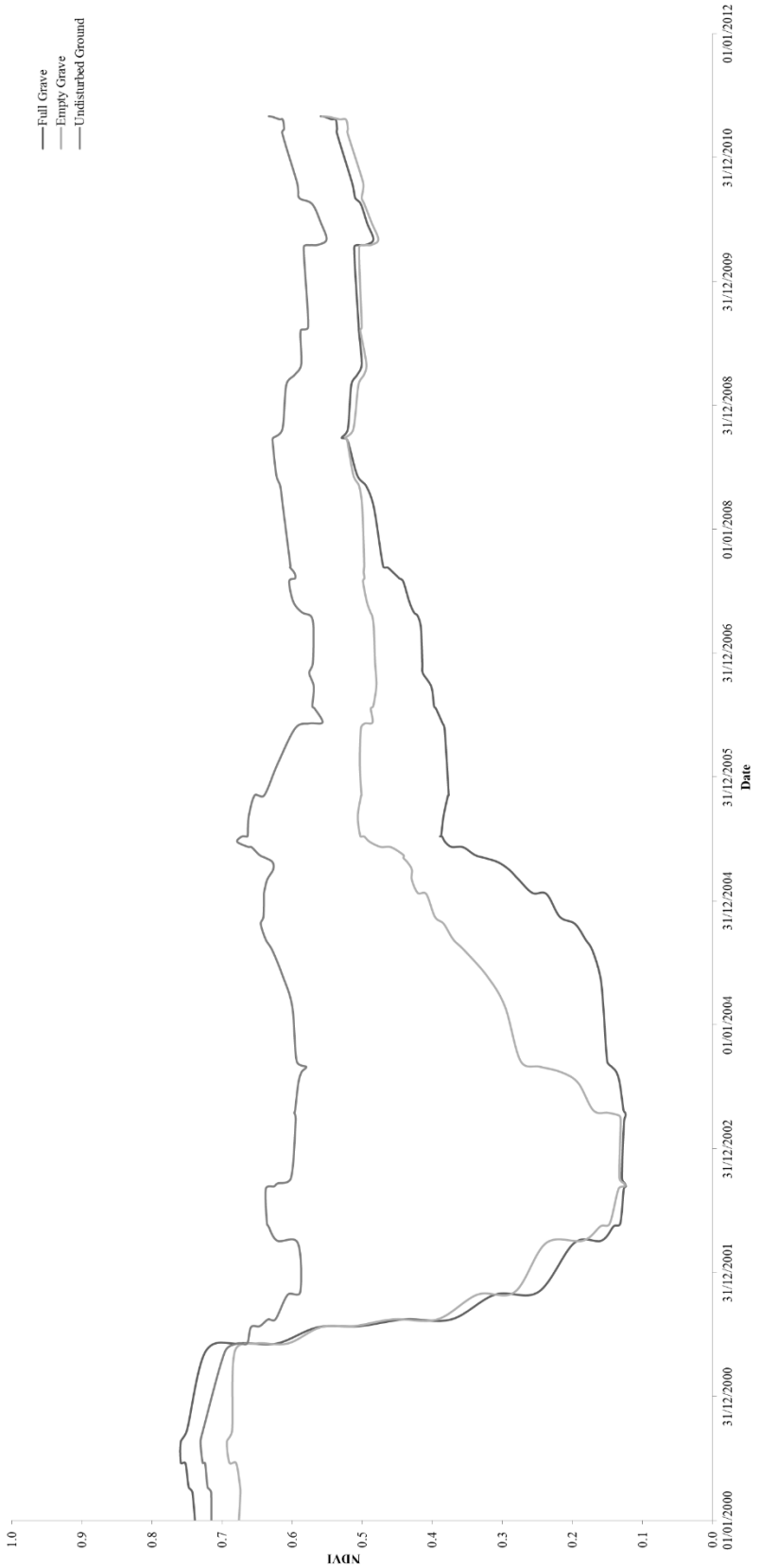

Figure 134 - Running Median NDVI (Interval 10) and Exponentially Smoothed (Damping Factor 0.5) median NDVI – 1997 to 2011.

6.4.4 Relationship between NDVI and Meteorological Variables at the Former RAF Pershore airfield

NDVI is known to be influenced by meteorological variables, therefore it was important to understand whether the NDVI observed had a strong relationship with such variables. The nearest weather station that recorded continuously throughout the study period (2001-2011) was the Meteorological Station located at Ross-On-Wye (51.9141, -2.5811, 41m above sea level), 28 miles south west of the site. Monthly meteorological data was downloaded from DATA.gov.uk, published by the Met Office and available through an Open Government Licence (Appendix 3). The archive reading comprised of the following variables, maximum temperature (TMax - ^{o}C), minimum temperature (TMin - ^{o}C), rainfall (mm – cumulative) and sun hours (hours – cumulative).

It is important to note that throughout the study period, a number of 'events' occurred which may have had an impact on the relationship between NDVI and the meteorological variables including; creation of the grave, and the recovery of the vegetation. Consequently, two phases were investigated: firstly, the relationship between meteorological variables and NDVI prior to grave creation (1997-2001) and secondly, the relationship between the variables and NDVI post grave creation (May 2001-2011).

Relationships were investigated between NDVI and the meteorological variables listed above, taking into account weather data one month prior to image acquisition. The sections presented below detail the relationships between meteorological variables and NDVI one month prior to image acquisition, for the two phases detailed above. For the data investigating the relationships between the NDVI and meteorological variables, two and three months prior to image acquisition, refer to Appendix 3.

6.4.4.1 The relationship between NDVI and meteorological variables for the period prior to grave creation (1997-2001)

This section presents the relationships that existed between NDVI and meteorological variables prior to grave creation. There was no evidence to suggest that any of the areas used within this study were disturbed prior to the known disturbance in 2001, therefore, it was expected that relationships between the three surface types (full and empty graves and the area of undisturbed ground) would be similar. Some variation may be observed due to

the location of the undisturbed ground (UDG) points, as these were local but not in close proximity to the graves.

The slope describing the linear relationship between NDVI and meteorological variables prior to the graves being created, were horizontal with slope values around zero (Table 27). The strongest linear relationships existed between the two grave surfaces and cumulative rainfall with r values of 0.259 (full grave) and 0.167 (empty grave), compared to the undisturbed grass where the correlation coefficient (r) was 0.251 (Table 27). The grave surfaces exhibited negative weak relationships with TMax, TMin and sun hours whereas, the undisturbed grass had a relatively weak negative relationship with TMin, TMax and sun hours. After plotting the scatter plots for each variable and NDVI, a trend line was added and r^2 values were generated for each surface type (Table 27). It was found that the r^2 values for all variables and surface types were low, the highest being 0.0085 (empty graves) and 0.067 (full graves) (Figure 135). The remainder of the r^2 values accounted for a maximum of 0.8% of the relationships between the grave surfaces and the meteorological variables. The original NDVI values and meteorological data used to derive these relationships are located in Appendix 3.

Table 27 - Relationship between NDVI and meteorological variables one month prior to image collection for the period prior to the creation of the grave.

FUNCTION		Full Grave	Empty Grave	Undisturbed Grass
SLOPE	NDVI vs TMax (^{o}C)	0.000	0.000	0.000
	NDVI vs TMin (^{o}C)	-0.001	-0.003	-0.004
	NDVI vs Cumul. Rainfall (mm)	0.001	0.000	0.001
	NDVI vs Sun Hours (hours)	0.000	0.001	0.000
CORREL (r)	NDVI vs TMax (^{o}C)	-0.007	0.000	-0.104
	NDVI vs TMin (^{o}C)	-0.037	-0.096	-0.137
	NDVI vs Cumul. Rainfall (mm)	0.259	0.167	0.251
	NDVI vs Sun Hours (hours)	0.061	0.292	-0.017
RSQ (r2 or %)	NDVI vs TMax (^{o}C)	0.000	0.000	0.011
	NDVI vs TMin (^{o}C)	0.001	0.009	0.019
	NDVI vs Cumul. Rainfall (mm)	0.067	0.028	0.063
	NDVI vs Sun Hours (hours)	0.004	0.085	0.000

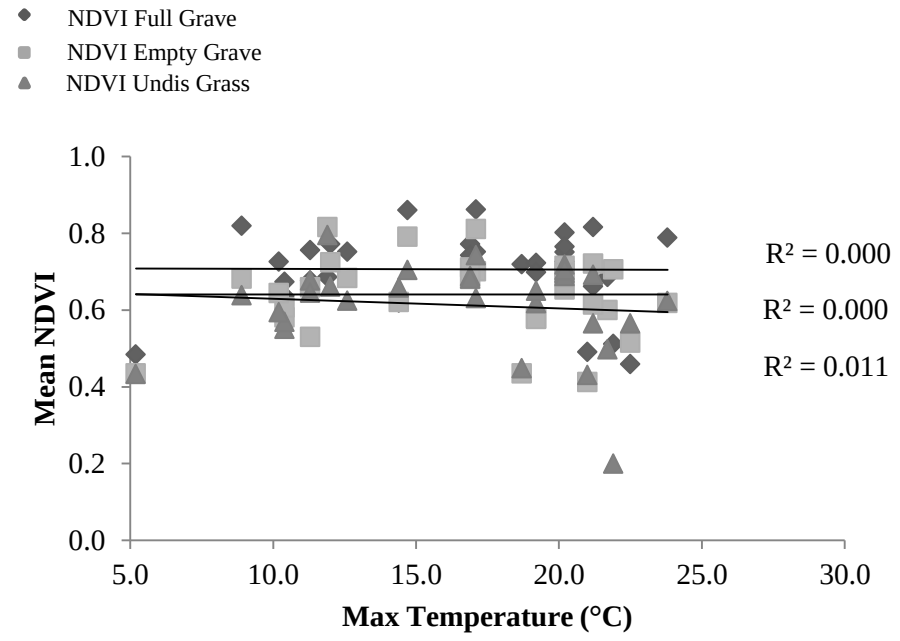
NDVI Full Grave
NDVI Empty Grave
NDVI Undis Grass
Mean NDVI
1.0
0.8
0.6
0.4
0.2
0.0
5.0
10.0
15.0
20.0
25.0
30.0
Max Temperature (°C)
R² = 0.000
R² = 0.000
R² = 0.011

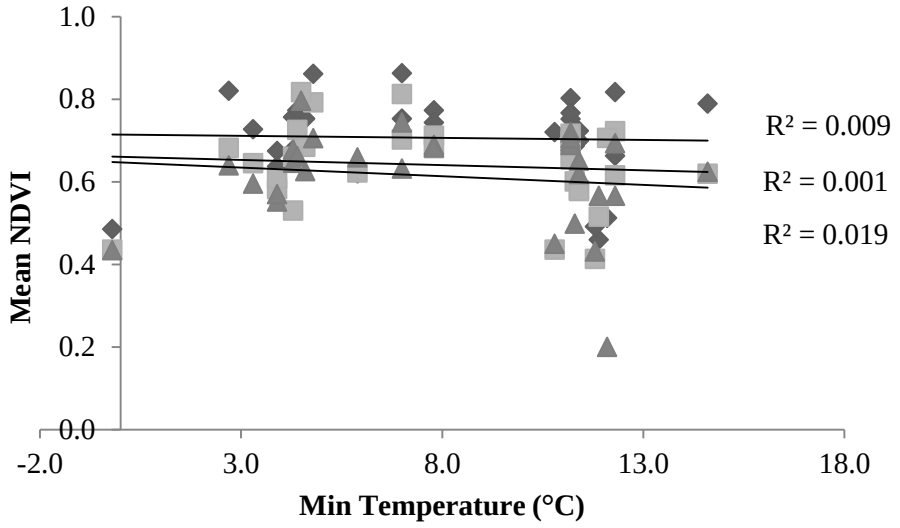
Mean NDVI
1.0
0.8
0.6
0.4
0.2
0.0
-2.0
3.0
8.0
13.0
18.0
Min Temperature (°C)
R² = 0.009
R² = 0.001
R² = 0.019

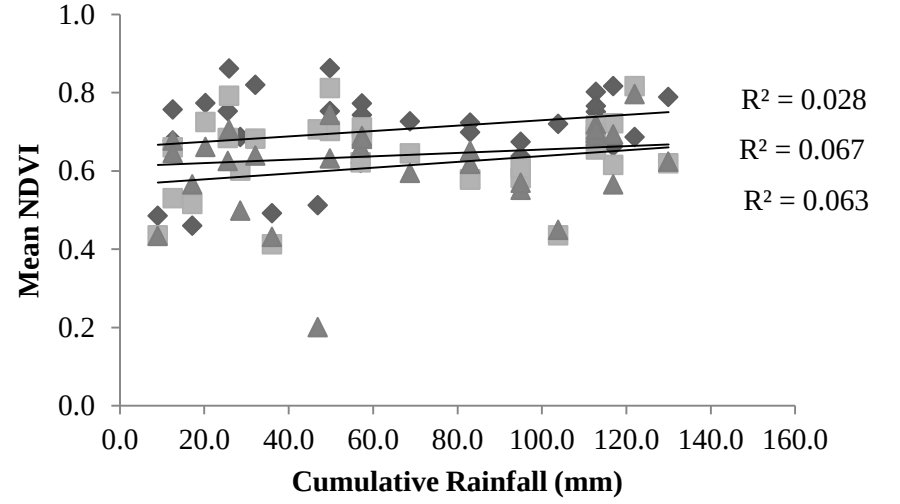
Mean NDVI
1.0
0.8
0.6
0.4
0.2
0.0
0.0
20.0
40.0
60.0
80.0
100.0
120.0
140.0
160.0
Cumulative Rainfall (mm)
R² = 0.028
R² = 0.067
R² = 0.063

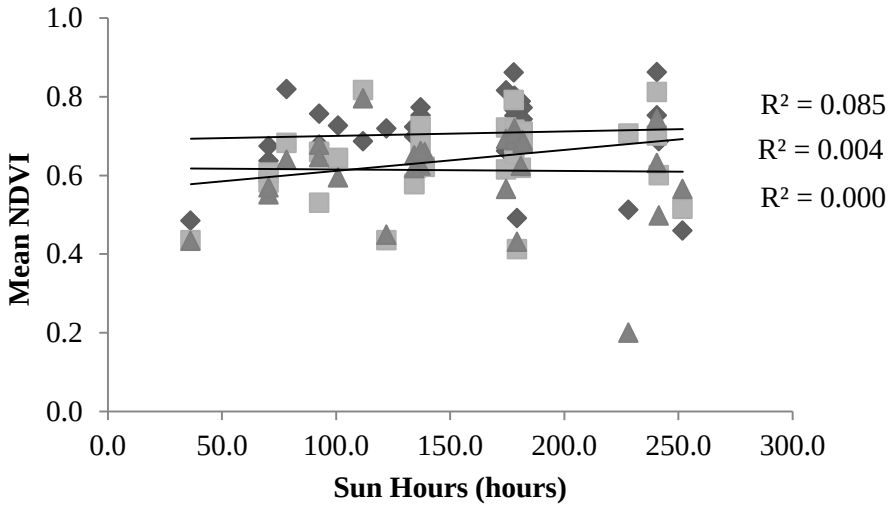

Figure 135 - Relationships between NDVI and meteorological variables one month prior to the image acquisition for the period prior to the graves being created (1997-2001).

6.4.4.2 The relationship between NDVI and meteorological variables for the period post creation of the grave (2001-2011)

Relationships between meteorological variables and NDVI were investigated, taking into account weather events one month prior to image acquisition, through the production of scatter plots, extraction of slope, calculation of correlation coefficients and r^2 values (Figure 136). A difference in the relationships was expected, particularly between the undisturbed ground and the two grave surfaces, as when they were created; soil was present on the surfaces rather than vegetation.

When the slope of the linear relationship was calculated for each scatter plot (Table 28

Table 28) it was found that the slope was negative for the relationships between TMax and TMin for all three surface types; the values were small and close to zero indicating horizontal trend lines (Table 28). The slope for the relationships for both cumulative rainfall and sun hours and NDVI, were zero for all surface types. The strongest linear correlation existed between the undisturbed grass and TMin (r = -0.247), sun hours (r = +0.169), TMax (r = -0.129) and cumulative rainfall (r = +0.013). In contrast, the grave surfaces had weaker

linear relationships, the strongest of which was TMin followed by TMax, cumulative rainfall and sun hours. It was found that taking into account weather data from one month prior to the satellite image acquisition, that the r^2 values were similar across all surface types. It was also observed that the relationship between the two grave surfaces and the weather variables were very similar, with the undisturbed ground having noticeably stronger relationships in comparison. The linear trend line was able to explain 4% of the relationship between NDVI and the grave surfaces, indicating that a complex relationship existed between the variables and the grave surfaces. However, as the relationships were found to be relatively weak overall, this suggests that the NDVI of surface types were not affected by the seasonal fluctuations in meteorological variables over the duration of the study period. The original NDVI and meteorological data is located in Appendix 3.

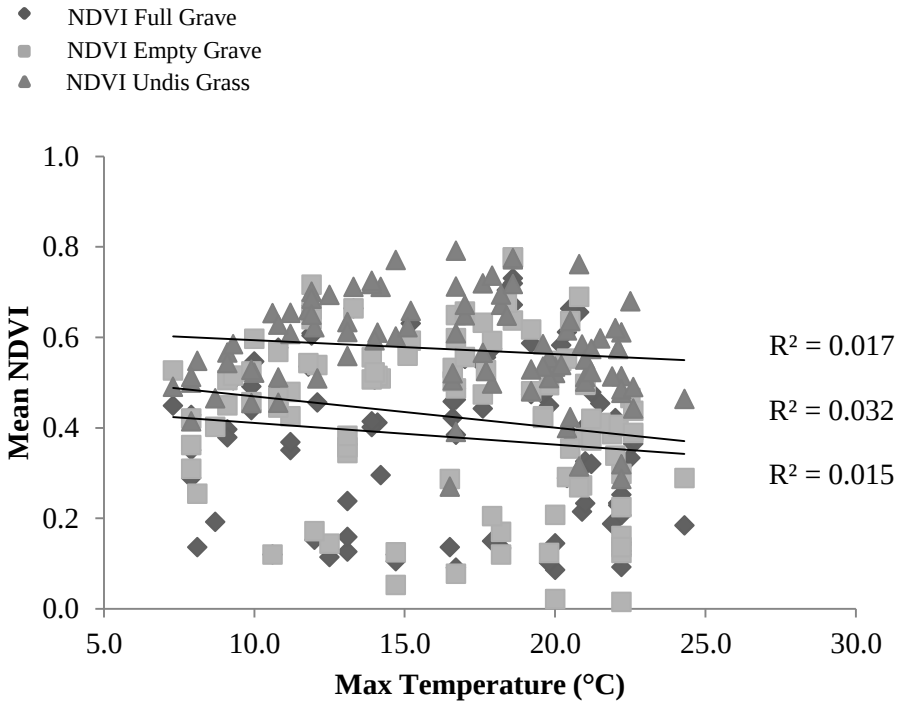

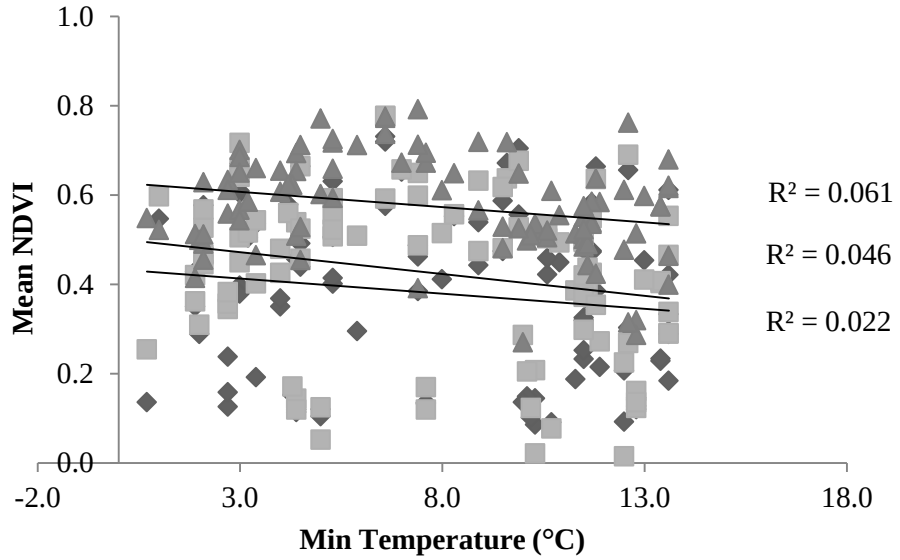
1.0
0.8
0.6
0.4
0.2
0.0
Mean NDVI
-2.0
3.0
8.0
13.0
18.0
Min Temperature (°C)
R² = 0.061
R² = 0.046
R² = 0.022

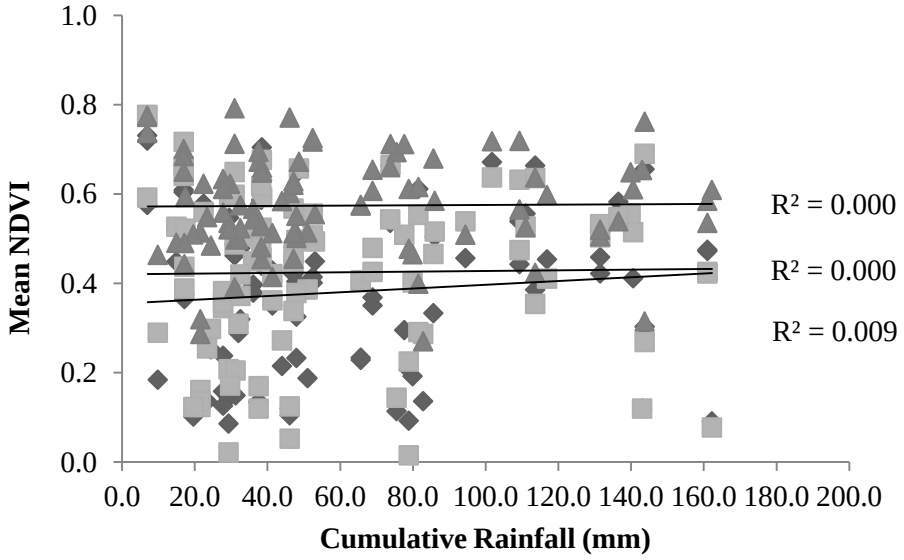
1.0
0.8
0.6
0.4
0.2
0.0
Mean NDVI
0.0 20.0 40.0 60.0 80.0 100.0 120.0 140.0 160.0 180.0 200.0
Cumulative Rainfall (mm)
R² = 0.000
R² = 0.000
R² = 0.009

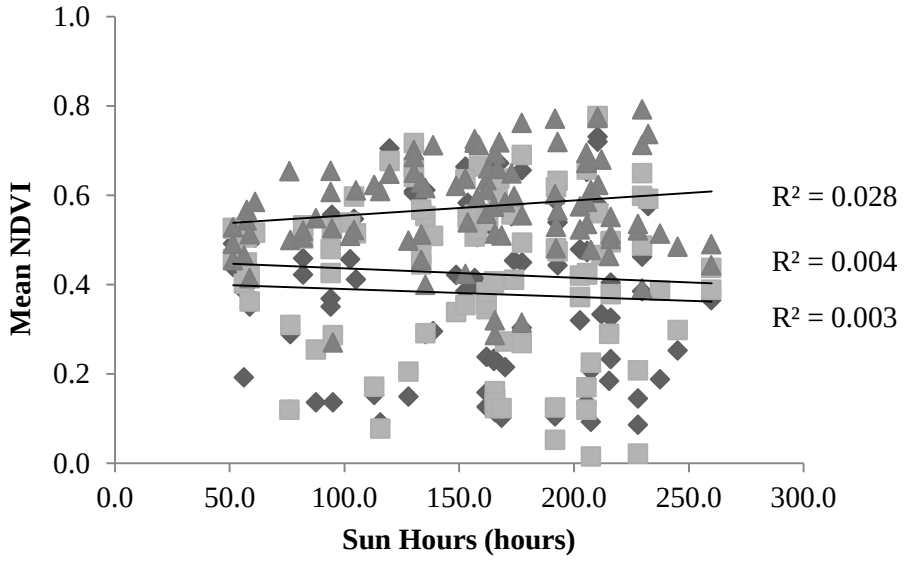
1.0
0.8
0.6
0.4
0.2
0.0
Mean NDVI
0.0 50.0 100.0 150.0 200.0 250.0 300.0
Sun Hours (hours)
R² = 0.028
R² = 0.004
R² = 0.003

Figure 136 - Relationships between NDVI and meteorological variables one month prior to the image acquisition for the period 2001-2011.

Table 28 - Relationship between NDVI and meteorological variables one month prior to image collection for the period 2001-2011.

FUNCTION		Full Grave	Empty Grave	Undisturbed Grass
SLOPE	NDVI vs TMax (^{o}C)	-0.005	-0.005	-0.005
	NDVI vs TMin (^{o}C)	-0.007	-0.010	-0.007
	NDVI vs Cumul. Rainfall (mm)	0.000	0.000	0.000
	NDVI vs Sun Hours (hours)	0.000	0.000	0.000
CORREL (r)	NDVI vs TMax (^{o}C)	-0.121	-0.179	-0.129
	NDVI vs TMin (^{o}C)	-0.147	-0.215	-0.247
	NDVI vs Cumul. Rainfall (mm)	0.094	0.017	0.013
	NDVI vs Sun Hours (hours)	-0.053	-0.064	0.169
RSQ (r2 or %)	NDVI vs TMax (^{o}C)	0.015	0.032	0.017
	NDVI vs TMin (^{o}C)	0.022	0.046	0.061
	NDVI vs Cumul. Rainfall (mm)	0.009	0.000	0.000
	NDVI vs Sun Hours (hours)	0.003	0.004	0.028

6.5 Discussion

6.5.1 Is NDVI influenced by the presence of mass graves containing mammalian matter and if so, for how long?

Through the research undertaken on the foot and mouth burial site at the Former RAF Pershore airfield, it was found that the presence of mass graves, both full and empty, influenced the NDVI of the vegetation on the grave surfaces, over a decadal time period.

Prior to the epidemic, the NDVI across all surfaces was stable, with fluctuations observed representative of seasonal changes. When the graves were created in 2001, the NDVI

reduced significantly in the areas containing graves, due to the presence of soil; this being indicative of large scale disturbance. The areas unaffected by the creation of the burials exhibited relatively high NDVI, which persisted throughout the duration of the study. The NDVI of both the full and empty grave surfaces took a considerable amount of time to recover, both in terms of vegetation cover and also vegetation stress, resulting in apparent equalisation of both graves by 6 years and 2 months post burial ($p>0.05$). This indicated that, when only using medium spatial resolution imagery (i.e. Landsat with 30m spatial resolution), the graves, both full and empty, could not be differentiated from either the undisturbed, control vegetation or each other. However, when NDVI derived from comparatively fine spatial resolution imagery (RapidEye) was assessed, it was found that although the NDVI for all surface types appears to have recovered, significance was observed, ranging from *** ($p<0.001$) to * ($p<0.05$), from 2009 through to 2011. Therefore, suggesting that the vegetation had not recovered or equalised, up to 9 years and 11 months post burial.

Comparable research was conducted by Kalacska et al. (2009) who used hyperspectral airborne imaging and field spectroscopy, to determine whether the spectral signature of a simulated mass grave (containing cattle), could be differentiated from surrounding vegetation and a control grave, over 16 months in the Costa Rican tropics. Similar to the Former RAF Pershore site it was found that the false grave colonised quicker than the true grave (containing cattle). However, Kalacska et al's (2009) research was conducted over 16 months whereas, this research considered changes in NDVI over a decadal time scale. At 16 months post burial, at the Former RAF Pershore, low NDVI continued to dominate the mass graves. The location of the experimental site accounts for the fact that colonisation occurred more readily in the tropics, compared to the temperate climes of rural Worcestershire. However, for both sites the presence of buried mammalian remains has inhibited vegetation growth and caused measureable vegetation stress at the grave surface which was visible in both the gradient of the Red Edge and through NDVI, regardless of geographical location. The impacts of these findings are such that, in tropical environments there may be a limited time window when vegetation stress could be used to aid the detection of mass graves. Whereas, in temperate environments this window appears to be up to 9 years and 11 months post burial, when calculating NDVI from both medium and fine spatial resolution imagery.

6.5.2 Are both full and empty mass graves detectable, using NDVI, up to 10 years post burial?

Both the full and empty mass graves were able to be differentiated from the native undisturbed ground up to 9 years, 11 months post burial, using variations in NDVI derived from fine spatial resolution imagery (RapidEye). Using medium spatial resolution from Landsat, the full and empty graves could be distinguished from the native vegetation up to 6 years, 2 months post burial; after which, the vegetation above the graves exhibited comparable stress to the undisturbed areas of the site.

Following the initial reduction in NDVI indicative of disturbance, NDVI was found to slowly increase for the full and empty graves, indicating vegetation growth and recovery. Through comparison of the NDVI trend over the full decadal time series, it was discovered that the NDVI of the full and empty graves recovered at varying rates, enabling them to be differentiated from each other and the undisturbed vegetation.

The NDVI values for the full and empty grave surfaces were similar during May 2001 and March 2002, with no significance observed ($p>0.05$). However, in April 2003, *** significance ($p<0.001$) was observed between the NDVI values the full and empty graves and the undisturbed vegetation. This suggests that soil, or stressed vegetation, dominated the surface of the full graves, whereas, the higher NDVI on the surface of the empty graves indicates possible vegetation colonisation. Varying levels of significance were observed between 2004 and 2007, enabling the differentiation between the full and empty graves and the undisturbed ground. However, July 2007, was the first instance where no significance ($p>0.05$) was observed between the undisturbed vegetation and the two grave surfaces.

Therefore, it can be said that when utilising medium spatial resolution imagery (Landsat 30m), between February 2003 and June 2006 (1 year, 10 months up to 5 years, 1 month post burial) full and empty burials were able to be differentiated, not only from the undisturbed ground, but also each other using NDVI. By July 2007 (6 years, 2 months post burial), the NDVI of vegetation above both the full and empty graves appeared to have equalised and was similar to the undisturbed vegetation. Post June 2008, the NDVI had equalised for all surface types, with any fluctuations observed being representative of seasonal changes. These findings were clearly evident when the median NDVI values for each surface type were smoothed using moving median and exponential smoothing; where the NDVI of the empty graves increased more rapidly than the full graves, indicating that the empty grave was colonising more readily than the full graves.

However, by calculating NDVI using comparably fine spatial resolution imagery from RapidEye (5m), the time frame within which significance was detected between the grave surfaces and the undisturbed ground, was able to be extended to 9 years, 11 months post burial.

6.5.3 What is the relationship between NDVI and the presence of a decadal mass grave?

It was found that the NDVI had complex relationships with meteorological variables prior to and post creation of the grave for all surface types. Two periods were considered, the period prior to the grave creation (1997-2001) and post creation (May 2001-2011). It was found that the strongest relationships existed between cumulative rainfall and NDVI for the full and empty grave surfaces and the undisturbed grass prior to grave creation. The differences in the order and strength of the relationships with NDVI were likely due to the placement of the sample points; the undisturbed grass was comprised of two groups of points from two separate areas of the site. Post grave creation (May 2001-2011), it was found that the relationship between the NDVI of the undisturbed grass and the meteorological variables, were stronger than the two grave surfaces. This is likely due to the fact that the relationship between soil and meteorological variables differs compared to the relationships that exist between weather and vegetation. The order, in terms of strength, of the relationships for the NDVI of the grave surfaces were identical whereby TMin was the strongest, followed by TMax, cumulative rainfall and sun hours. Overall, the relationships between NDVI and meteorological variable were complex and on the whole, weak. Therefore, suggesting that such variables have little effect on the NDVI observed throughout this decadal study.

6.6 Conclusions

From this research, it was found that NDVI derived from archive multispectral orbital imagery with medium spatial resolution, can be used to detect disturbance synonymous with the creation of mass graves, at the Former RAF Pershore.

From 1 year, 10 months up until 5 years, 1 month post burial, it was possible to differentiate the NDVI of full burials from empty burials, with significance observed ranging between *** (p<0.001) and ** (p<0.01); using medium spatial resolution imagery. At 6 years, 2

months post burial, the NDVI values were no longer found to be significant between the full and empty graves, or the undisturbed ground. Therefore, suggesting that the vegetation across the site had recovered and equalised. However, through utilising fine spatial resolution imagery from RapidEye (5m), it was possible to demonstrate that significance existed (*** $p<0.001$, ** $p<0.01$ and * $p<0.05$) between the control undisturbed vegetation and both grave surfaces post 2006 (5 years, 1 month post burial). The high levels of significance observed between the NDVI of the undisturbed, control vegetation compared to the full graves indicated, that full graves can be differentiated from undisturbed vegetation and empty graves, up to 9 years, 11 months post burial. These observations suggest that the presence of organic remains causes vegetation on the surface of graves to remain stressed, or sparsely colonised, for extended periods of time, compared to empty graves which have been found to recover and colonise sooner.

The findings presented refute statements by Kalacska and Bell (2006), Kalacska et al. (2009) and Leblanc et al. (2014) and proves that hyperspectral sensors are not necessary to locate areas of disturbance or differentiate between full and empty graves, specifically in temperate environments. Instead, the results obtained have demonstrated that medium spatial resolution archive imagery is appropriate for detecting targets that have a larger extent than the spatial resolution of the imagery. Also, the benefits of utilising complimentary sensors with fine spatial resolution have been demonstrated.

The following chapter will investigate this further by applying the methods used within the previous two chapters, to ascertain whether NDVI can be used to detect disturbance resulting from exhumations of known location human mass graves in Bosnia and Herzegovina.

7 The Detection of Clandestine Human Mass Graves in Bosnia and Herzegovina - A Multi-Platform Approach

This chapter assesses whether NDVI can be used to locate human clandestine mass graves in Bosnia and Herzegovina, through the detection of disturbance. As in Chapter 6, archive medium spatial resolution orbital imagery was used to derive NDVI profiles for human mass graves, over a time scale in excess of twenty years. In addition to imagery pre-dating the creation of the graves, imagery was acquired for the period post interment through to exhumation and post exhumation. This imagery was acquired to detect significant decreases in NDVI on the grave surface compared to surrounding undisturbed vegetation (control). In addition, archive RapidEye imagery with a fine spatial resolution of 5m was assessed for use on a mass grave, located on Cancari Road that was exhumed in 2009 to ascertain whether the disturbance caused by the exhumation process could be detected using variations in NDVI. This data was used to identify whether fine spatial resolution imagery is more applicable for the detection of human mass graves.

7.1 The Cancari Road Mass Graves

Cancari Road is located in the Zvornik Municipality in the Republika Srpska, Bosnia and Herzegovina (Figure 137 and Figure 138). During the conflict in the early to mid-1990s thirteen secondary mass graves (CR01 – CR13) were created along the Cancari Road, and contained in excess of 1900 individuals (ICTY 2010e). The graves were associated with the fall of Srebrenica and two primary mass graves, Branjevo Farm and Kozluk (Table 29). As a result of the conflict in the Former Yugoslavia an estimated 100,000 people perished with approximately 40,000 reported as missing (International Commission on Missing Persons 2014). The International Commission on Missing Persons (2014a) estimated that 70% of the individuals reported as missing have now been accounted for, however, efforts continue to locate remaining missing individuals.

Figure 137 - Map of Bosnia and Herzegovina with the location of Cancari Road indicated by the red box. Source: http://www.eoearth.org/files/192801_192900/192802/bk-map.gif [Accessed 18/03/2016]

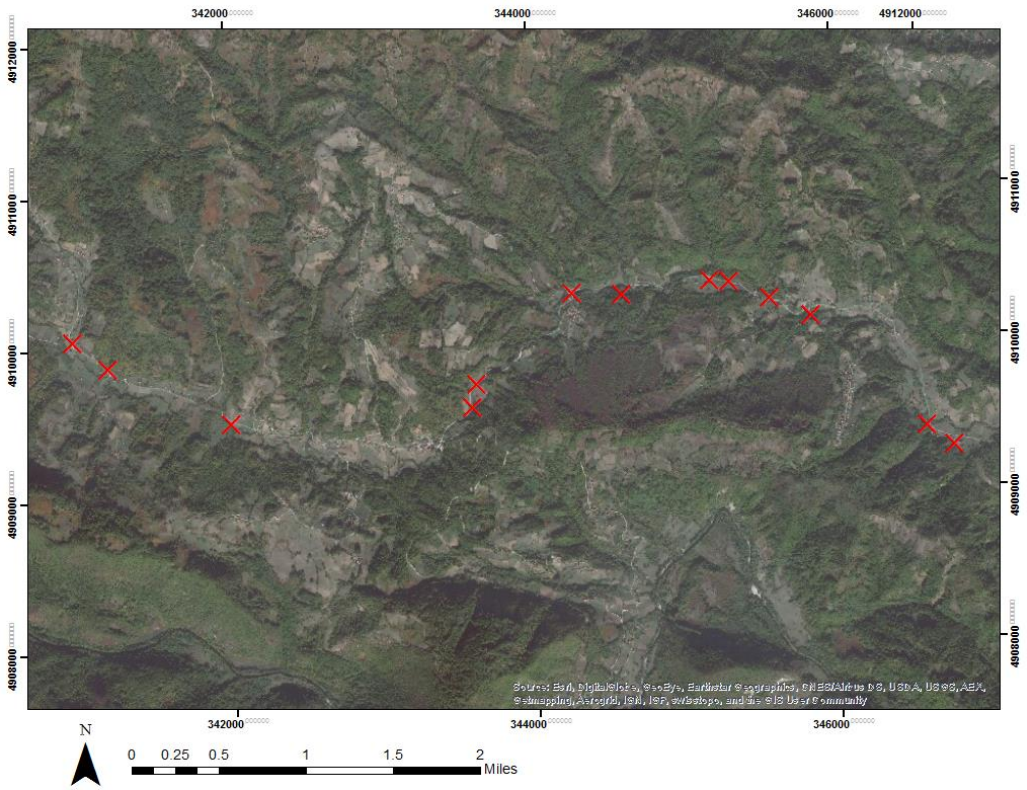

Figure 138 - The Cancari Road with the locations of the 13 secondary mass graves indicated by red crosses.

Much is known about the Cancari Road mass graves due to the extensive forensic investigations that have been undertaken including the search, location and exhumation of the graves. Additionally, experts in various fields including soil specialists and geologists have provided insights into the native geology on which the graves were created. The geology of and around the Cancari Road is amphibolite and limestone, with the soil being comprised of Mediterranean brown earths; a mixture of red-brown, sandy clay (ICTY 2011af; ICTY 2012d). The area surrounding the road is predominantly farmland, consisting of relatively small arable fields located in the valley floor with woodland dominating elevated areas (ICTY 2011af).

7.2 Rationale for the study location

As a result of the extensive forensic investigations surrounding the fate of individuals from the fall of Srebrenica, substantial quantities of documentary evidence were available for the Cancari Road mass graves including aerial photographs, exhumation records and individual grave reports. All were freely available via the United Nations ICTY Court Record Archives. The documentary evidence available indicated that mass graves 1-12 were created between the 7th September and 2nd October 1995; it is unknown when CR13 was created. However, the assumption is that this grave was also created around the same time as CR1-12. Each of the mass graves was exhumed at different times, the first in 1998 and the last in 2009, resulting in a series of known location mass graves, of different ages (Table 30).

Documentary evidence also detailed some of the sizes of the mass graves (post exhumation) indicating that the graves were relatively large (e.g. ranging between 14 and 17m long by 2.7 to 3.9m wide (ICTY 2012d) Table 29), with the grave footprint (area of disturbance from the creation of a grave) much larger. All of the graves were located in close proximity to Cancari Road and along a total distance of 6km. As a result of this, all of the mass graves were located within a single scene of orbital imagery. This was true also for RapidEye, which had the smallest spatial extent. Thus, any instrument related effects would consequently impact the entire scene, and therefore the graves equally, resulting in relative differences in NDVI within a single scene, being unaffected. Furthermore, there is intelligence to suggest that there may be additional undetected mass graves in the locality of Cancari Road that remain undisturbed (ICTY 2010e).

Table 29 - Dimensions of the Cancari Mass Graves

Mass Grave	Dimensions (m) L x W x D	Alleged Primary Grave	Reference
CR01	Unknown	Kozluk[1]	[1]ICMP 2014b
CR02	Unknown	Kozluk[2]	[2]ICMP 2014b
CR03	14 x 3.5 x 1.8[3]	Kozluk[4]	[3,4] ICTY 2011aa
CR04	15 x 3.2 x 1.6-2.5[5]	Branjevo Military Farm[6]	[5]ICTY 2012c; [6]ICMP 2014b
CR05	Unknown	Branjevo Military Farm[7]	[7]ICMP 2014b
CR06	17 x 3-3.6 x 1.5[8]	Branjevo Military Farm[9]	[8,9] ICTY 2012b
CR07	Unknown	Kozluk[10]	[10]ICMP 2014b
CR08	14 x 3.1-3.9 x 1.8[11]	Branjevo Military Farm[12]	[11,12] ICTY 2012d
CR09	16 x 2.7-3.7 x 2.1m[13]	Branjevo Military Farm[14]	[13]ICTY 2010d; [14]ICMP 2014b
CR10	Unknown	Branjevo Military Farm[15]	[15]ICMP 2014b
CR11	Unknown	Branjevo Military Farm[16]	[16]ICMP 2014b
CR12	13 x 3.8 x 1.2[17]	Branjevo Military Farm[18]	[17,18]ICTY 2011aa
CR13	Unknown	Kozluk[19]	[19]ICMP 2014b

Table 30 - Details regarding inhumation date, exhumation date and age of burial for the Cancari Road mass graves

Mass Grave	Inhumation Date	Examination/ Probe Date	Exhumation Date	Age of Burial (from 7 Sept 1995)
Cancari Road 1 (CR01)	7 September – 2 October 1995	16 June 1998	8-23 July 2009	13 years 10 months
Cancari Road 2 (CR02)	7 September – 2 October 1995	15 June 1998	6 - 12 August 2002	6 years 11 months
Cancari Road 3 (CR03)	7 September – 2 October 1995	-	27 May – 10 June 1998	2 years 8 months
Cancari Road 4 (CR04)	7 September – 2 October 1995	15 June 1998	12 August – 26 September 2008	12 years 11 months
Cancari Road 5 (CR05)	7 September – 2 October 1995	15 June 1998	12 August – 4 October 2002	6 years 11 months
Cancari Road 6 (CR06)	7 September – 2 October 1995	16 June 1998	8 October – 11 December 2008	13 years 1 month
Cancari Road 7 (CR07)	7 September – 2 October 1995	1996 (exact date unknown)	2 – 23 October 2002	7 years one month
Cancari Road 8 (CR08)	7 September – 2 October 1995	14 June 1998	20 October – 18 November 2008	13 years one month
Cancari Road 9 (CR09)	7 September – 2 October 1995	14 June 1998	22 October – 24 November 2007	12 years one month
Cancari Road 10 (CR10)	7 September – 2 October 1995	14 June 1998	8 June – 12 August 2006	10 years 9 months
Cancari Road 11 (CR11)	7 September – 2 October 1995	16 June 1998	28 August – 28 September 2001	6 years
Cancari Road 12 (CR12)	7 September – 2 October 1995	-	10 – 25 May 1998	2 years 8 months
Cancari Road 13 (CR13)	7 September – 2 October 1995	-	14 – 25 October 2002	7 years one month

7.3 Methods

7.3.1 Locating the Cancari Road Graves

Cancari Road and the mass graves were located using maps and reports submitted to the ICTY during the tribunals (ICMP 2005; ICTY 2011aa; ICTY 2011ac; ICTY 2011ad). Consulting with literature enabled the approximate location of graves CR01-CR13 to be identified. Summary reports published by the ICMP for CR04 (ICTY 2012c), CR06 (ICTY 2012b) and CR08 (ICTY 2012d) provided Military Grid Reference System (MGRS) coordinates which were inputted into a GIS (ArcMap). The locations of the graves were fine-tuned using aerial photomosaics and individual aerial photos showing areas of disturbed

ground, synonymous with creation of the graves (ICTY 2011a-2011z; ICTY 2011ae; ICTY 2012a). IKONOS imagery was also utilised as it showed the locations of CR13 and CR01 in relation to the rest of the graves (ICTY 2011ae). Refer to Appendix 4 for comparisons between the identified mass grave points and the grave footprints visible in the aerial photographs from October 1995.

7.3.2 Archive Satellite Imagery

To study fluctuations in NDVI of the vegetation on the surface of the Cancari Road mass graves prior to creation, during creation and post burial, a dense time series of 209 cloud free archive orbital multispectral scenes were acquired, from 1990 to 2014 (full list of imagery is provided in Appendix 4). The scenes were acquired from three platforms, Landsat (5 TM, 7 ETM+, 8 OLI), SPOT and RapidEye. The majority of the imagery, including SPOT and RapidEye along with 68 scenes of Landsat was obtained through a European Space Agency (ESA) data grant[4]. The remainder of the Landsat imagery was freely available from the USGS EarthExplorer interface. As the majority of the imagery was obtained from Landsat it was deemed the primary sensor; similar to the previous chapter. SPOT was the secondary sensor and RapidEye the tertiary. The number of archive orbital scenes downloaded for each year is presented in Figure 139 with the breakdown for the number of scenes per sensor and per year located in Appendix 4.

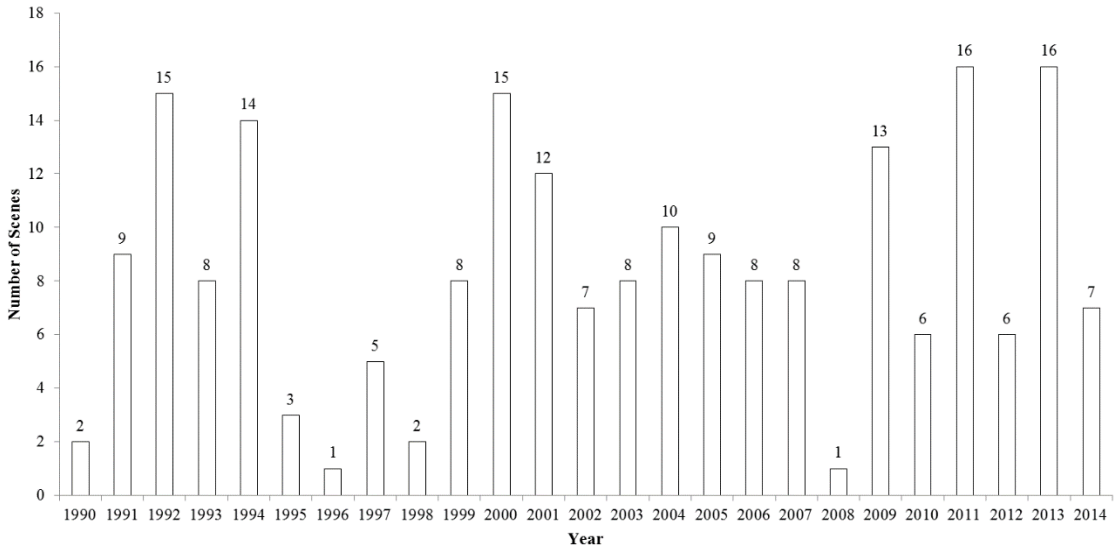

Figure 139 - The cloud-free archive orbital imagery scenes available per year.

[4] European Space Agency, Project ID: 26349

7.3.2.1 Archive Satellite Imagery Pre-Processing

All of the imagery underwent atmospheric correction, fine registration and NDVI calculation in ENVI. Due to the imagery having been acquired from various sources including USGS EarthExplorer and ESA, the levels of pre-processing carried out by the imagery provider varied. This is indicated by the processing level within Appendix 4. Once the required pre-processing was completed, the scenes were spatially subset for ease of computing using the spatial extent of a RapidEye image. The NDVI values for each grave were extracted using the extract multi values to points tool in ArcMap (Version 10.3). The pre-processing steps are summarised for each sensor within Figure 140.

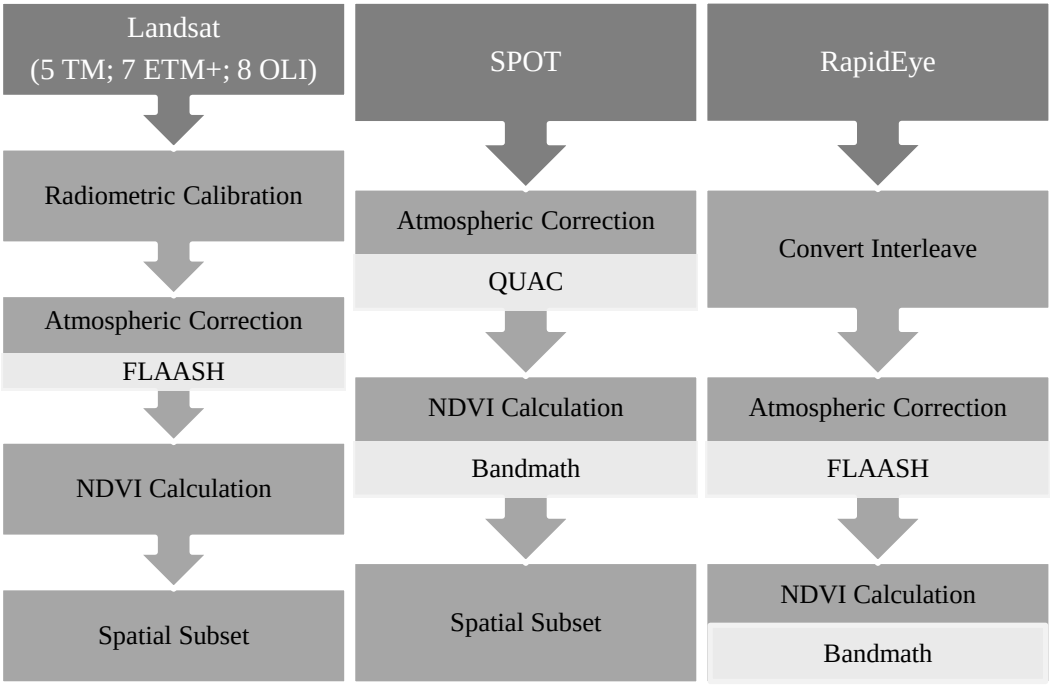

Figure 140 - Pre-processing stages for the orbital images from each sensor

7.3.2.1.2 Radiometric Calibration

The ENVI toolbox Radiometric Correction was used to radiometrically calibrate all of the Landsat imagery. The full extent of the scene and all bands were inputted and FLAASH settings were applied, resulting in a radiance image that had a BIL (band-interleaved-by-line) interleave, in floating point format (combining all bands into a single file) and a scale factor of 0.1. Neither SPOT nor RapidEye required radiometric calibration as the imagery requested from ESA was processed to Level3ortho and Level 3A (RapidEye Ortho product)

respectively; with all images radiometrically calibrated, sensor and geometrically corrected and orthorectified. However, it was necessary to convert the interleave type from the default for RapidEye (BSQ – Band Sequential) to BIL to carry out atmospheric correction.

7.3.2.1.3 Atmospheric Correction

FLAASH was used to atmospherically correct the Landsat and RapidEye imagery. After selecting the correct sensor type, the technical fields containing platform specific data, i.e. sensor altitude (km) were automatically updated. To apply the correct atmospheric parameters for each scene, the details of the flight date and time, located within the scene's metadata file, were inputted. The aerosol model chosen was consistently 'rural', as this described location of Cancari Road best in the context of its surroundings. On advice of technical staff at BlackBridge, the aerosol retrieval tool was not used during the atmospheric correction process, as it required wavelengths that were not recorded within the spectral range of the RapidEye imagery. The SPOT imagery was atmospherically corrected using QUAC, in ENVI (Version 5.3). The sensor type was specified as 'unknown' and the full extent of the image and all bands were considered during the correction process.

7.3.2.1.4 Fine Registration

The base (master) image selected was a RapidEye image, from the 28th June 2014, to which all images were registered using the Geometric Correction toolbox in ENVI (Version 5.3). Tie points were automatically generated using the general cross correlation matching method before being filtered. A minimum matching score of 0.7 was stated with a maximum error per tie point of 5.0. Polynomial warping, the default setting, was carried out on the warp image and the image was resampled using cubic convolution. The output pixel size was stated as being the same size as the imagery that was initially inputted (e.g. in the case of Landsat 30m x 30m). In some instances it was found that the image registration process described above did not register the images as accurately as was required for this study. Therefore, the ENVI header was manually edited for the images in question.

7.3.2.1.5 NDVI Calculation

NDVI was calculated for Landsat and SPOT using the ENVI spectral toolbox. As ENVI did not have a pre-set to automatically calculate NDVI for the RapidEye imagery, NDVI was

calculated manually using the following equations in Band Math (Equation 8). This took into account bands 3 and 5 for the RapidEye imagery which equated to the red and the near infrared bands respectively.

Equation 9 - NDVI Calculation for RapidEye Imagery (b5 = band 5, b3 = band 3)

$$NDVI = \frac{(float(b5) - b3)}{(b5 + b3)}$$

7.3.2.1.6 Subsetting the imagery

All imagery was subset to be equivalent to RapidEye which had the smallest spatial extent.

7.4 Results

7.4.1 Extraction of NDVI values for all graves post burial (1996-2014)

The NDVI values were extracted from the Cancari Road mass grave shapefiles in ArcMap (Version 10.3.1) using the extract multi-values to points tool and were plotted for the period post interment (1996-2014). NDVI values were extracted from 143 cloud free scenes and included imagery from all sensors; Landsat, SPOT and RapidEye. All graves followed the same trend in NDVI over the study period (Appendix 4).

Following the results obtained in Chapter 5 and 6, it was expected that low NDVI values would be observed immediately post interment and that this would persist for a number of years. However, low NDVI values were not observed in 1996 (approximately 1 year post burial) instead, NDVI remained relatively high ranging between 0.65 and 0.85 for all graves.

It was found that the NDVI of CR07 was found to be lower than the NDVI of the other mass graves throughout the study. It is believed that this is due to the proximity of the mass grave to the road (Figure 141). When utilising medium spatial resolution imagery (30m) to derive NDVI for graves close to roads or other non-vegetated areas, it is possible that pixels may become mixed therefore reducing the NDVI observed.

Figure 141 - Aerial photograph of the location of Cancari Road mass grave 7 (CR07) - showing the proximity of the grave to the road (ICTY 2011m).

During 2002 and 2008, multiple mass graves were exhumed along Cancari Road. Therefore, it was possible to plot the NDVI for each grave from 1996 either to 2002 or 2008, to ascertain how similar the grave profiles were to others of similar or the same age. The line plot in Figure 142 shows the NDVI from 1996 to the end of 2003 (one year post exhumation), for the four mass graves exhumed (CR02, CR05, CR07 and CR13) between August and October 2002. The two vertical lines represent the period during which the graves were exhumed. On first appearance the NDVI for all mass graves decreased which could suggest disturbance. Therefore, an additional plot was created which focussed from 2000 to the end of 2003 (Figure 143). Nevertheless, when the NDVI of the graves was compared to that from March 2001 the values from 2003 did not appear much lower post exhumation. The NDVI values in 1996 and 2003 despite disturbance in 1995 (interment) and also in 2003, are likely to be due to climatic factors rather than the disturbance itself. When considering the growing season in 2003, it was found that the NDVI rose steadily peaking in August, as would be expected at peak summer. This process was also carried out for three mass graves that were exhumed in 2008 (Appendix 4); for which the same results were obtained. Therefore, suggesting that plotting the NDVI of the mass graves over an extended period of time (1996 – 2009, one year post exhumation) was not sufficient to detect disturbance associated with either interment or exhumation when using medium spatial resolution imagery (Landsat and SPOT).

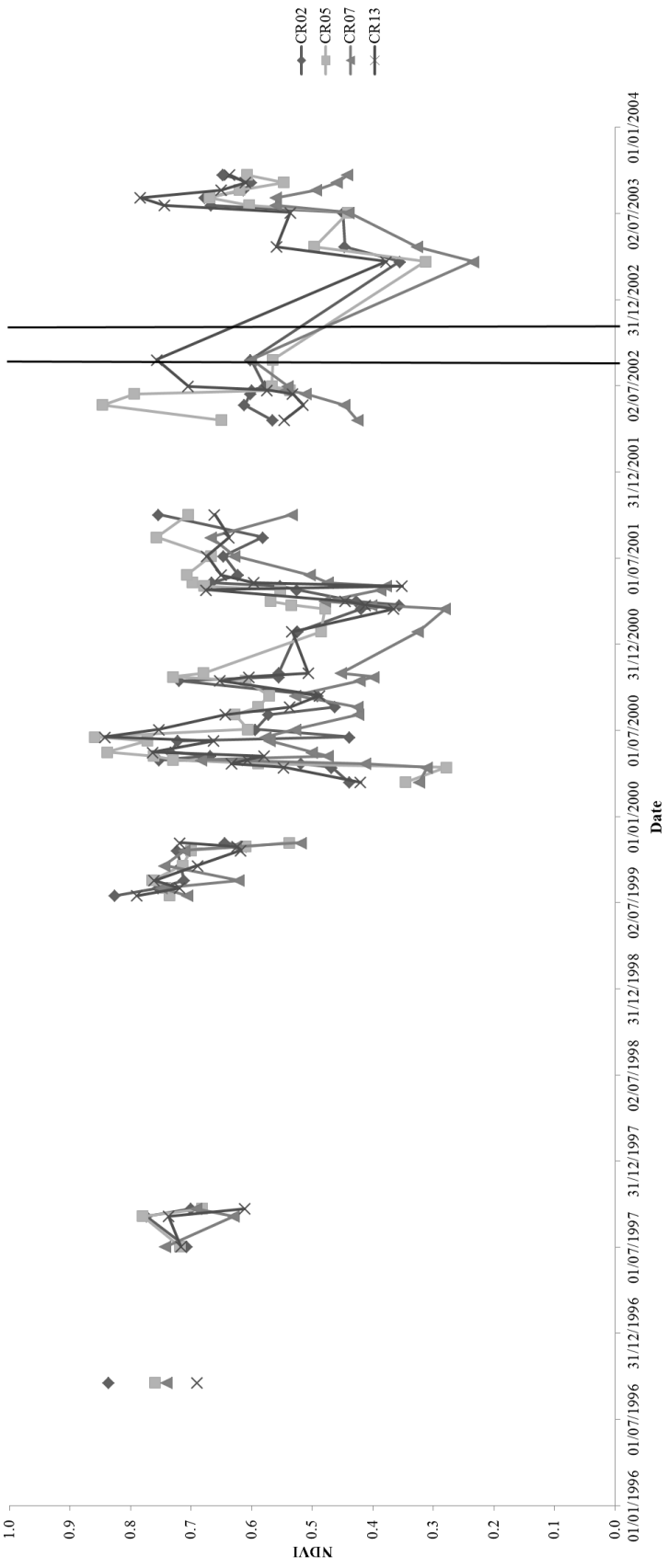

Figure 142 - NDVI of the Cancari Road mass graves exhumed in 2002. The period of exhumation is indicated by the two black vertical lines.

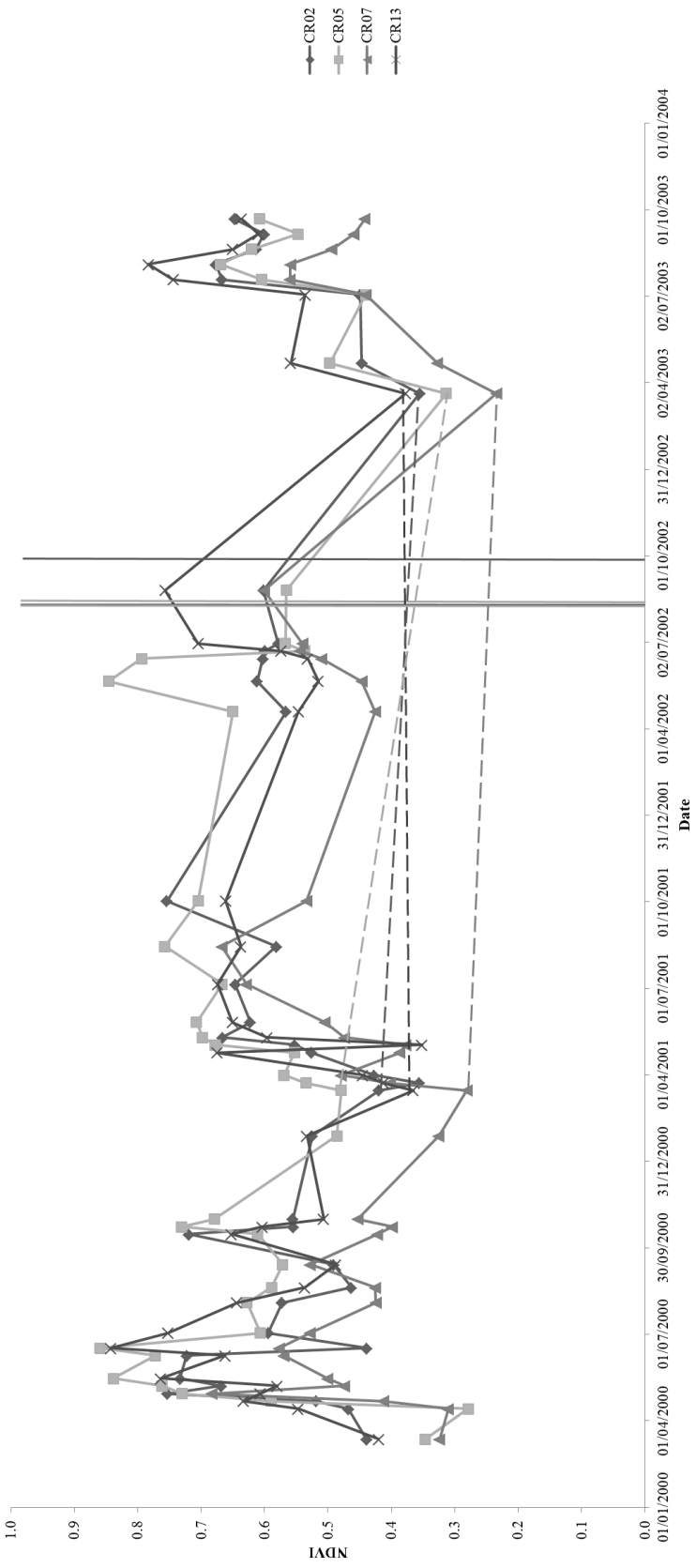

Figure 143 - NDVI of the Cancari Road mass graves exhumed in 2002, focussing on the years 2000-2003. The period of exhumation is represented by vertical lines. Dashed lines are for comparison between NDVI in March 2001 and April 2003.

7.4.2 Variations in NDVI at the grave surface during peak summer from 1991 to 2013

Rather than considering the complete NDVI time series for all graves to identify disturbance, the NDVI from one scene per year (from the summer months) for each grave was plotted individually, to ascertain whether a trend indicative of disturbance and recovery could be observed between 1991 and 2013. A similar approach was applied to data from the former RAF Pershore, which resulted in a trend, indicative of the recovery of vegetation post disturbance, to be observed over a decadal time period.

The time period chosen pre-dated the creation of the graves, accounted for the period post burial and also in some cases, post exhumation. Unfortunately, imagery was not available for the summer months during 1995. Control, non-grave points were extracted and plotted alongside the grave points to account for fluctuations in NDVI of native vegetation. Figure 144 is the graph produced for CR01.

As the graves had been exhumed at different times, each was plotted according to when it had been exhumed (Figure 144 – the remainder of the graphs are located in Appendix 4). The addition of the non-grave points also enabled the responses to be deemed as seasonal or non-seasonal and therefore potentially an indicator of disturbance (i.e. creation / exhumation of a grave).

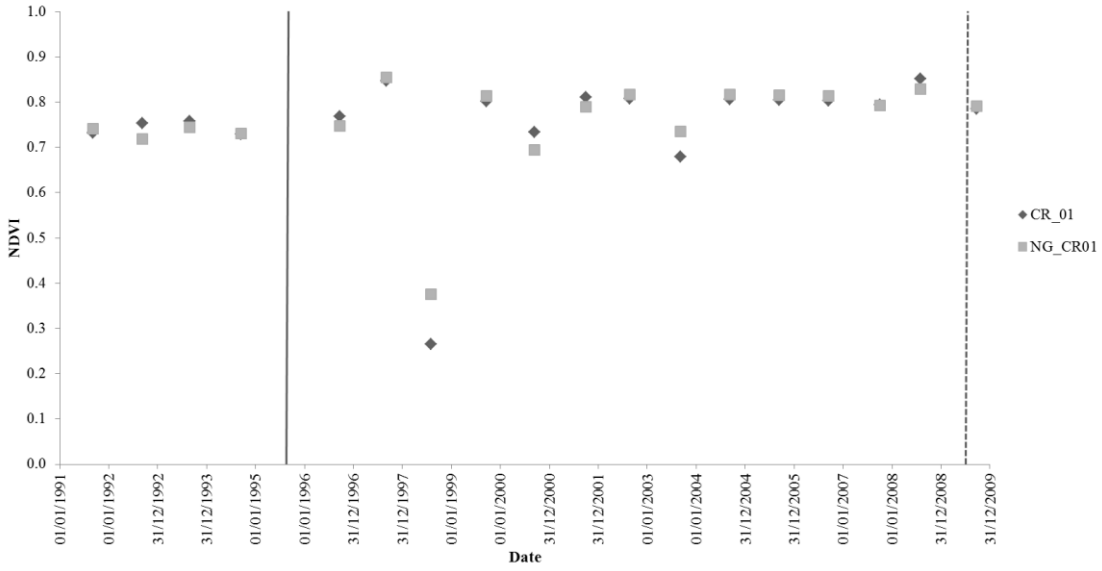

Figure 144 - Extracted NDVI at peak summer of Cancari Road Grave 1 (CR_01) and an area of background vegetation (NG_CR01) from 1991 through to 2009. Grey line = inhumation date; grey dashed line = exhumation date.

In August 1998, all graves (CR1 – CR13) exhibited very low NDVI for both the grave and non-grave points. This NDVI was calculated from a SPOT image rather than a Landsat (5 TM or 7 ETM+). Although many of the graves were probed in 1998, with the exception of CR03, CR12 and CR13, it is unlikely that this would have caused the observed drop in NDVI; as the disturbance to the grave surface would have been minimal. In addition, this was also observed in the NDVI values for the graves which had not been probed. Therefore this point is deemed a false positive. The vertical lines representing interment and exhumation date were added to the produced scatter plots, as it was expected that both grave creation and exhumation (represented by the solid and dashed lines respectively - Figure 144) would result in low NDVI values. However, this was not observed in the scatter plots for any of the graves. Moreover, it was expected that the non-grave points would exhibit a higher NDVI throughout the study period (up until exhumation) than the grave points, this was also not observed, with some of the grave points exhibiting higher NDVI. These assumptions were borne out of the previous chapter at Former RAF Pershore, where it was found that post interment there had been a steady recovery in NDVI values throughout the duration of the study.

In summary, focusing on one summer image per year both prior and post interment, using predominantly Landsat and SPOT medium spatial resolution imagery, the trends in NDVI indicative of disturbance and recovery could not be observed. This may be due to numerous factors including: error in the location of the graves; the effect of mixed pixels (specifically for the grave points) or that the graves were was too small in extent for the spatial resolution of the orbital platforms used. Consequently, a number of different approaches to locating the mass graves on the Cancari Road, focusing on the extraction of NDVI trends over time were undertaken with both medium and fine spatial resolution imagery.

7.4.3 Bracketing around 1995 to try to pinpoint inhumation of the Cancari Road mass graves

It is well documented that the Cancari Road mass graves are believed to have been created between 7th September and 2nd October 1995. This has been previously shown through aerial photographs acquired and archived by the ICTY. To try to locate the point of grave creation via a sudden drop in NDVI (Figure 145) around September and October 1995, archive imagery was acquired from which, after pre-processing, NDVI values for each grave were extracted and plotted over time, imagery for 1994 as well as February and March 1995 were considered. It was found that there was a lack of imagery during 1995 and 1996 for both

Landsat and SPOT, and thus the months of interment and one year post burial, could not be targeted. However, this approach did allow for a profile of undisturbed vegetation to be created in the areas where the graves were located. The NDVI for all grave areas peaked in or around July 1994; a curve was added to visualise the within year NDVI trend. The NDVI of the graves were found to vary in amplitude however, they all followed the same general trend throughout 1994 (Appendix 4).

All graves were subject to a minimum of two disturbance events, firstly during interment and secondly during exhumation. As a result of the analysis conducted at the Former RAF Pershore airfield (Chapter 6), it was anticipated that there would be a drop in NDVI during the creation of the graves, and following that, a slow, gradual recovery in the NDVI (Figure 145). However, the opposite was found, for all of the graves a relatively high NDVI was observed in the imagery closest to the inhumation dates (Figure 146).

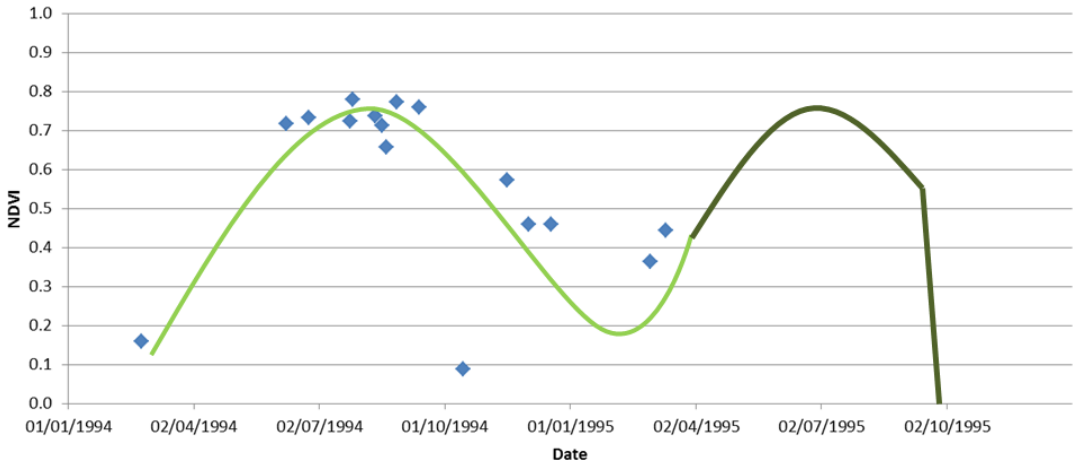

Figure 145 - Hypothesis for the sudden drop in NDVI around September - October 1995 - indicative of the creation of a grave.

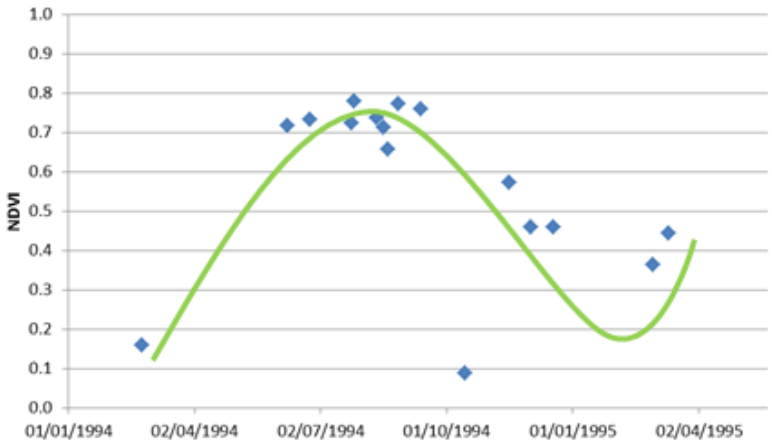

Figure 146 - NDVI Profile for CR01 from 1994 – 1995

7.4.4 Creation of a 40m radius buffer to locate the Cancari Road Mass Graves (April - November)

Previous attempts to detect a drop in NDVI around the time of burial were unsuccessful due to a lack of imagery in 1995 (year of burial) and 1996 (one year post burial). Following exhumation, it is believed that the grave sites were restored back to their original state (likely re-turfed); meaning that the drop in NDVI from vegetation to one representing soil, indicating disturbance, was not observed.

When plotting points for the mass grave and non-grave area it was found that on occasion, the NDVI of the mass grave exceeded that of the background vegetation. Therefore, a buffer with a radius of 40m (diameter 80m) was created for each mass grave within a GIS (ArcMap Version. 10.3.1), the centre of which was the mass grave point. At the outline of the buffer, eight new shapefiles were created (e.g. Figure 147). These were deemed non-grave points (maps for individual mass graves are located in Appendix 4). The equal distance of the non-grave points to the mass grave ensured that the background vegetation would be similar (in the case that the vegetation in the area was homogenous) and representative. Therefore, the NDVI of the mass graves could be directly compared to the non-grave points. A 40m (radius) buffer was selected, as the quoted error within Landsat pixels is ⅓ of the spatial resolution (i.e. the spatial resolution of Landsat is 30m, therefore the error is 10m). As can be seen from the example within Figure 147, the graves were in close proximity to the road (within 40m in many cases). Therefore, particularly in the case of the Landsat imagery with a spatial resolution of 30m, the roads and the surrounding vegetation could influence the pixels around the graves more than the graves themselves; lowering the NDVI.

The NDVI values were extracted in ArcMap using the ‘extract multi-values to points’ tool, as mentioned previously. The median and mean NDVI were calculated for each of the eight non-grave points and were plotted along with the extracted grave NDVI values. The median was selected as opposed to the mean, to visualise the trend in temporal NDVI, as it is less sensitive to outliers. The graphs relating to the mean NDVI are located in Appendix 4. The NDVI of the grave and non-grave points were plotted from 1996 (post burial) up until the date of exhumation (which varied per grave, refer to Table 30). These values were used to observe the changes in NDVI post interment and to determine whether or not the graves were distinguishable from the background (Figure 148 – the remainder of graphs are located in Appendix 4). It was found that none of the mass graves (CR01-CR13) could be distinguished from the non-grave areas using NDVI over time with medium spatial resolution imagery from Landsat or SPOT.

Figure 147 – Example 40m radius buffer at Cancari Road mass grave 2 (CR02) (NG: non-grave; CR: Cancari Road grave locations); for context a RapidEye image from 02/07/2012 used.

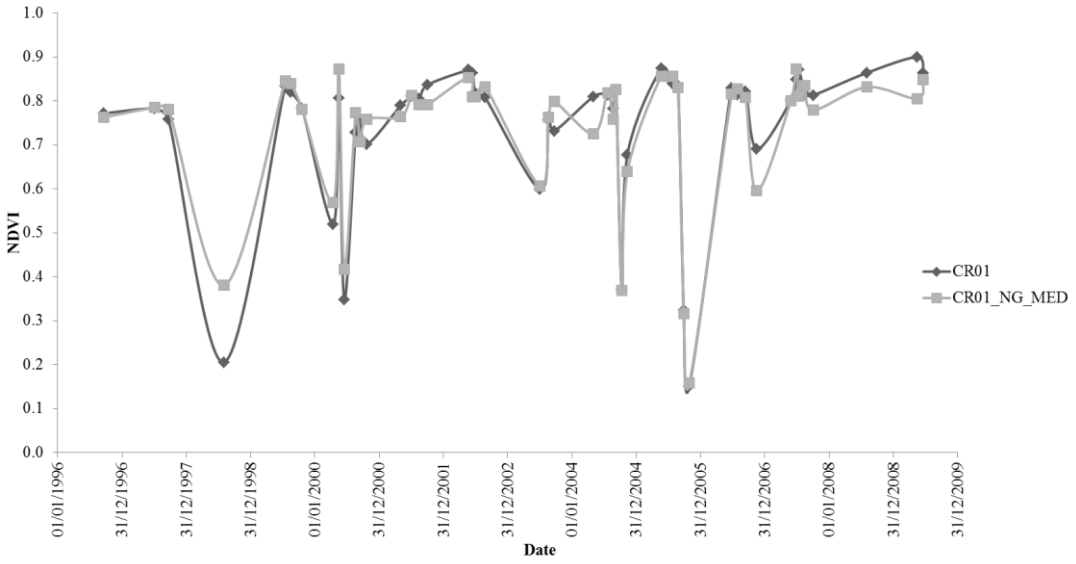

Figure 148 - Line plot showing NDVI of the Cancari Road mass grave (CR01) and the median of non-grave areas (CR01_NG_MED) throughout the period of interment (1996 - 2009)

7.4.5 Summary of results pertaining to the use of medium spatial resolution and variations in derived NDVI to locate human clandestine mass graves along Cancari Road

Landsat, a medium spatial resolution platform, was the primary sensor used to calculate NDVI for in excess of one hundred Landsat scenes focussed on the Cancari Road. The imagery was used to investigate whether variations in NDVI over time, could help detect the location of a grave at during interment, post burial and also during exhumation. It was anticipated that for a number of years post interment, the grave surfaces could be investigated to identify trends in NDVI. It was also anticipated that the gradual recovery of NDVI values over time would be observable for the pixel containing the grave. It was then hypothesised that these trends would help identify the location of unknown mass graves. However, medium spatial resolution imagery acquired by Landsat 5 TM, 7 ETM+ and 8 OLI was too coarse to detect the Cancari Road mass graves, even when the pixels containing the grave were plotted against areas of background vegetation (i.e. non-grave areas). None of the approaches detailed above, successfully or accurately, located a low NDVI signal indicative of disturbance, caused by creating a grave, or indeed even evidence of exhumation. The analysis was further limited by the lack of available imagery from 1995, when the burials were created. The approaches undertaken were unsuccessful largely due to the spatial resolution of the imagery, the size of the grave (being less than 30m) and the proximity of the graves to the road; resulting in mixed pixels. Imagery acquired by SPOT provided extremely low NDVI values, this was most evident in 1998, as a result many of the NDVI values derived from SPOT were categorised as anomalies and omitted from the dataset. As a result of findings above, fine spatial resolution was investigated for one of the Cancari Road mass graves exhumed in 2009. Analysis was not conducted on the remainder of the grave sites as they were exhumed prior to 2009, which pre-dates the RapidEye data received from ESA.

7.4.6 Case study into the applicability of fine spatial resolution imagery for the detection of a disturbance, indicative of mass grave exhumation

After it was discovered that the spatial resolution of Landsat imagery was too coarse to locate the area of disturbance indicative of mass grave creation or exhumation on the Cancari Road, fine spatial resolution imagery was considered. RapidEye imagery has been successfully utilised in a previous chapter, as well as used in the full time series presented in

an earlier section. The RapidEye imagery was obtained through an ESA data grant[5]. RapidEye has a spatial resolution of 5m, which is substantially finer than Landsat. Therefore, this section will investigate whether RapidEye imagery can be used to detect disturbance to aid in the location of mass graves.

The limiting factor with fine spatial resolution imagery, is that the technology is relatively new and as such the archives are not established and do not backdate to the Bosnian conflict in 1994. Therefore, graves such as those on Cancari Road cannot be studied over a long time series, or time period, at the present time. The graves were approximately 15 years old in 2009 when the first RapidEye imagery became available, following its launch in 2008 (29th August 2008 – Satellite Imaging Corporation 2016). The CR01 mass grave was exhumed during July 2009 therefore, using the imagery from the ESA data grant, it was possible to try to locate the disturbance caused by the exhumation. The results obtained from Chapter 5, illustrated the success of multi-spectral images being used to detect variations in NDVI on the surface of mass graves; particularly when the size of the grave exceeded the spatial resolution (pixel size) of the imagery. Therefore, the chance of disturbance being detected at CR01 using NDVI derived from RapidEye was high; with the extent of the exhumation being larger than the spatial resolution of the RapidEye imagery (5m x 5m). Furthermore, as CR01 was set back away from the road and the potential for mixed pixels was reduced.

7.4.6.1 Can NDVI derived from RapidEye imagery, with fine spatial resolution, detect disturbance indicative of a mass grave exhumation?

To locate CR01 through a reduction in NDVI from July 2009, NDVI values were extracted in ArcMap for all imagery available from 2009, including Landsat 5 TM and RapidEye imagery (Table 31). Although the spatial resolution of Landsat 5 TM was previously proved to be too coarse to detect the grave, it was included for comparison with the fine spatial resolution imagery. Furthermore, imagery was obtained on 20/07/2009 by both RapidEye and Landsat, enabling direct comparisons to be made.

The data contained in Table 32 was plotted and scaled for the year 2009. The NDVI values from the two platforms, Landsat and RapidEye, were plotted to allow differences in NDVI at the surface of CR01 to be visualised (Figure 142 and Figure 150). It was found that the NDVI derived from the Thematic Mapper (Landsat 5) was higher throughout 2009 compared to the RapidEye imagery. As has been mentioned above, on 20/07/2009 imagery was

[5] European Space Agency, Project ID: 26349

obtained by both satellites; within both images, a decrease in NDVI was observed, indicative of disturbance (Figure 142 and Figure 150).

Table 31 - Archive multispectral orbital imagery available to locate CR01 during 2009

Acquisition Date	Platform	Sensor	Resolution (m)	Source	Time in relation to Exhumation
15/04/2009	Landsat 5	TM	30	ESA	Prior to exhumation
17/05/2009	Landsat 5	TM	30	ESA	Prior to exhumation
18/06/2009	Landsat 5	TM	30	USGS	Prior to exhumation
14/07/2009	RapidEye-4	MSI	5	ESA	Exhumation
20/07/2009	RapidEye-5	MSI	5	ESA	Exhumation
20/07/2009	Landsat 5	TM	30	USGS	Exhumation
21/08/2009	Landsat 5	TM	30	ESA	Post exhumation
27/08/2009	RapidEye-5	MSI	5	ESA	Post exhumation
28/08/2009	RapidEye-1	MSI	5	ESA	Post exhumation
21/09/2009	RapidEye-1	MSI	5	ESA	Post exhumation
22/09/2009	Landsat 5	TM	30	USGS	Post exhumation
08/10/2009	Landsat 5	TM	30	USGS	Post exhumation
28/10/2009	RapidEye-5	MSI	5	ESA	Post exhumation

Table 32 - NDVI values extracted for CR01 from the 2009 archive orbital imagery (coincident imagery was available for 20/07/2009 for both RapidEye and Landsat – highlighted in yellow).

Platform	Acquisition Date	NDVI_CR01	Time in relation to Exhumation
Landsat 5	15/04/2009	0.786	Prior to exhumation
Landsat 5	17/05/2009	0.900	Prior to exhumation
Landsat 5	18/06/2009	0.863	Prior to exhumation
RapidEye-4	14/07/2009	0.472	Exhumation
RapidEye-5	20/07/2009	0.322	Exhumation
Landsat 5	20/07/2009	0.784	Exhumation
Landsat 5	21/08/2009	0.689	Post exhumation
RapidEye-5	27/08/2009	0.511	Post exhumation
RapidEye-1	28/08/2009	0.554	Post exhumation
RapidEye-1	21/09/2009	0.757	Post exhumation
Landsat 5	22/09/2009	0.802	Post exhumation
Landsat 5	08/10/2009	0.803	Post exhumation
RapidEye-5	28/10/2009	0.088	Post exhumation

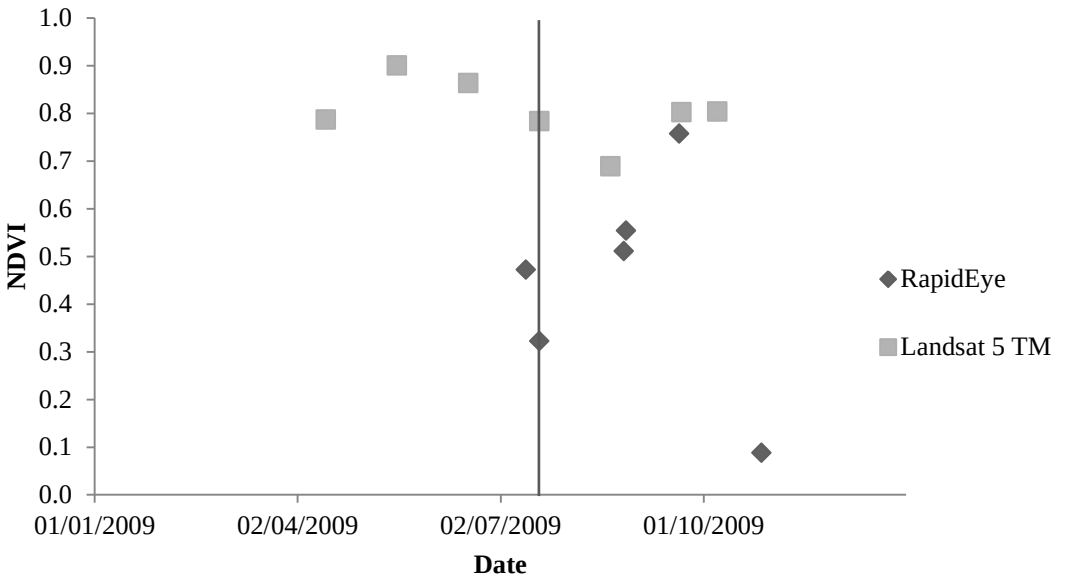

Figure 149 - Scatter plot comparing the NDVI values from both Landsat and RapidEye for CR01 during 2009 (date of exhumation indicated by the vertical line).

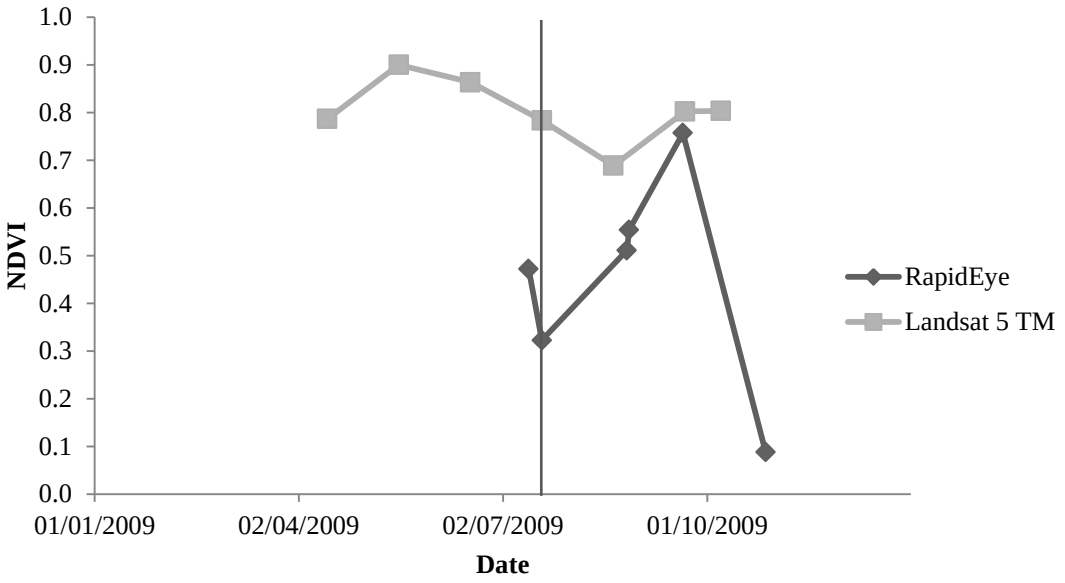

Figure 150 - Line plot comparing the NDVI values from Landsat and RapidEye for CR01 during 2009 (date of exhumation indicated by the vertical line).

As both platforms acquired imagery on 20/07/2009, which also coincided with the middle of the exhumation, direct comparisons between the NDVI values were made, as well as visual comparisons between the atmospherically corrected images. The two NDVI images, one derived from RapidEye and the other from Landsat 5 TM, are presented alongside the aerial photograph acquired around the time of burial in October 1995 (Figure 151). This

comparison allowed for the grave location, indicated by low NDVI, to be compared to the area of disturbed ground observed within the 1995 aerial photograph. In addition to the grave location, another low NDVI feature is observed within the imagery; this is a dwelling, masked by the title of the aerial photo. However, low NDVI persisted throughout all images within these pixels, indicating a consistently low NDVI feature which cannot therefore be a vegetated surface; this is also observed for features including roads and runways. As demonstrated in Figure 151, the spatial resolution of RapidEye imagery was sufficient to observe the area of low NDVI, indicative of disturbed earth, which was coincident with the exhumation of CR01. This was also visible in the atmospherically corrected RapidEye image where there is an area of obvious disturbance compared to the surrounding vegetation (Figure 152 and Figure 153). In contrast, the exhumation was not visually observed in either the NDVI or the atmospherically corrected Landsat 5 TM image.

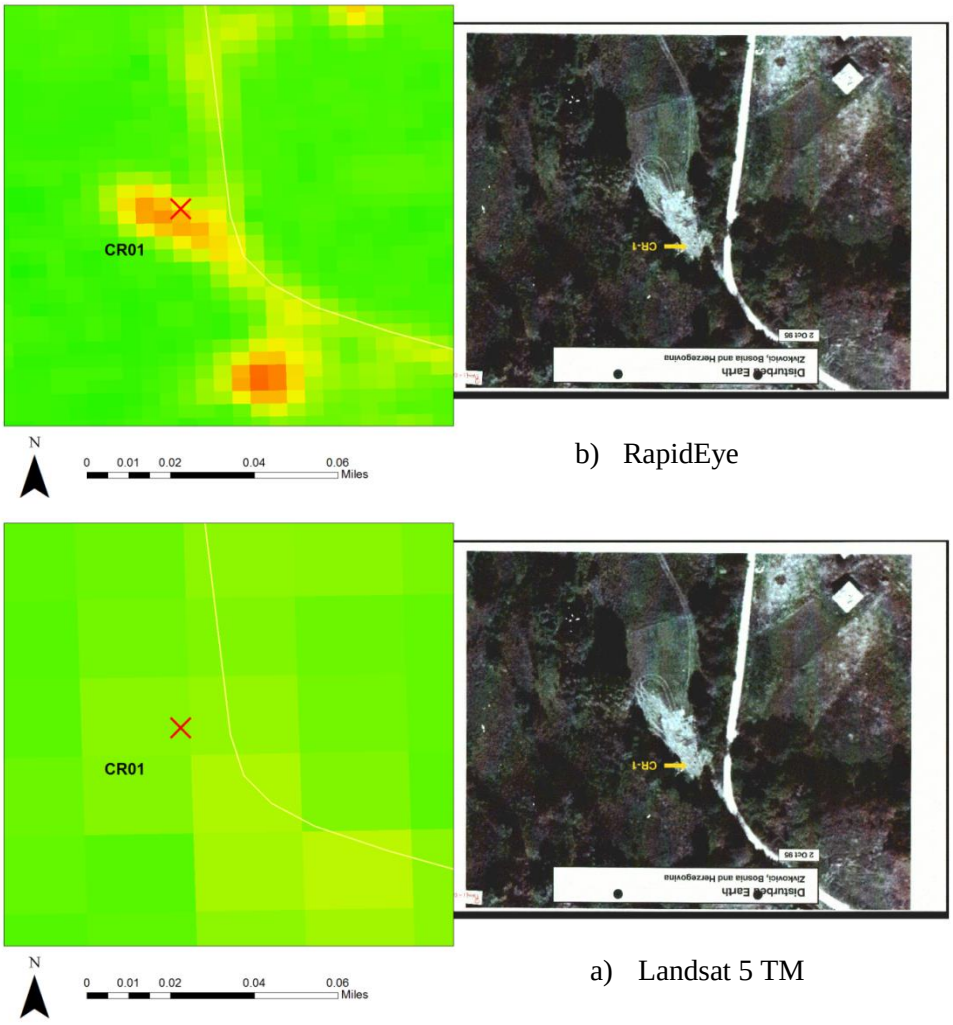

Figure 151 - NDVI images derived from a) RapidEye and b) Landsat 5 TM for 20/07/2009 located at the Cancari Road mass grave (CR01). Aerial photograph from ICTY 2011c. The low NDVI feature below the grave is the roof of a house.

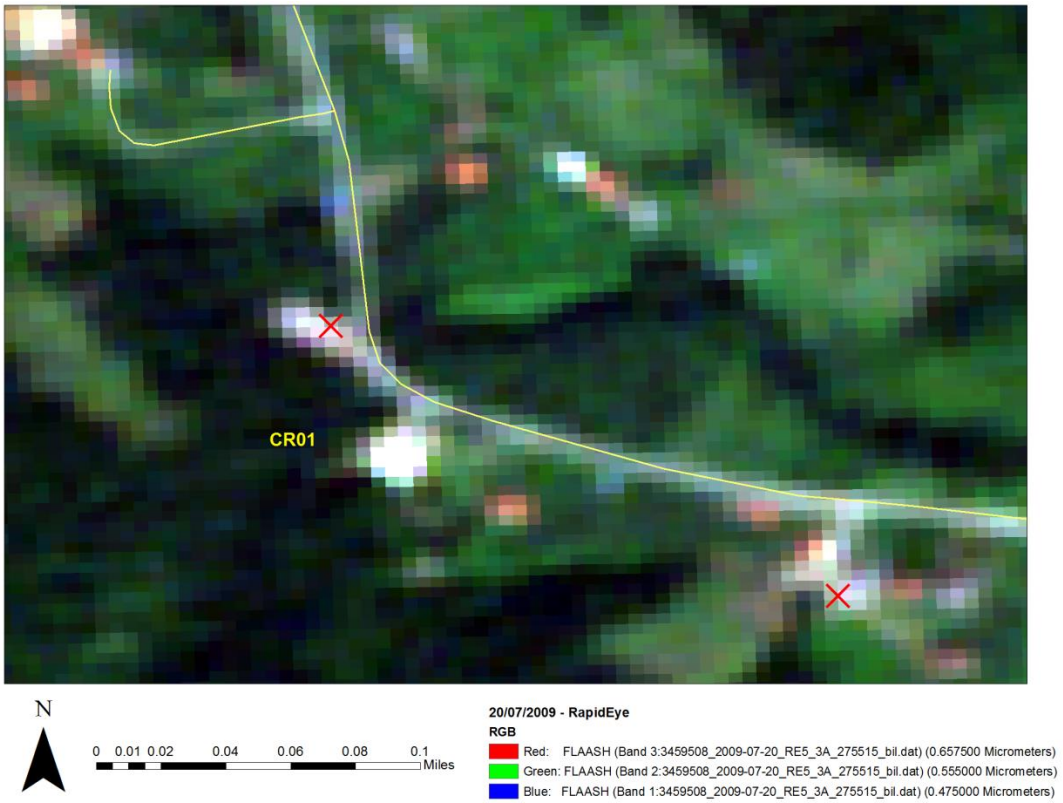

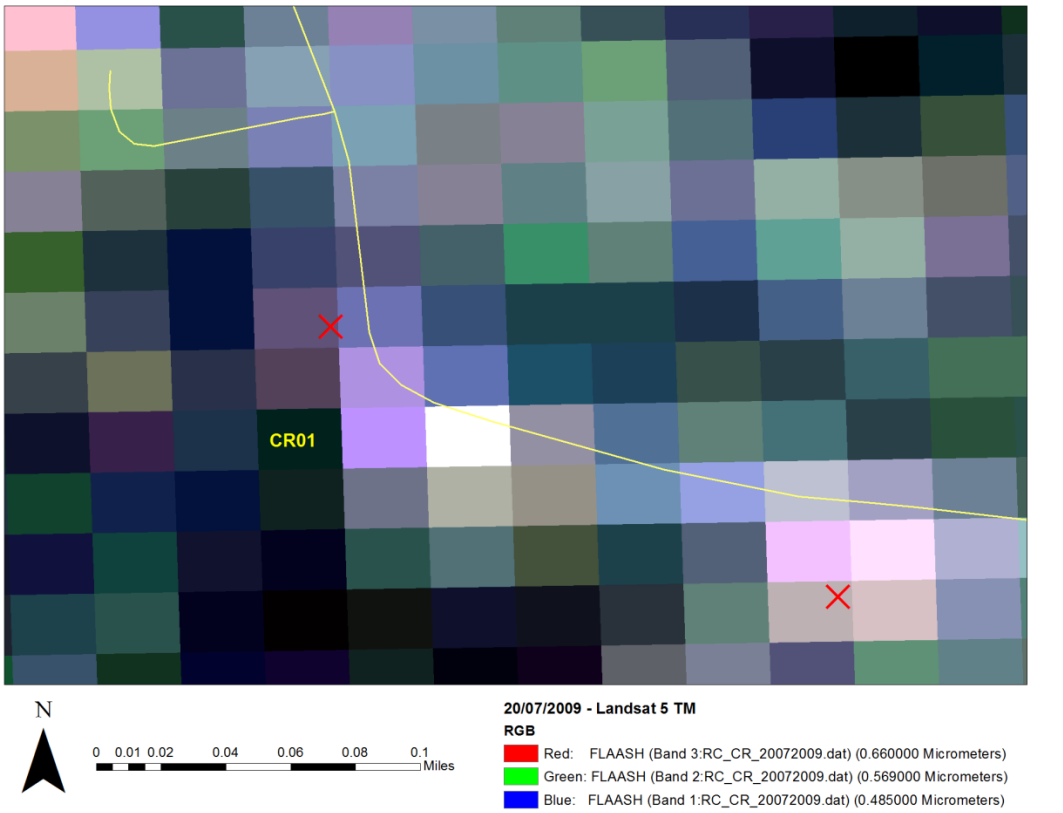

Figure 152 – Atmospherically corrected images of RapidEye (above) and Landsat 5 TM (below) for 20/07/2009 located at the Cancari Road mass grave (CR01).

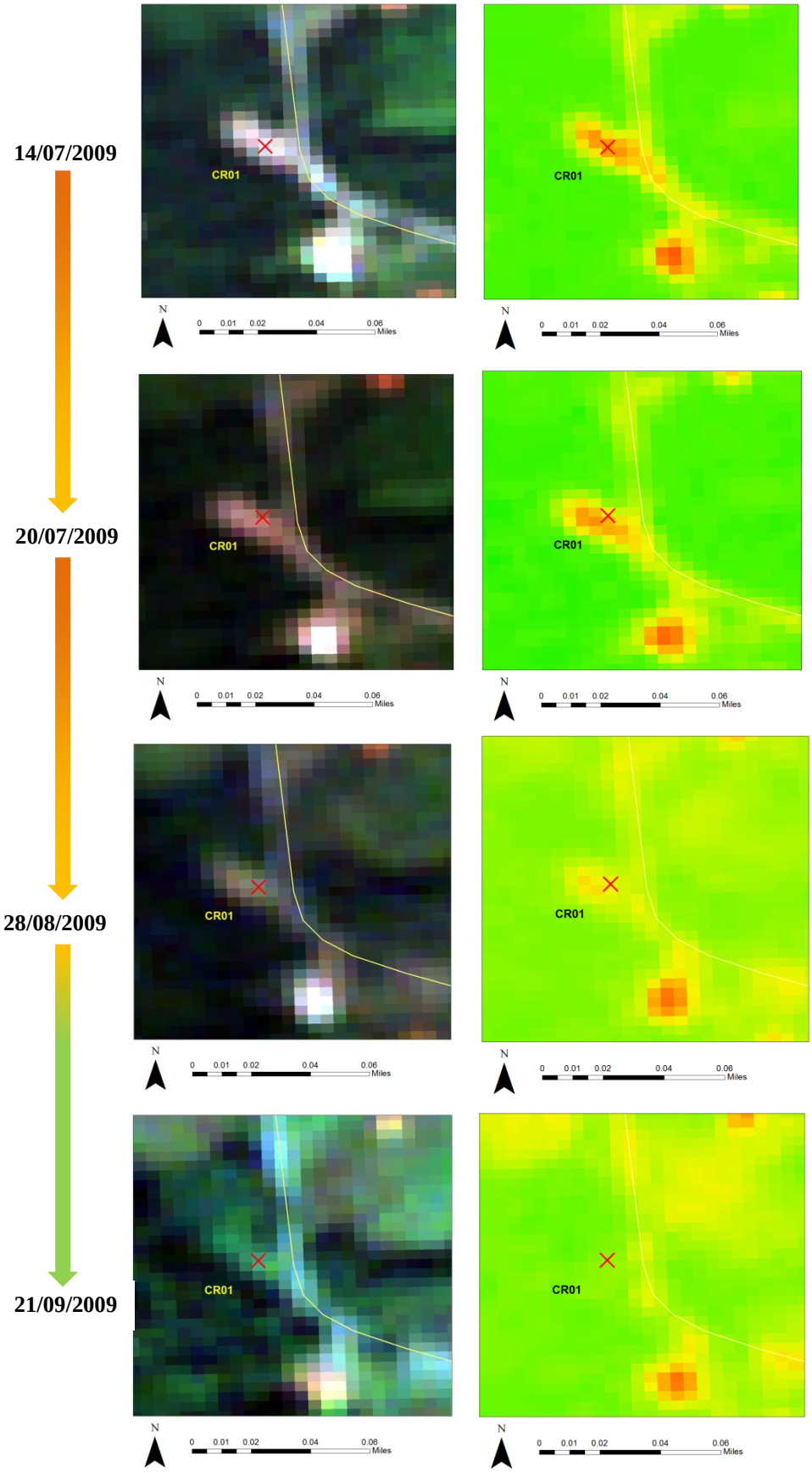

Figure 153 - FLAASH and NDVI timeline for 2009 using RapidEye imagery (FLAASH - left; NDVI - right). The persistently low NDVI feature below the grave is the roof of a house.

When the NDVI obtained from RapidEye was compared to the undisturbed, non-grave area it was found that during the period of exhumation, 8th to the 23rd July 2009, there was a clear difference between the NDVI of the two surfaces. The grave exhibited low NDVI, ranging from 0.4 to 0.3, whilst the non-grave points ranged between 0.8 and 0.9, indicating disturbance and healthy vegetation respectively (Figure 154).

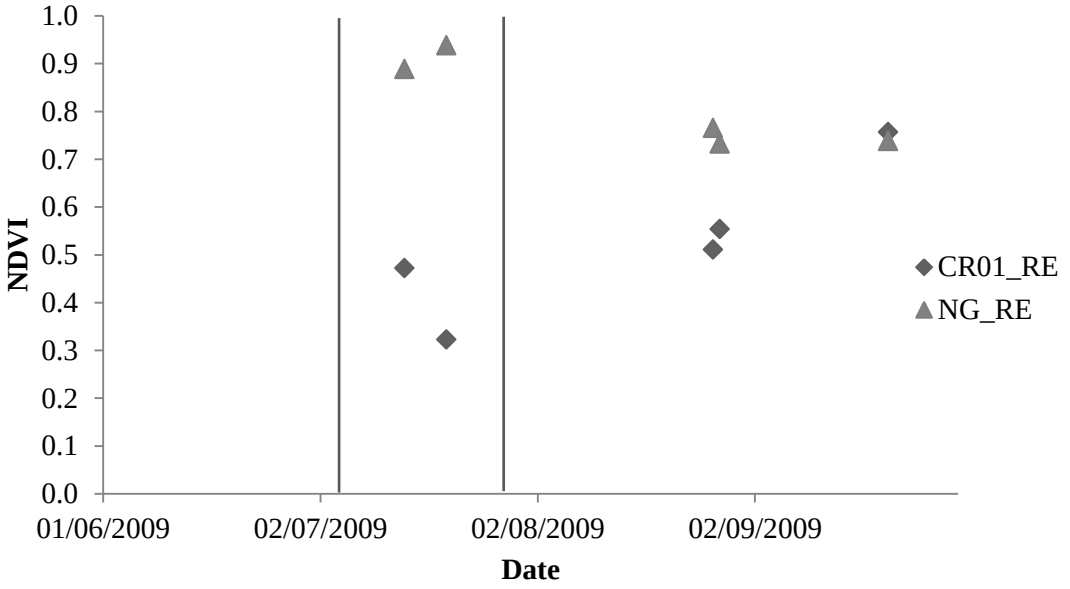

Figure 154 – Scatterplot comparing the NDVI of CR01 and a non-grave area (NG_RE) during 2009 (period of exhumation indicated between the vertical lines).

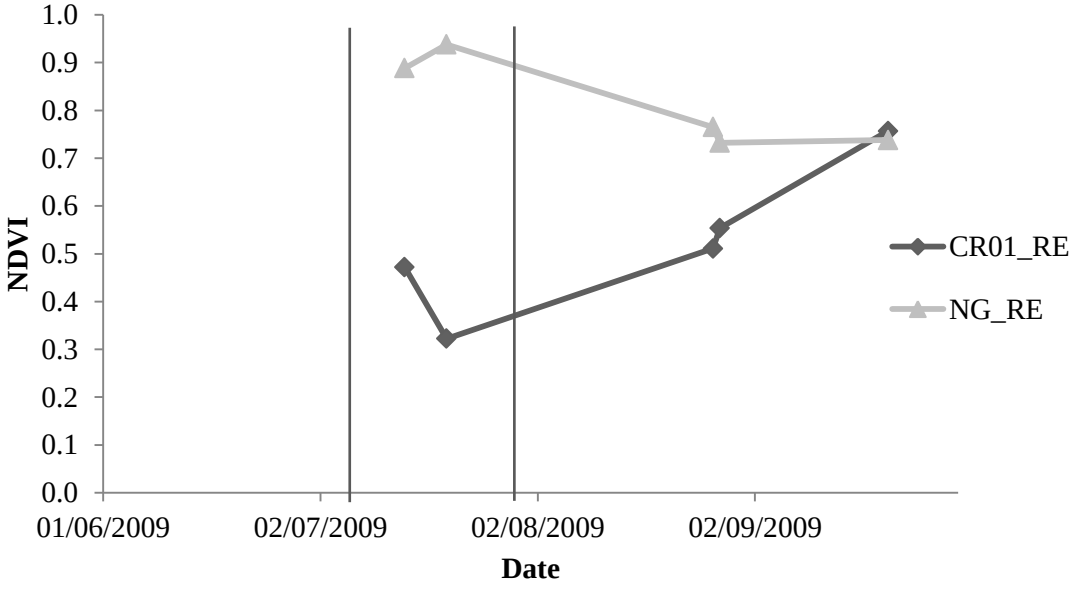

Figure 155 - Comparing the trend in NDVI between CR01 and the non-grave area during 2009 (period of exhumation indicated between the vertical lines).

When the trends in NDVI for the grave and non-grave surface were compared for 2009, it was found that the low NDVI observed during the exhumation of CR01 was short-lived, with the grave surface appearing to recover and become indistinguishable from the non-grave by September 2009 (Figure 155). The rapid recovery in NDVI post exhumation was unexpected, within such short time frames, considering the results from the two previous chapters and also by Kalacska et al. (2009). However, it has since been ascertained from ICTY exhumation reports that post exhumation, the mass grave sites were restored to their initial state. This included levelling and re-turfing the grave surfaces. This alone would account for the relatively high NDVI signal (NDVI ~0.7), indicative of the presence of relatively healthy vegetation at the grave surface, observed two months post exhumation. Therefore, it can be stated that fine spatial resolution imagery, in this case RapidEye, and derived NDVI, was successful in locating disturbance and consequently, the exhumation of the CR01 mass grave in July 2009.

When considering a longer time period from 2009 to 2015, it was found that the NDVI of both CR01 and the non-grave area followed the same trend, with the exception of mid-2011, 2012 and 2013, where the non-grave area appears to have been disturbed; suggesting a change in land use (Figure 156).

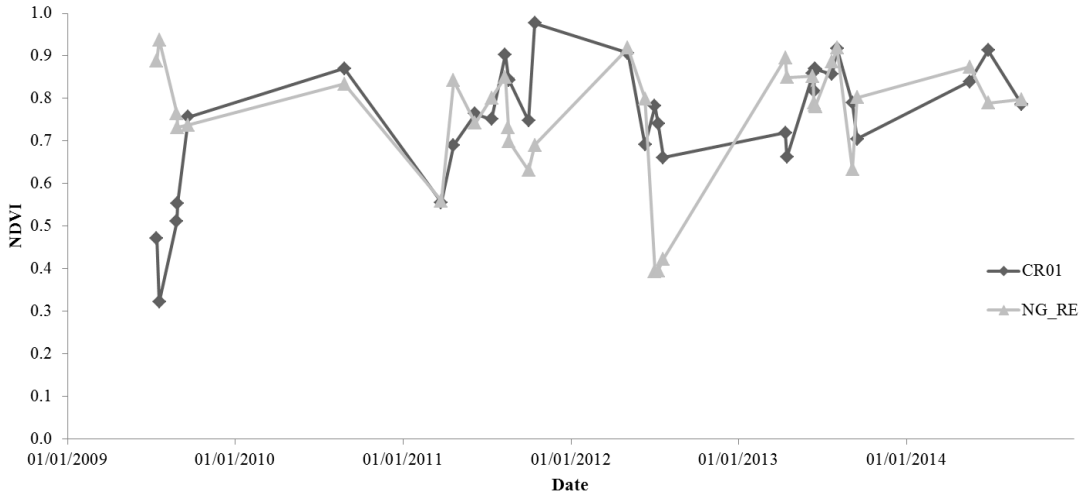

Figure 156 – Line plot showing the trend in NDVI for CR01 and a non-grave area from 2009 to 2015.

Unfortunately, RapidEye imagery was not available for CR01 prior to 14/07/2009. If it was available, it would have been used to provide an insight into whether the vegetation above CR01 had recovered and become indistinguishable from the surrounding vegetation, following the initial interment in 1995. Additionally, this data would have allowed for the trends in the variation of NDVI above the mass grave to be further understood and would have built upon the results obtained in Chapter 6.

This limitation will not be an issue for those searching for mass graves in the future, due to dramatic improvements in technology observed within remote sensing. However, it prevents the use of new, fine spatial resolution imagery being used to detect mass graves that are known to have been created and exhumed prior to August 2008 (prior to the launch of RapidEye); with comparably coarse resolution multispectral imagery being the only option.

7.4.6.2 Summary of results regarding the use of fine spatial resolution to detect disturbances

Using fine spatial resolution (5m) archive orbital imagery from the RapidEye platform, it was possible to visualise the disturbance associated with the exhumation of the Cancari Road 01 (CR01) mass grave through differences in NDVI. This research has also demonstrated that medium spatial resolution orbital imagery (Landsat) is not appropriate to be used for the detection of mass graves or disturbances on the Cancari Road. This due to a number of factors including: the spatial resolution of the imagery, that the mass graves were represented by a single pixel and the proximity of the graves to the road, resulting in mixed pixels. However, had the size of the graves or disturbance been larger, it is believed that variations in NDVI indicative of disturbance would have been detectable using Landsat imagery. The use of fine spatial resolution imagery, RapidEye, on a single mass grave (CR01) corroborated exhumation reports of a number of the mass graves along the Cancari Road, which stated that post exhumation the areas containing graves were restored. This was observed by the NDVI on the grave surface recovering rapidly and becoming indistinguishable from non-grave, vegetated areas within three months of the exhumation ceasing.

Although this study has focussed on the detection of disturbance synonymous with the exhumation of a mass grave, this approach, using fine spatial resolution RapidEye imagery, would also detect the disturbance synonymous with the creation of a mass grave. This is specific to the mass graves that have been exhumed in Bosnia. It is unlikely that a mass grave, post creation, would be re-turfed or levelled off, therefore, a recent grave, created

during or post 2009, could be detected as an area of comparatively low NDVI that persists for a longer period of time, similar to the results obtained in Chapter 6.

Theoretically, therefore it would be possible to differentiate between disturbances relating to the creation of a mass grave compared to an exhumation by considering the trend in recovery of NDVI over time. Disturbance resulting from the creation of a mass grave would be characterised by low NDVI, indicative of bare soil, that persists over a significant period of time i.e. years. In contrast, disturbance relating to an exhumation would be characterised by a momentary period of low NDVI that rapidly recovers, over the course of months rather than years, to become equivalent to surrounding non-grave vegetation. The latter scenario would require a relatively dense time series to enable detection, with images being considered over months, rather than years.

7.5 Discussion

7.5.1 Can NDVI derived from medium spatial resolution imagery, be used to detect disturbance associated with the creation, interment or exhumation of human mass graves?

It was found that the medium spatial resolution (Landsat) imagery was not suitable and was unable to locate disturbance associated with the creation, interment or exhumation of human mass graves along the Cancari Road. This was primarily due to the size of the mass graves (e.g. ranging between 14 and 17m long by 2.7 to 3.9m wide (ICTY 2012d) Table 29) as the spatial resolution of the orbital imagery was too coarse to differentiate between the graves and the surrounding area.

The results obtained have highlighted that both the size of the grave/ disturbance and the spatial resolution of the imagery is crucial for successful detection. To maximise the chance of successfully locating a grave, the disturbance would need to be represented by several pixels, rather than individual pixels. Therefore, fine spatial resolution imagery should be sought for all potential mass graves, even if this results in a mixture of medium and fine spatial resolution imagery being utilised. The benefits of this approach were demonstrated in Chapter 6, where a combination of Landsat and RapidEye were used, and successfully differentiated between full and empty graves, compared to undisturbed ground.

Had the extent of the mass graves been larger and located further away from the road, based on the results in Chapter 6, it is reasonable to assume that it is likely that medium spatial resolution imagery would have been able to detect disturbance associated with the creation, interment or exhumation.

7.5.2 Can NDVI derived from fine spatial resolution imagery, be used to detect disturbance associated with the creation, interment or exhumation of human mass graves?

Vegetation indices, specifically NDVI, derived from fine spatial resolution RapidEye imagery (5m) was successfully used to locate disturbance related to the exhumation of one of the Cancari Road mass graves (CR01) in 2009. The disturbance was characterised by a reduction in NDVI compared to the undisturbed vegetation surrounding the site; as previously observed for the former RAF Pershore mass graves. However, unlike the foot and mouth mass graves, the NDVI for CR01 appeared to recover within three months of the exhumation commencing. This was due to the restoration of the area post exhumation. If restoration had not been completed it is assumed that low NDVI would have persisted for an extended period of time and would have been able to be detected using RapidEye imagery.

Unfortunately, due to RapidEye having been launched in 2008, imagery does not exist prior to this date; therefore, the additional twelve Cancari Road mass graves could not be investigated using this imagery.

It appears that the finer the spatial resolution of the imagery, the more likely it is that a grave will be successfully detected. However, from an application and operational point of view, fine spatial resolution imagery is often costly, has a smaller spatial extent per scene and the temporal resolution (revisit time) may not be particularly fine. When attempting to locate human mass graves prior to the mid-2000s the options for archive multispectral imagery with a spatial resolution anywhere near appropriate to locate a mass grave is limited to Landsat (30m), SPOT (20m) and ASTER (15m).

Therefore, by using fine spatial resolution imagery, differences in the temporal NDVI signal above known location human mass graves could be used to identify undiscovered clandestine human mass graves or disturbances in Bosnia across large spatial areas.

7.5.3 Can vegetation stress be used to locate both primary and secondary mass graves?

It is well documented that the graves along the Cancari Road were secondary mass graves. Consequently, the applicability of the method presented within this chapter could be questioned in terms of its appropriateness to locate primary mass graves. The disturbance resulting from the creation of a grave is characterised by a large quantity of soil being removed and deposited around the grave location; creating a footprint that often exceeds the extend of the grave. This is the case for both primary and secondary mass graves. On this premise, it is reasonable to suggest that during creation, both primary and secondary mass graves, would be detectable through a low NDVI signal being observed, that occurs suddenly and persists for a period of time before recovering; with NDVI steadily increasing until it cannot be differentiated from surrounding undisturbed vegetation.

However, there are likely to be differences during the period post burial, up to exhumation, depending on whether the mass grave is primary or secondary. In the case of a primary mass grave, it is assumed that the grave would be backfilled with 'native' or local soil, removed during grave creation. When backfilled, the grave matrix would be mixed and the bare soil would dominate the grave surface. In addition, the individuals buried in a primary mass grave, in a context such as Bosnia and Herzegovina, are unlikely to be heavily decomposed prior to burial and as such, much of the decomposition process would occur within the grave structure. Therefore, the remains are likely to predominantly be whole body systems rather than disarticulated body parts. As a result, decomposition is likely to occur as described within literature but this is dependent on the conditions at the gravesite, the number of remains and therefore the thickness of the mass of individuals.

In the case of secondary mass graves, the backfill is likely to be a mixture of native soil and also traces from the primary grave location (classed as non-native or exotic), which would result in a complex matrix that is incomparable to the undisturbed matrix surrounding the grave. The human remains within secondary mass graves are likely to contain partially decomposed and disarticulated remains, depending on the duration of interment within the primary grave; as opposed to whole body systems. The decomposition that takes place within a secondary mass grave would therefore differ from a primary mass grave. The effect that this has on a grave surface and in turn, vegetation has not been previously investigated. However, if the remains were not already skeletonised, it is likely that the human remains would continue to decompose if the conditions within the grave were optimal.

With further research, focusing on vegetation stress above mass graves during the period post burial up until exhumation, it may be possible to demonstrate that primary and secondary mass graves can be differentiated.

Similar to the creation of a burial, the exhumation is a period of disturbance characterised by a low NDVI signal, dominating pixel(s) at the location of the mass grave. This is likely to also be larger than the true extent of the mass grave. However, unlike the process of interment, exhumations particularly in the context of Bosnia and Herzegovina are carried out under the instruction of a Court of Law (ICTY) and therefore the grave, once all human remains are exhumed, is restored back to its original state (i.e. prior to the exhumation being carried out). As a result the low NDVI signal which is anticipated to persist for an extended period post burial may not occur following an exhumation.

Although it has not been possible in this study to successfully demonstrate the utility of medium spatial resolution satellite imagery and derived NDVI to locate human mass graves in Bosnia and Herzegovina. Studies undertaken in Chapters 5 and 6, as well as work by Kalacska et al. (2009), have demonstrated that there is a period of time (variable in length) when the vegetation above a mass grave appears to be affected and/ or stressed by the presence of buried mammalian remains. Consequently, there is no tangible reason why both primary and secondary mass graves, particularly around the time of burial creation and exhumation, could not be detected using NDVI derived from orbital imagery. Thus, it is anticipated that multispectral imagery with an appropriate, finer, spatial resolution (RapidEye, IKONOS and ASTER) would able to successfully detect the low NDVI anomalies resulting from the disturbance. In light of this, further research is required which utilises fine spatial resolution imagery to closely track vegetation stress above human mass graves, to understand how vegetation stress over time can be used to detect human mass graves.

7.6 Conclusion

This research has found that NDVI derived from medium spatial resolution orbital imagery (30m), was too coarse to successfully differentiate human secondary mass graves on Cancari Road from the surrounding undisturbed vegetation around the time of burial (due to a lack of imagery available) or around the time of exhumation. However, fine spatial resolution orbital imagery from RapidEye was successful in detecting the disturbance resulting from the exhumation of CR01 in July 2009. It was also found that shortly following exhumation,

the mass grave exhibited a vegetation signal, with relatively high NDVI, rather than one representative of soil. This was due to the fact that the mass grave was restored to its original state, prior to exhumation and therefore, it can be assumed that vegetation removed during the exhumation was replaced afterwards.

Therefore, it is possible that disturbance caused via grave creation and exhumation could be differentiated, with grave creation being characterised by low NDVI for a prolonged period of time (due to the presence of soil). Whereas, disturbance caused by exhumation, particularly in the context of Bosnia and Herzegovina, would be characterised by low NDVI being observed for a short period of time, followed by a gradual increase in NDVI; indicative of the re-turfed grass recovering.

Due to the relatively coarse spatial resolution of the Landsat imagery (30m) investigations into trends in NDVI over seasons and years could not be undertaken. It is anticipated that if imagery had been available with a spatial resolution equivalent to RapidEye (5m), a detailed study could have been conducted. This will not be an issue for the detection of human mass graves created post late 2000s, where the technology has been, and will continue to be, improved with fine spatial and temporal resolution imagery becoming commonplace worldwide.

In conclusion it can be said that the issue, in the case of the Cancari Road mass graves, was one of spatial resolution and the size of the mass graves. Consequently, it is suggested that the area of interest should be larger than the spatial resolution of the imagery used for a potential grave to be located. If the size of the grave is unknown, as is likely in many cases, the finest spatial resolution imagery available should be utilised alongside complimentary techniques and the evidence available. NDVI is a useful vegetation index to locate disturbances and mass graves, as in the case of CR01 discussed above, and the East Holme and Former RAF Pershore airfield sites, discussed in Chapters 5 and 6. However, more research is required on known location human mass graves using fine spatial resolution imagery prior to it being utilised in forensic casework to avoid false positives.

8 Discussion

8.1 Summary of findings

This research aimed to evaluate the utility of archive multispectral satellite imagery to monitor temporal changes in vegetation stress as a means to detect clandestine human mass graves in temperate environments. The studies presented in Chapters 5 through to 7, have successfully demonstrated the potential that exists for fine and medium spatial resolution, multispectral orbital imagery and derived NDVI, to be used to detect disturbances synonymous with the creation and exhumation of mass graves.

The study undertaken at the East Holme experimental mass grave site, detailed within Chapter 5, found that both the full and empty grave could be differentiated from an area of control, undisturbed ground up to 121 days post burial. It was found that NDVI collected from the surface of the graves was unaffected by the presence of the buried mammalian remains throughout the study. This is likely due to the length of the study, which was relatively short, and also that it was undertaken when the ambient temperature was decreasing steadily, potentially inhibiting vegetation colonisation on the grave surface. It was found that the NDVI was most affected by meteorological variables including temperature and dew point, with precipitation having a lesser impact in comparison. However, although the study was short, the disturbance resulting from grave creation was detectable for the duration of the study through both NDVI and geophysical surveys (electromagnetic and resistance). At 70 days during October 2013 the percentage difference in geophysical response, from both the electromagnetic and resistance, peaked. This coincided with a period where climatic events including increased cumulative precipitation and decreased ambient temperatures were recorded. Consequently, it appears that the results obtained from the geophysical surveys were influenced heavily by climatic factors and in the case of this research, enabled the graves to be more readily detected. Significance (*** $p<0.001$) between the grave surfaces and the control, undisturbed vegetation via NDVI was also observed throughout the duration of the study. Consequently, NDVI would not aid in the differentiation between a full or an empty grave up to 121 days post burial, however, both graves were able to be differentiated from the undisturbed vegetation surrounding them.

The decadal study undertaken at the Former RAF Pershore found that NDVI derived from archive multispectral, orbital imagery with medium spatial resolution could be used to detect disturbance synonymous with the creation of mass graves. The NDVI of the full and empty burials could be differentiated from 1 year, 10 months up until 5 years, 1 month, with the

significance observed ranging between *** ($p<0.001$) and ** ($p<0.01$). At 6 years, 2 months post burial no significance between the surface types was observed, inferring that the vegetation above the graves had recovered following the disturbance in 2001. However, through utilising fine spatial resolution imagery from RapidEye (5m), significance *** ($p<0.001$) was found to exist between the NDVI of the undisturbed, control vegetation and both the full and empty graves up to 9 years, 11 months post burial (for seven out of the ten RapidEye observations). This demonstrated the potential for fine and medium spatial resolution multispectral orbital imagery, to be used for the detection of human mass graves up to almost a decade post burial.

The final study was undertaken on secondary human mass graves along the Cancari Road, in Bosnia and Herzegovina. The NDVI derived from medium spatial resolution imagery, was too coarse to successfully locate disturbances as a result of creation or exhumation of the mass graves. This was primarily due to the size of the mass graves being relatively small (e.g. ranging between 14 and 17m long by 2.7 to 3.9m wide (ICTY 2012d)) compared to the spatial resolution of the Landsat imagery (30m +/- 15m). The proximity of the graves to the road, and other non-vegetated features including buildings with consistently low NDVI, also proved problematic as this resulted in mixed pixels. However, fine spatial resolution imagery from RapidEye (5m) was successful in detecting the disturbance resulting from the exhumation of CR01 in July 2009. Using the archive RapidEye imagery it was found that the mass grave (CR01) was restored to its original state (i.e. re-turfed), this being observed through low NDVI during exhumation and relatively high NDVI post exhumation, which persisted for the remainder of the study.

It has been demonstrated throughout the studies in Chapters 5, 6 and 7, that NDVI is a useful vegetation index to aid in the detection of disturbance synonymous with the creation or exhumation of mass graves. However, to maximise the success of detecting a mass grave using NDVI derived from multispectral orbital imagery, it is vital to consider the spatial resolution of the imagery chosen and for this to be considered alongside the suspected extent of the mass grave. As a rule of thumb, the extent of the grave should exceed the spatial resolution of the imagery used for a mass grave to be successfully detected. If the size of the mass grave is unknown, as is likely in most cases, the finest spatial resolution imagery available should be utilised. This may be problematic for older mass graves, created prior to the 2000's as the spatial resolution of the available archive imagery is relatively coarse and likely to be of similar resolution to Landsat. However, moving forward this technological limitation will no longer exist as the discipline of remote sensing and available orbital platforms is advancing at a rapid rate.

8.2 Comparison of findings to literature

Remote sensing has been suggested as a useful technique for locating mass graves within literature (Davenport 2001; ICMP 2005; Kalacska and Bell 2006; Kalacska et al. 2009; Cox et al. 2008b; Raymond 2012; Wang et al. 2013; Leblanc et al. 2014; Schuldenrein et al. 2017; Corcoran et al. 2018; Evers et al. 2018) however, very little research has been conducted to assess its applicability and appropriateness. Published research to date has focussed solely on the spectral characterisation of both mass and single graves, using airborne hyperspectral imaging, supported by field spectroscopy campaigns (Kalacska and Bell 2006; Kalacska et al. 2009; Leblanc et al. 2014; Corcoran et al. 2018; Evers et al. 2018). When this research is compared to existing published research, regarding the location of mass graves using remote sensing, it is important to note that it is not directly comparable to those focussed on hyperspectral imagery. This research is the first of its kind to assess the use of multispectral orbital imagery, by monitoring three experimental sites over varying time scales, from the date of interment up to 20 years post burial, using various multispectral platform of varying spatial resolution. In the published literature to date, multispectral orbital imagery was deemed inappropriate for use due to its wide spectral bands leading to a supposed high error rate in detection. However, research has not been undertaken to assess the use of such imagery. In addition to spectral resolution, the spatial resolution of orbital multispectral imagery has been questioned however, temporal resolution has not. Kalacska et al. 2009 stated that the spatial resolution of multispectral imagery was too coarse therefore providing justification for the use of airborne hyperspectral imagery. However, it should be noted that the spatial resolution achieved by the airborne hyperspectral sensor was 5m, which is equivalent to the imagery acquired by RapidEye, a multispectral orbital platform. This has been successfully used to locate the disturbance caused by the exhumation of the CR01 mass grave in Bosnia and Herzegovina.

It is important to consider research by Kalacska et al. (2009) during which both a cattle mass grave and an empty grave were monitored over 16 months in Costa Rica. Four spectral datasets were acquired using hand held field spectroscopy and one hyperspectral image was collected via an airborne sensor, one month post burial. Due to the tropical climate, the colonisation of the vegetation on both grave surfaces was rapid in comparison to this study, undertaken in a temperate environment; therefore, Kalacska et al. (2009) were able to observe the effect that the presence of buried organic remains had on the colonising vegetation at the grave surface. This was then able to be compared to the vegetation that colonised the surface of the empty grave. It was found that the presence of buried mammalian remains inhibited vegetation colonisation on the cattle grave surface and that the

vegetation was also more stressed compared to the control, empty grave; this was observed through the red edge. This research supports Kalacska et al's (2009) findings, whereby the presence of buried mammalian remains inhibited vegetation growth and caused measureable vegetation stress at the grave surface, regardless of geographical location. Using a combination of fine and medium spatial resolution imagery, the variations in vegetation stress of the grave surfaces compared to the undisturbed areas of the Former RAF Pershore airfield, persisted up to 9 years, 11 months post burial. In contrast, the Costa Rican study was undertaken over a period of 16 months (Kalacska et al. 2009). Kalacska et al. (2009) suggested that further research was required to examine the effect of spatial resolution on the ability to locate mass graves. This research has demonstrated that selecting a platform with an appropriate spatial resolution, is critical to the successful detection of mass graves. This research supports Kalacska et al's (2009) statement that when a grave occupies several pixels, it is likely to be detected. This was demonstrated through the use of Landsat imagery (30m spatial resolution) at the Former RAF Pershore, where the Foot and Mouth mass graves occupied approximately 10 pixels and were successfully detected and monitored over a decadal time period. This was also true for CR01, where the mass grave occupied multiple RapidEye pixels (5m spatial resolution). Therefore, the success of detecting a mass grave using imagery from either multi or hyperspectral remote sensing platforms is dependent on the spatial resolution of the imagery and size of the grave, as well as its proximity to other features such as roads. If a grave is believed to be located in close proximity to a road or building (i.e. the Cancari Road mass graves), fine spatial resolution is required, to avoid mixed pixels.

This research challenges claims that multispectral imagery is unsuitable for use in mass grave detection by demonstrating how vegetation stress over time, derived from temporal NDVI trends can be used to successfully locate human mass graves specifically in temperate environments. Proof-of-concept was demonstrated for both a small scale proxy mass grave, as well as a large scale mass grave from the Foot and Mouth epidemic. Therefore, rather than spectrally characterising a mass grave using a handful of hyperspectral images, variations in temporal NDVI can be monitored to derive the NDVI signal of a mass grave up to 20 years post burial (in the case of human mass graves in Bosnia and Herzegovina). This research suggests that relative differences in NDVI within a given area could help locate a mass grave and identify disturbance. The NDVI of a mass grave has been shown to be lower than that of an empty grave and undisturbed ground, as a result of the presence of buried organic remains; specifically at the Former RAF Pershore. In contrast to Kalacska et al's (2009) conclusions, this research has demonstrated that when orbital multispectral imagery with an

appropriate spatial resolution is used, it is possible to differentiate between a mass grave containing mammalian remains, from an empty grave until to 9 years, 11 months post burial.

In conclusion, using archive multispectral satellite imagery within forensic investigations allows for retrospective observations of areas of interest i.e. disturbance that may be indicative of a mass grave and therefore its location. Hyperspectral imagery is relatively new, expensive to acquire, as it is predominantly acquired via airborne platform and as such it is unlikely that archive imagery exists for a specific area. Furthermore, it has not yet been demonstrated how long post burial hyperspectral imagery can be used to differentiate between a full and empty grave, compared to undisturbed ground. Therefore, this research has demonstrated that the retrospective investigation of proxy and human mass graves is possible using medium and fine spatial resolution orbital multispectral imagery. Whereby the period prior to grave creation, post burial, during exhumation and also post exhumation can be observed and characterised through variations in NDVI. Orbital multispectral imagery is available from established earth observation missions including, Landsat and SPOT with archives spanning the last 25 years. However, satellite technology has developed at a rapid pace over the past 30 years and this trend is set to continue. Therefore, in the coming years more data will be available with finer spatial and temporal resolution and worldwide coverage.

This research has both societal and humanitarian impact, as it will enable those deemed missing, presumed buried in mass graves to be located and subsequently identified; providing closure for families and relatives. The detection of such sites will enable evidence to be recovered for use in criminal proceedings; providing justice for both the victims and their relatives. Furthermore, the use of orbital imagery enables mass graves to be detected regardless of physical and political boundaries, which could revolutionise the search and detection of mass graves in the future. Such imagery will ensure that atrocities in the future, as well as the recent past, do not go unnoticed and that those responsible will be held accountable.

This study provides the international forensic and justice community with a new approach to mass grave detection in temperate environments. In addition, the imagery could also be used to corroborate or refute witness statements and testimonies. By utilising remote sensing imagery, as part of the suite of techniques employed in the search for mass graves, less forensic personnel would be put at risk, enabling the planning and much of the search to be carried out remotely. This would result in a targeted and efficient approach during deployment. The use of pre-existing multispectral orbital imagery would also be a cost effective option, compared to many other forms of remote sensing data including airborne

hyperspectral imagery. The successful application of orbital multispectral remote sensing for the detection of mass graves in the future is reliant on additional research, and the remote sensing and forensic community working together to nurture a mutually beneficial relationship which provides forensic investigators access to archive imagery at relatively low cost.

8.3 Recommendations for future research

To further develop and understand the applicability of multispectral orbital imagery and derived vegetation indices for use in the detection of mass graves, additional research is required. The recommendations detailed below are a result of reflecting on all chapters and the challenges faced whilst undertaking this research.

Throughout the studies undertaken the presence of a mass grave has been indicated by a sudden drop in NVDI, indicating a surface of relatively healthy vegetation becoming an area dominated by soil. This allows disturbance to be detected, which in the context of mass graves could be indicative of the creation, disturbance or exhumation.

Consequently, the logical progression for this research is to study the applicability of methods that have been specifically designed to detect change within time series, preferably of orbital multispectral imagery, at pixel level. Once such method is BFAST (Breaks for Additive Season and Trend), developed by Verbesselt et al. (2010) which focusses on the detection of changes or disturbances, known as breakpoints, within time series data at pixel level. BFAST is globally applicable, each pixel is analysed individually without the setting of thresholds. Various changes including phenological, abrupt and gradual are able to be detected. Mass grave detection would likely require the detection of abrupt change which is defined as "…a step change caused by disturbances such as deforestation, floods, and fires…" (Verbesselt et al. 2010, p.2971), as opposed to phenological or gradual change.

BFAST detects disturbances within time series data by automatically detecting a stable history period to model the season-trend variation against. Two periods are defined, the first being a 'history period', this is the data that is analysed for stability to enable the modelling of normal vegetation dynamics. The second period is a 'monitoring period'; this is the data that will be analysed for disturbances. As an example, in the case of mass graves in Bosnia and Herzegovina, the history period could be from 1990-1992, with a monitoring period of 1993-1997. Therefore, some prior knowledge such as suspected burial/ disturbance/ exhumations dates, or periods of known combat etc. are required to identify an appropriate

history period; however, it is likely that this information would have been gathered at the outset of the forensic investigation.

The code required to process time series data using the bfast package is open source and available from http://bfast.R-Forge.R-project.org/, with the processing being carried out in R. An advantage of BFAST is that imagery downloaded from EROS ESPA, in its compressed image and metadata form, is able to be processed without any pre-processing. Furthermore, BFAST was designed to be able to analyse time series of vegetation indices, including NDVI. By analysing time series using BFAST the process for detecting mass graves could potentially be semi-automated, allowing for large numbers of image files spanning months / years to be stacked and analysed pixel by pixel; producing an output which identifies pixels with the most change.

On undertaking additional studies to test BFAST for the detection of breakpoints and therefore disturbance at the surface of mass graves, it is important to understand the impact of mixed pixels on the detection of breakpoints; how pure does a pixel need to be in order for disturbance within it to be detected?

Imagery from a range of multispectral orbital sensors should also be studied and evaluated for use in the detection of mass graves. Depending on when atrocities occurred, it is likely that imagery from a variety of multispectral sensors may be available. Therefore, additional sensors acquiring imagery in the red and NIR spectral bands, should be considered for human mass grave detection. Table 33 details both live and expired multispectral orbital platforms and sensors that could be investigated for use in the detection of mass graves. All platforms and their respective sensors acquire imagery in both the red and NIR bands thus allowing NDVI and a range of alternative vegetation indices such as EVI, SAVI, MSAVI, NDMI among others to be calculated. Also detailed within Table 33 is the spatial and temporal resolution (repeat period) of each sensor; it can be seen that both become finer as technology improves. Thus, the potential for using such imagery and technology for future forensic investigations and applications is vast.

An additional investigation stemming from this doctoral study is the phenological response of vegetation above mass graves and the determination of how/ whether it differs from the surrounding undisturbed vegetation. There is currently no published research that considers the seasonal signal of human mass graves over extended temporal periods. By undertaking a phenological study, the long term temporal NDVI signal of human clandestine mass graves could be understood, in different temperate environments and could aid in the detection of graves when the inhumation date is unknown. This research has illustrated that vegetation

above a grave containing buried organic remains is significantly different to vegetation above both empty graves and also areas of undisturbed ground over prolonged periods of time; this being measured by vegetation stress (i.e. NDVI). Therefore, post the initial abrupt drop in NDVI during grave creation, once the vegetation begins to colonise and recover; there is an opportunity to study vegetation phenology. To aid in this study, a moving kernel alongside logical operators and morphological filters (i.e. erosion and dilation) could be employed to undertake pixel based analysis of phenological change within time series data over extended temporal periods. This could potentially allow for the automation of human mass grave detection, measured by pixel-level fluctuations in seasonal and yearly NDVI.

Table 33 - Details of orbital multispectral platforms and sensors that could be used for the detection of mass graves.

Platform	Sensor	Spectral Bands		Spatial Resolution (m)	Repeat Period (days)	Launched	Decommissioned	Red Edge Band (nm)	Data Available From:
		Red (nm)	NIR (nm)						
ASTER	Multispectral	630-690	780-860	15	16	1999	-	-	USGS
DMC	Multispectral	630-690	770-900	32	3-4	2002	-	-	DMCii
DMC-2	Multispectral	630-690	770-900	22	3-4	2005	-	-	DMCii
EO-1	ALI	630-690	775-805	30	16	2000	-	-	USGS
FORMOSAT-2	RSI	630-690	760-900	8	1	2004	-	-	ESA-Taiwan
GeoEye-1	Multispectral	655-690	780-920	1.84	3	2008	-	-	DigitalGlobe
GeoEye-2 (WorldView-4)	Multispectral	655-690	780-920	1.36 / 1.0	<3	2016	-	705-745	DigitalGlobe
IKONOS (1 + 2)	Multispectral	632-698	757-853	3.2	11	1999	-	-	DigitalGlobe
Landsat 5	TM	630-690	760-790	30	16	1984	Jun-13	-	USGS and ESA
Landsat 7	ETM+	630-690	760-790	30	16	1999	-	-	USGS and ESA
Landsat 8	OLI	640-670	850-880	30	16	2013	-	-	USGS and ESA
ORBVIEW-3	MSS	630-690	760-900	4	3	2003	2007	-	DigitalGlobe
Pleiades – 1A	Multispectral	600-720	750-950	2	1	2011	-	-	AIRBUS Defence & Space
Pleiades – 1B	Multispectral	600-720	750-950	2	1	2012	-	-	AIRBUS Defence & Space
QuickBird	Multispectral	630-690	760-900	2.4	3	2001	Jan-15	-	DigitalGlobe
RapidEye	MS	630-685	760-850	5	1	2008	-	690-730	BlackBridge
Sentinel 2A	MSI	630-690	780-920	10	5	2015	-	Yes (x3 @ 20m)	AIRBUS Defence & Space and ESA
SPOT 1	XS	610-680	780-890	20	1-4	1986	Dec-90	-	AIRBUS Defence & Space
SPOT 2	XS	610-680	780-890	20	1-4	1990	Jul-09	-	AIRBUS Defence & Space
SPOT 3	XS	610-680	780-890	20	1-4	1993	Nov-97	-	AIRBUS Defence & Space
SPOT 4	XS	610-680	780-890	20	1-4	1998	Jul-13	-	AIRBUS Defence & Space
SPOT 5	XS	610-680	780-890	10	2-3	2002	Jul-05	-	AIRBUS Defence & Space
SPOT 6	XS	625-695	760-890	8	26	2012	-	-	AIRBUS Defence & Space
SPOT 7	XS	625-695	760-890	6	1	2014	-	-	AIRBUS Defence & Space
SSOT	Multispectral	620-690	760-890	5.8	37	2011	-	-	EADS and ASTRIUM
WorldView-2	MSS	630-690	770-895	1.84	1.1	2009	-	705-745nm	DigitalGlobe
WorldView-3	MSS	630-690	770-895	1.24	<1	2014	-	705-745nm	DigitalGlobe

9 Conclusion

The detection and location of clandestine human mass graves has posed a huge challenge to forensic investigators and is a task that remains at the forefront of international forensics. This research aimed to evaluate the use of archive multispectral satellite imagery to monitor temporal changes in vegetation stress as a means to detect clandestine human mass graves in temperate environments. This research has proven that there is promise in the use of archive medium and fine spatial resolution, multispectral orbital imagery and derived NDVI at three sites and over varying temporal time scales ranging from the time of burial up to 20 years post burial, in temperate environments.

A dense time series of archive multispectral imagery and derived NDVI, has been successfully utilised to detect disturbances caused by the creation of a Foot and Mouth mass grave containing mammalian remains, as well as enabling the differentiation between full and empty burials and undisturbed ground up to 9 years and 11 months post burial. The same method, when applied to known location secondary human mass graves along Cancari Road in Bosnia and Herzegovina, indicated that medium spatial resolution imagery (i.e. 30m Landsat) was too coarse to locate the relatively small mass graves (e.g. ranging between 14 and 17m long by 2.7 to 3.9m wide (ICTY 2012d) Table 29). However, NDVI calculated from fine spatial resolution (5m) multispectral imagery from RapidEye successfully located disturbance caused by the exhumation of one of the Cancari Road mass graves CR01, in July 2009. Therefore, indicating that the spatial resolution of the imagery used and also the size of the mass grave are limiting factors in the success of locating a mass grave. Thus, it is critical that careful consideration is given to the spatial resolution of multispectral imagery and that this should heavily influence the choice of the multispectral platform and sensor used by forensic investigators. As a rule of thumb, for a mass grave to be successfully detected, the potential mass grave should exceed the spatial resolution of the imagery used. If the size of the mass grave is unknown, as is likely in most cases, the finest spatial resolution imagery available should be selected.

In conclusion, the author considers this research as being pivotal as it has the potential to revolutionise the way clandestine human mass graves are detected in the future. With further research, multispectral orbital remote sensing could become a frequent, routine tool used to detect clandestine human mass graves, providing forensic investigators with crucial evidence for criminal proceedings. However, most importantly, the detection of these graves will provide closure and justice for families and relatives of the missing.

10 References

Agapiou, A., Alexakis, D.D., Sarris, A. and Hadjimitsis, D.G., 2014. Evaluating the potentials of Sentinel-2 for archaeological perspective. Remote Sensing, 6 (3), 2176-2194

Agapiou, A., Hadjimitsis, G. and Alexakis, D.D., 2013. Development of an image-based method for the detection of archaeological buried relics using multi-temporal satellite imagery. International Journal of Remote Sensing, 34 (16), 5979-5996

Aktaruzzaman, M.D., Schmitt, T.G. and Hagen, H., 2011. Modelling urban flooding by filtering LiDAR data. Journal of Urban Technology [online], 18 (4), 97-112

Anderson, A., Cox, M., Flavel, A., Hanson, I., Hedly, M., Laver, J., Perman, A., Viner, M., and Wright, R., 2008. Protocols for the Investigation of Mass Graves. In: Cox, M., Flavel, A., Hanson, I., Laver, J. and Wessling, R., The Scientific Investigation of Mass Graves: Towards Protocols and Standard Operating Procedures. New York: Cambridge University Press, 39-108

Anderson, G., Pukall, B., Allred, C.L., Jeong, L.S., Hoke, M., Chetwyndm J.H., Adler-Golden, S.M., Berk, A., Bernstein, L.S., Richtmeier, S.C., Acharya, P.K. and Matthew, M.W., 1999. FLAASH and MODTRAN-4: State of the art atmospheric correction for hyperspectral data. IEEE Aerospace Conference: Proceedings, 4, 177-181

ASTRIUM., 2015. SPOT 6/ SPOT 7 Technical Sheet [online]. Available from: http://www2.geo-airbusds.com/files/pmedia/public/r12317_9_spot6-7_technical_sheet.pdf [Accessed 18 May 2015]

Baier, W. and Rando, C., 2016. Developing the use of Structure-from-Motion in mass grave documentation. Forensic Science International, 261, 19-25

Bannari, A., Morin, D., Bonn, F. and Huete, A.R., 1995. A review of vegetation indices. Remote Sensing Reviews, 13 (1-2), 95-120

Baraybar, J.P. and Gasior, M., 2006. Forensic anthropology and the most probable cause of death in cases of violations against International Humanitarian Law: An example from Bosnia and Herzegovina. Journal of Forensic Sciences [online], 51 (1), 103-108

Barrett, E.C., 1999. Introduction to Environmental Remote Sensing. 4th edition. New York: Routledge

Bethell, P. H. and Carver, M. O. H., 1987. Detection and enhancement of decayed inhumations at Sutton Hoo. In: Boddington, A., Garland, A. N. and Janaway, R. C., eds. Death, Decay and Reconstruction: Approaches to Archaeology and Forensic Science. Manchester, UK: Manchester University Press, 10–21

Bevan, B.W., 1991. The search for graves. Geophysics [online], 59 (9), 1310-1319

Bevernage, B. and Colaert, L., 2014. History from the grave? Politics of time in Spanish mass grave exhumations. Memory Studies, 7 (4), 440-456

BlackBridge., 2013. Satellite Imagery Product Specifications: Version 6.0 [online]. BlackBridge: UK. Available from: http://BlackBridge.com/rapideye/upload/RE_Product_Specifications_ENG.pdf [Accessed 28 March 2015]

Bock, J.H. and Norris, D.O., 1997. Forensic botany: An underutilised resource. Journal of Forensic Sciences [online], 42 (3), 364-367

Brilis, G.M., Gerlach, C.L. and Waasbergen, R.J., 2000. Remote sensing tools assist in environmental forensics. Part I: Traditional methods. Journal of Environmental Forensics [online], 1, 63-67

Brkic, H., Strinovic, D., Kubat, M. and Petrovecki, V., 2000. Odontological identification of human remains from mass graves in Croatia. International Journal of Legal Medicine, 114, 19-22

Brkic, H., Strinovic, D., Slaus, M., Skavic, J., Zecevic, D. and Milicevic, M., 1997. Dental identification of war victims from Petrinja in Croatia. International Journal of Legal Medicine, 110, 47-51

Bray, E., 1996. The use of geophysics or the detection of clandestine burials: some research and experimentation. Unpublished MSc Dissertation: Department of Archaeological Sciences, University of Bradford, UK.

Brown, A.G., 2006. The use of forensic botany and geology in war crimes investigations in NE Bosnia. Forensic Science International, 163, 204-210

Brown, M.E., Pinzon, J.E., Didan, K., Morisette, J.T. and Tucker, C.J., 2006. Evaluation of the consistency of long term NDVI time series derived from AVHRR, SPOT-vegetation, SeaWiFS, MODIS and Landsat ETM+ Sensors. IEEE Transactions on Geoscience and Remote Sensing [online], 44 (7), 1787-1793

Buck, S.C., 2003. Searching for graves using geophysical technology: Field tests with ground penetrating radar, magnetometry and electrical resistivity. Journal of Forensic Sciences [online], 48 (1), 5-11

Carccianiga, M., Bottacin, S. and Cattaneo, C., 2012. Vegetation dynamics as a tool for detecting clandestine graves. Journal of Forensic Sciences [online], 57 (4), 983-988

Campbell, J.B. and Wynne, R.H., 2011. Introduction to Remote Sensing. 5th edition. New York: Guildford Press

Carter, D.O. and Tibbett, M., 2009. Cadaver decomposition and soil: processes. In: Tibbett, M. and Carter, D.O., eds. Soil Analysis in Forensic Taphonomy: Chemical and Biological Effects of Buried Human Remains. Florida: CRC Press, 29-52

Carter, D.O., Yellowlees, D. and Tibbett, M., 2007. Cadaver decomposition in terrestrial ecosystems. Naturwissenschaften, 94, 12-24

Carter, D.O., Yellowlees, D. and Tibbett, M., 2010. Moisture can be the dominant environmental parametre governing cadaver decomposition in soil. Forensic Science International, 200, 60-66

Cheetham, P., 2005. Forensic geophysical survey. In: Hunter, J.R. and Cox, M. (eds). Forensic Archaeology: Advances in Theory and Practice. London: Routledge, 62-95

Cheetham, P., Cox, M., Flavel, A., Hanson, I., Haynie, T., Oxlee, D. and Wessling, R., 2008. Search, Location, Excavation and Recovery. In: Cox, M., Flavel, A., Hanson, I., Laver, J. and Wessling, R., 2008. The Scientific Investigation of Mass Graves: Towards Protocols and Standard Operating Procedures. New York, Cambridge University Press, 183-267

Cleland, E.E., Chuine, I., Menzel, A., Mooney, H.A. and Schwartz, M.D., 2007. Shifting plant phenology in response to global change. TRENDS in Ecology and Evolution, 22 (7), 354-365

Committee on Scientific Accomplishments of Earth Observations from Space, 2008. Earth Observations from Space: The First 50 Years of Scientific Achievements. Washington: National Academic Press

Congram, D.R., 2008. A Clandestine Burial in Costa Rica: Prospection and Excavation. Journal of Forensic Sciences [online], 53 (4), 793-796

Connor, M. and Scott, D.D., 2001. Paradigms and perpetrators. Historical Archaeology [online], 35 (1), 1-6

Conyers, L.B., 2006. Ground penetrating radar techniques to discover and map historic graves. Historical Archaeology, 40 (3), 64-73

Corcoran, K.A., Mundorff, A.Z., White, D.A., and Emch, M.L., 2018. A novel application of terrestrial LIDAR to characterize elevation change at human grave surfaces in support of narrowing down possible unmarked grave locations. Forensic Science International, 289, 320-328

Cox, M., Flavel, A. and Hanson, I., 2008a. Introduction and context. In: Cox, M., Flavel, A., Hanson, I., Laver, J. and Wessling, R., 2008. The Scientific Investigation of Mass Graves: Towards Protocols and Standard Operating Procedures. New York: Cambridge University Press, 1-28

Cox, M., Flavel, A., Hanson, I., Laver, J. and Wessling, R., 2008b. The Scientific Investigation of Mass Graves: Towards Protocols and Standard Operating Procedures. New York: Cambridge University Press

Coyle, H.M., Lee, C.L., Lin, W.Y., Lee, H.C. and Palmbach, T.M., 2005. Forensic botany: Using plant evidence to aid in forensic death investigation. Croatian Medical Journal [online], 46 (4), 606-612

Crowley, G., 2010. DMC Data Product Manual [online]. DMC International Imaging: Surrey, UK. Available from: http://earth.esa.int/documents/10174/1987716/DMC-Data-Product-Manual.pdf [Accessed 10 March 2015]

Cunningham, S., Kirkland, S., and Ross, A., 2011. Bone weathering of juvenile-sized remains in the North Carolina Piedmont. In: Ross, A., and Abel, S., editors. The juvenile skeleton in forensic abuse investigations. New York: Springer Press, 179-196

Dalan, R.A., De Vore, S.L. and Clay, R.B., 2010. Geophysical identification of unmarked historic graves. Geoarchaeology: An International Journal, 25 (5), 572-601

Dalva, M., Kalacska, M.E., Moore, T.R. and Constopoulous, A., 2012. Detecting graves with methane. Geoderma [online], 189-190, 18-27

Dalva, M., Moore, T.R., Kalacska, M.E., Leblanc, G. and Constopoulous, A., 2015. Nitrous oxide, methane and carbon dioxide dynamics from experimental pig graves. Forensic Science International, 247, 41-47

Davenport, G.C., 2001. Remote sensing applications in forensic investigations. Historical Archaeology [online], 35 (1), 87-100

Davis, J.L., Heginbottom, J.A., Annan, A.P., Daniels, R.S., Berdal, B.P., Bergan, T., Duncan, K.E., Lewin, P.K., Oxford, J.S., Roberts, N., Skehel, J.J. and Smith, C.R., 2000. Ground penetrating radar surveys to locate 1918 Spanish flu victims in permafrost. Journal of Forensic Sciences, 45 (1), 68-76

Deering, D.W., 1978. Rangeland reflectance characteristics measured by aircraft and spacecraft sensors, Ph.D. Dissertation, Texas A&M University, College Station, TX.

De Jong, R., Bai, Z.G., Dent, D.L., Schaepman, M.E., de Bruin, S. and de Wit, A., 2009. Enhanced assessment of global land degradation. 33th International Symposium on Remote Sensing of Environment (ISRSE). Stresa, Italy

De Jong, R., De Bruin, S., De Wit, A., Schaepman, M.E. and Dent, D.L., 2011. Analysis of monotonic greening and browning trends from global NDVI time series. Remote Sensing of Environment, 115, 692-702

Dekeirsschieter, J., Verheggen, F.J., Gohy, M., Hubrecht, F., Bourguignon, L., Lognay, G. and Haubruge, E., 2009. Cadaveric volatile organic compounds released by decaying pig carcasses (Sus domesticus L.) in different biotopes. Forensic Science International [online], 189, 46-53

Dent, B.B., Forbes, S.L. and Stuart, B.H., 2004. Review of human decomposition processes in soil. Environmental Geology [online], 45, 576-585

Det Norske Veritas, 2003. *Independent Environmental and Public Health Risk Assessment of DEFRA Foot and Mouth Disposal Site (No. 20073900).* London, Det Norske Veritas

Didan, K., 2014. MODIS Land – Vegetation Indices [online]. NASA Goddard Space Flight Center. Available from: http://modis-land.gsfc.nasa.gov/vi.html [Accessed 18 May 2015]

Dirkmaat, D., 2012. A Companion to Forensic Anthropology. Chichester: West Sussex: Wiley-Blackwell

Djuric, M., Dunjic, D., Djonic, D. and Skinner, M., 2007. Identification of victims from two mass graves in Serbia – A critical evaluation of classical markers of identity. Forensic Science International, 172, 125-129

Doolittle, J.A. and Bellantoni, N.F., 2010. The search for graves with ground penetrating radar in Connecticut. Journal of Archaeological Science, 37, 941-949

Eastman, J.R., Sangermano, F., Machado, E.A., Rogan, J. and Anyamba, A., 2013. Global trends in seasonality of Normalized Difference Vegetation Index (NDVI), 1982-2011. Remote Sensing [online], 5, 4799-4818

Ellis, P.S.J. and Wright, R., 2016. War Crimes: Site Investigation. In: Byard, R. and Payne-James, P., eds. Encyclopedia of Forensic and Legal Medicine. London: Elsevier, 665-671

Evers, R., and Masters, P., 2018. The application of low-altitude near-infrared aerial photography for detecting clandestine burials using a UAV and low-cost unmodified digital camera. Forensic Science International, 289, 408-418.

EXELIS, 2015. About the Atmospheric Correction Module [online]. Available from: http://www.exelisvis.com/docs/AboutAtmosphericCorrectionModule.html [Accessed 7 May 2015]

EXELIS, 2015b. QUAC Background [online]. Available from: http://www.exelisvis.com/docs/backgroundquac.html [Accessed 7 May 2015]

EXELIS, 2015c. FLAASH Background [online]. Available from: http://www.exelisvis.com/docs/backgroundflaash.html [Accessed 7 May 2015]

EXELIS, 2015d. Broadband Greenness [online]. Available from: http://www.exelisvis.com/docs/broadbandgreenness.html [Accessed 7 May 2015]

EXELIS, 2015e. Narrowband Greenness [online]. Available from: http://www.exelisvis.com/docs/narrowbandgreenness.html [Accessed 7 May 2015]

Fernandez-Alvarez, J., Rubio-Melendi, D., Martinez-Velasco, A., Pringle, J.K., and Aguilera, H., 2016. Case Report: Discovery of a mass grave from the Spanish Civil War using Ground Penetrating Radar and forensic archaeology. Forensic Science International, 267, e10-e17.

Fontanelli, G., Paloscia, S., Zribi, M. and Chahbi, A., 2013. Sensitive analysis of X-band SAR to wheat and barley leaf area index in the Merguellil Basin. Remote Sensing Letters [online], 4 (11), 1101-1116

Forbes, S.L., Troobnikoff, A.N., Ueland, M., Nizio, K.D. and Perrault, K.A., 2016. Profiling the decomposition odour at the grave surface before and after probing. Forensic Science International, 259, 193-199

France. D.L., Griffin, T.J., Swanberg, J.G., Lindemann, J.W., Davenport, G.C., Trammell, V., Armbrust, C.T., Kondratieff, B., Nelson, A., Castello, K. and Hopkins, D., 1992. A multidisciplinary approach to the detection of clandestine graves. Journal of Forensic Sciences [online], 37 (6), 1445-1458

France. D.L., Griffin, T.J., Swanberg, J.G., Lindemann, J.W., Davenport, G.C., Trammell, V., Armbrust, C.T., Kondratieff, B., Nelson, A., Castello, K., Hopkins, D., Adair, T., 1996. NecroSearch Revisited: Further Multidisciplinary Approaches to the Detection of Clandestine Graves. *In:* Haglund, W.D., Sorg, M.H., eds. *Forensic Taphonomy: The Postmortem Fate of Human* Remains. Boca Raton, FL: CRC Press, 497-510

Garrido-Varas, C. and Intriago Leiva, M., 2012. Case Report – Managing commingled remains from mass graves: Considerations, implications and recommendations from a human rights case in Chile. Journal of Forensic Sciences [online], 219, 19-24

Gibson, P.J., 2000. Introductory Remote Sensing: Principles and Concepts. Oxon: Routledge

Gonzalez-Aguilera, D., Crespo-Matellan, E., Hernandez-Lopez, D. and Rodriguez-Gonzalvez, P., 2013. Automated urban analysis based on LiDAR-derived building models. IEEE Transactions on Geoscience and Remote Sensing [online], 51 (3), 1844-1851

Grip, W.M., Grip, R.W. and Morrison, R.D., 2000. Application of aerial photography and photogrammetry in environmental forensic investigations. Journal of Environmental Forensics [online], 1, 121-129

Groen, W.J. M., Marquez-Grant, N. and Janaway, R. C., 2015. Forensic Archaeology – A Global Perspective. Chichester, West Sussex: John Wiley and Sons Ltd

Groen, W.J. M., Marquez-Grant, N. and Janaway, R. C ., 2015a. Introduction. In: Groen, W.J. M., Marquez-Grant, N. and Janaway, R. C., eds. Forensic Archaeology – A Global Perspective. Chichester, West Sussex: John Wiley and Sons Ltd, Ii-Ixvii

Gupta, N., 2013. Local communities, national governments and forensic and archaeological investigations of human rights violations. Archaeologies: Journal of the World Archaeological Congress [online], 9 (1), 106-131

Haglund, W.D., 2002. Recent mass graves. In: Haglund, W.D. and Sorg, M.H., eds. Advances in Forensic Taphonomy: Method, Theory and Archaeological Perspectives. New York: CRC Press, 243-261

Haglund, W.D., Connor, M. and Scott, D.D., 2001. The archaeology of contemporary mass graves. Historical Archaeology [online], 35 (1), 57-69

Haglund, W.D. and Sorg, M.H., eds. 2002. Advances in Forensic Taphonomy: Method, Theory and Archaeological Perspectives. New York: CRC Press, 243-261

Hammon, W.S., McMechan, G.A. and Zeng, X., 2000. Forensic GPR: Finite-difference simulations of responses from buried human remains. Journal of Applied Geophysics, 45, 171-186

Hanson, I.D., 2004. The importance of stratigraphy in forensic investigation. In: Pye, K., and Croft, D.J., (eds.). Forensic Geoscience: Principles, Techniques and Applications. London: Geological Society Special Publications, 232, 39-47

Harrington, R.J., 1999. Forensic Monitoring Project Report: Hrastova Glavica Cave Recovery State Commission on Missing Persons (7 through 16 December 1998). Boston: Physicians for Human Rights

Harris, T. L., Drake, J., Wyndham, J.M., Wolfinbarger, S.R., Lott, S.D., and Lerner, M., 2018. Geospatial Evidence in International Human Rights Litigation: Technical and Legal Considerations. Available from: https://mcmprodaaas.s3.amazonaws.com/s3fs-public/reports/Geospatial%20Evidence%20in%20International%20Human%20Rights%20Litigation.pdf?82fMnrKB1Y92OEsgMEIWhFIhOW80cFQo [Accessed 02 August 2018]

Hansen, J.D., Pringle, J.K. and Goodwin, J., 2014. GPR and bulk ground resistivity surveys in graveyards: Locating unmarked burials in contrasting soil types. Forensic Science International, 237, 14-29

Hochrein, M.J., 2002. An Autopsy of the Grave: Recognising, Collecting and Preserving Forensic Geotaphonomic Evidence. In: Haglund, W.D. and Sorg, M.H., eds. Advances in Forensic Taphonomy: Method, Theory and Archaeological Perspectives. New York: CRC Press, 45-70

Holben, B.N., 1986. Characteristics of maximum-value composite images from temporal AVHRR data. International Journal of Remote Sensing, 7 (11), 1417-1434

Horler, D.N.H., Dockray, M., and Barber, J., 1983. The red edge of plant leaf reflectance. International Journal of Remote Sensing, 4 (2), 273-288.

Hou, W., Gao, J., Wu, S. and Dai, E., 2015. Interannual variations in growing season NDVI and its correlation with climate variables in the Southwestern Karst Region of China. Remote Sensing, 7, 11105-11124

Huete, A.R., 1988. A soil-adjusted vegetation index (SAVI). Remote Sensing of Environment, 25, 295-309

Hunter, J.R., Brickley, M.B., Bourgeois, J., Bouts, W., Bourguignon, L., Hubrecht, F., De Winne, J., Van Haaster, H., Hakbijl, T., De Jong, H., Smits, L., Van Wijngaarden, LH. and Luschen, M., 2001. Forensic archaeology, forensic anthropology and human rights in Europe. Science and Justice [online], 41 (3), 173-178

Hunter, J.R. and Cox, M. (eds)., 2005. Forensic Archaeology: Advances in Theory and Practice. London: Routledge

International Commission on Missing Persons., 2004. Batajnica Summary Report: Forensic Monitoring Activities. Sarajevo: Report ICMP.FSD.16.04.2.doc

International Commission on Missing Persons., 2005. Location of Mass Graves Using Non-Invasive Remote Sensing Equipment, Geophysics, and Satellite Imagery. Sarajevo: International Commission on Missing Persons. Report ICMP.FSD.33.05.doc.

International Commission on Missing Persons., 2014a. The missing [online]. Sarajevo: International Commission on Missing Persons. Available from: http://www.icmp.int/the-missing [Accessed 24 January 2016]

International Commission on Missing Persons., 2014b. Bosnia and Herzegovina. Missing Persons from the Armed Conflicts of the 1990s: A Stocktaking [online]. Sarajevo: International Commission on Missing Persons. Available from: http://www.icmp.int/?resources=missing-persons-from-the-armed-conflict-of-the-1990s-a-stocktaking-on-the-effort-to-locate-and-identify-missing-persons-in-bosnia-and-herzegovina [Accessed 25 January 2016]

ICTY., 2009a. Report on Autopsies of Human Remains from Cancari Road Site 3, August-September 1998 by C H Lawrence, MB.BS, BSc (Med), FRCPA [online]. The Hague: United Nations ICTY Court Records. Available from: http://icr.icty.org/LegalRef/CMSDocStore/Public/English/Exhibit/NotIndexable/IT-04-81/ACE85617R0000341189.pdf [Accessed 20 January 2015]

ICTY., 2009b. Report on Autopsies of Human Remains from Cancari Road Site 12, August 1998 by C H Lawrence, MB.BS, BSc (Med), FRCPA [online]. The Hague: United Nations ICTY Court Records. Available from: http://icr.icty.org/LegalRef/CMSDocStore/Public/English/Exhibit/NotIndexable/IT-04-81/ACE87149R0000343245.pdf [Accessed 20 January 2015]

ICTY., 2010a. Exhumation record for Cancari Road 4 (Kamenica 4 – KA04ZVO) [online]. The Hague: United Nations ICTY Court Records. Available from: http://icr.icty.org/LegalRef/CMSDocStore/Public/English/Exhibit/NotIndexable/IT-05-88%232/ACE89880R0000399313.pdf [Accessed 6 February 2015]

ICTY., 2010b. Exhumation record for Cancari Road 6 (Kamenica 6 – KA06ZVO) [online]. The Hague: United Nations ICTY Court Records. Available from: http://icr.icty.org/LegalRef/CMSDocStore/Public/English/Exhibit/NotIndexable/IT-05-88%232/ACE89882R0000399315.pdf [Accessed 6 February 2015]

ICTY., 2010c. Exhumation record for Cancari Road 8 (Kamenica 8 – KA08ZVO) [online]. The Hague: United Nations ICTY Court Records. Available from: http://icr.icty.org/LegalRef/CMSDocStore/Public/English/Exhibit/NotIndexable/IT-05-88%232/ACE89885R0000399318.pdf [Accessed 6 February 2015]

ICTY., 2010d. Exhumation record for Cancari Road 9 (Kamenica 9 – KA09ZVO) [online]. The Hague: United Nations ICTY Court Records. Available from: http://icr.icty.org/LegalRef/CMSDocStore/Public/English/Exhibit/NotIndexable/IT-05-88%232/ACE89886R0000395290.pdf [Accessed 6 February 2015]

ICTY., 2010e. Report titled, "Update to the Summary of Forensic Evidence – Exhumation of the Graves and Surface Remains Recoveries Related to Srebrenica and Zepa – April 2010," by Dusan JANC, dated 21 April 2010 [online]. The Hague: United Nations ICTY Court Records. Available from:

http://icr.icty.org/LegalRef/CMSDocStore/Public/English/Exhibit/NotIndexable/IT-05-88%232/ACE89854R0000395251.pdf [Accessed 15 February 2015]

ICTY., 2011a. Aerial image titled Cancari-Kamenica Road Segment, A3-size panorama (with markings CR-2 to CR-12).tif [photograph]. The Hague: United Nations ICTY Court Records. Available from: http://icr.icty.org/LegalRef/CMSDocStore/Public/English/Exhibit/Indexable/IT-05-88%232/ACE88621R0000393434.tif [Accessed 10 January 2015].

ICTY., 2011b. Aerial image titled Disturbed Earth, Zivkovici dated 7 Sep 95 (no markings).tif [photograph]. The Hague: United Nations ICTY Court Records. Available from: http://icr.icty.org/LegalRef/CMSDocStore/Public/English/Exhibit/Indexable/IT-05-88%232/ACE88622R0000393435.tif [Accessed 10 January 2015].

ICTY., 2011c. Aerial image titled Disturbed Earth, Zivkovici dated 2 Oct 95 (with marking CR-1).tif [photograph]. The Hague: United Nations ICTY Court Records. Available from: http://icr.icty.org/LegalRef/CMSDocStore/Public/English/Exhibit/Indexable/IT-05-88%232/ACE88623R0000393436.tif [Accessed 10 January 2015].

ICTY., 2011d. Aerial image titled Disturbed Earth, Ravne dated 7 Sep 95 (no markings).tif [photograph]. The Hague: United Nations ICTY Court Records. Available from: http://icr.icty.org/LegalRef/CMSDocStore/Public/English/Exhibit/Indexable/IT-05-88%232/ACE88624R0000393437.tif [Accessed 10 January 2015].

ICTY., 2011e. Aerial image titled Disturbed Earth, Ravne dated 2 Oct 95 (with marking CR-2).tif [photograph]. The Hague: United Nations ICTY Court Records. Available from: http://icr.icty.org/LegalRef/CMSDocStore/Public/English/Exhibit/Indexable/IT-05-88%232/ACE88625R0000393438.tif [Accessed 10 January 2015].

ICTY., 2011f. Aerial image titled Disturbed Earth, Ravne dated 7 Sep 95 (no markings).tif [photograph]. The Hague: United Nations ICTY Court Records. Available from: http://icr.icty.org/LegalRef/CMSDocStore/Public/English/Exhibit/Indexable/IT-05-88%232/ACE88626R0000393439.tif [Accessed 10 January 2015].

ICTY., 2011g. Aerial image titled Disturbed Earth, Ravne dated 2 Oct 95 (with marking CR-3).tif [photograph]. The Hague: United Nations ICTY Court Records. Available from: http://icr.icty.org/LegalRef/CMSDocStore/Public/English/Exhibit/Indexable/IT-05-88%232/ACE88627R0000393440.tif [Accessed 10 January 2015].

ICTY., 2011h. Aerial image titled Disturbed Earth, Ravne dated 7 Sep 95 (no markings).tif [photograph]. The Hague: United Nations ICTY Court Records. Available from: http://icr.icty.org/LegalRef/CMSDocStore/Public/English/Exhibit/Indexable/IT-05-88%232/ACE88628R0000393441.tif [Accessed 10 January 2015].

ICTY., 2011i. Aerial image titled Disturbed Earth, Ravne dated 2 Oct 95 (with marking CR-4 & CR-5).tif [photograph]. The Hague: United Nations ICTY Court Records. Available from: http://icr.icty.org/LegalRef/CMSDocStore/Public/English/Exhibit/Indexable/IT-05-88%232/ACE88629R0000393442.tif [Accessed 10 January 2015].

ICTY., 2011j. Aerial image titled Disturbed Earth, Redzici dated 7 Sep 95 (no markings).tif [photograph]. The Hague: United Nations ICTY Court Records. Available from: http://icr.icty.org/LegalRef/CMSDocStore/Public/English/Exhibit/Indexable/IT-05-88%232/ACE88630R0000393443.tif [Accessed 10 January 2015].

ICTY., 2011k. Aerial image titled Disturbed Earth, Redzici dated 2 Oct 95 (with marking CR-6).tif [photograph]. The Hague: United Nations ICTY Court Records. Available from: http://icr.icty.org/LegalRef/CMSDocStore/Public/English/Exhibit/Indexable/IT-05-88%232/ACE88631R0000393444.tif [Accessed 10 January 2015].

ICTY., 2011l. Aerial image titled Disturbed Earth, Redzici dated 7 Sep 95 (no markings).tif [photograph]. The Hague: United Nations ICTY Court Records. Available from: http://icr.icty.org/LegalRef/CMSDocStore/Public/English/Exhibit/Indexable/IT-05-88%232/ACE88632R0000393445.tif [Accessed 10 January 2015].

ICTY., 2011m. Aerial image titled Disturbed Earth, Redzici dated 2 Oct 95 (with marking CR-7).tif [photograph]. The Hague: United Nations ICTY Court Records. Available from: http://icr.icty.org/LegalRef/CMSDocStore/Public/English/Exhibit/Indexable/IT-05-88%232/ACE88633R0000393446.tif [Accessed 10 January 2015].

ICTY., 2011n. Aerial image titled Disturbed Earth, Bakraci dated 2 Oct 95 (with marking CR-8).tif [photograph]. The Hague: United Nations ICTY Court Records. Available from: http://icr.icty.org/LegalRef/CMSDocStore/Public/English/Exhibit/Indexable/IT-05-88%232/ACE88634R0000393447.tif [Accessed 10 January 2015].

ICTY., 2011o. Aerial image titled Disturbed Earth, Bakraci dated 7 Sep 95 (no markings).tif [photograph]. The Hague: United Nations ICTY Court Records. Available from: http://icr.icty.org/LegalRef/CMSDocStore/Public/English/Exhibit/Indexable/IT-05-88%232/ACE88635R0000393448.tif [Accessed 10 January 2015].

ICTY., 2011p. Aerial image titled Disturbed Earth, Bakraci dated 27 Sep 95 (no markings).tif [photograph]. The Hague: United Nations ICTY Court Records. Available from: http://icr.icty.org/LegalRef/CMSDocStore/Public/English/Exhibit/Indexable/IT-05-88%232/ACE88636R0000393449.tif [Accessed 10 January 2015].

ICTY., 2011q. Aerial image titled Disturbed Earth, Bakraci dated 2 Oct 95 (with marking CR-9).tif [photograph]. The Hague: United Nations ICTY Court Records. Available from: http://icr.icty.org/LegalRef/CMSDocStore/Public/English/Exhibit/Indexable/IT-05-88%232/ACE88637R0000393450.tif [Accessed 10 January 2015].

ICTY., 2011r. Aerial image titled Disturbed Earth, Kamenica dated 7 Sep 95 (no markings).tif [photograph]. The Hague: United Nations ICTY Court Records. Available from: http://icr.icty.org/LegalRef/CMSDocStore/Public/English/Exhibit/Indexable/IT-05-88%232/ACE88638R0000393451.tif [Accessed 10 January 2015].

ICTY., 2011s. Aerial image titled Disturbed Earth, Kamenica dated 27 Sep 95 (no markings).tif [photograph]. The Hague: United Nations ICTY Court Records. Available from: http://icr.icty.org/LegalRef/CMSDocStore/Public/English/Exhibit/Indexable/IT-05-88%232/ACE88639R0000393452.tif [Accessed 10 January 2015].

ICTY., 2011t. Aerial image titled Disturbed Earth, Kamenica dated 2 Oct 95 (with marking CR-10).tif [photograph]. The Hague: United Nations ICTY Court Records. Available from: http://icr.icty.org/LegalRef/CMSDocStore/Public/English/Exhibit/Indexable/IT-05-88%232/ACE88640R0000393453.tif [Accessed 10 January 2015].

ICTY., 2011u. Aerial image titled Disturbed Earth, Cancari dated 7 Sep 95 (no markings).tif [photograph]. The Hague: United Nations ICTY Court Records. Available from: http://icr.icty.org/LegalRef/CMSDocStore/Public/English/Exhibit/Indexable/IT-05-88%232/ACE88641R0000393454.tif [Accessed 10 January 2015].

ICTY., 2011v. Aerial image titled Disturbed Earth, Cancari dated 27 Sep 95 (no markings).tif [photograph]. The Hague: United Nations ICTY Court Records. Available from: http://icr.icty.org/LegalRef/CMSDocStore/Public/English/Exhibit/Indexable/IT-05-88%232/ACE88642R0000393455.tif [Accessed 10 January 2015].

ICTY., 2011w. Aerial image titled Disturbed Earth, Cancari dated 2 Oct 95 (with marking CR-11).tif [photograph]. The Hague: United Nations ICTY Court Records. Available from: http://icr.icty.org/LegalRef/CMSDocStore/Public/English/Exhibit/Indexable/IT-05-88%232/ACE88643R0000393456.tif [Accessed 10 January 2015].

ICTY., 2011x. Aerial image titled Disturbed Earth, Cancari dated 7 Sep 95 (no markings) marked by JR.tif [photograph]. The Hague: United Nations ICTY Court Records. Available from: http://icr.icty.org/LegalRef/CMSDocStore/Public/English/Exhibit/Indexable/IT-05-88%232/ACE88644R0000393457.tif [Accessed 10 January 2015].

ICTY., 2011y. Aerial image titled Disturbed Earth, Cancari dated 27 Sep 95 (no markings).tif [photograph]. The Hague: United Nations ICTY Court Records. Available from: http://icr.icty.org/LegalRef/CMSDocStore/Public/English/Exhibit/Indexable/IT-05-88%232/ACE88645R0000393458.tif [Accessed 10 January 2015].

ICTY., 2011z. Aerial image titled Disturbed Earth, Cancari dated 2 Oct 95 (with marking CR-12).tif [photograph]. The Hague: United Nations ICTY Court Records. Available from: http://icr.icty.org/LegalRef/CMSDocStore/Public/English/Exhibit/Indexable/IT-05-88%232/ACE88646R0000393459.tif [Accessed 10 January 2015].

ICTY., 2011aa. Exhumations in Eastern Bosnia in 1998 by Emeritus Professor Richard Wright, 12 May 1999 [online]. The Hague: United Nations ICTY Court Records. Available from: http://icr.icty.org/LegalRef/CMSDocStore/Public/English/Exhibit/NotIndexable/IT-95-5%2318/ACE112795R0000457121.pdf [Accessed 25 February 2015]

ICTY., 2011ab. Expert Report of Jose BARAYBAR: Anthropology Examination of Human Remains from Eastern Bosnia 1999 [online]. The Hague: United Nations ICTY Court Records. Available from: http://icr.icty.org/LegalRef/CMSDocStore/Public/English/Exhibit/NotIndexable/IT-95-5%2318/ACE112725R0000457046.TIF [Accessed 25 February 2015]

ICTY., 2011ac. Map of Cancari Road Secondary Graves 1-12.tif [map]. The Hague: United Nations ICTY Court Records. Available from: http://icr.icty.org/LegalRef/CMSDocStore/Public/English/Exhibit/Indexable/IT-05-88%232/ACE88476R0000393250.tif [Accessed 9 January 2015].

ICTY., 2011ad. Map of Srebrenica Primary and Secondary Mass Graves [map]. The Hague: United Nations ICTY Court Records. Available from: http://icr.icty.org/LegalRef/CMSDocStore/Public/English/Exhibit/Indexable/IT-05-88%232/ACE89063R0000394032.tif [Accessed 11 January 2015].

ICTY., 2011ae. 17 IKONOS satellite images and overview map showing the locations of and links between primary and secondary graves.tif [photograph]. The Hague: United Nations ICTY Court Records. Available from: http://icr.icty.org/LegalRef/CMSDocStore/Public/English/Exhibit/NotIndexable/IT-05-88%232/ACE89062R0000394031.pdf [Accessed 11 January 2015].

ICTY., 2011af. Statement of Antony BROWN from the Department of Geography, Exeter University, Soil Report regarding Cancari Road, Kozluk, Branjevo Farm, Hodzici Road and Lazete, dated 26 February 1999 [online]. The Hague: United Nations ICTY Court Records. Available from: http://icr.icty.org/LegalRef/CMSDocStore/Public/English/Exhibit/NotIndexable/IT-05-88%232/ACE88302R0000392997.TIF [Accessed 20 January 2015]

ICTY., 2011ag. Report titled, "Srebrenica Investigation, Summary of Forensic Evidence – Execution Points and Mass Graves 2001", by Dean MANNING [online]. The Hague: United Nations ICTY Court Records. Available from: http://icr.icty.org/LegalRef/CMSDocStore/Public/English/Exhibit/NotIndexable/IT-05-88%232/ACE89174R0000394171.pdf [Accessed 15 February 2015]

ICTY., 2011ah. Updated Summary of Forensic Evidence Exhumation of mass graves, prepared by Dean MANNING, with Annex, dated 27 November 2007 [online]. The Hague: United Nations ICTY Court Records. Available from: http://icr.icty.org/LegalRef/CMSDocStore/Public/English/Exhibit/NotIndexable/IT-05-88%232/ACE89057R0000394025.pdf [Accessed 15 February 2015]

ICTY., 2012a. Booklet Entitled Srebrenica Mass Graves – Primary and Secondary Mass Grave Aerial Imagery [online]. The Hague: United Nations ICTY Court Records. Available from: http://icr.icty.org/LegalRef/CMSDocStore/Public/English/Exhibit/NotIndexable/IT-95-5%2318/ACE120536R0000469616.pdf [Accessed 1 February 2015]

ICTY., 2012b. Corrected ICMP Summary Report on Cancari Road 6, created from 8 to 10 August 2008 [online]. The Hague: United Nations ICTY Court Records. Available from: http://icr.icty.org/LegalRef/CMSDocStore/Public/English/Exhibit/NotIndexable/IT-95-5%2318/ACE120604R0000469691.pdf [Accessed 6 February 2015]

ICTY., 2012c. ICMP Summary Report Cancari Road 04, BiH – ICMP Site Code: R-ZVO.CR04. [online]. The Hague: United Nations ICTY Court Records. Available from: http://icr.icty.org/LegalRef/CMSDocStore/Public/English/Exhibit/NotIndexable/IT-95-5%2318/ACE113251R0000457615.pdf [Accessed 6 February 2015]

ICTY., 2012d. ICMP Summary Report on Cancari Road 8 (Kamenica 8 – KAM08ZVO) [online]. The Hague: United Nations ICTY Court Records. Available from: http://icr.icty.org/LegalRef/CMSDocStore/Public/English/Exhibit/NotIndexable/IT-95-5%2318/ACE113252R0000457616.pdf [Accessed 6 February 2015]

Jackson, R.D. and Huete, A.R., 1991. Interpreting vegetation indices. Preventative Veterinary Medicine, 11, 185-200

Jankauskas, R., Barkus, A., Urbanavieius, V. and Garmus, A., 2005. Forensic archaeology in Lithuania: the Tuskulenai mass grave. Acta Medica Lituanica [online], 12 (1), 70-74

Jervis, J.R. and Pringle, J.K., 2014. A study of the effect of seasonal climatic factors on the electrical resistivity response of three experimental graves. Journal of Applied Geophysics, 108, 53-60

Jervis, J.R., Pringle, J.K., Cassella, J.P. and Tuckwell, G.W., 2009a. Using soil and groundwater to understand resistivity surveys over a simulated clandestine grave. In: Ritz, K., Dawson, L. and Miller, D., eds. Criminal and Environmental Soil Forensics. Dordrecht, Netherlands: Springer, 271-284

Jervis, J.R., Pringle, J.K. and Tuckwell, G.W., 2009b. Time-lapse resistivity surveys over simulated clandestine graves. Forensic Science International, 192, 7-13

Jessee, E. and Skinner, M., 2005. A typology of mass grave and mass grave related sites. Forensic Science International [online], 152, 55-59

Jin, S., and Sader, S.A., 2005. Comparison of time series tasselled cap wetness and the normalised difference moisture index in detecting forest disturbances. Remote Sensing of Environment, 94, 364-372

Joseph, G., 2005. Fundamentals of Remote Sensing. 2nd edition. India: Orient BlackSwan/ Universities Press

Juerges, A., Pringle, J.K., Jervis, J.R. and Masters, P., 2010. Comparisons of magnetic and electrical resistivity surveys over simulated clandestine graves in contrasting burial environments. Near Surface Geophysics, 8, 529-539

Julien, Y., Sobrino, J.A. and Verhoef, W., 2006. Changes in land surface temperatures and NDVI values over Europe between 1982 and 1999. Remote Sensing of Environment, 103, 43-55

Kalacska, M. and Bell, L.S., 2006. Remote sensing as a tool for the detection of clandestine mass graves. Canadian Society of Forensic Science Journal [online], 39 (1), 1-13

Kalacska, M.E., Bell, L.S., Sanchez-Azofeifa, G.A. and Caelli, T., 2009. The application of remote sensing for detecting mass graves: An experimental animal case study from Costa Rica. Journal of Forensic Sciences [online], 54, 159-166

Komar, D., 2001. Differential decay rates in singe, multiple, and mass graves in Bosnia. Proceedings of the American Academy of Forensic Sciences Annual Meeting, 7, 242-243

Komar, D., 2008. Patterns of mortuary practice associated with Genocide. Current Anthropology, 49 (1), 123-133

Leblanc, G., Kalacska, M. and Soffer, R., 2014. Technical Note – Detection of single graves by airborne hyperspectral imaging. Forensic Science International, 245, 17-23

Lillesand, T., Kiefer, R.W. and Chipman, J., 2008. Remote Sensing and Image Interpretation. 6th edition. USA: John Wiley and Sons

Litherland, S., Marquez-Grant, N. and Roberts, J., 2012. Forensic Archaeology. In: Marquez-Grant, N. and Roberts, J., eds. Forensic Ecology Handbook: From Crime Scene to Court. West Sussex, UK: John Wiley and Sons, 23-48

Liu, H.Q., and Huete, A.R., 1995. A feedback based modification of the NDV I to minimize canopy background and atmospheric noise. IEEE Transactions on Geoscience and Remote Sensing, 33, 457-465

Manning, D. P., 2003. Prosecutor v. Slobodan Milosevic IT-02-54-T. Witness Statement – Investigations Team Leader Dean Paul Manning.ICTY.

Mant, A.K., 1987. Knowledge Acquired from Post-War Exhumations. In: Boddington, A., Garland, A.N. and Janaway, R.C., eds. Death, Decay and Reconstruction: Approaches to Archaeology and Forensic Science. Manchester, UK: Manchester University Press, 65-78

Mather, P. M., 2004. Computer Processing of Remotely-Sensed Images. 3rd edition. Sussex: John Wiley and Sons

Matsushita, B., Yang, W., Chen, J., Onda, Y., and Qiu, G., 2007. Sensitivity of the Enhanced Vegetation Index (EVI) and Normalized Difference Vegetation Index (NDVI) to Topographic Effects: A Case Study in High-Density Cypress Forest. Sensors (Basel)., 7 (11), 2636-2651

Matuszewski, S., Hall, M.J.R., Moreau, G., Schonely, K.G., Tarone, A.M., and Villet, M.H., 2019. Pigs vs. people: the use of pigs as analogues for humans in forensic entomology and taphonomy research. International Journal of Legal Medicine [online], 1-18

McGray, D., 2001. Unearthing grave offences. Foreign Policy [online], 126, 86-87

MacLellan, C., 2006. Guidelines for Post Processing GER 1500 Spectral Data Files using a FSF Excel Template. NERC Field Spectroscopy Facility: Edinburgh

Miller, P.S., 1996. Disturbances in the soil: Finding buried bodies and other evidence using ground penetrating radar. Journal of Forensic Sciences [online], 41 (4), 648-652

MODTRAN5., 2015. Top 10 Most Frequently Asked Questions About MODTRAN [online]. Available from: http://modtran5.com/faqs/index.html [Accessed 7 May 2015]

Molina, C.M., Pringle, J.K., Saumett, M. and Evans, G.T., 2016. Geophysical monitoring of simulated graves with resistivity, magnetic susceptibility, conductivity and GPR in Colombia, South America. Forensic Science International, 261, 106-115

Molina, C.M., Pringle, J.K., Saumett, M. and Hernandez, O., 2015. Preliminary result of sequential monitoring of simulated clandestine graves in Colombia, South America, using ground penetrating radar and botany. Forensic Science International, 248, 61-70

Morawitz, D.F., Blewett, T.M., Cohen, A. and Alberti, M., 2006. Using NDVI to assess vegetative land cover change in central Puget Sound. Environmental Monitoring and Assessment, 114, 86-106

Morse, D., Crusoe, D. and Smith, H.G., 1976. Forensic archaeology. Journal of Forensic Sciences, 21 (2), 323-332

NASA., 2011. Landsat 7 Science Data Users Handbook [online]. NASA: USA. Available from: http://landsathandbook.gsfc.nasa.gov/pdfs/Landsat7_Handbook.pdf [Accessed 18 April 2015]

NASA., 2015. MODIS – Moderate Resolution Imaging Spectroradiometre [online]. Available from: http://modis.gsfc.nasa.gov/about/specifications.php [Accessed 18 May 2015]

NOAA SIS., 2013. Advanced Very High Resolution Radiometre – AVHRR [online]. Available from: http://noaasis.noaa.gov/NOAASIS/ml/avhrr.html [Accessed 18 May 2015]

NERC FSF., 2016. GER1500 System. Edinburgh: NERC FSF. Available from: http://fsf.nerc.ac.uk/instruments/ger1500.shtml [Accessed 1 August 2014]

Nobes, D.C., 2000. Case Report: The search for "Yvonne": A case example of the delineation of a grave using near-surface geophysical methods. Journal of Forensic Sciences [online], 45 (3), 715-721

Norton, E.A., 2010. The Application of In Situ Reflectance Spectroscopy for the Detection of Mass Graves. Thesis (MSc). Cranfield University

Nunez, C., Baeta, M., Palencia-Madrid, L., Herrasti, L., Etxeberria, F. and de Pancorbo, M.M., 2015. A grave in my garden. Genetic identification of Spanish civil war victims buried in two mass graves in Espinosa de los Monteros (Burgos, Spain). Forensic Science International: Genetics Supplement Series, 19, 272-279

Orlando, L. and Marchesi, E., 2001. Georadar as a tool to identify and characterise solid waste dump deposits. Journal of Applied Geophysics, 48, 163-174

Owsley, D.W., 1995. Techniques for locating burials, with emphasis on the probe. Journal of Forensic Sciences [online], 40 (5), 735-740

Owsley, D.W., Strinovic, D., Slaus, M., Kollmann, D.D. and Richardson, M.L., 1996. Recovery and Identification of Civilian: Victims of War in Croatia [online]. United States – Department of the Interior. Available from: https://www.hsdl.org/?abstract&did=781470 [Accessed 2 February 2015]

Oxford English Dictionary., 2018. [online] Available from: http://www.oed.com/view/Entry/80989?rskey=OGDdM5&result=1#eid [Accessed 4 November 2018]

Powell, K., 2004. Detecting buried human remains using near-surface geophysical instruments. Exploration Geophysics [online], 35, 88-92

Pringle, J.K., Giubertoni, M., Cassidy, N.J., Wisniewski, K.D., Hansen, J.D., Linford, N.T. and Daniels, R.M., 2015. The use of magnetic susceptibility as a forensic search tool. Forensic Science International, 246, 31-42

Pringle J.K., Jervis, J.R., Hansen J.D., Jones G.M., Cassidy N.J. and Cassella J.P., 2012. Geophysical monitiroing of simulated clandestine graves using electrical and ground-penetrating radar methods: 0-3 years after burial. Journal of Forensic Sciences [online], 57 (6) 1467-1486

Pringle, J.K. and Jervis, J.R., 2010. Case Report: Electrical resistivity survey to search for a recent clandestine burial of a homicide victim, UK. Forensic Science International [online], 202, 1-7

Pringle, J.K., Jervis, J., Cassella, J.P. and Cassidy, N.J., 2008. Technical Note: Time-lapse geophysical investigations over a simulated urban clandestine grave. Journal of Forensic Sciences [online], 53 (6), 1405-1416

Pringle, J.K., Ruffell, A., Jervis, J.R., Donnelly, L., McKinley, J., Hansen, J., Morgan, R., Pirrie, D. and Harrison, M., 2012. The use of geoscience methods for terrestrial forensic searches. Earth-Science Reviews, 114, 108-123

Qi, J., Chehbouni, A., Huete, A.R., Kerr, Y.H., and Sorooshian, S., 1994. A modified soil adjusted vegetation index. Remote Sensing of Environment, 48 (2), 119-126

Raymond, N. The ethical quandaries around George Clooney's satellites over Sudan, 2012. [radio interview]. Q.CBC Radio. 4 April 2012 [last accessed 28 January 2014]. Available from: http://www.cbc.ca/player/Radio/Q/ID/2219451352/?page=28

Rees, W.G., 1990. Introduction. In: Rees, W.G., *Topics in Remote Sensing 1: Physical Principles of Remote Sensing*. , Cambridge: Cambridge University Press, 1-7

Richardson, A.D., Keenan, T.F., Migliavacca, M., Ryu, Y., Sonnentag, O. and Toomey, M., 2013. Review – Climate change, phenology, and phonological control of vegetation feedbacks to the climate system. Agricultural and Forest Meteorology, 169, 156-173

Rios, L., Casaado Ovejero, J.I. and Prieto, J.P., 2010. Case Report: Identification process in mass graves from the Spanish Civil War I. Forensic Science International [online], 199, 27-36

Rios, L., Garcia-Rubio, A., Martinez, B., Alonso, A. and Puente, J., 2012. Case Report: Identification process in mass graves from the Spanish Civil War II. Forensic Science International [online], 219, 4-9

Rodriguez, W.C. and Bass, W.M., 1985. Decomposition of buried bodies and methods that may aid in their location. Journal of Forensic Sciences, 30, 836-852

Roerink, G.J. and Menenti, M., 2000. Reconstructing cloudfree NDVI composites using fourier analysis of time series. International Journal of Remote Sensing, 21 (9), 1911-1917

Rubio-Melendi, D., Gonzalez-Quiros, A., Roberts, D., Carmen Garcia Garcia, M., Dominguez, A.C., Pringle, J.K., and Fernandez-Alvarez, J., 2018. Case Report: GPR and ERT detection and characterisation of a mass burial, Spanish Civil War, Northern Spain. Forensic Science International, 287, e1-e9.

Rubio-Melendi, D., Gonzalez-Quiros, A., Roberts, D., Carmen Garcia Garcia, M., Dominguez, A.C., Pringle, J.K., and Fernandez-Alvarez, J., 2018. Case Report: GPR and ERT detection and characterisation of a mass burial, Spanish Civil War, Northern Spain. Forensic Science International, 287, e1-e9.

Ruffell, A., 2002. Review: Remote detection and identification of organic remains: An assessment of archaeological potential. Archaeological Prospection [online], 9, 115-122

Ruffell, A., Donnelly, C., Carver, N., Murphy, E., Murray, E. and McCambridge., 2009. Suspect burial excavation procedure: A cautionary tale. Forensic Science International, 183, e11-e16

Ruffell, A. and Kulessa, B., 2009. Application of geophysical techniques in identifying illegally buried toxic waste. Environmental Forensics, 10, 196-207

Ruffell, A., McCabe, A., Donnelly, C. and Sloan, B., 2009. Location and assessment of and historic mass grave (150-160 years old) using geographic and ground penetrating radar investigation, NW Ireland. Journal of Forensic Sciences, 54 (2), 382-394

Ruffell, A. and McKinley, J., 2005. Forensic geosciences: Applications of geology, geomorphology and geophysics to criminal investigations. Earth-Science Reviews, 69, 235-247

Ruwanpura, P.R., Perera, U.C.P., Wijayaweera, H.T.K. and Chandrasiri, N., 2006. Adaptation of archaeological techniques in forensic mass grave exhumation: the experience of 'Chemmani' excavation in northern Sri Lanka. Ceylon Medical Journal, 51 (3), 98-102

Sabins, F.F., 1997. *Remote Sensing: Principles and Interpretation*. New York: W.H. Freeman and Company

Satellite Imaging Corporation., 2016. RapidEye Satellite Sensor [online]. Texas, USA: Satellite Imaging Corporation. Available from: www.satimagingcorp.com/satellite-sensors/other-satellite-sensors/rapideye [Accessed 22 March 2016]

Schaepan, M.E., 2009. Imaging Spectrometers. In: Warner, T.A., Nellis, M.D. and Foody, G.M., eds. The SAGE Handbook of Remote Sensing. London: SAGE Publications Ltd, 166-178

Schmitt, S., 2002. Mass Graves and the Collection of Forensic Evidence: Genocide, War Crimes and Crimes Against Humanity. In: Haglund, W.D. and Sorg, M.H., eds. Advances in Forensic Taphonomy: Method, Theory and Archaeological Perspectives. New York: CRC Press, 277-292

Schuldenrein, J., Trimble, M.K., Malin-Boyce, S., and Smith, M., 2017. Geoarchaeology, Forensics, and the Prosecution of Saddam Hussein: A Case Study from the Iraq War (2003–2011). Geoarchaeology: An International Journal, 32, 130-156

Schultz, J.J., 2007. Using ground penetrating radar to locate clandestine graves of homicide victims: Forming forensic archaeology partnerships with law enforcement. Homicide Studies [online], 11 (1), 15-29

Schultz, J.J., Collins, M.E. and Falsetti, A.B., 2006. Sequential monitoring of burials containing large pig cadavers using ground-penetrating radar. Journal of Forensic Sciences, 51 (3), 607-616

Schultz, J.J. and Dupras, T.L., 2008. The contribution of forensic archaeology to homicide investigations. Homicide Studies [online], 12, 399-413

Scott, J. and Hunter, J.R., 2004. Environmental influences on resistivity mapping for the location of clandestine graves. In: Pye, K. and Croft, D.J., (eds). Forensic Geoscience: Principles, Techniques and Applications. London: Geological Society, 232, 33-38

Shaw, G.A. and Burke, H.K., 2003. Spectral imaging for remote sensing. Lincoln Laboratory Journal [online], 14 (1), 1-26

Sims, D.A. and Gamon, J.A., 2002. Relationships between leaf pigment content and spectral reflectance across a wide range of species, leaf structures and developmental stages. Remote Sensing of Environment, 81, 337-354

Simmons, T., 2002. Taphonomy of a Karstic Cave Execution Site at Hrgar, Bosnia-Herzegovina. In: Haglund, W.D. and Sorg, M.H., eds. Advances in Forensic Taphonomy: Method, Theory and Archaeological Perspectives. New York: CRC Press, 264-275

Skinner, M., Alempijevic, D. and Djuric-Srejic, M., 2003. Guidelines for international bio-archaeology monitors of mass grave exhumations. Forensic Science International [online], 134, 81-92

Skinner, M.F., 1987. Planning the archaeological recovery of evidence from recent mass graves. Forensic Science International [online], 34, 267-287

Skinner, M. and Sterenberg, J., 2005. Turf wars: Authority and responsibility for the investigation of mass graves. Forensic Science International [online], 151, 221-232

Slaus, M., Strinovic, D., Pecina-Slaus, N,. Brkic, H., Balicevic, D., Petrovecki, V. and Pecina, T, C., 2007. Identification and analysis of human remains recovered from wells from the 1991 War in Croatia**.** Forensic Science International, 171, 37-43

SPOT Image., 2010. SPOT Satellite Technical Data [online]. Available from: http://www2.geo-airbusds.com/files/pmedia/public/r329_9_spotsatellitetechnicaldata_en_sept2010.pdf [Accessed 18 May 2015]

SPOT Image., 2010. Resolutions and spectral modes [online]. SPOT Image: France. Available from: http://www2.geo-airbusds.com/files/pmedia/public/r451_9_resolutionspectralmodes_uk_sept2010.pdf [Accessed 20 April 2015]

Steadman, D.W. and Haglund, W.D., 2005. The scope of anthropological contributions to human rights investigations. Journal of Forensic Sciences [online], 50 (1), 1-8

Steele, C., 2008. Archaeology and the forensic investigation of recent mass graves: Ethical issues for a new practice of archaeology. Archaeologies: Journal of the World Archaeological Congress [online], 4 (3), 414-428

Stover, E., Haglund, W.D. and Samuels, M., 2003. Exhumation of mass graves in Iraq: Considerations for forensic investigations, humanitarian needs, and the demands of justice. The Journal of the American Medical Association [online], 290 (5), 663-666

Stover, E. and Ryan, M., 2001. Breaking bread with the dead. Historical Archaeology [online], 35 (1), 7-25

Szleszkowski, L., Thannhauser, A., Szwagrzyk, K., Konczewski, P., Kawecki, J. and Swiatek, B., 2014. Exhumation research concerning the victims of political repressions in 1945-1956 in Poland: A new direction in forensic medicine. Forensic Science International [online], 235, e1-6

The Prosecutor v Radovan Karadzic (Prosecution motion to amend exhibits P04771 and P04772) IT-95-5/18-T (25 September 2013)

Thenkabail, P.S., Smith, R.B. and Pauw, E.D., 2000. Hyperspectral vegetation indices and their relationships with agricultural crop characteristics. Remote Sensing of Environment [online], 71, 158-182

Tillack, A., Clasen, A., Kleinschmit, B. and Forster., 2014. Estimation of the seasonal leaf area index in an alluvial forest using high-resolution satellite-based vegetation indices. Remote Sensing of Environment [online], 141, 52-63

Touzi, R., Lopes, A., Bruniquel, J. and Vachon, P.W., 1999. Coherence Estimation for SAR Imagery. IEEE Transactions on Geoscience and Remote Sensing, 37 (1), 134-149

Tucker, C.J., 1979. Red and photographic infrared linear combinations for monitoring vegetation. Remote Sensing of Environment, 8 (2), 127-150

Tuller, H. and Duric, M., 2006. Keeping the pieces together: Comparison of mass grave excavation methodology. Forensic Science International [online], 156, 192-200

Tuller., H.H., 2012. Mass Graves and Human Rights: Latest Developments, Methods, and Lessons Learned. In: Dirkmaat, D., 2012. A Companion to Forensic Anthropology. Chichester: West Sussex: Wiley-Blackwell, 157-174

Tyagi, P. and Bhosle, U., 2011. Atmospheric correction of remotely sensed images in spatial and transform domain. International Journal of Image Processing, 5 (5), 564-579

United Nations, 1991. Manual on the effective prevention and investigation of extra-legal, arbitrary and summary executions [online]. New York: United Nations. Available from: https://www.ncjrs.gov/pdffiles1/Digitization/133673NCJRS.pdf [Accessed 12 March 2014]

U.S. Geological Survey., 2016. Frequently Asked Questions about the Landsat Missions [online]. U.S. Geological Survey: USA. Available from: http://landsat.usgs.gov/band_designations_landsat_satellites.php [Accessed 4 April 2016]

U.S. Geological Survey., 2018. Landsat 4-7 Surface Reflectance (LEDAPS) Product Guide - Version 1.0 [online]. U.S. Geological Survey: USA. Available from: https://landsat.usgs.gov/sites/default/files/documents/ledaps_product_guide.pdf [Accessed 19 January 2019]

U.S. Geological Survey., 2017. Product Guide: Landsat Surface Reflectance-Derived Spectral Indices - Version 3.6 [online]. U.S. Geological Survey: USA. Available from: https://landsat.usgs.gov/sites/default/files/documents/si_product_guide.pdf [Accessed 2 December 2018]

U.S. Geological Survey., 2018b. User Guide – Earth Resources Observation and Sciences (EROS) Center Science Processing Architecture (ESPA) On Demand Interface - Version 4.4 [online]. U.S. Geological Survey: USA. Available from: https://landsat.usgs.gov/sites/default/files/documents/espa_odi_userguide.pdf [Accessed 2 December 2018]

Van Belle, L.E., Carter, D.O. and Forbes, S.L., 2009. Measurement of ninhydrin reactive nitrogen influx into gravesoil during aboveground and belowground carcass (Sus domesticus) decomposition. Forensic Science International, 193, 37–41

Vanezis, P., 1999. Investigation of clandestine graves resulting from human rights abuses. Journal of Clinical Forensic Medicine, 6 (4), 238-242

Van Zyl, J. and Kim, Y., 2011. Synthetic Aperature Radar Polarimetry. New Jersey: John Wiley and Sons Ltd

Vass, A.A., 2012. Odor mortis. Forensic Science International, 222, 234-241

Vass, A.A., Smith, R.R., Thompson, C.V., Burnett, M.N.,Dulgerian, N. and Eckenrode, B.A., 2008. Odor analysis of decomposing buried human remains. Journal of Forensic Sciences, 53 (2), 384-391

Vass, A.A., Smith, R.R., Thompson, C.V., Burnett, M.N., Wolf, D.A., Synstelien, J.A., Dulgerian, N. and Eckenrode, B.A., 2004. Decompositional odor analysis database. Journal of Forensic Sciences [online], 49, 760-769

Vass, A.A., Thompson, C.V. and Wise, M.W., 2010. A new forensics tool: Development of an advanced sensor for detecting clandestine graves. USA: U.S. Department of Justice. 2007-DN-R-104.

Verbesselt, J., Hyndman, R., Newnham, G., and Culvenor, D., 2010. Detecting trend and seasonal changes in satellite image time series. Remote Sensing of Environment, 114, 106-115

Verbesselt, J., Hyndman, R., Zeileis, A., and Culvenor, D., 2010. Phenological change detection while accounting for abrupt and gradual trends in satellite image time series. Remote Sensing of Environment, 114, 2970-2980

Verbesselt, J., Zeileis, A., and Harold, M., 2012. Near real-time disturbance detection using satellite image time series. Remote Sensing of Environment, 123, 98-108

Wang, B.Y., Raymond, N.A., Gould, G. and Baker, I., 2013. Problems from hell, solution in the heavens? : Identifying obstacles and opportunities for employing geospatial technologies to document and mitigate mass atrocities. Stability: International Journal of Security and Development [online], 2 (3), 1-18

Watters, M. and Hunter, J.R., 2004. Geophysics and burials: Field experience and software development. In: Pye, K. and Croft, D.J., eds. Forensic Geosciences: Principles, Techniques and Applications. London: Geological Society Special Publications, 232, 21-31

Whitehurst, A.S., Awatantran, A., Blair, B,J., Hofton, M,A. and Dubayah, R., 2013. Characterization of canopy layering in forested ecosystems using full waveform LiDAR. Remote Sensing [online], 5 (4), 2014-2036

Wilson, E.H., and Sader, S.A., 2002. Detection of forest harvest type using multiple dates of Landsat TM imagery. Remote Sensing of Environment, 80, 385-396

Worcestershire County Council, 2011. *Worcestershire Waste Core Strategy Background Document – Waste Sites in Worcestershire* [online]. Worcestershire County Council. Available from: http://www.worcestershire.gov.uk/cms/pdf/2011.02.28%20Waste%20sites%20background%20doc.pdf

Zancajo-Blazquez, S., Gonzalez-Aguilera, D., Gonzalez-Jorge, H. and Hernandez-Lopez, D., 2015. An automatic image-based modelling method applied to forensic infography. PLOS ONE, 10 (3), 1-15

Zhou, J., Hu, G., Jia, L. and Menenti, M., 2012. Evaluation of Harmonic Analysis of Time Series (HANTS): Impact of gaps on time series reconstruction. In: 2nd International

Workshop on Earth Observation and Remote Sensing Applications, 8-11th June 2012. Shanghai, China, 31-35

Zhou, J., Jia, L., Hu, G. and Menenti, M., 2013. A global evaluation of harmonic analysis of time series under distinct gap conditions. EARSeL Proceedings, 12, 58-66

Zwiggelaar, R., 1998. A review of spectral properties of plants and their potential use for crop/weed discrimination in row-crops. Crop Protection, 1 (3), 189-206

Appendix 1 for Chapter 4

Landsat Data Product Specifications

Table 1-1 - Landsat Mission Characteristics (Source: NASA 2011)

System	Launch (End of Service)	Instruments	Resolution (m)	Alt. km	Revisit Interval
Landsat 5	01/03/1984	MSS TM	80 30	705	16
Landsat 6	05/10/1993 (05/10/1993)	ETM	15 (pan) 30 (ms)	705	16
Landsat 7	15/04/1999	ETM+	15 (pan) 30 (ms)	705	16
Landsat 8	11/02/2013	OLI TIRS	15 (pan) 30 (ms) 100 (TIR)	705	16

Table 1-2 – Landsat 5 – 8 spectral bands, ground pixel size and spectral resolution (Source: U.S. Geological Survey 2018)

Satellite	Spectral Bands	Ground Pixel Size (m)	Spectral Resolution (nm)
Thematic Mapper (TM) Landsat 5	B1	30	450-520
	B2		520-600
	B3		630-690
	B4		760-900
	B5		1550-1750
	B6	120	10400-12500
	B7	30	2080-2350
Enhanced Thematic Mapper (ETM+)	B1	30	450-520
	B2		520-600
	B3		630-690
	B4		770-900
	B5		1550-1750
	B6	60	10400-12500
	B7	30	2080-2350
	B8	15	520-900
Operational Land Imager (OLI)	B1	30	452-512
	B2		533-590
	B3		636-673
	B4		851-879
	B5		1566-1651
	B6	100	10600-12510
	B7	30	21070-22940
	B8	15	503-676

Table 1-3 - Landsat Ecosystem Disturbance Adaptive Processing System Algorithm Details (Source: USGS 2018)

Parameter	**Landsat 4-5, 7 (LEDAPS)**
Global Coverage	Yes
Top Of Atmosphere Reflectance	Visible (Bands 1–5,7)
Top Of Atmosphere Brightness Temperature	Thermal (Band 6)
Spectral Range	Visible (1–5, 7) bands
Radiative transfer model	6S
Thermal correction level	Top Of Atmosphere only
Thermal band units	Kelvin
Pressure	NCEP Grid
Water vapour	NCEP Grid
Air temperature	NCEP Grid
DEM	Global Climate Model DEM
Ozone	OMI/TOMS
AOT	Correlation between chlorophyll absorption and bound water absorption of scene
Sun angle	Scene center from input metadata
View zenith angle	From input metadata
Undesirable zenith angle correction	SR not processed when solar zenith angle > 76 degrees
Pan band processed?	No
XML metadata?	Yes
Brightness temperature calculated	Yes (Band 6 TM/ETM+)
Cloud mask	Internal algorithm; CFmask
Data format	INT16
Fill values	-9999
QA bands	Cloud Adjacent cloud Cloud shadow DDV Fill Land water Snow Atmospheric opacity

Table 1-4 - DMC Data Product Specifications (Source: Crowley 2010).

Product	**Description**
L0R	Raw satellite data split into the 3 spectral bands (NIR, Red and Green) with a radiometric correction applied to all bands.

Table 1-5 - DMC Imager Information (Source: Crowley 2010).

DMC	Imager	Imager Type	GSD at Nadir	Spectral Bands	Spectral Bandwidth (nm)
UK-DMC	SLIM-6	Optical	31.822m	NIR Red Green	770-900
					630-690
					520-600
UK-DMC2	SLIM-6-22	Optical	22.001m	NIR Red Green	770-900
					630-690
					520-600

Table 1-6 - UK-DMC Orbit Information (Source: Crowley 2010)

Parameter	Nominal Value
Orbit Type	Sun synchronous
Altitude	686km
Inclination	98.2^{o}
Orbital Period	98.4min
LTAN	10:15 UTC
Orbital Velocity	$7.5 kms^{-1}$
Ground Velocity	$6.8 kms^{-1}$

Table 1-7 - UK-DMC2 Orbit Information (Source: Crowley 2010)

Parameter	Nominal Value
Orbit Type	Sun synchronous
Altitude	659km
Inclination	98.06^{o}
Orbital Period	97.9min
LTAN	10:45 UTC
Orbital Velocity	$7.5 kms^{-1}$
Ground Velocity	$6.8 kms^{-1}$

Table 1-8 - SPOT 1-5 spectral bands, ground pixel size and spectral resolution (Source: SPOT Image 2010).

SPOT Satellite	Spectral Bands	Ground Pixel Size (m)	Spectral Resolution (nm)
SPOT 5	P: Panchromatic	2.5m or 5m	480-710
	B1: Green	10 m	500-590
	B2: Red		610-680
	B3: NIR		780-890
	B4: SWIR	20m	1580-1750
SPOT 4	M: Monospectral	10m	610-680
	B1: Green	20m	500-590
	B2: Red		610-680
	B3: NIR		780-890
	B4: SWIR		1580-1750
SPOT 1, 2 & 3	P: Panchromatic	10	510-730
	B1: Green	20m	500-590
	B2: Red		610-680
	B3: NIR		780-890

Table 1-9 - RapidEye Satellite Mission Information (Source: BlackBridge 2013)

Mission Characteristic	Information
Number of satellites	5
Spacecraft lifetime	Over 7 years
Orbital altitude	630km in sun-synchronous orbit
Equator crossing time	11:00 am local time (approximately)
Sensor type	Multi-spectral push broom imager
Spectral Bands	Capable of capturing all of the following spectral bands: Blue 440-510nm Green 520-590nm Red 630-685nm Red Edge 690-730nm NIR 760-850nm
Ground sampling distance (at nadir)	6.5m
Pixel sixe (orthorectified)	5m
Swath width	77km
On board data storage	Up to 1500km of image data per orbit
Revisit time	Daily (off-nadir) / 5.5 days (at nadir)
Image capture capacity	5 million sq km/day
Camera dynamic range	12 bit

Table 1-10 - RapidEye Satellite Image Product Specifications (Source: BlackBridge 2013)

Level	Description
3A	RapidEye Ortho Product – Radiometric, sensor and geometric corrections applied to the data. The product accuracy depends on the quality of the ground control and DEMs used. Product is processed as an individual 25 km by 25 km tile.

Table 1-11 – Imagery attributes for Product L3A (Source: BlackBridge 2013)

PRODUCT ATTRIBUTE	DESCRIPTION
Product Components and Format	RapidEye Ortho image product consists of the following file components: Image File – GeoTIFF file that contains image data and geolocation information Metadata File – XML format metadata file Browse Image File – GeoTIFF format Unusable Data Mask (UDM) file – GeoTIFF format
Product Orientation	Map North up
Product Framing	Image Tile (image tiles are based on a worldwide, 24km by 24km fixed grid system (see Appendix B for full tile grid definition). To each 24km by 24km grid square, a 500m overlap is added to produce a 25km by 25km image tile. Image tiles are black-filled 1km beyond the order polygon used during order placement. Tiles only partially covered by an image take will be also be black-filled in areas containing no valid image data.
Pixel spacing	5m
Bit Depth	16-bit unsigned integers.
Product Size	Tile size is 25km (5000 lines) by 25km (5000 columns). 250 Mbytes per Tile for 5 bands at 5m pixel spacing.
Geometric Corrections	Sensor-related effects are corrected using sensor telemetry and a sensor model, bands are co-registered, and spacecraft-related effects are corrected using attitude telemetry and best available ephemeris data. Orthorectified using GCPs and fine DEMs (30m to 90m posting)
Horizontal Datum	WGS84
Map Projection	Universal Transverse Mercator (UTM)
Resampling Kernel	Cubic Convolution (default), MTF, or Nearest Neighbour

Location of the AOI within the scene

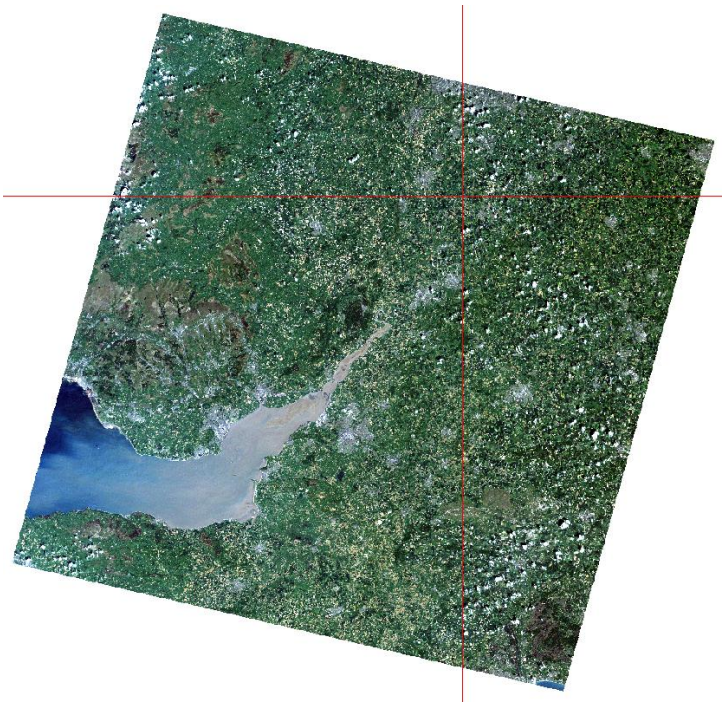

Figure 1-1 - Location of the Former RAF Pershore airfield within a Landsat 5 TM scene (site located at the red crosshair).

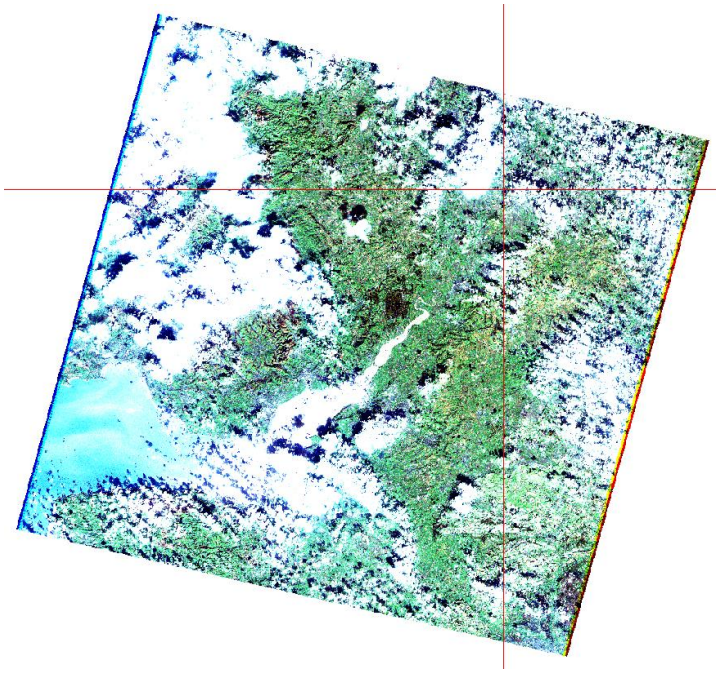

Figure 1-2 - Location of the Former RAF Pershore airfield within a Landsat 7 ETM+ scene (site located at the red crosshair).

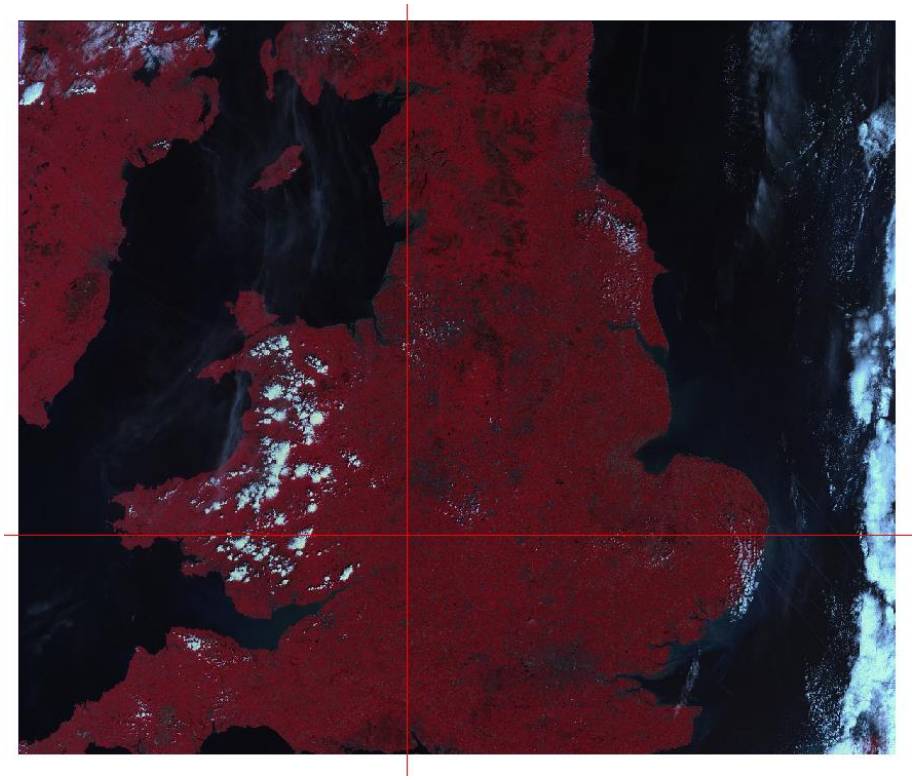

Figure 1-3 - Location of the Former RAF Pershore airfield within a DMC scene (site located at the red crosshair).

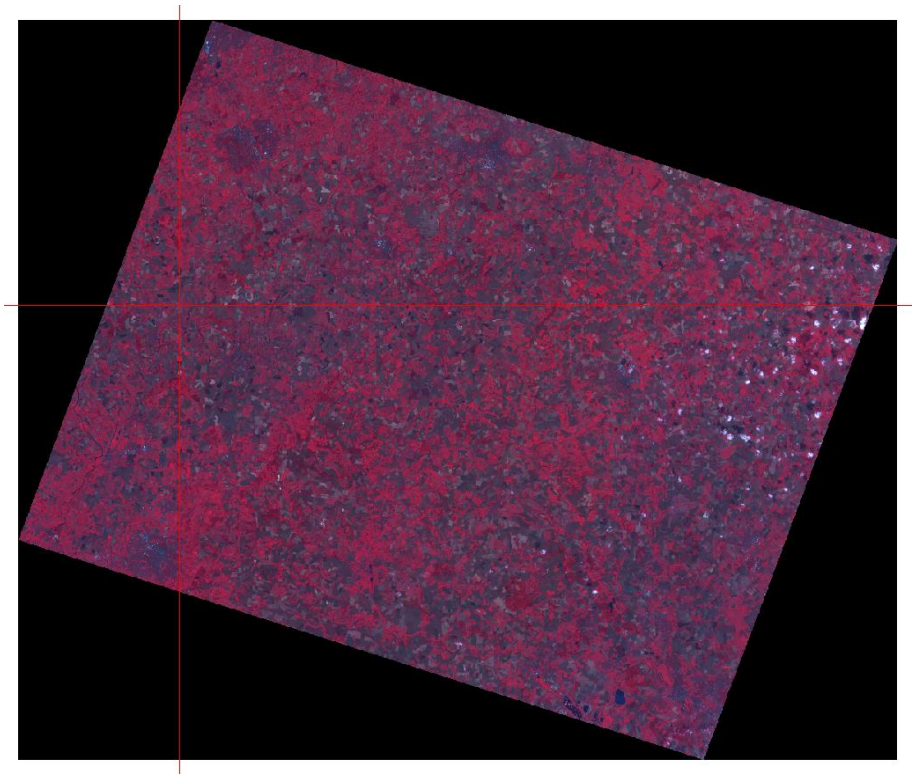

Figure 1-4 - Location of the Former RAF Pershore airfield within a SPOT scene (site located at the red crosshair).

Figure 1-5 - Location of the Former RAF Pershore airfield within a RapidEye scene (site located at the red crosshair).

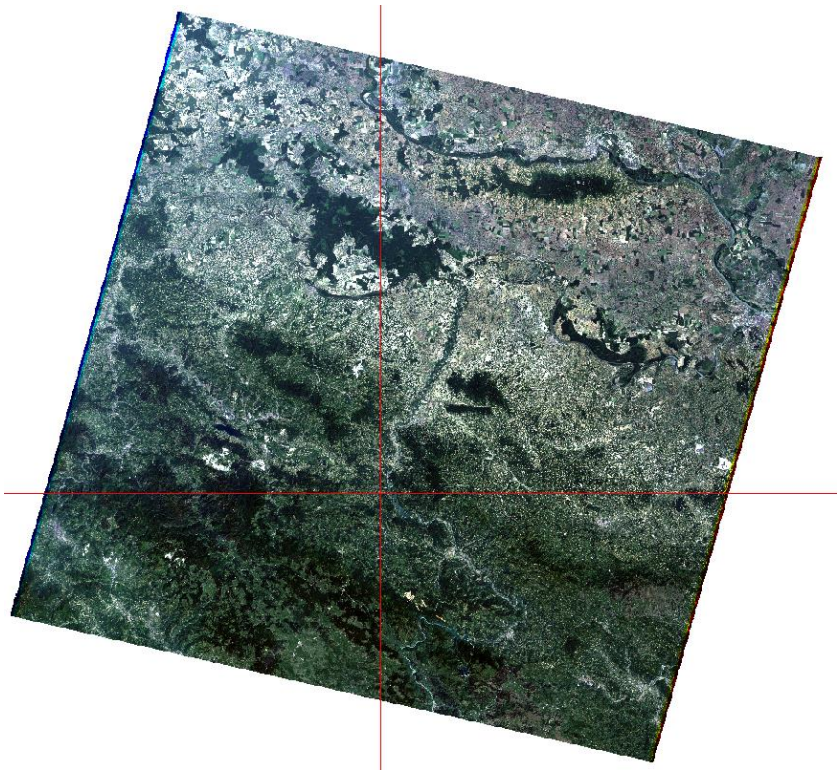

Figure 1-6 - Location of Cancari Road within a Landsat 5 TM scene (Cancari Road mass located at the red crosshair).

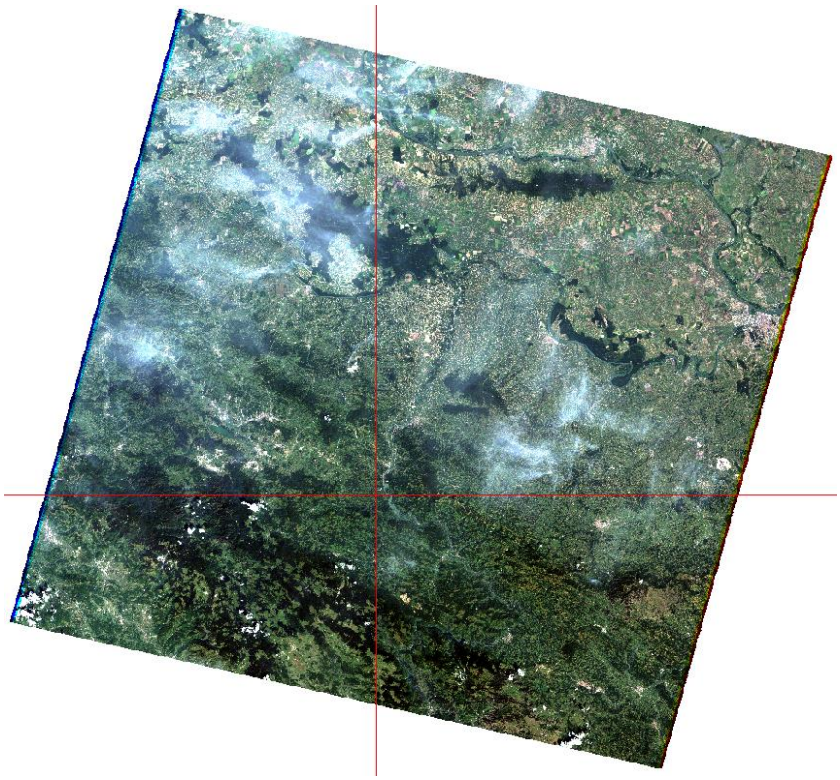

Figure 1-7 - Location of Cancari Road within a Landsat 7 ETM+ scene (Cancari Road mass located at the red crosshair).

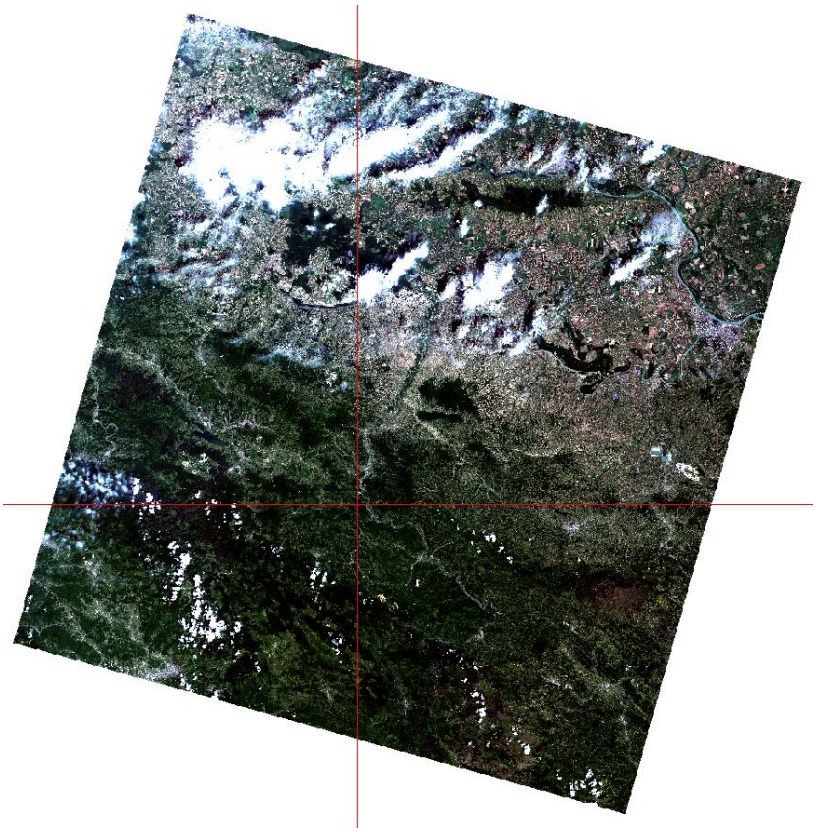

Figure 1-8 - Location of Cancari Road within a Landsat 8 OLI scene (Cancari Road mass located at the red crosshair).

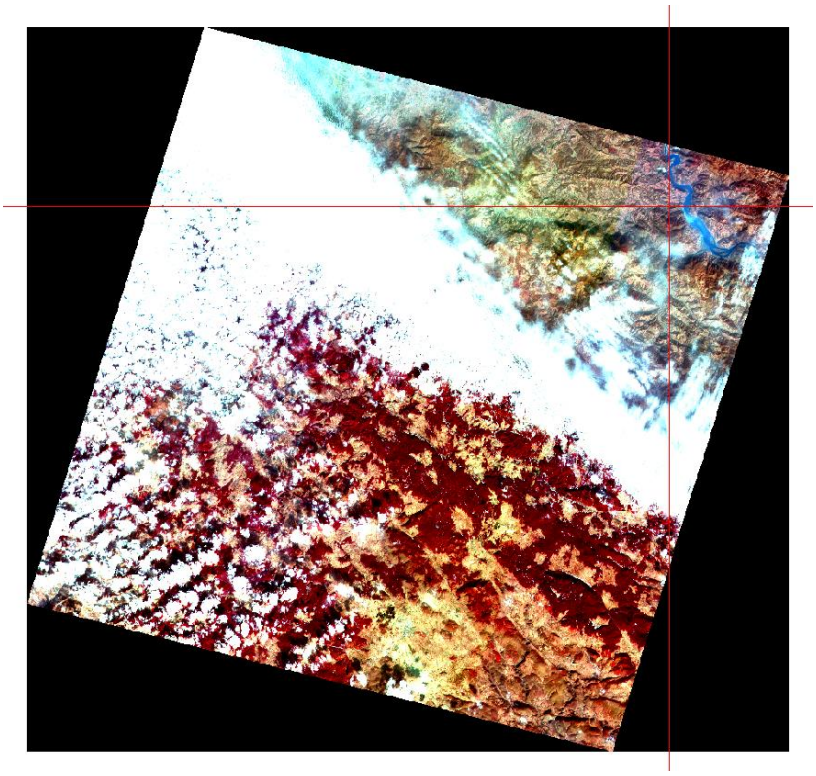

Figure 1-9 - Location of Cancari Road within a SPOT scene (Cancari Road mass located at the red crosshair).

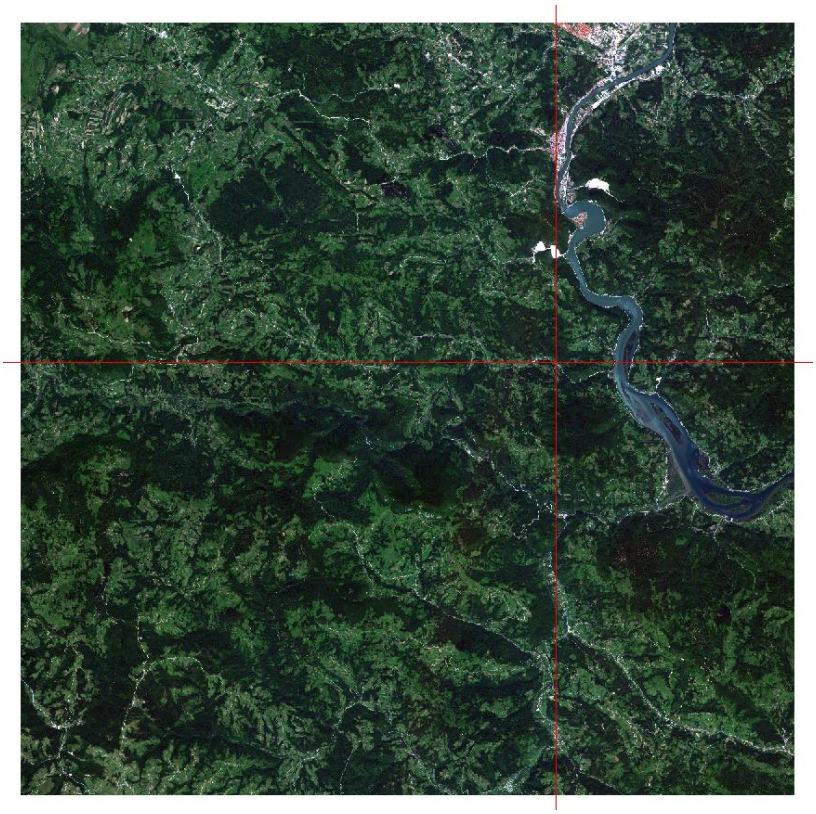

Figure 1-10 - Location of Cancari Road within a RapidEye scene (Cancari Road mass located at the red crosshair).

ENVI pre-processing screenshots

Radiometric Calibration

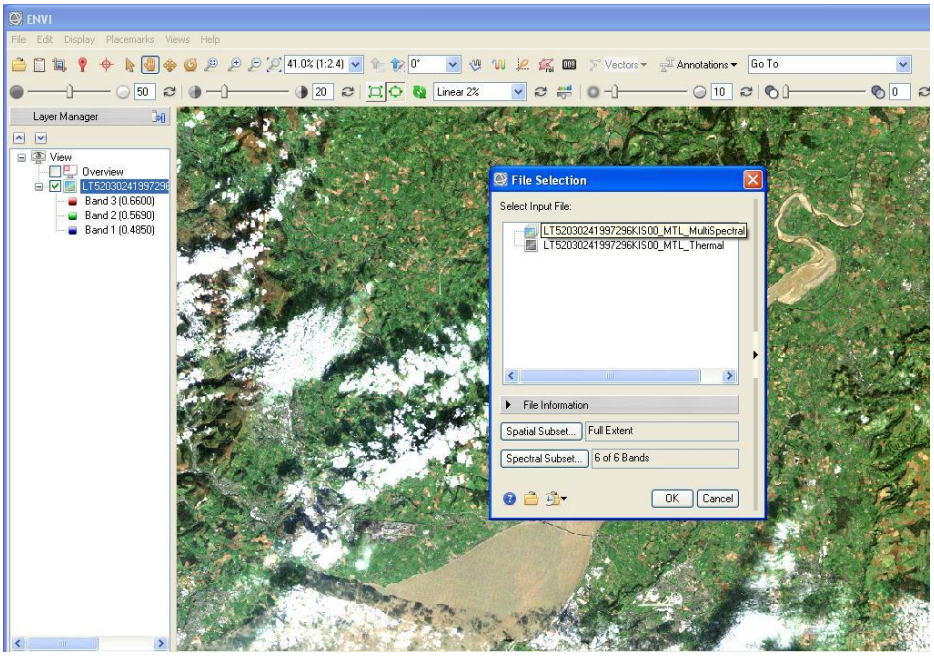

Figure 1-11 - Radiometric calibration - multispectral file selection.

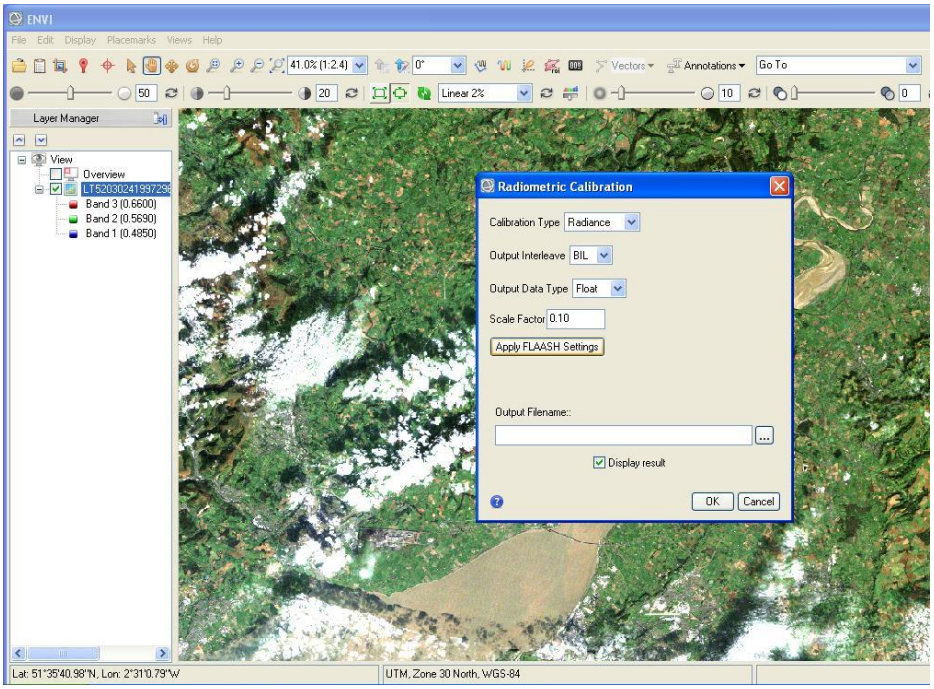

Figure 1-12 - Radiometric calibration – applying FLAASH settings.

Atmospheric Correction – FLAASH

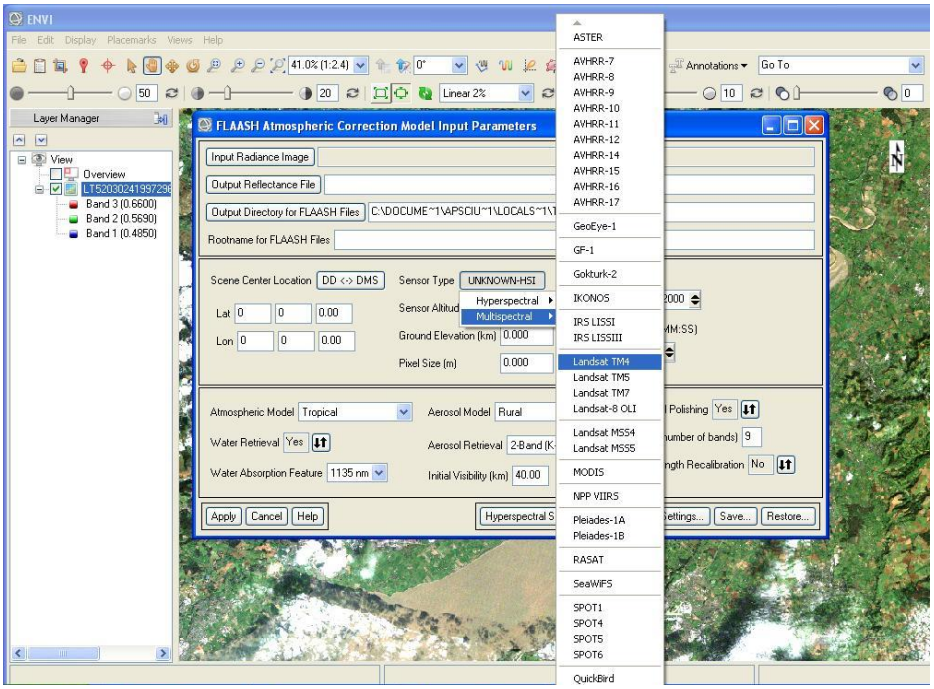

Figure 1-13 - Atmospheric Correction - FLAASH - Sensor Type Selection.

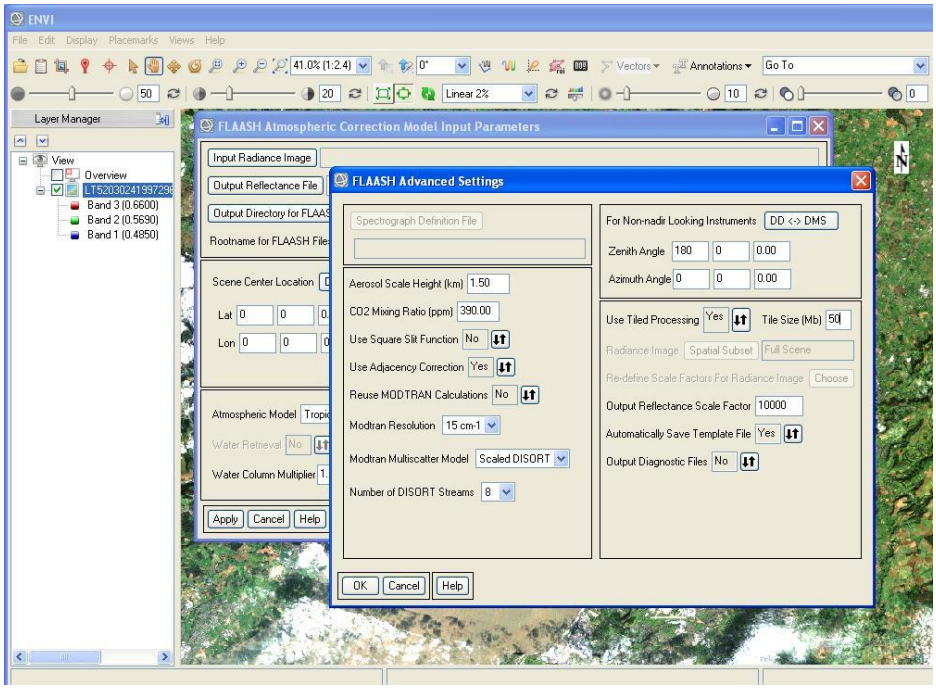

Figure 1-14 - Atmospheric Correction - FLAASH - Advanced Settings.

Image Registration Workflow

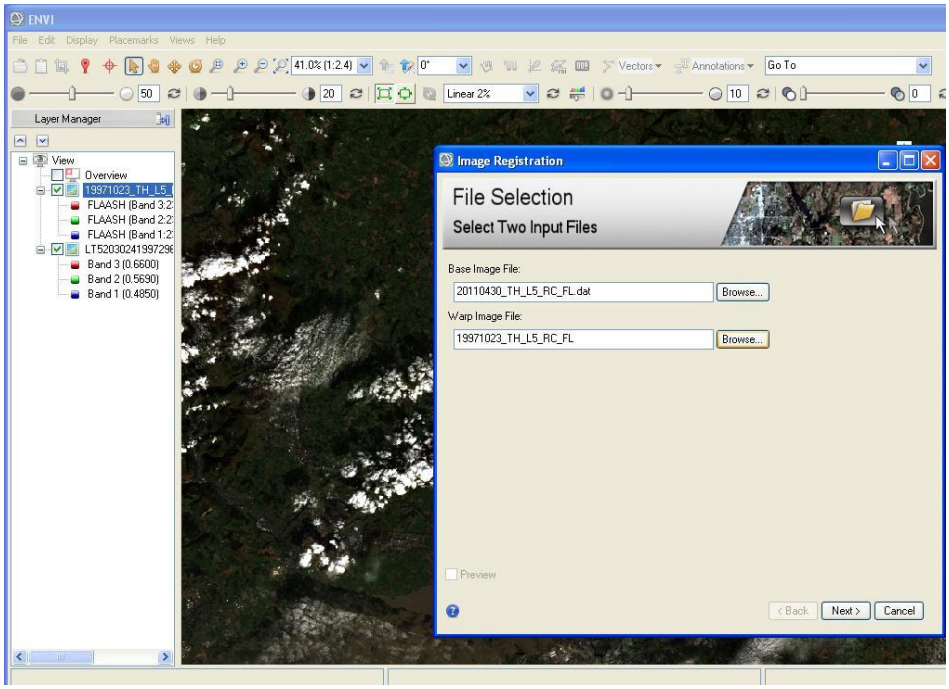

Figure 1-15 - Image registration workflow - File selection.

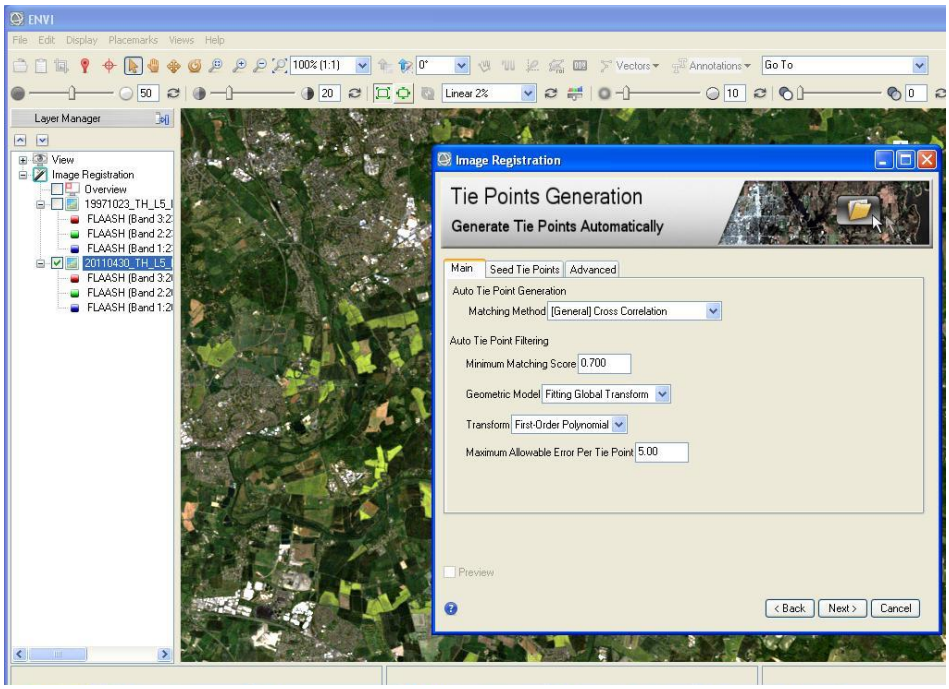

Figure 1-16 - Image registration workflow - Tie point generation.

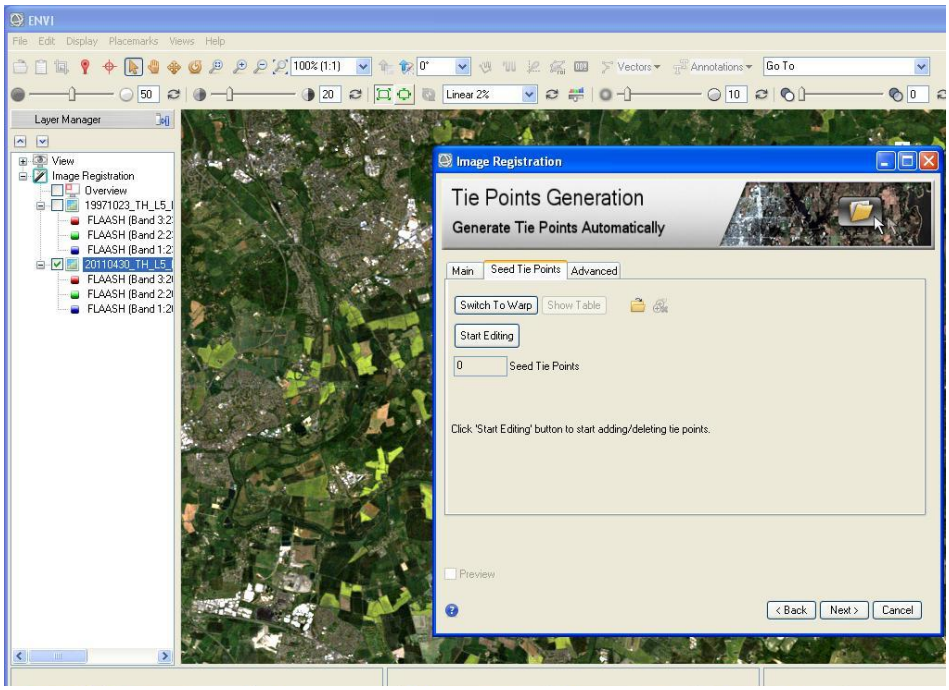

Figure 1-17 - Image registration workflow - Seed tie points.

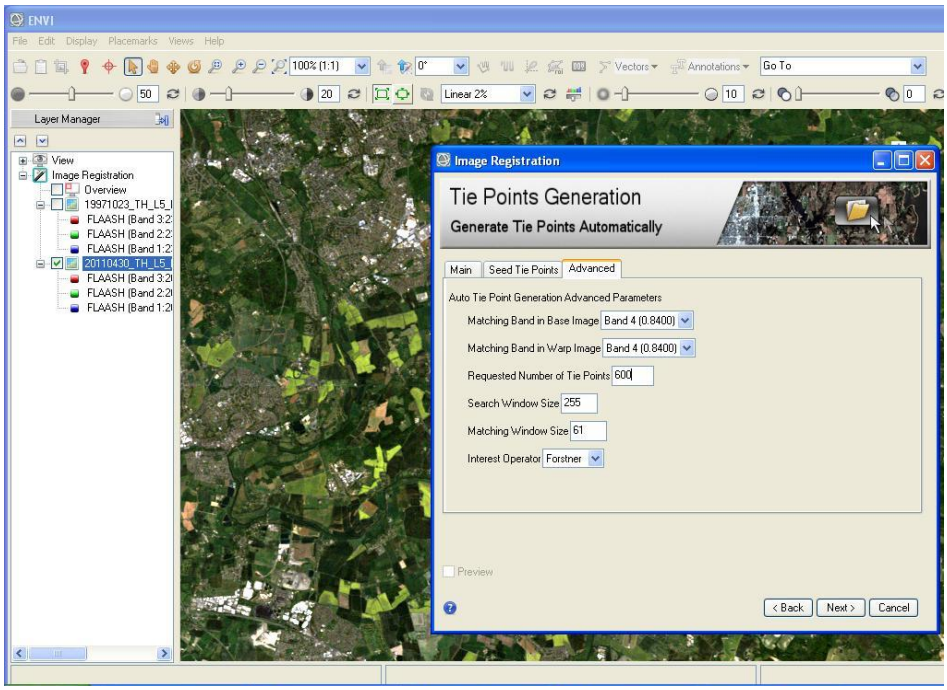

Figure 1-18 - Image registration workflow - Tie point generation advanced settings.

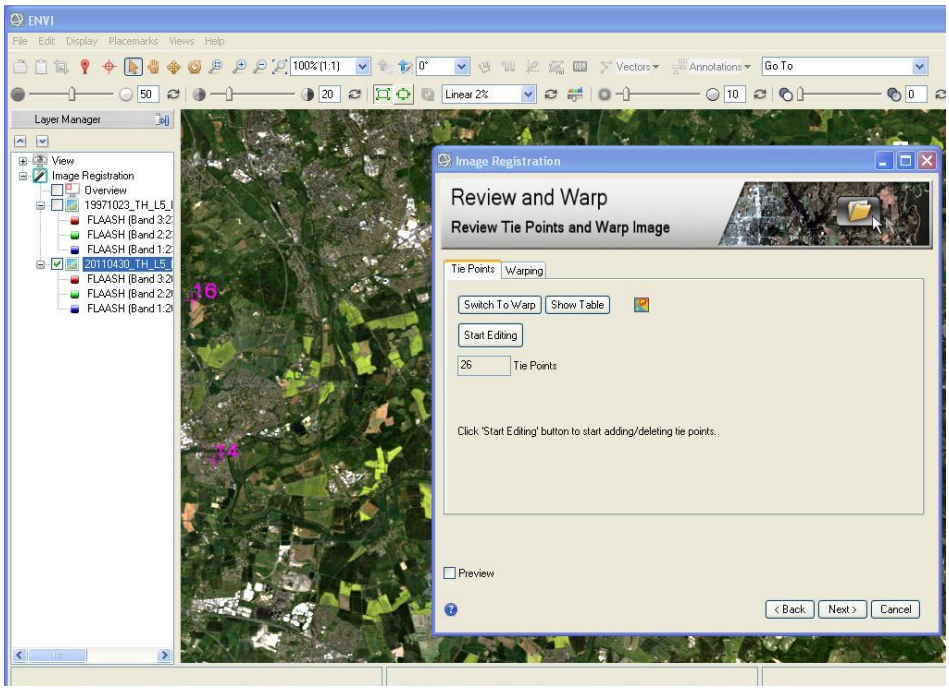

Figure 1-19 - Image registration workflow - Review tie points.

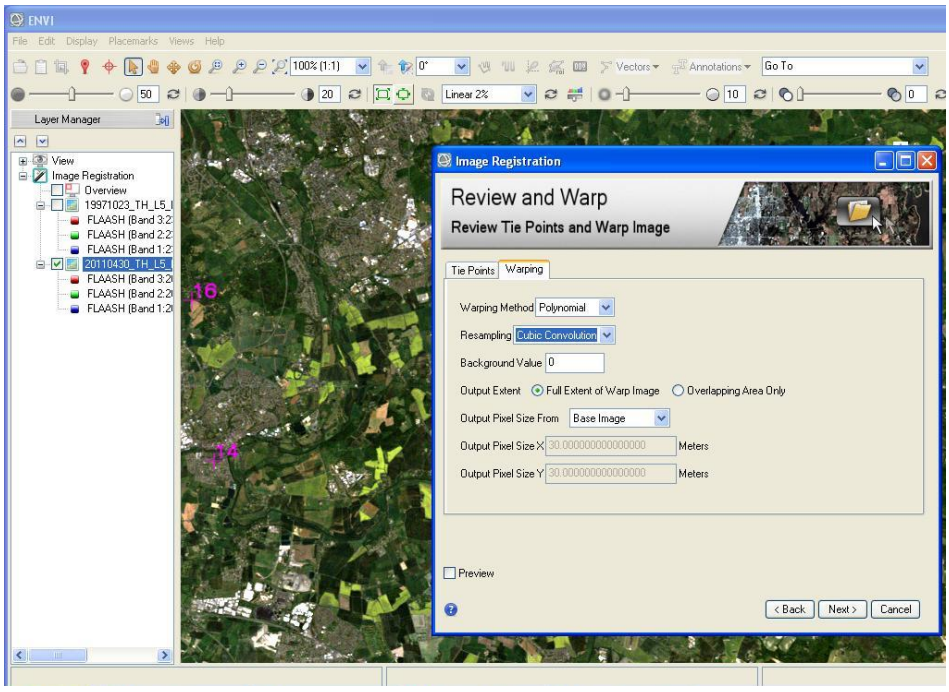

Figure 1-20 - Image registration workflow - Warp settings.

NDVI Calculation

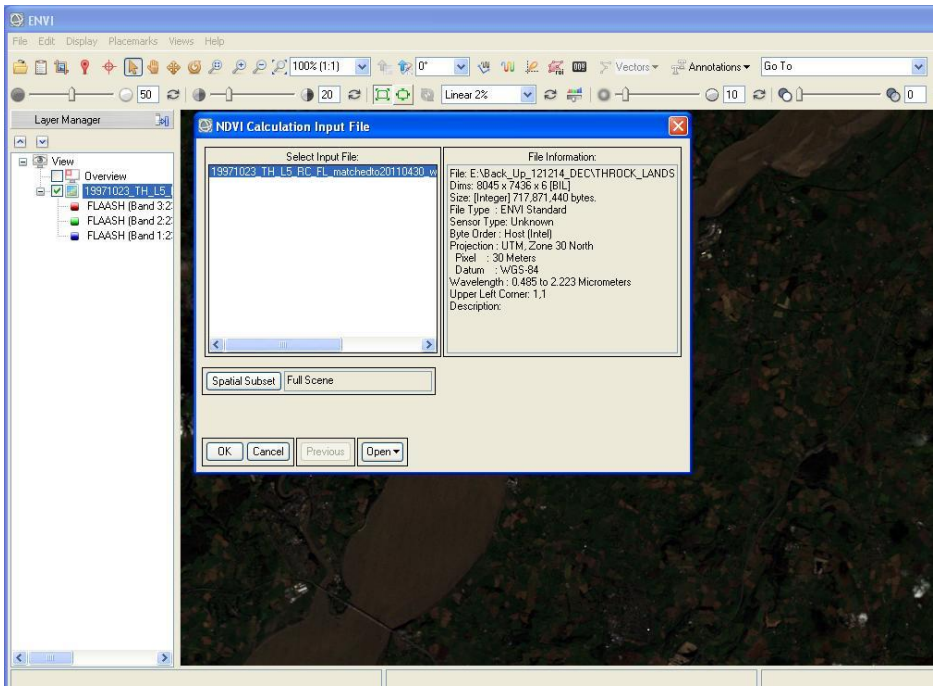

Figure 1-21 - NDVI calculation - Input file.

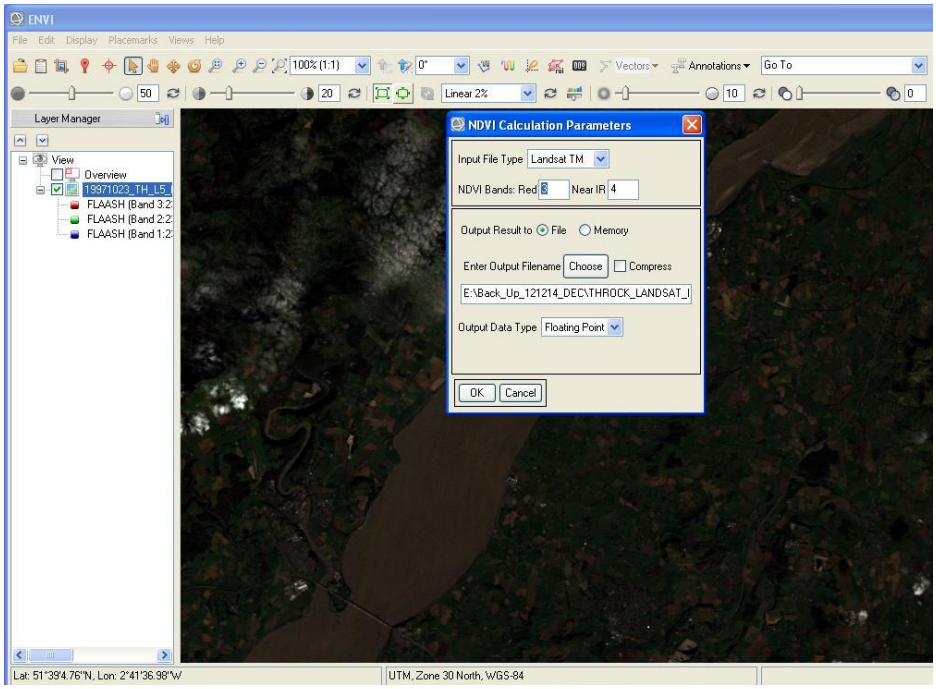

Figure 1-22 - NDVI calculation - parameters.

Appendix 2 for Chapter 5

GER1500 Technical Specifications

Table 2-12 - GER1500 Instrument Technical Specifications (Source: NERC FSF 2016)

Spectral Range	350-1050nm
Spectral Resolution FWHM	3.2nm @ 700nm
Bandwidth	1.5nm @ 700nm
Field of View	3^o, 15^o 2pi
Integration times	5ms & up
Detector Arrays	512 Si Array
Foreoptics Available	4^o & 8^o
Environmental Limits	-10 to 50^oC
Instrument Weight	4.5lbs or 2 kg
Battery Weight	0.5lbs or 0.23kg
Stand Alone Measurements	Standard
Noise Equivalent Radiance w/cm2/nm/sr @ 1sec	0.5 x10-9 @ 700nm

MATLAB Code used to process and convolve the GER1500 spectra

Importing .sig files into MATLAB

The function importsvc is used to import the .sig files into the MATLAB workspace. The command that was used to import all .sig files within the current directory was as follows:

```
[tar, ref] = importsvc('*.sig')
```

On import the spectra are stored in two separate structure arrays, one containing the target spectra (tar) and the second containing the reference spectra (ref), the format of which can be seen in Figure 2-23. Note that the tar array contains a field called 'pair' this links the tar spectra with the corresponding reference panel spectra, which allows for the reflectance, both relative and absolute to be calculated.

```
tar =

1x116 struct array with fields:

    name
    datetime
    header
    pair
    wavelength
    data


ref =

1x116 struct array with fields:

    name
    datetime
    header
    wavelength
    data
```

Figure 2-23 - Screenshot of the example 'tar' and 'ref' structure array formats and fields after carrying out the 'importsvc' function.

Calculating Relative Reflectance

In order to calculate the relative reflectance measured by the GER1500 for each sample point, the function relativereflectance is used. This function calculates relative reflectance spectra by dividing each target spectrum by its corresponding reference spectrum. The command used for calculating relative reflectance is:

```
R_rel = relativereflectance(tar, ref)
```

This command creates a structure array called R_rel in the workspace which contains the relative reflectance values for each sample.

Calculating Absolute Reflectance

As part of the process to calculate absolute reflectance the relative reflectance is multiplied by the reflectance of the panel used to record the reference spectra. As a result the reference panel calibration data has to be imported into MATLAB in order to be used in the calculation. Therefore, the function importpanelcal is used in the following command:

```
p = importpanelcal('FSF Ref Panel Cal Data 2013_3.xls', 'SRT #033')
```

Where p is the new structure array containing information relating to the reference panel's calibration spectrum (calibration of which is carried out by NERC FSF routinely), this can then be used in the calculation of absolute reflectance. In order to visually inspect the calibration panel spectrum, the function plot was used to plot the calibration spectrum using the following command:

```
plot (p.wavelength, 100*p.data)
```

The absolute reflectance was then calculated using the function absolutereflectance in the following command:

```
R_abs = absolutereflectance (R_rel, p)
```

A structure array (R_abs) is created on completion of this calculation which contains the absolute reflectance of all sample points. The absolute reflectance recorded by the GER1500 can be plotted using the function plot in the following command:

```
plot([R_abs.wavelength], 100*[R_abs.data])
```

Smoothing

The absolute reflectance data (R_abs) is then smoothed using a Savitzky-Golay filter, sgsmooth, as part of the following function:

```
s_smoothed = sgsmooth(R_abs)
```

After the data is smoothed it is contained within the s_smoothed structure array.

Comparison of GER1500 spectra with the Landsat 5 TM Satellite Instrument

The GER1500 can be considered a hyperspectral instrument when compared to Landsat 5 TM which is a multispectral orbital instrument. Thus, in order to calculate NDVI from the GER1500 that is comparable to Landsat 5 TM the GER1500 spectra are convolved using the Landsat 5 TM spectral response bands.

$$S_{LR}(\lambda) = \int_0^{\infty} S_{HR}(\lambda_{\text{source}}) f_{LR}(\lambda - \lambda_{\text{source}}) \mathrm{d}\lambda_{\text{source}}$$

Figure 2-24 - Equation whereby the spectral resolution of an instrument can be reduced in order to compare to a lower spectral resolution instrument. Source: Robinson and Mac Arthur, 2012: p22.

The spectral response functions for Landsat 5 TM were inputted into MATLAB using the following command:

LANDSAT5TM = Band('http://fsf.nerc.ac.uk/user_group/bands/Landsat5TM.xml')

This command loaded the spectral response functions into a structure array named LANDSAT5TM which was used to convolve the GER1500 spectral data into Landsat 5 TM comparable spectral bands. The function convolve is used to reduce the spectral resolution of the GER1500 to match the bands of Landsat 5 TM in the following command which creates the structure array 'convolved':

convolved = convolve(s_smoothed, LANDSAT5TM)

Export data from MATLAB into Excel File

This process was carried out for spectral data contained in the structure arrays R_abs, R_rel, s_smoothed and the convolved data. To arrange wavelength values and spectral data into a matrix where wavelength values are contained within the first column and spectral data are in the second the following command was carried out:

e.g. B = [R_abs(1).wavelength, [R_abs.data]]

It is imperative that the name of the structure array (in the example above, 'B') is changed each time the command is used to avoid overwriting data. To write this matrix to an excel file (.xls) the following command was used:

e.g. xlswrite('convolved_051213.xls', B)

This command writes the matrix into an .xls file that is created in the current directory folder; this file can then be opened in Microsoft Excel. Once opened the file will contain data in the following layout (Figure 2-25).

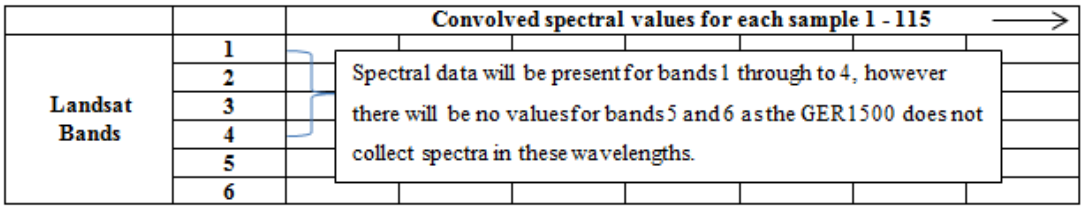

Figure 2-25 - Example layout of .xls file after using the xlswrite command.

Once convolved, smoothed values are opened in Microsoft Excel, the NDVI can be calculated using the following equation, Landsat 5 TM's red and NIR bands are bands 3 and 4 respectively.

Table 2-13 - IDorset weather station mean daily ambient temperatures and mean daily BGL temperature recorded by TinyTag data loggers

Date	IDORSET Station Mean Ambient Temperature (°C)	Pig Grave TinyTag		Empty Grave TinyTag
		30cm BGL (°C)	50cm BGL (°C)	50cm BGL (°C)
06/08/2013	17.8	18.9	15.1	24.0
07/08/2013	17.3	17.8	15.6	19.5
08/08/2013	18.3	17.9	16.9	18.7
09/08/2013	19.7	18.9	17.9	18.4
10/08/2013	17.6	19.0	18.6	18.2
11/08/2013	19.3	19.6	19.0	18.1
12/08/2013	17.1	19.7	19.4	18.1
13/08/2013	17.1	19.3	19.5	17.8
14/08/2013	16.4	19.3	19.6	17.6
15/08/2013	19.2	19.5	19.6	17.5
16/08/2013	18.9	19.8	19.8	17.6
17/08/2013	15.9	19.1	19.9	17.5
18/08/2013	19.3	19.2	19.6	17.2
19/08/2013	18.4	19.5	19.7	17.3
20/08/2013	17.6	19.5	19.8	17.2
21/08/2013	17.7	19.9	19.9	17.3
22/08/2013	20.0	20.6	20.2	17.4
23/08/2013	20.4	21.2	20.6	17.7
24/08/2013	17.3	20.9	20.9	17.9
25/08/2013	16.6	19.8	20.6	17.6
26/08/2013	19.5	20.2	20.2	17.3
27/08/2013	18.8	20.6	20.4	17.4
28/08/2013	17.9	20.5	20.5	17.5
29/08/2013	18.7	20.8	20.6	17.5
30/08/2013	18.5	20.8	20.7	17.6
31/08/2013	17.3	21.0	20.7	17.7
01/09/2013	15.7	20.4	20.7	17.6
02/09/2013	17.8	20.4	20.5	17.4
03/09/2013	18.6	20.9	20.5	17.5
04/09/2013	17.1	21.2	20.8	17.7
05/09/2013	18.8	21.2	20.9	17.8
06/09/2013	16.2	21.2	21.0	17.8
07/09/2013	13.7	20.3	20.7	17.6
08/09/2013	11.5	19.3	20.2	17.2
09/09/2013	15.5	18.6	19.5	16.7
10/09/2013	14.9	18.1	19.1	16.4

Date	IDORSET Station Mean Ambient Temperature (°C)	Pig Grave TinyTag		Empty Grave TinyTag
		30cm BGL (°C)	50cm BGL (°C)	50cm BGL (°C)
11/09/2013	14.2	17.6	18.7	16.2
12/09/2013	17.4	17.9	18.4	16.0
13/09/2013	18.2	18.5	18.5	16.2
14/09/2013	13.6	17.9	18.5	16.4
15/09/2013	12.4	16.6	18.1	16.0
16/09/2013	12.3	15.8	17.3	15.5
17/09/2013	14.1	15.3	16.7	15.1
18/09/2013	13.5	15.9	16.5	15.0
19/09/2013	14.5	15.4	16.4	15.0
20/09/2013	14.1	15.3	16.2	14.8
21/09/2013	14.3	15.6	16.1	14.7
22/09/2013	19.4	16.8	16.4	
23/09/2013	16.1	17.4	17.0	
24/09/2013	15.5	17.1	17.2	
25/09/2013	16.8	17.2	17.2	
26/09/2013	15.6	17.2	17.3	
27/09/2013	15.4	16.8	17.2	
28/09/2013	16.4	16.7	17.0	
29/09/2013	16.4	16.6	16.9	
30/09/2013	15.4	16.7	16.9	
01/10/2013	16.5	16.8	16.9	
02/10/2013	17.9	17.3	17.0	
03/10/2013	18.2	17.3	17.2	
04/10/2013	16.5	17.5	17.3	
05/10/2013	14.8	17.0	17.2	
06/10/2013	13.2	16.1	16.9	
07/10/2013	14.6	15.9	16.5	
08/10/2013	18.8	16.6	16.5	
09/10/2013	14.2	16.4	16.7	
10/10/2013	9.7	14.7	16.3	
11/10/2013	11.2	13.8	15.5	
12/10/2013	11.8	14.3	15.1	
13/10/2013	10.5	13.9	15.0	
14/10/2013	10.6	13.4	14.6	
15/10/2013	9.8	12.8	14.1	
16/10/2013	11.3	12.9	13.7	
17/10/2013	15.8	13.8	13.6	
18/10/2013	14.5	14.3	13.9	

Date	IDORSET Station Mean Ambient Temperature (°C)	Pig Grave TinyTag		Empty Grave TinyTag
		30cm BGL (°C)	50cm BGL (°C)	50cm BGL (°C)
19/10/2013	16.5	14.7	14.2	
20/10/2013	15.2	14.6	14.3	
21/10/2013	16.3	14.7	14.3	
22/10/2013	16.6	15.1	14.5	
23/10/2013	12.3	14.9	14.6	
24/10/2013	10.1	13.4	14.2	
25/10/2013	16.7	14.2	13.9	
26/10/2013	14.9	14.5	14.1	
27/10/2013	13.9	14.1	14.1	
28/10/2013	13.2	14.0	14.0	
29/10/2013	9.4	12.6	13.5	
30/10/2013	8.3	11.3	12.6	
31/10/2013	13.3	12.2	12.3	
01/11/2013	13.2	12.6	12.5	
02/11/2013	12.3	12.5	12.7	
03/11/2013	10.6	11.4	12.3	
04/11/2013	8.3	11.5	11.9	
05/11/2013	8.4	11.0	11.7	
06/11/2013	12.5	11.5	11.6	
07/11/2013	9.8	12.1	12.0	
08/11/2013	7.9	11.0	11.8	
09/11/2013	6.8	10.2	11.2	
10/11/2013	7.4	10.1	10.8	
11/11/2013	11.0	10.3	10.7	
12/11/2013	8.4	11.5	11.0	
13/11/2013	5.7	10.5	11.2	
14/11/2013	8.1	10.0	10.7	
15/11/2013	6.5	8.5	10.0	
16/11/2013	5.2	7.7	9.2	
17/11/2013	8.7	8.6	9.0	
18/11/2013	8.8	9.2	9.4	
19/11/2013	2.5	8.3	9.4	
20/11/2013	3.9	6.9	8.6	
21/11/2013	5.9	6.9	8.1	
22/11/2013	4.8	6.1	7.7	
23/11/2013	4.7	5.6	7.3	
24/11/2013	4.3	5.5	6.9	
25/11/2013	6.0	6.1	6.9	

Date	IDORSET Station Mean Ambient Temperature (°C)	Pig Grave TinyTag		Empty Grave TinyTag
		30cm BGL (°C)	50cm BGL (°C)	50cm BGL (°C)
26/11/2013	3.0	5.9	7.0	
27/11/2013	7.3	6.2	6.9	
28/11/2013	9.3	7.3	7.3	
29/11/2013	9.1	7.8	7.8	
30/11/2013	4.6	7.1	7.9	
01/12/2013	3.2	5.9	7.3	
02/12/2013	8.3	6.4	7.0	
03/12/2013	6.4	6.8	7.2	
04/12/2013	4.8	7.0	7.4	
05/12/2013	4.4	6.1	7.2	
06/12/2013	6.9	6.3	7.0	
07/12/2013	8.7	7.1	7.1	
08/12/2013	7.7	7.3	7.4	
09/12/2013	7.3	7.5	7.6	
10/12/2013	6.2	7.3	7.6	
11/12/2013	5.5	6.9	7.5	
12/12/2013	9.3	7.2	7.4	
13/12/2013	9.5	8.5	7.9	
14/12/2013	8.4	8.1	8.2	
15/12/2013	9.1	8.9	8.4	
16/12/2013	10.4	10.0	9.0	
17/12/2013	6.4	9.7	9.4	
18/12/2013	7.5	9.1	9.2	
19/12/2013	5.9	8.7	8.9	
20/12/2013	6.5	7.8	8.4	
21/12/2013	10.5	8.6	8.3	
22/12/2013	8.3	8.8	8.7	
23/12/2013	9.8	8.4	8.5	
24/12/2013	8.4	9.1	8.7	
25/12/2013	4.3	7.9	8.5	
26/12/2013	5.3	7.2	7.9	
27/12/2013	9.7	7.7	7.7	
28/12/2013	4.2	7.2	7.7	
29/12/2013	5.0	6.7	7.4	
30/12/2013	9.4	7.3	7.2	
31/12/2013	8.9	7.7	7.6	

Table 2- 14 - Convolved NDVI values for each surface type on 19th August 2013.

No.	Convolved NDVI				
	Pig Grass	Pig Soil	Empty Grass	Empty Soil	Undisturbed Grass
1	0.3108	0.2917	0.277	0.1217	0.5641
2	0.2484	0.177	0.2885	0.1136	0.6317
3	0.1771	0.0919	0.245	0.2385	0.5882
4	0.2502	0.0642	0.2422	0.1218	0.6171
5	0.2963	0.1095	0.2993	0.1219	0.5025
6	0.2875	0.3682	0.281	0.1631	0.592
7	0.2797	0.1233	0.2842	0.1136	0.7742
8	0.2846	0.0947	0.257	0.2909	0.7606
9	0.2632	0.1304	0.2896	0.095	0.5889
10	0.3022	0.0985	0.2841	0.1608	0.4273
11	0.2827	0.104	0.2274	0.1157	0.5926
12	0.2987	0.1197	0.2805	0.1515	0.6892
13	0.2317	0.127	0.3327	0.1045	0.6755
14	0.2735	0.1315		0.1718	0.519
15	0.2988	0.1314		0.375	0.6983
16	0.2612	0.1378		0.1251	0.6961
17	0.2635	0.2109		0.1594	0.6533
18	0.3112	0.2363		0.2268	0.6546
19	0.4588				0.5943
20					0.6262
21					0.7352
22					0.5496
23					0.5539
24					0.6649
25					0.6541
26					0.6521
27					0.6166
28					0.6802
29					0.6634
30					0.5294
31					0.6304
32					0.6405
33					0.4663
34					0.6554
35					0.564
36					0.6781
37					0.6688
38					0.6549
39					0.5587
40					0.5822
41					0.6454
42					0.6105
43					0.6402
44					0.6634
45					0.6211
46					0.6581
47					0.4917

Table 2-15 - Convolved NDVI values for each surface type on 22nd August 2013.

No.	Convolved NDVI				
	Pig Grass	Pig Soil	Empty Grass	Empty Soil	Undisturbed Grass
1	0.3052	0.3243	0.1143	-0.0025	0.2995
2	0.2454	0.1572	0.1472	0.1047	0.5274
3	0.1667	0.1079	0.263	0.1064	0.6018
4	0.2653	0.1061	0.1116	0.2262	0.5637
5	0.2912	0.15	0.2541	0.2794	0.5254
6	0.2804	0.1271	0.1345	0.1247	0.4859
7	0.2892	0.1314	0.1388	0.2387	0.6295
8	0.262	0.1004	0.115	0.2711	0.7354
9	0.2733	0.1199	0.2321	0.2844	0.7326
10	0.1016	0.0926	0.2961	0.0848	0.5971
11	0.2771	0.0944	0.2748	0.1405	0.4144
12	0.2211	0.1234	0.167	0.0996	0.7005
13	0.2435	0.1108	0.2697	0.2731	0.6885
14	0.2723	0.1276		0.1069	0.5398
15	0.245	0.1184		0.2541	0.6659
16	0.283	0.1323		0.3587	0.7071
17	0.3239	0.2781		0.257	0.6366
18	0.4364	0.2702		0.1181	0.6723
19					0.5972
20					0.6669
21					0.5721
22					0.5142
23					0.6351
24					0.6283
25					0.6703
26					0.6387
27					0.6718
28					0.6339
29					0.5308
30					0.6024
31					0.6239
32					0.4762
33					0.5652
34					0.6414
35					0.657
36					0.6386
37					0.5586
38					0.5514
39					0.5888
40					0.5791
41					0.6427
42					0.6216
43					0.6216
44					0.6323
45					0.4492

Table 2-16 - Convolved NDVI values for each surface type on 10th October 2013.

No.	Convolved NDVI				
	Pig Grass	Pig Soil	Empty Grass	Empty Soil	Undisturbed Grass
1	0.4088	0.54	0.2793	0.0844	0.4653
2	0.3155	0.1812	0.2658	0.0877	0.6656
3	0.293	0.1282	0.2694	0.3292	0.4487
4	0.3243	0.1087	0.3074	0.0935	0.5998
5	0.3067	0.1141	0.092	0.0911	0.5832
6	0.2781	0.1233	0.2944	0.1561	0.7736
7	0.2997	0.131	0.0964	0.0774	0.7417
8	0.3998	0.1224	0.2622	0.2645	0.4305
9	0.317	0.1446	0.3677	0.0739	0.4385
10	0.3543	0.0915	0.3019	0.1082	0.5692
11	0.3161	0.1555	0.208	0.0807	0.7412
12	0.2816	0.0946	0.2904	0.0921	0.5501
13	0.1579	0.1144	0.4503	0.1108	0.6907
14	0.3392	0.1103		0.2934	0.7115
15	0.2482	0.1052		0.4558	0.7224
16	0.3103	0.123		0.1184	0.6527
17	0.3788	0.1418		0.1245	0.7275
18	0.7277	0.1968		0.1776	0.556
19					0.7521
20					0.7748
21					0.6602
22					0.6448
23					0.669
24					0.7722
25					0.5701
26					0.7296
27					0.7629
28					0.7096
29					0.5824
30					0.6316
31					0.8169
32					0.6041
33					0.6301
34					0.6343
35					0.7176
36					0.8257
37					0.7968
38					0.5838
39					0.7995
40					0.7046
41					0.617
42					0.6081
43					0.7278
44					0.7556
45					0.6638
46					0.7056

Table 2-17 - Convolved NDVI values for each surface type on 5th December 2013.

No.	Convolved NDVI				
	Pig Grass	Pig Soil	Empty Grass	Empty Soil	Undisturbed Grass
1	0.3808	0.6939	0.1542	0.6593	0.3915
2	0.4343	0.3754	0.1942	0.1208	0.4585
3	0.2005	0.197	0.4371	0.1349	0.3647
4	0.5513	0.1231	0.162	0.6953	0.6561
5	0.5159	0.162	0.3946	0.4574	0.4072
6	0.4566	0.2067	0.4427	0.3574	0.6472
7	0.362	0.1504	0.1307	0.3935	0.5807
8	0.1864	0.5048	0.1633	0.3718	0.6444
9	0.1151	0.2157	0.317	0.6358	0.7103
10	0.3274	0.1753	0.4415	0.1663	0.5124
11	0.4729	0.1697	0.3728	0.1339	0.3962
12	0.4598	0.1795	0.1888	0.1503	0.6113
13	0.4634	0.4486	0.428	0.3544	0.6661
14	0.2721	0.192		0.1251	0.5748
15	0.4092	0.5452		0.3061	0.6704
16	0.3676	0.1415		0.707	0.6483
17	0.3204	0.1665		0.3007	0.6822
18	0.4158	0.2508		0.148	0.6871
19	0.3597				0.6794
20					0.6302
21					0.6714
22					0.7045
23					0.6279
24					0.5877
25					0.5998
26					0.7193
27					0.6208
28					0.7232
29					0.634
30					0.646
31					0.6745
32					0.463
33					0.7246
34					0.6532
35					0.4734
36					0.5195
37					0.5925
38					0.6784
39					0.733
40					0.471
41					0.7297
42					0.6542
43					0.527
44					0.5172
45					0.6816
46					0.6237
47					0.6542

Figure 2-26 - Photograph of grave A (pig grave) taken on 8th August 2013

Figure 2-27- Photograph of grave B (empty, control grave) taken on 8th August 2013.

Figure 2-28 - Photograph of grave A (pig grave) taken on 18th September 2013.

Figure 2-29 - Photograph of grave B (empty, control grave) taken on 18th September 2013.

Figure 2-30 - Photograph of grave A (pig grave) taken on 13th October 2013.

Figure 2-31 - Photograph of grave B (empty, control grave) taken on 13th October 2013.

Figure 2-32 - Photograph of grave A (pig grave) taken on 5th October 2013.

Figure 2-33 - Photograph of grave B (empty, control grave) taken on 5th December 2013.

Statistical Significance

19th August 2013 - Undisturbed Vegetation vs Pig Grave – Grass

F-Test Two-Sample for Variances	*Variable 1*	*Variable 2*
Mean	0.62074249	0.283161945
Variance	0.005140126	0.002834906
Observations	47	19
df	46	18
F	1.813155918	
P(F<=f) one-tail	0.084830543	
F Critical one-tail	2.045042636	
t-Test: Two-Sample Assuming Equal Variances		
Mean	0.62074249	0.283161945
Variance	0.005140126	0.002834906
Observations	47	19
Pooled Variance	0.004491783	
Hypothesized Mean Difference	0	
df	64	
t Stat	18.52771172	
P(T<=t) one-tail	0.00000000	
t Critical one-tail	1.669013025	
P(T<=t) two-tail	0.000000000	
t Critical two-tail	1.997729654	

Undisturbed Vegetation vs Pig Grave – Soil

F-Test Two-Sample for Variances	*Variable 1*	*Variable 2*
Mean	0.62074249	0.152664564
Variance	0.005140126	0.006060001
Observations	47	18
df	46	17
F	0.848205584	
P(F<=f) one-tail	0.317952101	
F Critical one-tail	0.540553869	
t-Test: Two-Sample Assuming Unequal Variances		
Mean	0.62074249	0.152664564
Variance	0.005140126	0.006060001
Observations	47	18
Hypothesized Mean Difference	0	
df	29	
t Stat	22.16335976	
P(T<=t) one-tail	4.98569E-20	
t Critical one-tail	1.699127027	
P(T<=t) two-tail	0.000000000	
t Critical two-tail	2.045229642	

Undisturbed Vegetation vs Empty Grave – Grass

F-Test Two-Sample for Variances	*Variable 1*	*Variable 2*
Mean	0.62074249	0.276041059
Variance	0.005140126	0.000759072
Observations	47	13
df	46	12
F	6.771595975	
P(F<=f) one-tail	0.000484794	
F Critical one-tail	2.4097209	
t-Test: Two-Sample Assuming Unequal Variances		
Mean	0.62074249	0.276041059
Variance	0.005140126	0.000759072
Observations	47	13
Hypothesized Mean Difference	0	
df	52	
t Stat	26.61374422	
P(T<=t) one-tail	2.92564E-32	
t Critical one-tail	1.674689154	
P(T<=t) two-tail	0.000000000	
t Critical two-tail	2.006646805	

Undisturbed Vegetation vs Empty Grave – Soil

F-Test Two-Sample for Variances	*Variable 1*	*Variable 2*
Mean	0.62074249	0.165030315
Variance	0.005140126	0.005463058
Observations	47	18
df	46	17
F	0.940888049	
P(F<=f) one-tail	0.415637313	
F Critical one-tail	0.540553869	
t-Test: Two-Sample Assuming Unequal Variances		
Mean	0.62074249	0.165030315
Variance	0.005140126	0.005463058
Observations	47	18
Hypothesized Mean Difference	0	
df	30	
t Stat	22.42772456	
P(T<=t) one-tail	1.33777E-20	
t Critical one-tail	1.697260887	
P(T<=t) two-tail	0.000000000	
t Critical two-tail	2.042272456	

Pig Grave – Grass vs Empty Grave – Grass

F-Test Two-Sample for Variances	*Variable 1*	*Variable 2*
Mean	0.283161945	0.276041059
Variance	0.002834906	0.000759072
Observations	19	13
df	18	12
F	3.734701415	
P(F<=f) one-tail	0.012085303	
F Critical one-tail	2.568427596	
t-Test: Two-Sample Assuming Unequal Variances		
Mean	0.283161945	0.276041059
Variance	0.002834906	0.000759072
Observations	19	13
Hypothesized Mean Difference	0	
df	28	
t Stat	0.494225208	
P(T<=t) one-tail	0.312501202	
t Critical one-tail	1.701130934	
P(T<=t) two-tail	0.63	
t Critical two-tail	2.048407142	

Pig Grave – Soil vs Empty Grave – Soil

F-Test Two-Sample for Variances	*Variable 1*	*Variable 2*
Mean	0.152664564	0.165030315
Variance	0.006060001	0.005463058
Observations	18	18
df	17	17
F	1.109268869	
P(F<=f) one-tail	0.416591994	
F Critical one-tail	2.271892889	
t-Test: Two-Sample Assuming Equal Variances		
Mean	0.152664564	0.165030315
Variance	0.006060001	0.005463058
Observations	18	18
Pooled Variance	0.005761529	
Hypothesized Mean Difference	0	
df	34	
t Stat	-0.488734331	
P(T<=t) one-tail	0.31408378	
t Critical one-tail	1.690924255	
P(T<=t) two-tail	0.63	
t Critical two-tail	2.032244509	

22nd August 2013

Undisturbed Vegetation vs Pig Grave – Grass

F-Test Two-Sample for Variances	*Variable 1*	*Variable 2*
Mean	0.598503408	0.265707895
Variance	0.007215964	0.004476772
Observations	45	18
df	44	17
F	1.611867801	
P(F<=f) one-tail	0.142764227	
F Critical one-tail	2.091762116	
t-Test: Two-Sample Assuming Equal Variances		
Mean	0.605299006	0.263384871
Variance	0.005257343	0.004653363
Observations	44	17
Pooled Variance	0.005093552	
Hypothesized Mean Difference	0	
df	59	
t Stat	16.77616058	
P(T<=t) one-tail	1.98813E-24	
t Critical one-tail	1.671093032	
P(T<=t) two-tail	0.000000000	
t Critical two-tail	2.000995378	

Undisturbed Vegetation vs Pig Grave – Soil

F-Test Two-Sample for Variances	*Variable 1*	*Variable 2*
Mean	0.598503408	0.148460011
Variance	0.007215964	0.004685147
Observations	45	18
df	44	17
F	1.540178742	
P(F<=f) one-tail	0.167422574	
F Critical one-tail	2.091762116	
t-Test: Two-Sample Assuming Equal Variances		
Mean	0.605299006	0.138116272
Variance	0.005257343	0.002931729
Observations	44	17
Pooled Variance	0.004626668	
Hypothesized Mean Difference	0	
df	59	
t Stat	24.05129687	
P(T<=t) one-tail	1.74858E-32	
t Critical one-tail	1.671093032	
P(T<=t) two-tail	0.000000000	

t Critical two-tail	2.000995378

Undisturbed Vegetation vs Empty Grave – Grass

F-Test Two-Sample for Variances	*Variable 1*	*Variable 2*
Mean	0.598503408	0.193706166
Variance	0.007215964	0.005118259
Observations	45	13
df	44	12
F	1.409847469	
P(F<=f) one-tail	0.265933594	
F Critical one-tail	2.414639324	
t-Test: Two-Sample Assuming Equal Variances		
Mean	0.605299006	0.200327432
Variance	0.005257343	0.004961808
Observations	44	12
Pooled Variance	0.005197141	
Hypothesized Mean Difference	0	
df	54	
t Stat	17.24905183	
P(T<=t) one-tail	6.32668E-24	
t Critical one-tail	1.673564906	
P(T<=t) two-tail	0.000000000	
t Critical two-tail	2.004879288	

Undisturbed Vegetation vs Empty Grave – Soil

F-Test Two-Sample for Variances	*Variable 1*	*Variable 2*
Mean	0.598503408	0.184788267
Variance	0.007215964	0.009410727
Observations	45	18
df	44	17
F	0.766780737	
P(F<=f) one-tail	0.234633721	
F Critical one-tail	0.53746851	
t-Test: Two-Sample Assuming Unequal Variances		
Mean	0.605299006	0.184788267
Variance	0.005257343	0.009410727
Observations	44	18
Hypothesized Mean Difference	0	
df	25	
t Stat	16.59231684	
P(T<=t) one-tail	2.6287E-15	
t Critical one-tail	1.708140761	
P(T<=t) two-tail	0.000000000	
t Critical two-tail	2.059538553	

Pig Grave – Grass vs Empty Grave – Grass

F-Test Two-Sample for Variances	*Variable 1*	*Variable 2*
Mean	0.193706166	0.265707895
Variance	0.005118259	0.004476772
Observations	13	18
df	12	17
F	1.143292332	
P(F<=f) one-tail	0.390278611	
F Critical one-tail	2.380654162	
t-Test: Two-Sample Assuming Equal Variances		
Mean	0.193706166	0.265707895
Variance	0.005118259	0.004476772
Observations	13	18
Pooled Variance	0.004742215	
Hypothesized Mean Difference	0	
df	29	
t Stat	-2.872628072	
P(T<=t) one-tail	0.00376836	
t Critical one-tail	1.699127027	
P(T<=t) two-tail	0.01	
t Critical two-tail	2.045229642	

Pig Grave – Soil vs Empty Grave – Soil

F-Test Two-Sample for Variances	*Variable 1*	*Variable 2*
Mean	0.184788267	0.148460011
Variance	0.009410727	0.004685147
Observations	18	18
df	17	17
F	2.008629935	
P(F<=f) one-tail	0.080294997	
F Critical one-tail	2.271892889	
t-Test: Two-Sample Assuming Equal Variances		
Mean	0.184788267	0.148460011
Variance	0.009410727	0.004685147
Observations	18	18
Pooled Variance	0.007047937	
Hypothesized Mean Difference	0	
df	34	
t Stat	1.298179599	
P(T<=t) one-tail	0.101481532	
t Critical one-tail	1.690924255	
P(T<=t) two-tail	0.20	
t Critical two-tail	2.032244509	

10th October 2013

Undisturbed Vegetation vs Pig Grave – Grass

F-Test Two-Sample for Variances	*Variable 1*	*Variable 2*
Mean	0.663451623	0.336501934
Variance	0.010144719	0.012747904
Observations	46	18
df	45	17
F	0.795795065	
P(F<=f) one-tail	0.263531704	
F Critical one-tail	0.539042116	
t-Test: Two-Sample Assuming Unequal Variances		
Mean	0.663451623	0.336501934
Variance	0.010144719	0.012747904
Observations	46	18
Hypothesized Mean Difference	0	
df	28	
t Stat	10.72829057	
P(T<=t) one-tail	9.97007E-12	
t Critical one-tail	1.701130934	
P(T<=t) two-tail	0.000000000	
t Critical two-tail	2.048407142	

Undisturbed Vegetation vs Pig Grave – Soil

F-Test Two-Sample for Variances	*Variable 1*	*Variable 2*
Mean	0.663451623	0.151471367
Variance	0.010144719	0.010161262
Observations	46	18
df	45	17
F	0.99837195	
P(F<=f) one-tail	0.474110226	
F Critical one-tail	0.539042116	
t-Test: Two-Sample Assuming Unequal Variances		
Mean	0.663451623	0.151471367
Variance	0.010144719	0.010161262
Observations	46	18
Hypothesized Mean Difference	0	
df	31	
t Stat	18.27275484	
P(T<=t) one-tail	1.87207E-18	
t Critical one-tail	1.695518783	
P(T<=t) two-tail	0.000000000	
t Critical two-tail	2.039513446	

Undisturbed Vegetation vs Empty Grave – Grass

F-Test Two-Sample for Variances	*Variable 1*	*Variable 2*
Mean	0.663451623	0.268080668
Variance	0.010144719	0.00927193
Observations	46	13
df	45	12
F	1.094132376	
P(F<=f) one-tail	0.459062737	
F Critical one-tail	2.412127847	
t-Test: Two-Sample Assuming Equal Variances		
Mean	0.663451623	0.268080668
Variance	0.010144719	0.00927193
Observations	46	13
Pooled Variance	0.009960974	
Hypothesized Mean Difference	0	
df	57	
t Stat	12.61183997	
P(T<=t) one-tail	1.9594E-18	
t Critical one-tail	1.672028888	
P(T<=t) two-tail	0.000000000	
t Critical two-tail	2.002465459	

Undisturbed Vegetation vs Empty Grave – Soil

F-Test Two-Sample for Variances	*Variable 1*	*Variable 2*
Mean	0.663451623	0.156628855
Variance	0.010144719	0.011663112
Observations	46	18
df	45	17
F	0.869812333	
P(F<=f) one-tail	0.341712629	
F Critical one-tail	0.539042116	
t-Test: Two-Sample Assuming Unequal Variances		
Mean	0.663451623	0.156628855
Variance	0.010144719	0.011663112
Observations	46	18
Hypothesized Mean Difference	0	
df	29	
t Stat	17.1978516	
P(T<=t) one-tail	4.69798E-17	
t Critical one-tail	1.699127027	
P(T<=t) two-tail	0.000000000	
t Critical two-tail	2.045229642	

Pig Grave – Grass vs Empty Grave – Grass

F-Test Two-Sample for Variances	*Variable 1*	*Variable 2*
Mean	0.336501934	0.268080668
Variance	0.012747904	0.00927193
Observations	18	13
df	17	12
F	1.374892136	
P(F<=f) one-tail	0.291361121	
F Critical one-tail	2.582838906	
t-Test: Two-Sample Assuming Equal Variances		
Mean	0.336501934	0.268080668
Variance	0.012747904	0.00927193
Observations	18	13
Pooled Variance	0.01130957	
Hypothesized Mean Difference	0	
df	29	
t Stat	1.767645397	
P(T<=t) one-tail	0.043821092	
t Critical one-tail	1.699127027	
P(T<=t) two-tail	0.09	
t Critical two-tail	2.045229642	

Pig Grave – Soil vs Empty Grave – Soil

F-Test Two-Sample for Variances	*Variable 1*	*Variable 2*
Mean	0.156628855	0.151471367
Variance	0.011663112	0.010161262
Observations	18	18
df	17	17
F	1.147801557	
P(F<=f) one-tail	0.389766934	
F Critical one-tail	2.271892889	
t-Test: Two-Sample Assuming Equal Variances		
Mean	0.156628855	0.151471367
Variance	0.011663112	0.010161262
Observations	18	18
Pooled Variance	0.010912187	
Hypothesized Mean Difference	0	
df	34	
t Stat	0.148116561	
P(T<=t) one-tail	0.441562866	
t Critical one-tail	1.690924255	
P(T<=t) two-tail	0.88	
t Critical two-tail	2.032244509	

5th December 2013

Undisturbed Vegetation vs Pig Grave – Grass

F-Test Two-Sample for Variances	*Variable 1*	*Variable 2*
Mean	0.606897914	0.372178638
Variance	0.009885902	0.013236518
Observations	47	19
df	46	18
F	0.746865795	
P(F<=f) one-tail	0.209425668	
F Critical one-tail	0.545591776	
t-Test: Two-Sample Assuming Unequal Variances		
Mean	0.606897914	0.372178638
Variance	0.009885902	0.013236518
Observations	47	19
Hypothesized Mean Difference	0	
df	29	
t Stat	7.79373776	
P(T<=t) one-tail	6.76963E-09	
t Critical one-tail	1.699127027	
P(T<=t) two-tail	0.000000000	
t Critical two-tail	2.045229642	

Undisturbed Vegetation vs Pig Grave – Soil

F-Test Two-Sample for Variances	*Variable 1*	*Variable 2*
Mean	0.606897914	0.272122788
Variance	0.009885902	0.027894497
Observations	47	18
df	46	17
F	0.354403316	
P(F<=f) one-tail	0.002668788	
F Critical one-tail	0.540553869	
t-Test: Two-Sample Assuming Equal Variances		
Mean	0.606897914	0.272122788
Variance	0.009885902	0.027894497
Observations	47	18
Pooled Variance	0.014745364	
Hypothesized Mean Difference	0	
df	63	
t Stat	9.946125369	
P(T<=t) one-tail	7.72976E-15	
t Critical one-tail	1.669402222	
P(T<=t) two-tail	0.000000000	
t Critical two-tail	1.998340543	

Undisturbed Vegetation vs Empty Grave – Grass

F-Test Two-Sample for Variances	*Variable 1*	*Variable 2*
Mean	0.606897914	0.294388185
Variance	0.009885902	0.016740242
Observations	47	13
df	46	12
F	0.590547169	
P(F<=f) one-tail	0.09969272	
F Critical one-tail	0.507745785	
t-Test: Two-Sample Assuming Unequal Variances		
Mean	0.606897914	0.294388185
Variance	0.009885902	0.016740242
Observations	47	13
Hypothesized Mean Difference	0	
df	16	
t Stat	8.07421847	
P(T<=t) one-tail	2.45915E-07	
t Critical one-tail	1.745883676	
P(T<=t) two-tail	0.000000000	
t Critical two-tail	2.119905299	

Undisturbed Vegetation vs Empty Grave – Soil

F-Test Two-Sample for Variances	*Variable 1*	*Variable 2*
Mean	0.606897914	0.345440663
Variance	0.009885902	0.044260147
Observations	47	18
df	46	17
F	0.223359002	
P(F<=f) one-tail	2.53238E-05	
F Critical one-tail	0.540553869	
t-Test: Two-Sample Assuming Equal Variances		
Mean	0.606897914	0.345440663
Variance	0.009885902	0.044260147
Observations	47	18
Pooled Variance	0.019161492	
Hypothesized Mean Difference	0	
df	63	
t Stat	6.814194545	
P(T<=t) one-tail	2.10404E-09	
t Critical one-tail	1.669402222	
P(T<=t) two-tail	0.00000	
t Critical two-tail	1.998340543	

Pig Grave – Grass vs Empty Grave – Grass

F-Test Two-Sample for Variances	*Variable 1*	*Variable 2*
Mean	0.294388185	0.372178638
Variance	0.016740242	0.013236518
Observations	13	19
df	12	18
F	1.264701339	
P(F<=f) one-tail	0.316862923	
F Critical one-tail	2.342066798	
t-Test: Two-Sample Assuming Equal Variances		
Mean	0.294388185	0.372178638
Variance	0.016740242	0.013236518
Observations	13	19
Pooled Variance	0.014638007	
Hypothesized Mean Difference	0	
df	30	
t Stat	-1.786318137	
P(T<=t) one-tail	0.042079545	
t Critical one-tail	1.697260887	
P(T<=t) two-tail	0.08	
t Critical two-tail	2.042272456	

Pig Grave – Soil vs Empty Grave – Soil

F-Test Two-Sample for Variances	*Variable 1*	*Variable 2*
Mean	0.345440663	0.272122788
Variance	0.044260147	0.027894497
Observations	18	18
df	17	17
F	1.586698157	
P(F<=f) one-tail	0.175206584	
F Critical one-tail	2.271892889	
t-Test: Two-Sample Assuming Equal Variances		
Mean	0.345440663	0.272122788
Variance	0.044260147	0.027894497
Observations	18	18
Pooled Variance	0.036077322	
Hypothesized Mean Difference	0	
df	34	
t Stat	1.158014446	
P(T<=t) one-tail	0.127464089	
t Critical one-tail	1.690924255	
P(T<=t) two-tail	0.25	
t Critical two-tail	2.032244509	

Table 2-18 - Meteorological data used to derive the relationships between NDVI of the grass halves of the graves and surface type one week prior to GER100 data collection.

Date	NDVI Pig Grave Grass	NDVI Empty Grave Grass	NDVI Undis Grass	Mean Air Temperature (°C)	Mean Humidity (%)	Mean Dew Point (°C)	Mean Wind Speed (km/h)	Mean Pressure (hPa)	Cumul. Rainfall (mm)
19/08/13	0.2832	0.27604	0.6207	17.70	79.29	13.73	3.14	1018.36	0.83
22/08/13	0.2657	0.19371	0.5985	18.14	77.86	13.83	3.00	1019.57	0.81
10/10/13	0.3365	0.26808	0.6635	15.74	79.71	11.90	2.14	1022.29	3.90
05/12/13	0.3722	0.29439	0.6069	6.49	74.57	2.46	1.43	1012.71	0.00

Table 2-19 - Meteorological data used to derive the relationships between NDVI of the soil halves of the graves and surface type one week prior to GER100 data collection.

Date	NDVI Pig Grave Soil	NDVI Empty Grave Soil	NDVI Undis Grass	Mean Air Temperature (°C)	Mean Humidity (%)	Mean Dew Point (°C)	Mean Wind Speed (km/h)	Mean Pressure (hPa)	Cumul. Rainfall (mm)
19/08/13	0.1527	0.16503	0.6207	17.70	79.29	13.73	3.14	1018.36	0.83
22/08/13	0.1485	0.18479	0.5985	18.14	77.86	13.83	3.00	1019.57	0.81
10/10/13	0.1515	0.15663	0.6635	15.74	79.71	11.90	2.14	1022.29	3.90
05/12/13	0.2721	0.34544	0.6069	6.49	74.57	2.46	1.43	1012.71	0.00

Table 2-20 - Meteorological data used to derive the relationships between NDVI of the grass halves of the graves and surface type two weeks prior to GER100 data collection.

Date	NDVI Pig Grave Grass	NDVI Empty Grave Grass	NDVI Undis Grass	Mean Air Temperature (°C)	Mean Humidity (%)	Mean Dew Point (°C)	Mean Wind Speed (km/h)	Mean Pressure (hPa)	Cumul. Rainfall (mm)
19/08/13	0.2832	0.2760	0.6207	18.01	75.79	13.23	2.71	1018.54	2.71
22/08/13	0.2657	0.1937	0.5985	18.04	74.43	12.97	2.64	1020.68	0.89
10/10/13	0.3365	0.2681	0.6635	15.98	80.86	12.39	2.93	1015.07	15.70
05/12/13	0.3722	0.2944	0.6069	5.81	74.50	1.74	2.14	1015.93	0.50

Table 2-21 - Description of the direction and strength of the linear relationship between NDVI calculated from convolved GER1500 data on the grass half of the experimental graves and meteorological variables (two weeks prior to data collection).

FUNCTION		Pig Grave Grass	Empty Grave Grass	Undisturbed Grass
SLOPE	NDVI vs Temp	-0.01	0.00	0.00
	NDVI vs Humidity	0.00	0.00	0.01
	NDVI vs Dew Point	-0.01	0.00	0.00
	NDVI vs Wind Speed	-0.07	-0.04	0.06
	NDVI vs Pressure	-0.02	-0.01	-0.01
	NDVI vs Cumul. Rainfall	0.00	0.00	0.00
CORREL (r)	NDVI vs Temp	-0.88	-0.60	0.21
	NDVI vs Humidity	0.23	0.23	0.99
	NDVI vs Dew Point	0.99	-0.55	0.31
	NDVI vs Wind Speed	0.86	-0.32	0.67
	NDVI vs Pressure	0.56	-0.79	-0.69
	NDVI vs Cumul. Rainfall	0.25	0.17	0.98
RSQ (r^2 or %)	NDVI vs Temp	0.77 77%	0.36 36%	0.04 4%
	NDVI vs Humidity	0.05 5%	0.05 5%	0.98 98%
	NDVI vs Dew Point	0.67 67%	0.31 31%	0.10 10%
	NDVI vs Wind Speed	0.26 26%	0.10 10%	0.45 45%
	NDVI vs Pressure	0.78 78%	0.62 62%	0.48 48%
	NDVI vs Cumul. Rainfall	0.05 5%	0.03 3%	0.95 95%

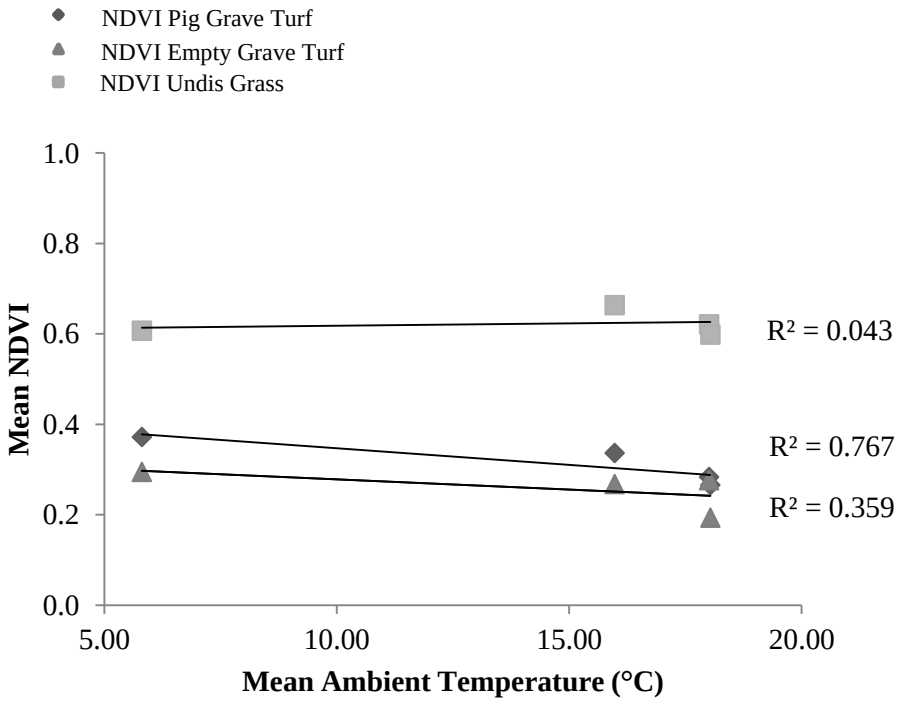

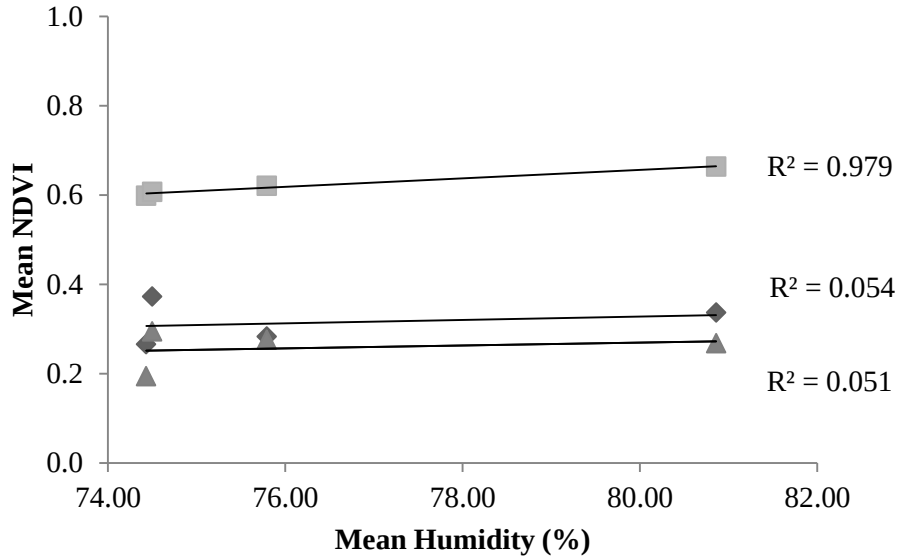
1.0
0.8
0.6
0.4
0.2
0.0
Mean NDVI
74.00
76.00
78.00
80.00
82.00
Mean Humidity (%)
R² = 0.979
R² = 0.054
R² = 0.051

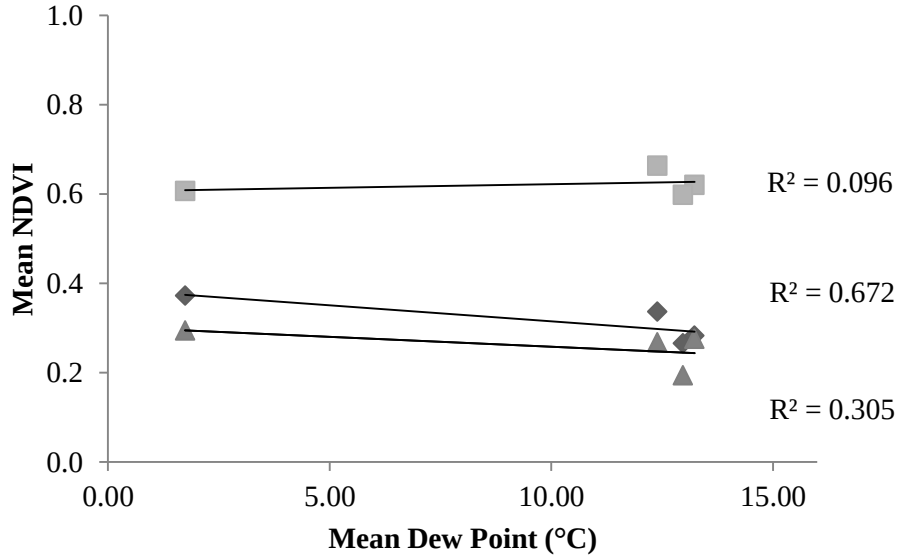
1.0
0.8
0.6
0.4
0.2
0.0
Mean NDVI
0.00
5.00
10.00
15.00
Mean Dew Point (°C)
R² = 0.096
R² = 0.672
R² = 0.305

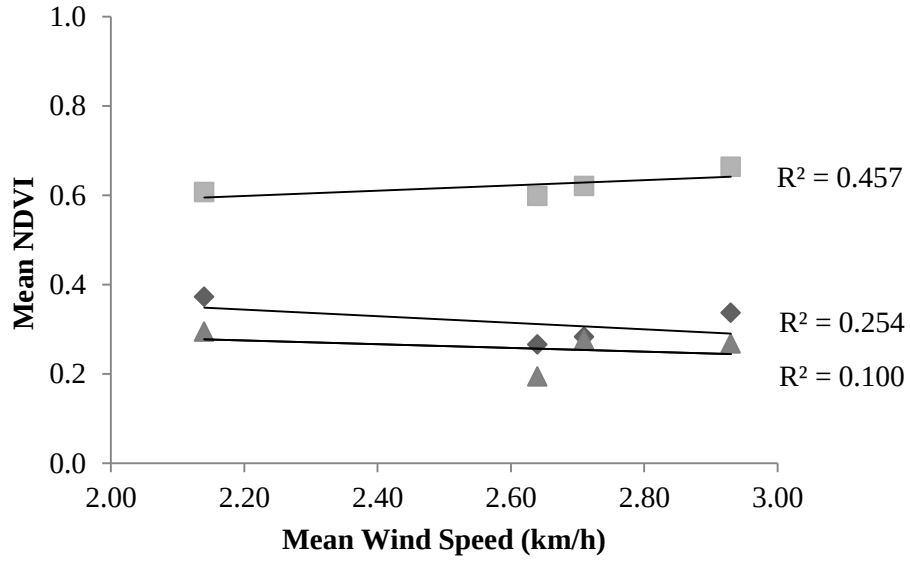
1.0
0.8
0.6
0.4
0.2
0.0
Mean NDVI
2.00
2.20
2.40
2.60
2.80
3.00
Mean Wind Speed (km/h)
R² = 0.457
R² = 0.254
R² = 0.100

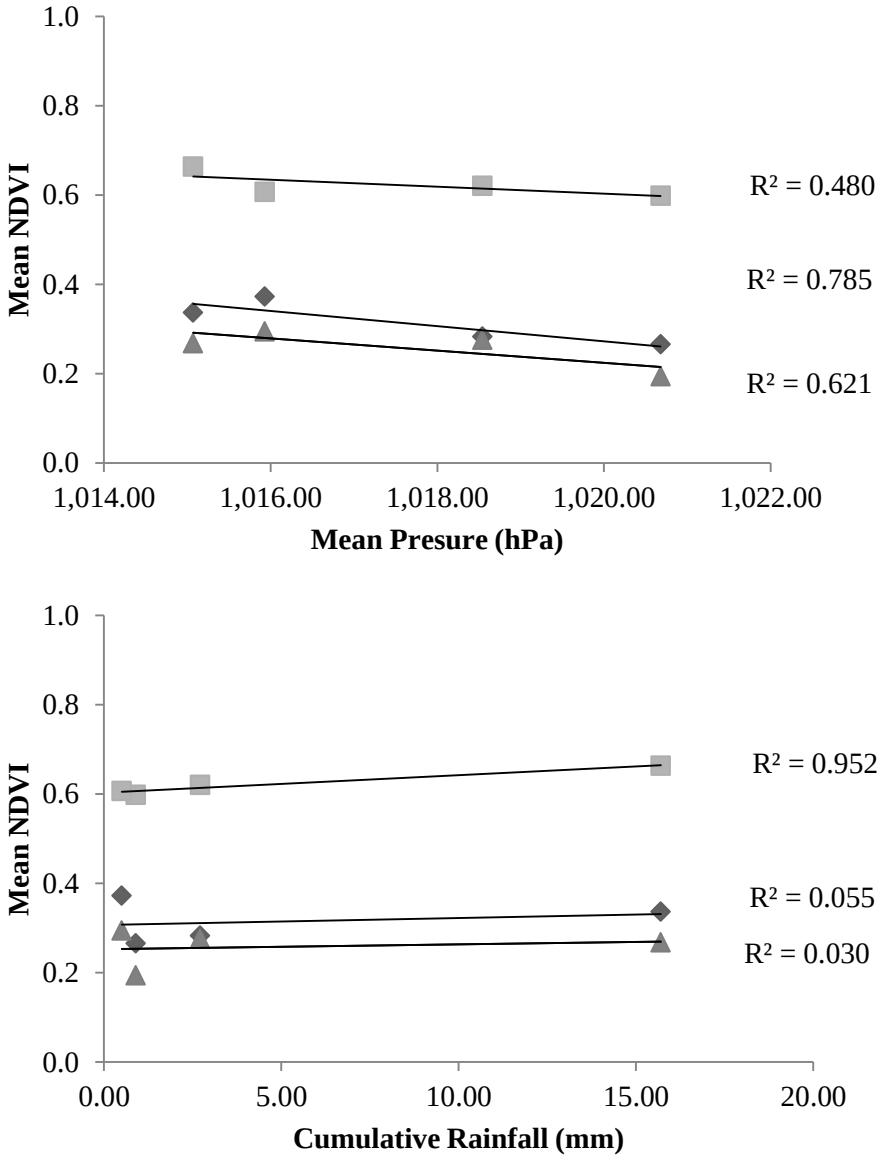

Figure 2-34 - Scatter plots illustrating the linear relationships between NDVI of the grass half of the graves and meteorological variables two weeks prior to spectra collection.

Table 2-22 - Meteorological data used to derive the relationships between NDVI of the soil halves of the graves and surface type two weeks prior to GER100 data collection.

Date	NDVI Pig Grave Soil	NDVI Empty Grave Soil	NDVI Undis Grass	Mean Air Temperature (°C)	Mean Humidity (%)	Mean Dew Point (°C)	Mean Wind Speed (km/h)	Mean Pressure (hPa)	Cumul. Rainfall (mm)
19/08/13	0.1527	0.1650	0.6207	18.01	75.79	13.23	2.71	1018.54	2.71
22/08/13	0.1485	0.1848	0.5985	18.04	74.43	12.97	2.64	1020.68	0.89
10/10/13	0.1515	0.1566	0.6635	15.98	80.86	12.39	2.93	1015.07	15.70
05/12/13	0.2721	0.3454	0.6069	5.81	74.50	1.74	2.14	1015.93	0.50

Table 2-23 - Description of the direction and strength of the linear relationship between NDVI calculated from convolved GER1500 data on the soil half of the experimental graves and meteorological variables (two weeks prior to data collection).

FUNCTION		Pig Grave Soil	Empty Grave Soil	Undisturbed Grass
SLOPE	NDVI vs Temp	-0.01	-0.01	0.00
	NDVI vs Humidity	-0.01	-0.02	0.01
	NDVI vs Dew Point	-0.01	-0.02	0.00
	NDVI vs Wind Speed	-0.17	-0.26	0.06
	NDVI vs Pressure	-0.01	-0.01	-0.01
	NDVI vs Cumul. Rainfall	0.00	-0.01	0.00
CORREL (r)	NDVI vs Temp	-0.99	-0.96	0.21
	NDVI vs Humidity	-0.40	-0.51	0.99
	NDVI vs Dew Point	0.99	-0.99	0.31
	NDVI vs Wind Speed	0.86	-0.96	0.67
	NDVI vs Pressure	0.56	-0.31	-0.69
	NDVI vs Cumul. Rainfall	0.25	-0.50	0.98
RSQ (r^2 or %)	NDVI vs Temp	0.97 97%	0.92 92%	0.04 4%
	NDVI vs Humidity	0.16 16%	0.26 26%	0.98 98%
	NDVI vs Dew Point	1.00 100%	0.97 97%	0.10 10%
	NDVI vs Wind Speed	0.86 86%	0.93 93%	0.45 45%
	NDVI vs Pressure	0.19 19%	0.10 10%	0.48 48%
	NDVI vs Cumul. Rainfall	0.16 16%	0.25 25%	0.95 95%

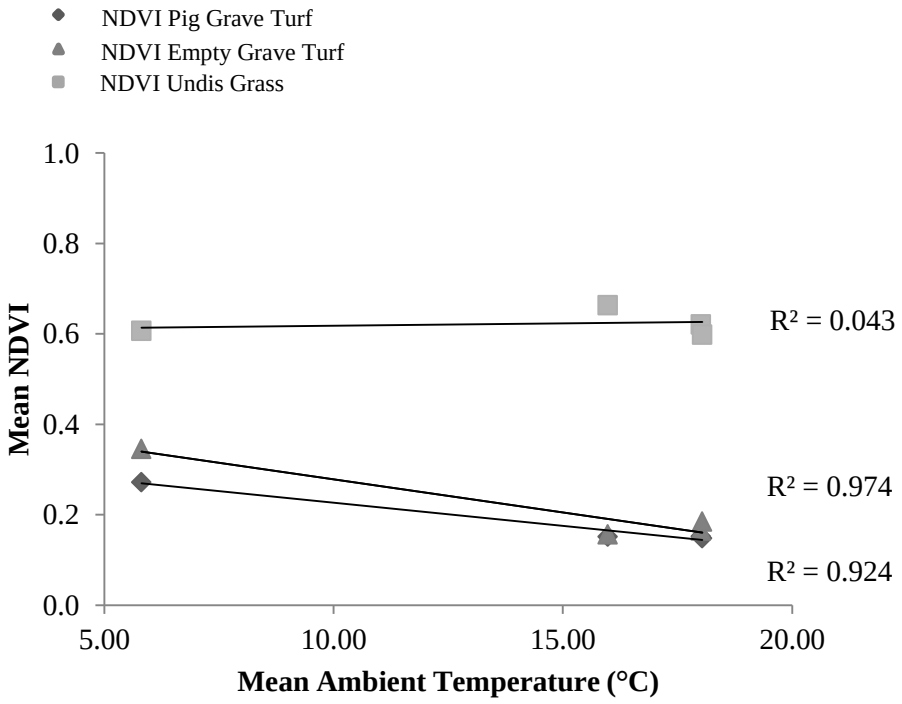

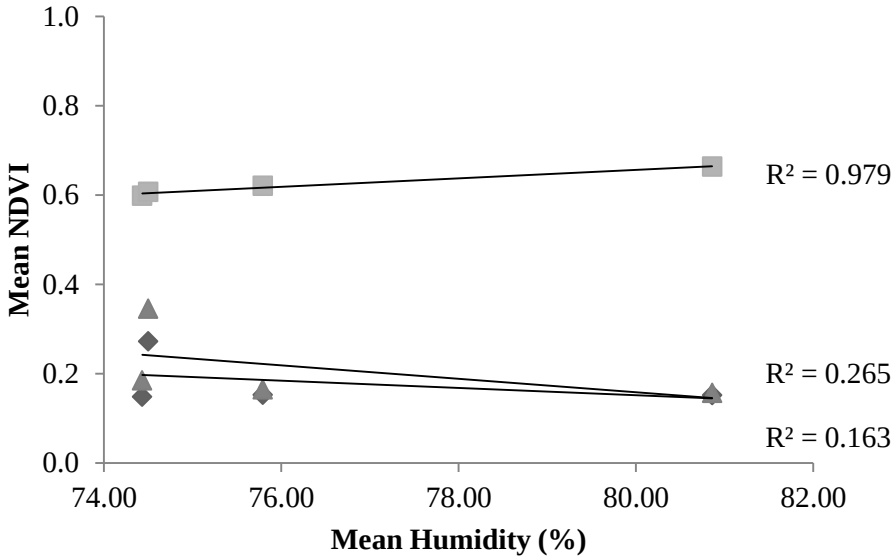
1.0
0.8
0.6
0.4
0.2
0.0
Mean NDVI
R² = 0.979
R² = 0.265
R² = 0.163
74.00
76.00
78.00
80.00
82.00
Mean Humidity (%)

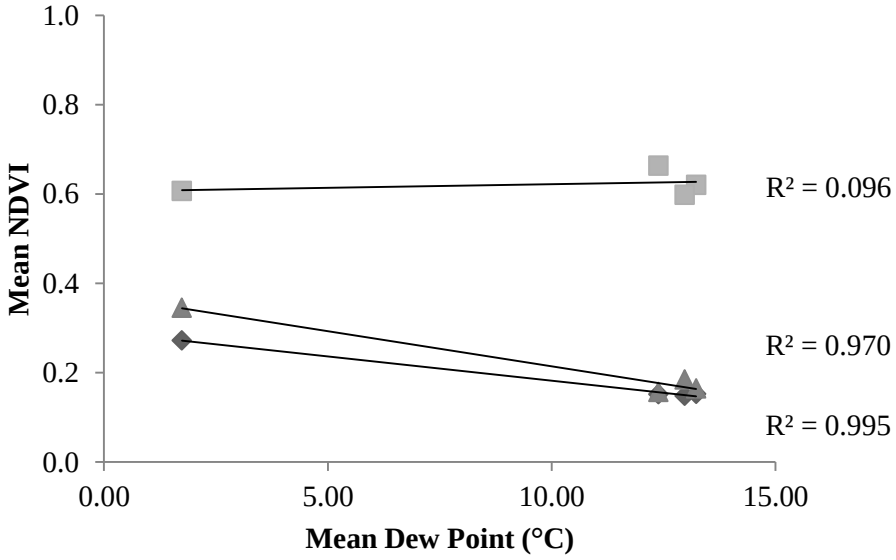
1.0
0.8
0.6
0.4
0.2
0.0
Mean NDVI
R² = 0.096
R² = 0.970
R² = 0.995
0.00
5.00
10.00
15.00
Mean Dew Point (°C)

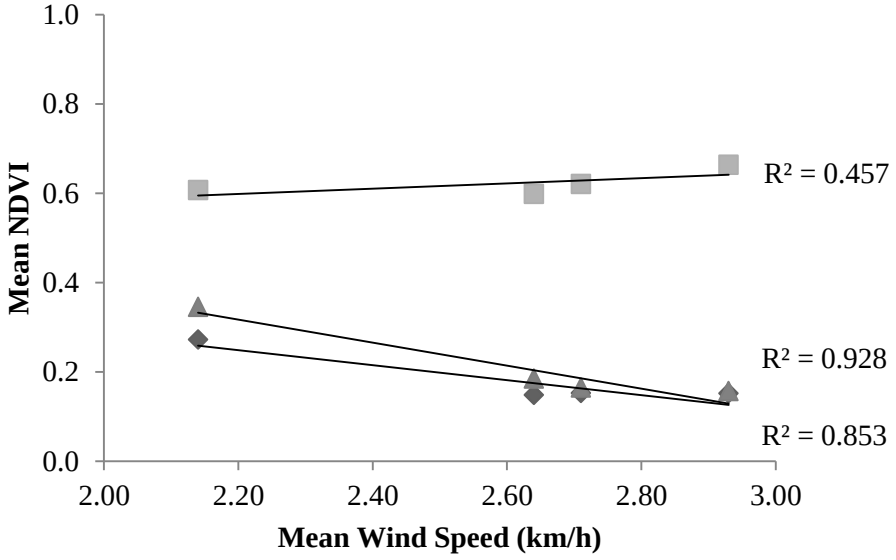
1.0
0.8
0.6
0.4
0.2
0.0
Mean NDVI
R² = 0.457
R² = 0.928
R² = 0.853
2.00
2.20
2.40
2.60
2.80
3.00
Mean Wind Speed (km/h)

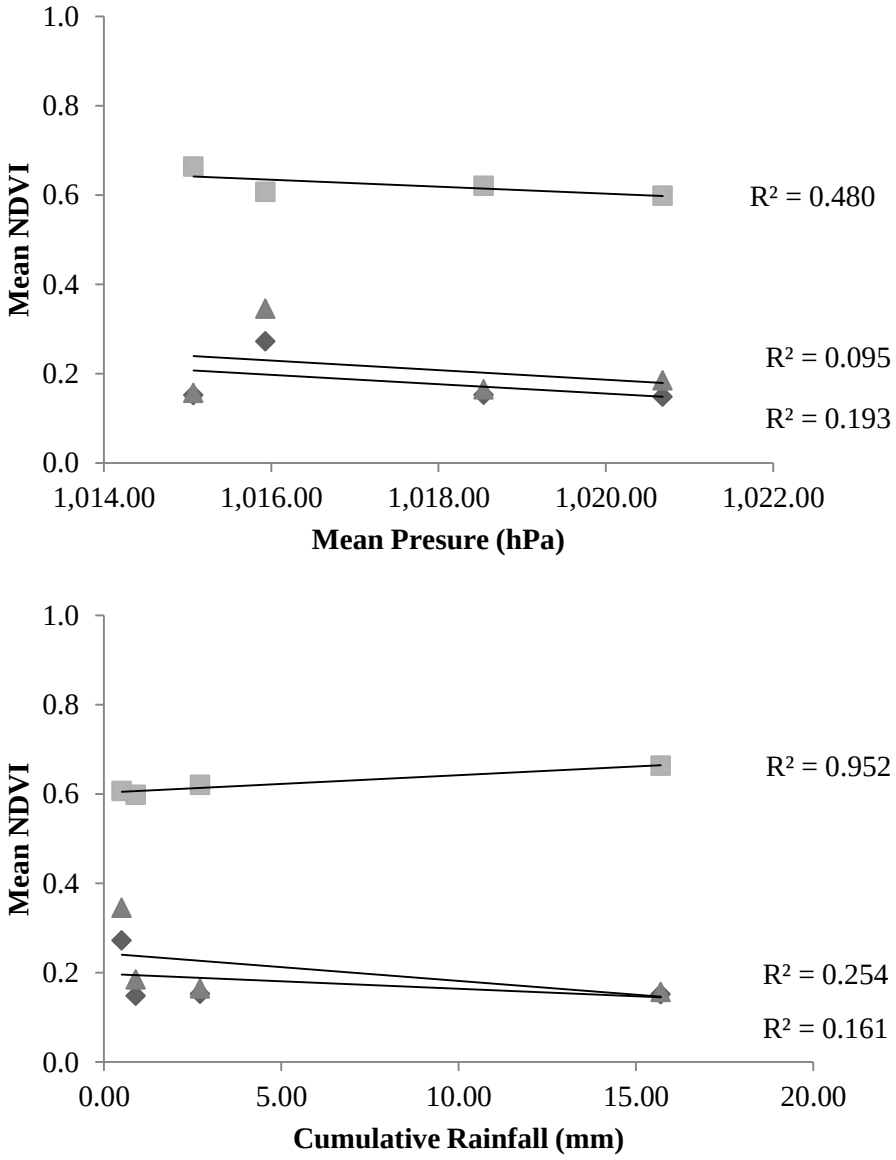

Figure 2-35 - Scatter plots illustrating the linear relationships between NDVI of the soil half of the graves and meteorological variables two weeks prior to spectra collection.

Table 2-24 - Meteorological data used to derive the relationships between NDVI of the grass halves of the graves and surface type four weeks prior to GER100 data collection.

Date	NDVI Pig Grave Grass	NDVI Empty Grave Grass	NDVI Undis Grass	Mean Air Temperature (°C)	Mean Humidity (%)	Mean Dew Point (°C)	Mean Wind Speed (km/h)	Mean Pressure (hPa)	Cumul. Rainfall (mm)
19/08/13	0.2832	0.27604	0.6207	18.67	77.82	14.36	2.89	1016.04	5.08
22/08/13	0.2657	0.19371	0.5985	18.42	76.86	13.89	2.86	1017.02	5.08
10/10/13	0.3365	0.26808	0.6635	15.56	80.54	11.96	2.61	1013.59	19.98
05/12/13	0.3722	0.29439	0.6069	6.49	76.96	2.90	1.93	1015.68	22.50

Table 2-25 - Description of the direction and strength of the linear relationship between NDVI calculated from convolved GER1500 data on the grass half of the experimental graves and meteorological variables (four weeks prior to data collection).

FUNCTION		Pig Grave Grass	Empty Grave Grass	Undisturbed Grass
SLOPE	NDVI vs Temp	-0.01	0.00	0.00
	NDVI vs Humidity	0.01	0.01	0.02
	NDVI vs Dew Point	-0.01	0.00	0.00
	NDVI vs Wind Speed	-0.10	-0.06	0.01
	NDVI vs Pressure	-0.02	-0.02	-0.02
	NDVI vs Cumul. Rainfall	0.01	0.00	0.00
CORREL	NDVI vs Temp	-0.91	-0.60	0.14
	NDVI vs Humidity	0.23	0.25	0.99
	NDVI vs Dew Point	1.00	-0.58	0.19
	NDVI vs Wind Speed	1.00	-0.60	0.11
	NDVI vs Pressure	0.19	-0.53	-0.95
	NDVI vs Cumul. Rainfall	-0.83	0.63	0.42
RSQ	NDVI vs Temp	0.83 83%	0.36 36%	0.02 2%
	NDVI vs Humidity	0.05 5%	0.06 6%	0.99 99%
	NDVI vs Dew Point	0.78 78%	0.33 33%	0.04 4%
	NDVI vs Wind Speed	0.85 85%	0.36 36%	0.01 1%
	NDVI vs Pressure	0.34 34%	0.28 28%	0.90 90%
	NDVI vs Cumul. Rainfall	0.94 94%	0.39 39%	0.18 18%

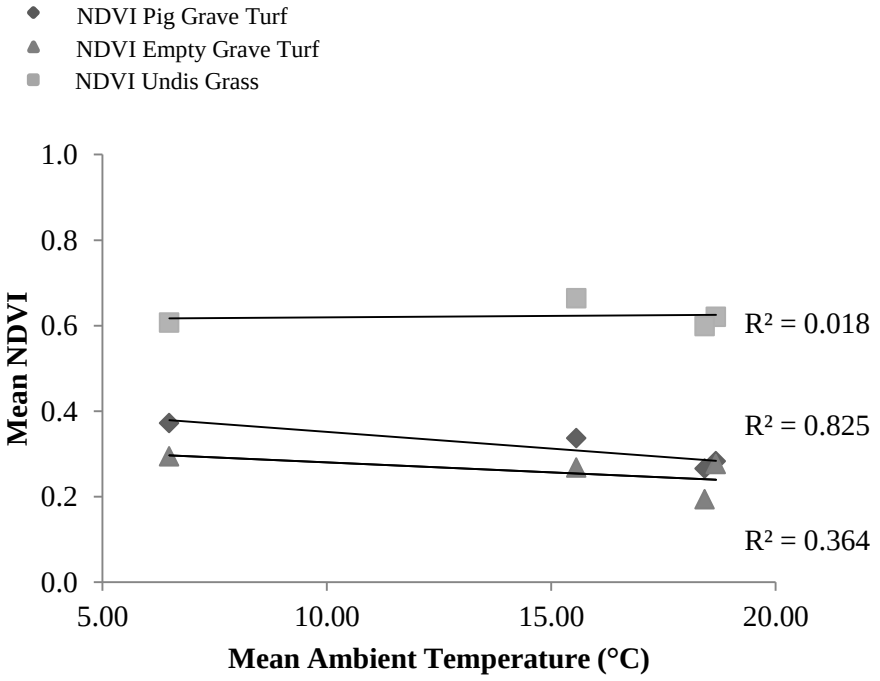

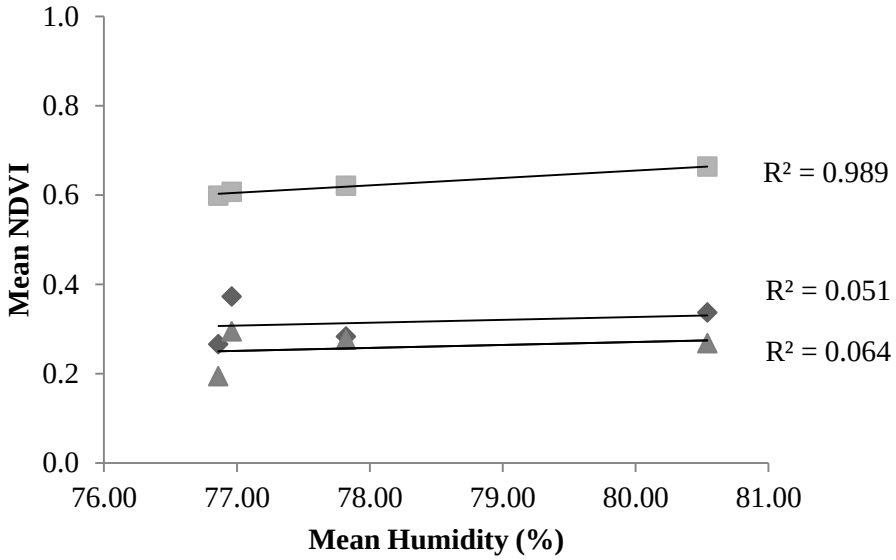
1.0
0.8
0.6
0.4
0.2
0.0
Mean NDVI
R² = 0.989
R² = 0.051
R² = 0.064
76.00
77.00
78.00
79.00
80.00
81.00
Mean Humidity (%)

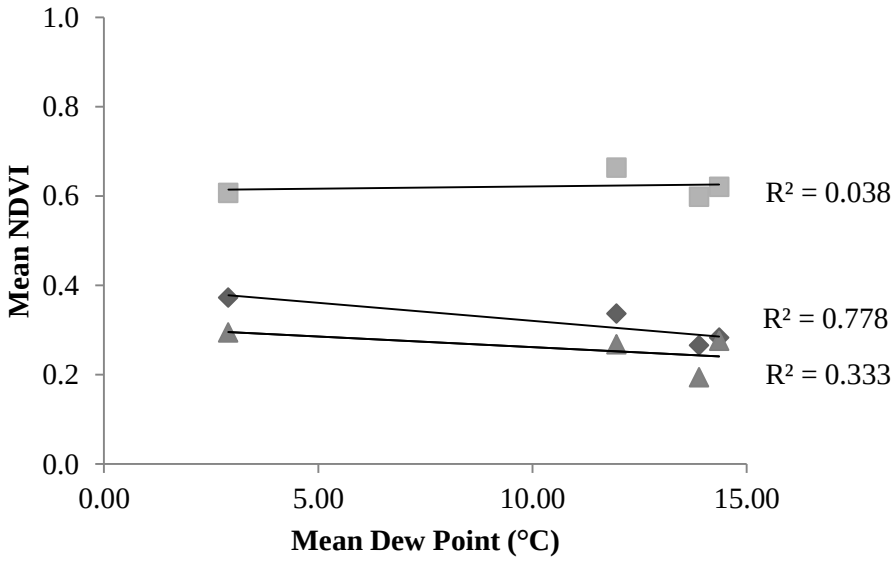
1.0
0.8
0.6
0.4
0.2
0.0
Mean NDVI
R² = 0.038
R² = 0.778
R² = 0.333
0.00
5.00
10.00
15.00
Mean Dew Point (°C)

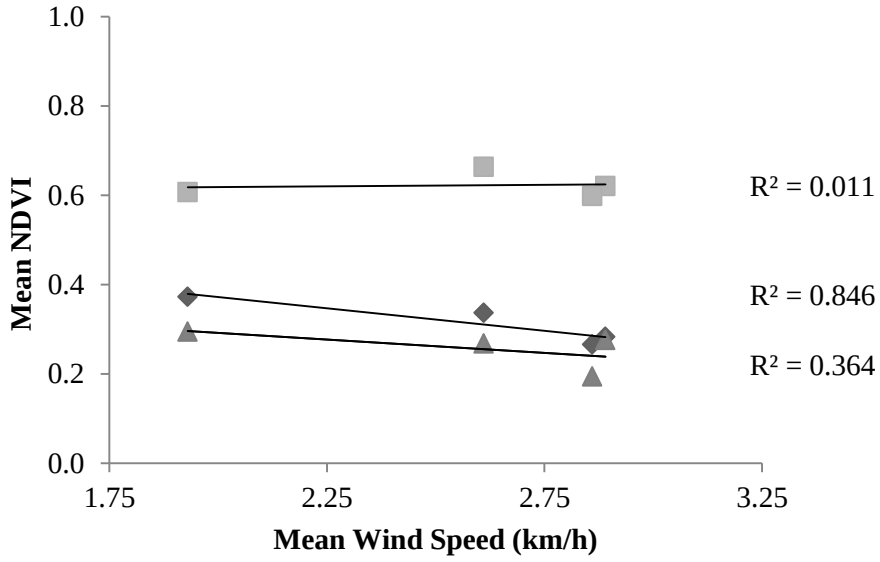
1.0
0.8
0.6
0.4
0.2
0.0
Mean NDVI
R² = 0.011
R² = 0.846
R² = 0.364
1.75
2.25
2.75
3.25
Mean Wind Speed (km/h)

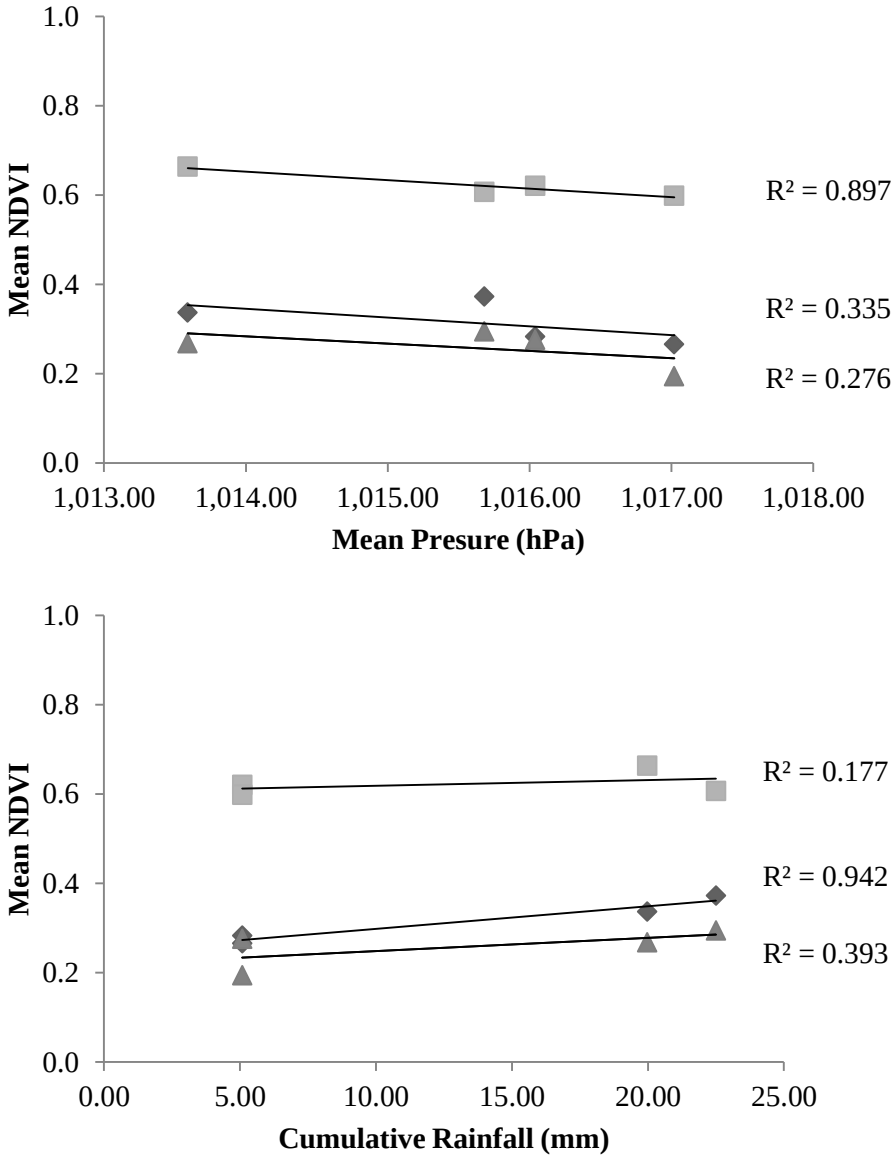

Figure 2-36 - Scatter plots illustrating the linear relationships between NDVI of the grass half of the graves and meteorological variables four weeks prior to spectra collection.

Table 2-26 - Meteorological data used to derive the relationships between NDVI of the soil halves of the graves and surface type four weeks prior to GER100 data collection.

Date	NDVI Pig Grave Soil	NDVI Empty Grave Soil	NDVI Undis Grass	Mean Air Temp (°C)	Mean Humidity (%)	Mean Dew Point (°C)	Mean Wind Speed (km/h)	Mean Pressure (hPa)	Cumul. Rainfall (mm)
19/08/13	0.1527	0.16503	0.6207	18.67	77.82	14.36	2.89	1016.04	5.08
22/08/13	0.1485	0.18479	0.5985	18.42	76.86	13.89	2.86	1017.02	5.08
10/10/13	0.1515	0.15663	0.6635	15.56	80.54	11.96	2.61	1013.59	19.98
05/12/13	0.2721	0.34544	0.6069	6.49	76.96	2.90	1.93	1015.68	22.50

Table 2-27 - Description of the direction and strength of the linear relationship between NDVI calculated from convolved GER1500 data on the soil half of the experimental graves and meteorological variables (four weeks prior to data collection).

FUNCTION		Pig Grave Soil	Empty Grave Soil	Undisturbed Grass
SLOPE	NDVI vs Temp	-0.01	-0.01	0.00
	NDVI vs Humidity	-0.01	-0.03	0.02
	NDVI vs Dew Point	-0.01	-0.02	0.00
	NDVI vs Wind Speed	-0.13	-0.18	0.01
	NDVI vs Pressure	0.00	0.01	-0.02
	NDVI vs Cumul. Rainfall	0.00	0.01	0.00
CORREL	NDVI vs Temp	-0.97	-0.94	0.14
	NDVI vs Humidity	-0.41	-0.52	0.99
	NDVI vs Dew Point	1.00	-0.96	0.19
	NDVI vs Wind Speed	1.00	-0.93	0.11
	NDVI vs Pressure	0.19	0.16	-0.95
	NDVI vs Cumul. Rainfall	-0.83	0.59	0.42
RSQ	NDVI vs Temp	0.94 94%	0.88 88%	0.02 2%
	NDVI vs Humidity	0.17 17%	0.27 27%	0.99 99%
	NDVI vs Dew Point	0.96 96%	0.92 92%	0.04 4%
	NDVI vs Wind Speed	0.92 92%	0.86 86%	0.01 1%
	NDVI vs Pressure	0.00 0%	0.03 3%	0.90 90%
	NDVI vs Cumul. Rainfall	0.45 45%	0.34 34%	0.18 18%

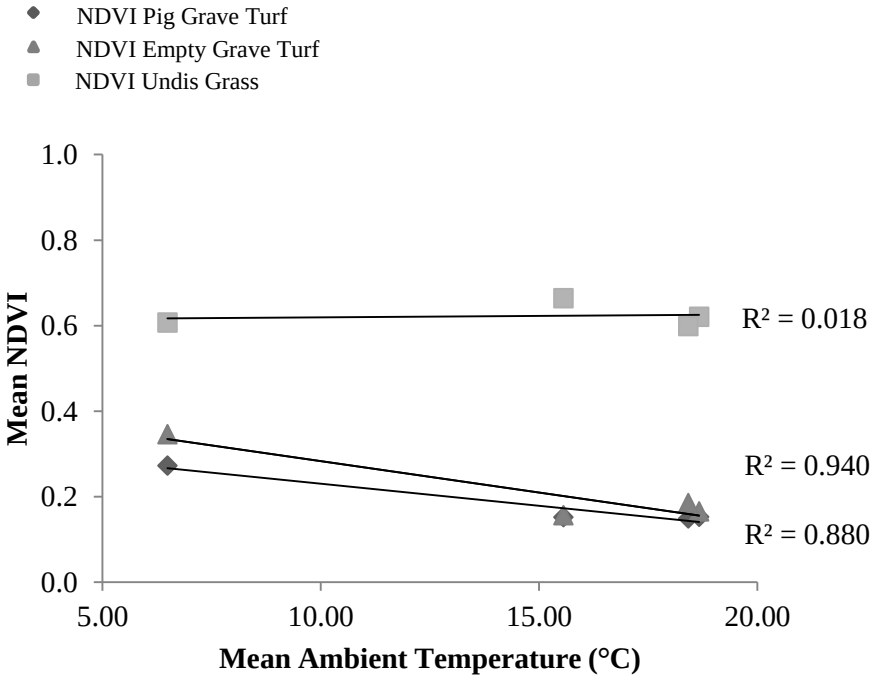

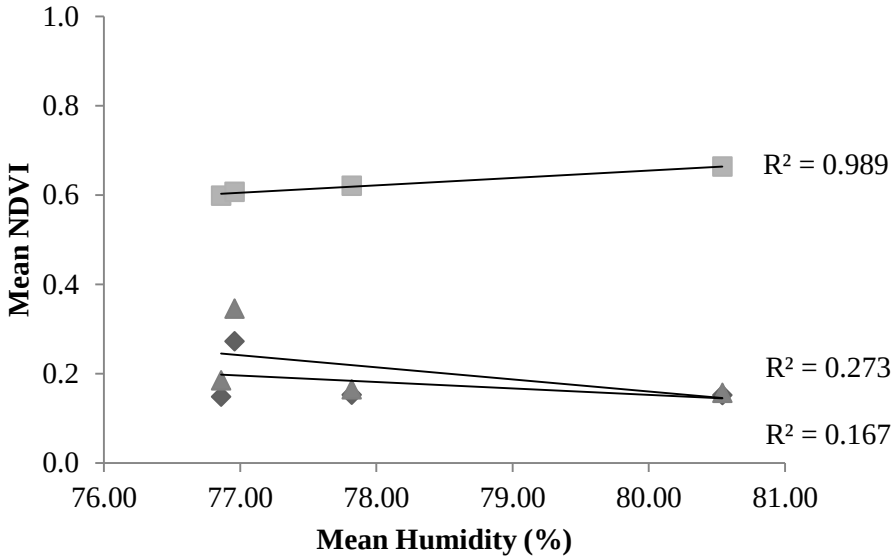
1.0
0.8
0.6
0.4
0.2
0.0
Mean NDVI
R² = 0.989
R² = 0.273
R² = 0.167
76.00
77.00
78.00
79.00
80.00
81.00
Mean Humidity (%)

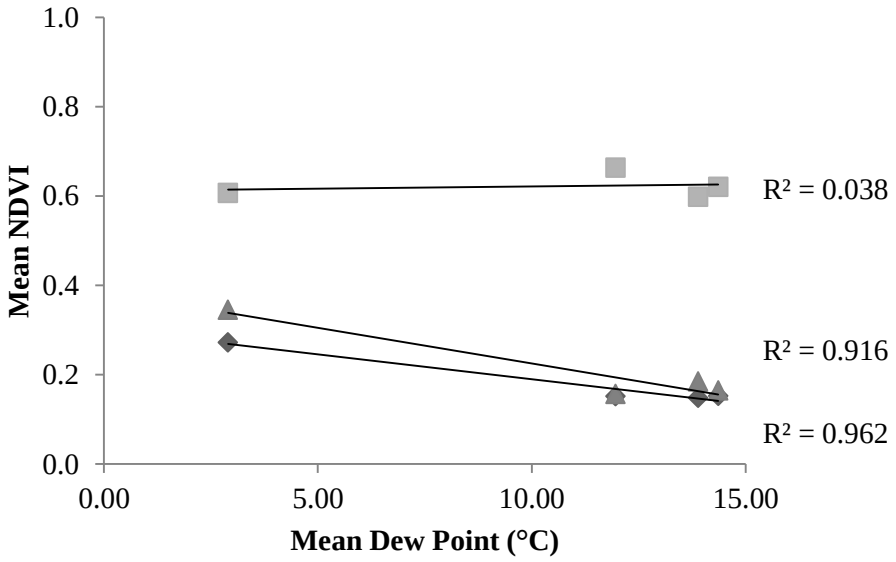
1.0
0.8
0.6
0.4
0.2
0.0
Mean NDVI
R² = 0.038
R² = 0.916
R² = 0.962
0.00
5.00
10.00
15.00
Mean Dew Point (°C)

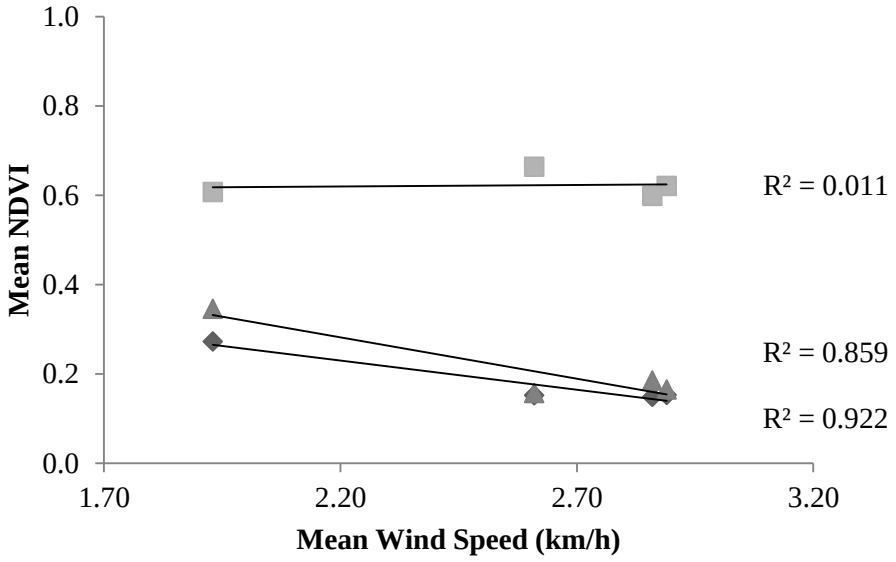
1.0
0.8
0.6
0.4
0.2
0.0
Mean NDVI
R² = 0.011
R² = 0.859
R² = 0.922
1.70
2.20
2.70
3.20
Mean Wind Speed (km/h)

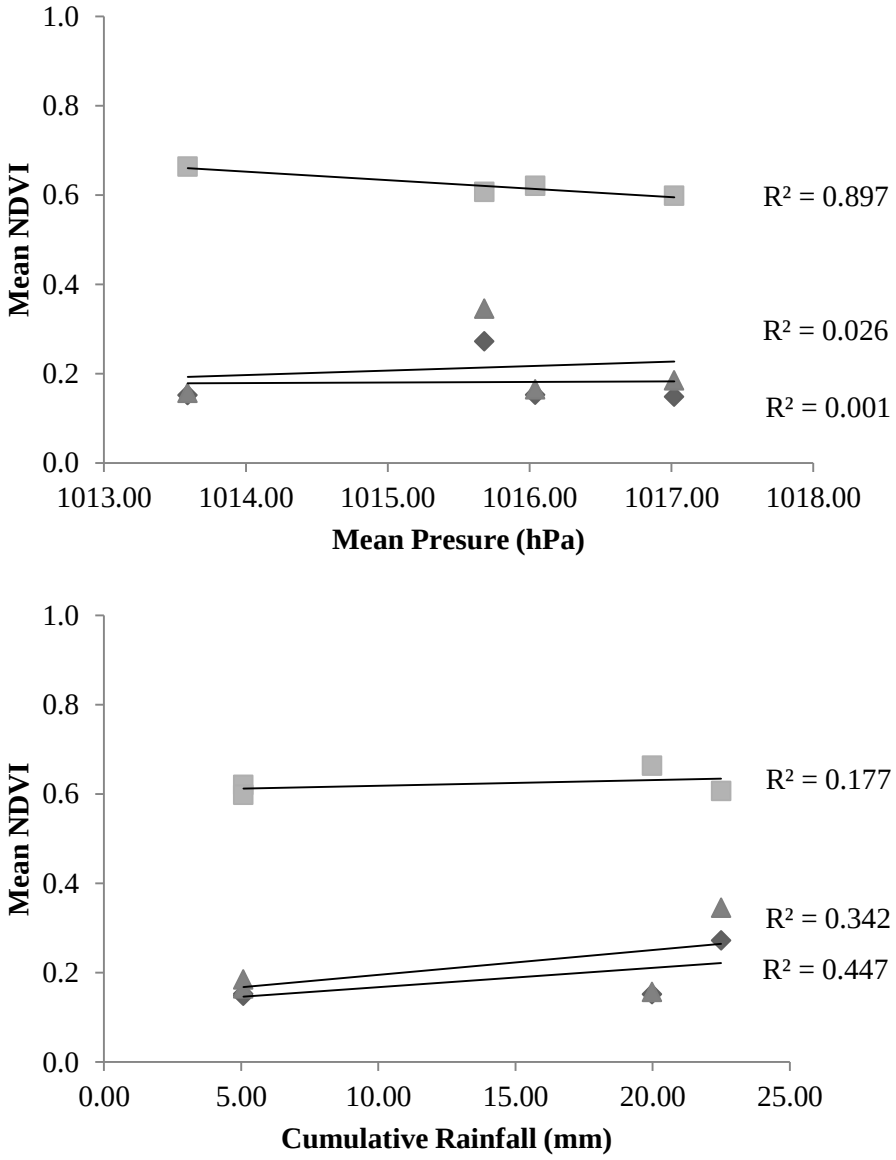

Figure 2-37 - Scatter plots illustrating the linear relationships between NDVI of the soil half of the graves and meteorological variables four weeks prior to spectra collection.

Appendix 3 for Chapter 6

Table 3-28 - Satellite imagery used for NDVI extraction at the Former RAF Pershore airfield.

Acquisition Date	Platform	Sensor	Source	Processing Level	Spatial Resolution (m)
15/02/1990	Landsat 5	TM	USGS EPSA	L1	30
06/05/1990	Landsat 5	TM	USGS EPSA	L1	30
22/05/1990	Landsat 5	TM	USGS EPSA	L1	30
25/07/1990	Landsat 5	TM	USGS EPSA	L1	30
01/08/1990	Landsat 5	TM	USGS EPSA	L1	30
13/10/1990	Landsat 5	TM	USGS EPSA	L1	30
05/11/1990	Landsat 5	TM	USGS EPSA	L1	30
13/08/1991	Landsat 5	TM	USGS EPSA	L1	30
20/08/1991	Landsat 5	TM	USGS EPSA	L1	30
29/08/1991	Landsat 5	TM	USGS EPSA	L1	30
30/09/1991	Landsat 5	TM	USGS EPSA	L1	30
09/04/1992	Landsat 5	TM	USGS EPSA	L1	30
27/05/1992	Landsat 5	TM	USGS EPSA	L1	30
30/07/1992	Landsat 5	TM	USGS EPSA	L1	30
06/08/1992	Landsat 5	TM	USGS EPSA	L1	30
15/08/1992	Landsat 5	TM	USGS EPSA	L1	30
07/09/1992	Landsat 5	TM	USGS EPSA	L1	30
03/11/1992	Landsat 5	TM	USGS EPSA	L1	30
23/02/1993	Landsat 5	TM	USGS EPSA	L1	30
06/06/1993	Landsat 5	TM	USGS EPSA	L1	30
15/06/1993	Landsat 5	TM	USGS EPSA	L1	30
21/10/1993	Landsat 5	TM	USGS EPSA	L1	30
11/07/1994	Landsat 5	TM	USGS EPSA	L1	30
02/04/1995	Landsat 5	TM	USGS EPSA	L1	30
04/05/1995	Landsat 5	TM	USGS EPSA	L1	30
24/05/1995	Landsat 5	TM	USGS EPSA	L1	30
28/06/1995	Landsat 5	TM	USGS EPSA	L1	30
30/07/1995	Landsat 5	TM	USGS EPSA	L1	30
15/08/1995	Landsat 5	TM	USGS EPSA	L1	30
10/03/1996	Landsat 5	TM	USGS EPSA	L1	30
04/04/1996	Landsat 5	TM	USGS EPSA	L1	30
13/05/1996	Landsat 5	TM	USGS EPSA	L1	30
25/07/1996	Landsat 5	TM	USGS EPSA	L1	30
29/10/1996	Landsat 5	TM	USGS EPSA	L1	30
18/02/1997	Landsat 5	TM	USGS EPSA	L1	30
06/03/1997	Landsat 5	TM	USGS EPSA	L1	30
22/03/1997	Landsat 5	TM	USGS EPSA	L1	30
07/04/1997	Landsat 5	TM	USGS EPSA	L1	30
25/05/1997	Landsat 5	TM	USGS EPSA	L1	30

Acquisition Date	Platform	Sensor	Source	Processing Level	Spatial Resolution (m)
01/06/1997	Landsat 5	TM	ESA	L1	30
17/06/1997	Landsat 5	TM	ESA	L1	30
19/07/1997	Landsat 5	TM	USGS EPSA	L1	30
09/08/1997	SPOT 2	HRV	ESA	L3	20
14/09/1997	Landsat 5	TM	USGS EPSA	L1	30
21/09/1997	Landsat 5	TM	USGS EE	L1	30
22/11/1997	SPOT 2	HRV	ESA	L3	20
04/03/1998	SPOT 1	HRV	ESA	L3	20
09/03/1998	Landsat 5	TM	USGS EPSA	L1	30
19/05/1998	Landsat 5	TM	USGS EE	L1	30
16/08/1998	Landsat 5	TM	USGS EE	L1	30
17/09/1998	Landsat 5	TM	USGS EPSA	L1	30
19/10/1998	Landsat 5	TM	USGS EPSA	L1	30
26/10/1998	Landsat 5	TM	USGS EPSA	L1	30
28/03/1999	Landsat 5	TM	USGS EPSA	L1	30
03/09/1999	SPOT 2	HRV	ESA	L3	20
04/09/1999	Landsat 5	TM	USGS EPSA	L1	30
05/10/1999	Landsat 7	ETM+	USGS EPSA	L1	30
06/10/1999	Landsat 5	TM	USGS EPSA	L1	30
13/10/1999	Landsat 5	TM	USGS EPSA	L1	30
14/10/1999	Landsat 7	ETM+	USGS EPSA	L1	30
06/11/1999	Landsat 5	TM	USGS EE	L1	30
09/01/2000	Landsat 5	TM	ESA	L1	30
26/02/2000	Landsat 5	TM	USGS EE	L1	30
22/03/2000	Landsat 7	ETM+	ESA	L1	30
07/04/2000	Landsat 7	ETM+	USGS ESPA	L1	30
30/04/2000	Landsat 5	TM	USGS EE	L1	30
17/06/2000	Landsat 7	ETM+	USGS ESPA	L1	30
18/06/2000	Landsat 5	TM	USGS EPSA	L1	30
20/08/2000	Landsat 7	ETM+	USGS ESPA	L1	30
01/11/2000	Landsat 5	TM	USGS EE	L1	30
26/12/2000	Landsat 5	TM	USGS EE	L1	30
27/01/2001	Landsat 5	TM	USGS EE	L1	30
12/05/2001	Landsat 7	ETM+	USGS ESPA	L1	30
05/06/2001	Landsat 5	TM	USGS EPSA	L1	30
05/06/2001	SPOT 2	HRV	ESA	L3	20
23/07/2001	Landsat 5	TM	USGS EPSA	L1	30
26/07/2001	SPOT 2	HRV	ESA	L3	20
15/08/2001	Landsat 5	TM	USGS EPSA	L1	30
15/08/2001	SPOT 2	HRV	ESA	L3	20
27/10/2001	Landsat 5	TM	USGS EPSA	L1	30
04/11/2001	Landsat 7	ETM+	USGS ESPA	L1	30
22/12/2001	Landsat 5	TM	USGS EE	L1	30

Acquisition Date	Platform	Sensor	Source	Processing Level	Spatial Resolution (m)
28/03/2002	Landsat 7	ETM+	USGS ESPA	L1	30
04/04/2002	Landsat 7	ETM+	USGS ESPA	L1	30
24/05/2002	SPOT 2	HRV	ESA	L3	20
15/07/2002	SPOT 2	HRV	ESA	L3	20
04/09/2002	Landsat 7	ETM+	USGS ESPA	L1	30
11/09/2002	Landsat 7	ETM+	USGS ESPA	L1	30
20/09/2002	Landsat 7	ETM+	USGS ESPA	L1	30
06/10/2002	Landsat 7	ETM+	USGS ESPA	L1	30
07/11/2002	Landsat 7	ETM+	USGS EE	L1	30
18/02/2003	Landsat 7	ETM+	USGS EE	L1	30
22/03/2003	Landsat 7	ETM+	USGS ESPA	L1	30
07/04/2003	Landsat 7	ETM+	USGS ESPA	L1	30
16/04/2003	Landsat 7	ETM+	USGS ESPA	L1	30
23/04/2003	Landsat 7	ETM+	USGS ESPA	L1	30
13/07/2003	Landsat 7	ETM+	USGS EE	L1	30
14/08/2003	Landsat 5	TM	USGS EPSA	L1	30
30/08/2003	Landsat 5	TM	USGS EPSA	L1	30
15/09/2003	Landsat 5	TM	USGS EPSA	L1	30
23/02/2004	SPOT 2	HRV	ESA	L3	20
23/05/2004	DMC	MSI	DMCii	L0R	32
07/08/2004	Landsat 5	TM	USGS EPSA	L1	30
08/09/2004	Landsat 5	TM	USGS EPSA	L1	30
24/10/2004	DMC	MSI	DMCii	L0R	32
14/11/2004	SPOT 2	HRV	ESA	L3	20
20/01/2005	SPOT 2	HRV	ESA	L3	20
23/01/2005	Landsat 5	TM	USGS EPSA	L1	30
03/03/2005	Landsat 5	TM	USGS EPSA	L1	30
02/04/2005	SPOT 2	HRV	ESA	L3	20
24/04/2005	SPOT 2	HRV	ESA	L3	20
06/05/2005	Landsat 5	TM	USGS EPSA	L1	30
15/05/2005	Landsat 5	TM	USGS EPSA	L1	30
07/06/2005	Landsat 5	TM	USGS EPSA	L1	30
08/06/2005	SPOT 2	HRV	ESA	L3	20
23/06/2005	Landsat 5	TM	USGS EPSA	L1	30
08/07/2005	DMC	MSI	DMCii	L0R	32
09/07/2005	Landsat 5	TM	USGS EPSA	L1	30
10/07/2005	SPOT 4	HRVIR	ESA	L3	20
06/09/2005	DMC	MSI	DMCii	L0R	32
07/11/2005	Landsat 5	TM	USGS EPSA	L1	30
07/11/2005	SPOT 2	HRV	ESA	L3	20
09/02/2006	SPOT 2	HRV	ESA	L3	20
07/06/2006	Landsat 5	TM	USGS EPSA	L1	30
10/06/2006	Landsat 5	TM	USGS EPSA	L1	30

Acquisition Date	Platform	Sensor	Source	Processing Level	Spatial Resolution (m)
12/07/2006	Landsat 5	TM	USGS EE	L1	30
21/07/2006	Landsat 5	TM	USGS EPSA	L1	30
28/07/2006	Landsat 5	TM	USGS EPSA	L1	30
23/09/2006	Landsat 5	TM	USGS EPSA	L1	30
03/11/2006	SPOT 5	HRV2_X	ESA	L3	20
02/12/2006	SPOT 4	HRVIR	ESA	L3	20
18/03/2007	Landsat 5	TM	USGS EPSA	L1	30
19/04/2007	Landsat 5	TM	USGS EPSA	L1	30
01/05/2007	DMC	MSI	DMCii	L0R	32
01/06/2007	DMC	MSI	DMCii	L0R	32
31/07/2007	Landsat 5	TM	USGS EPSA	L1	30
09/08/2007	Landsat 5	TM	USGS EPSA	L1	30
25/08/2007	Landsat 5	TM	USGS EPSA	L1	30
10/09/2007	Landsat 5	TM	USGS EPSA	L1	30
13/09/2007	SPOT 4	HRVIR	ESA	L3	20
04/03/2008	DMC	MSI	DMCii	L0R	32
06/05/2008	DMC	MSI	DMCii	L0R	32
08/06/2008	Landsat 5	TM	USGS EPSA	L1	30
19/09/2008	Landsat 5	TM	USGS EPSA	L1	30
26/09/2008	SPOT 4	HRVIR	ESA	L3	20
21/10/2008	Landsat 5	TM	USGS EPSA	L1	30
02/03/2009	DMC	MSI	DMCii	L0R	32
30/03/2009	Landsat 5	TM	USGS EPSA	L1	30
01/05/2009	Landsat 5	TM	USGS EPSA	L1	30
09/08/2009	SPOT 4	HRVIR	ESA	L3	20
19/08/2009	RapidEye	MSI	ESA	3A	5
21/08/2009	Landsat 5	TM	USGS EE	L1	30
02/11/2009	Landsat 5	TM	USGS EE	L1	30
11/04/2010	Landsat 5	TM	USGS EPSA	L1	30
17/04/2010	RapidEye	MSI	ESA	3A	5
18/04/2010	Landsat 5	TM	USGS EPSA	L1	30
04/05/2010	Landsat 5	TM	USGS EPSA	L1	30
21/06/2010	Landsat 5	TM	USGS EPSA	L1	30
16/08/2010	RapidEye	MSI	ESA	3A	5
02/09/2010	Landsat 5	TM	USGS EPSA	L1	30
18/09/2010	Landsat 5	TM	USGS EE	L1	30
25/09/2010	Landsat 5	TM	USGS EPSA	L1	30
20/10/2010	Landsat 5	TM	USGS EPSA	L1	30
14/03/2011	RapidEye	MSI	ESA	3A	5
25/03/2011	RapidEye	MSI	ESA	3A	5
21/04/2011	Landsat 5	TM	USGS EE	L1	30
22/04/2011	RapidEye	MSI	ESA	3A	5

23/04/2011	RapidEye	MSI	ESA	3A	5
Acquisition Date	**Platform**	**Sensor**	**Source**	**Processing Level**	**Spatial Resolution (m)**
30/04/2011	Landsat 5	TM	USGS EPSA	L1	30
02/05/2011	RapidEye	MSI	ESA	3A	5
03/05/2011	RapidEye	MSI	ESA	3A	5
14/07/2011	RapidEye	MSI	ESA	3A	5

Statistical Significance – Landsat 5TM & 7ETM+

16/06/1999

Undisturbed Vegetation vs Full Grave

F-Test Two-Sample for Variances	*Variable 1*	*Variable 2*
Mean	0.685716667	0.779
Variance	0.025066299	0.000324277
Observations	30	15
df	29	14
F	77.29899942	
P(F<=f) one-tail	3.13912E-11	
F Critical one-tail	2.313868369	
t-Test: Two-Sample Assuming Unequal Variances		
Mean	0.685716667	0.779
Variance	0.025066299	0.000324277
Observations	30	15
Hypothesized Mean Difference	0	
df	30	
t Stat	-3.18619727	
P(T<=t) one-tail	0.001677893	
t Critical one-tail	1.697260887	
P(T<=t) two-tail	0.003355787	
t Critical two-tail	2.042272456	

Undisturbed Vegetation vs Empty Grave

F-Test Two-Sample for Variances	*Variable 1*	*Variable 2*
Mean	0.685716667	0.6966
Variance	0.025066299	0.006156929
Observations	30	10
df	29	9
F	4.071234073	
P(F<=f) one-tail	0.016030203	
F Critical one-tail	2.868783172	
t-Test: Two-Sample Assuming Unequal Variances		
Mean	0.685716667	0.6966
Variance	0.025066299	0.006156929
Observations	30	10
Hypothesized Mean Difference	0	
df	32	
t Stat	-0.28568858	
P(T<=t) one-tail	0.38847893	
t Critical one-tail	1.693888748	
P(T<=t) two-tail	0.776957859	
t Critical two-tail	2.036933343	

Empty Grave vs Full Grave

F-Test Two-Sample for Variances	*Variable 1*	*Variable 2*
Mean	0.6966	0.779
Variance	0.006156929	0.000324277
Observations	10	15
df	9	14
F	18.98662618	
P(F<=f) one-tail	0.000002281	
F Critical one-tail	2.645790735	
t-Test: Two-Sample Assuming Unequal Variances		
Mean	0.6966	0.779
Variance	0.006156929	0.000324277
Observations	10	15
Hypothesized Mean Difference	0	
df	10	
t Stat	-3.26400924	
P(T<=t) one-tail	0.004258084	
t Critical one-tail	1.812461123	
P(T<=t) two-tail	0.008516169	
t Critical two-tail	2.228138852	

12/08/2000

Undisturbed Vegetation vs Full Grave

F-Test Two-Sample for Variances	*Variable 1*	*Variable 2*
Mean	0.405443333	0.497613333
Variance	0.012618749	0.00066512
Observations	30	15
df	29	14
F	18.97214392	
P(F<=f) one-tail	4.10437E-07	
F Critical one-tail	2.313868369	
t-Test: Two-Sample Assuming Unequal Variances		
Mean	0.405443333	0.497613333
Variance	0.012618749	0.00066512
Observations	30	15
Hypothesized Mean Difference	0	
df	35	
t Stat	-4.274436393	
P(T<=t) one-tail	7.00706E-05	
t Critical one-tail	1.689572458	
P(T<=t) two-tail	0.000140141	
t Critical two-tail	2.030107928	

Undisturbed Vegetation vs Empty Grave

F-Test Two-Sample for Variances	*Variable 1*	*Variable 2*
Mean	0.405443333	0.43045
Variance	0.012618749	0.004133685
Observations	30	10
df	29	9
F	3.052663361	
P(F<=f) one-tail	0.04127167	
F Critical one-tail	2.868783172	
t-Test: Two-Sample Assuming Unequal Variances		
Mean	0.405443333	0.43045
Variance	0.012618749	0.004133685
Observations	30	10
Hypothesized Mean Difference	0	
df	28	
t Stat	-0.86591345	
P(T<=t) one-tail	0.19694848	
t Critical one-tail	1.701130934	
P(T<=t) two-tail	0.393896959	
t Critical two-tail	2.048407142	

Empty Grave vs Full Grave

F-Test Two-Sample for Variances	*Variable 1*	*Variable 2*
Mean	0.43045	0.497613333
Variance	0.004133685	0.00066512
Observations	10	15
df	9	14
F	6.214947955	
P(F<=f) one-tail	0.001337136	
F Critical one-tail	2.645790735	
t-Test: Two-Sample Assuming Unequal Variances		
Mean	0.43045	0.497613333
Variance	0.004133685	0.00066512
Observations	10	15
Hypothesized Mean Difference	0	
df	11	
t Stat	-3.13933113	
P(T<=t) one-tail	0.004709815	
t Critical one-tail	1.795884819	
P(T<=t) two-tail	0.009419629	
t Critical two-tail	2.20098516	

12/05/2001

Undisturbed Vegetation vs Full Grave

F-Test Two-Sample for Variances	*Variable 1*	*Variable 2*
Mean	0.693623333	0.1138
Variance	0.02505656	0.000249694
Observations	30	15
df	29	14
F	100.3489516	
P(F<=f) one-tail	0.0000000	
F Critical one-tail	2.313868369	
t-Test: Two-Sample Assuming Unequal Variances		
Mean	0.693623333	0.1138
Variance	0.02505656	0.000249694
Observations	30	15
Hypothesized Mean Difference	0	
df	30	
t Stat	19.86599468	
P(T<=t) one-tail	4.07237E-19	
t Critical one-tail	1.697260887	
P(T<=t) two-tail	0.000000000	
t Critical two-tail	2.042272456	

Undisturbed Vegetation vs Empty Grave

F-Test Two-Sample for Variances	*Variable 1*	*Variable 2*
Mean	0.693623333	0.14402
Variance	0.02505656	0.001792684
Observations	30	10
df	29	9
F	13.97712022	
P(F<=f) one-tail	0.000136553	
F Critical one-tail	2.868783172	
t-Test: Two-Sample Assuming Unequal Variances		
Mean	0.693623333	0.14402
Variance	0.02505656	0.001792684
Observations	30	10
Hypothesized Mean Difference	0	
df	37	
t Stat	17.25544255	
P(T<=t) one-tail	1.38781E-19	
t Critical one-tail	1.68709362	
P(T<=t) two-tail	0.00000000	
t Critical two-tail	2.026192463	

Empty Grave vs Full Grave

F-Test Two-Sample for Variances	*Variable 1*	*Variable 2*
Mean	0.14402	0.1138
Variance	0.001792684	0.000249694
Observations	10	15
df	9	14
F	7.179515522	
P(F<=f) one-tail	0.000638775	
F Critical one-tail	2.645790735	
t-Test: Two-Sample Assuming Unequal Variances		
Mean	0.14402	0.1138
Variance	0.001792684	0.000249694
Observations	10	15
Hypothesized Mean Difference	0	
df	11	
t Stat	2.15904137	
P(T<=t) one-tail	0.026896991	
t Critical one-tail	1.795884819	
P(T<=t) two-tail	0.053793981	
t Critical two-tail	2.20098516	

28/03/2002

Undisturbed Vegetation vs Full Grave

F-Test Two-Sample for Variances	*Variable 1*	*Variable 2*
Mean	0.65374	0.119793333
Variance	0.0277124	0.000111611
Observations	30	15
df	29	14
F	248.295262	
P(F<=f) one-tail	0.000000	
F Critical one-tail	2.313868369	
t-Test: Two-Sample Assuming Unequal Variances		
Mean	0.65374	0.119793333
Variance	0.0277124	0.000111611
Observations	30	15
Hypothesized Mean Difference	0	
df	29	
t Stat	17.49763454	
P(T<=t) one-tail	2.97016E-17	
t Critical one-tail	1.699127027	
P(T<=t) two-tail	0.000000000	
t Critical two-tail	2.045229642	

Undisturbed Vegetation vs Empty Grave

F-Test Two-Sample for Variances	*Variable 1*	*Variable 2*
Mean	0.65374	0.1197
Variance	0.0277124	0.000384669
Observations	30	10
df	29	9
F	72.04221741	
P(F<=f) one-tail	0.000000	
F Critical one-tail	2.868783172	
t-Test: Two-Sample Assuming Unequal Variances		
Mean	0.65374	0.1197
Variance	0.0277124	0.000384669
Observations	30	10
Hypothesized Mean Difference	0	
df	31	
t Stat	17.21622992	
P(T<=t) one-tail	1.01013E-17	
t Critical one-tail	1.695518783	
P(T<=t) two-tail	0.000000000	
t Critical two-tail	2.039513446	

Empty Grave vs Full Grave

F-Test Two-Sample for Variances	*Variable 1*	*Variable 2*
Mean	0.1197	0.119793333
Variance	0.000384669	0.000111611
Observations	10	15
df	9	14
F	3.446524426	
P(F<=f) one-tail	0.018973986	
F Critical one-tail	2.645790735	
t-Test: Two-Sample Assuming Unequal Variances		
Mean	0.1197	0.119793333
Variance	0.000384669	0.000111611
Observations	10	15
Hypothesized Mean Difference	0	
df	13	
t Stat	-0.01377509	
P(T<=t) one-tail	0.494609288	
t Critical one-tail	1.770933396	
P(T<=t) two-tail	0.989218576	
t Critical two-tail	2.160368656	

16/04/2003

Undisturbed Vegetation vs Full Grave

F-Test Two-Sample for Variances	*Variable 1*	*Variable 2*
Mean	0.611506667	0.1583
Variance	0.026134692	0.000309487
Observations	30	15
df	29	14
F	84.44516346	
P(F<=f) one-tail	1.70722E-11	
F Critical one-tail	2.313868369	
t-Test: Two-Sample Assuming Unequal Variances		
Mean	0.611506667	0.1583
Variance	0.026134692	0.000309487
Observations	30	15
Hypothesized Mean Difference	0	
df	30	
t Stat	15.17627758	
P(T<=t) one-tail	6.42375E-16	
t Critical one-tail	1.697260887	
P(T<=t) two-tail	0.000000000	
t Critical two-tail	2.042272456	

Undisturbed Vegetation vs Empty Grave

F-Test Two-Sample for Variances	*Variable 1*	*Variable 2*
Mean	0.611506667	0.35664
Variance	0.026134692	0.004001056
Observations	30	10
df	29	9
F	6.531948658	
P(F<=f) one-tail	0.002878135	
F Critical one-tail	2.868783172	
t-Test: Two-Sample Assuming Unequal Variances		
Mean	0.611506667	0.35664
Variance	0.026134692	0.004001056
Observations	30	10
Hypothesized Mean Difference	0	
df	37	
t Stat	7.148180397	
P(T<=t) one-tail	9.00368E-09	
t Critical one-tail	1.68709362	
P(T<=t) two-tail	0.000000018	
t Critical two-tail	2.026192463	

Empty Grave vs Full Grave

F-Test Two-Sample for Variances	*Variable 1*	*Variable 2*
Mean	0.35664	0.1583
Variance	0.004001056	0.000309487
Observations	10	15
df	9	14
F	12.92802009	
P(F<=f) one-tail	2.37047E-05	
F Critical one-tail	2.645790735	
t-Test: Two-Sample Assuming Unequal Variances		
Mean	0.35664	0.1583
Variance	0.004001056	0.000309487
Observations	10	15
Hypothesized Mean Difference	0	
df	10	
t Stat	9.669508522	
P(T<=t) one-tail	1.08055E-06	
t Critical one-tail	1.812461123	
P(T<=t) two-tail	0.000002161	
t Critical two-tail	2.228138852	

08/09/2004

Undisturbed Vegetation vs Full Grave

F-Test Two-Sample for Variances	*Variable 1*	*Variable 2*
Mean	0.67957	0.3333667
Variance	0.0394913	0.0029095
Observations	30	15
df	29	14
F	13.57303463	
P(F<=f) one-tail	3.56077E-06	
F Critical one-tail	2.313868369	
t-Test: Two-Sample Assuming Unequal Variances		
Mean	0.67957	0.3333667
Variance	0.0394913	0.0029095
Observations	30	15
Hypothesized Mean Difference	0	
df	37	
t Stat	8.908262595	
P(T<=t) one-tail	4.85832E-11	
t Critical one-tail	1.68709362	
P(T<=t) two-tail	0.000000000	
t Critical two-tail	2.026192463	

Undisturbed Vegetation vs Empty Grave

F-Test Two-Sample for Variances	*Variable 1*	*Variable 2*
Mean	0.67957	0.46574
Variance	0.0394913	0.006666296
Observations	30	10
df	29	9
F	5.924024391	
P(F<=f) one-tail	0.004161919	
F Critical one-tail	2.868783172	
t-Test: Two-Sample Assuming Unequal Variances		
Mean	0.67957	0.46574
Variance	0.0394913	0.006666296
Observations	30	10
Hypothesized Mean Difference	0	
df	36	
t Stat	4.801827918	
P(T<=t) one-tail	1.37432E-05	
t Critical one-tail	1.688297714	
P(T<=t) two-tail	0.000027486	
t Critical two-tail	2.028094001	

Empty Grave vs Full Grave

F-Test Two-Sample for Variances	*Variable 1*	*Variable 2*
Mean	0.46574	0.333366667
Variance	0.006666296	0.002909541
Observations	10	15
df	9	14
F	2.291184798	
P(F<=f) one-tail	0.079539148	
F Critical one-tail	2.645790735	
t-Test: Two-Sample Assuming Equal Variances		
Mean	0.46574	0.333366667
Variance	0.006666296	0.002909541
Observations	10	15
Pooled Variance	0.004379576	
Hypothesized Mean Difference	0	
df	23	
t Stat	4.899594288	
P(T<=t) one-tail	2.99202E-05	
t Critical one-tail	1.713871528	
P(T<=t) two-tail	0.000059840	
t Critical two-tail	2.06865761	

15/05/2005

Undisturbed Vegetation vs Full Grave

F-Test Two-Sample for Variances	*Variable 1*	*Variable 2*
Mean	0.725096667	0.414306667
Variance	0.033100464	0.002437868
Observations	30	15
df	29	14
F	13.57762892	
P(F<=f) one-tail	3.55312E-06	
F Critical one-tail	2.313868369	
t-Test: Two-Sample Assuming Unequal Variances		
Mean	0.725096667	0.414306667
Variance	0.033100464	0.002437868
Observations	30	15
Hypothesized Mean Difference	0	
df	37	
t Stat	8.73518104	
P(T<=t) one-tail	7.99306E-11	
t Critical one-tail	1.68709362	
P(T<=t) two-tail	0.00000000	
t Critical two-tail	2.026192463	

Undisturbed Vegetation vs Empty Grave

F-Test Two-Sample for Variances	*Variable 1*	*Variable 2*
Mean	0.725096667	0.55574
Variance	0.033100464	0.009130516
Observations	30	10
df	29	9
F	3.625256718	
P(F<=f) one-tail	0.023715068	
F Critical one-tail	2.868783172	
t-Test: Two-Sample Assuming Unequal Variances		
Mean	0.725096667	0.55574
Variance	0.033100464	0.009130516
Observations	30	10
Hypothesized Mean Difference	0	
df	30	
t Stat	3.771498228	
P(T<=t) one-tail	0.000356297	
t Critical one-tail	1.697260887	
P(T<=t) two-tail	0.00071259	
t Critical two-tail	2.042272456	

Empty Grave vs Full Grave

F-Test Two-Sample for Variances	*Variable 1*	*Variable 2*
Mean	0.55574	0.414306667
Variance	0.009130516	0.002437868
Observations	10	15
df	9	14
F	3.745287568	
P(F<=f) one-tail	0.013578566	
F Critical one-tail	2.645790735	
t-Test: Two-Sample Assuming Unequal Variances		
Mean	0.55574	0.414306667
Variance	0.009130516	0.002437868
Observations	10	15
Hypothesized Mean Difference	0	
df	12	
t Stat	4.312520785	
P(T<=t) one-tail	0.00050467	
t Critical one-tail	1.782287556	
P(T<=t) two-tail	0.00100934	
t Critical two-tail	2.17881283	

10/06/2006

Undisturbed Vegetation vs Full Grave

F-Test Two-Sample for Variances	*Variable 1*	*Variable 2*
Mean	0.71895	0.53853333
Variance	0.024741124	0.00244213
Observations	30	15
df	29	14
F	10.13094527	
P(F<=f) one-tail	2.22182E-05	
F Critical one-tail	2.313868369	
t-Test: Two-Sample Assuming Unequal Variances		
Mean	0.71895	0.53853333
Variance	0.024741124	0.00244213
Observations	30	15
Hypothesized Mean Difference	0	
df	38	
t Stat	5.74123379	
P(T<=t) one-tail	6.44664E-07	
t Critical one-tail	1.68595446	
P(T<=t) two-tail	0.000001289	
t Critical two-tail	2.024394164	

Undisturbed Vegetation vs Empty Grave

F-Test Two-Sample for Variances	*Variable 1*	*Variable 2*
Mean	0.71895	0.63216
Variance	0.024741124	0.00604086
Observations	30	10
df	29	9
F	4.095629123	
P(F<=f) one-tail	0.015704543	
F Critical one-tail	2.868783172	
t-Test: Two-Sample Assuming Unequal Variances		
Mean	0.71895	0.63216
Variance	0.024741124	0.00604086
Observations	30	10
Hypothesized Mean Difference	0	
df	32	
t Stat	2.296071778	
P(T<=t) one-tail	0.014184674	
t Critical one-tail	1.693888748	
P(T<=t) two-tail	0.028369348	
t Critical two-tail	2.036933343	

Empty Grave vs Full Grave

F-Test Two-Sample for Variances	*Variable 1*	*Variable 2*
Mean	0.63216	0.538533333
Variance	0.00604086	0.002442134
Observations	10	15
df	9	14
F	2.473599285	
P(F<=f) one-tail	0.062474723	
F Critical one-tail	2.645790735	
t-Test: Two-Sample Assuming Unequal Variances		
Mean	0.63216	0.538533333
Variance	0.00604086	0.002442134
Observations	10	15
Hypothesized Mean Difference	0	
df	14	
t Stat	3.380894497	
P(T<=t) one-tail	0.002239982	
t Critical one-tail	1.761310136	
P(T<=t) two-tail	0.004479964	
t Critical two-tail	2.144786688	

31/07/2007

Undisturbed Vegetation vs Full Grave

F-Test Two-Sample for Variances	*Variable 1*	*Variable 2*
Mean	0.538853333	0.582606667
Variance	0.013096357	0.001364372
Observations	30	15
df	29	14
F	9.598816264	
P(F<=f) one-tail	3.09283E-05	
F Critical one-tail	2.313868369	
t-Test: Two-Sample Assuming Unequal Variances		
Mean	0.538853333	0.582606667
Variance	0.013096357	0.001364372
Observations	30	15
Hypothesized Mean Difference	0	
df	39	
t Stat	-1.905015545	
P(T<=t) one-tail	0.032085575	
t Critical one-tail	1.684875122	
P(T<=t) two-tail	0.064171150	
t Critical two-tail	2.02269092	

Undisturbed Vegetation vs Empty Grave

F-Test Two-Sample for Variances	*Variable 1*	*Variable 2*
Mean	0.538853333	0.54782
Variance	0.013096357	0.003005168
Observations	30	10
df	29	9
F	4.357944421	
P(F<=f) one-tail	0.012663065	
F Critical one-tail	2.868783172	
t-Test: Two-Sample Assuming Unequal Variances		
Mean	0.538853333	0.54782
Variance	0.013096357	0.003005168
Observations	30	10
Hypothesized Mean Difference	0	
df	33	
t Stat	-0.330277502	
P(T<=t) one-tail	0.371638999	
t Critical one-tail	1.692360309	
P(T<=t) two-tail	0.743277998	
t Critical two-tail	2.034515297	

Empty Grave vs Full Grave

F-Test Two-Sample for Variances	*Variable 1*	*Variable 2*
Mean	0.54782	0.582606667
Variance	0.003005168	0.001364372
Observations	10	15
df	9	14
F	2.202601809	
P(F<=f) one-tail	0.089613747	
F Critical one-tail	2.645790735	
t-Test: Two-Sample Assuming Unequal Variances		
Mean	0.54782	0.582606667
Variance	0.003005168	0.001364372
Observations	10	15
Hypothesized Mean Difference	0	
df	14	
t Stat	-1.758169768	
P(T<=t) one-tail	0.050274956	
t Critical one-tail	1.761310136	
P(T<=t) two-tail	0.100549912	
t Critical two-tail	2.144786688	

08/06/2008

Undisturbed Vegetation vs Full Grave

F-Test Two-Sample for Variances	*Variable 1*	*Variable 2*
Mean	0.718016667	0.671653333
Variance	0.027889938	0.001293264
Observations	30	15
df	29	14
F	21.56553955	
P(F<=f) one-tail	1.77029E-07	
F Critical one-tail	2.313868369	
t-Test: Two-Sample Assuming Unequal Variances		
Mean	0.718016667	0.671653333
Variance	0.027889938	0.001293264
Observations	30	15
Hypothesized Mean Difference	0	
df	34	
t Stat	1.454631459	
P(T<=t) one-tail	0.077470939	
t Critical one-tail	1.690924255	
P(T<=t) two-tail	0.154941877	
t Critical two-tail	2.032244509	

Undisturbed Vegetation vs Empty Grave

F-Test Two-Sample for Variances	*Variable 1*	*Variable 2*
Mean	0.718016667	0.63686
Variance	0.027889938	0.005485105
Observations	30	10
df	29	9
F	5.084668125	
P(F<=f) one-tail	0.007309329	
F Critical one-tail	2.868783172	
t-Test: Two-Sample Assuming Unequal Variances		
Mean	0.718016667	0.63686
Variance	0.027889938	0.005485105
Observations	30	10
Hypothesized Mean Difference	0	
df	35	
t Stat	2.110868901	
P(T<=t) one-tail	0.020999533	
t Critical one-tail	1.689572458	
P(T<=t) two-tail	0.041999065	
t Critical two-tail	2.030107928	

Empty Grave vs Full Grave

F-Test Two-Sample for Variances	*Variable 1*	*Variable 2*
Mean	0.63686	0.671653333
Variance	0.005485105	0.001293264
Observations	10	15
df	9	14
F	4.241287537	
P(F<=f) one-tail	0.008024595	
F Critical one-tail	2.645790735	
t-Test: Two-Sample Assuming Unequal Variances		
Mean	0.63686	0.671653333
Variance	0.005485105	0.001293264
Observations	10	15
Hypothesized Mean Difference	0	
df	12	
t Stat	-1.38102702	
P(T<=t) one-tail	0.096223848	
t Critical one-tail	1.782287556	
P(T<=t) two-tail	0.192447696	
t Critical two-tail	2.17881283	

01/05/2009

Undisturbed Vegetation vs Full Grave

F-Test Two-Sample for Variances	*Variable 1*	*Variable 2*
Mean	0.6584	0.63082
Variance	0.030558262	0.000954502
Observations	30	15
df	29	14
F	32.01488443	
P(F<=f) one-tail	1.27436E-08	
F Critical one-tail	2.313868369	
t-Test: Two-Sample Assuming Unequal Variances		
Mean	0.6584	0.63082
Variance	0.030558262	0.000954502
Observations	30	15
Hypothesized Mean Difference	0	
df	32	
t Stat	0.838362865	
P(T<=t) one-tail	0.204022897	
t Critical one-tail	1.693888748	
P(T<=t) two-tail	0.408045793	
t Critical two-tail	2.036933343	

Undisturbed Vegetation vs Empty Grave

F-Test Two-Sample for Variances	*Variable 1*	*Variable 2*
Mean	0.6584	0.5928
Variance	0.030558262	0.007101609
Observations	30	10
df	29	9
F	4.303005495	
P(F<=f) one-tail	0.01323639	
F Critical one-tail	2.868783172	
t-Test: Two-Sample Assuming Unequal Variances		
Mean	0.6584	0.5928
Variance	0.030558262	0.007101609
Observations	30	10
Hypothesized Mean Difference	0	
df	33	
t Stat	1.577739425	
P(T<=t) one-tail	0.062082351	
t Critical one-tail	1.692360309	
P(T<=t) two-tail	0.124164701	
t Critical two-tail	2.034515297	

Empty Grave vs Full Grave

F-Test Two-Sample for Variances	*Variable 1*	*Variable 2*
Mean	0.5928	0.63082
Variance	0.007101609	0.000954502
Observations	10	15
df	9	14
F	7.44012167	
P(F<=f) one-tail	0.000529678	
F Critical one-tail	2.645790735	
t-Test: Two-Sample Assuming Unequal Variances		
Mean	0.5928	0.63082
Variance	0.007101609	0.000954502
Observations	10	15
Hypothesized Mean Difference	0	
df	11	
t Stat	-1.366782278	
P(T<=t) one-tail	0.099488848	
t Critical one-tail	1.795884819	
P(T<=t) two-tail	0.198977695	
t Critical two-tail	2.20098516	

25/09/2010

Undisturbed Vegetation vs Full Grave

F-Test Two-Sample for Variances	*Variable 1*	*Variable 2*
Mean	0.636643333	0.663666667
Variance	0.032346652	0.001354758
Observations	30	15
df	29	14
F	23.87633011	
P(F<=f) one-tail	9.03348E-08	
F Critical one-tail	2.313868369	
t-Test: Two-Sample Assuming Unequal Variances		
Mean	0.636643333	0.663666667
Variance	0.032346652	0.001354758
Observations	30	15
Hypothesized Mean Difference	0	
df	34	
t Stat	-0.790528127	
P(T<=t) one-tail	0.217349517	
t Critical one-tail	1.690924255	
P(T<=t) two-tail	0.434699033	
t Critical two-tail	2.032244509	

Undisturbed Vegetation vs Empty Grave

F-Test Two-Sample for Variances	*Variable 1*	*Variable 2*
Mean	0.636643333	0.6357
Variance	0.032346652	0.008621993
Observations	30	10
df	29	9
F	3.751644226	
P(F<=f) one-tail	0.021154279	
F Critical one-tail	2.868783172	
t-Test: Two-Sample Assuming Unequal Variances		
Mean	0.636643333	0.6357
Variance	0.032346652	0.008621993
Observations	30	10
Hypothesized Mean Difference	0	
df	31	
t Stat	0.021414956	
P(T<=t) one-tail	0.491525946	
t Critical one-tail	1.695518783	
P(T<=t) two-tail	0.983051892	
t Critical two-tail	2.039513446	

Empty Grave vs Full Grave

F-Test Two-Sample for Variances	*Variable 1*	*Variable 2*
Mean	0.6357	0.663666667
Variance	0.008621993	0.001354758
Observations	10	15
df	9	14
F	6.364230901	
P(F<=f) one-tail	0.001186684	
F Critical one-tail	2.645790735	
t-Test: Two-Sample Assuming Unequal Variances		
Mean	0.6357	0.663666667
Variance	0.008621993	0.001354758
Observations	10	15
Hypothesized Mean Difference	0	
df	11	
t Stat	-0.906159073	
P(T<=t) one-tail	0.192135643	
t Critical one-tail	1.795884819	
P(T<=t) two-tail	0.384271285	
t Critical two-tail	2.20098516	

30/04/2011

Undisturbed Vegetation vs Full Grave

F-Test Two-Sample for Variances	*Variable 1*	*Variable 2*
Mean	0.649723333	0.6038667
Variance	0.010602044	0.0005772
Observations	30	15
df	29	14
F	18.36852923	
P(F<=f) one-tail	5.06891E-07	
F Critical one-tail	2.313868369	
t-Test: Two-Sample Assuming Unequal Variances		
Mean	0.649723333	0.6038667
Variance	0.010602044	0.0005772
Observations	30	15
Hypothesized Mean Difference	0	
df	35	
t Stat	2.316464596	
P(T<=t) one-tail	0.013255001	
t Critical one-tail	1.689572458	
P(T<=t) two-tail	0.026510001	
t Critical two-tail	2.030107928	

Undisturbed Vegetation vs Empty Grave

F-Test Two-Sample for Variances	*Variable 1*	*Variable 2*
Mean	0.649723333	0.64031
Variance	0.010602044	0.00086125
Observations	30	10
df	29	9
F	12.3100671	
P(F<=f) one-tail	0.000231131	
F Critical one-tail	2.868783172	
t-Test: Two-Sample Assuming Unequal Variances		
Mean	0.649723333	0.64031
Variance	0.010602044	0.00086125
Observations	30	10
Hypothesized Mean Difference	0	
df	38	
t Stat	0.449004743	
P(T<=t) one-tail	0.327989284	
t Critical one-tail	1.68595446	
P(T<=t) two-tail	0.655978568	
t Critical two-tail	2.024394164	

Empty Grave vs Full Grave

F-Test Two-Sample for Variances	*Variable 1*	*Variable 2*
Mean	0.64031	0.603866667
Variance	0.00086125	0.000577185
Observations	10	15
df	9	14
F	1.492155087	
P(F<=f) one-tail	0.24212229	
F Critical one-tail	2.645790735	
t-Test: Two-Sample Assuming Unequal Variances		
Mean	0.64031	0.603866667
Variance	0.00086125	0.000577185
Observations	10	15
Hypothesized Mean Difference	0	
df	17	
t Stat	3.264766256	
P(T<=t) one-tail	0.002282109	
t Critical one-tail	1.739606726	
P(T<=t) two-tail	0.004564218	
t Critical two-tail	2.109815578	

Statistical Significance – RapidEye

19/08/2009

Undisturbed Vegetation vs Full Grave

F-Test Two-Sample for Variances	*Variable 1*	*Variable 2*
Mean	0.761738667	0.655465467
Variance	0.006001706	0.001606063
Observations	30	15
df	29	14
F	3.73690531	
P(F<=f) one-tail	0.005987306	
F Critical one-tail	2.313868369	
t-Test: Two-Sample Assuming Unequal Variances		
Mean	0.761738667	0.655465467
Variance	0.006001706	0.001606063
Observations	30	15
Hypothesized Mean Difference	0	
df	43	
t Stat	6.064070162	
P(T<=t) one-tail	1.47513E-07	
t Critical one-tail	1.681070703	
P(T<=t) two-tail	0.000000295	
t Critical two-tail	2.016692199	

Undisturbed Vegetation vs Empty Grave

F-Test Two-Sample for Variances	*Variable 1*	*Variable 2*
Mean	0.761738667	0.6898004
Variance	0.006001706	0.001509531
Observations	30	10
df	29	9
F	3.975873934	
P(F<=f) one-tail	0.017384257	
F Critical one-tail	2.868783172	
t-Test: Two-Sample Assuming Unequal Variances		
Mean	0.761738667	0.6898004
Variance	0.006001706	0.001509531
Observations	30	10
Hypothesized Mean Difference	0	
df	31	
t Stat	3.83972582	
P(T<=t) one-tail	0.000284571	
t Critical one-tail	1.695518783	
P(T<=t) two-tail	0.000569142	
t Critical two-tail	2.039513446	

Full Grave vs Empty Grave

F-Test Two-Sample for Variances	*Variable 1*	*Variable 2*
Mean	0.655465467	0.6898004
Variance	0.001606063	0.001509531
Observations	15	10
df	14	9
F	1.063948268	
P(F<=f) one-tail	0.477746871	
F Critical one-tail	3.025472724	
t-Test: Two-Sample Assuming Equal Variances		
Mean	0.655465467	0.6898004
Variance	0.001606063	0.001509531
Observations	15	10
Pooled Variance	0.00156829	
Hypothesized Mean Difference	0	
df	23	
t Stat	-2.12372685	
P(T<=t) one-tail	0.022332424	
t Critical one-tail	1.713871528	
P(T<=t) two-tail	0.044664847	
t Critical two-tail	2.06865761	

17/04/2010

Undisturbed Vegetation vs Full Grave

F-Test Two-Sample for Variances	*Variable 1*	*Variable 2*
Mean	0.628198267	0.576748867
Variance	0.003704773	0.000908941
Observations	30	15
df	29	14
F	4.075922162	
P(F<=f) one-tail	0.003884661	
F Critical one-tail	2.313868369	
t-Test: Two-Sample Assuming Unequal Variances		
Mean	0.628198267	0.576748867
Variance	0.003704773	0.000908941
Observations	30	15
Hypothesized Mean Difference	0	
df	43	
t Stat	3.791988103	
P(T<=t) one-tail	0.000230796	
t Critical one-tail	1.681070703	
P(T<=t) two-tail	0.000461591	
t Critical two-tail	2.016692199	

Undisturbed Vegetation vs Empty Grave

F-Test Two-Sample for Variances	*Variable 1*	*Variable 2*
Mean	0.628198267	0.5675089
Variance	0.003704773	0.001151771
Observations	30	10
df	29	9
F	3.216588169	
P(F<=f) one-tail	0.034991421	
F Critical one-tail	2.868783172	
t-Test: Two-Sample Assuming Unequal Variances		
Mean	0.628198267	0.5675089
Variance	0.003704773	0.001151771
Observations	30	10
Hypothesized Mean Difference	0	
df	28	
t Stat	3.92838549	
P(T<=t) one-tail	0.000254498	
t Critical one-tail	1.701130934	
P(T<=t) two-tail	0.000508997	
t Critical two-tail	2.048407142	

Empty Grave vs Full Grave

F-Test Two-Sample for Variances	*Variable 1*	*Variable 2*
Mean	0.5675089	0.576748867
Variance	0.001151771	0.000908941
Observations	10	15
df	9	14
F	1.267156984	
P(F<=f) one-tail	0.333438066	
F Critical one-tail	2.645790735	
t-Test: Two-Sample Assuming Unequal Variances		
Mean	0.5675089	0.576748867
Variance	0.001151771	0.000908941
Observations	10	15
Hypothesized Mean Difference	0	
df	18	
t Stat	-0.69693792	
P(T<=t) one-tail	0.247372501	
t Critical one-tail	1.734063607	
P(T<=t) two-tail	0.494745003	
t Critical two-tail	2.10092204	

16/08/2010

Undisturbed Vegetation vs Full Grave

F-Test Two-Sample for Variances	*Variable 1*	*Variable 2*
Mean	0.6204385	0.421541267
Variance	0.003796737	0.000989878
Observations	30	15
df	29	14
F	3.83555861	
P(F<=f) one-tail	0.005265701	
F Critical one-tail	2.313868369	
t-Test: Two-Sample Assuming Unequal Variances		
Mean	0.6204385	0.421541267
Variance	0.003796737	0.000989878
Observations	30	15
Hypothesized Mean Difference	0	
df	43	
t Stat	14.33366416	
P(T<=t) one-tail	2.77143E-18	
t Critical one-tail	1.681070703	
P(T<=t) two-tail	5.54287E-18	
t Critical two-tail	2.016692199	

Undisturbed Vegetation vs Empty Grave

F-Test Two-Sample for Variances	*Variable 1*	*Variable 2*
Mean	0.6204385	0.3384699
Variance	0.003796737	0.001820849
Observations	30	10
df	29	9
F	2.08514587	
P(F<=f) one-tail	0.123687266	
F Critical one-tail	2.868783172	
t-Test: Two-Sample Assuming Unequal Variances		
Mean	0.6204385	0.3384699
Variance	0.003796737	0.001820849
Observations	30	10
Hypothesized Mean Difference	0	
df	22	
t Stat	16.0499118	
P(T<=t) one-tail	0.0000000	
t Critical one-tail	1.7171444	
P(T<=t) two-tail	0.0000000	
t Critical two-tail	2.0738731	

Empty Grave vs Full Grave

F-Test Two-Sample for Variances	*Variable 1*	*Variable 2*
Mean	0.3384699	0.421541267
Variance	0.001820849	0.000989878
Observations	10	15
df	9	14
F	1.839467763	
P(F<=f) one-tail	0.147925571	
F Critical one-tail	2.645790735	
t-Test: Two-Sample Assuming Equal Variances		
Mean	0.3384699	0.421541267
Variance	0.001820849	0.000989878
Observations	10	15
Pooled Variance	0.001315041	
Hypothesized Mean Difference	0	
df	23	
t Stat	-5.6112205	
P(T<=t) one-tail	0.0000052	
t Critical one-tail	1.7138715	
P(T<=t) two-tail	0.0000104	
t Critical two-tail	2.0686576	

14/03/2011

Undisturbed Vegetation vs Full Grave

F-Test Two-Sample for Variances	*Variable 1*	*Variable 2*
Mean	0.454434967	0.439140267
Variance	0.002658899	0.001034753
Observations	30	15
df	29	14
F	2.569596217	
P(F<=f) one-tail	0.032789185	
F Critical one-tail	2.313868369	
t-Test: Two-Sample Assuming Unequal Variances		
Mean	0.454434967	0.439140267
Variance	0.002658899	0.001034753
Observations	30	15
Hypothesized Mean Difference	0	
df	41	
t Stat	1.218271917	
P(T<=t) one-tail	0.115042441	
t Critical one-tail	1.682878002	
P(T<=t) two-tail	0.230084882	
t Critical two-tail	2.01954097	

Undisturbed Vegetation vs Empty Grave

F-Test Two-Sample for Variances	*Variable 1*	*Variable 2*
Mean	0.454434967	0.4567403
Variance	0.002658899	0.00016304
Observations	30	10
df	29	9
F	16.30821467	
P(F<=f) one-tail	7.15614E-05	
F Critical one-tail	2.868783172	
t-Test: Two-Sample Assuming Unequal Variances		
Mean	0.454434967	0.4567403
Variance	0.002658899	0.00016304
Observations	30	10
Hypothesized Mean Difference	0	
df	37	
t Stat	-0.22504824	
P(T<=t) one-tail	0.411590044	
t Critical one-tail	1.68709362	
P(T<=t) two-tail	0.823180087	
t Critical two-tail	2.026192463	

Full Grave vs Empty Grave

F-Test Two-Sample for Variances	*Variable 1*	*Variable 2*
Mean	0.439140267	0.4567403
Variance	0.001034753	0.00016304
Observations	15	10
df	14	9
F	6.34660596	
P(F<=f) one-tail	0.004300318	
F Critical one-tail	3.025472724	
t-Test: Two-Sample Assuming Unequal Variances		
Mean	0.439140267	0.4567403
Variance	0.001034753	0.00016304
Observations	15	10
Hypothesized Mean Difference	0	
df	20	
t Stat	-1.90577016	
P(T<=t) one-tail	0.035578062	
t Critical one-tail	1.724718243	
P(T<=t) two-tail	0.071156123	
t Critical two-tail	2.085963447	

25/03/2011

Undisturbed Vegetation vs Full Grave

F-Test Two-Sample for Variances	*Variable 1*	*Variable 2*
Mean	0.5278934	0.4912512
Variance	0.003351889	0.000348659
Observations	30	15
df	29	14
F	9.613671367	
P(F<=f) one-tail	3.06375E-05	
F Critical one-tail	2.313868369	
t-Test: Two-Sample Assuming Unequal Variances		
Mean	0.5278934	0.4912512
Variance	0.003351889	0.000348659
Observations	30	15
Hypothesized Mean Difference	0	
df	39	
t Stat	3.153967437	
P(T<=t) one-tail	0.001548367	
t Critical one-tail	1.684875122	
P(T<=t) two-tail	0.003096734	
t Critical two-tail	2.02269092	

Undisturbed Vegetation vs Empty Grave

F-Test Two-Sample for Variances	*Variable 1*	*Variable 2*
Mean	0.5278934	0.5243862
Variance	0.003351889	0.000138815
Observations	30	10
df	29	9
F	24.14640979	
P(F<=f) one-tail	1.34422E-05	
F Critical one-tail	2.868783172	
t-Test: Two-Sample Assuming Unequal Variances		
Mean	0.5278934	0.5243862
Variance	0.003351889	0.000138815
Observations	30	10
Hypothesized Mean Difference	0	
df	35	
t Stat	0.312929431	
P(T<=t) one-tail	0.378095697	
t Critical one-tail	1.689572458	
P(T<=t) two-tail	0.756191394	
t Critical two-tail	2.030107928	

Full Grave vs Empty Grave

F-Test Two-Sample for Variances	*Variable 1*	*Variable 2*
Mean	0.4912512	0.5243862
Variance	0.000348659	0.000138815
Observations	15	10
df	14	9
F	2.511674143	
P(F<=f) one-tail	0.08408145	
F Critical one-tail	3.025472724	
t-Test: Two-Sample Assuming Equal Variances		
Mean	0.4912512	0.5243862
Variance	0.000348659	0.000138815
Observations	15	10
Pooled Variance	0.000266546	
Hypothesized Mean Difference	0	
df	23	
t Stat	-4.97137508	
P(T<=t) one-tail	2.50372E-05	
t Critical one-tail	1.713871528	
P(T<=t) two-tail	0.00005007	
t Critical two-tail	2.06865761	

22/04/2011

Undisturbed Vegetation vs Full Grave

F-Test Two-Sample for Variances	*Variable 1*	*Variable 2*
Mean	0.700558033	0.670094467
Variance	0.002347941	0.000821634
Observations	30	15
df	29	14
F	2.857647222	
P(F<=f) one-tail	0.020843971	
F Critical one-tail	2.313868369	
t-Test: Two-Sample Assuming Unequal Variances		
Mean	0.700558033	0.670094467
Variance	0.002347941	0.000821634
Observations	30	15
Hypothesized Mean Difference	0	
df	42	
t Stat	2.64112606	
P(T<=t) one-tail	0.005777232	
t Critical one-tail	1.681952357	
P(T<=t) two-tail	0.011554464	
t Critical two-tail	2.018081703	

Undisturbed Vegetation vs Empty Grave

F-Test Two-Sample for Variances	*Variable 1*	*Variable 2*
Mean	0.700558033	0.7168026
Variance	0.002347941	0.000626854
Observations	30	10
df	29	9
F	3.745592642	
P(F<=f) one-tail	0.021269035	
F Critical one-tail	2.868783172	
t-Test: Two-Sample Assuming Unequal Variances		
Mean	0.700558033	0.7168026
Variance	0.002347941	0.000626854
Observations	30	10
Hypothesized Mean Difference	0	
df	31	
t Stat	-1.36828135	
P(T<=t) one-tail	0.090530058	
t Critical one-tail	1.695518783	
P(T<=t) two-tail	0.181060115	
t Critical two-tail	2.039513446	

Full Grave vs Empty Grave

F-Test Two-Sample for Variances	*Variable 1*	*Variable 2*
Mean	0.670094467	0.7168026
Variance	0.000821634	0.000626854
Observations	15	10
df	14	9
F	1.310726045	
P(F<=f) one-tail	0.348675384	
F Critical one-tail	3.025472724	
t-Test: Two-Sample Assuming Equal Variances		
Mean	0.670094467	0.7168026
Variance	0.000821634	0.000626854
Observations	15	10
Pooled Variance	0.000745416	
Hypothesized Mean Difference	0	
df	23	
t Stat	-4.19052838	
P(T<=t) one-tail	0.000175101	
t Critical one-tail	1.713871528	
P(T<=t) two-tail	0.000350201	
t Critical two-tail	2.06865761	

23/04/2011

Undisturbed Vegetation vs Full Grave

F-Test Two-Sample for Variances	*Variable 1*	*Variable 2*
Mean	0.685062933	0.609035933
Variance	0.002873375	0.000442457
Observations	30	15
df	29	14
F	6.494138273	
P(F<=f) one-tail	0.00031302	
F Critical one-tail	2.313868369	
t-Test: Two-Sample Assuming Unequal Variances		
Mean	0.685062933	0.609035933
Variance	0.002873375	0.000442457
Observations	30	15
Hypothesized Mean Difference	0	
df	41	
t Stat	6.7925586849	
P(T<=t) one-tail	0.0000000162	
t Critical one-tail	1.6828780021	
P(T<=t) two-tail	0.0000000324	
t Critical two-tail	2.0195409704	

Undisturbed Vegetation vs Empty Grave

F-Test Two-Sample for Variances	*Variable 1*	*Variable 2*
Mean	0.685062933	0.6620874
Variance	0.002873375	0.000335352
Observations	30	10
df	29	9
F	8.568231736	
P(F<=f) one-tail	0.00100176	
F Critical one-tail	2.868783172	
t-Test: Two-Sample Assuming Unequal Variances		
Mean	0.685062933	0.6620874
Variance	0.002873375	0.000335352
Observations	30	10
Hypothesized Mean Difference	0	
df	38	
t Stat	2.0204223151	
P(T<=t) one-tail	0.0252144424	
t Critical one-tail	1.6859544602	
P(T<=t) two-tail	0.0504288847	
t Critical two-tail	2.0243941639	

Full Grave vs Empty Grave

F-Test Two-Sample for Variances	*Variable 1*	*Variable 2*
Mean	0.609035933	0.6620874
Variance	0.000442457	0.000335352
Observations	15	10
df	14	9
F	1.31937932	
P(F<=f) one-tail	0.344835753	
F Critical one-tail	3.025472724	
t-Test: Two-Sample Assuming Equal Variances		
Mean	0.609035933	0.6620874
Variance	0.000442457	0.000335352
Observations	15	10
Pooled Variance	0.000400546	
Hypothesized Mean Difference	0	
df	23	
t Stat	-6.4930189023	
P(T<=t) one-tail	0.0000006309	
t Critical one-tail	1.7138715277	
P(T<=t) two-tail	0.0000012618	
t Critical two-tail	2.0686576104	

02/05/2011

Undisturbed Vegetation vs Full Grave

F-Test Two-Sample for Variances	*Variable 1*	*Variable 2*
Mean	0.772633833	0.730937333
Variance	0.002339831	0.000796976
Observations	30	15
df	29	14
F	2.935887271	
P(F<=f) one-tail	0.018504195	
F Critical one-tail	2.313868369	
t-Test: Two-Sample Assuming Unequal Variances		
Mean	0.772633833	0.730937333
Variance	0.002339831	0.000796976
Observations	30	15
Hypothesized Mean Difference	0	
df	42	
t Stat	3.641288567	
P(T<=t) one-tail	0.000369212	
t Critical one-tail	1.681952357	
P(T<=t) two-tail	0.000738424	
t Critical two-tail	2.018081703	

Undisturbed Vegetation vs Empty Grave

F-Test Two-Sample for Variances	*Variable 1*	*Variable 2*
Mean	0.772633833	0.7767144
Variance	0.002339831	0.000429441
Observations	30	10
df	29	9
F	5.448543263	
P(F<=f) one-tail	0.005677738	
F Critical one-tail	2.868783172	
t-Test: Two-Sample Assuming Unequal Variances		
Mean	0.772633833	0.7767144
Variance	0.002339831	0.000429441
Observations	30	10
Hypothesized Mean Difference	0	
df	35	
t Stat	-0.37105491	
P(T<=t) one-tail	0.356416615	
t Critical one-tail	1.689572458	
P(T<=t) two-tail	0.71283323	
t Critical two-tail	2.030107928	

Full Grave vs Empty Grave

F-Test Two-Sample for Variances	*Variable 1*	*Variable 2*
Mean	0.730937333	0.7767144
Variance	0.000796976	0.000429441
Observations	15	10
df	14	9
F	1.855842122	
P(F<=f) one-tail	0.17663797	
F Critical one-tail	3.025472724	
t-Test: Two-Sample Assuming Equal Variances		
Mean	0.730937333	0.7767144
Variance	0.000796976	0.000429441
Observations	15	10
Pooled Variance	0.000653158	
Hypothesized Mean Difference	0	
df	23	
t Stat	-4.38747333	
P(T<=t) one-tail	0.000107162	
t Critical one-tail	1.713871528	
P(T<=t) two-tail	0.000214325	
t Critical two-tail	2.06865761	

03/05/2011

Undisturbed Vegetation vs Full Grave

F-Test Two-Sample for Variances	*Variable 1*	*Variable 2*
Mean	0.774999533	0.719240267
Variance	0.002631912	0.001709727
Observations	30	15
df	29	14
F	1.539375652	
P(F<=f) one-tail	0.198613499	
F Critical one-tail	2.313868369	
t-Test: Two-Sample Assuming Equal Variances		
Mean	0.774999533	0.719240267
Variance	0.002631912	0.001709727
Observations	30	15
Pooled Variance	0.002331666	
Hypothesized Mean Difference	0	
df	43	
t Stat	3.651605815	
P(T<=t) one-tail	0.000351146	
t Critical one-tail	1.681070703	
P(T<=t) two-tail	0.000702292	
t Critical two-tail	2.016692199	

Undisturbed Vegetation vs Empty Grave

F-Test Two-Sample for Variances	*Variable 1*	*Variable 2*
Mean	0.774999533	0.7765084
Variance	0.002631912	0.00034689
Observations	30	10
df	29	9
F	7.587167892	
P(F<=f) one-tail	0.001615949	
F Critical one-tail	2.868783172	
t-Test: Two-Sample Assuming Unequal Variances		
Mean	0.774999533	0.7765084
Variance	0.002631912	0.00034689
Observations	30	10
Hypothesized Mean Difference	0	
df	38	
t Stat	-0.13637216	
P(T<=t) one-tail	0.446123504	
t Critical one-tail	1.68595446	
P(T<=t) two-tail	0.892247008	
t Critical two-tail	2.024394164	

Full Grave vs Empty Grave

F-Test Two-Sample for Variances	*Variable 1*	*Variable 2*
Mean	0.719240267	0.7765084
Variance	0.001709727	0.00034689
Observations	15	10
df	14	9
F	4.928730608	
P(F<=f) one-tail	0.010544913	
F Critical one-tail	3.025472724	
t-Test: Two-Sample Assuming Unequal Variances		
Mean	0.719240267	0.7765084
Variance	0.001709727	0.00034689
Observations	15	10
Hypothesized Mean Difference	0	
df	21	
t Stat	-4.69677966	
P(T<=t) one-tail	6.15024E-05	
t Critical one-tail	1.720742903	
P(T<=t) two-tail	0.000123005	
t Critical two-tail	2.079613845	

14/07/2011

Undisturbed Vegetation vs Full Grave

F-Test Two-Sample for Variances	*Variable 1*	*Variable 2*
Mean	0.4808331	0.586850067
Variance	0.005657979	0.000404814
Observations	30	15
df	29	14
F	13.9767404	
P(F<=f) one-tail	2.95458E-06	
F Critical one-tail	2.313868369	
t-Test: Two-Sample Assuming Unequal Variances		
Mean	0.4808331	0.586850067
Variance	0.005657979	0.000404814
Observations	30	15
Hypothesized Mean Difference	0	
df	36	
t Stat	-7.220448762	
P(T<=t) one-tail	8.45197E-09	
t Critical one-tail	1.688297714	
P(T<=t) two-tail	0.0000000169	
t Critical two-tail	2.028094001	

Undisturbed Vegetation vs Empty Grave

F-Test Two-Sample for Variances	*Variable 1*	*Variable 2*
Mean	0.4808331	0.6175974
Variance	0.005657979	0.001279437
Observations	30	10
df	29	9
F	4.422242958	
P(F<=f) one-tail	0.012029809	
F Critical one-tail	2.868783172	
t-Test: Two-Sample Assuming Unequal Variances		
Mean	0.4808331	0.6175974
Variance	0.005657979	0.001279437
Observations	30	10
Hypothesized Mean Difference	0	
df	33	
t Stat	-7.686991831	
P(T<=t) one-tail	3.74983E-09	
t Critical one-tail	1.692360309	
P(T<=t) two-tail	0.0000000075	
t Critical two-tail	2.034515297	

Full Grave vs Empty Grave

F-Test Two-Sample for Variances	*Variable 1*	*Variable 2*
Mean	0.586850067	0.6175974
Variance	0.000404814	0.001279437
Observations	15	10
df	14	9
F	0.316400164	
P(F<=f) one-tail	0.026488181	
F Critical one-tail	0.377958841	
t-Test: Two-Sample Assuming Equal Variances		
Mean	0.586850067	0.6175974
Variance	0.000404814	0.001279437
Observations	15	10
Pooled Variance	0.000747058	
Hypothesized Mean Difference	0	
df	23	
t Stat	-2.755535762	
P(T<=t) one-tail	0.005630421	
t Critical one-tail	1.713871528	
P(T<=t) two-tail	0.0112608426	
t Critical two-tail	2.06865761	

Table 3-29 - Monthly meteorological data for the Ross-on-Wye station

Year	Month	TMax (°C)	TMin (°C)	Rain (mm)	Sun Hours
1997	Jan	5.2	-0.2	9.0	36.3
1997	Feb	10.4	3.9	95.0	70.5
1997	Mar	12.6	4.6	25.6	137.1
1997	Apr	14.7	4.8	25.9	177.9
1997	May	17.1	7.0	49.8	240.6
1997	Jun	18.7	10.8	103.9	122.2
1997	Jul	22.5	11.9	17.2	251.9
1997	Aug	23.8	14.6	130.0	181.1
1997	Sep	18.8	10.1	21.7	145.6
1997	Oct	14.4	5.9	57.1	138.9
1997	Nov	11.8	6.0	95.5	48.5
1997	Dec	9.0	3.5	60.9	44.1
1998	Jan	8.1	3.0	124.3	48.1
1998	Feb	11.3	4.3	12.6	92.7
1998	Mar	12.1	5.1	75.6	84.6
1998	Apr	11.9	4.5	122.0	111.9
1998	May	19.2	8.7	9.9	243.3
1998	Jun	18.5	11.3	89.4	152.3
1998	Jul	20.3	12.1	16.4	177.2
1998	Aug	21.7	11.3	28.6	241.5
1998	Sep	19.2	11.4	83.0	134.4
1998	Oct	14.2	7.6	108.8	96.9
1998	Nov	9.9	3.3	50.1	78.9
1998	Dec	9.2	2.5	60.5	34.7
1999	Jan	9.2	3.2	129.1	50.7
1999	Feb	8.9	2.7	32.1	78.4
1999	Mar	11.2	3.9	47.2	100.4
1999	Apr	14.0	5.9	75.4	151.2
1999	May	17.5	9.4	55.6	149.1
1999	Jun	19.3	9.4	49.2	200.2
1999	Jul	24.0	13.1	6.4	261.7
1999	Aug	21.2	12.3	116.9	174.6
1999	Sep	20.2	11.2	112.8	178.3
1999	Oct	14.8	6.9	82.6	129.6
1999	Nov	10.9	4.9	43.0	70.3
1999	Dec	8.6	0.6	100.2	62.2
2000	Jan	8.4	0.5	21.9	54.7
2000	Feb	10.2	3.3	68.8	100.9
2000	Mar	12.0	4.4	20.3	137.2
2000	Apr	12.2	4.1	172.0	143.3
2000	May	16.9	7.8	57.4	181.9
2000	Jun	20.2	11.4	31.4	177.2
2000	Jul	21.0	11.8	36.1	179.3
2000	Aug	21.9	12.1	46.9	228.1
2000	Sep	19.4	11.2	85.1	122.6
2000	Oct	14.0	7.1	137.5	94.7
2000	Nov	10.2	4.4	144.5	59.0
2000	Dec	8.6	3.9	177.0	54.5
2001	Jan	6.4	1.0	60.6	67.5
2001	Feb	8.5	1.1	76.1	92.0
2001	Mar	8.7	2.3	103.3	81.1
2001	Apr	12.5	4.4	75.6	165.7
2001	May	18.2	7.6	37.6	205.5
2001	Jun	20.0	10.3	29.4	228.0
2001	Jul	22.2	12.5	78.9	207.4
2001	Aug	21.5	13.1	62.5	190.9
2001	Sep	17.9	10.1	31.3	127.9
2001	Oct	16.7	10.7	162.3	115.7
2001	Nov	11.3	3.9	33.4	63.2
2001	Dec	7.1	0.3	16.4	74.4
2002	Jan	9.2	2.9	79.2	40.8
2002	Feb	10.6	4.4	143.1	76.1
2002	Mar	12.0	4.3	29.8	113.0
2002	Apr	14.7	5.0	46.2	191.8
2002	May	16.5	8.0	81.9	192.1
2002	Jun	19.1	10.1	23.0	184.9
2002	Jul	21.0	11.8	55.9	202.0
2002	Aug	22.2	12.8	21.6	165.6
2002	Sep	19.8	10.2	19.7	168.6
2002	Oct	14.2	6.6	183.2	108.3
2002	Nov	12.1	6.5	110.8	64.5
2002	Dec	8.2	4.2	105.4	33.6
2003	Jan	7.8	2.1	52.5	91.7
2003	Feb	8.1	0.7	23.5	87.7
2003	Mar	13.1	2.7	27.9	162.0
2003	Apr	15.4	5.0	36.5	195.6

Year	Month	TMax (°C)	TMin (°C)	Rain (mm)	Sun Hours
2003	May	16.7	8.2	35.7	221.5
2003	Jun	21.9	11.3	51.1	237.6
2003	Jul	22.1	13.4	65.7	165.2
2003	Aug	24.3	13.6	9.9	215.4
2003	Sep	20.6	8.7	11.7	165.6
2003	Oct	13.8	4.9	46.4	138.8
2003	Nov	11.6	5.3	77.8	65.2
2003	Dec	8.7	2.1	83.8	45.4
2004	Jan	8.7	3.4	80.0	56.3
2004	Feb	8.7	2.9	29.6	96.2
2004	Mar	10.8	3.3	42.3	110.5
2004	Apr	14.2	5.9	77.7	138.7
2004	May	18.1	8.0	36.6	203.1
2004	Jun	21.1	11.7	36.0	248.9
2004	Jul	20.9	11.9	44.1	170.1
2004	Aug	22.5	13.6	85.7	212.1
2004	Sep	19.8	10.9	53.1	177.5
2004	Oct	14.1	8.0	140.6	105.1
2004	Nov	11.1	5.2	30.4	48.2
2004	Dec	9.1	3.0	36.1	57.5
2005	Jan	9.6	3.8	27.1	61.1
2005	Feb	7.9	2.0	32.1	76.5
2005	Mar	11.2	4.0	69.0	94.1
2005	Apr	13.9	5.3	52.5	156.8
2005	May	16.7	7.4	31.0	229.8
2005	Jun	21.0	11.5	48.0	216.1
2005	Jul	22.2	13.0	60.7	224.1
2005	Aug	22.2	11.5	24.5	245.2
2005	Sep	20.7	11.4	67.1	174.4
2005	Oct	16.6	10.6	131.6	82.1
2005	Nov	10.1	2.5	68.4	77.2
2005	Dec	8.5	1.1	65.2	50.8
2006	Jan	7.3	2.1	15.0	51.5
2006	Feb	6.7	1.2	30.8	68.0
2006	Mar	9.3	2.5	67.2	101.0
2006	Apr	14.0	5.3	17.5	157.9
2006	May	17.6	8.9	109.4	193.0
2006	Jun	22.6	11.6	17.2	259.9

Year	Month	TMax (°C)	TMin (°C)	Rain (mm)	Sun Hours
2006	Jul	26.8	14.4	34.3	309.6
2006	Aug	21.5	13.0	117.0	174.0
2006	Sep	21.5	12.6	57.6	157.7
2006	Oct	16.5	10.0	82.9	95.1
2006	Nov	12.1	4.4	94.5	102.6
2006	Dec	9.3	4.5	105.5	40.3
2007	Jan	10.5	4.8	66.6	60.3
2007	Feb	9.3	3.2	86.1	61.2
2007	Mar	11.8	3.4	73.8	162.7
2007	Apr	17.9	6.6	7.0	232.4
2007	May	17.0	8.3	139.9	172.9
2007	Jun	20.2	11.7	136.6	153.7
2007	Jul	19.6	11.7	161.1	205.8
2007	Aug	21.2	11.5	32.6	202.7
2007	Sep	18.9	10.1	49.1	153.6
2007	Oct	14.9	7.5	37.4	100.3
2007	Nov	11.2	3.6	51.2	75.9
2007	Dec	8.4	2.6	68.0	42.1
2008	Jan	10.3	3.9	101.7	44.1
2008	Feb	10.0	1.0	29.5	104.3
2008	Mar	10.7	3.7	100.2	125.6
2008	Apr	13.3	4.5	73.9	158.6
2008	May	18.6	9.6	101.8	167.6
2008	Jun	19.6	10.4	22.0	237.6
2008	Jul	21.6	12.5	86.8	195.2
2008	Aug	20.4	13.6	81.6	135.3
2008	Sep	17.7	9.9	111.1	94.7
2008	Oct	14.1	6.5	62.4	130.8
2008	Nov	10.6	4.8	76.2	62.7
2008	Dec	7.1	1.4	49.0	63.8
2009	Jan	6.4	0.1	71.7	54.4
2009	Feb	7.9	1.9	41.4	58.8
2009	Mar	12.0	2.8	24.7	142.9
2009	Apr	15.2	5.3	38.6	166.9
2009	May	17.5	8.2	37.7	224.3
2009	Jun	20.9	10.4	102.6	209.8
2009	Jul	20.8	12.6	143.8	177.4
2009	Aug	21.1	12.9	22.0	173.5

Year	Month	TMax (^{o}C)	TMin (^{o}C)	Rain (mm)	Sun Hours
2009	Sep	19.0	10.5	23.3	145.8
2009	Oct	15.7	8.8	49.5	94.3
2009	Nov	11.4	6.7	168.1	64.2
2009	Dec	6.1	0.3	86.0	50.0
2010	Jan	4.7	-1.7	73.4	65.8
2010	Feb	6.9	0.7	47.3	66.9
2010	Mar	10.8	2.1	47.2	133.5
2010	Apr	15.1	4.2	22.5	210.7
2010	May	17.0	7.0	48.7	205.7
2010	Jun	22.1	10.6	21.2	249.5
2010	Jul	22.0	13.6	47.2	148.8
2010	Aug	20.5	11.8	113.7	152.8
2010	Sep	18.4	9.9	38.5	119.7
2010	Oct	14.5	6.8	45.9	116.6
2010	Nov	8.6	2.3	61.4	59.0
2010	Dec	2.8	-4.3	21.1	27.2
2011	Jan	6.9	1.3	65.7	50.3
2011	Feb	9.9	4.5	38.4	51.5
2011	Mar	11.9	3.0	17.0	130.4
2011	Apr	18.6	6.6	7.0	210.4
2011	May	17.5	8.4	39.0	219.9
2011	Jun	19.2	9.5	38.3	192.3

Table 3-30 - Mean NDVI for the different surface types and the meteorological variables from the Ross on Wye meteorological station (one month prior to imagery collection) to derive relationships between NDVI and meteorological variables (1997-2011).

Imagery Date	Mean NDVI Full Grave	Mean NDVI Empty Grave	Mean NDVI Undisturbed Grass	Tmax (^{o}C)	Tmin (^{o}C)	Cumulative Rainfall (mm)	Sun Hours (Hours)
18/02/1997	0.484	0.435	0.433	5.2	-0.2	9.0	36.3
06/03/1997	0.637	0.581	0.551	10.4	3.9	95.0	70.5
22/03/1997	0.674	0.607	0.570	10.4	3.9	95.0	70.5
07/04/1997	0.752	0.684	0.625	12.6	4.6	25.6	137.1
25/05/1997	0.861	0.792	0.705	14.7	4.8	25.9	177.9
01/06/1997	0.862	0.812	0.743	17.1	7.0	49.8	240.6
17/06/1997	0.752	0.701	0.631	17.1	7.0	49.8	240.6
19/07/1997	0.719	0.435	0.449	18.7	10.8	103.9	122.2
09/08/1997	0.459	0.515	0.565	22.5	11.9	17.2	251.9
14/09/1997	0.789	0.619	0.623	23.8	14.6	130.0	181.1
22/11/1997	0.620	0.622	0.659	14.4	5.9	57.1	138.9
04/03/1998	0.677	0.530	0.677	11.3	4.3	12.6	92.7
09/03/1998	0.756	0.660	0.646	11.3	4.3	12.6	92.7
19/05/1998	0.687	0.816	0.796	11.9	4.5	122.0	111.9
17/09/1998	0.686	0.600	0.498	21.7	11.3	28.6	241.5
19/10/1998	0.723	0.578	0.618	19.2	11.4	83.0	134.4
26/10/1998	0.699	0.577	0.651	19.2	11.4	83.0	134.4
28/03/1999	0.819	0.682	0.639	8.9	2.7	32.1	78.4
03/09/1999	0.662	0.615	0.565	21.2	12.3	116.9	174.6
04/09/1999	0.816	0.722	0.692	21.2	12.3	116.9	174.6
05/10/1999	0.802	0.716	0.719	20.2	11.2	112.8	178.3
06/10/1999	0.751	0.697	0.697	20.2	11.2	112.8	178.3
13/10/1999	0.726	0.654	0.689	20.2	11.2	112.8	178.3
14/10/1999	0.766	0.686	0.705	20.2	11.2	112.8	178.3
22/03/2000	0.726	0.644	0.595	10.2	3.3	68.8	100.9
07/04/2000	0.773	0.725	0.661	12.0	4.4	20.3	137.2
17/06/2000	0.772	0.711	0.689	16.9	7.8	57.4	181.9
18/06/2000	0.743	0.681	0.682	16.9	7.8	57.4	181.9
20/08/2000	0.491	0.412	0.431	21.0	11.8	36.1	179.3
22/09/2000	0.512	0.706	0.200	21.9	12.1	46.9	228.1
12/05/2001	0.114	0.144	0.694	12.5	4.4	75.6	165.7
05/06/2001	0.135	0.119	0.672	18.2	7.6	37.6	205.5
05/06/2001	0.132	0.170	0.694	18.2	7.6	37.6	205.5
23/07/2001	0.145	0.207	0.521	20.0	10.3	29.4	228.0
26/07/2001	0.086	0.021	0.536	20.0	10.3	29.4	228.0
15/08/2001	0.092	0.015	0.611	22.2	12.5	78.9	207.4
15/08/2001	0.207	0.225	0.477	22.2	12.5	78.9	207.4
27/10/2001	0.149	0.205	0.498	17.9	10.1	31.3	127.9
04/11/2001	0.091	0.077	0.609	16.7	10.7	162.3	115.7

Imagery Date	Mean NDVI Full Grave	Mean NDVI Empty Grave	Mean NDVI Undisturbed Grass	Tmax (^{o}C)	Tmin (^{o}C)	Cumulative Rainfall (mm)	Sun Hours (Hours)
28/03/2002	0.120	0.120	0.654	10.6	4.4	143.1	76.1
04/04/2002	0.152	0.171	0.622	12.0	4.3	29.8	113.0
17/05/2002	0.120	0.125	0.602	14.7	5.0	46.2	191.8
24/05/2002	0.105	0.052	0.771	14.7	5.0	46.2	191.8
04/09/2002	0.146	0.161	0.320	22.2	12.8	21.6	165.6
11/09/2002	0.120	0.123	0.514	22.2	12.8	21.6	165.6
20/09/2002	0.128	0.136	0.286	22.2	12.8	21.6	165.6
06/10/2002	0.101	0.123	0.510	19.8	10.2	19.7	168.6
22/03/2003	0.136	0.254	0.548	8.1	0.7	23.5	87.7
07/04/2003	0.126	0.344	0.633	13.1	2.7	27.9	162.0
16/04/2003	0.158	0.357	0.612	13.1	2.7	27.9	162.0
23/04/2003	0.238	0.383	0.558	13.1	2.7	27.9	162.0
13/07/2003	0.187	0.386	0.514	21.9	11.3	51.1	237.6
14/08/2003	0.228	0.403	0.576	22.1	13.4	65.7	165.2
30/08/2003	0.233	0.407	0.574	22.1	13.4	65.7	165.2
15/09/2003	0.184	0.289	0.464	24.3	13.6	9.9	215.4
23/02/2004	0.192	0.402	0.465	8.7	3.4	80.0	56.3
23/05/2004	0.295	0.509	0.712	14.2	5.9	77.7	138.7
07/08/2004	0.215	0.272	0.584	20.9	11.9	44.1	170.1
08/09/2004	0.333	0.466	0.680	22.5	13.6	85.7	212.1
24/10/2004	0.449	0.494	0.555	19.8	10.9	53.1	177.5
14/11/2004	0.411	0.515	0.610	14.1	8.0	140.6	105.1
20/01/2005	0.397	0.505	0.567	9.1	3.0	36.1	57.5
23/01/2005	0.379	0.449	0.543	9.1	3.0	36.1	57.5
03/03/2005	0.289	0.310	0.500	7.9	2.0	32.1	76.5
02/04/2005	0.351	0.425	0.607	11.2	4.0	69.0	94.1
24/04/2005	0.368	0.479	0.654	11.2	4.0	69.0	94.1
06/05/2005	0.401	0.507	0.718	13.9	5.3	52.5	156.8
15/05/2005	0.414	0.556	0.725	13.9	5.3	52.5	156.8
07/06/2005	0.487	0.598	0.712	16.7	7.4	31.0	229.8
08/06/2005	0.462	0.649	0.792	16.7	7.4	31.0	229.8
23/06/2005	0.385	0.487	0.391	16.7	7.4	31.0	229.8
08/07/2005	0.404	0.497	0.512	21.0	11.5	48.0	216.1
09/07/2005	0.326	0.495	0.551	21.0	11.5	48.0	216.1
10/07/2005	0.233	0.378	0.502	21.0	11.5	48.0	216.1
06/09/2005	0.252	0.298	0.485	22.2	11.5	24.5	245.2
07/11/2005	0.422	0.503	0.505	16.6	10.6	131.6	82.1
07/11/2005	0.458	0.532	0.520	16.6	10.6	131.6	82.1
09/02/2006	0.449	0.527	0.490	7.3	2.1	15.0	51.5
25/05/2006	0.506	0.523	0.593	14.0	5.3	17.5	157.9
07/06/2006	0.442	0.474	0.565	17.6	8.9	109.4	193.0

Imagery Date	Mean NDVI Full Grave	Mean NDVI Empty Grave	Mean NDVI Undisturbed Grass	Tmax (^{o}C)	Tmin (^{o}C)	Cumulative Rainfall (mm)	Sun Hours (Hours)
10/06/2006	0.539	0.632	0.719	17.6	8.9	109.4	193.0
21/07/2006	0.365	0.388	0.443	22.6	11.6	17.2	259.9
28/07/2006	0.375	0.437	0.490	22.6	11.6	17.2	259.9
23/09/2006	0.454	0.410	0.597	21.5	13.0	117.0	174.0
03/11/2006	0.136	0.287	0.270	16.5	10.0	82.9	95.1
02/12/2006	0.456	0.539	0.509	12.1	4.4	94.5	102.6
18/03/2007	0.505	0.516	0.585	9.3	3.2	86.1	61.2
19/04/2007	0.535	0.543	0.660	11.8	3.4	73.8	162.7
01/05/2007	0.575	0.592	0.736	17.9	6.6	7.0	232.4
01/06/2007	0.553	0.557	0.648	17.0	8.3	139.9	172.9
31/07/2007	0.583	0.548	0.539	20.2	11.7	136.6	153.7
09/08/2007	0.472	0.425	0.535	19.6	11.7	161.1	205.8
25/08/2007	0.475	0.422	0.585	19.6	11.7	161.1	205.8
10/09/2007	0.479	0.420	0.574	21.2	11.5	32.6	202.7
13/09/2007	0.320	0.372	0.523	21.2	11.5	32.6	202.7
04/03/2008	0.546	0.597	0.521	10.0	1.0	29.5	104.3
06/05/2008	0.664	0.664	0.712	13.3	4.5	73.9	158.6
08/06/2008	0.672	0.637	0.718	18.6	9.6	101.8	167.6
19/09/2008	0.611	0.553	0.615	20.4	13.6	81.6	135.3
26/09/2008	0.289	0.291	0.399	20.4	13.6	81.6	135.3
21/10/2008	0.556	0.528	0.525	17.7	9.9	111.1	94.7
02/03/2009	0.350	0.362	0.414	7.9	1.9	41.4	58.8
30/03/2009	0.428	0.420	0.512	7.9	1.9	41.4	58.8
01/05/2009	0.631	0.593	0.658	15.2	5.3	38.6	166.9
09/08/2009	0.303	0.269	0.314	20.8	12.6	143.8	177.4
19/08/2009	0.655	0.690	0.762	20.8	12.6	143.8	177.4
11/04/2010	0.452	0.445	0.455	10.8	2.1	47.2	133.5
17/04/2010	0.577	0.568	0.628	10.8	2.1	47.2	133.5
18/04/2010	0.481	0.467	0.511	10.8	2.1	47.2	133.5
04/05/2010	0.578	0.559	0.622	15.1	4.2	22.5	210.7
21/06/2010	0.652	0.657	0.672	17.0	7.0	48.7	205.7
16/08/2010	0.422	0.338	0.620	22.0	13.6	47.2	148.8
02/09/2010	0.386	0.354	0.423	20.5	11.8	113.7	152.8
25/09/2010	0.664	0.636	0.637	20.5	11.8	113.7	152.8
20/10/2010	0.704	0.677	0.648	18.4	9.9	38.5	119.7
14/03/2011	0.439	0.457	0.454	9.9	4.5	38.4	51.5
25/03/2011	0.491	0.524	0.528	9.9	4.5	38.4	51.5
22/04/2011	0.670	0.717	0.701	11.9	3.0	17.0	130.4
23/04/2011	0.609	0.662	0.685	11.9	3.0	17.0	130.4
30/04/2011	0.604	0.640	0.650	11.9	3.0	17.0	130.4
02/05/2011	0.731	0.777	0.773	18.6	6.6	7.0	210.4

03/05/2011	0.719	0.777	0.775	18.6	6.6	7.0	210.4
14/07/2011	0.587	0.618	0.481	19.2	9.5	38.3	192.3

Table 3-31 - Mean NDVI for the different surface types and the meteorological variables from the Ross on Wye meteorological station (two months prior to imagery collection) to derive relationships between NDVI and meteorological variables (1997-2011).

Imagery Date	Mean NDVI Full Grave	Mean NDVI Empty Grave	Mean NDVI Undisturbed Grass	Tmax (^{o}C)	Tmin (^{o}C)	Cumulative Rainfall (mm)	Sun Hours (Hours)
18/02/1997	0.484	0.435	0.433	7.8	1.9	52.0	53.4
06/03/1997	0.637	0.581	0.551	7.8	1.9	52.0	53.4
22/03/1997	0.674	0.607	0.570	7.8	1.9	52.0	53.4
07/04/1997	0.752	0.684	0.625	11.5	4.3	60.3	103.8
25/05/1997	0.861	0.792	0.705	13.7	4.7	25.8	157.5
01/06/1997	0.862	0.812	0.743	15.9	5.9	37.9	209.3
17/06/1997	0.752	0.701	0.631	15.9	5.9	37.9	209.3
19/07/1997	0.719	0.435	0.449	17.9	8.9	76.9	181.4
09/08/1997	0.459	0.515	0.565	20.6	11.4	60.6	187.1
14/09/1997	0.789	0.619	0.623	23.2	13.3	73.6	216.5
22/11/1997	0.620	0.622	0.659	21.3	12.4	75.9	163.4
04/03/1998	0.677	0.530	0.677	9.7	3.7	68.5	70.4
09/03/1998	0.756	0.660	0.646	9.7	3.7	68.5	70.4
19/05/1998	0.687	0.816	0.796	12.0	4.8	98.8	98.3
17/09/1998	0.686	0.600	0.498	21.0	11.7	22.5	209.4
19/10/1998	0.723	0.578	0.618	20.5	11.4	55.8	188.0
26/10/1998	0.699	0.577	0.651	20.5	11.4	55.8	188.0
28/03/1999	0.819	0.682	0.639	9.1	3.0	80.6	64.6
03/09/1999	0.662	0.615	0.565	22.6	12.7	61.7	218.2
04/09/1999	0.816	0.722	0.692	22.6	12.7	61.7	218.2
05/10/1999	0.802	0.716	0.719	20.7	11.8	114.9	176.5
06/10/1999	0.751	0.697	0.697	20.7	11.8	114.9	176.5
13/10/1999	0.726	0.654	0.689	20.7	11.8	114.9	176.5
14/10/1999	0.766	0.686	0.705	20.7	11.8	114.9	176.5
22/03/2000	0.726	0.644	0.595	9.3	1.9	45.4	77.8
07/04/2000	0.773	0.725	0.661	11.1	3.9	44.6	119.1
17/06/2000	0.772	0.711	0.689	14.6	6.0	114.7	162.6
18/06/2000	0.743	0.681	0.682	14.6	6.0	114.7	162.6
20/08/2000	0.491	0.412	0.431	20.6	11.6	33.8	178.3
22/09/2000	0.512	0.706	0.200	21.5	12.0	41.5	203.7
12/05/2001	0.114	0.144	0.694	10.6	3.4	89.5	123.4
05/06/2001	0.135	0.119	0.672	15.4	6.0	56.6	185.6
05/06/2001	0.132	0.170	0.694	15.4	6.0	56.6	185.6
23/07/2001	0.145	0.207	0.521	19.1	9.0	33.5	216.8
26/07/2001	0.086	0.021	0.536	19.1	9.0	33.5	216.8
15/08/2001	0.092	0.015	0.611	21.1	11.4	54.2	217.7
15/08/2001	0.207	0.225	0.477	21.1	11.4	54.2	217.7
27/10/2001	0.149	0.205	0.498	19.7	11.6	46.9	159.4
04/11/2001	0.091	0.077	0.609	17.3	10.4	96.8	121.8

Imagery Date	Mean NDVI Full Grave	Mean NDVI Empty Grave	Mean NDVI Undisturbed Grass	Tmax (°C)	Tmin (°C)	Cumulative Rainfall (mm)	Sun Hours (Hours)
28/03/2002	0.120	0.120	0.654	9.9	3.7	111.2	58.5
04/04/2002	0.152	0.171	0.622	11.3	4.4	86.5	94.6
17/05/2002	0.120	0.125	0.602	13.4	4.7	38.0	152.4
24/05/2002	0.105	0.052	0.771	13.4	4.7	38.0	152.4
04/09/2002	0.146	0.161	0.320	21.6	12.3	38.8	183.8
11/09/2002	0.120	0.123	0.514	21.6	12.3	38.8	183.8
20/09/2002	0.128	0.136	0.286	21.6	12.3	38.8	183.8
06/10/2002	0.101	0.123	0.510	21.0	11.5	20.7	167.1
22/03/2003	0.136	0.254	0.548	8.0	1.4	38.0	89.7
07/04/2003	0.126	0.344	0.633	10.6	1.7	25.7	124.9
16/04/2003	0.158	0.357	0.612	10.6	1.7	25.7	124.9
23/04/2003	0.238	0.383	0.558	10.6	1.7	25.7	124.9
13/07/2003	0.187	0.386	0.514	19.3	9.8	43.4	229.6
14/08/2003	0.228	0.403	0.576	22.0	12.4	58.4	201.4
30/08/2003	0.233	0.407	0.574	22.0	12.4	58.4	201.4
15/09/2003	0.184	0.289	0.464	23.2	13.5	37.8	190.3
23/02/2004	0.192	0.402	0.465	8.7	2.8	81.9	50.9
23/05/2004	0.295	0.509	0.712	12.5	4.6	60.0	124.6
07/08/2004	0.215	0.272	0.584	21.0	11.8	40.1	209.5
08/09/2004	0.333	0.466	0.680	21.7	12.8	64.9	191.1
24/10/2004	0.449	0.494	0.555	21.2	12.3	69.4	194.8
14/11/2004	0.411	0.515	0.610	17.0	9.5	96.9	141.3
20/01/2005	0.397	0.505	0.567	10.1	4.1	33.3	52.9
23/01/2005	0.379	0.449	0.543	10.1	4.1	33.3	52.9
03/03/2005	0.289	0.310	0.500	8.8	2.9	29.6	68.8
02/04/2005	0.351	0.425	0.607	9.6	3.0	50.6	85.3
24/04/2005	0.368	0.479	0.654	9.6	3.0	50.6	85.3
06/05/2005	0.401	0.507	0.718	12.6	4.7	60.8	125.5
15/05/2005	0.414	0.556	0.725	12.6	4.7	60.8	125.5
07/06/2005	0.487	0.598	0.712	15.3	6.4	41.8	193.3
08/06/2005	0.462	0.649	0.792	15.3	6.4	41.8	193.3
23/06/2005	0.385	0.487	0.391	15.3	6.4	41.8	193.3
08/07/2005	0.404	0.497	0.512	18.9	9.5	39.5	223.0
09/07/2005	0.326	0.495	0.551	18.9	9.5	39.5	223.0
10/07/2005	0.233	0.378	0.502	18.9	9.5	39.5	223.0
06/09/2005	0.252	0.298	0.485	22.2	12.3	42.6	234.7
07/11/2005	0.422	0.503	0.505	18.7	11.0	99.4	128.3
07/11/2005	0.458	0.532	0.520	18.7	11.0	99.4	128.3
09/02/2006	0.449	0.527	0.490	7.9	1.6	40.1	51.2
25/05/2006	0.506	0.523	0.593	11.7	3.9	42.4	129.5
07/06/2006	0.442	0.474	0.565	15.8	7.1	63.5	175.5

Imagery Date	Mean NDVI Full Grave	Mean NDVI Empty Grave	Mean NDVI Undisturbed Grass	Tmax (°C)	Tmin (°C)	Cumulative Rainfall (mm)	Sun Hours (Hours)
10/06/2006	0.539	0.632	0.719	15.8	7.1	63.5	175.5
21/07/2006	0.365	0.388	0.443	20.1	10.3	63.3	226.5
28/07/2006	0.375	0.437	0.490	20.1	10.3	63.3	226.5
23/09/2006	0.454	0.410	0.597	24.2	13.7	75.7	241.8
03/11/2006	0.136	0.287	0.270	19.0	11.3	70.3	126.4
02/12/2006	0.456	0.539	0.509	14.3	7.2	88.7	98.9
18/03/2007	0.505	0.516	0.585	9.9	4.0	76.4	60.8
19/04/2007	0.535	0.543	0.660	10.6	3.3	80.0	112.0
01/05/2007	0.575	0.592	0.736	14.9	5.0	40.4	197.6
01/06/2007	0.553	0.557	0.648	17.5	7.5	73.5	202.7
31/07/2007	0.583	0.548	0.539	18.6	10.0	138.3	163.3
09/08/2007	0.472	0.425	0.535	19.9	11.7	148.9	179.8
25/08/2007	0.475	0.422	0.585	19.9	11.7	148.9	179.8
10/09/2007	0.479	0.420	0.574	20.4	11.6	96.9	204.3
13/09/2007	0.320	0.372	0.523	20.4	11.6	96.9	204.3
04/03/2008	0.546	0.597	0.521	10.2	2.5	65.6	74.2
06/05/2008	0.664	0.664	0.712	12.0	4.1	87.1	142.1
08/06/2008	0.672	0.637	0.718	16.0	7.1	87.9	163.1
19/09/2008	0.611	0.553	0.615	21.0	13.1	84.2	165.3
26/09/2008	0.289	0.291	0.399	21.0	13.1	84.2	165.3
21/10/2008	0.556	0.528	0.525	19.1	11.8	96.4	115.0
02/03/2009	0.350	0.362	0.414	7.2	1.0	56.6	56.6
30/03/2009	0.428	0.420	0.512	7.2	1.0	56.6	56.6
01/05/2009	0.631	0.593	0.658	13.6	4.1	31.7	154.9
09/08/2009	0.303	0.269	0.314	20.9	11.5	123.2	193.6
19/08/2009	0.655	0.690	0.762	20.9	11.5	123.2	193.6
11/04/2010	0.452	0.445	0.455	8.9	1.4	47.3	100.2
17/04/2010	0.577	0.568	0.628	8.9	1.4	47.3	100.2
18/04/2010	0.481	0.467	0.511	8.9	1.4	47.3	100.2
04/05/2010	0.578	0.559	0.622	13.0	3.2	34.9	172.1
21/06/2010	0.652	0.657	0.672	16.1	5.6	35.6	208.2
16/08/2010	0.422	0.338	0.620	22.1	12.1	34.2	199.2
02/09/2010	0.386	0.354	0.423	21.3	12.7	80.5	150.8
25/09/2010	0.664	0.636	0.637	21.3	12.7	80.5	150.8
20/10/2010	0.704	0.677	0.648	19.5	10.9	76.1	136.3
14/03/2011	0.439	0.457	0.454	8.4	2.9	52.1	50.9
25/03/2011	0.491	0.524	0.528	8.4	2.9	52.1	50.9
22/04/2011	0.670	0.717	0.701	10.9	3.8	27.7	91.0
23/04/2011	0.609	0.662	0.685	10.9	3.8	27.7	91.0
30/04/2011	0.604	0.640	0.650	10.9	3.8	27.7	91.0
02/05/2011	0.731	0.777	0.773	15.3	4.8	12.0	170.4

Table 3-32 - Relationship between NDVI and meteorological variables two months prior to image collection for the period prior to the creation of the grave (1997-2001).

FUNCTION		Full Grave	Empty Grave	Undisturbed Grass
SLOPE	NDVI vs TMax (^{o}C)	-0.001	-0.001	-0.002
	NDVI vs TMin (^{o}C)	-0.003	-0.002	-0.003
	NDVI vs Cumul. Rainfall (mm)	0.001	0.001	0.002
	NDVI vs Sun Hours (hours)	0.000	0.000	0.000
CORREL (r)	NDVI vs TMax (^{o}C)	-0.061	-0.035	-0.086
	NDVI vs TMin (^{o}C)	-0.120	-0.100	-0.109
	NDVI vs Cumul. Rainfall (mm)	0.234	0.196	0.462
	NDVI vs Sun Hours (hours)	0.104	0.121	-0.040
RSQ (r^2 or %)	NDVI vs TMax (^{o}C)	0.004	0.001	0.007
	NDVI vs TMin (^{o}C)	0.014	0.010	0.012
	NDVI vs Cumul. Rainfall (mm)	0.055	0.039	0.214
	NDVI vs Sun Hours (hours)	0.011	0.015	0.002

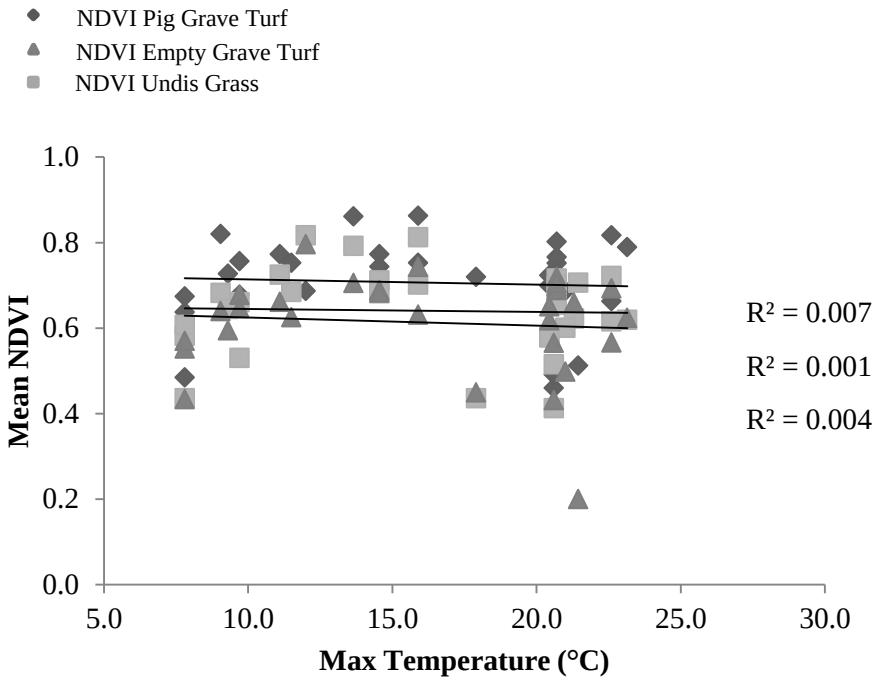

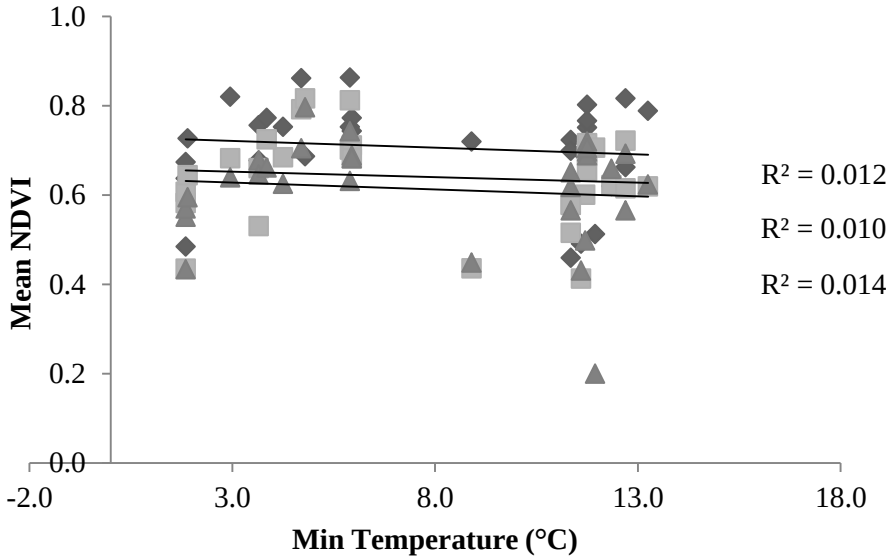

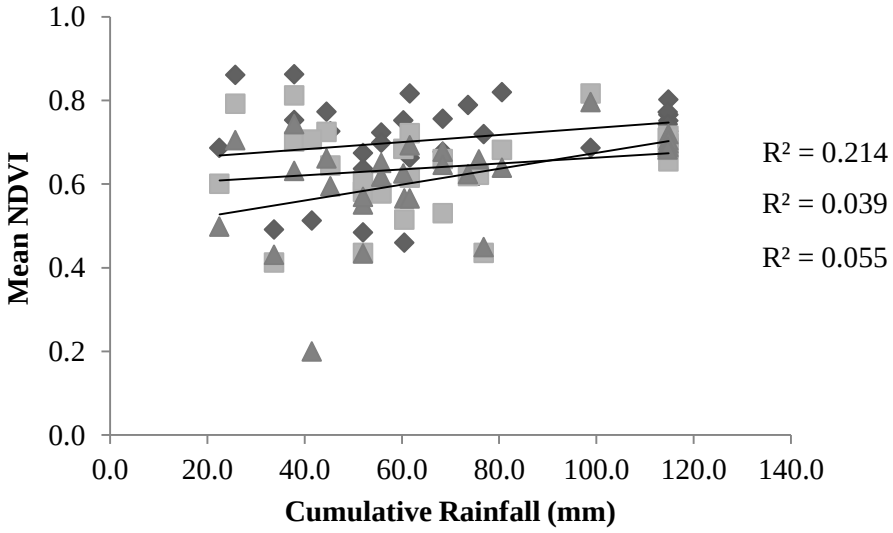

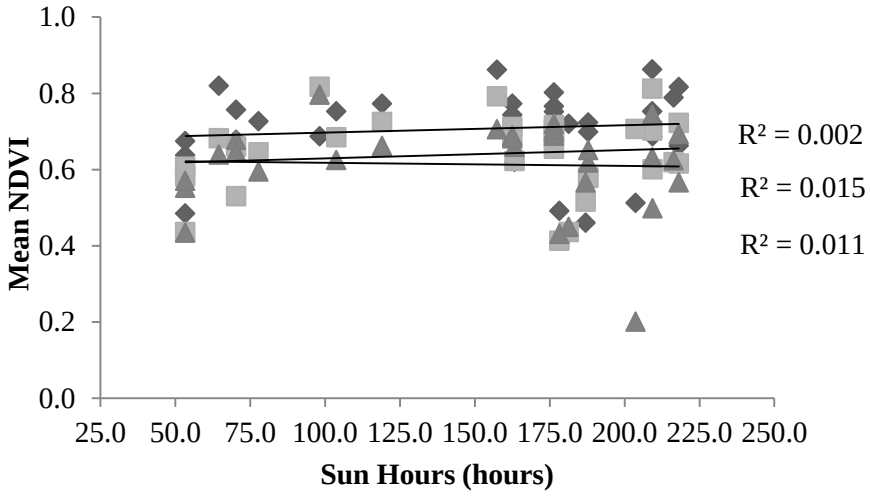

Figure 3-38 – Scatter plots showing the linear relationships between NDVI and meteorological variables two months prior to image acquisition prior to grave creation (1997-2001).

Table 3-33 - Relationship between NDVI and meteorological variables two months prior to image collection for the period 2001-2008.

FUNCTION		Full Grave	Empty Grave	Undisturbed Grass
SLOPE	NDVI vs TMax (^{o}C)	-0.005	-0.007	-0.005
	NDVI vs TMin (^{o}C)	-0.007	-0.010	-0.008
	NDVI vs Cumul. Rainfall (mm)	0.001	0.000	0.000
	NDVI vs Sun Hours (hours)	0.000	0.000	0.000
CORREL (r)	NDVI vs TMax (^{o}C)	-0.127	-0.197	-0.224
	NDVI vs TMin (^{o}C)	-0.143	-0.218	-0.301
	NDVI vs Cumul. Rainfall (mm)	0.127	0.015	-0.068
	NDVI vs Sun Hours (hours)	-0.102	-0.135	-0.008
RSQ (r^2 or %)	NDVI vs TMax (^{o}C)	0.016	0.039	0.050
	NDVI vs TMin (^{o}C)	0.020	0.048	0.091
	NDVI vs Cumul. Rainfall (mm)	0.016	0.000	0.005
	NDVI vs Sun Hours (hours)	0.010	0.018	0.000

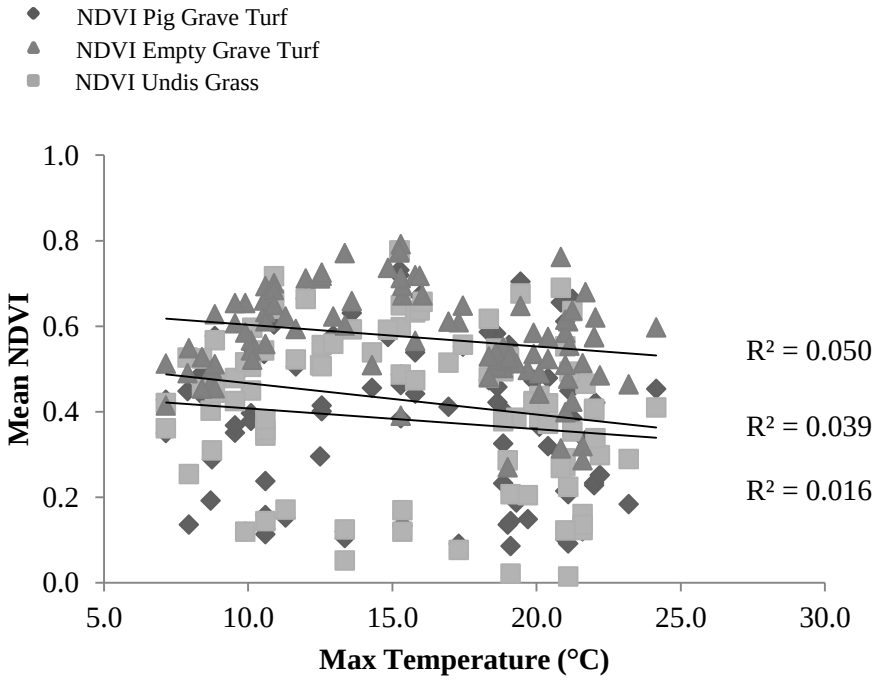

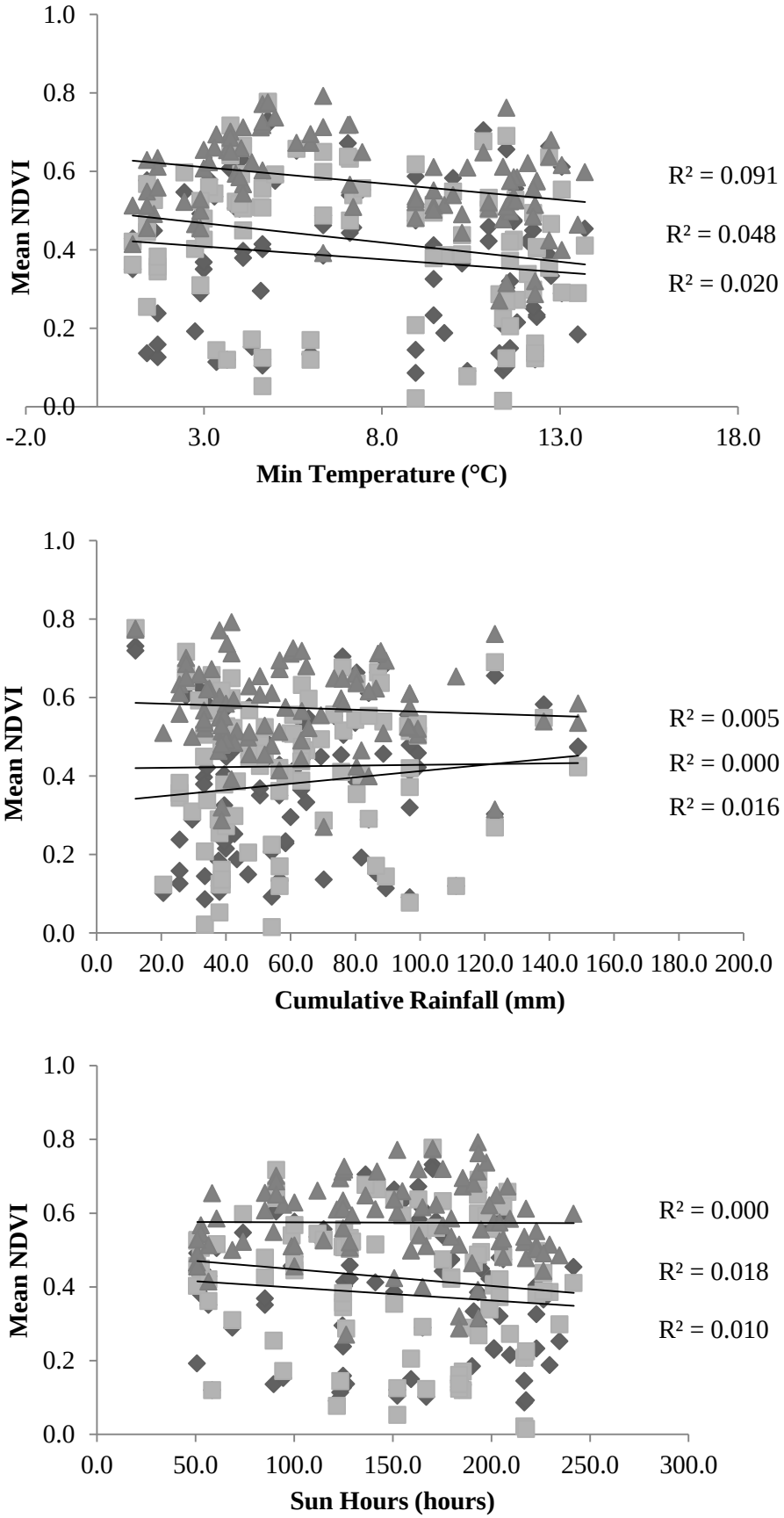

Figure 3-39 - Scatter plots showing the linear relationships between NDVI and meteorological variables two months prior to the image acquisition for the period 2001-2008.

Table 3-34 - Mean NDVI for the different surface types and the meteorological variables from the Ross on Wye meteorological station (three months prior to imagery collection) to derive relationships between NDVI and meteorological variables (1997-2011).

Imagery Date	Mean NDVI Full Grave	Mean NDVI Empty Grave	Mean NDVI Undisturbed Grass	Tmax (^{o}C)	Tmin (^{o}C)	Cumulative Rainfall (mm)	Sun Hours (Hours)
18/02/1997	0.484	0.435	0.433	7.8	1.9	52.0	53.4
06/03/1997	0.637	0.581	0.551	7.8	1.9	52.0	53.4
22/03/1997	0.674	0.607	0.570	7.8	1.9	52.0	53.4
07/04/1997	0.752	0.684	0.625	9.4	2.8	43.2	81.3
25/05/1997	0.861	0.792	0.705	12.6	4.4	48.8	128.5
01/06/1997	0.862	0.812	0.743	14.8	5.5	33.8	185.2
17/06/1997	0.752	0.701	0.631	14.8	5.5	33.8	185.2
19/07/1997	0.719	0.435	0.449	16.8	7.5	59.9	180.2
09/08/1997	0.459	0.515	0.565	19.4	9.9	57.0	204.9
14/09/1997	0.789	0.619	0.623	21.7	12.4	83.7	185.1
22/11/1997	0.620	0.622	0.659	19.0	10.2	69.6	155.2
04/03/1998	0.677	0.530	0.677	9.5	3.6	65.9	61.6
09/03/1998	0.756	0.660	0.646	9.5	3.6	65.9	61.6
19/05/1998	0.687	0.816	0.796	11.8	4.6	70.1	96.4
17/09/1998	0.686	0.600	0.498	20.2	11.6	44.8	190.3
19/10/1998	0.723	0.578	0.618	20.4	11.6	42.7	184.4
26/10/1998	0.699	0.577	0.651	20.4	11.6	42.7	184.4
28/03/1999	0.819	0.682	0.639	9.1	2.8	73.9	54.6
03/09/1999	0.662	0.615	0.565	21.5	11.6	57.5	212.2
04/09/1999	0.816	0.722	0.692	21.5	11.6	57.5	212.2
05/10/1999	0.802	0.716	0.719	21.8	12.2	78.7	204.9
06/10/1999	0.751	0.697	0.697	21.8	12.2	78.7	204.9
13/10/1999	0.726	0.654	0.689	21.8	12.2	78.7	204.9
14/10/1999	0.766	0.686	0.705	21.8	12.2	78.7	204.9
22/03/2000	0.726	0.644	0.595	9.1	1.5	63.6	72.6
07/04/2000	0.773	0.725	0.661	10.2	2.7	37.0	97.6
17/06/2000	0.772	0.711	0.689	13.7	5.4	83.2	154.1
18/06/2000	0.743	0.681	0.682	13.7	5.4	83.2	154.1
20/08/2000	0.491	0.412	0.431	19.4	10.3	41.6	179.5
22/09/2000	0.512	0.706	0.200	21.0	11.8	38.1	194.9
12/05/2001	0.114	0.144	0.694	9.9	2.6	85.0	112.9
05/06/2001	0.135	0.119	0.672	13.1	4.8	72.2	150.8
05/06/2001	0.132	0.170	0.694	13.1	4.8	72.2	150.8
23/07/2001	0.145	0.207	0.521	16.9	7.4	47.5	199.7
26/07/2001	0.086	0.021	0.536	16.9	7.4	47.5	199.7
15/08/2001	0.092	0.015	0.611	20.1	10.1	48.6	213.6
15/08/2001	0.207	0.225	0.477	20.1	10.1	48.6	213.6
27/10/2001	0.149	0.205	0.498	20.5	11.9	57.6	175.4
04/11/2001	0.091	0.077	0.609	18.7	11.3	85.4	144.8

Imagery Date	Mean NDVI Full Grave	Mean NDVI Empty Grave	Mean NDVI Undisturbed Grass	Tmax (^{o}C)	Tmin (^{o}C)	Cumulative Rainfall (mm)	Sun Hours (Hours)
28/03/2002	0.120	0.120	0.654	9.0	2.5	79.6	63.8
04/04/2002	0.152	0.171	0.622	10.6	3.9	84.0	76.6
17/05/2002	0.120	0.125	0.602	12.4	4.6	73.0	127.0
24/05/2002	0.105	0.052	0.771	12.4	4.6	73.0	127.0
04/09/2002	0.146	0.161	0.320	20.8	11.6	33.5	184.2
11/09/2002	0.120	0.123	0.514	20.8	11.6	33.5	184.2
20/09/2002	0.128	0.136	0.286	20.8	11.6	33.5	184.2
06/10/2002	0.101	0.123	0.510	21.0	11.6	32.4	178.7
22/03/2003	0.136	0.254	0.548	8.0	2.3	60.5	71.0
07/04/2003	0.126	0.344	0.633	9.7	1.8	34.6	113.8
16/04/2003	0.158	0.357	0.612	9.7	1.8	34.6	113.8
23/04/2003	0.238	0.383	0.558	9.7	1.8	34.6	113.8
13/07/2003	0.187	0.386	0.514	18.0	8.2	41.1	218.2
14/08/2003	0.228	0.403	0.576	20.2	11.0	50.8	208.1
30/08/2003	0.233	0.407	0.574	20.2	11.0	50.8	208.1
15/09/2003	0.184	0.289	0.464	22.8	12.8	42.2	206.1
23/02/2004	0.192	0.402	0.465	9.7	3.6	80.5	55.6
23/05/2004	0.295	0.509	0.712	11.2	4.0	49.9	115.1
07/08/2004	0.215	0.272	0.584	20.0	10.5	38.9	207.4
08/09/2004	0.333	0.466	0.680	21.5	12.4	55.3	210.4
24/10/2004	0.449	0.494	0.555	21.1	12.1	61.0	186.6
14/11/2004	0.411	0.515	0.610	18.8	10.8	93.1	164.9
20/01/2005	0.397	0.505	0.567	11.4	5.4	69.0	70.3
23/01/2005	0.379	0.449	0.543	11.4	5.4	69.0	70.3
03/03/2005	0.289	0.310	0.500	8.9	2.9	31.8	65.0
02/04/2005	0.351	0.425	0.607	9.6	3.3	42.7	77.2
24/04/2005	0.368	0.479	0.654	9.6	3.3	42.7	77.2
06/05/2005	0.401	0.507	0.718	11.0	3.8	51.2	109.1
15/05/2005	0.414	0.556	0.725	11.0	3.8	51.2	109.1
07/06/2005	0.487	0.598	0.712	13.9	5.6	50.8	160.2
08/06/2005	0.462	0.649	0.792	13.9	5.6	50.8	160.2
23/06/2005	0.385	0.487	0.391	13.9	5.6	50.8	160.2
08/07/2005	0.404	0.497	0.512	17.2	8.1	43.8	200.9
09/07/2005	0.326	0.495	0.551	17.2	8.1	43.8	200.9
10/07/2005	0.233	0.378	0.502	17.2	8.1	43.8	200.9
06/09/2005	0.252	0.298	0.485	21.8	12.0	44.4	228.5
07/11/2005	0.422	0.503	0.505	19.8	11.2	74.4	167.2
07/11/2005	0.458	0.532	0.520	19.8	11.2	74.4	167.2
09/02/2006	0.449	0.527	0.490	8.6	1.9	49.5	59.8
25/05/2006	0.506	0.523	0.593	10.0	3.0	38.5	109.0
07/06/2006	0.442	0.474	0.565	13.6	5.6	64.7	150.6

Imagery Date	Mean NDVI Full Grave	Mean NDVI Empty Grave	Mean NDVI Undisturbed Grass	Tmax (°C)	Tmin (°C)	Cumulative Rainfall (mm)	Sun Hours (Hours)
10/06/2006	0.539	0.632	0.719	13.6	5.6	64.7	150.6
21/07/2006	0.365	0.388	0.443	18.1	8.6	48.0	203.6
28/07/2006	0.375	0.437	0.490	18.1	8.6	48.0	203.6
23/09/2006	0.454	0.410	0.597	23.6	13.0	56.2	247.8
03/11/2006	0.136	0.287	0.270	19.8	11.9	85.8	142.3
02/12/2006	0.456	0.539	0.509	16.7	9.0	78.3	118.5
18/03/2007	0.505	0.516	0.585	9.7	4.2	86.1	53.9
19/04/2007	0.535	0.543	0.660	10.5	3.8	75.5	94.7
01/05/2007	0.575	0.592	0.736	13.0	4.4	55.6	152.1
01/06/2007	0.553	0.557	0.648	15.6	6.1	73.6	189.3
31/07/2007	0.583	0.548	0.539	18.4	8.9	94.5	186.3
09/08/2007	0.472	0.425	0.535	18.9	10.6	145.9	177.5
25/08/2007	0.475	0.422	0.585	18.9	10.6	145.9	177.5
10/09/2007	0.479	0.420	0.574	20.3	11.6	110.1	187.4
13/09/2007	0.320	0.372	0.523	20.3	11.6	110.1	187.4
04/03/2008	0.546	0.597	0.521	9.6	2.5	66.4	63.5
06/05/2008	0.664	0.664	0.712	11.3	3.1	67.9	129.5
08/06/2008	0.672	0.637	0.718	14.2	5.9	92.0	150.6
19/09/2008	0.611	0.553	0.615	20.5	12.2	63.5	189.4
26/09/2008	0.289	0.291	0.399	20.5	12.2	63.5	189.4
21/10/2008	0.556	0.528	0.525	19.9	12.0	93.2	141.7
02/03/2009	0.350	0.362	0.414	7.1	1.1	54.0	59.0
30/03/2009	0.428	0.420	0.512	7.1	1.1	54.0	59.0
01/05/2009	0.631	0.593	0.658	11.7	3.3	34.9	122.9
09/08/2009	0.303	0.269	0.314	19.7	10.4	94.7	203.8
19/08/2009	0.655	0.690	0.762	19.7	10.4	94.7	203.8
11/04/2010	0.452	0.445	0.455	7.5	0.4	56.0	88.7
17/04/2010	0.577	0.568	0.628	7.5	0.4	56.0	88.7
18/04/2010	0.481	0.467	0.511	7.5	0.4	56.0	88.7
04/05/2010	0.578	0.559	0.622	10.9	2.3	39.0	137.0
21/06/2010	0.652	0.657	0.672	14.3	4.4	39.5	183.3
16/08/2010	0.422	0.338	0.620	20.4	10.4	39.0	201.3
02/09/2010	0.386	0.354	0.423	21.5	12.0	60.7	183.7
25/09/2010	0.664	0.636	0.637	21.5	12.0	60.7	183.7
20/10/2010	0.704	0.677	0.648	20.3	11.8	66.5	140.4
14/03/2011	0.439	0.457	0.454	6.5	0.5	41.7	43.0
25/03/2011	0.491	0.524	0.528	6.5	0.5	41.7	43.0
22/04/2011	0.670	0.717	0.701	9.6	2.9	40.4	77.4
23/04/2011	0.609	0.662	0.685	9.6	2.9	40.4	77.4
30/04/2011	0.604	0.640	0.650	9.6	2.9	40.4	77.4
02/05/2011	0.731	0.777	0.773	13.5	4.7	20.8	130.8

Table 3-35 - Relationship between NDVI and meteorological variables three months prior to image collection for the period prior to the creation of the grave (1997-2001).

FUNCTION		Full Grave	Empty Grave	Undisturbed Grass
SLOPE	NDVI vs TMax (^{o}C)	-0.001	0.000	-0.001
	NDVI vs TMin (^{o}C)	-0.002	-0.002	-0.002
	NDVI vs Cumul. Rainfall (mm)	0.001	0.001	0.003
	NDVI vs Sun Hours (hours)	0.000	0.000	0.000
CORREL (r)	NDVI vs TMax (^{o}C)	-0.045	-0.023	-0.062
	NDVI vs TMin (^{o}C)	-0.085	-0.068	-0.082
	NDVI vs Cumul. Rainfall (mm)	0.229	0.104	0.412
	NDVI vs Sun Hours (hours)	0.031	0.064	-0.019
RSQ (r^2 or %)	NDVI vs TMax (^{o}C)	0.002	0.001	0.004
	NDVI vs TMin (^{o}C)	0.007	0.005	0.007
	NDVI vs Cumul. Rainfall (mm)	0.052	0.011	0.170
	NDVI vs Sun Hours (hours)	0.001	0.004	0.000

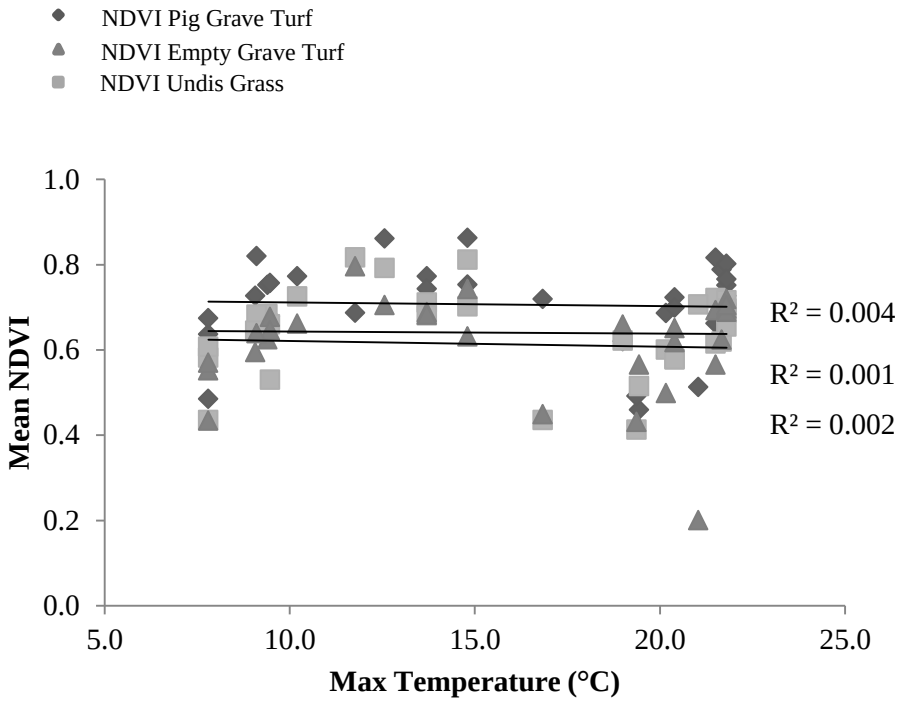

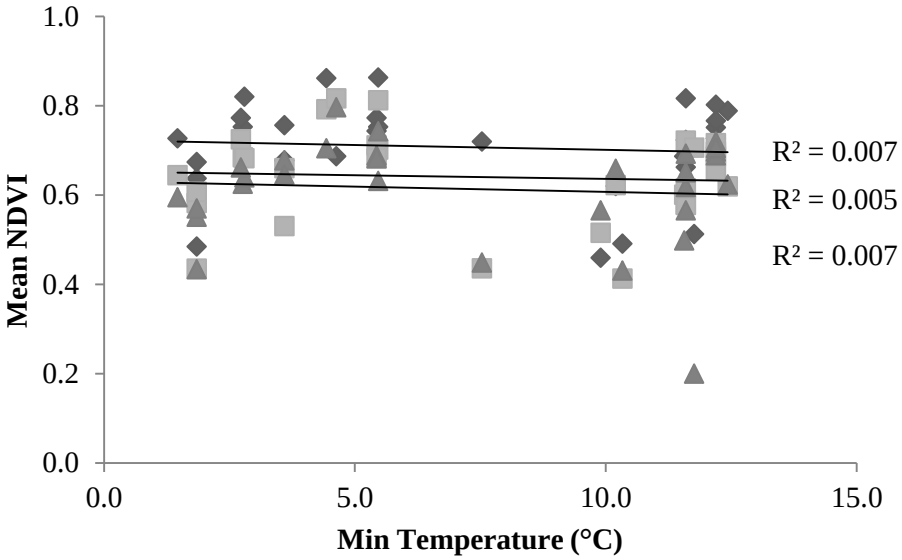

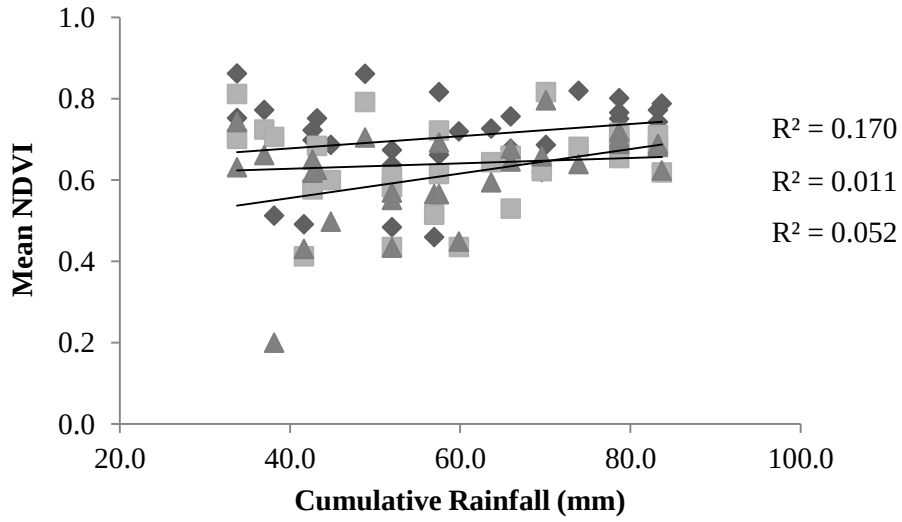

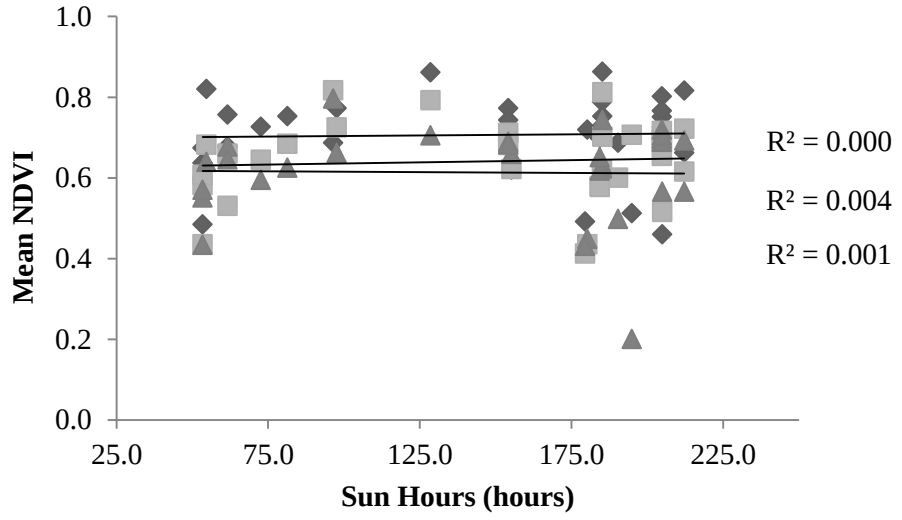

Figure 3-40 - Scatter plots showing the linear relationships between NDVI and meteorological variables three months prior to image acquisition prior to grave creation (1997-2001).

Table 3-36 - Relationship between NDVI and meteorological variables three months prior to image collection for the period 2001-2011.

FUNCTION		Full Grave	Empty Grave	Undisturbed Grass
SLOPE	NDVI vs TMax (^{o}C)	-0.005	-0.007	-0.006
	NDVI vs TMin (^{o}C)	-0.007	-0.010	-0.009
	NDVI vs Cumul. Rainfall (mm)	0.000	0.000	0.000
	NDVI vs Sun Hours (hours)	0.000	-0.001	0.000
CORREL (r)	NDVI vs TMax (^{o}C)	-0.138	-0.203	-0.279
	NDVI vs TMin (^{o}C)	-0.156	-0.217	-0.313
	NDVI vs Cumul. Rainfall (mm)	0.043	-0.063	0.002
	NDVI vs Sun Hours (hours)	-0.134	-0.178	-0.151
RSQ (r^2 or %)	NDVI vs TMax (^{o}C)	0.019	0.041	0.078
	NDVI vs TMin (^{o}C)	0.024	0.047	0.098
	NDVI vs Cumul. Rainfall (mm)	0.002	0.004	0.000
	NDVI vs Sun Hours (hours)	0.018	0.032	0.023

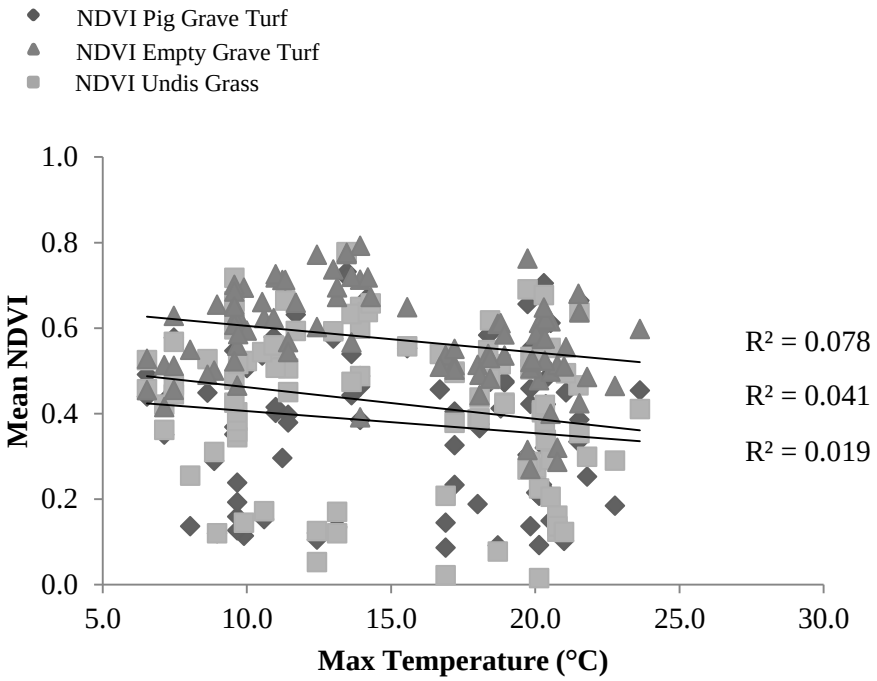

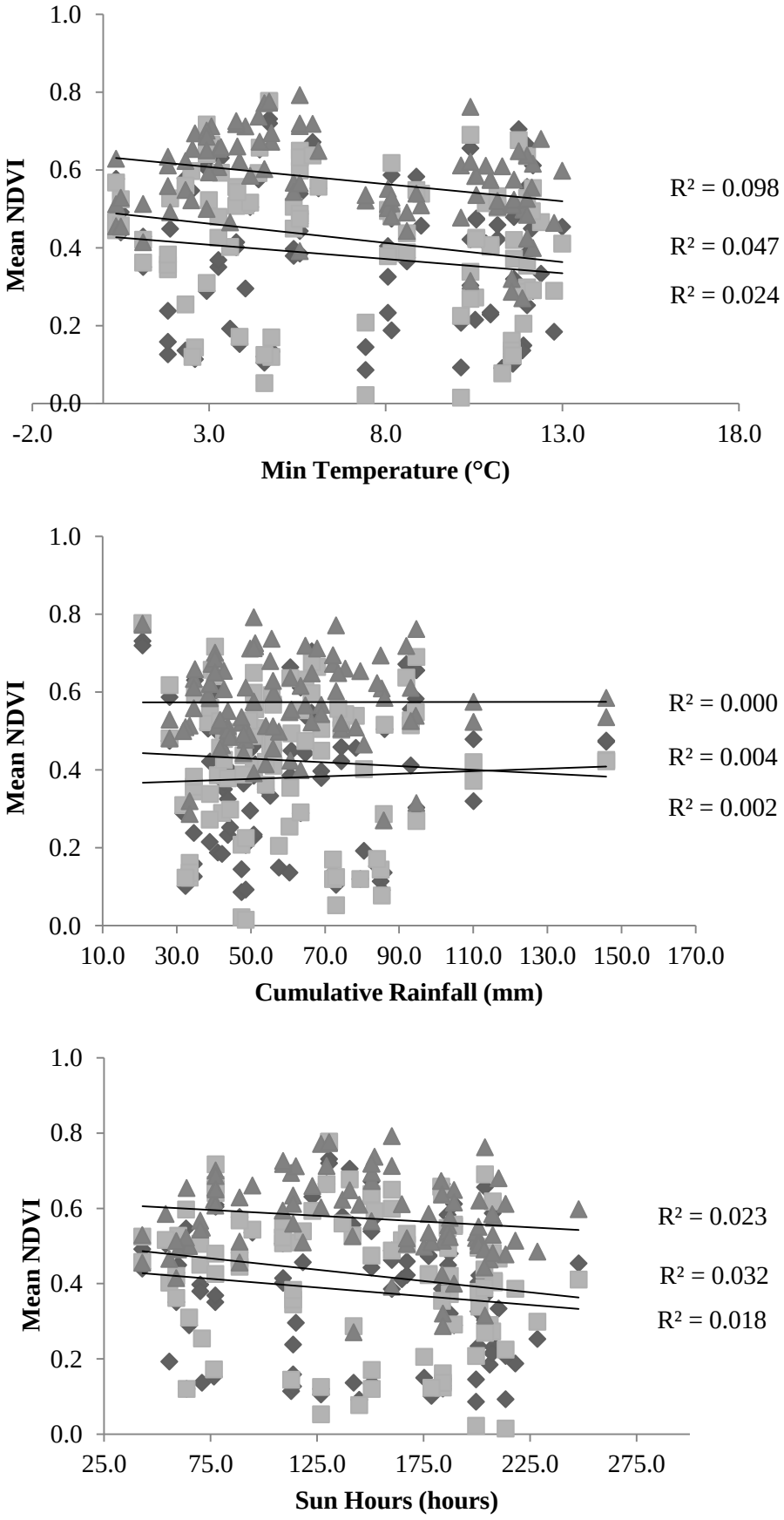

Figure 3-41 - Scatter plots showing the linear relationships between NDVI and meteorological variables three months prior to image acquisition post grave creation (2001 – 2011)

Appendix 4 for Chapter 7

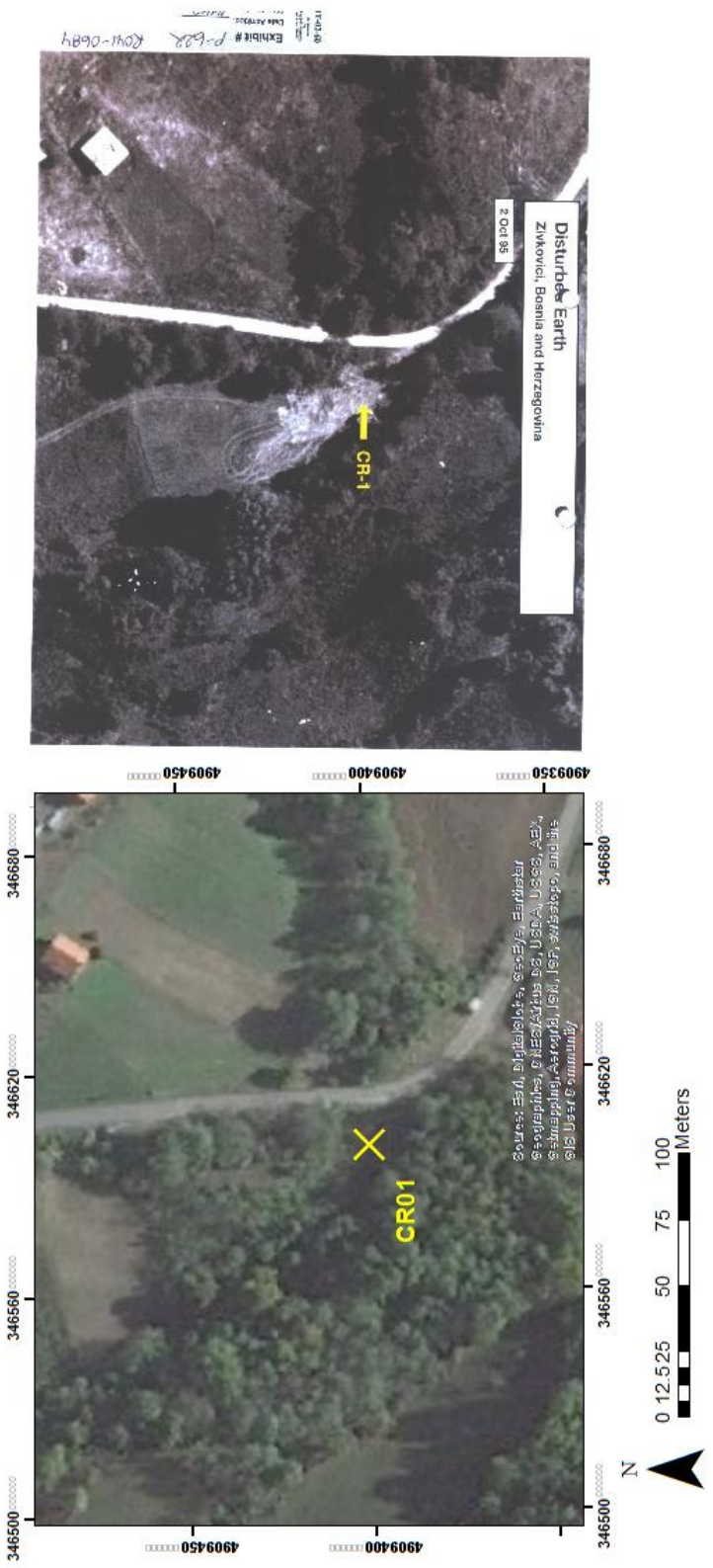

Figure 4-42 - Comparison of an aerial photograph (right) of disturbed earth from October 1995 (ICTY 2011c) and the shapefile (left) created for CR01.

Figure 4-43 - Comparison of an aerial photograph (right) of disturbed earth from October 1995 (ICTY 2011e) and the shapefile (left) created for CR02.

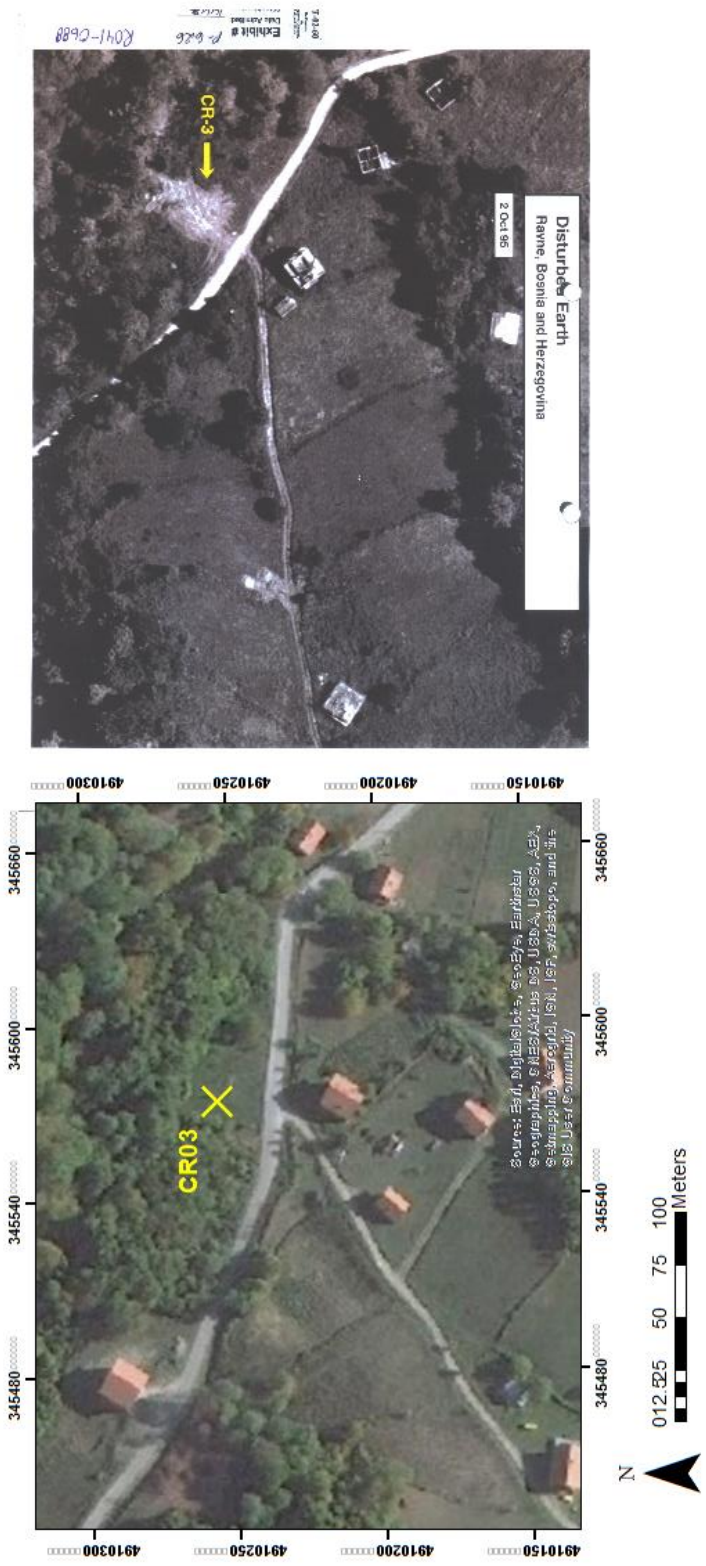

Figure 4-44 - Comparison of an aerial photograph (right) of disturbed earth from October 1995 (ICTY 2011g) and the shapefile (left) created for CR03.

Figure 4-45 - Comparison of an aerial photograph (right) of disturbed earth from October 1995 (ICTY 2011i) and the shapefile (left) created for CR04 and CR05.

Figure 4-46 - Comparison of an aerial photograph (right) of disturbed earth from October 1995 (ICTY 2011k) and the shapefile (left) created for CR06.

Figure 4-47 - Comparison of an aerial photograph (right) of disturbed earth from October 1995 (ICTY 2011m) and the shapefile (left) created for CR07.

Figure 4-48 - Comparison of an aerial photograph (right) of disturbed earth from October 1995 (ICTY 2011n) and the shapefile (left) created for CR08.

Figure 4-49 - Comparison of an aerial photograph (right) of disturbed earth from October 1995 (ICTY 2011q) and the shapefile (left) created for CR09.

Figure 4-50 - Comparison of an aerial photograph (right) of disturbed earth from October 1995 (ICTY 2011t) and the shapefile (left) created for CR10.

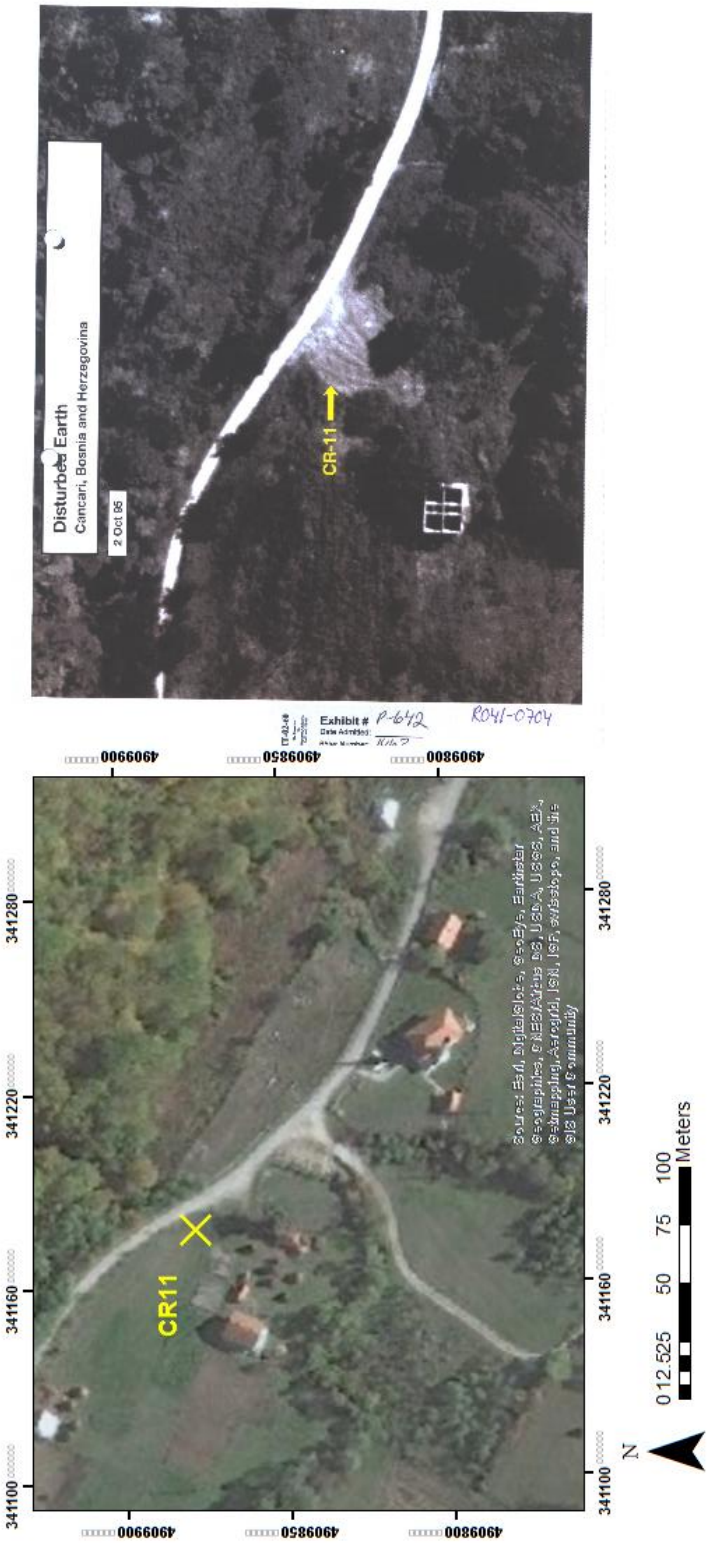

Figure 4-51 - Comparison of an aerial photograph (right) of disturbed earth from October 1995 (ICTY 2011w) and the shapefile (left) created for CR11.

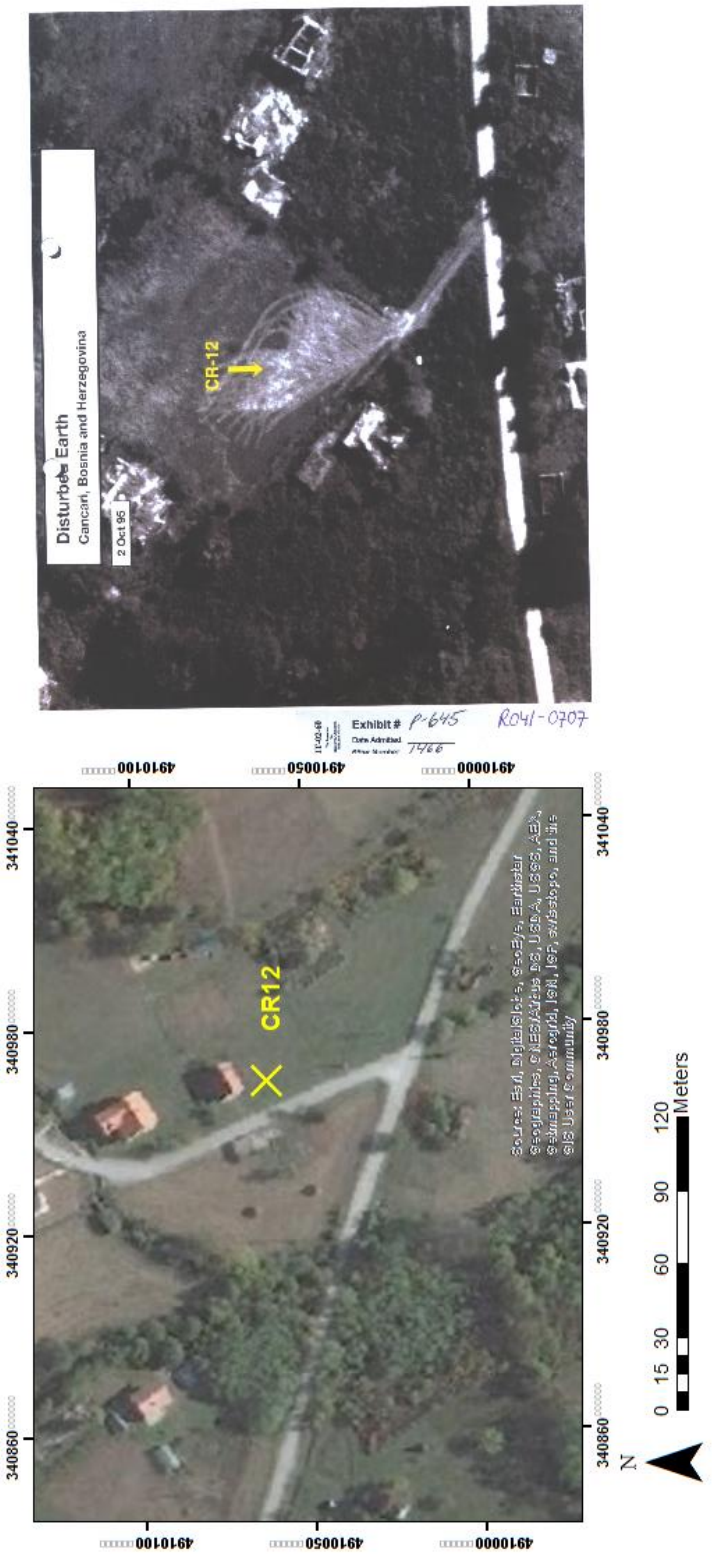

Figure 4-52 - Comparison of an aerial photograph (right) of disturbed earth from October 1995 (ICTY 2011z) and the shapefile (left) created for CR12.

Table 4-37 - Archive multispectral orbital imagery downloaded and processed for the Cancari Road mass graves. Processing levels: L1 – Level 1L3 – Level 3.

Acquisition Date	Platform	Sensor	Source	Processing Level	Spatial Resolution (m)
23/02/1990	SPOT-2	HRV	ESA	L3	20
16/03/1990	SPOT-2	HRV	ESA	L3	20
13/03/1991	Landsat 5	TM	ESA	L1	30
30/04/1991	Landsat 5	TM	ESA	L1	30
01/06/1991	Landsat 5	TM	ESA	L1	30
17/06/1991	Landsat 5	TM	USGS	L1	30
19/07/1991	Landsat 5	TM	ESA	L1	30
20/08/1991	Landsat 5	TM	ESA	L1	30
05/09/1991	Landsat 5	TM	USGS	L1	30
23/10/1991	Landsat 5	TM	ESA	L1	30
30/10/1991	SPOT-2	HRV	ESA	L3	20
28/02/1992	Landsat 5	TM	ESA	L1	30
31/03/1992	Landsat 5	TM	ESA	L1	30
02/05/1992	Landsat 5	TM	ESA	L1	30
09/06/1992	SPOT-2	HRV	ESA	L3	20
20/06/1992	SPOT-2	HRV	ESA	L3	20
23/06/1992	SPOT-1	HRV	ESA	L3	20
06/08/1992	Landsat 5	TM	ESA	L1	30
06/08/1992	Landsat 5	TM	ESA	L1	30
22/08/1992	Landsat 5	TM	ESA	L1	30
22/08/1992	Landsat 5	TM	ESA	L1	30
01/09/1992	SPOT-2	HRV	ESA	L3	20
07/09/1992	Landsat 5	TM	ESA	L1	30
09/10/1992	Landsat 5	TM	ESA	L1	30
25/10/1992	Landsat 5	TM	ESA	L1	30
10/11/1992	Landsat 5	TM	ESA	L1	30
01/04/1993	SPOT-2	HRV	ESA	L3	20
06/04/1993	SPOT-2	HRV	ESA	L3	20
11/05/1993	SPOT-1	HRV	ESA	L3	20
21/05/1993	Landsat 5	TM	USGS	L1	30
06/06/1993	Landsat 5	TM	ESA	L1	30
22/06/1993	Landsat 5	TM	ESA	L1	30
25/08/1993	Landsat 5	TM	ESA	L1	30
03/12/1993	SPOT-2	HRV	ESA	L3	20
23/02/1994	SPOT-2	HRV	ESA	L3	20
09/06/1994	Landsat 5	TM	USGS	L1	30
25/06/1994	Landsat 5	TM	USGS	L1	30
25/07/1994	SPOT-2	HRV	ESA	L3	20
27/07/1994	Landsat 5	TM	USGS	L1	30
12/08/1994	Landsat 5	TM	USGS	L1	30
17/08/1994	SPOT-3	HRV	ESA	L3	20

Acquisition Date	Platform	Sensor	Source	Processing Level	Spatial Resolution (m)
20/08/1994	SPOT-2	HRV	ESA	L3	20
28/08/1994	Landsat 5	TM	USGS	L1	30
13/09/1994	Landsat 5	TM	USGS	L1	30
15/10/1994	Landsat 5	TM	USGS	L1	30
16/11/1994	Landsat 5	TM	ESA	L1	30
02/12/1994	Landsat 5	TM	ESA	L1	30
18/12/1994	Landsat 5	TM	ESA	L1	30
28/02/1995	SPOT-2	HRV	ESA	L3	20
11/03/1995	SPOT-2	HRV	ESA	L3	20
19/11/1995	Landsat 5	TM	ESA	L1	30
18/09/1996	Landsat 5	TM	ESA	L1	30
25/02/1997	Landsat 5	TM	ESA	L1	30
14/04/1997	Landsat 5	TM	ESA	L1	30
03/07/1997	Landsat 5	TM	ESA	L1	30
05/09/1997	Landsat 5	TM	ESA	L1	30
21/09/1997	Landsat 5	TM	ESA	L1	30
02/08/1998	SPOT-4	HRVIR	ESA	L3	20
03/08/1998	SPOT-4	HRVIR	ESA	L3	20
17/07/1999	Landsat 7	ETM+	USGS	L1	30
02/08/1999	Landsat 7	ETM+	ESA	L1	30
18/08/1999	Landsat 7	ETM+	USGS	L1	30
19/09/1999	Landsat 7	ETM+	ESA	L1	30
21/10/1999	Landsat 7	ETM+	ESA	L1	30
29/10/1999	Landsat 5	TM	ESA	L1	30
06/11/1999	Landsat 7	ETM+	USGS	L1	30
08/12/1999	Landsat 7	ETM+	USGS	L1	30
13/03/2000	Landsat 7	ETM+	ESA	L1	30
14/04/2000	Landsat 7	ETM+	USGS	L1	30
22/04/2000	Landsat 5	TM	ESA	L1	30
30/04/2000	Landsat 7	ETM+	ESA	L1	30
08/05/2000	Landsat 5	TM	ESA	L1	30
16/05/2000	Landsat 7	ETM+	USGS	L1	30
09/06/2000	Landsat 5	TM	ESA	L1	30
17/06/2000	Landsat 7	ETM+	USGS	L1	30
03/07/2000	Landsat 7	ETM+	ESA	L1	30
04/08/2000	Landsat 7	ETM+	ESA	L1	30
20/08/2000	Landsat 7	ETM+	USGS	L1	30
13/09/2000	Landsat 5	TM	ESA	L1	30
15/10/2000	Landsat 5	TM	ESA	L1	30
23/10/2000	Landsat 7	ETM+	USGS	L1	30
31/10/2000	Landsat 5	TM	ESA	L1	30
27/01/2001	Landsat 7	ETM+	USGS	L1	30
16/03/2001	Landsat 7	ETM+	USGS	L1	30

Acquisition Date	Platform	Sensor	Source	Processing Level	Spatial Resolution (m)
24/03/2001	Landsat 5	TM	ESA	L1	30
01/04/2001	Landsat 7	ETM+	ESA	L1	30
25/04/2001	Landsat 5	TM	ESA	L1	30
03/05/2001	Landsat 7	ETM+	USGS	L1	30
11/05/2001	Landsat 5	TM	ESA	L1	30
27/05/2001	Landsat 5	TM	ESA	L1	30
06/07/2001	Landsat 7	ETM+	USGS	L1	30
14/07/2001	Landsat 5	TM	ESA	L1	30
15/08/2001	Landsat 5	TM	ESA	L1	30
02/10/2001	Landsat 5	TM	ESA	L1	30
30/01/2002	Landsat 7	ETM+	USGS	L1	30
20/04/2002	Landsat 7	ETM+	USGS	L1	30
22/05/2002	Landsat 7	ETM+	USGS	L1	30
15/06/2002	Landsat 5	TM	USGS	L1	30
23/06/2002	Landsat 7	ETM+	USGS	L1	30
01/07/2002	Landsat 5	TM	USGS	L1	30
26/08/2002	Landsat 7	ETM+	USGS	L1	30
22/03/2003	Landsat 7	ETM+	USGS	L1	30
23/04/2003	Landsat 7	ETM+	USGS	L1	30
04/07/2003	Landsat 5	TM	USGS	L1	30
20/07/2003	Landsat 5	TM	USGS	L1	30
05/08/2003	Landsat 5	TM	USGS	L1	30
21/08/2003	Landsat 5	TM	USGS	L1	30
06/09/2003	Landsat 5	TM	USGS	L1	30
22/09/2003	Landsat 5	TM	USGS	L1	30
16/03/2004	Landsat 5	TM	ESA	L1	30
03/05/2004	Landsat 5	TM	ESA	L1	30
06/07/2004	Landsat 5	TM	USGS	L1	30
22/07/2004	Landsat 5	TM	USGS	L1	30
07/08/2004	Landsat 5	TM	USGS	L1	30
23/08/2004	Landsat 5	TM	USGS	L1	30
08/09/2004	Landsat 5	TM	USGS	L1	30
10/10/2004	Landsat 5	TM	USGS	L1	30
26/10/2004	Landsat 5	TM	USGS	L1	30
11/11/2004	Landsat 5	TM	USGS	L1	30
04/04/2005	Landsat 5	TM	ESA	L1	30
20/04/2005	Landsat 5	TM	USGS	L1	30
22/05/2005	Landsat 5	TM	USGS	L1	30
25/07/2005	Landsat 5	TM	USGS	L1	30
10/08/2005	Landsat 5	TM	USGS	L1	30
26/08/2005	Landsat 5	TM	USGS	L1	30
11/09/2005	Landsat 5	TM	USGS	L1	30
27/09/2005	Landsat 5	TM	USGS	L1	30

Acquisition Date	Platform	Sensor	Source	Processing Level	Spatial Resolution (m)
29/10/2005	Landsat 5	TM	USGS	L1	30
23/04/2006	Landsat 5	TM	USGS	L1	30
09/05/2006	Landsat 5	TM	USGS	L1	30
26/06/2006	Landsat 5	TM	USGS	L1	30
12/07/2006	Landsat 5	TM	USGS	L1	30
28/07/2006	Landsat 5	TM	USGS	L1	30
14/09/2006	Landsat 5	TM	USGS	L1	30
30/09/2006	Landsat 5	TM	USGS	L1	30
17/11/2006	Landsat 5	TM	ESA	L1	30
21/02/2007	Landsat 5	TM	ESA	L1	30
12/05/2007	Landsat 5	TM	ESA	L1	30
28/05/2007	Landsat 5	TM	USGS	L1	30
13/06/2007	Landsat 5	TM	USGS	L1	30
29/06/2007	Landsat 5	TM	USGS	L1	30
15/07/2007	Landsat 5	TM	ESA	L1	30
16/08/2007	Landsat 5	TM	USGS	L1	30
03/10/2007	Landsat 5	TM	ESA	L1	30
02/08/2008	Landsat 5	TM	ESA	L1	30
15/04/2009	Landsat 5	TM	ESA	L1	30
17/05/2009	Landsat 5	TM	ESA	L1	30
18/06/2009	Landsat 5	TM	USGS	L1	30
14/07/2009	RapidEye-4	MSI	ESA	3A	5
20/07/2009	RapidEye-5	MSI	ESA	3A	30
20/07/2009	Landsat 5	TM	USGS	L1	5
21/08/2009	Landsat 5	TM	ESA	L1	30
27/08/2009	RapidEye-5	MSI	ESA	3A	5
28/08/2009	RapidEye-1	MSI	ESA	3A	5
21/09/2009	RapidEye-1	MSI	ESA	3A	5
22/09/2009	Landsat 5	TM	USGS	L1	30
08/10/2009	Landsat 5	TM	USGS	L1	30
28/10/2009	RapidEye-5	MSI	ESA	3A	5
18/04/2010	Landsat 5	TM	ESA	L1	30
23/07/2010	Landsat 5	TM	USGS	L1	30
24/08/2010	Landsat 5	TM	USGS	L1	30
27/08/2010	RapidEye-3	MSI	ESA	3A	5
09/09/2010	Landsat 5	TM	USGS	L1	30
11/10/2010	Landsat 5	TM	ESA	L1	30
25/03/2011	RapidEye-3	MSI	ESA	3A	5
21/04/2011	Landsat 5	TM	ESA	L1	30
21/04/2011	RapidEye-1	MSI	ESA	3A	5
07/05/2011	Landsat 5	TM	ESA	L1	30
07/06/2011	RapidEye-1	MSI	ESA	3A	5
08/06/2011	Landsat 5	TM	USGS	L1	30

Acquisition Date	Platform	Sensor	Source	Processing Level	Spatial Resolution (m)
10/07/2011	Landsat 5	TM	USGS	L1	30
13/07/2011	RapidEye-3	MSI	ESA	3A	5
11/08/2011	Landsat 5	TM	USGS	L1	30
12/08/2011	RapidEye-4	MSI	ESA	3A	5
18/08/2011	RapidEye-1	MSI	ESA	3A	5
20/08/2011	RapidEye-3	MSI	ESA	3A	5
27/08/2011	Landsat 5	TM	USGS	L1	30
28/09/2011	Landsat 5	TM	USGS	L1	30
02/10/2011	RapidEye-3	MSI	ESA	3A	5
15/10/2011	RapidEye-2	MSI	ESA	3A	5
04/05/2012	RapidEye-4	MSI	ESA	3A	5
11/06/2012	RapidEye-3	MSI	ESA	3A	5
02/07/2012	RapidEye-1	MSI	ESA	3A	5
10/07/2012	RapidEye-4	MSI	ESA	3A	5
21/07/2012	RapidEye-1	MSI	ESA	3A	5
18/10/2012	RapidEye-4	MSI	ESA	3A	5
13/04/2013	RapidEye-5	MSI	ESA	3A	5
16/04/2013	RapidEye-3	MSI	ESA	3A	5
28/05/2013	Landsat 8	OLI	USGS	L1	30
11/06/2013	RapidEye-2	MSI	ESA	3A	5
14/06/2013	RapidEye-5	MSI	ESA	3A	5
15/06/2013	RapidEye-1	MSI	ESA	3A	5
17/06/2013	RapidEye-3	MSI	ESA	3A	5
15/07/2013	Landsat 8	OLI	USGS	L1	30
23/07/2013	RapidEye-1	MSI	ESA	3A	5
03/08/2013	RapidEye-2	MSI	ESA	3A	5
16/08/2013	Landsat 8	OLI	USGS	L1	30
01/09/2013	Landsat 8	OLI	USGS	L1	30
06/09/2013	RapidEye-3	MSI	ESA	3A	5
16/09/2013	RapidEye-3	MSI	ESA	3A	5
19/10/2013	Landsat 8	OLI	USGS	L1	30
22/12/2013	Landsat 8	OLI	USGS	L1	30
12/03/2014	Landsat 8	OLI	USGS	L1	30
13/04/2014	Landsat 8	OLI	USGS	L1	30
19/05/2014	RapidEye-1	MSI	ESA	3A	5
28/06/2014	RapidEye-3	MSI	ESA	3A	5
02/07/2014	Landsat 8	OLI	USGS	L1	30
09/09/2014	RapidEye-5	MSI	ESA	3A	5
09/09/2014	Landsat 8	OLI	USGS	L1	30

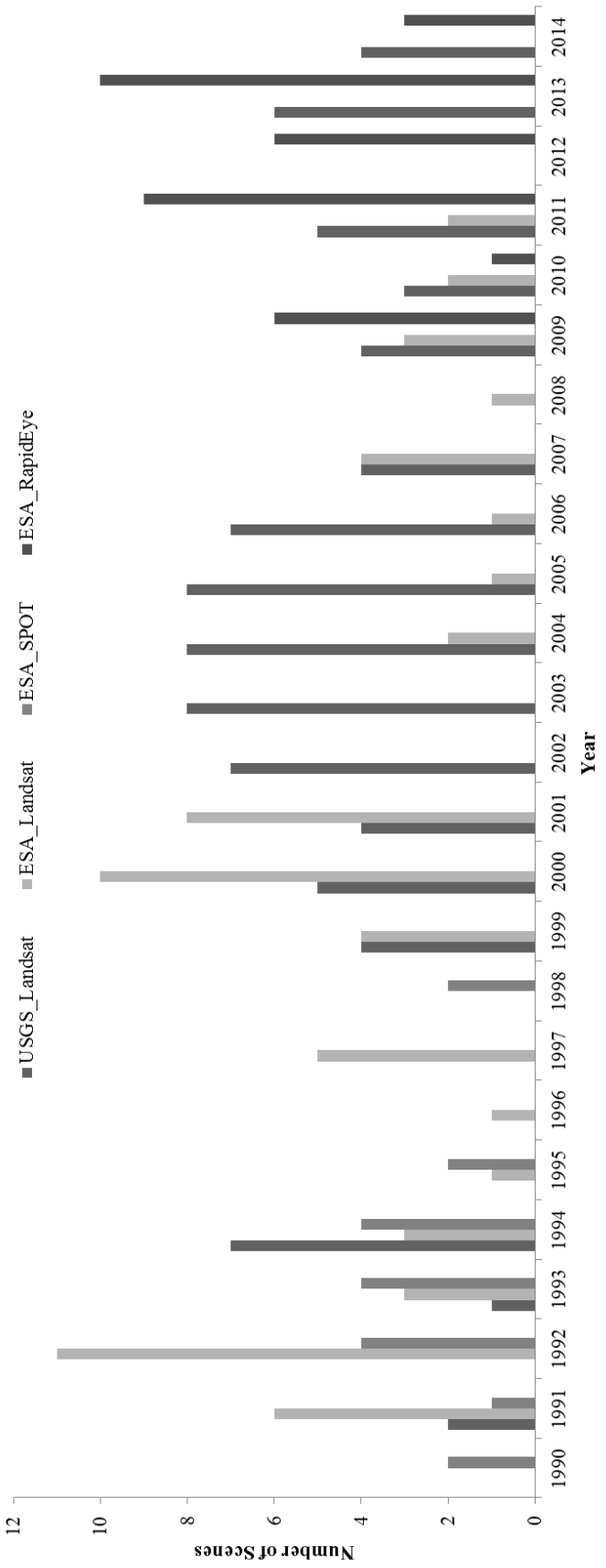

Figure 4-53 - Bar chart showing the sensors and numbers of scenes used per year.

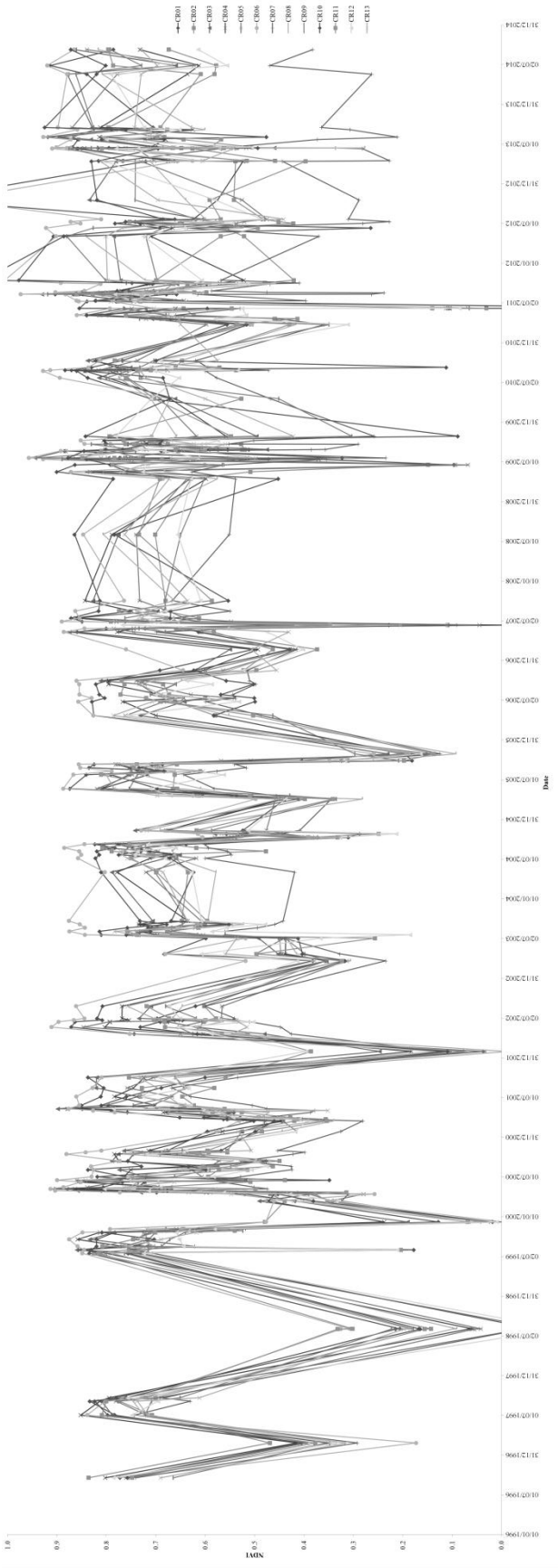

Figure 4-54 - NDVI profile for all of the Cancari Road mass graves from 1996 – 2014 derived from all sensors.

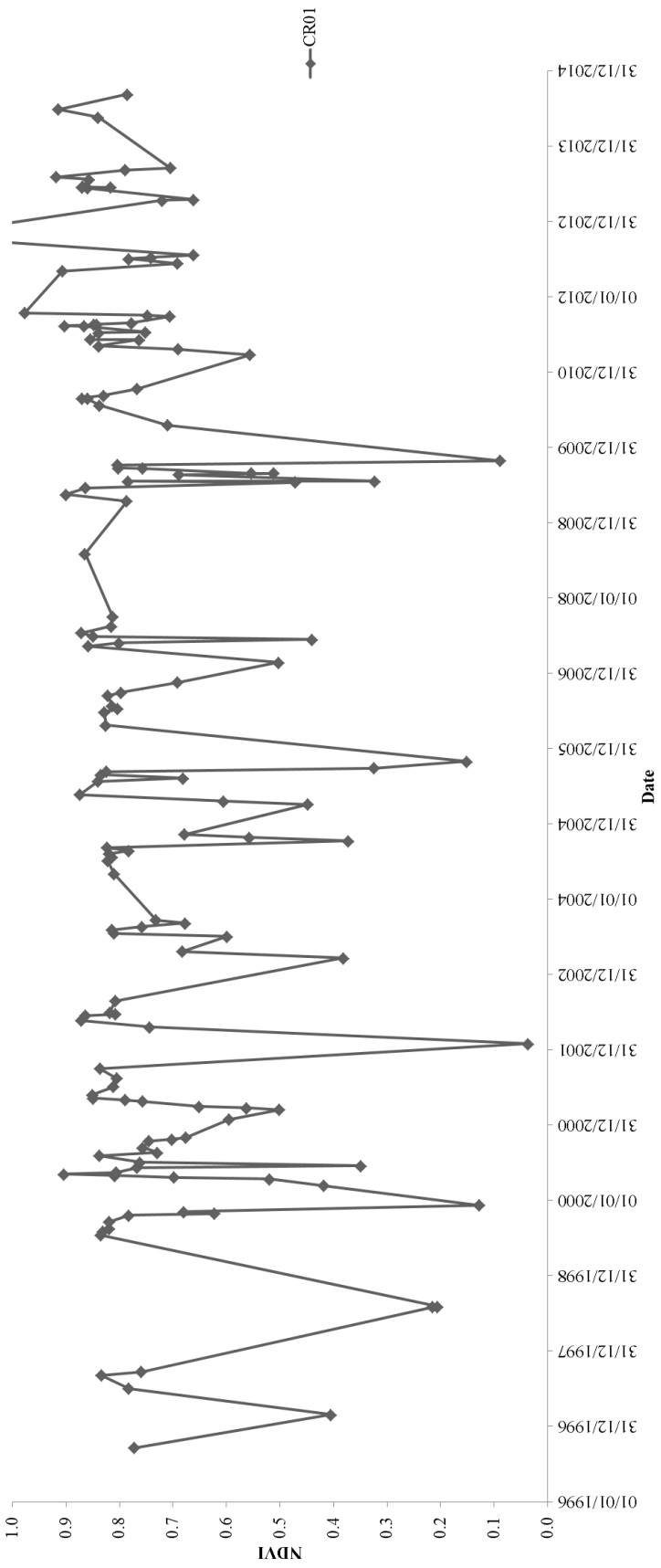

Figure 4-55 - Line plot showing the extracted NDVI profile, derived from all sensors, for the CR01 mass grave plotted from 1996 (post burial) to 2014 (post exhumation).

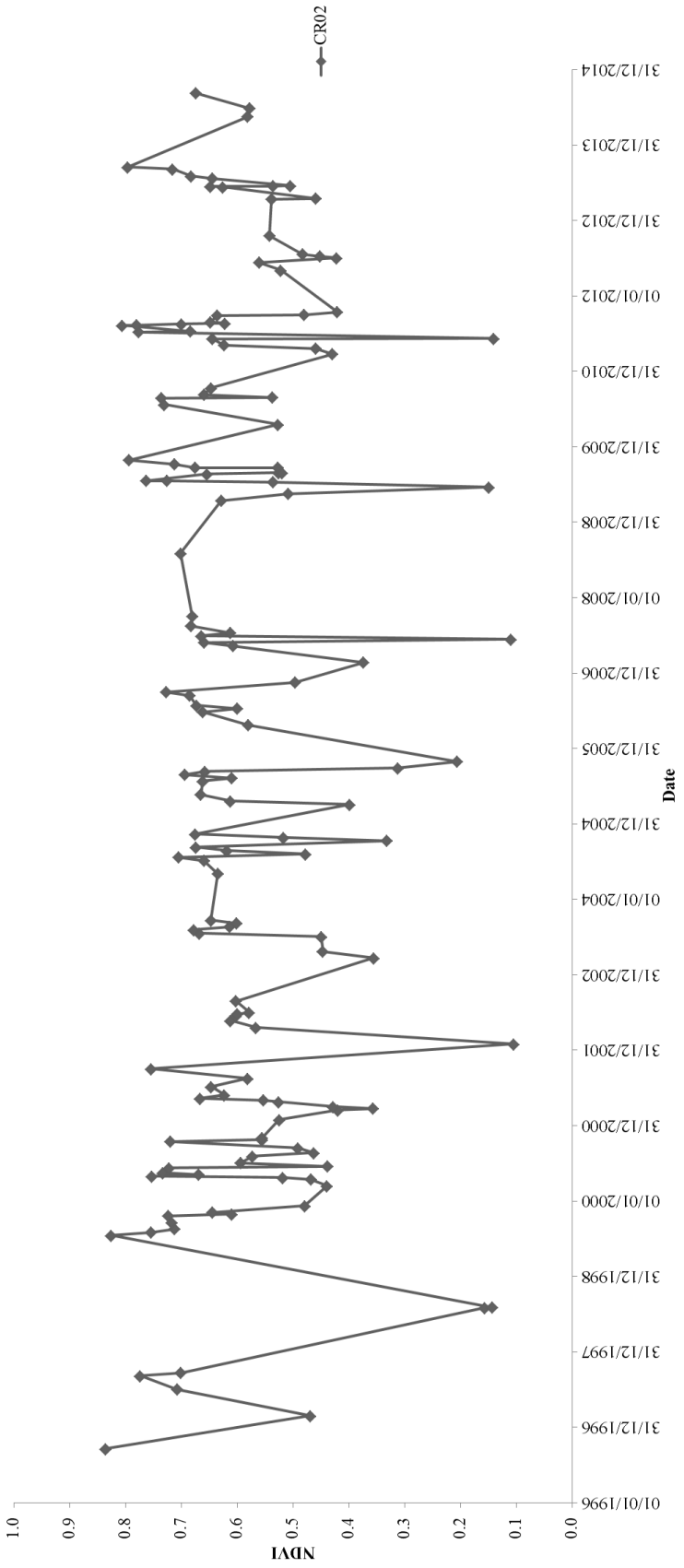

Figure 4-56 - Line plot showing the extracted NDVI profile, derived from all sensors, for the CR02 mass grave plotted from 1996 (post burial) to 2014 (post exhumation).

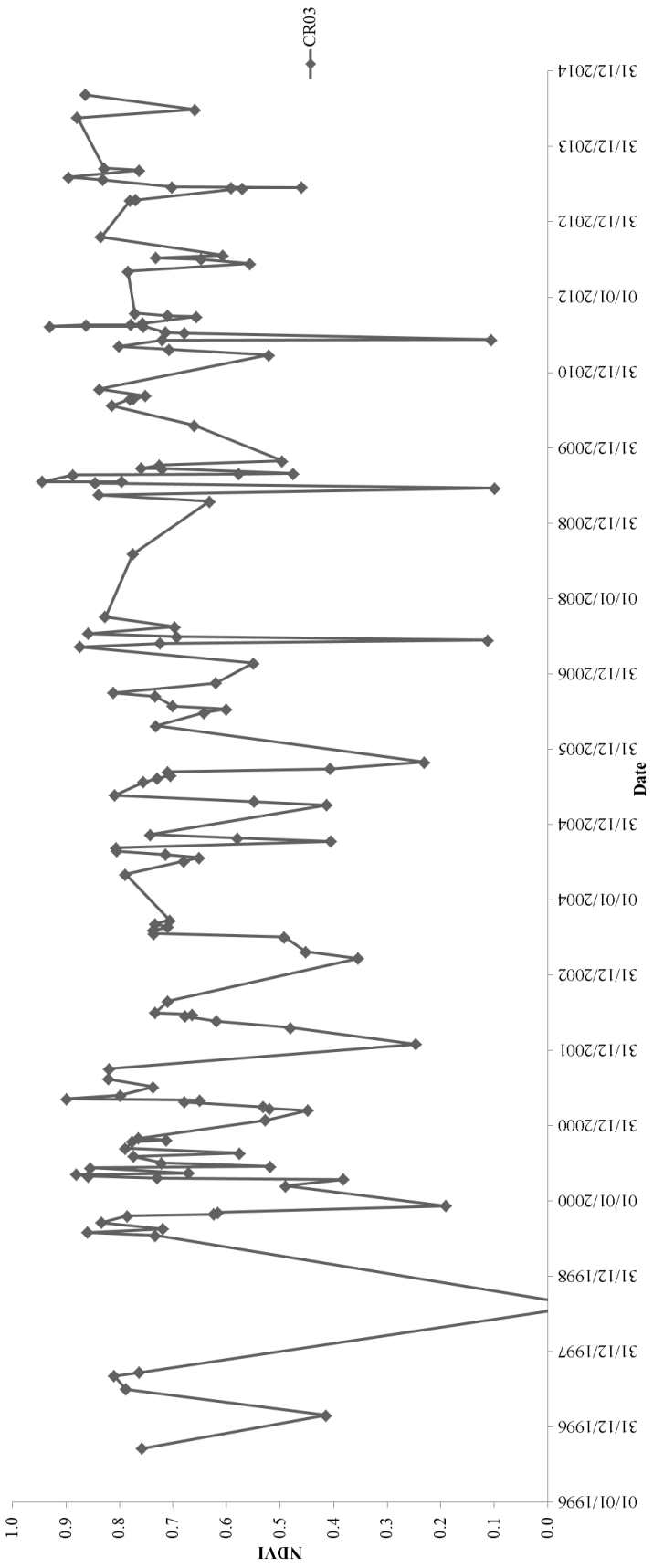

Figure 4-57 - Line plot showing the extracted NDVI profile, derived from all sensors, for the CR03 mass grave plotted from 1996 (post burial) to 2014 (post exhumation).

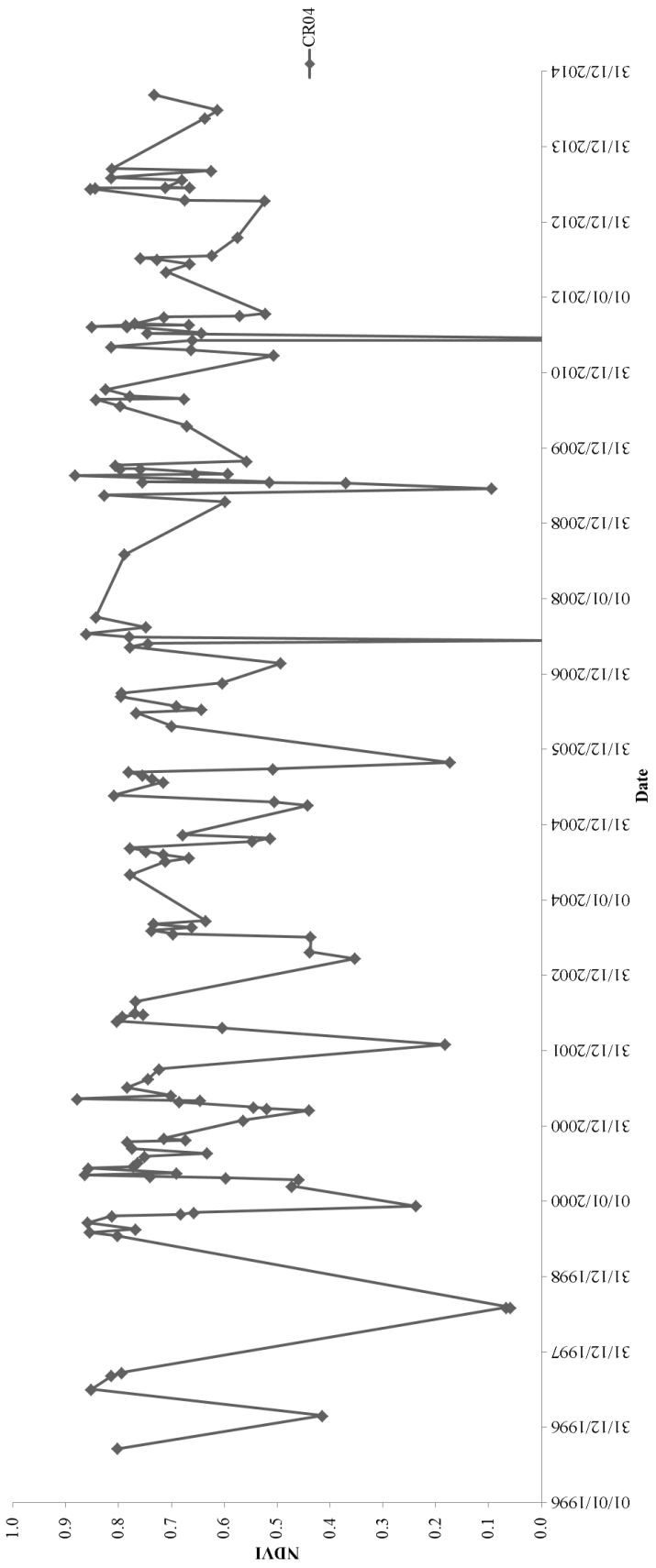

Figure 4-58 - Line plot showing the extracted NDVI profile, derived from all sensors, for the CR04 mass grave plotted from 1996 (post burial) to 2014 (post exhumation).

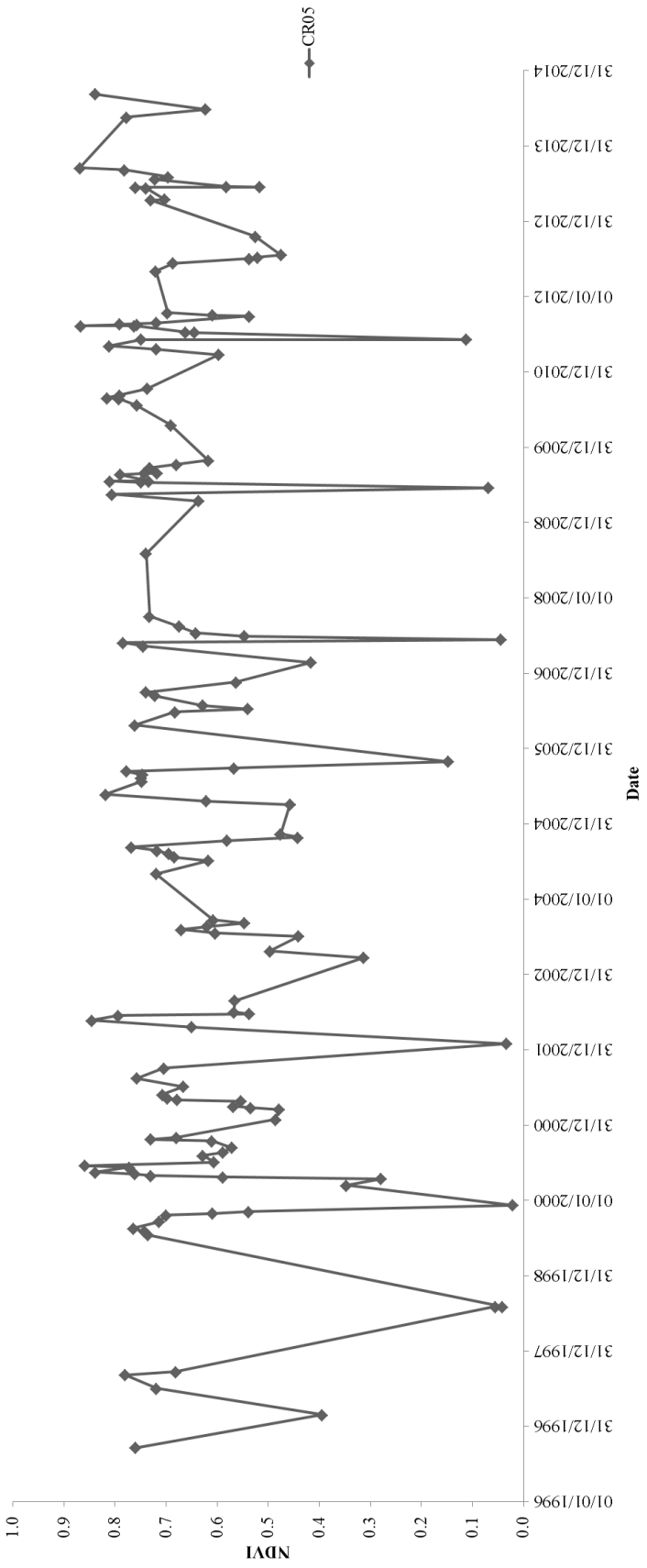

Figure 4-59 – Line plot showing the extracted NDVI profile, derived from all sensors, for the CR05 mass grave plotted from 1996 (post burial) to 2014 (post exhumation).

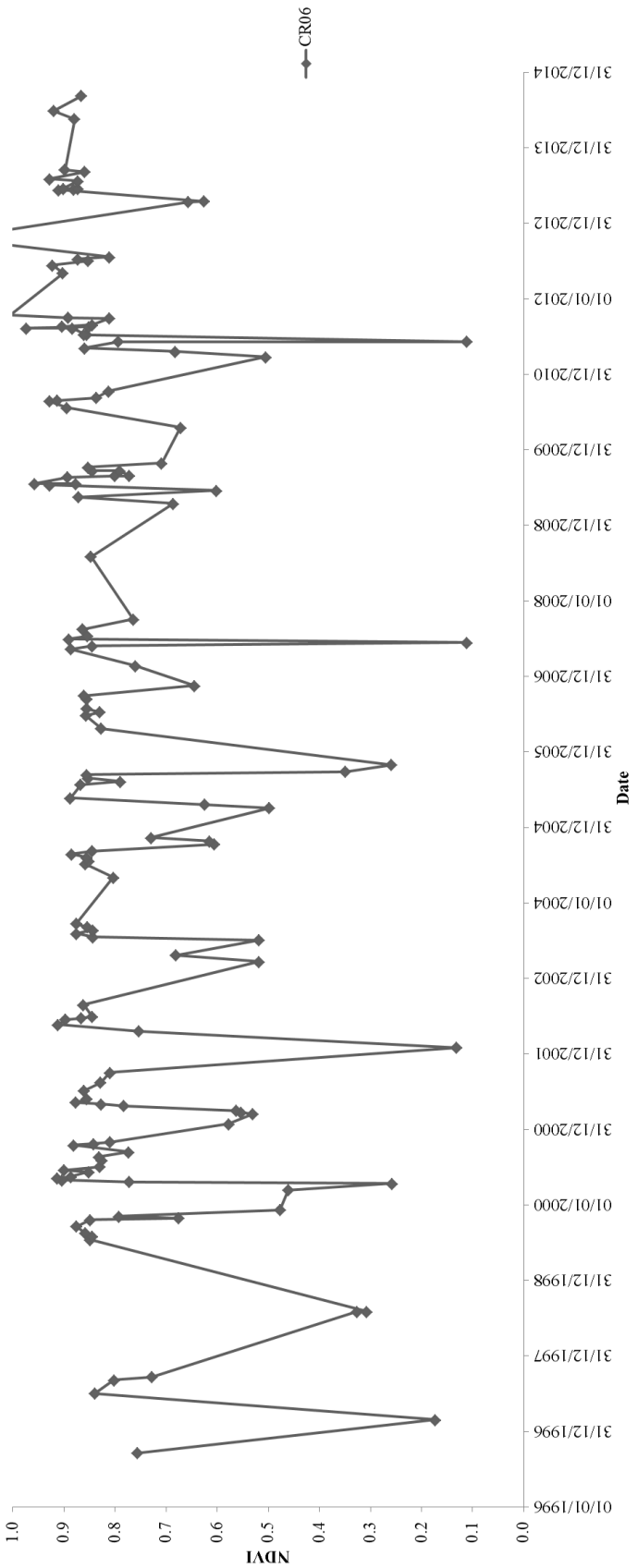

Figure 4-60 - Line plot showing the extracted NDVI profile, derived from all sensors, for the CR06 mass grave plotted from 1996 (post burial) to 2014 (post exhumation).

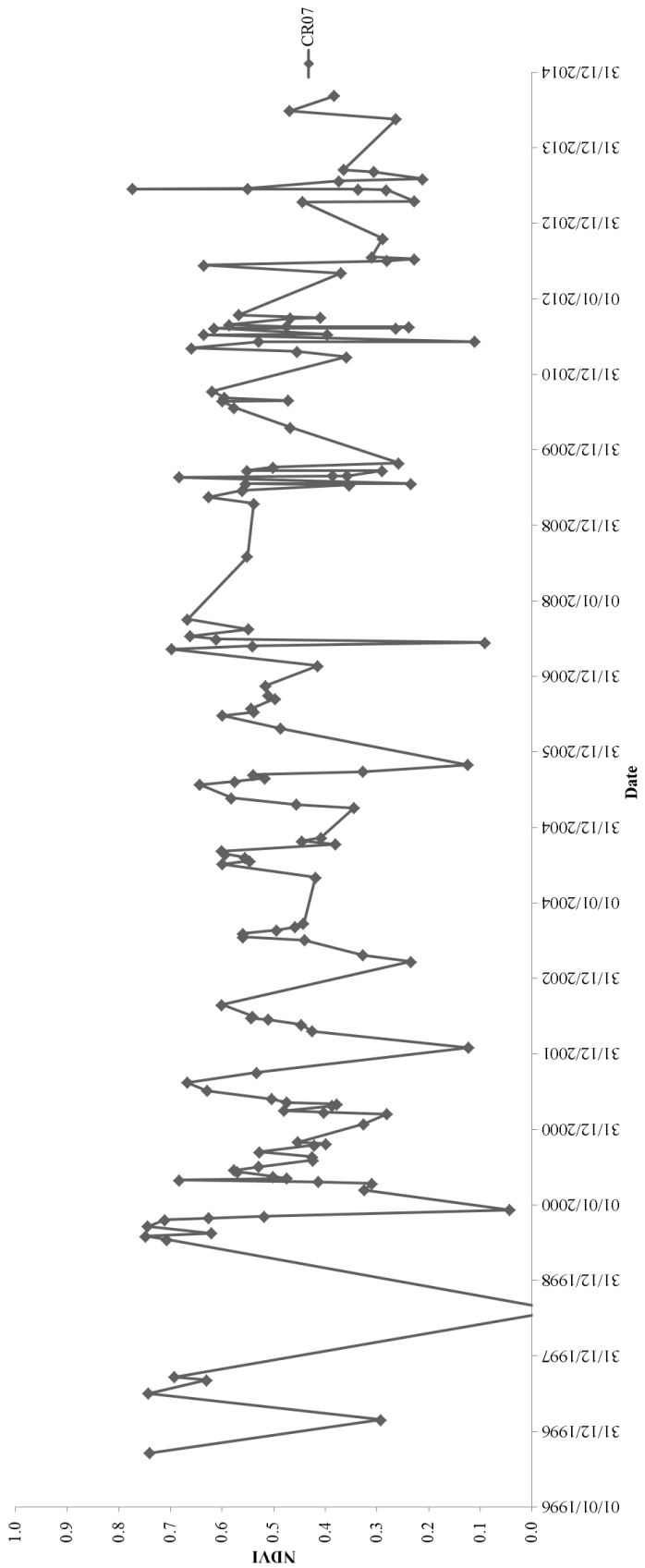

Figure 4-61 - Line plot showing the extracted NDVI profile, derived from all sensors, for the CR07 mass grave plotted from 1996 (post burial) to 2014 (post exhumation).

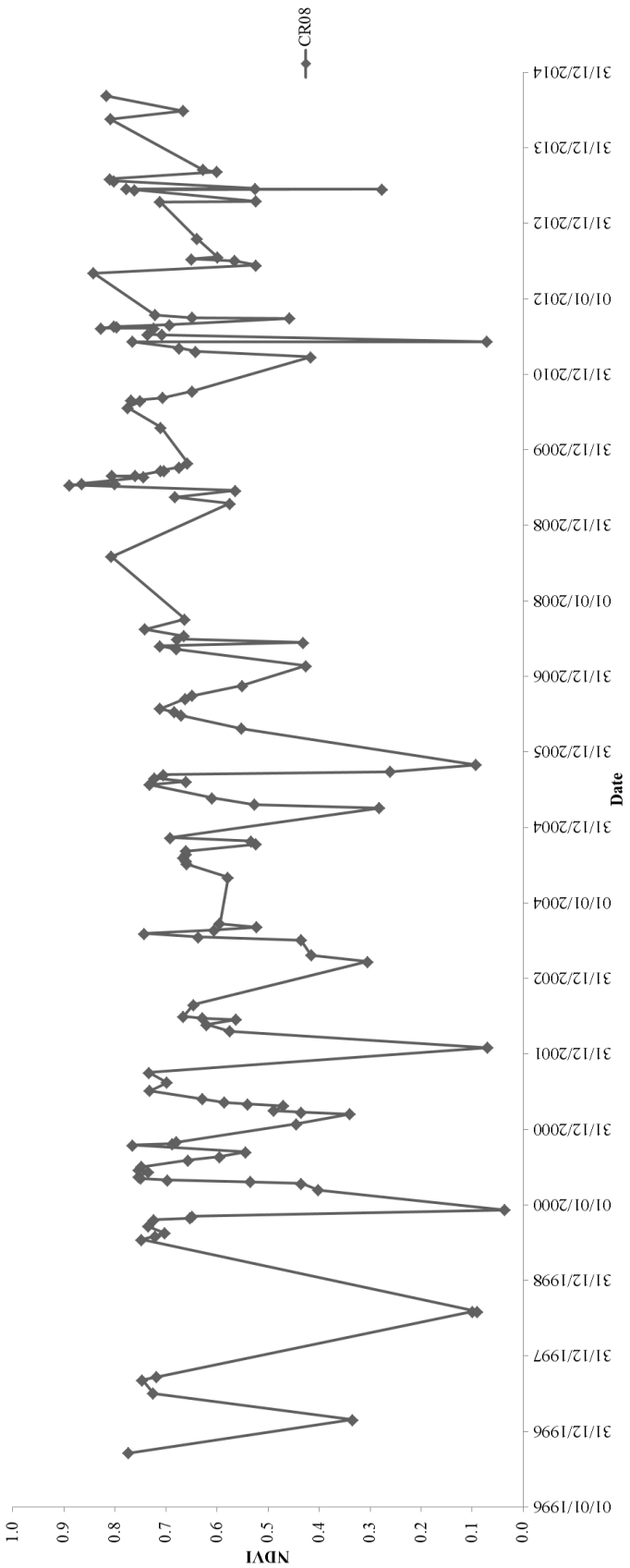

Figure 4-62 - Line plot showing the extracted NDVI profile, derived from all sensors, for the CR08 mass grave plotted from 1996 (post burial) to 2014 (post exhumation).

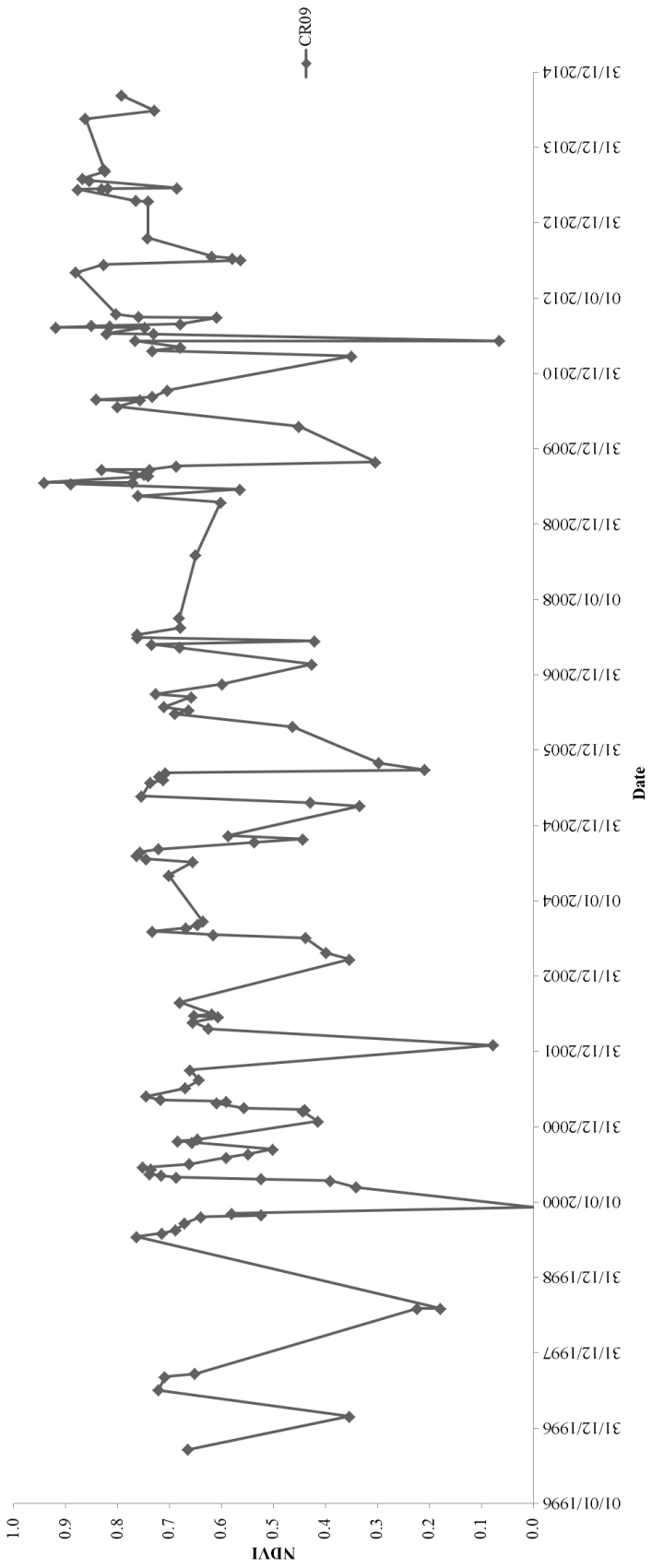

Figure 4-63 - Line plot showing the extracted NDVI profile, derived from all sensors, for the CR09 mass grave plotted from 1996 (post burial) to 2014 (post exhumation).

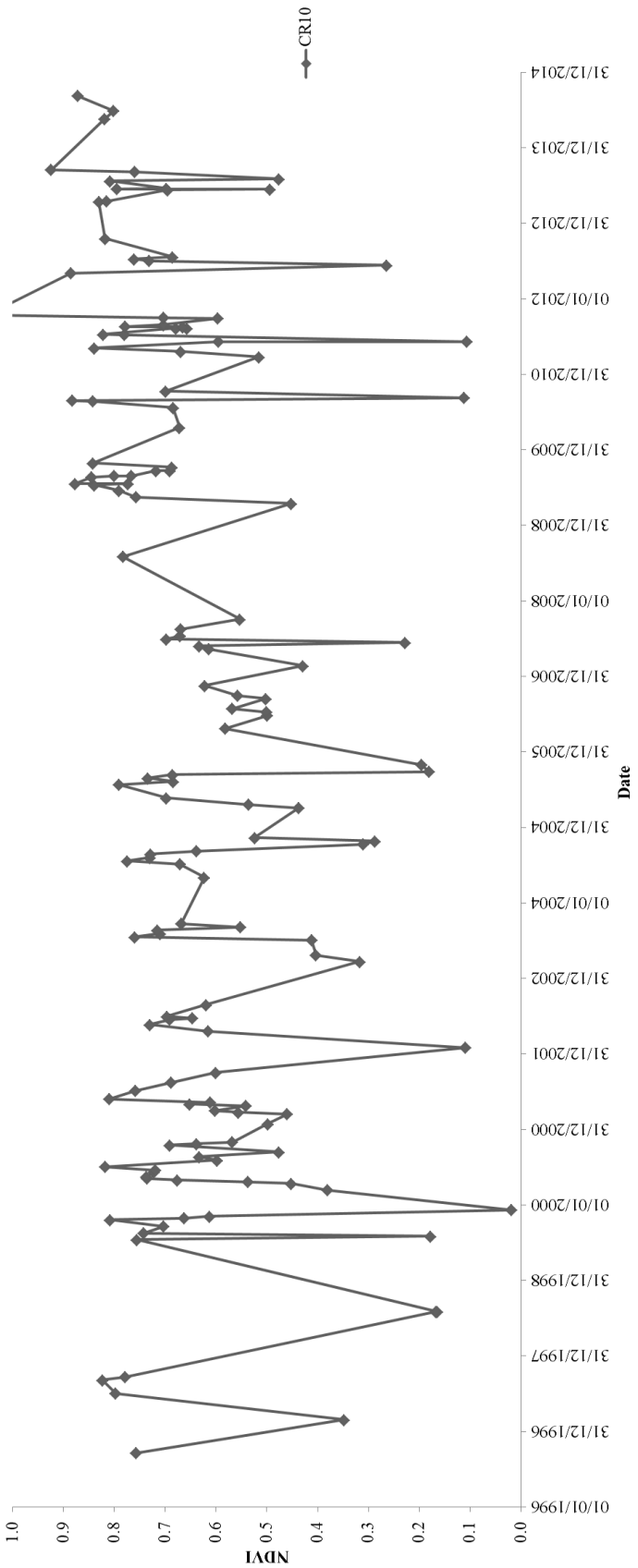

Figure 4-64 - Line plot showing the extracted NDVI profile, derived from all sensors, for the CR10 mass grave plotted from 1996 (post burial) to 2014 (post exhumation).

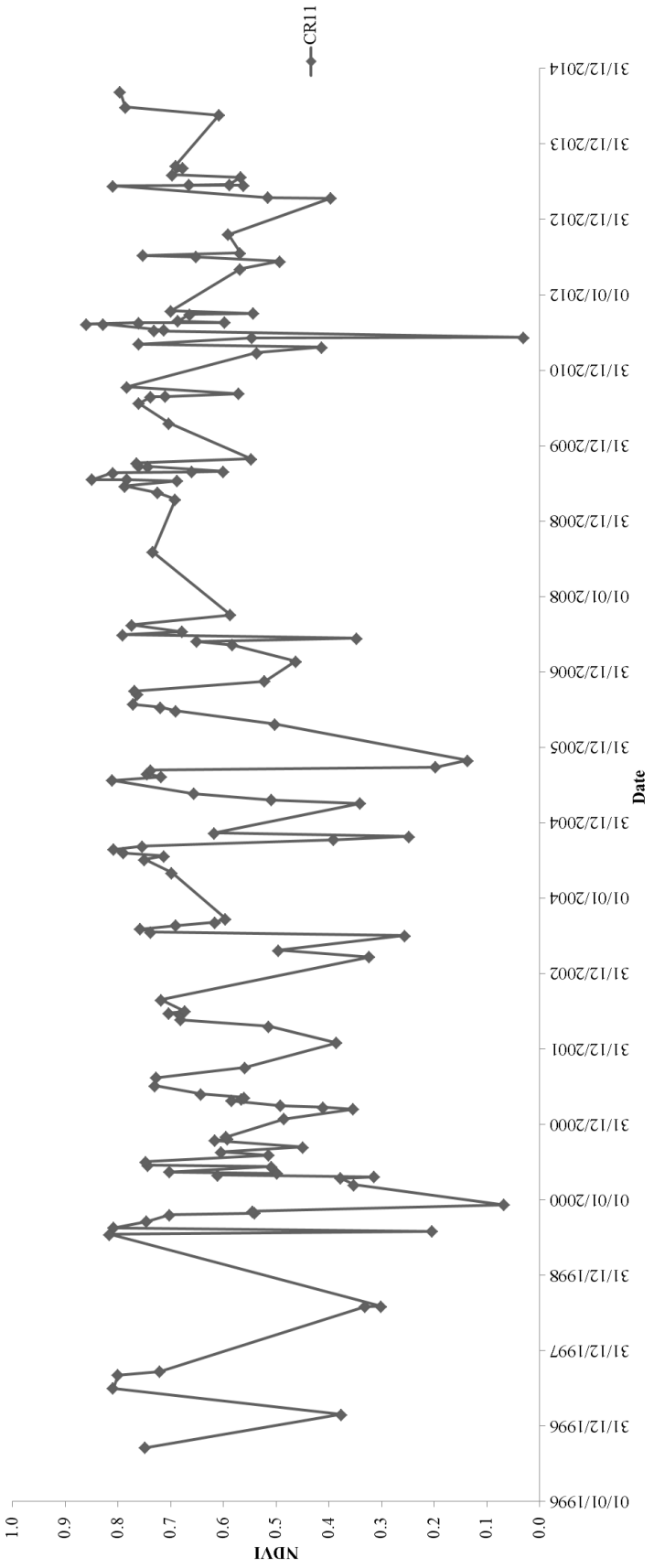

Figure 4-65 - Line plot showing the extracted NDVI profile, derived from all sensors, for the CR11 mass grave plotted from 1996 (post burial) to 2014 (post exhumation).

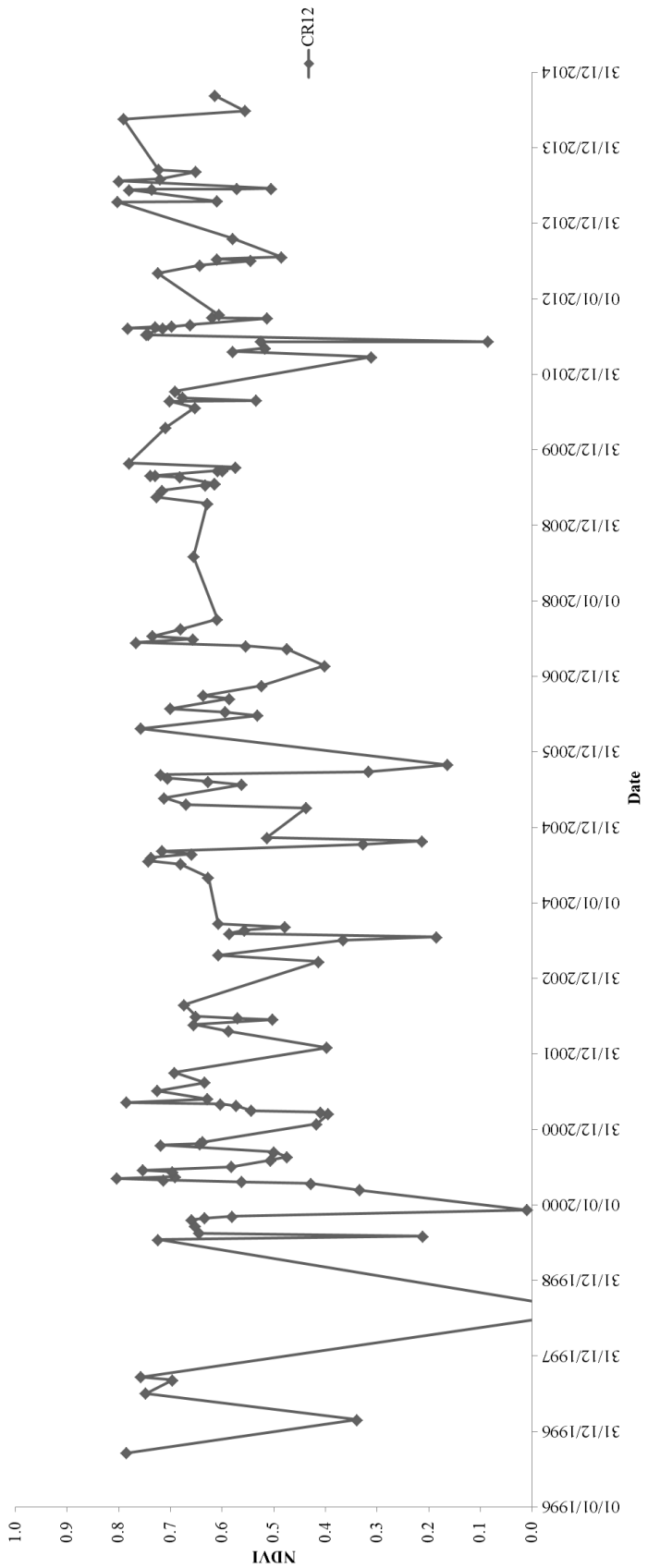

Figure 4-66 - Line plot showing the extracted NDVI profile, derived from all sensors, for the CR12 mass grave plotted from 1996 (post burial) to 2014 (post exhumation).

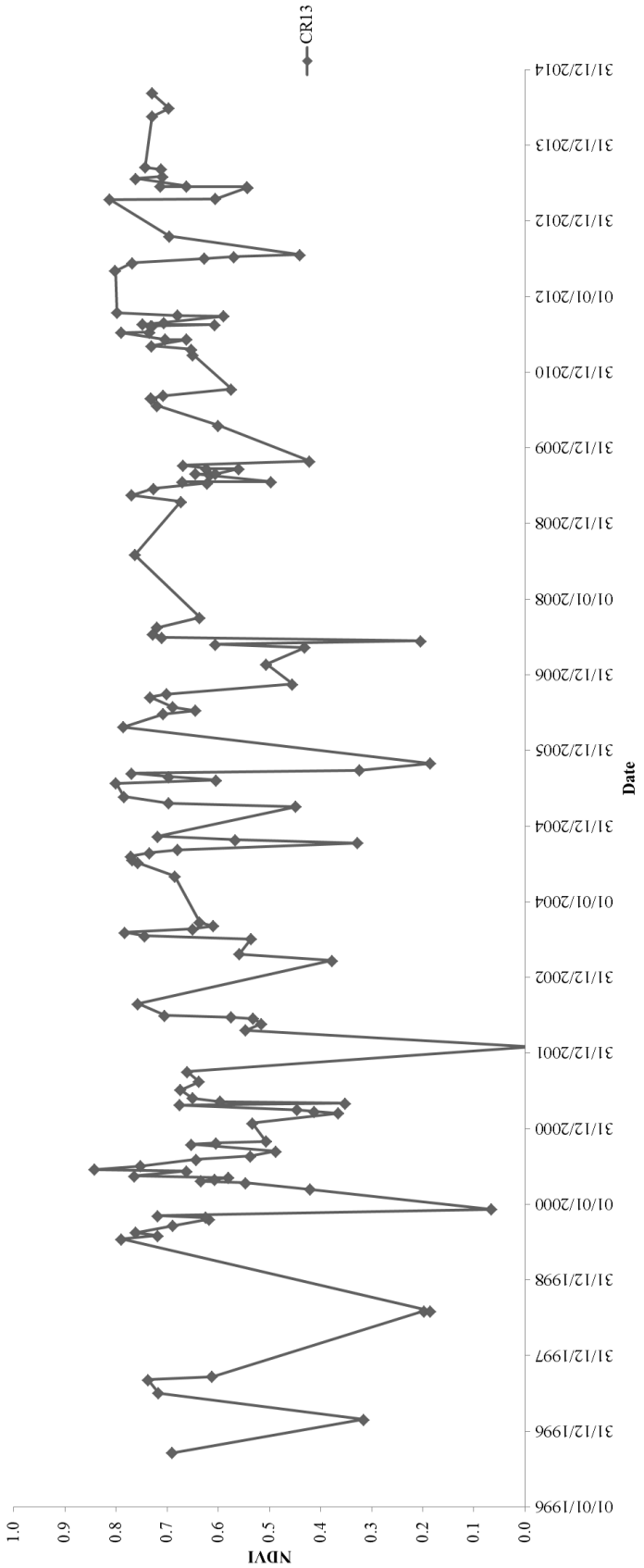

Figure 4-67 - Line plot showing the extracted NDVI profile, derived from all sensors, for the CR13 mass grave plotted from 1996 (post burial) to 2014 (post exhumation).

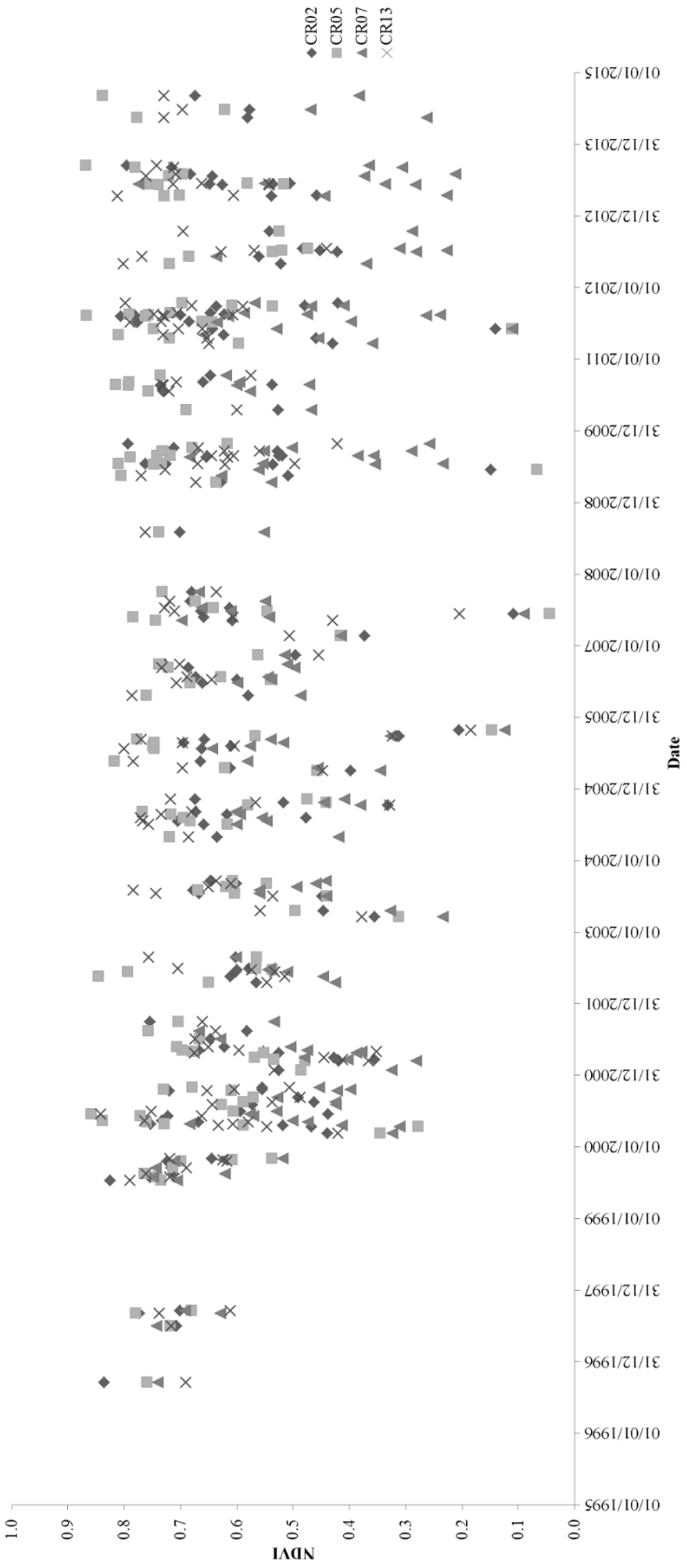

Figure 4-68 - Scatter plot showing the Cancari Road mass graves which were exhumed in 2002 and the extracted NDVI from all sensors (1995 – 2015). Anomalies (negative) NDVI values from SPOT were omitted.

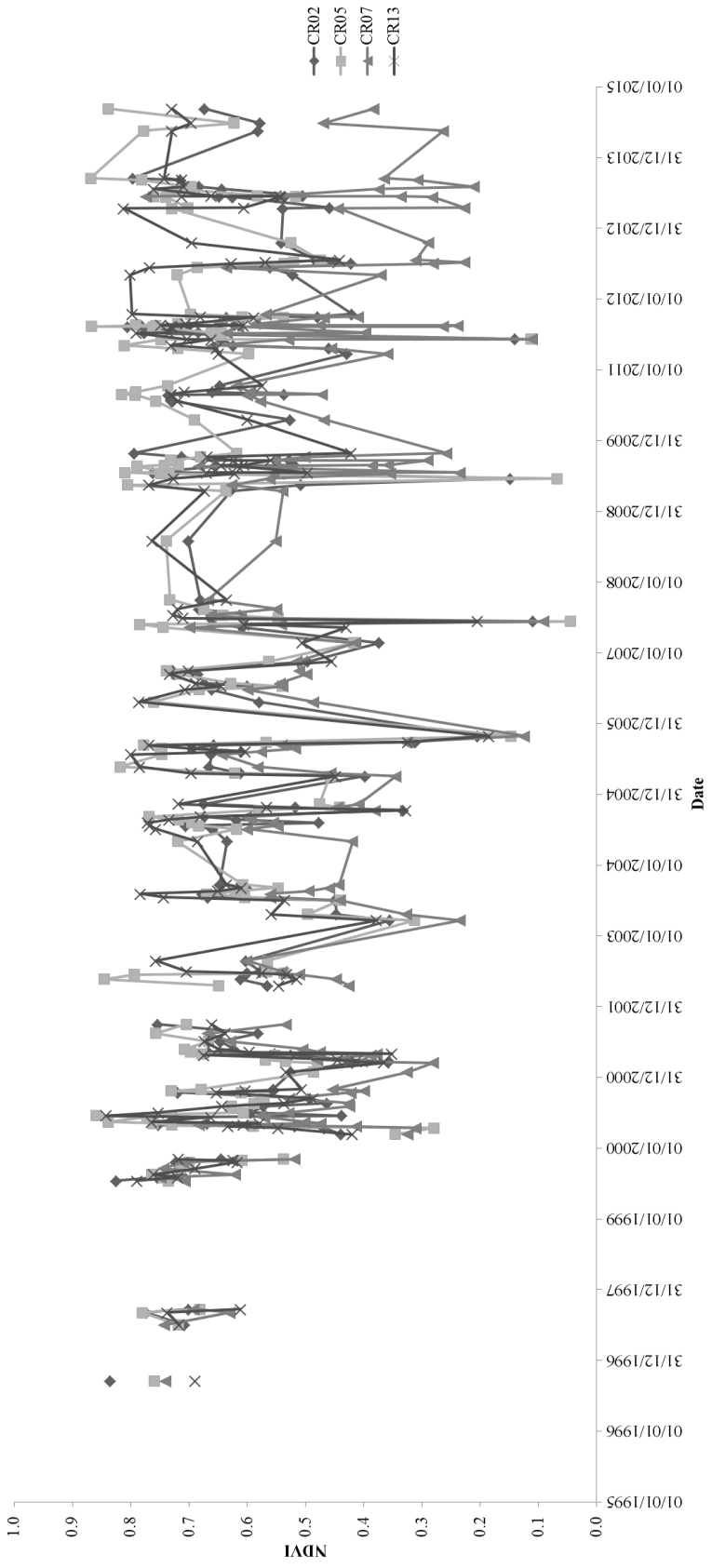

Figure 4-69 - Line plot showing the Cancari Road mass graves which were exhumed in 2002 and the extracted NDVI from all sensors (1995 – 2015). Anomalies (negative) NDVI values were omitted.

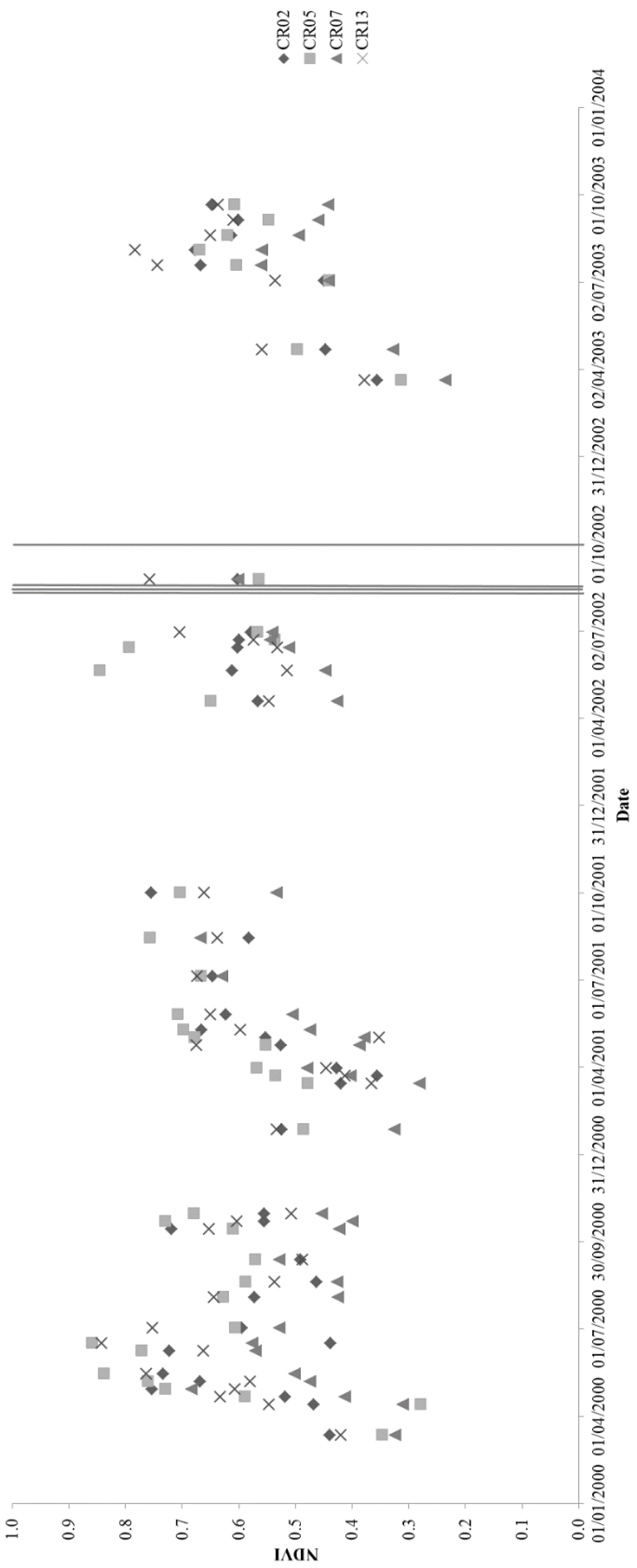

Figure 70 - Scatter plot showing the Cancari Road mass graves which were exhumed in 2002 and the extracted NDVI from all sensors (2000 – 2004). Anomalies (negative) NDVI values (from SPOT) are omitted. The excavation dates for each grave are represented by the vertical lines.

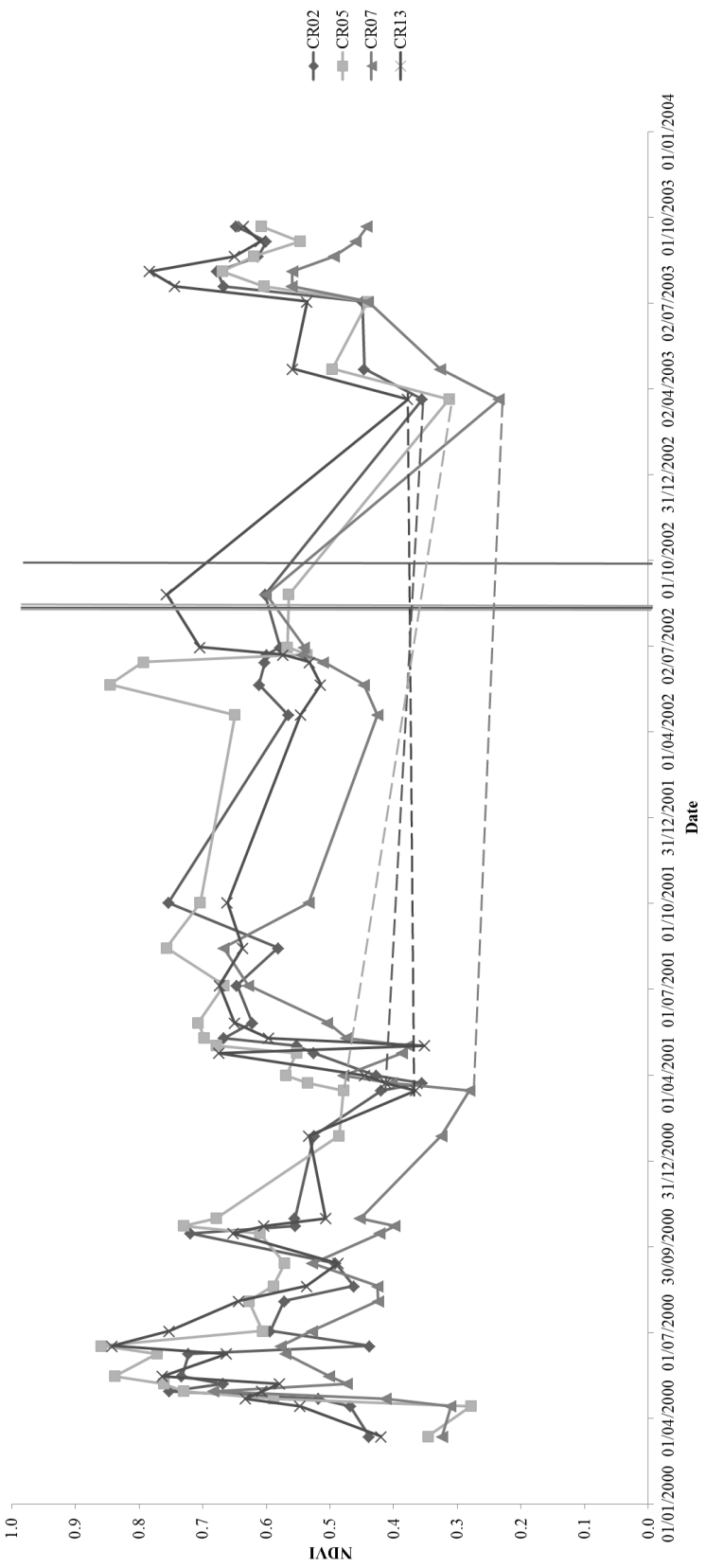

Figure 71 - Line plot showing the Cancari Road mass graves which were exhumed in 2002 and the extracted NDVI from all sensors (2000 – 2004). Anomalies (negative) NDVI values (from SPOT) are omitted. The excavation dates for each grave are represented by the vertical lines. Dashed lines compare NDVI values for each grave from August 2000 and April 2003.

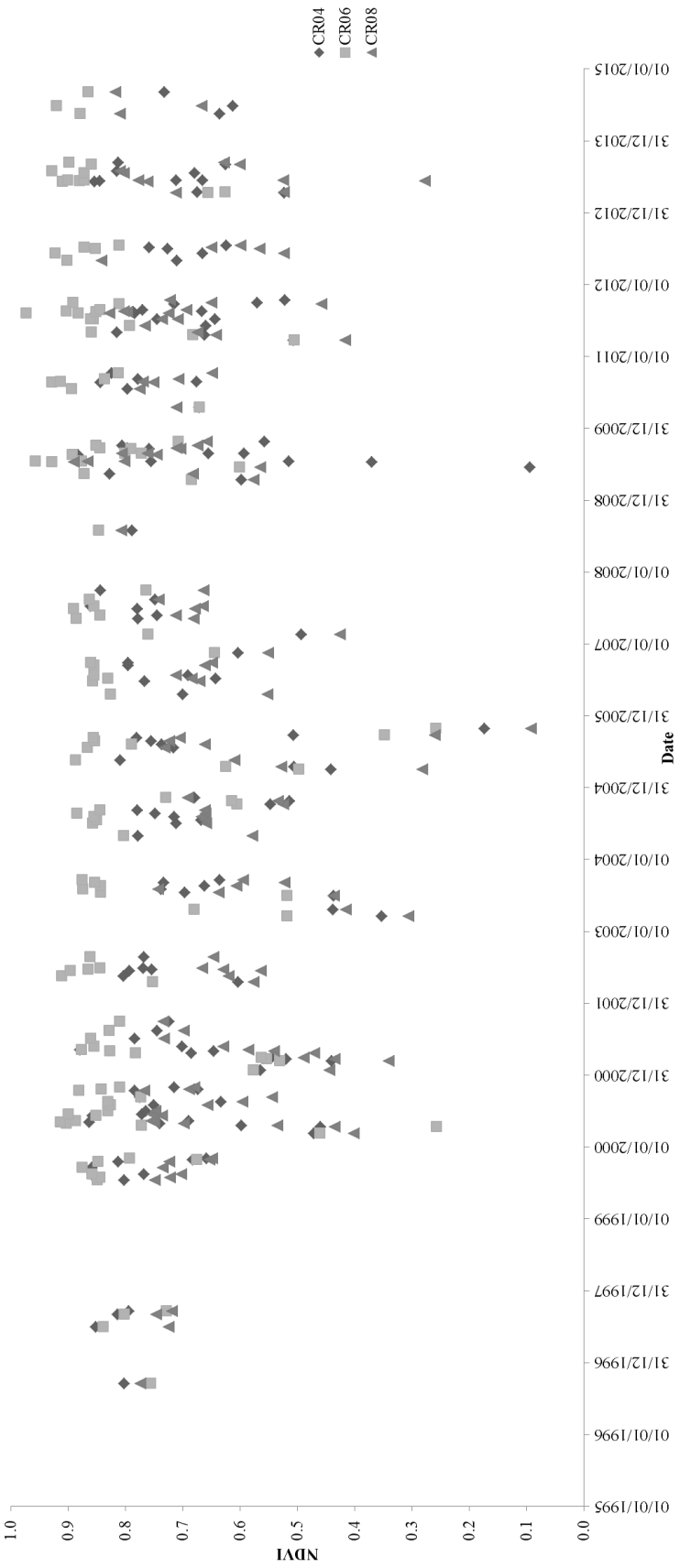

Figure 72 - Scatter plot showing the Cancari Road mass graves which were exhumed in 2008 and the extracted NDVI from all sensors (1995 – 2015). Anomalies (negative) NDVI values (from SPOT) were omitted.

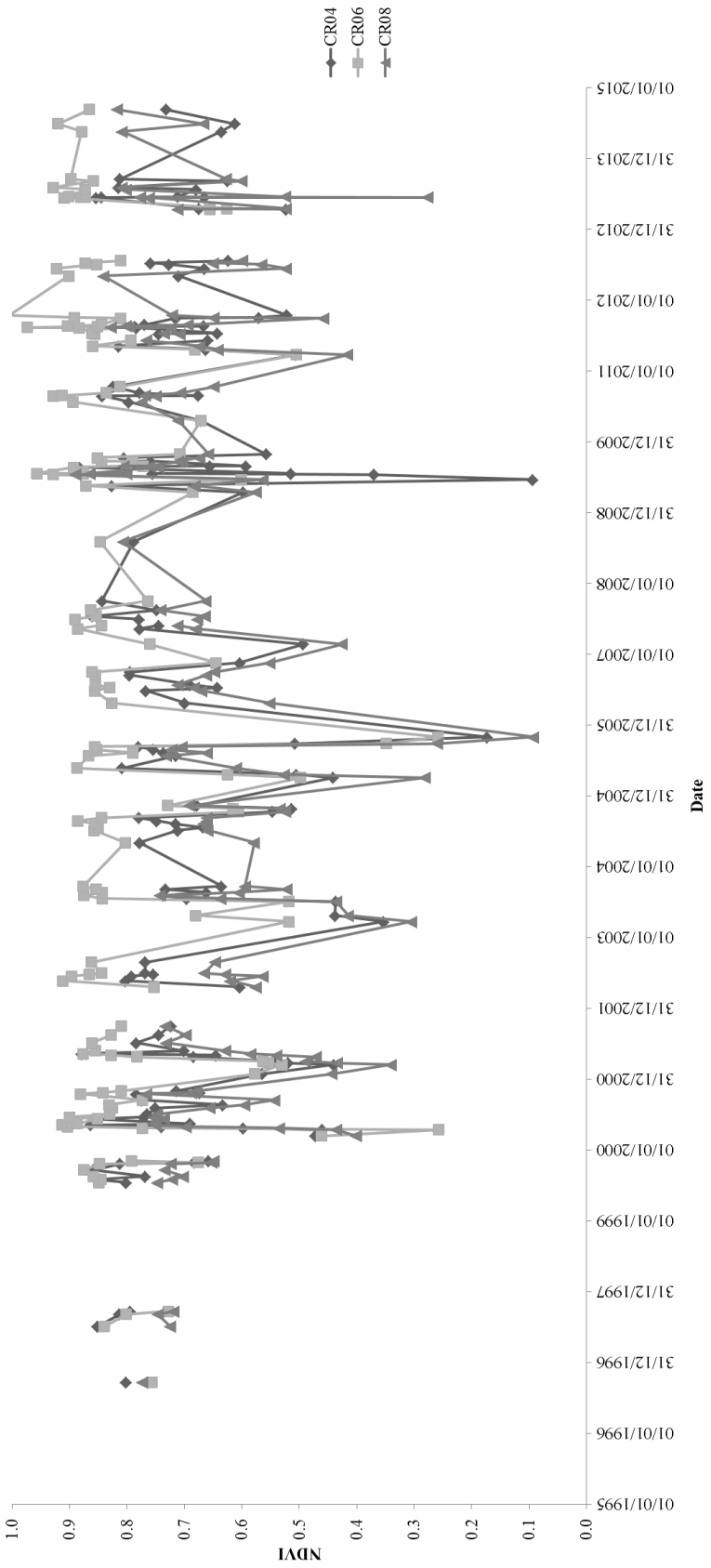

Figure 4-73 - Line plot showing the Cancari Road mass graves which were exhumed in 2008 and the extracted NDVI from all sensors (1995 – 2015). Anomalies (negative) NDVI values (from SPOT) were omitted.

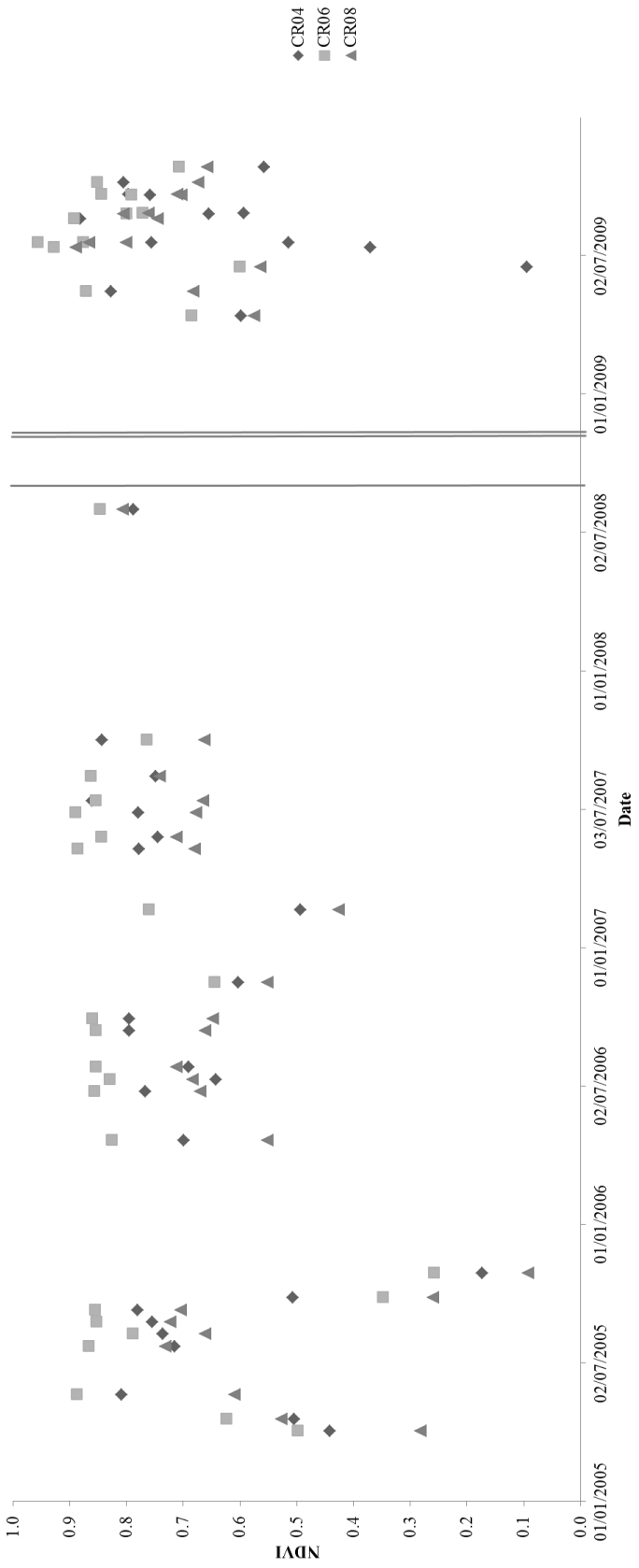

Figure 4-74 - Scatter plot showing the Cancari Road mass graves which were exhumed in 2008 and the extracted NDVI from all sensors (2005 – 2009). Anomalies (negative) NDVI values (from SPOT) are omitted. The excavation dates for each grave are represented by the vertical lines.

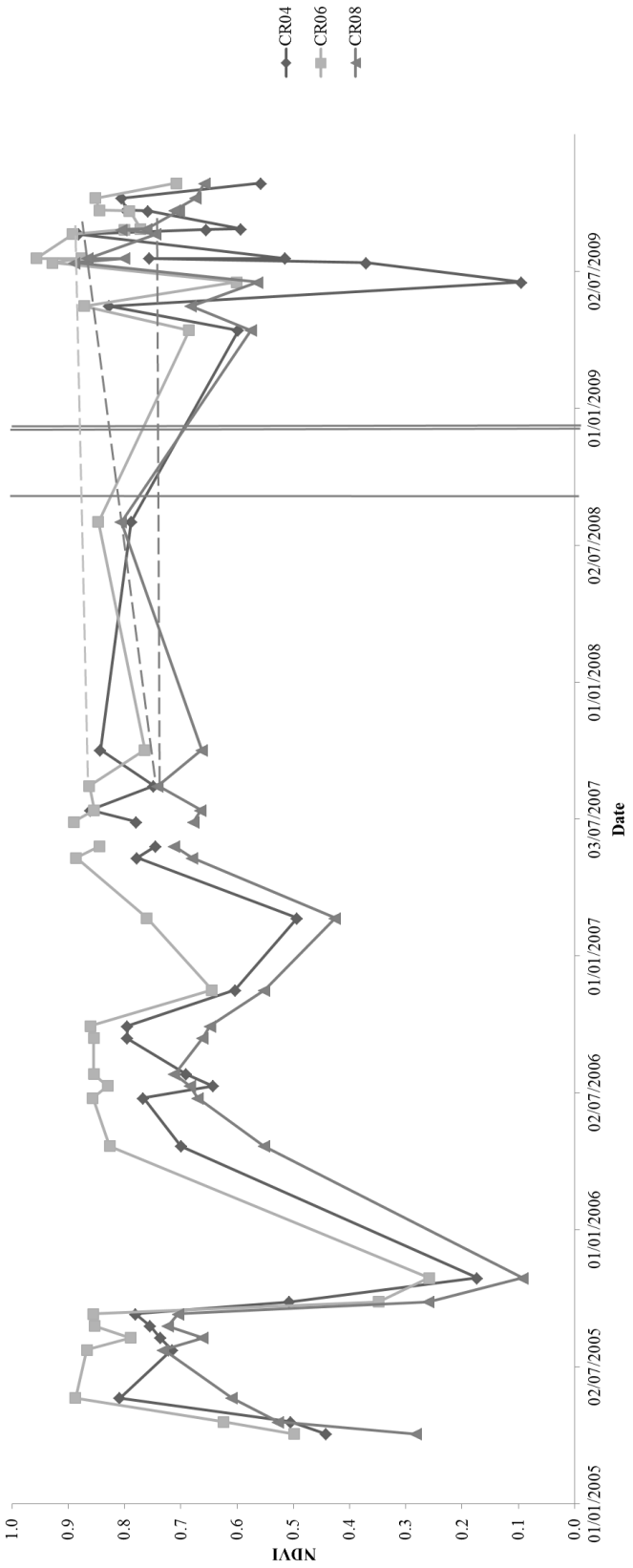

Figure 4-75 - Line plot showing the Cancari Road mass graves which were exhumed in 2008 and the extracted NDVI from all sensors (2005 – 2009). Anomalies (negative) NDVI values (from SPOT) are omitted. The excavation dates for each grave are represented by the vertical lines. Dashed lines compare NDVI values for each grave from August 2007 and August 2009.

Table 4-38 - NDVI for each of the Cancari Road mass graves from 1991 - 2012 around peak summer.

Sensor	Date Acquired	NDVI												
		CR01	CR02	CR03	CR04	CR05	CR06	CR07	CR08	CR09	CR10	CR11	CR12	CR13
Landsat 5 TM	05/09/1991	0.731	0.666	0.628	0.626	0.652	0.789	0.547	0.644	0.565	0.629	0.623	0.665	0.657
Landsat 5 TM	07/09/1992	0.754	0.665	0.811	0.805	0.682	0.804	0.568	0.629	0.596	0.635	0.668	0.590	0.591
Landsat 5 TM	25/08/1993	0.758	0.662	0.743	0.729	0.610	0.777	0.601	0.599	0.529	0.654	0.643	0.663	0.585
Landsat 5 TM	13/09/1994	0.730	0.762	0.702	0.688	0.620	0.840	0.570	0.663	0.614	0.655	0.713	0.679	0.646
Landsat 5 TM	18/09/1996	0.769	0.799	0.789	0.812	0.699	0.785	0.715	0.764	0.661	0.737	0.744	0.773	0.686
Landsat 5 TM	05/09/1997	0.846	0.758	0.809	0.815	0.731	0.806	0.680	0.762	0.692	0.786	0.805	0.726	0.723
SPOT-4	03/08/1998	0.265	0.287	-0.002	0.128	0.119	0.332	0.130	0.075	0.153	0.208	0.267	-0.115	0.158
Landsat 7 ETM	19/09/1999	0.802	0.737	0.835	0.838	0.723	0.847	0.719	0.754	0.686	0.749	0.752	0.691	0.695
Landsat 5 TM	13/09/2000	0.734	0.520	0.770	0.741	0.583	0.743	0.507	0.587	0.533	0.595	0.501	0.525	0.497
Landsat 5 TM	02/10/2001	0.811	0.713	0.805	0.781	0.698	0.793	0.578	0.730	0.659	0.678	0.596	0.678	0.656
Landsat 7 ETM	26/08/2002	0.808	0.602	0.710	0.768	0.565	0.862	0.600	0.646	0.680	0.620	0.718	0.673	0.757
Landsat 5 TM	06/09/2003	0.679	0.601	0.754	0.708	0.600	0.841	0.485	0.593	0.668	0.552	0.593	0.461	0.545
Landsat 5 TM	08/09/2004	0.806	0.663	0.811	0.769	0.751	0.832	0.614	0.678	0.746	0.638	0.746	0.709	0.662
Landsat 5 TM	11/09/2005	0.805	0.680	0.732	0.772	0.760	0.847	0.587	0.711	0.728	0.686	0.729	0.706	0.719
Landsat 5 TM	14/09/2006	0.802	0.690	0.760	0.802	0.742	0.850	0.538	0.711	0.697	0.502	0.741	0.593	0.680
Landsat 5 TM	03/10/2007	0.794	0.676	0.823	0.800	0.737	0.760	0.660	0.655	0.685	0.585	0.663	0.614	0.621
Landsat 5 TM	02/08/2008	0.852	0.691	0.798	0.789	0.742	0.842	0.661	0.783	0.675	0.777	0.713	0.660	0.709
Landsat 5 TM	22/09/2009	0.784	0.677	0.778	0.773	0.736	0.841	0.581	0.732	0.752	0.691	0.740	0.629	0.596
Landsat 5 TM	09/09/2010	0.792	0.676	0.768	0.761	0.776	0.843	0.637	0.727	0.750	0.112	0.596	0.687	0.664
Landsat 5 TM	28/09/2011	0.690	0.630	0.680	0.706	0.604	0.778	0.514	0.509	0.602	0.597	0.654	0.559	0.560
RapidEye-4	18/10/2012	1.002	0.823	0.910	0.894	0.482	0.984	0.604	0.557	0.608	0.722	0.711	0.555	0.811
RapidEye-3	01/09/2013	0.882	0.857	0.771	0.804	0.806	0.966	0.563	0.723	0.810	0.749	0.719	0.629	0.719

Table 4-39 - NDVI for areas of undisturbed vegetation (NG) for each of the Cancari Road mass graves from 1991 - 2012 around peak summer.

Sensor	Date Acquired	NDVI												
		NG_CR01	NG_CR02	NG_CR03	NG_CR04	NG_CR05	NG_CR06	NG_CR07	NG_CR08	NG_CR09	NG_CR10	NG_CR11	NG_CR12	NG_CR13
Landsat 5 TM	05/09/1991	0.740	0.707	0.617	0.598	0.653	0.789	0.608	0.680	0.620	0.703	0.657	0.650	0.682
Landsat 5 TM	07/09/1992	0.718	0.697	0.801	0.804	0.738	0.805	0.649	0.692	0.633	0.621	0.686	0.594	0.653
Landsat 5 TM	25/08/1993	0.743	0.663	0.740	0.738	0.675	0.751	0.688	0.662	0.586	0.645	0.669	0.689	0.605
Landsat 5 TM	13/09/1994	0.730	0.767	0.695	0.674	0.643	0.856	0.666	0.676	0.645	0.675	0.733	0.661	0.676
Landsat 5 TM	18/09/1996	0.747	0.769	0.792	0.823	0.742	0.795	0.778	0.765	0.707	0.692	0.768	0.764	0.697
Landsat 5 TM	05/09/1997	0.854	0.772	0.823	0.817	0.761	0.800	0.776	0.795	0.735	0.768	0.803	0.788	0.728
SPOT-4	03/08/1998	0.376	0.371	0.080	0.184	0.141	0.386	0.231	0.175	0.222	0.240	0.334	0.017	0.206
Landsat 7 ETM	19/09/1999	0.813	0.784	0.810	0.813	0.747	0.830	0.743	0.783	0.737	0.750	0.765	0.721	0.701
Landsat 5 TM	13/09/2000	0.695	0.567	0.724	0.710	0.627	0.751	0.577	0.606	0.558	0.565	0.544	0.521	0.477
Landsat 5 TM	02/10/2001	0.789	0.705	0.782	0.784	0.725	0.768	0.652	0.747	0.683	0.670	0.648	0.677	0.679
Landsat 7 ETM	26/08/2002	0.816	0.692	0.710	0.772	0.691	0.849	0.645	0.700	0.731	0.626	0.707	0.740	0.730
Landsat 5 TM	06/09/2003	0.735	0.683	0.675	0.649	0.611	0.826	0.567	0.613	0.686	0.637	0.579	0.506	0.558
Landsat 5 TM	08/09/2004	0.816	0.718	0.736	0.752	0.744	0.834	0.639	0.694	0.757	0.716	0.720	0.738	0.655
Landsat 5 TM	11/09/2005	0.816	0.744	0.718	0.783	0.746	0.838	0.650	0.710	0.763	0.705	0.735	0.732	0.727
Landsat 5 TM	14/09/2006	0.814	0.727	0.727	0.796	0.770	0.836	0.629	0.715	0.750	0.647	0.730	0.629	0.712
Landsat 5 TM	03/10/2007	0.792	0.701	0.761	0.773	0.761	0.757	0.701	0.690	0.703	0.657	0.675	0.644	0.663
Landsat 5 TM	02/08/2008	0.829	0.711	0.822	0.813	0.775	0.812	0.743	0.805	0.716	0.757	0.758	0.670	0.717
Landsat 5 TM	22/09/2009	0.791	0.733	0.726	0.748	0.724	0.835	0.644	0.737	0.764	0.695	0.732	0.653	0.635
Landsat 5 TM	09/09/2010	0.807	0.754	0.743	0.789	0.768	0.853	0.703	0.759	0.743	0.106	0.615	0.729	0.699
Landsat 5 TM	28/09/2011	0.717	0.667	0.637	0.664	0.608	0.753	0.603	0.549	0.629	0.573	0.651	0.576	0.591
RapidEye-4	18/10/2012	0.919	0.837	0.794	0.816	0.689	0.969	0.759	0.570	0.662	0.599	0.741	0.526	0.757
RapidEye-3	01/09/2013	0.911	0.901	0.786	0.812	0.825	0.970	0.677	0.720	0.836	0.756	0.724	0.663	0.767

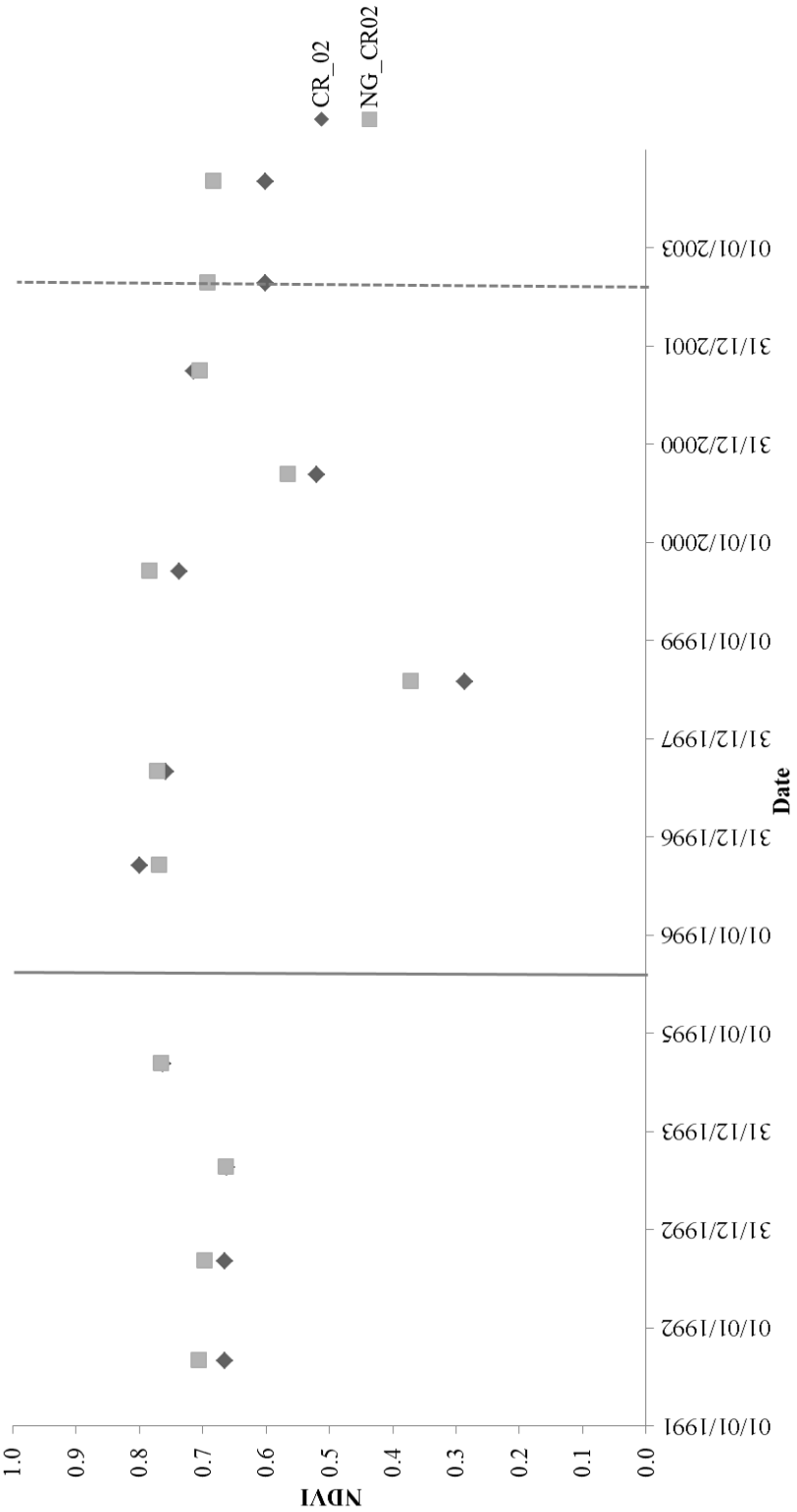

11

Figure 4-76 - NDVI of CR02 and a non-grave area (NG_CR02). Grey line = inhumation date; grey dashed line = exhumation date.

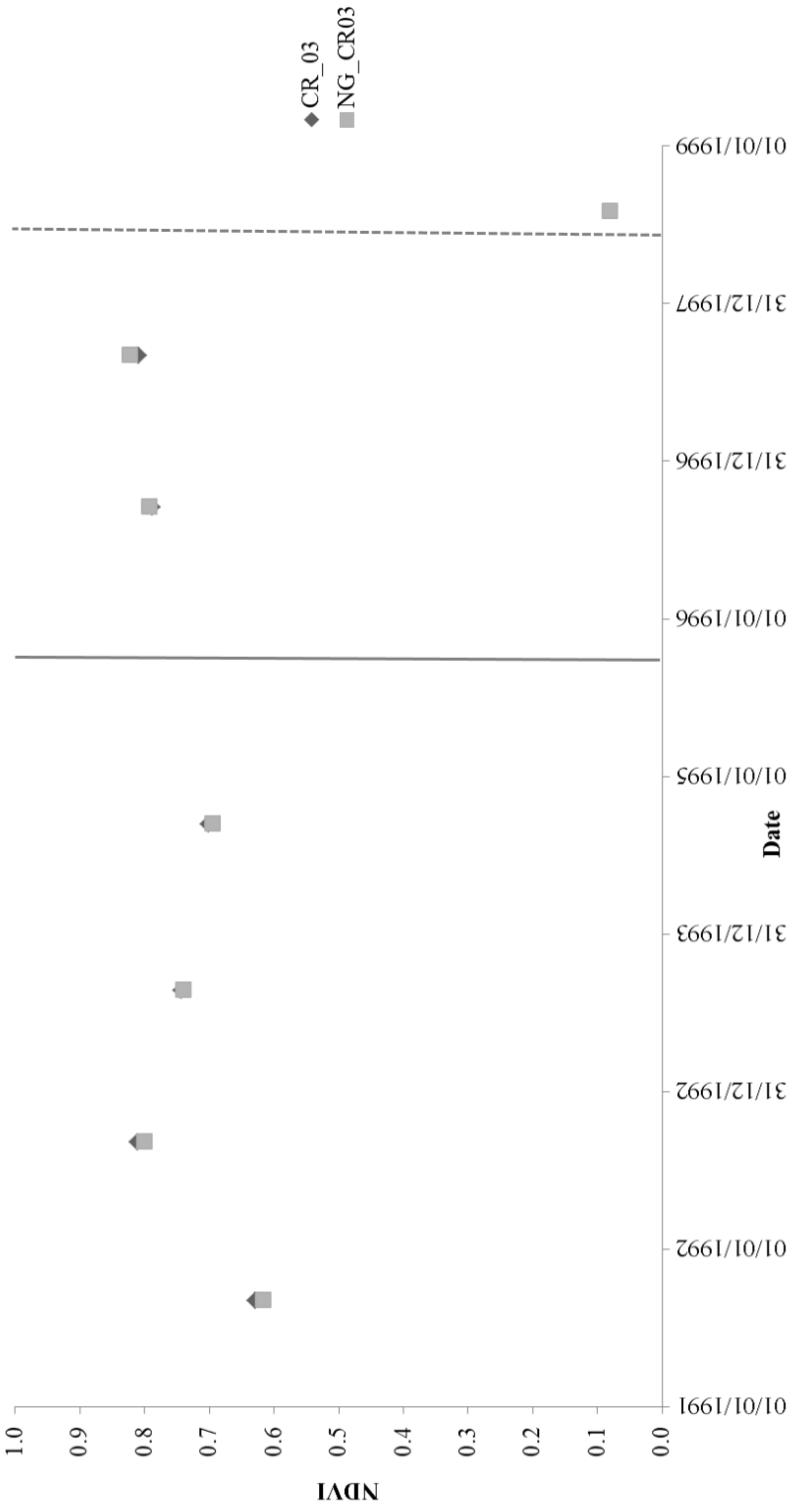

Figure 4-77 - NDVI of CR03 and a non-grave area (NG_CR03). Grey line = inhumation date; grey dashed line = exhumation date.

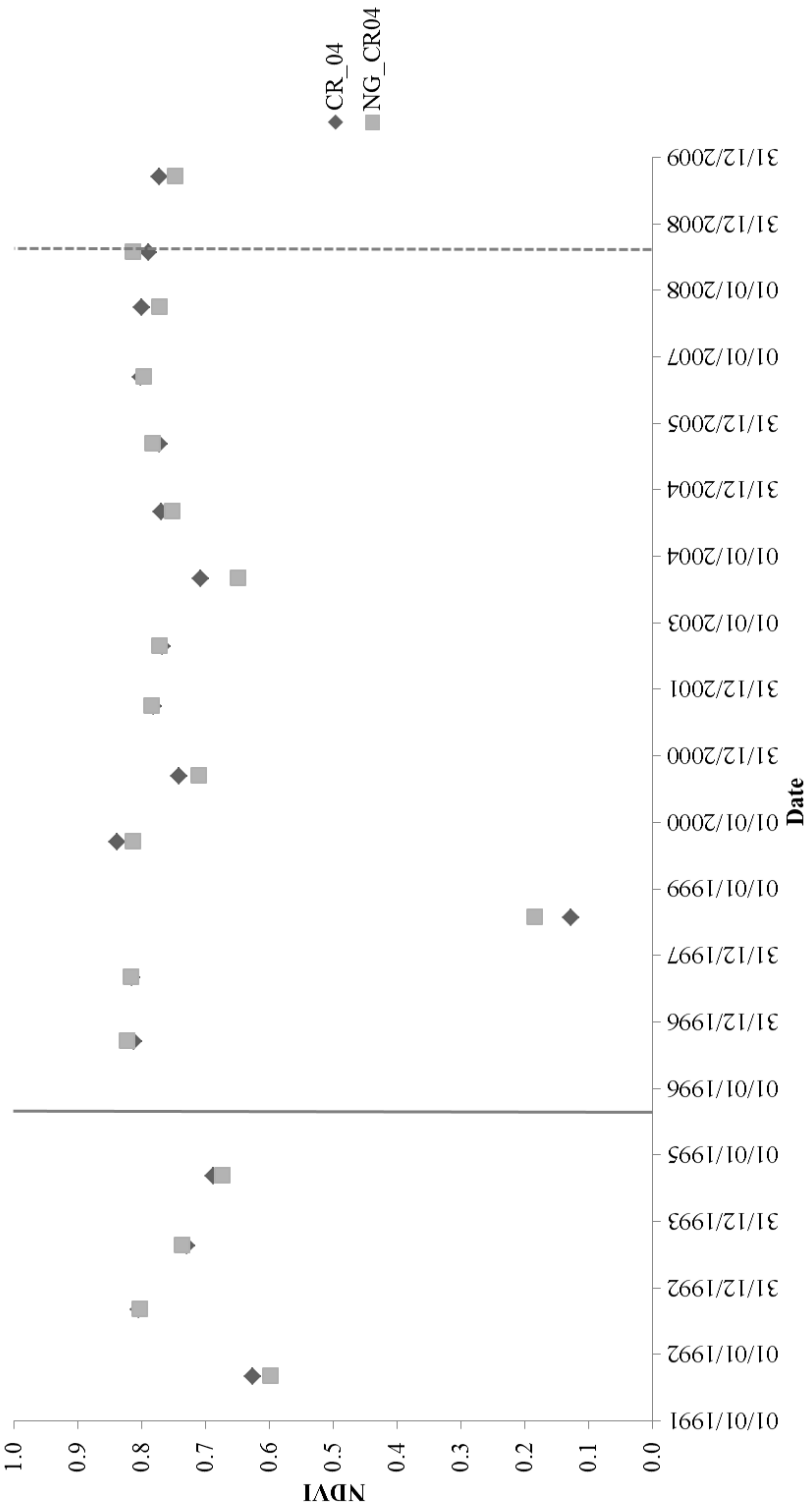

Figure 4-78 - NDVI of CR04 and a non-grave area (NG_CR04). Grey line = inhumation date; grey dashed line = exhumation date.

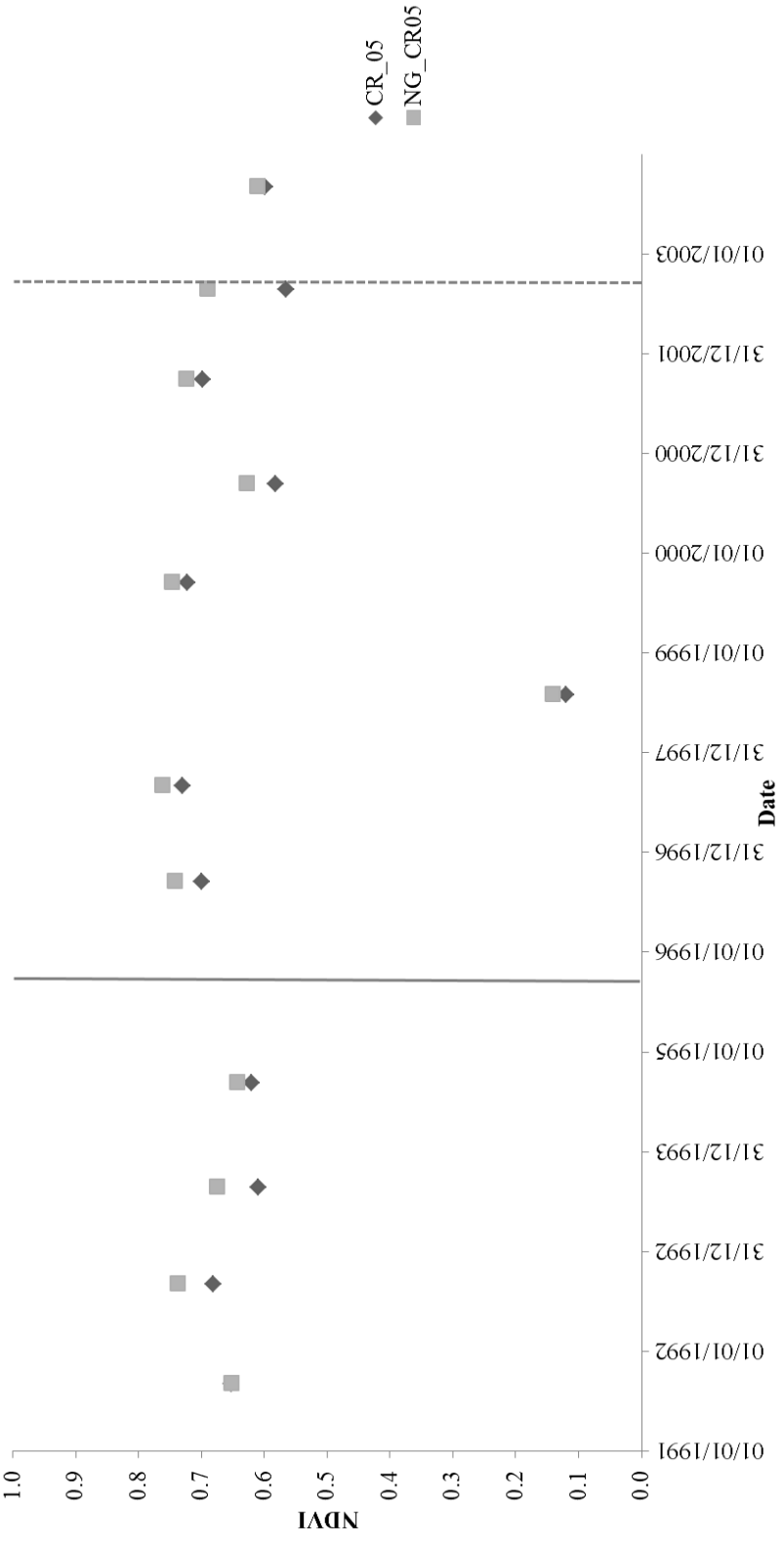

Figure 4-79 - NDVI of CR05 and a non-grave area (NG_CR05). Grey line = inhumation date; grey dashed line = exhumation date.

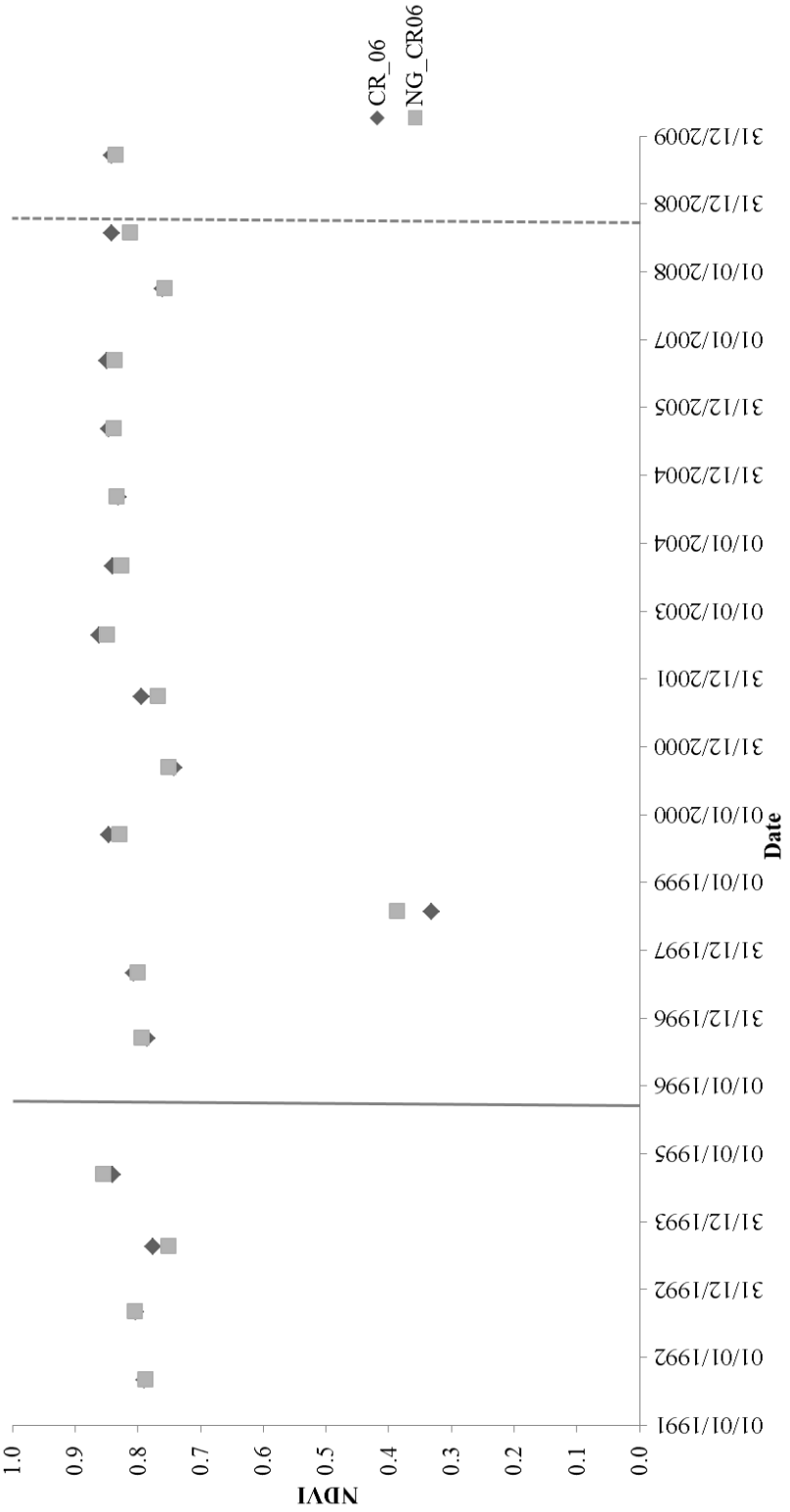

Figure 4-80 - NDVI of CR06 and a non-grave area (NG_CR06). Grey line = inhumation date; grey dashed line = exhumation date.

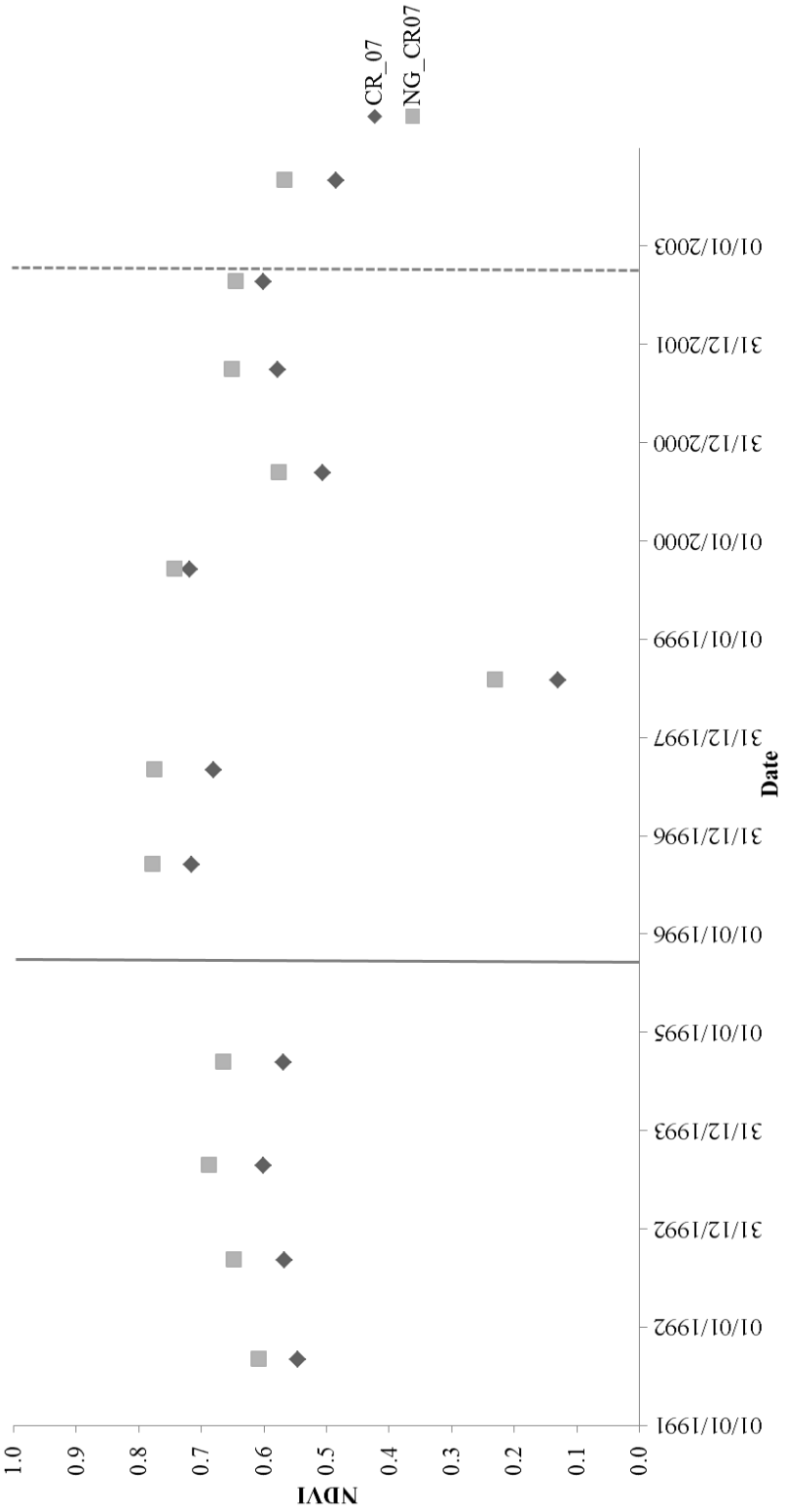

Figure 4-81 - NDVI of CR07 and a non-grave area (NG_CR07). Grey line = inhumation date; grey dashed line = exhumation date.

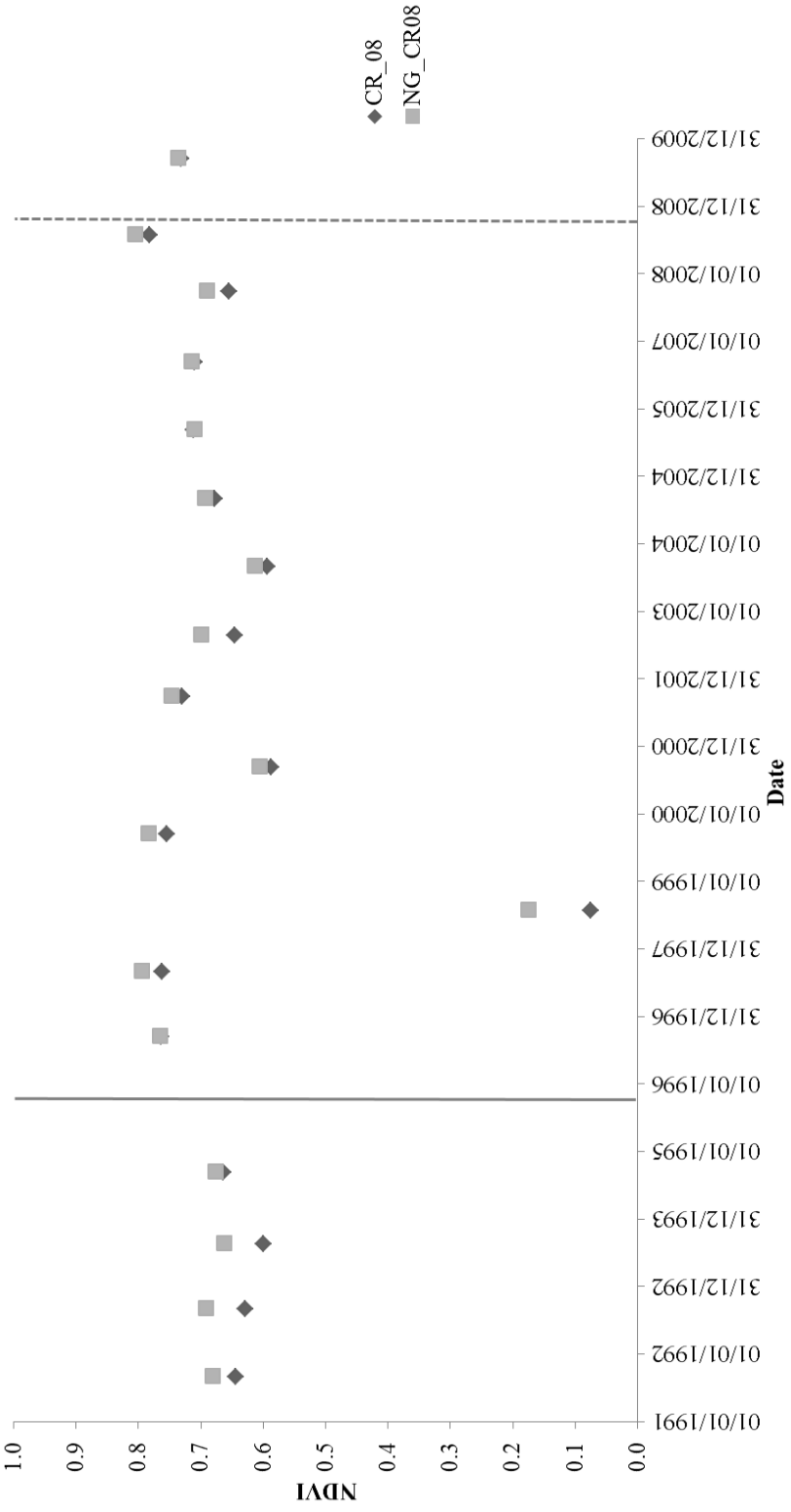

Figure 4-82 - NDVI of CR08 and a non-grave area (NG_CR08). Grey line = inhumation date; grey dashed line = exhumation date.

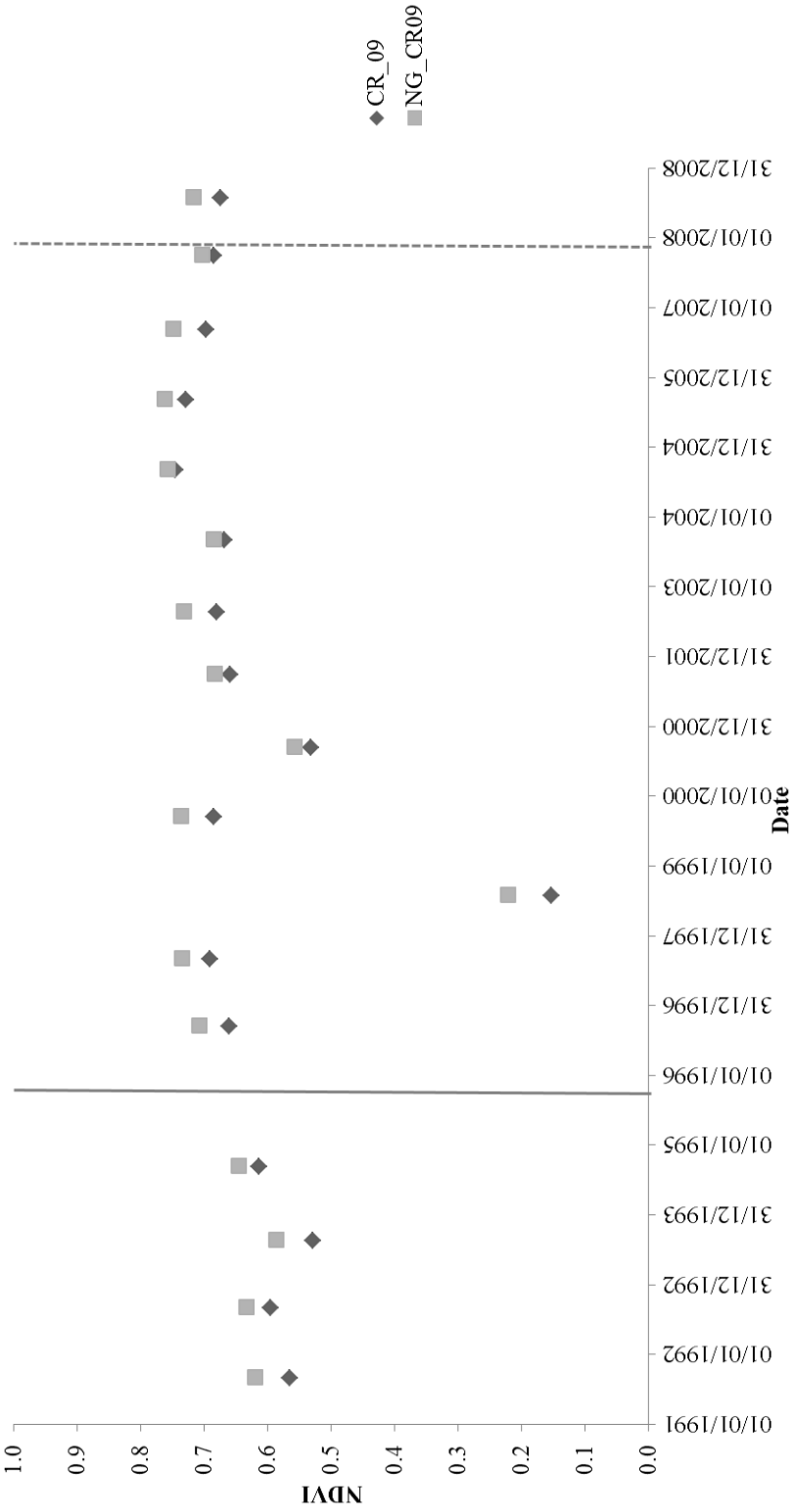

Figure 4-83 - NDVI of CR09 and a non-grave area (NG_CR09). Grey line = inhumation date; grey dashed line = exhumation date.

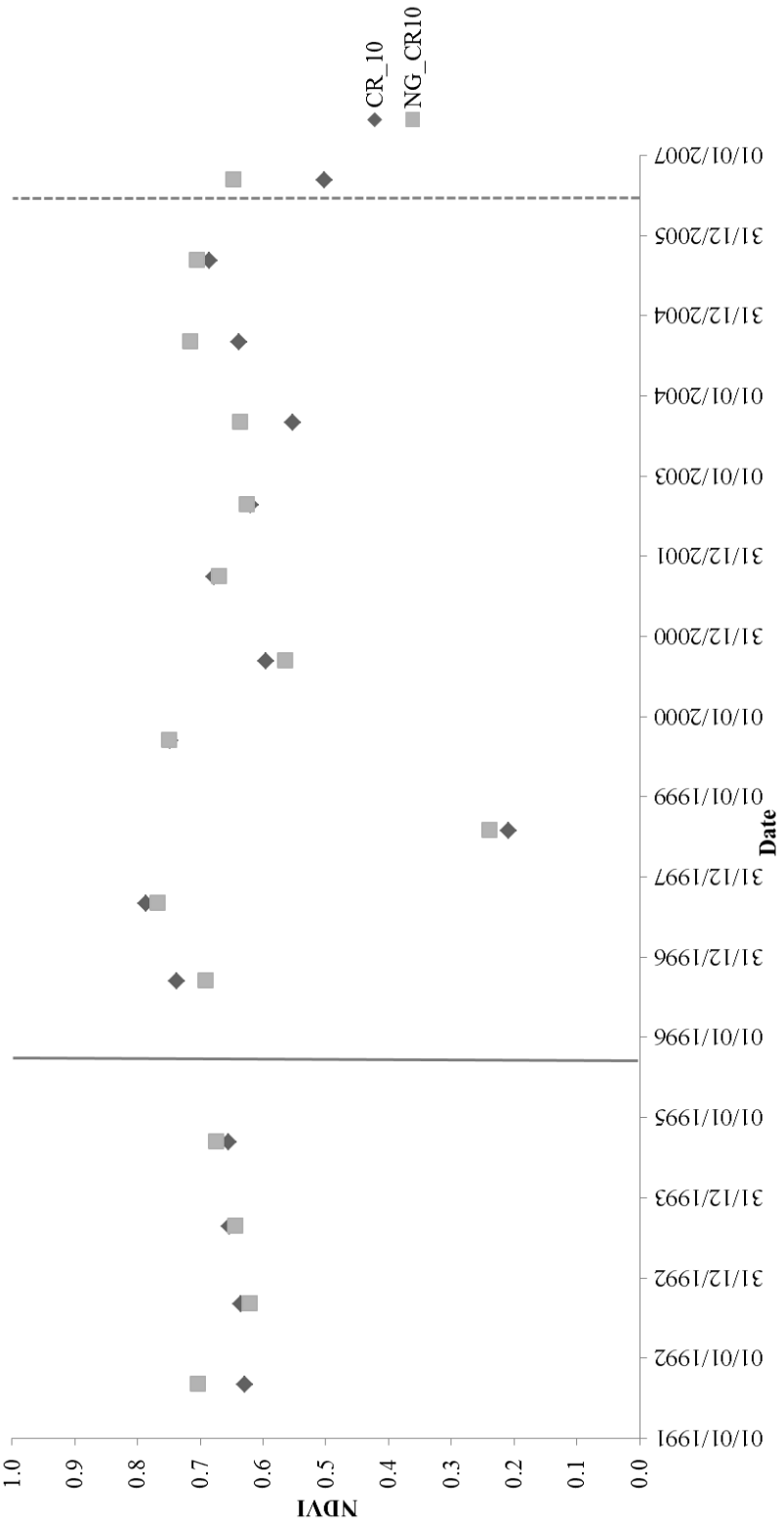

Figure 4-84 - NDVI of CR10 and a non-grave area (NG_CR10). Grey line = inhumation date; grey dashed line = exhumation date.

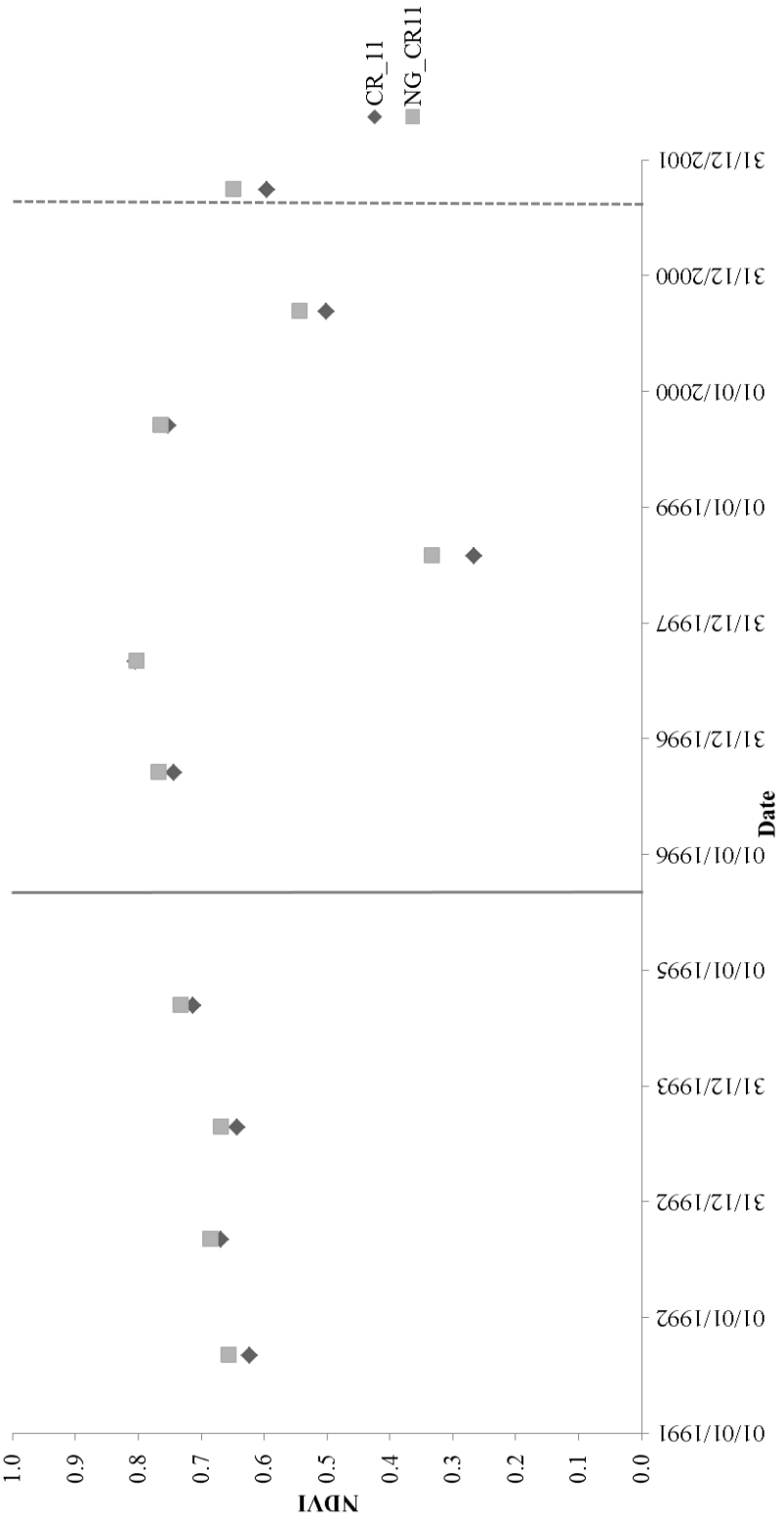

Figure 4-85 - NDVI of CR11 and a non-grave area (NG_CR11). Grey line = inhumation date; grey dashed line = exhumation date.

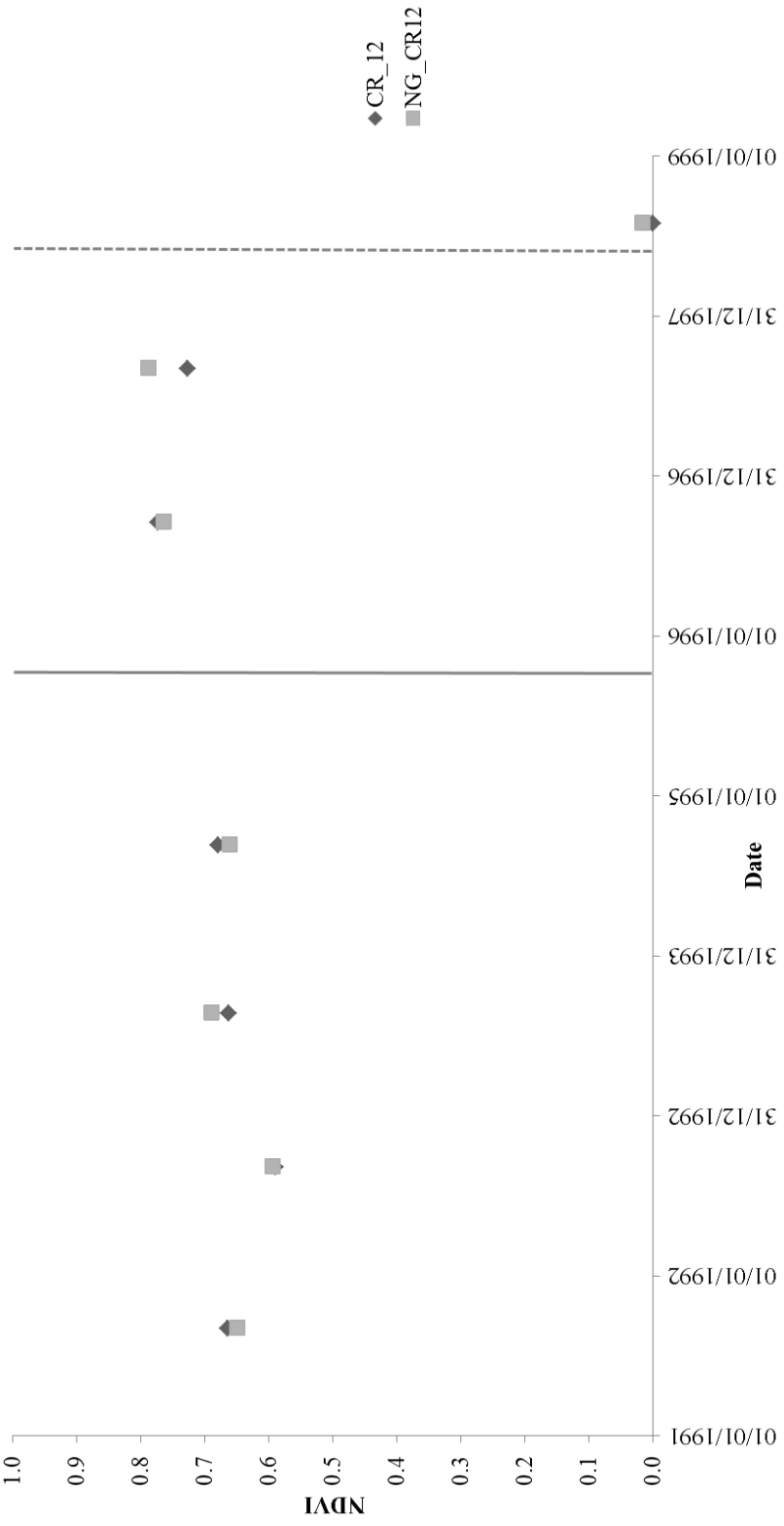

Figure 4-86 - NDVI of CR12 and a non-grave area (NG_CR12). Grey line = inhumation date; grey dashed line = exhumation date.

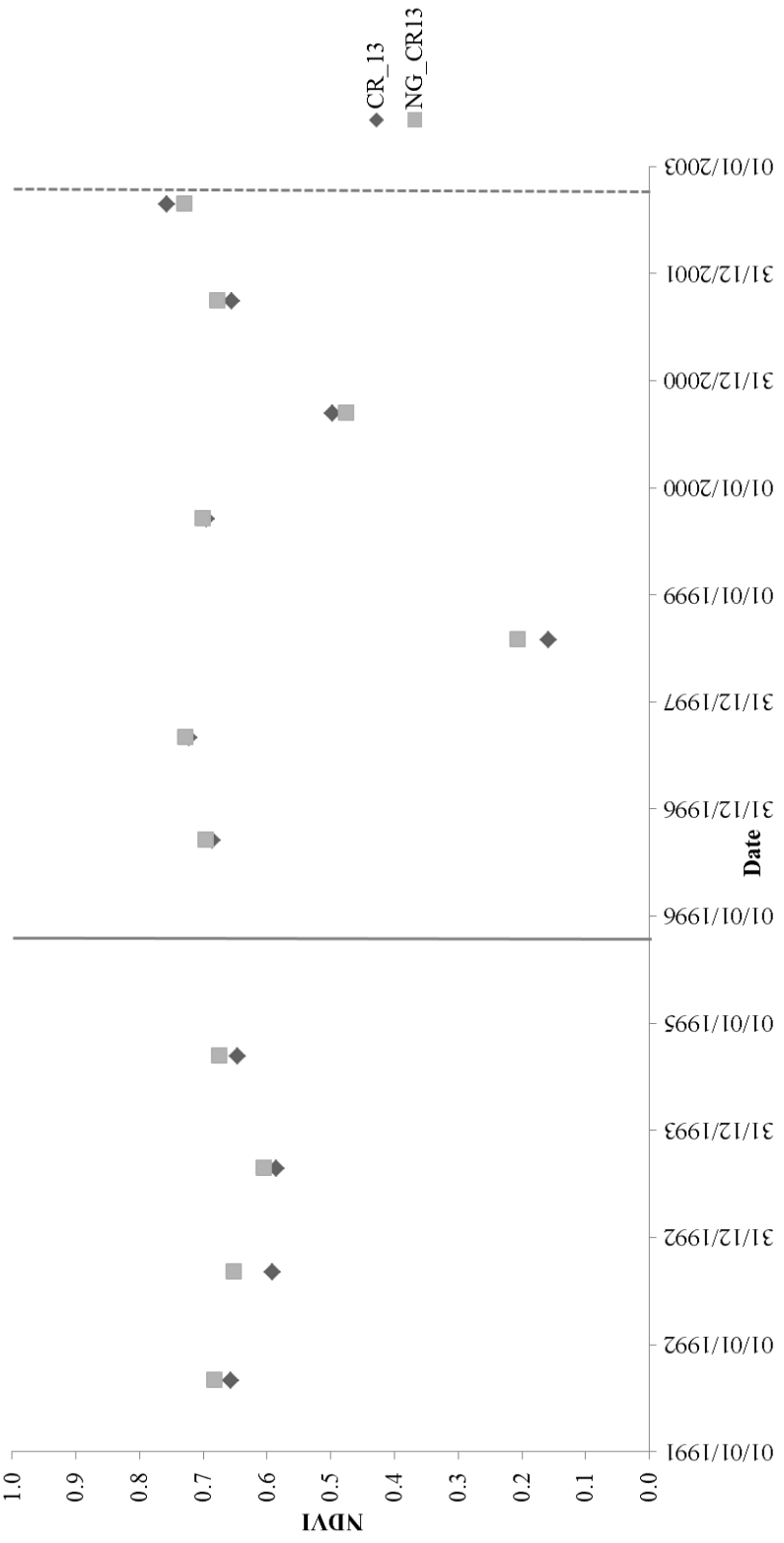

Figure 4-87 - NDVI of CR13 and a non-grave area (NG_CR13). Grey line = inhumation date; grey dashed line = exhumation date.

Table 4-40 - NDVI extracted for each of the Cancari Road mass graves for the period prior to burial.

Platform	Date Acquired	NDVI												
		CR01	CR02	CR03	CR04	CR05	CR06	CR07	CR08	CR09	CR10	CR11	CR12	CR13
SPOT-2	23/02/1994	0.159	0.197	0.269	0.195	0.205	0.137	0.220	0.203	0.324	0.264	0.263	0.243	0.178
Landsat 5	09/06/1994	0.717	0.776	0.742	0.749	0.674	0.863	0.616	0.757	0.692	0.766	0.782	0.721	0.795
Landsat 5	25/06/1994	0.732	0.759	0.679	0.708	0.553	0.840	0.627	0.738	0.633	0.722	0.771	0.711	0.713
SPOT-2	25/07/1994	0.724	0.699	0.731	0.685	0.660	0.818	0.621	0.726	0.656	0.746	0.742	0.704	0.717
Landsat 5	27/07/1994	0.779	0.729	0.715	0.707	0.609	0.850	0.615	0.663	0.657	0.695	0.759	0.774	0.773
Landsat 5	12/08/1994	0.736	0.588	0.613	0.481	0.581	0.805	0.558	0.632	0.603	0.646	0.693	0.661	0.693
SPOT-3	17/08/1994	0.713	0.682	0.704	0.549	0.586	0.793	0.484	0.677	0.739	0.699	0.745	0.711	0.682
SPOT-2	20/08/1994	0.658	0.635	0.688	0.580	0.601	0.804	0.560	0.689	0.730	0.653	0.721	0.613	0.639
Landsat 5	28/08/1994	0.773	0.757	0.709	0.694	0.628	0.824	0.601	0.689	0.609	0.686	0.727	0.743	0.298
Landsat 5	13/09/1994	0.760	0.781	0.675	0.728	0.595	0.815	0.526	0.640	0.553	0.655	0.740	0.744	0.667
Landsat 5	15/10/1994	0.088	0.064	0.178	0.123	0.084	0.105	0.092	0.159	0.297	0.572	0.195	0.178	0.093
Landsat 5	16/11/1994	0.573	0.462	0.379	0.343	0.321	0.328	0.258	0.322	0.243	0.423	0.507	0.503	0.364
Landsat 5	02/12/1994	0.459	0.510	0.478	0.578	0.543	0.548	0.444	0.493	0.532	0.488	0.511	0.470	0.389
Landsat 5	18/12/1994	0.460	0.640	0.497	0.611	0.526	0.868	0.398	0.475	0.768	0.522	0.370	0.490	0.460
SPOT-2	28/02/1995	0.363	0.371	0.454	0.386	0.434	0.206	0.361	0.354	0.404	0.417	0.160	0.160	0.354
SPOT-2	11/03/1995	0.444	0.374	0.490	0.410	0.434	0.368	0.341	0.379	0.399	0.391	0.398	0.427	0.407

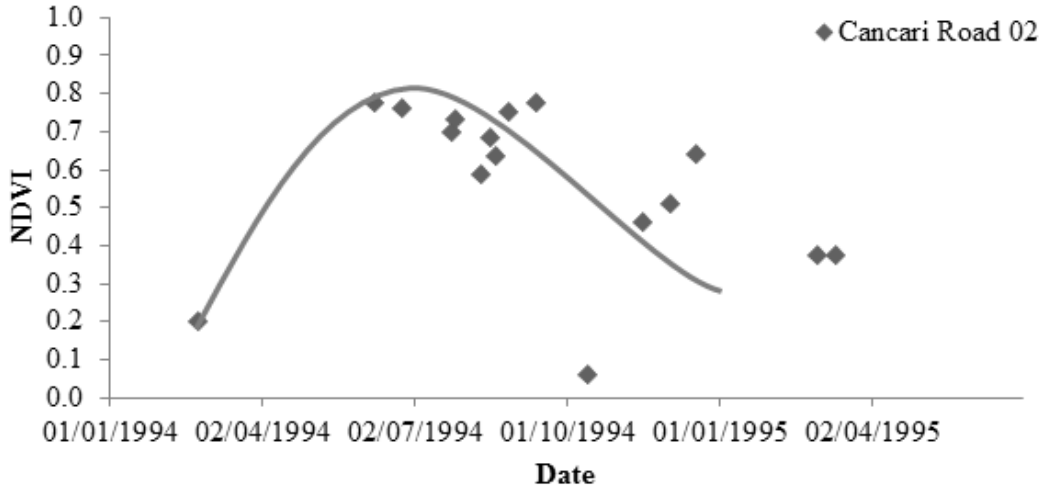

Figure 4-88 - Extracted NDVI for the year prior to creation of the CR02.

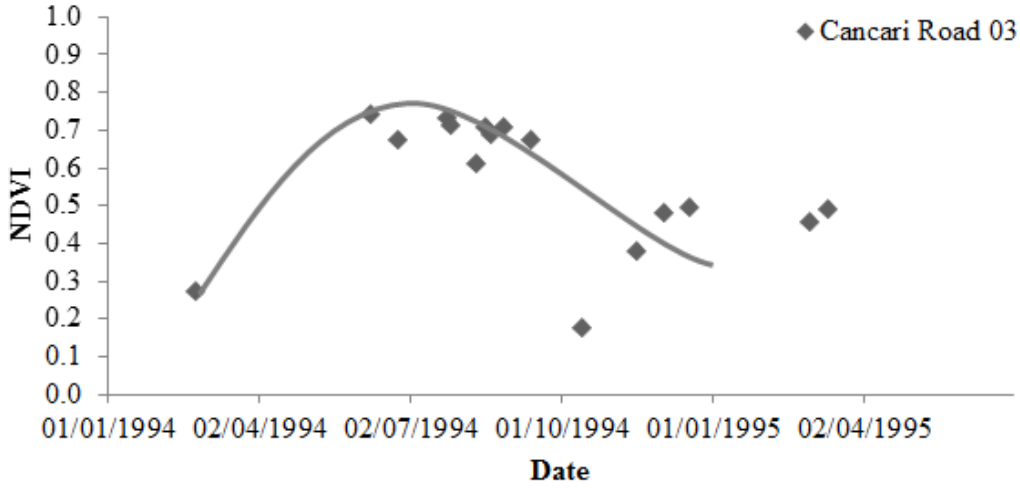

Figure 4-89 - Extracted NDVI for the year prior to creation of the CR03.

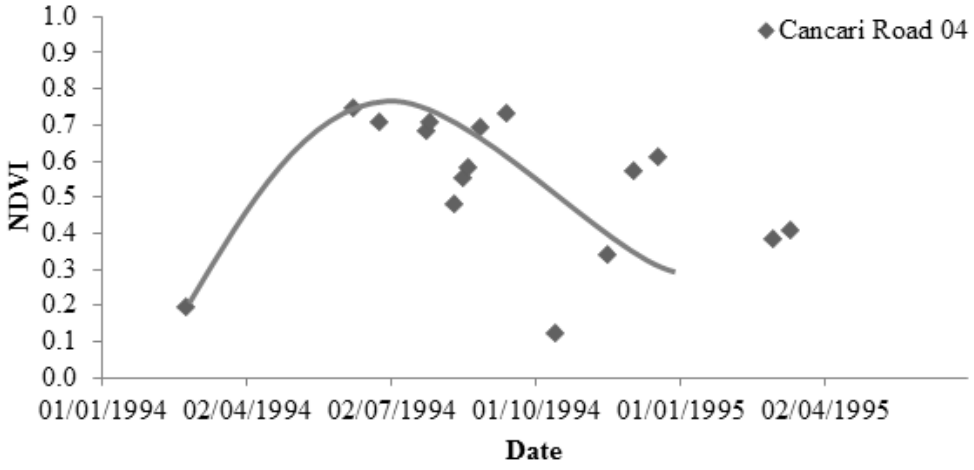

Figure 4-90 - Extracted NDVI for the year prior to creation of the CR04.

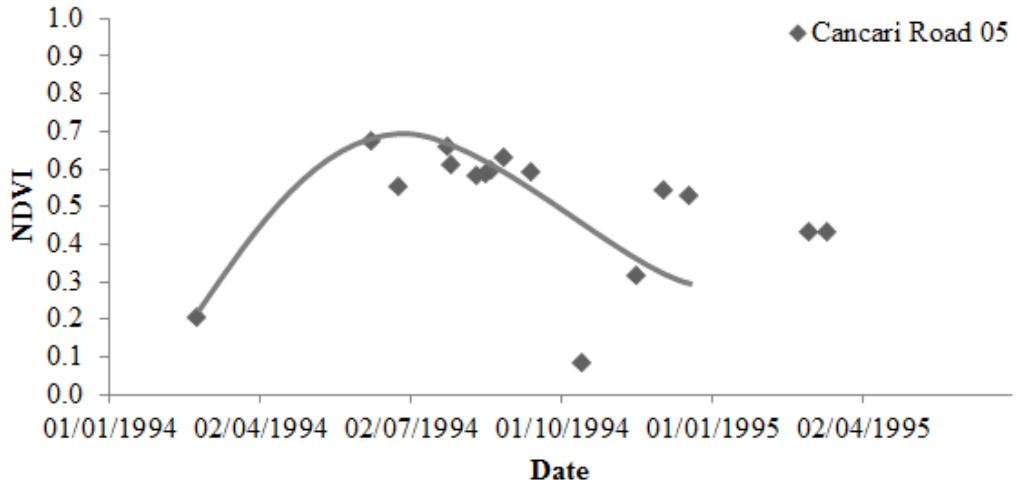

Figure 4-91 - Extracted NDVI for the year prior to creation of the CR05.

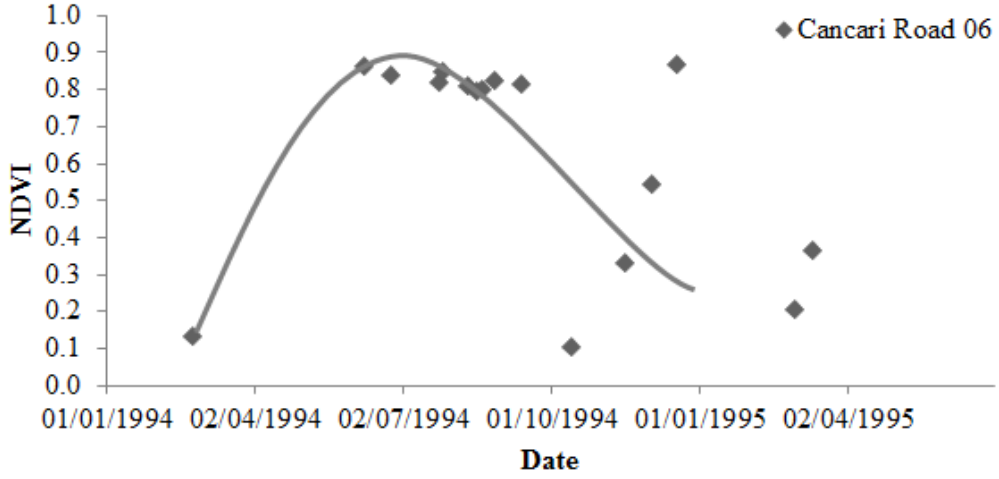

Figure 4-92 - Extracted NDVI for the year prior to creation of the CR06.

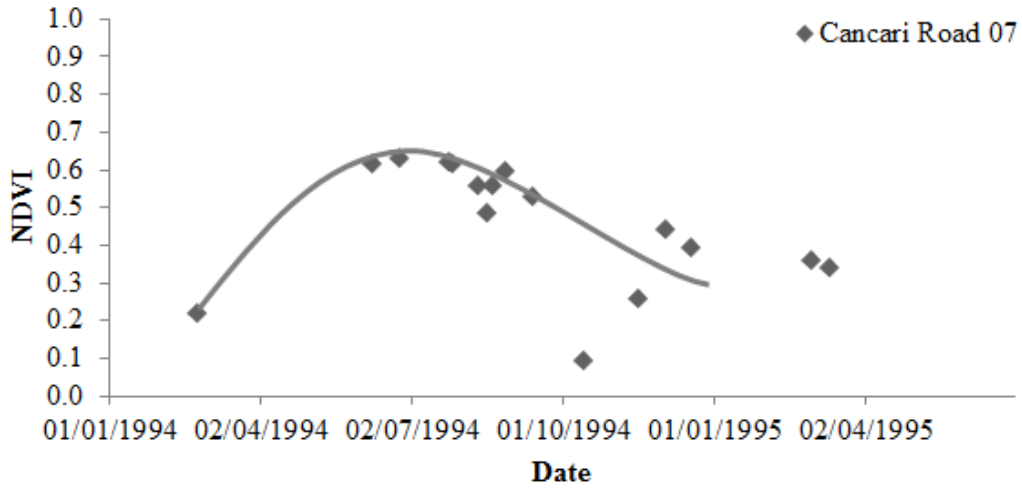

Figure 4-93 - Extracted NDVI for the year prior to creation of the CR07.

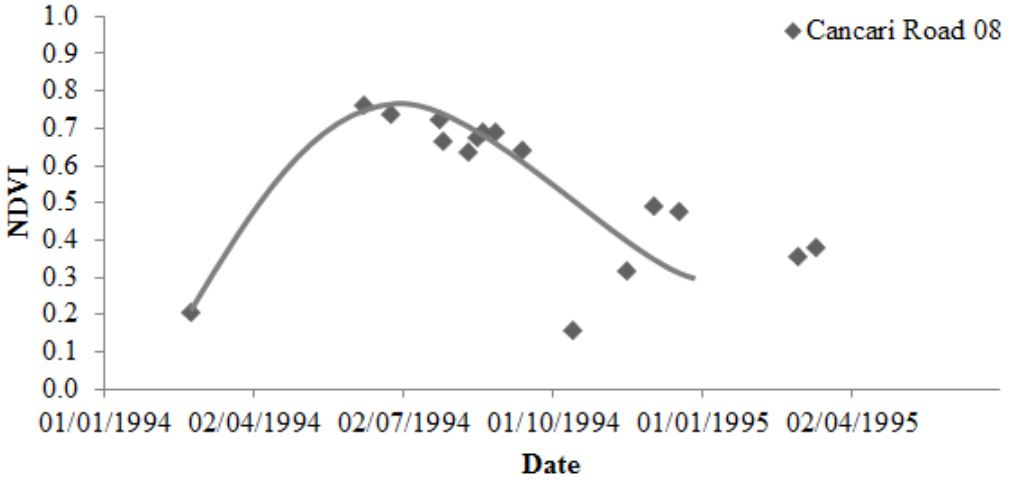

Figure 4-94 - Extracted NDVI for the year prior to creation of the CR08.

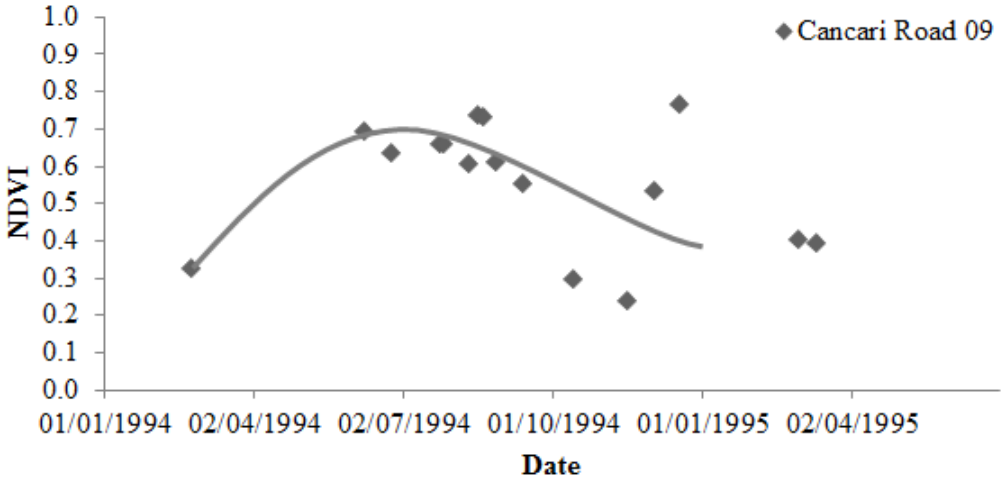

Figure 4-95 - Extracted NDVI for the year prior to creation of the CR09.

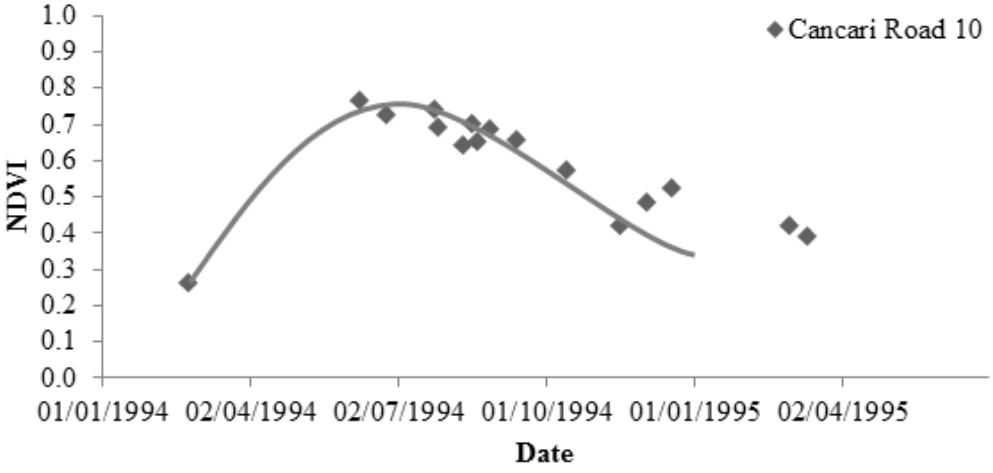

Figure 4-96 - Extracted NDVI for the year prior to creation of the CR10.

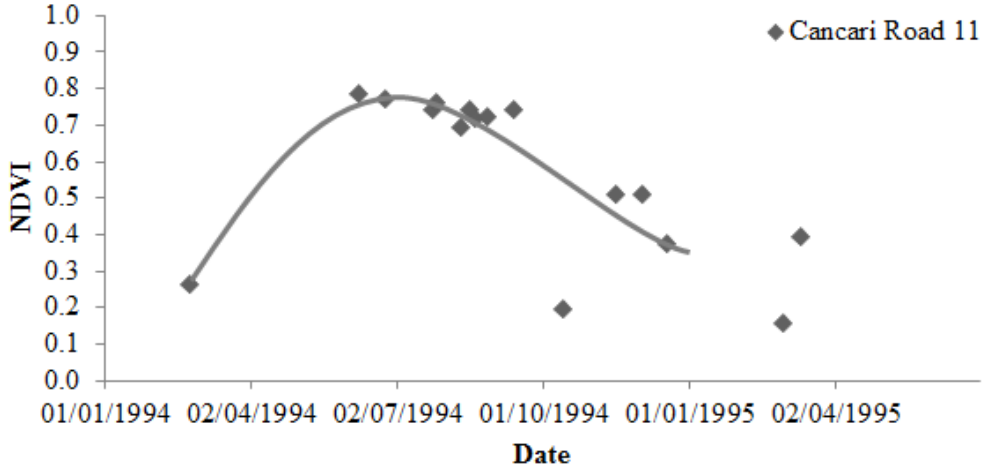

Figure 4-97 - Extracted NDVI for the year prior to creation of the CR11.

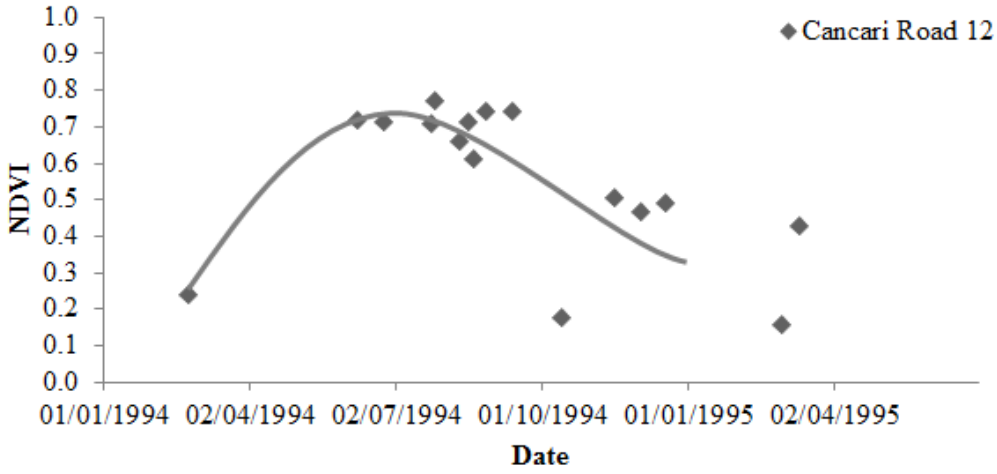

Figure 4-98 - Extracted NDVI for the year prior to creation of the CR12.

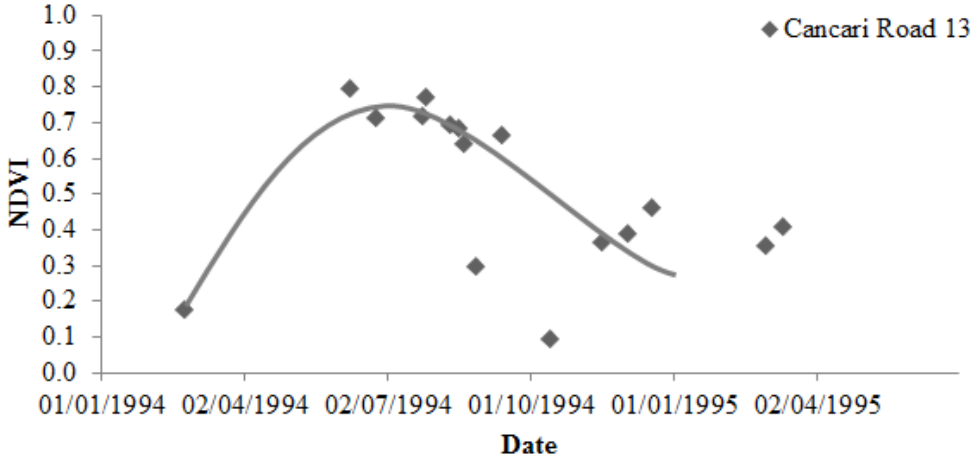

Figure 4-99 - Extracted NDVI for the year prior to creation of the CR13.

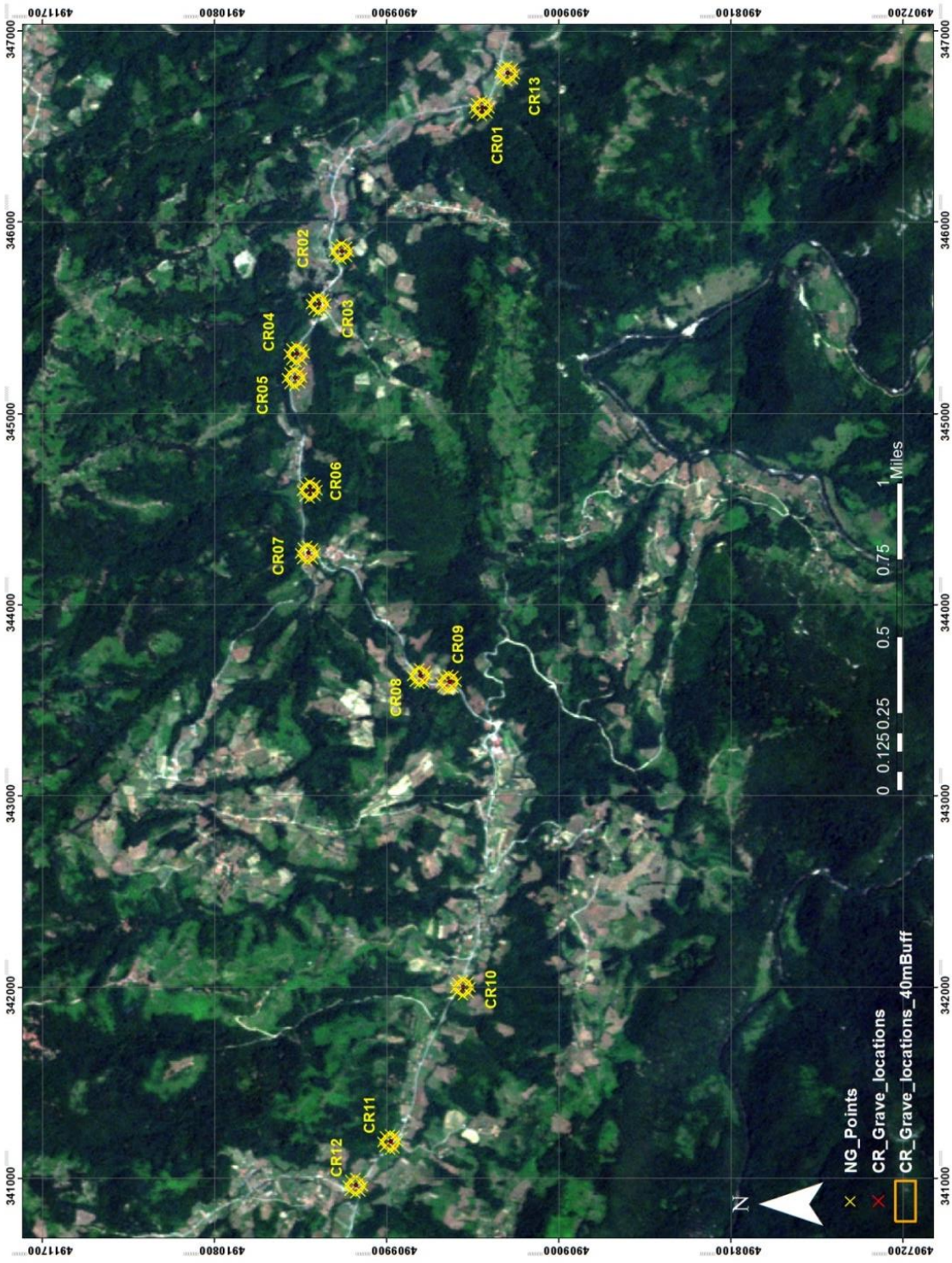

Figure 4-100 - Map showing CR1-CR13 with the 40m buffer (yellow) used to extract NDVI for the non-grave areas and the central point used to extract the mass grave.

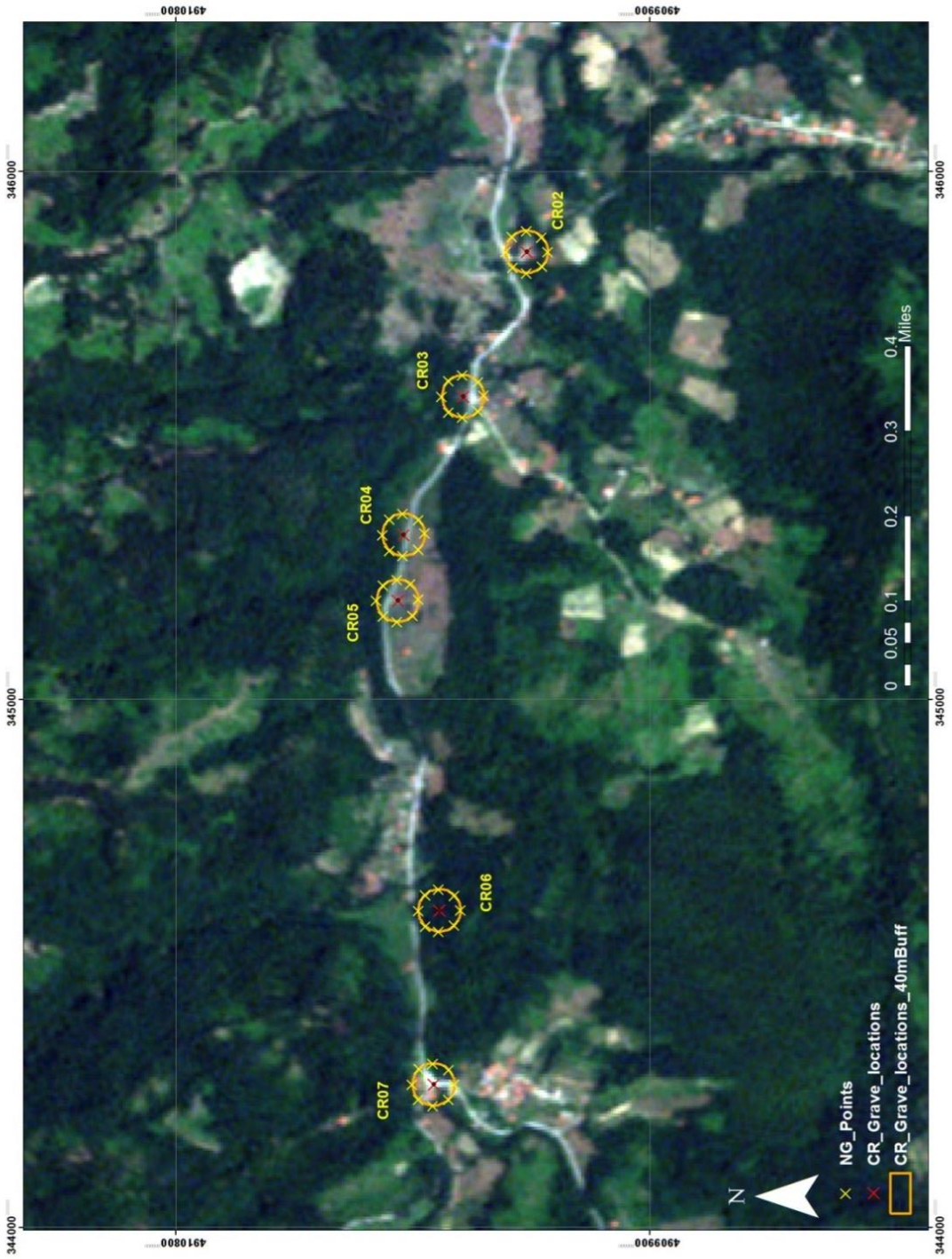

Figure 4-101 - Zoomed-in map showing CR2-CR7 with the 40m buffer (yellow) used to extract NDVI for the non-grave areas and the central point used to extract the mass grave.

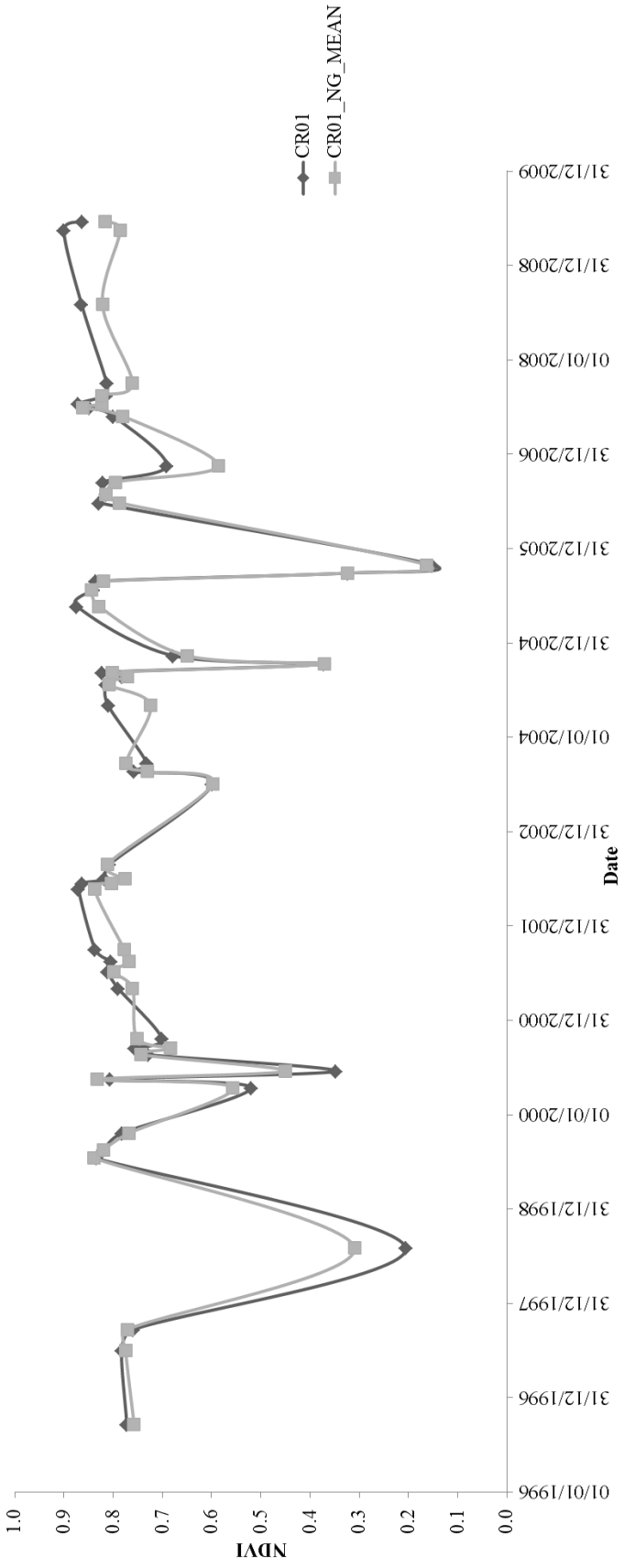

Figure 4-102 - Line plot showing NDVI throughout period of interment for Cancari Road 01 and mean NDVI of local non-grave areas (NG_Mean).

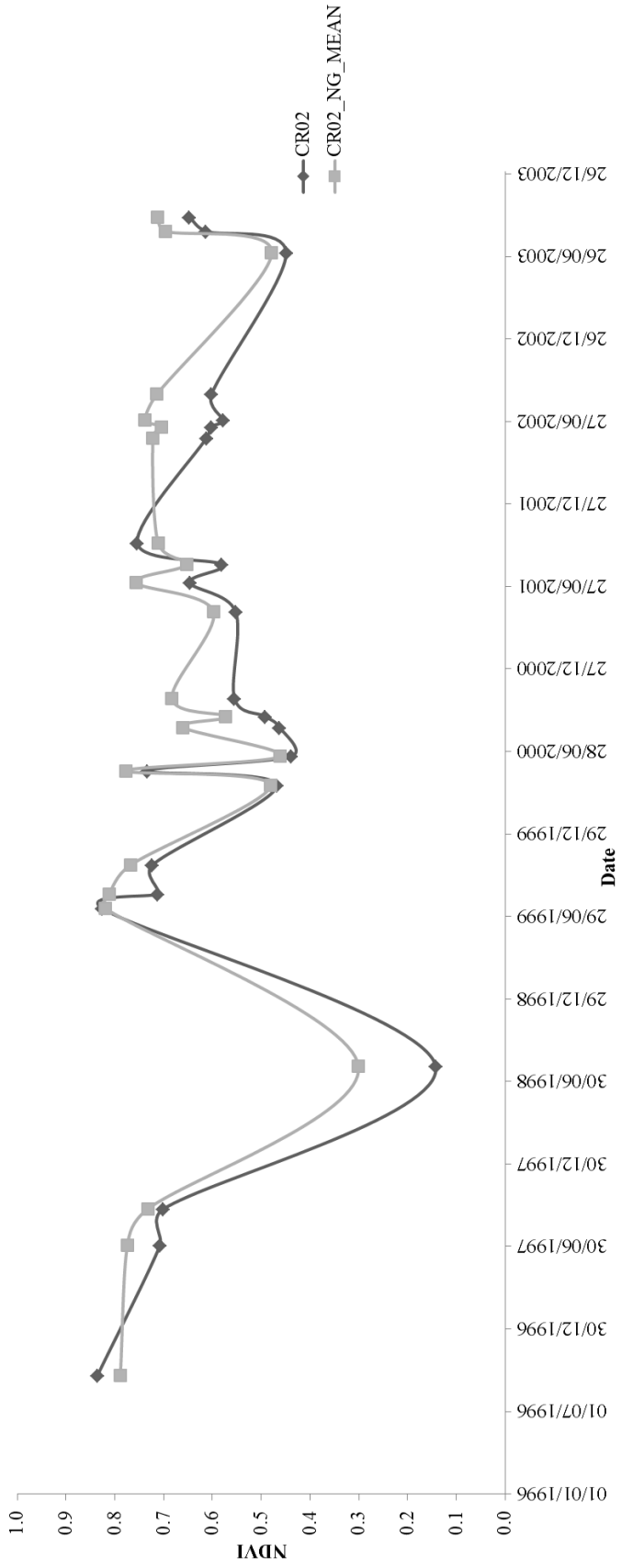

Figure 103 - Line plot showing NDVI throughout period of interment for Cancari Road 02 and mean NDVI of local non-grave areas.

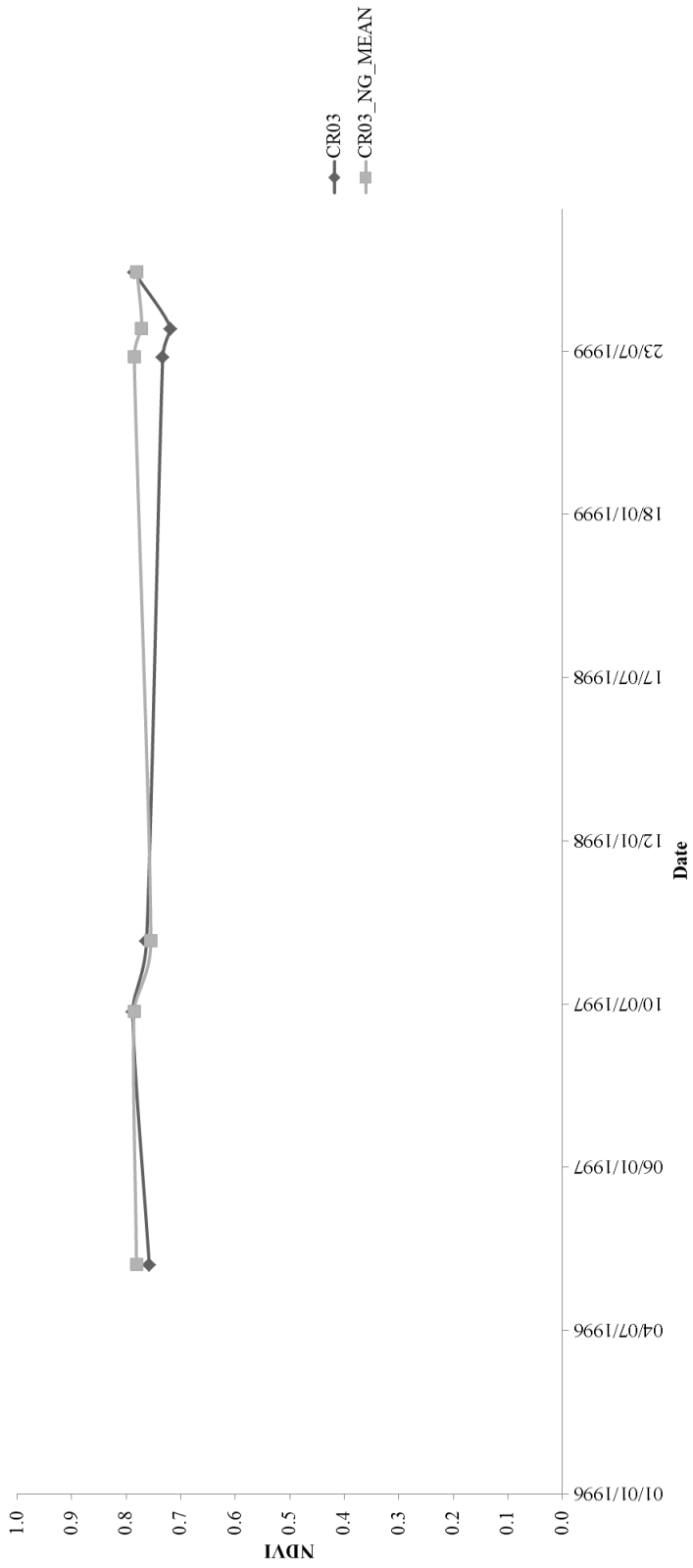

Figure 4-104 - Line plot showing NDVI throughout period of interment for Cancari Road 03 and mean NDVI of local non-grave areas.

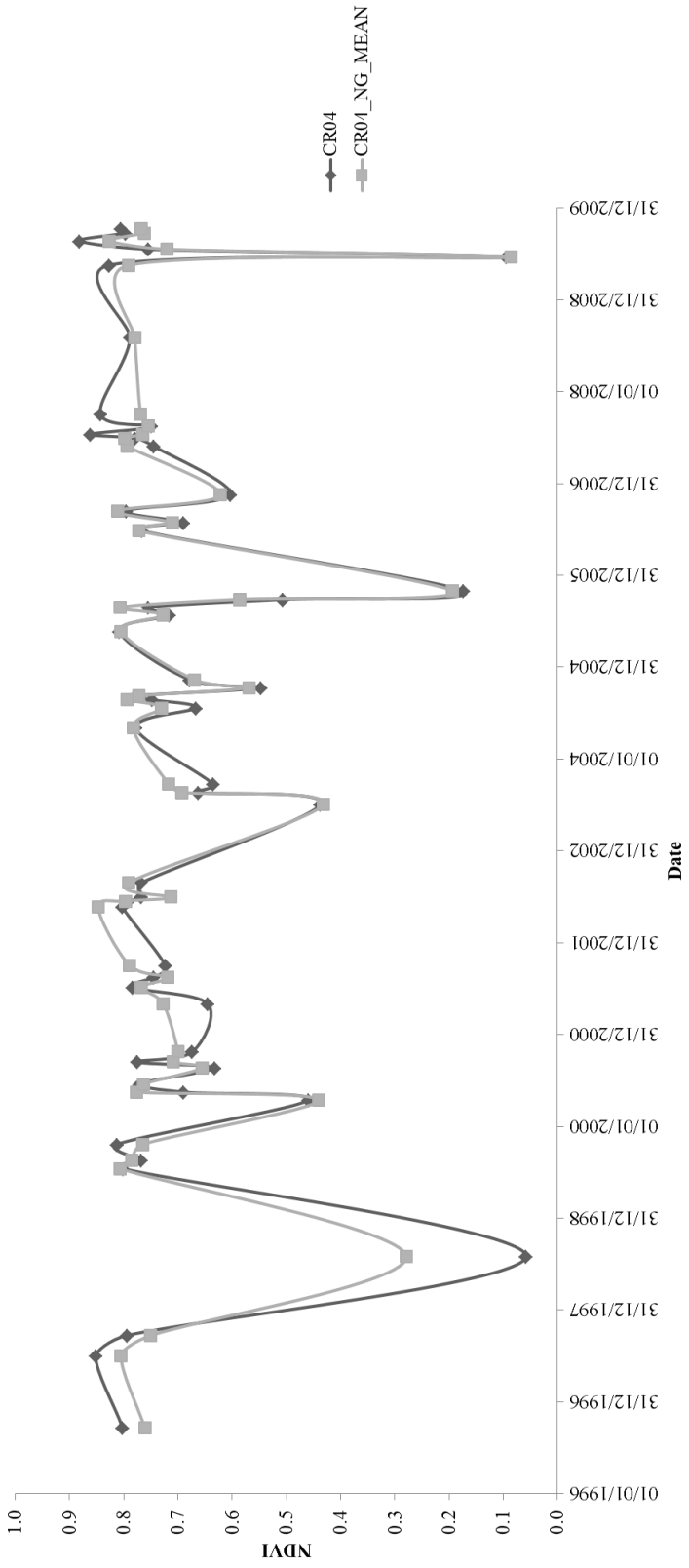

Figure 4-105 - Line plot showing NDVI throughout period of interment for Cancari Road 04 and mean NDVI of local non-grave areas.

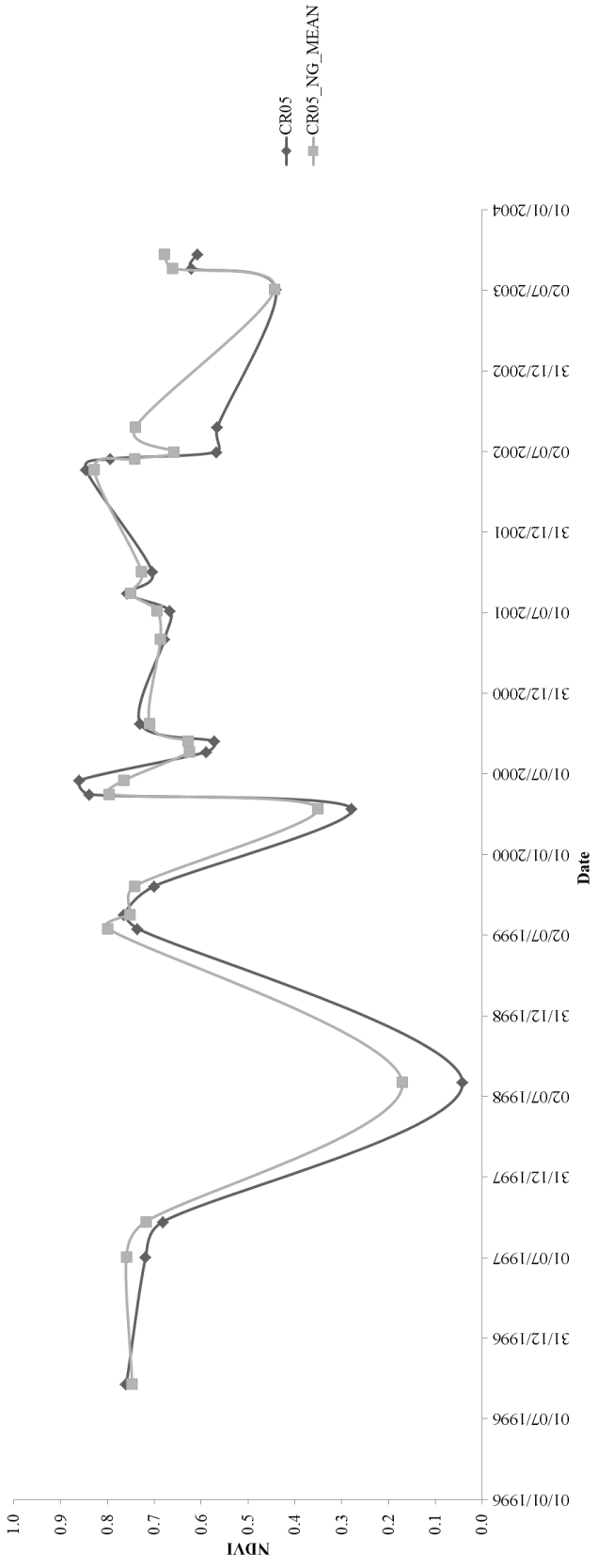

Figure 4-106 - Line plot showing NDVI throughout period of interment for Cancari Road 05 and mean NDVI of local non-grave areas.

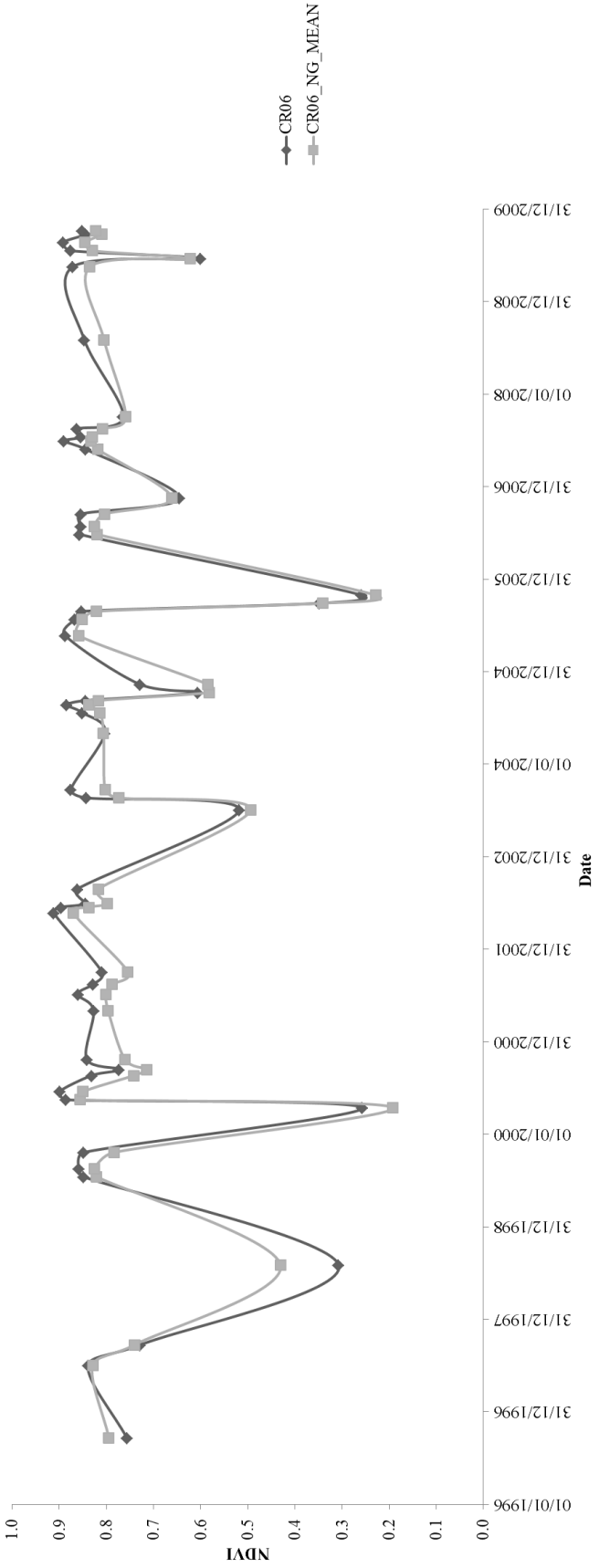

Figure 4-107 - Line plot showing NDVI throughout period of interment for Cancari Road 06 and mean NDVI of local non-grave areas.

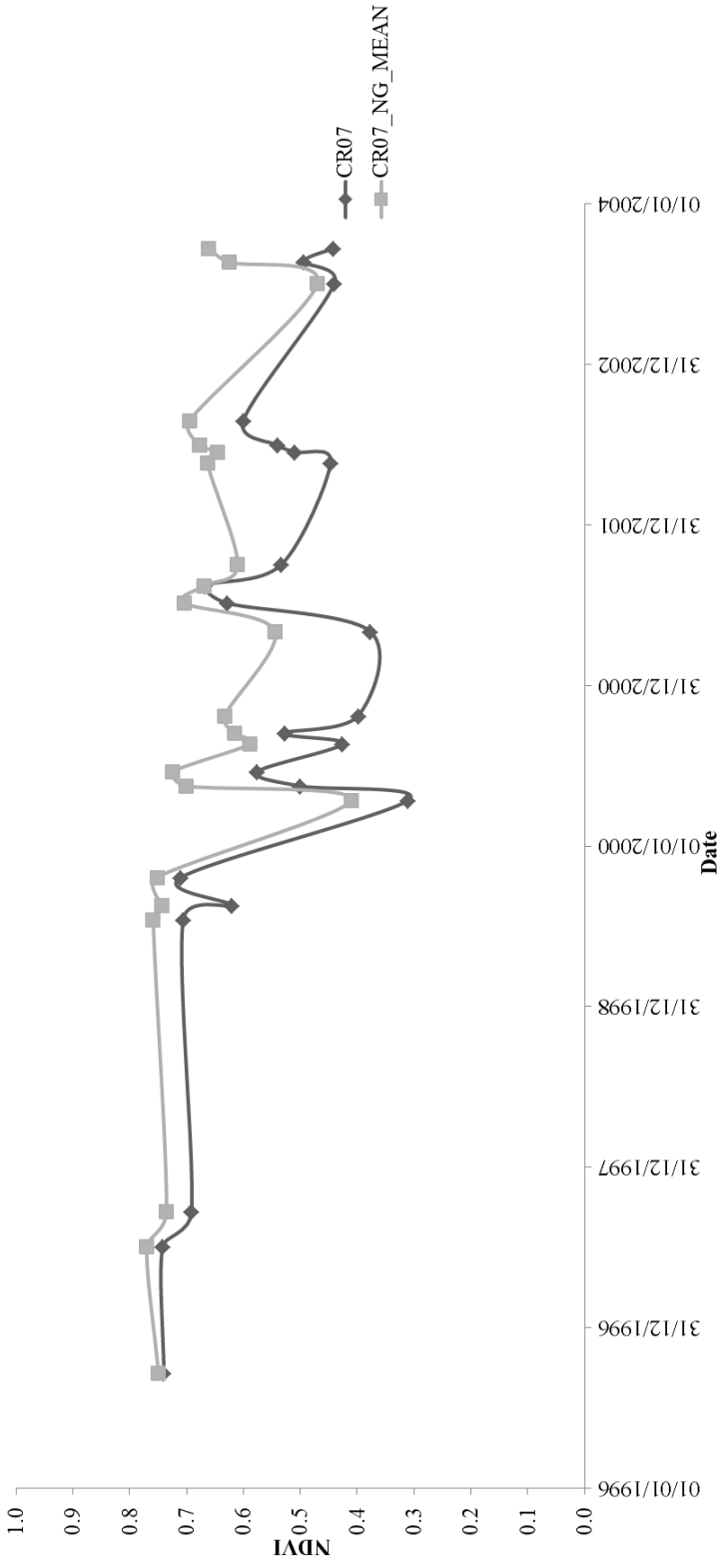

Figure 4-108 - Line plot showing NDVI throughout period of interment for Cancari Road 07 and mean NDVI of local non-grave areas.

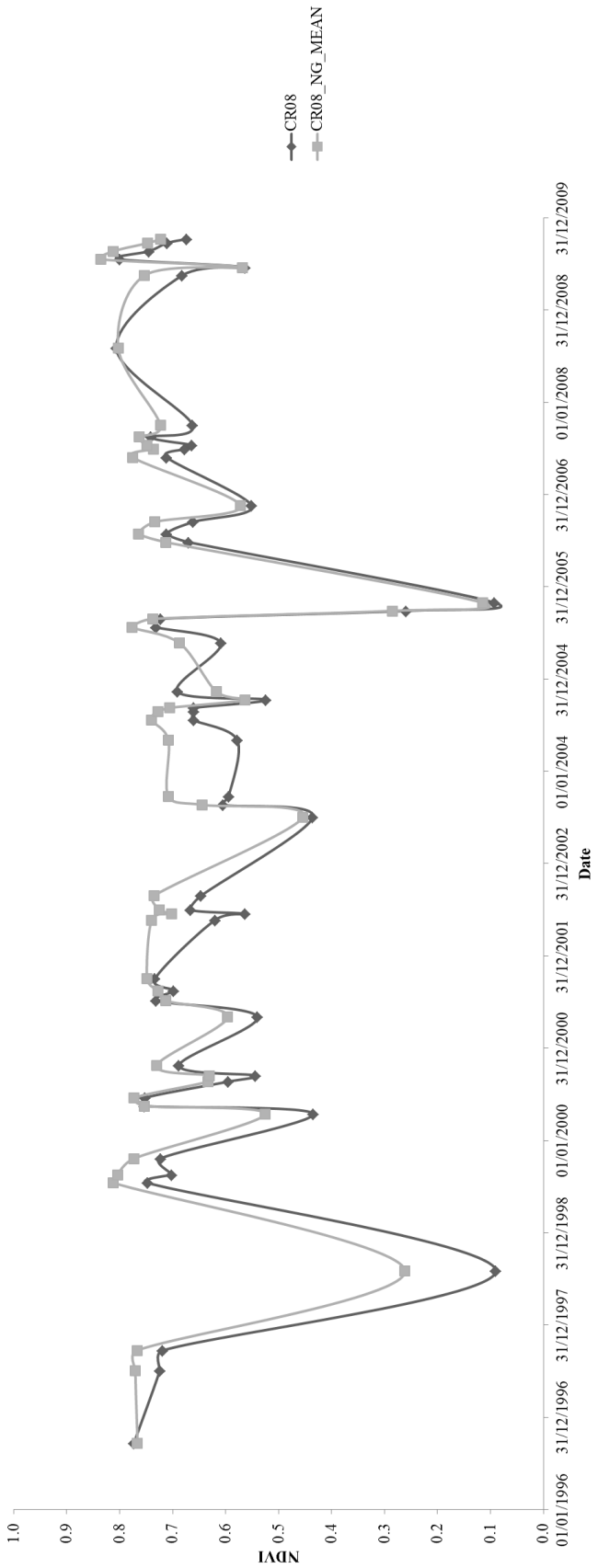

Figure 4-109 - Line plot showing NDVI throughout period of interment for Cancari Road 08 and mean NDVI of local non-grave areas.

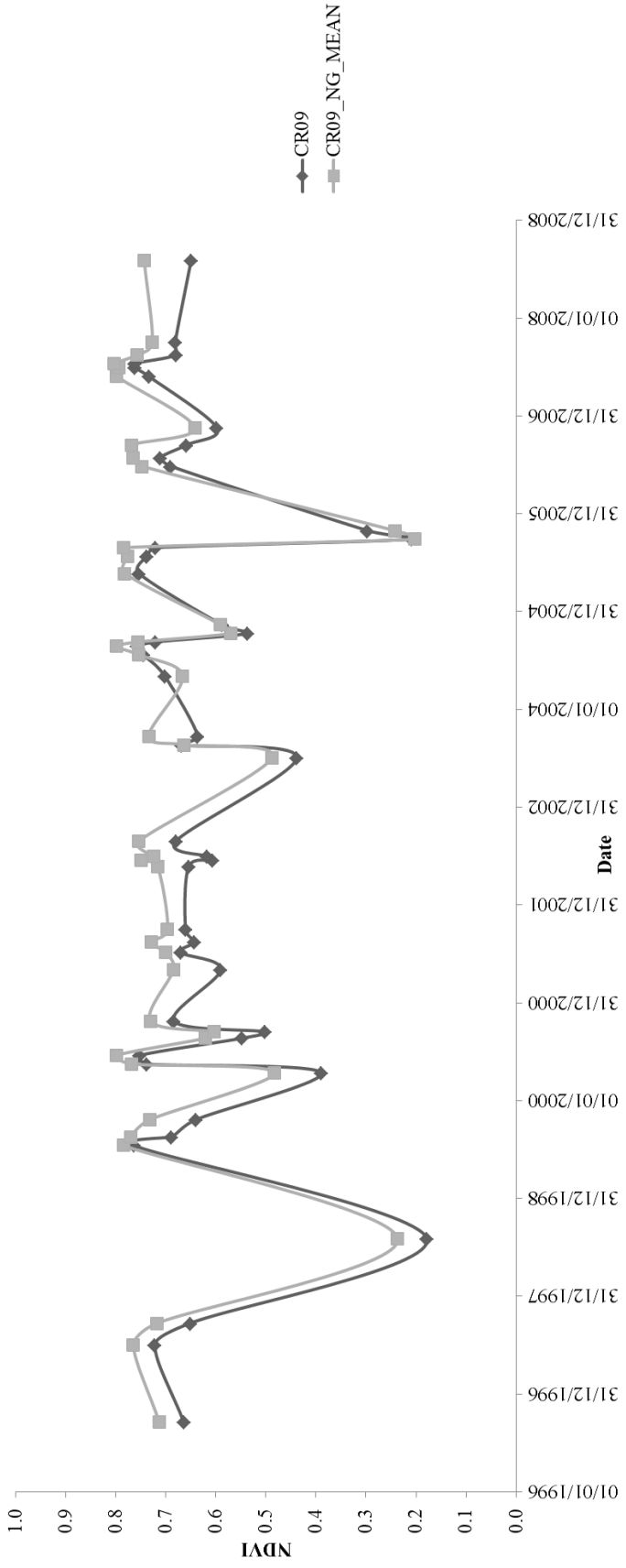

Figure 4-110 - Line plot showing NDVI throughout period of interment for Cancari Road 09 and mean NDVI of local non-grave areas.

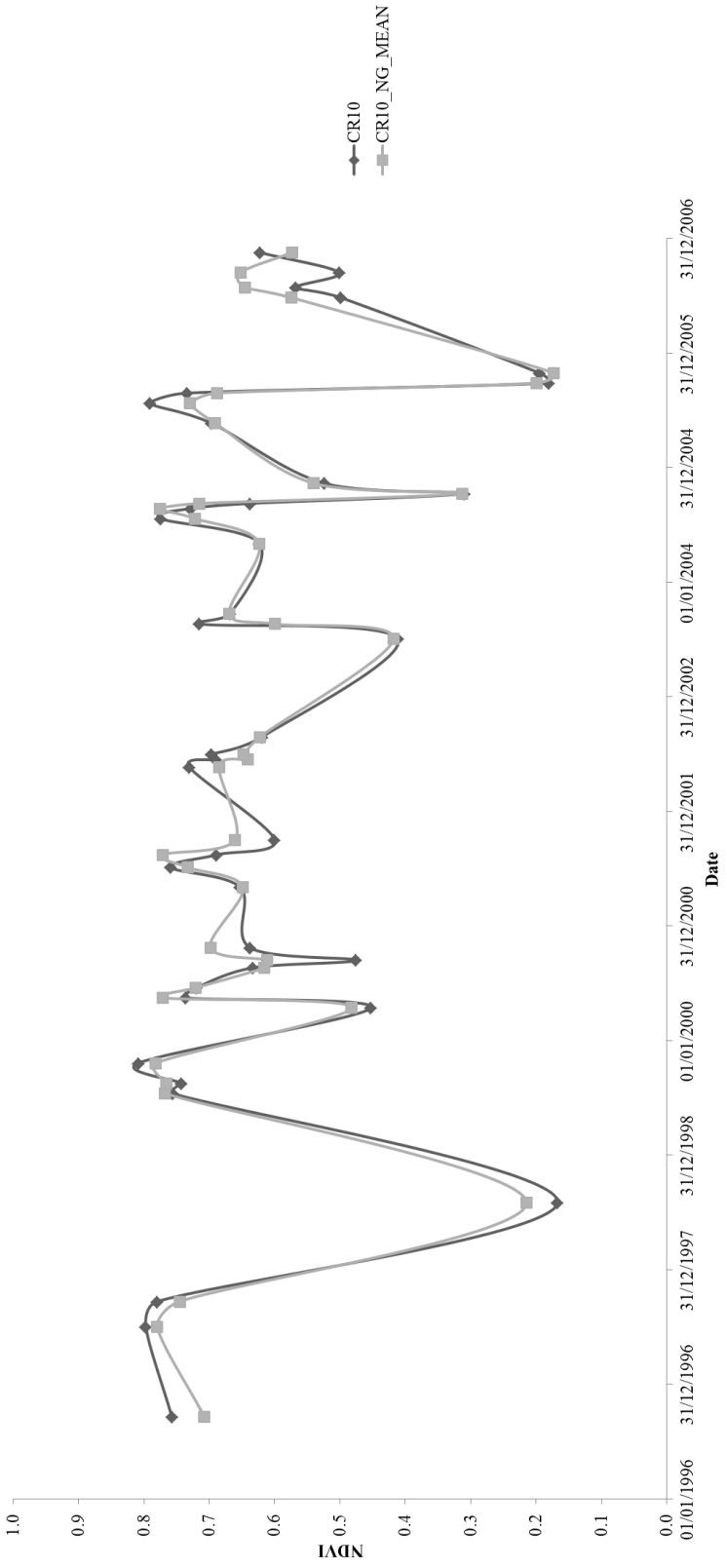

Figure 4-111 - Line plot showing NDVI throughout period of interment for Cancari Road 10 and mean NDVI of local non-grave areas.

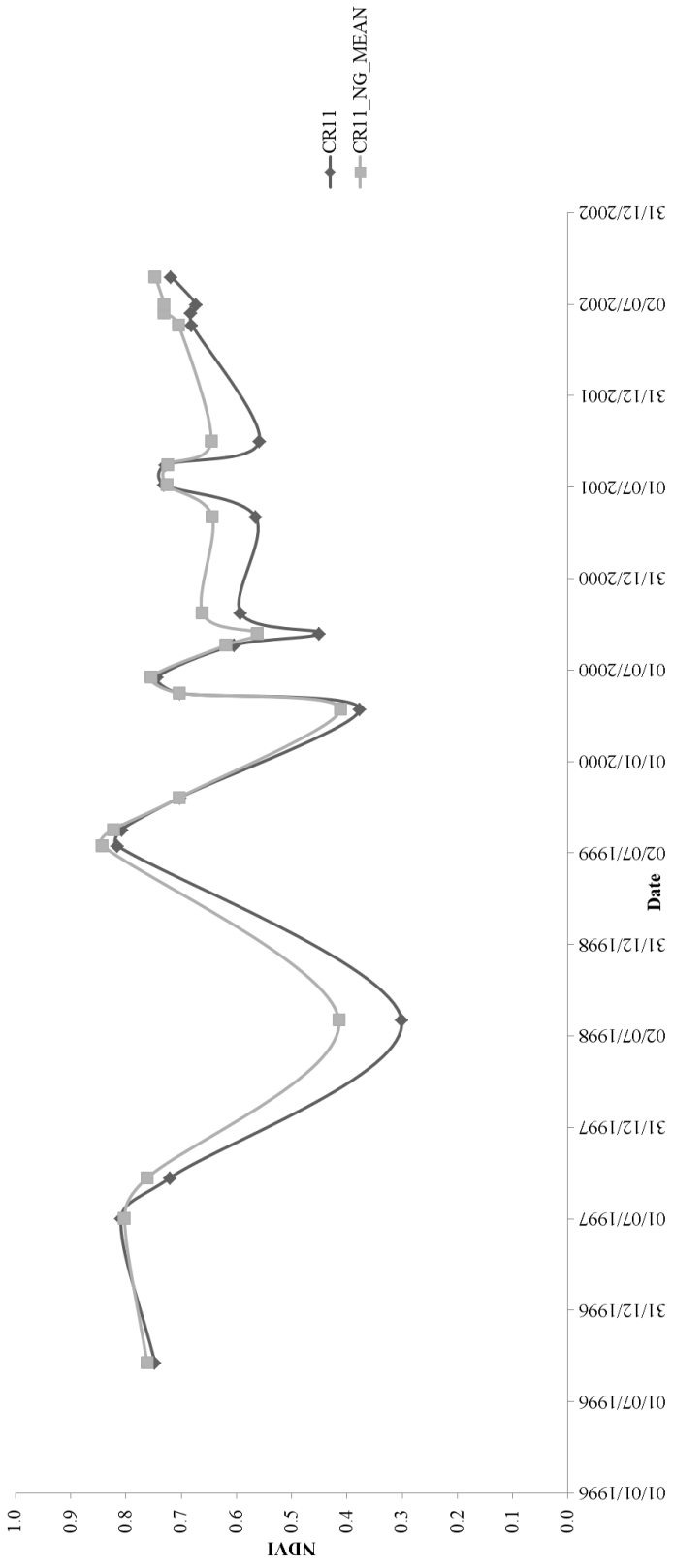

Figure 4-112 - Line plot showing NDVI throughout period of interment for Cancari Road 11 and mean NDVI of local non-grave areas.

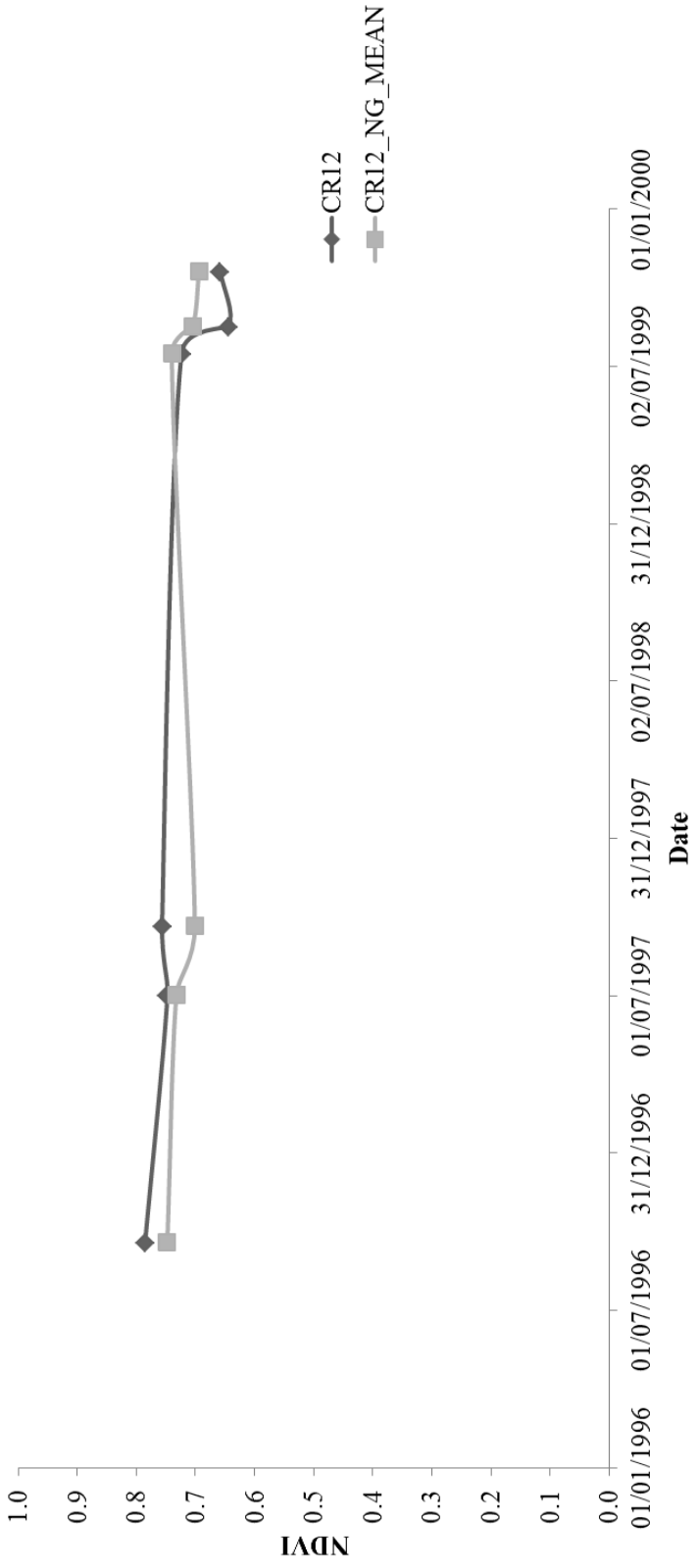

Figure 4-113 - Line plot showing NDVI throughout period of interment for Cancari Road 12 and mean NDVI of local non-grave areas.

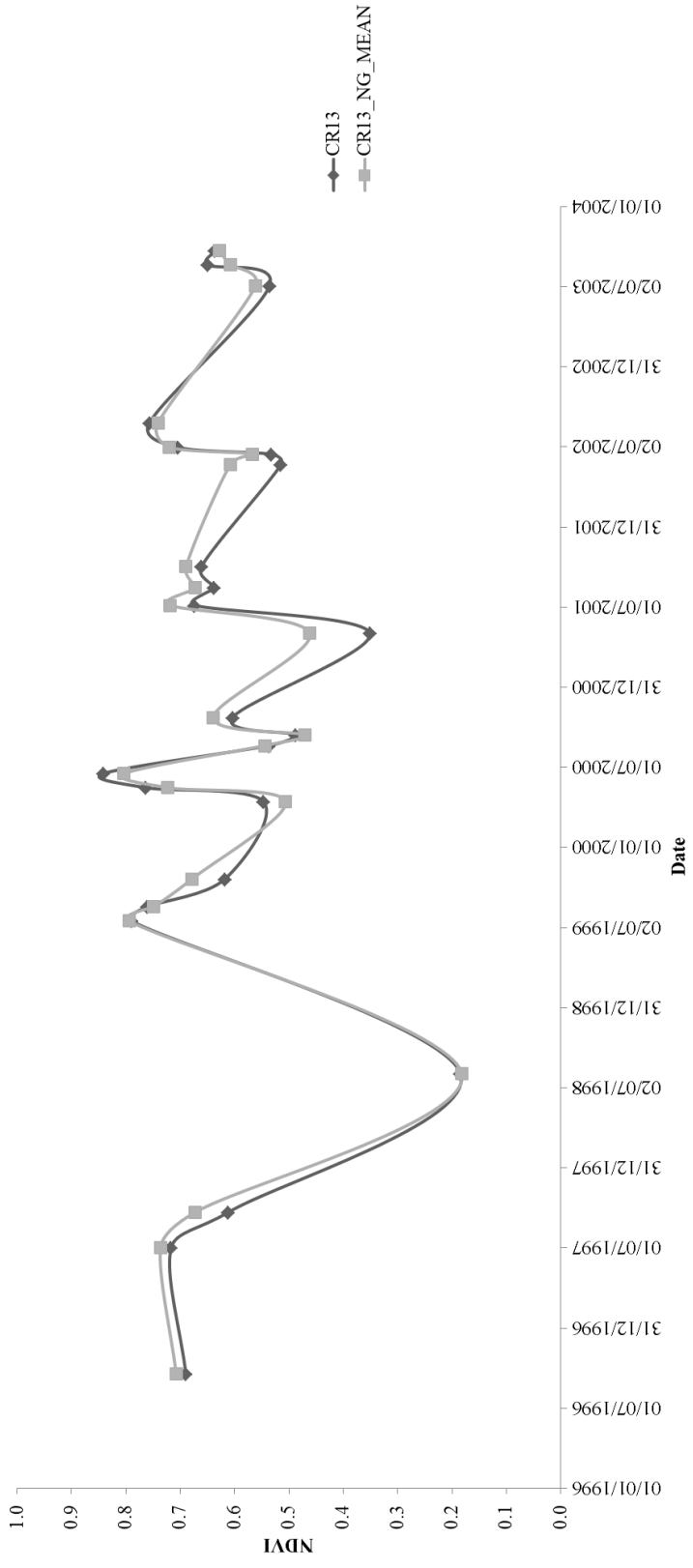

Figure 4-114 - Line plot showing NDVI throughout period of interment for Cancari Road 13 and mean NDVI of local non-grave areas.

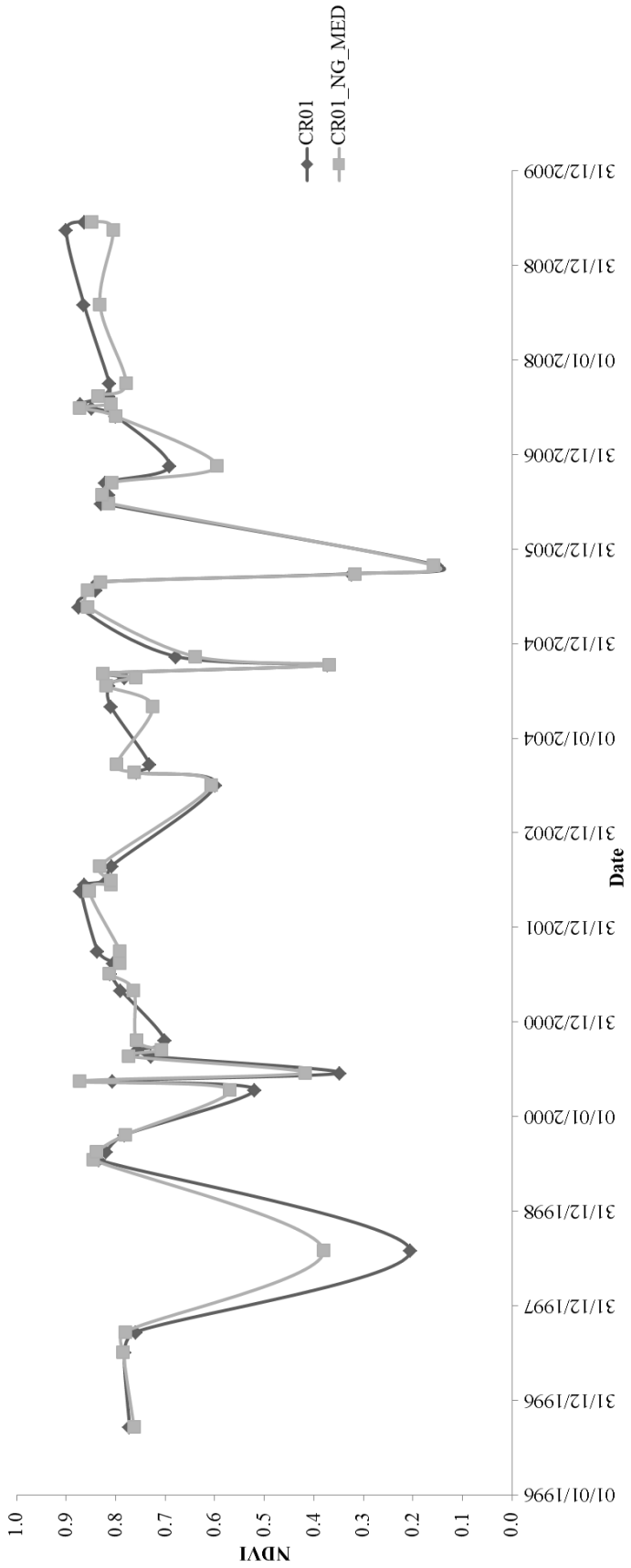

Figure 4-115 - Line plot showing NDVI throughout period of interment for Cancari Road 01 and median NDVI of local non-grave areas.

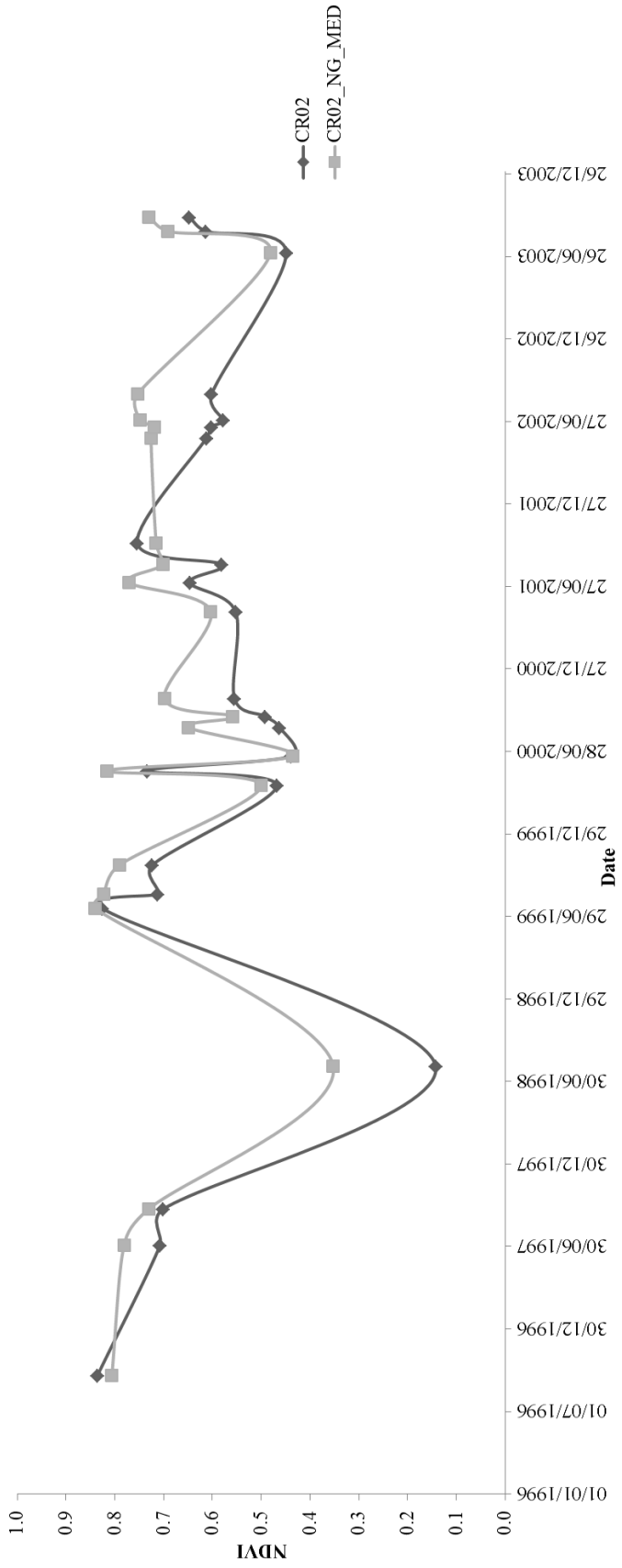

Figure 4-116 - Line plot showing NDVI throughout period of interment for Cancari Road 02 and median NDVI of local non-grave areas.

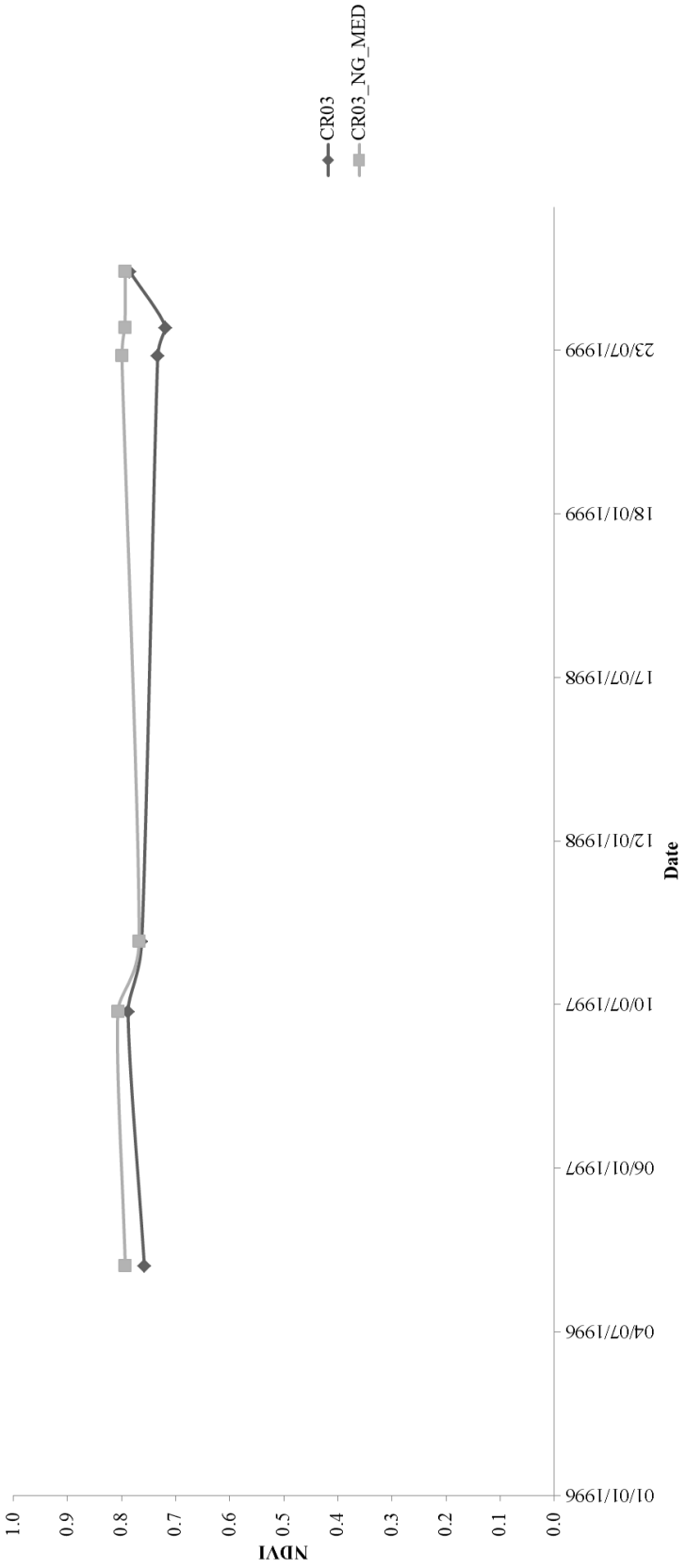

Figure 4-117 - Line plot showing NDVI throughout period of interment for Cancari Road 03 and median NDVI of local non-grave areas.

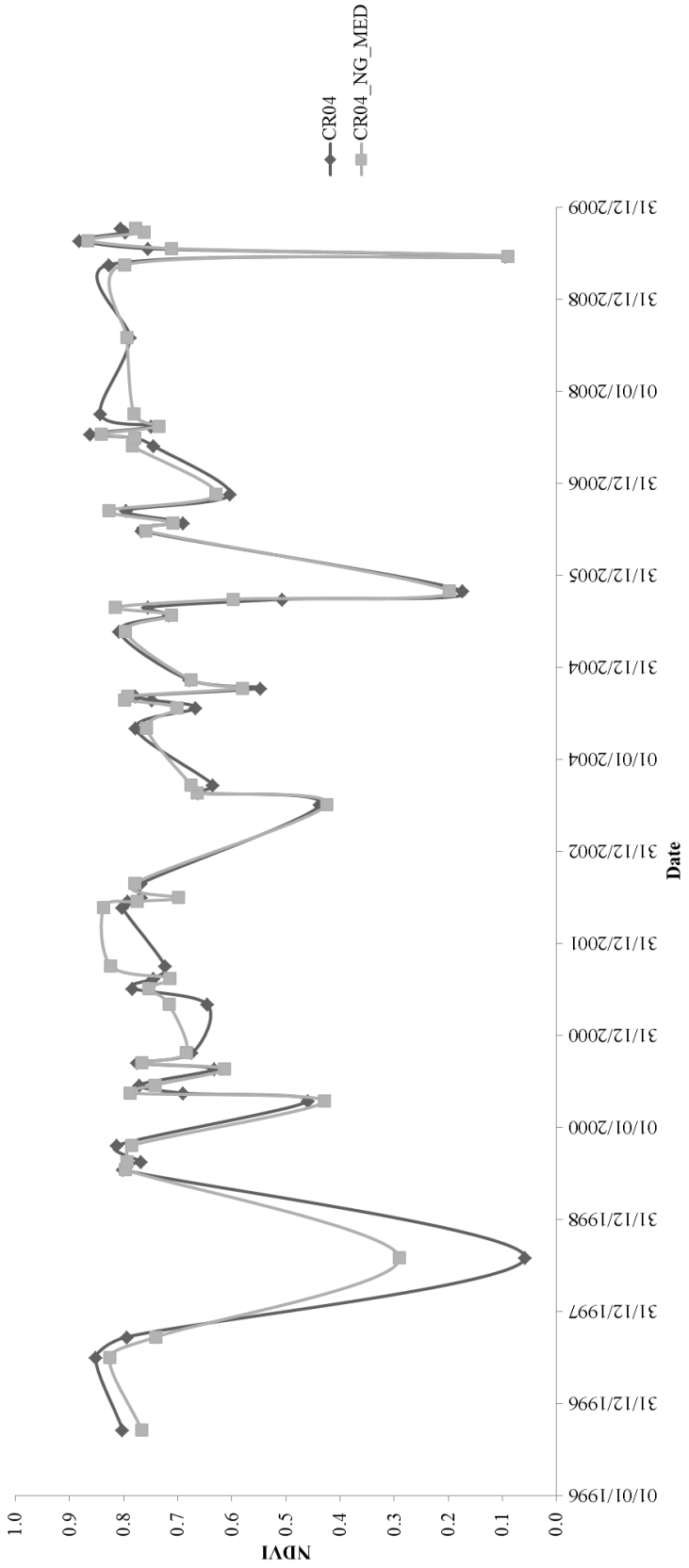

Figure 4-118 - Line plot showing NDVI throughout period of interment for Cancari Road 04 and median NDVI of local non-grave areas.

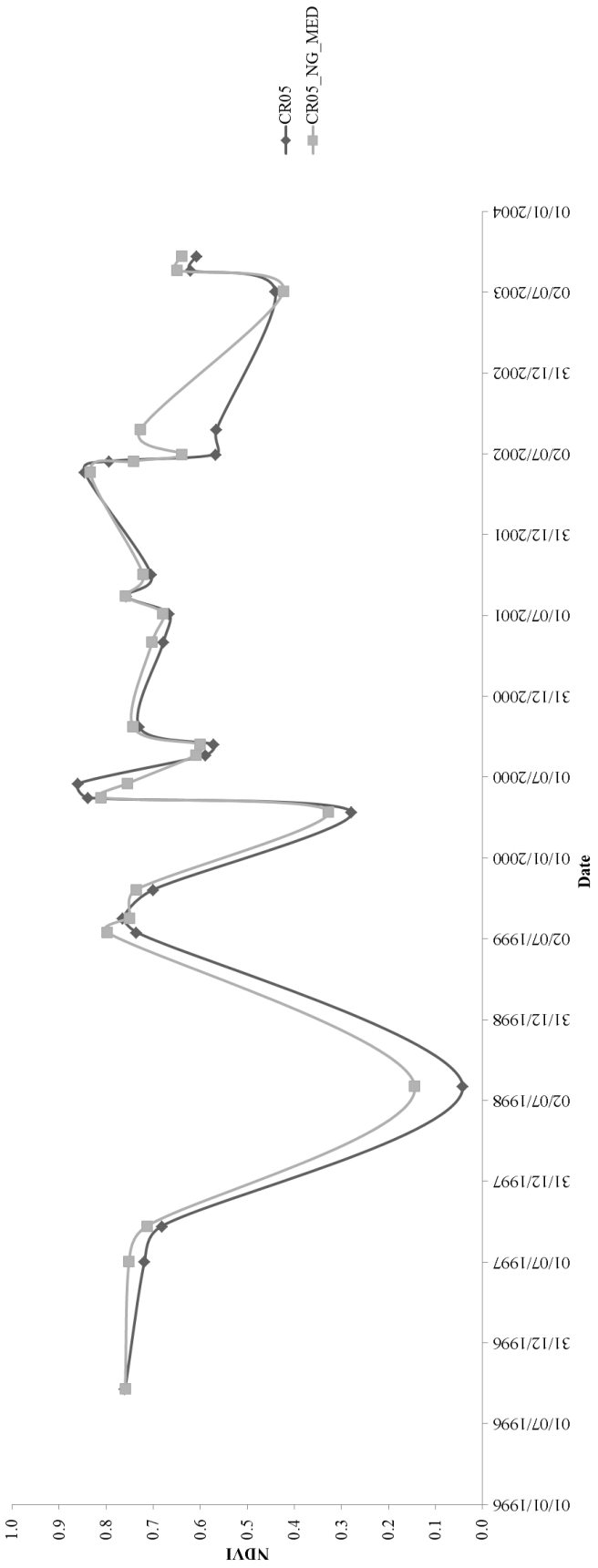

Figure 4-119 - Line plot showing NDVI throughout period of interment for Cancari Road 05 and median NDVI of local non-grave areas.

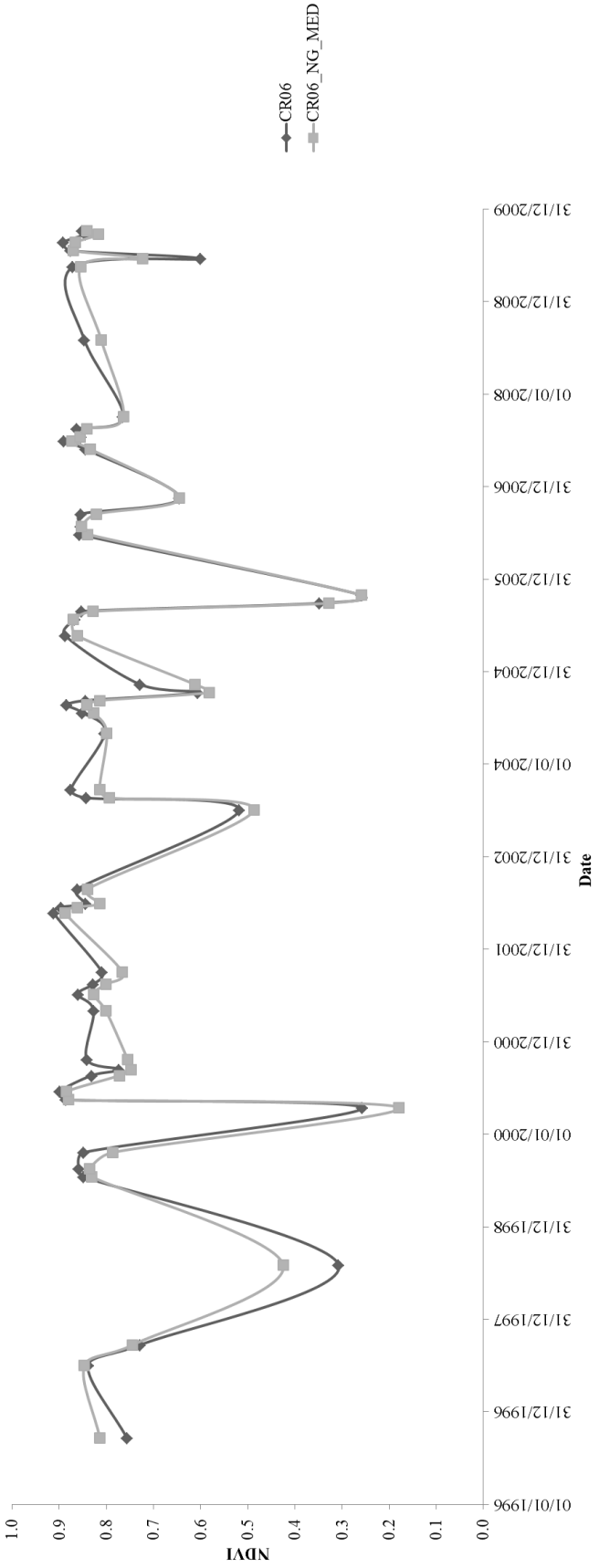

Figure 4-120 - Line plot showing NDVI throughout period of interment for Cancari Road 06 and median NDVI of local non-grave areas.

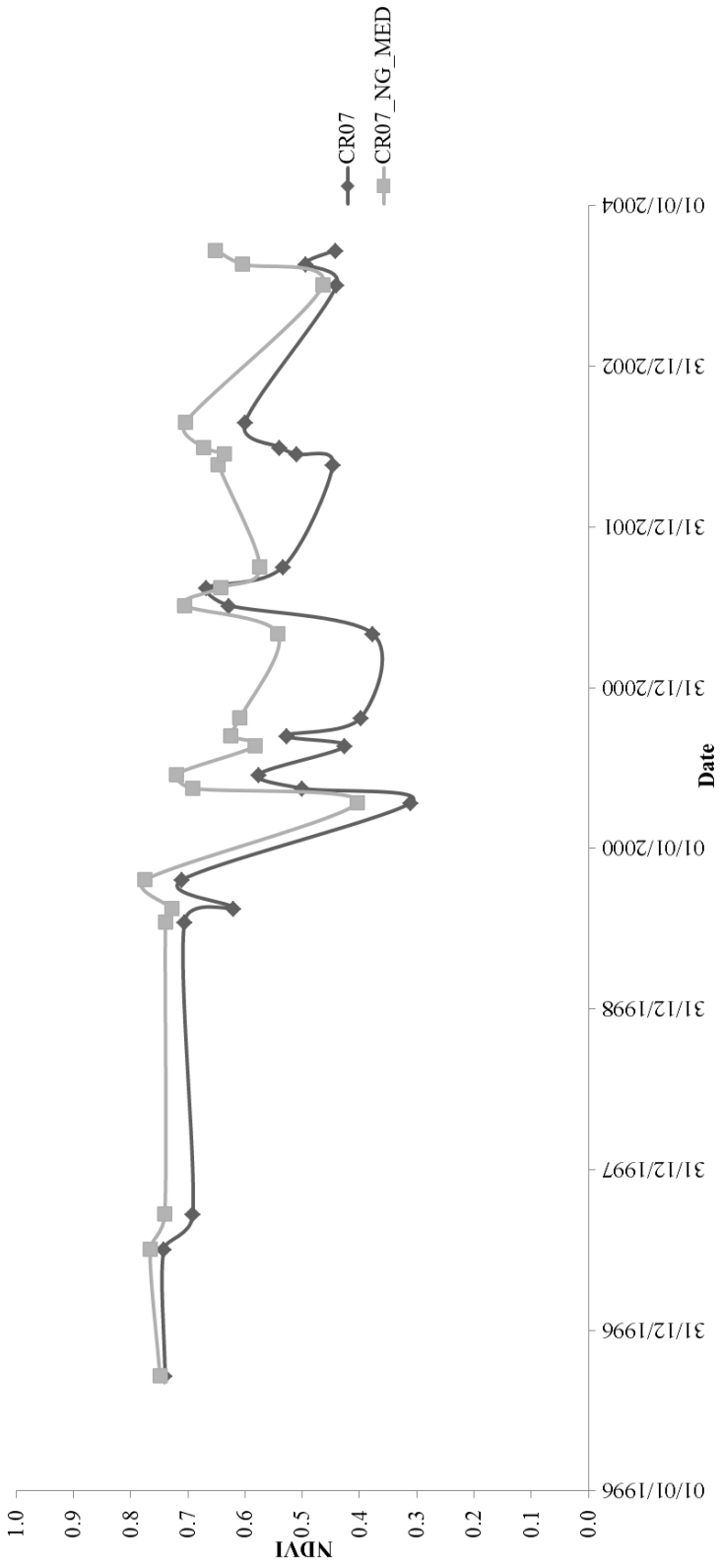

Figure 4-121 - Line plot showing NDVI throughout period of interment for Cancari Road 07 and median NDVI of local non-grave areas.

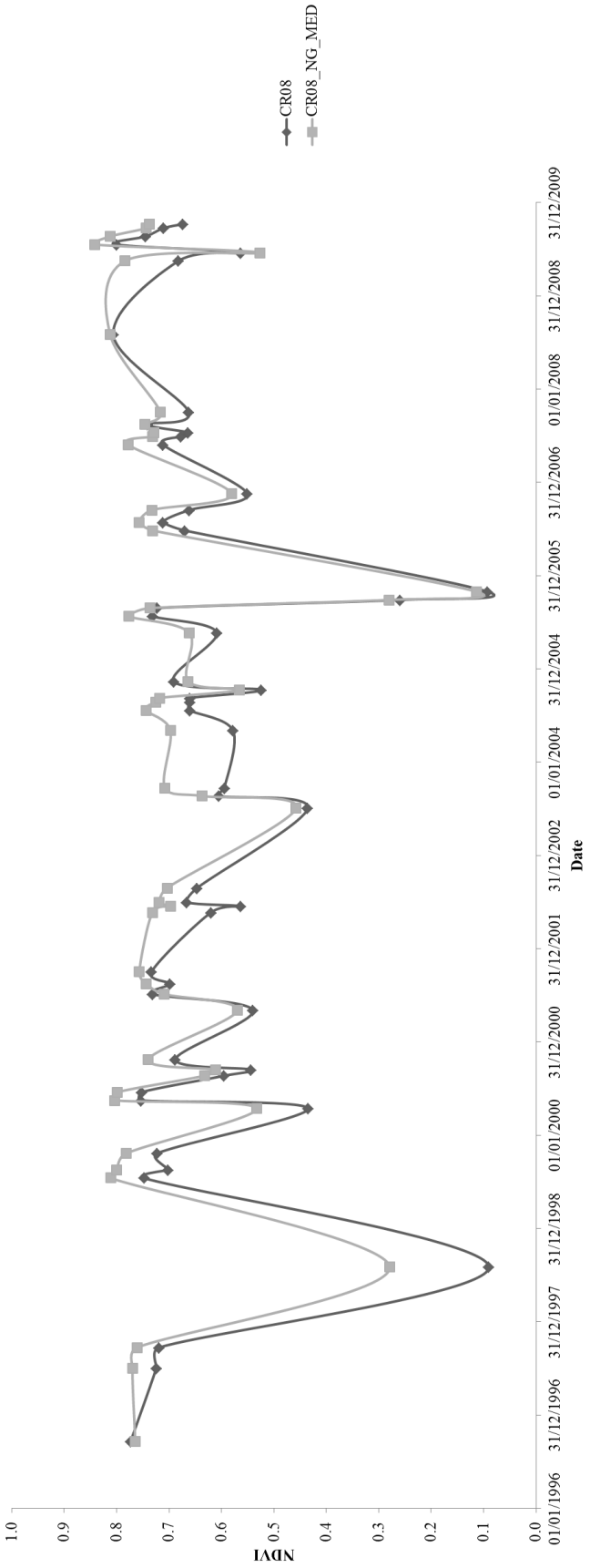

Figure 4-122 - Line plot showing NDVI throughout period of interment for Cancari Road 08 and median NDVI of local non-grave areas.

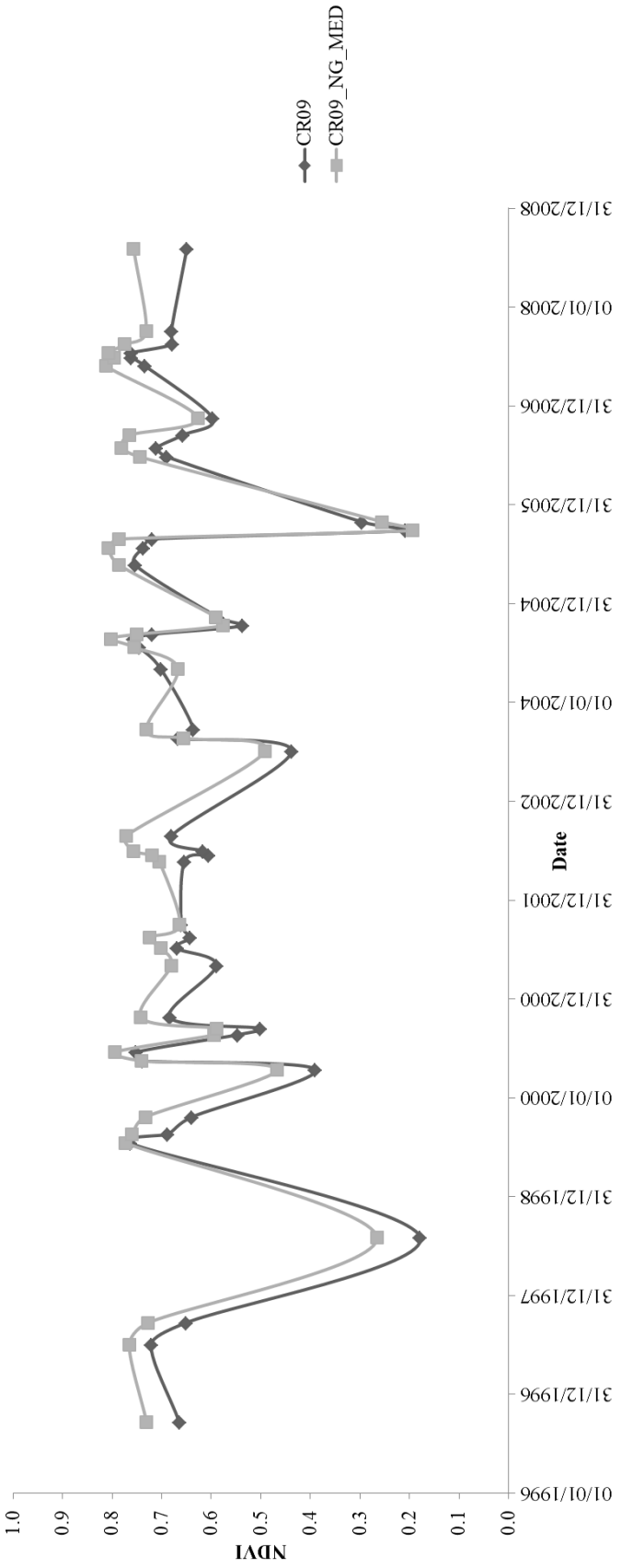

Figure 4-123 - Line plot showing NDVI throughout period of interment for Cancari Road 09 and median NDVI of local non-grave areas.

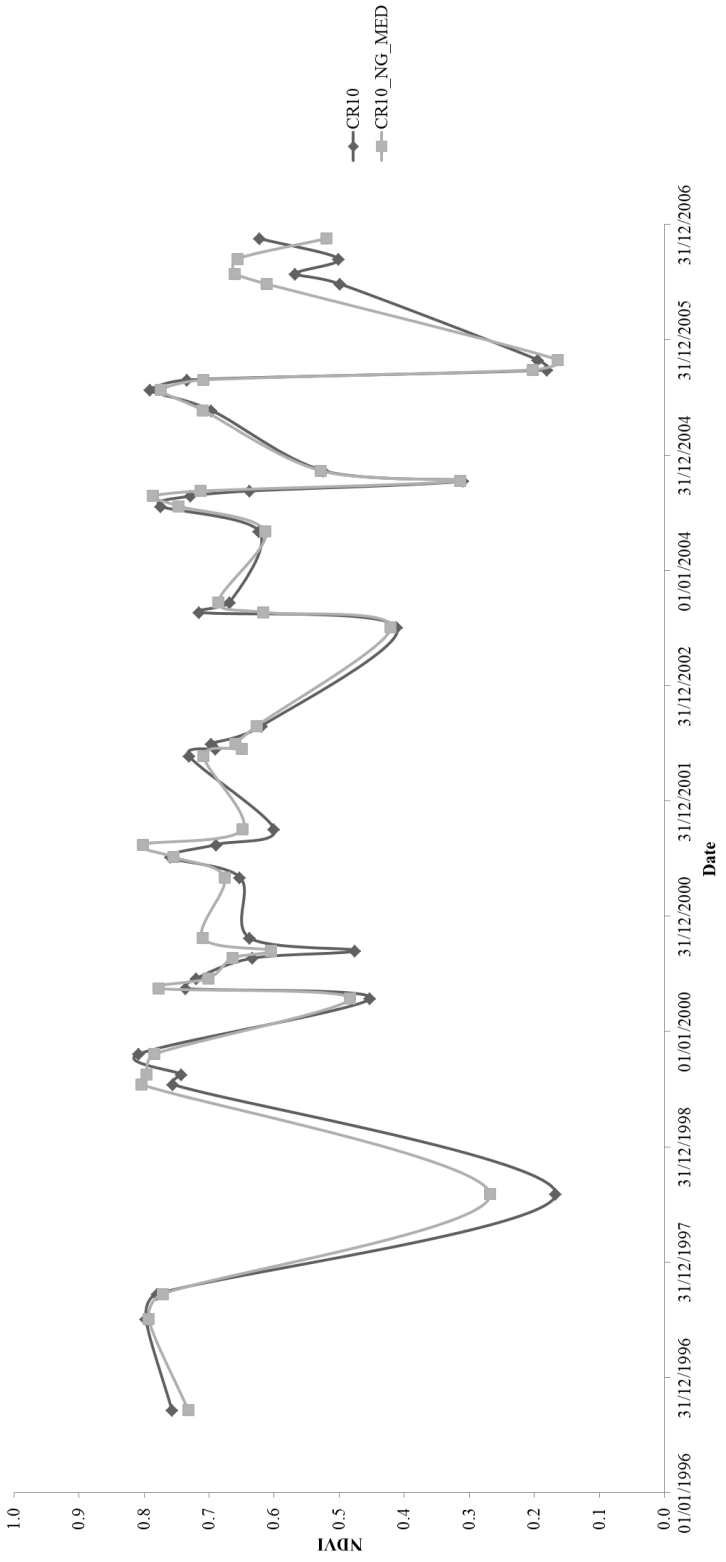

Figure 4-124 - Line plot showing NDVI throughout period of interment for Cancari Road 10 and median NDVI of local non-grave areas.

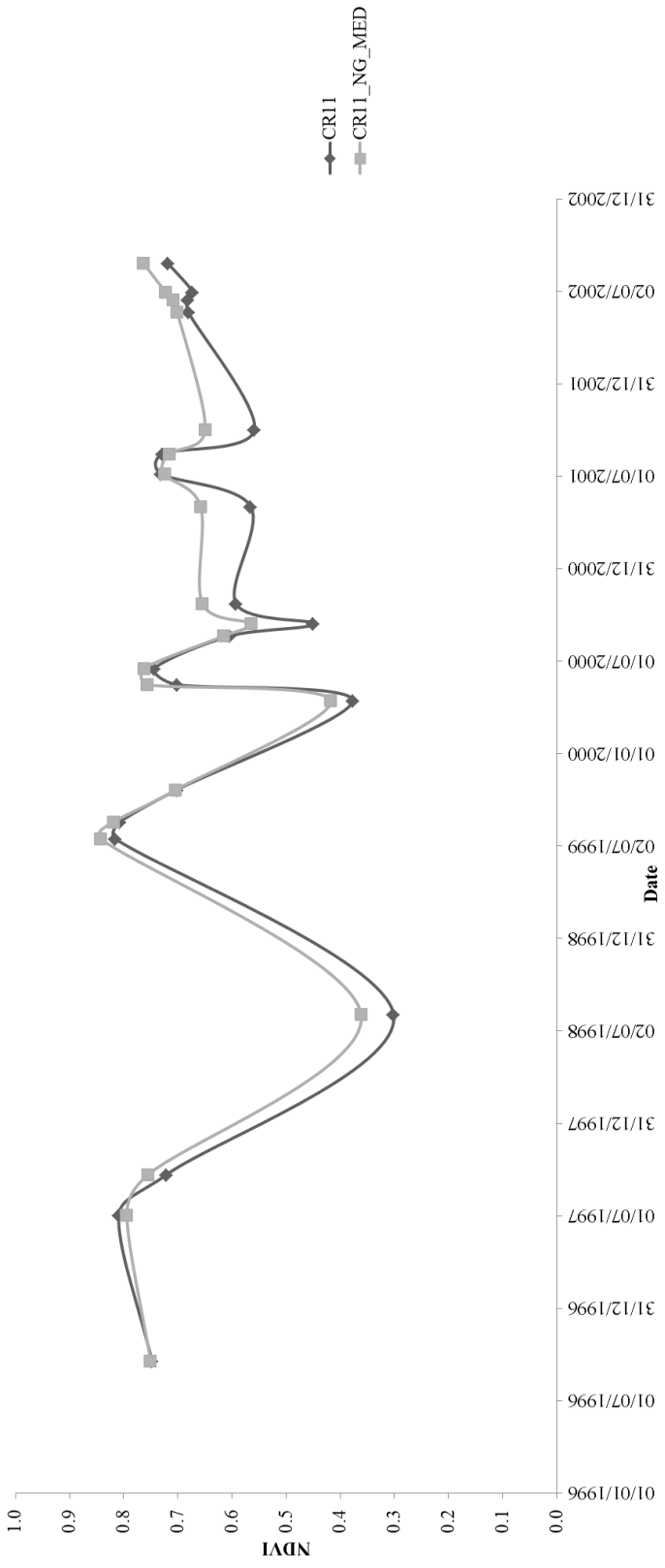

Figure 4-125 - Line plot showing NDVI throughout period of interment for Cancari Road 11 and median NDVI of local non-grave areas.

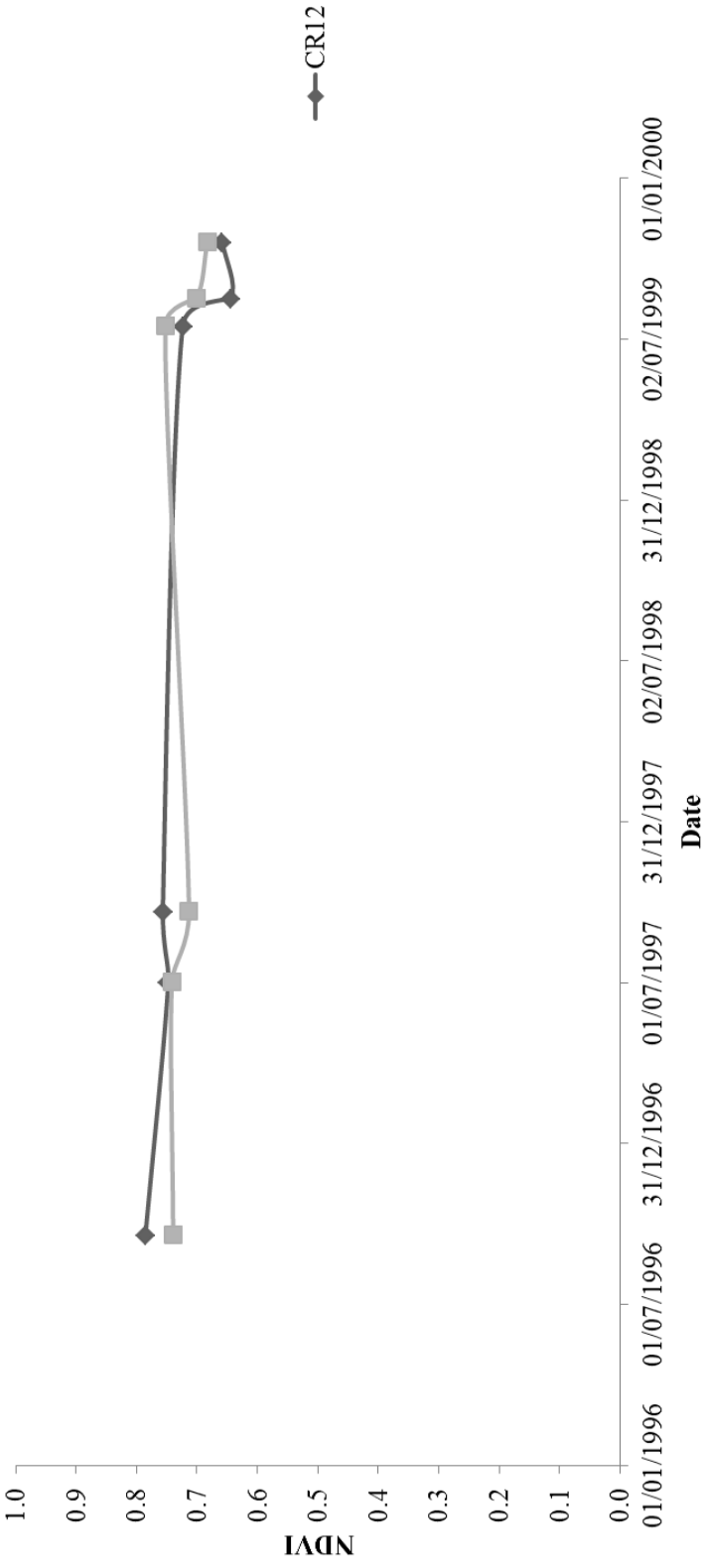

Figure 4-126 - Line plot showing NDVI throughout period of interment for Cancari Road 12 and median NDVI of local non-grave areas.

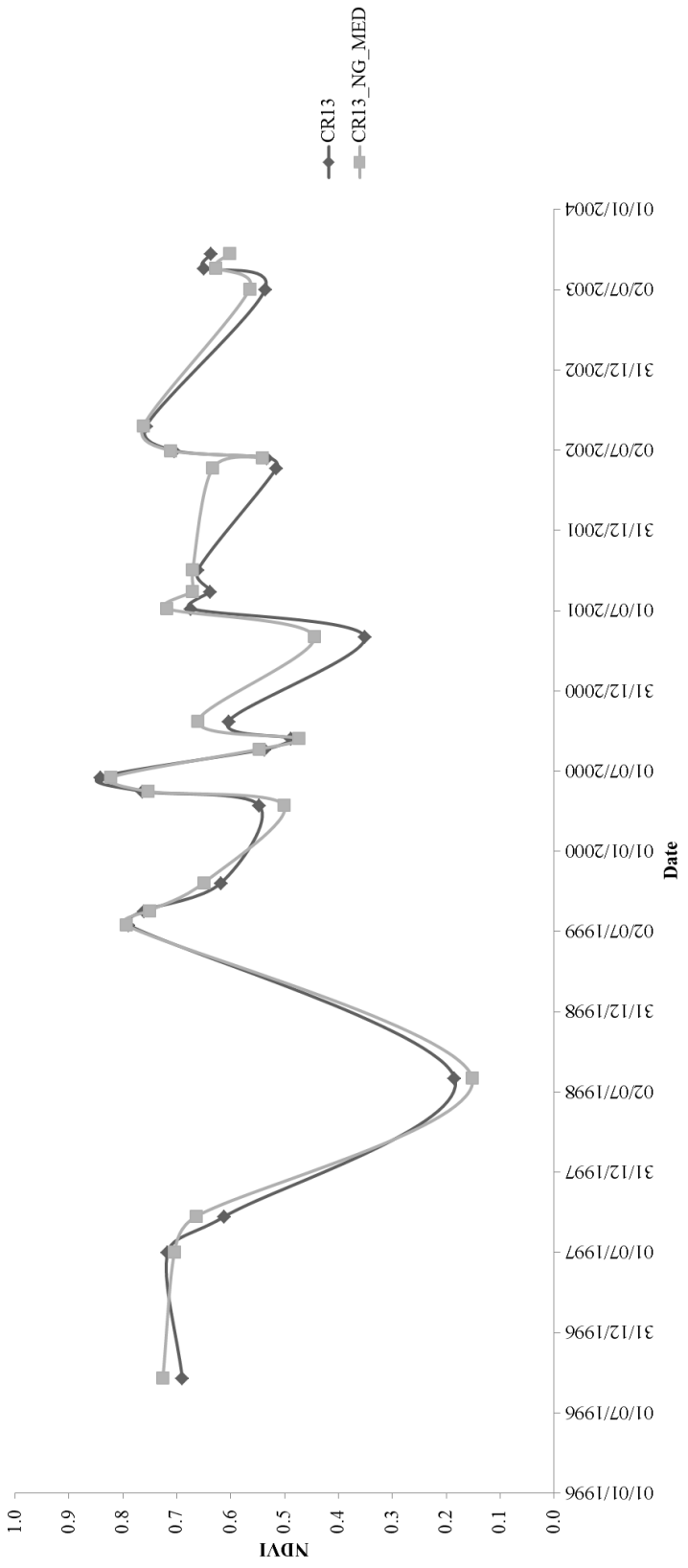

Figure 4-127 - Line plot showing NDVI throughout period of interment for Cancari Road 13 and median NDVI of local non-grave areas.

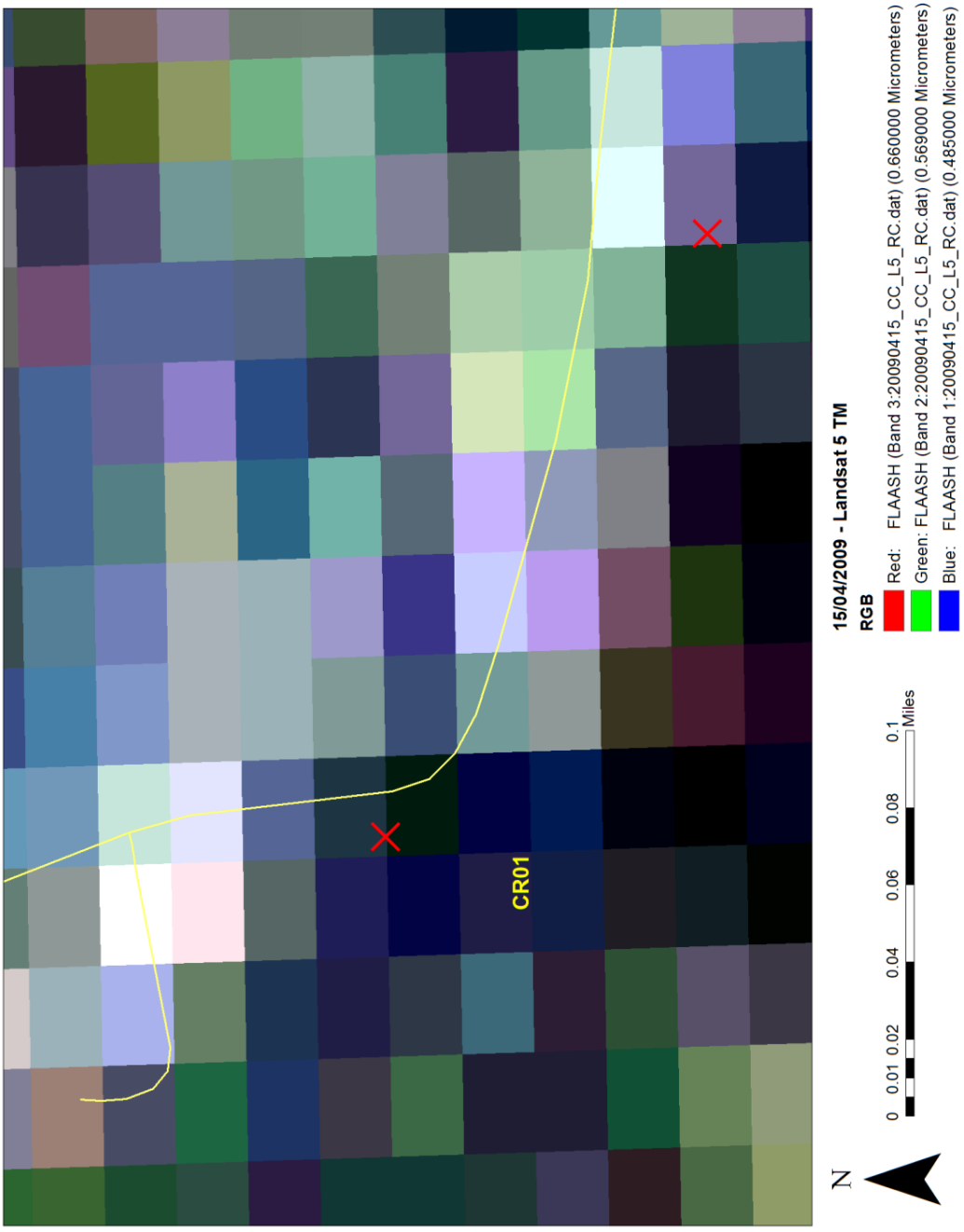

Figure 4-128 - Landsat 5 TM FLAASH image for 15/04/2009 showing CR01 – CR13 is also represented by a red X.

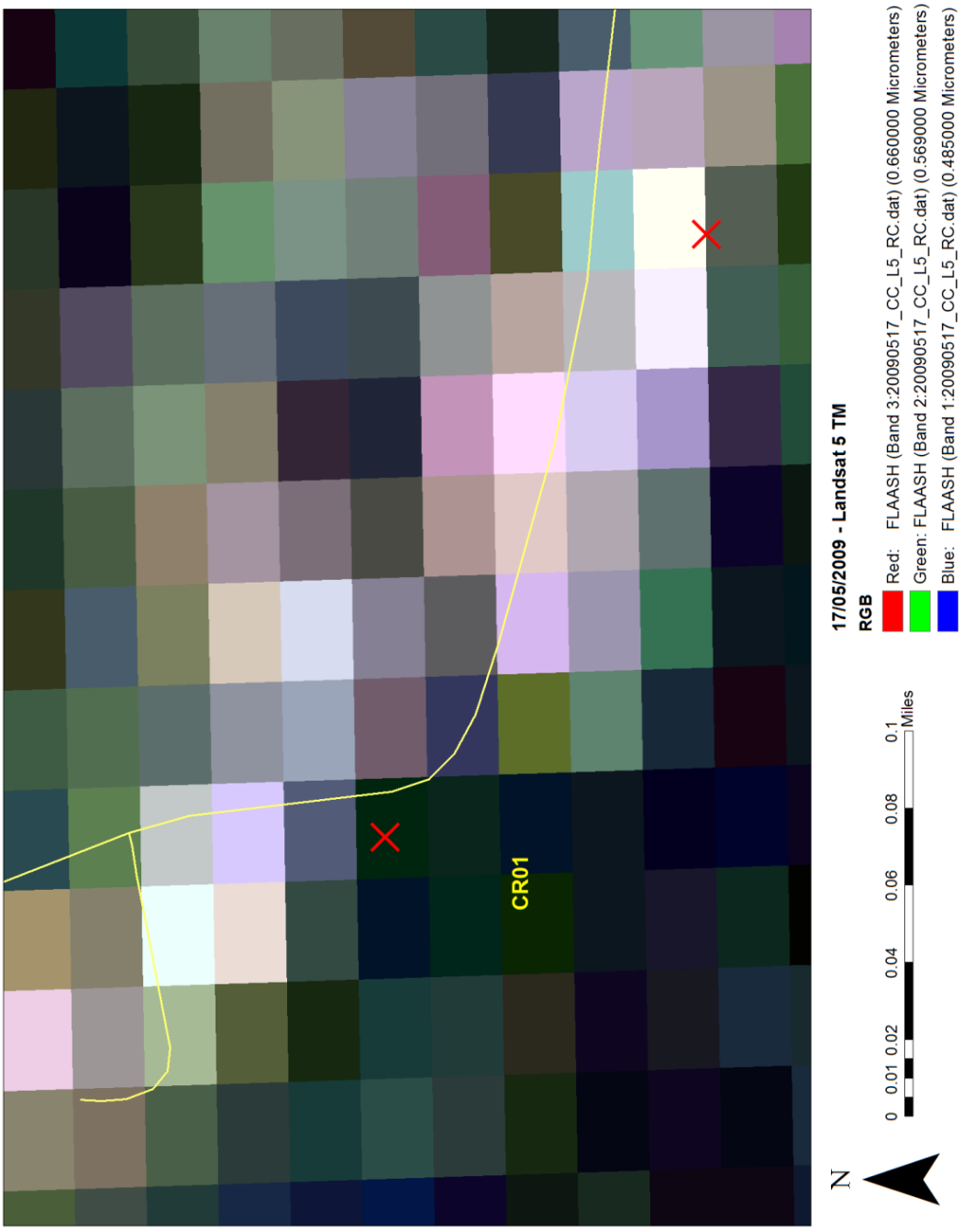

Figure 4-129 - Landsat 5 TM FLAASH image for 17/05/2009 showing CR01 - CR13 is also represented by a red X.

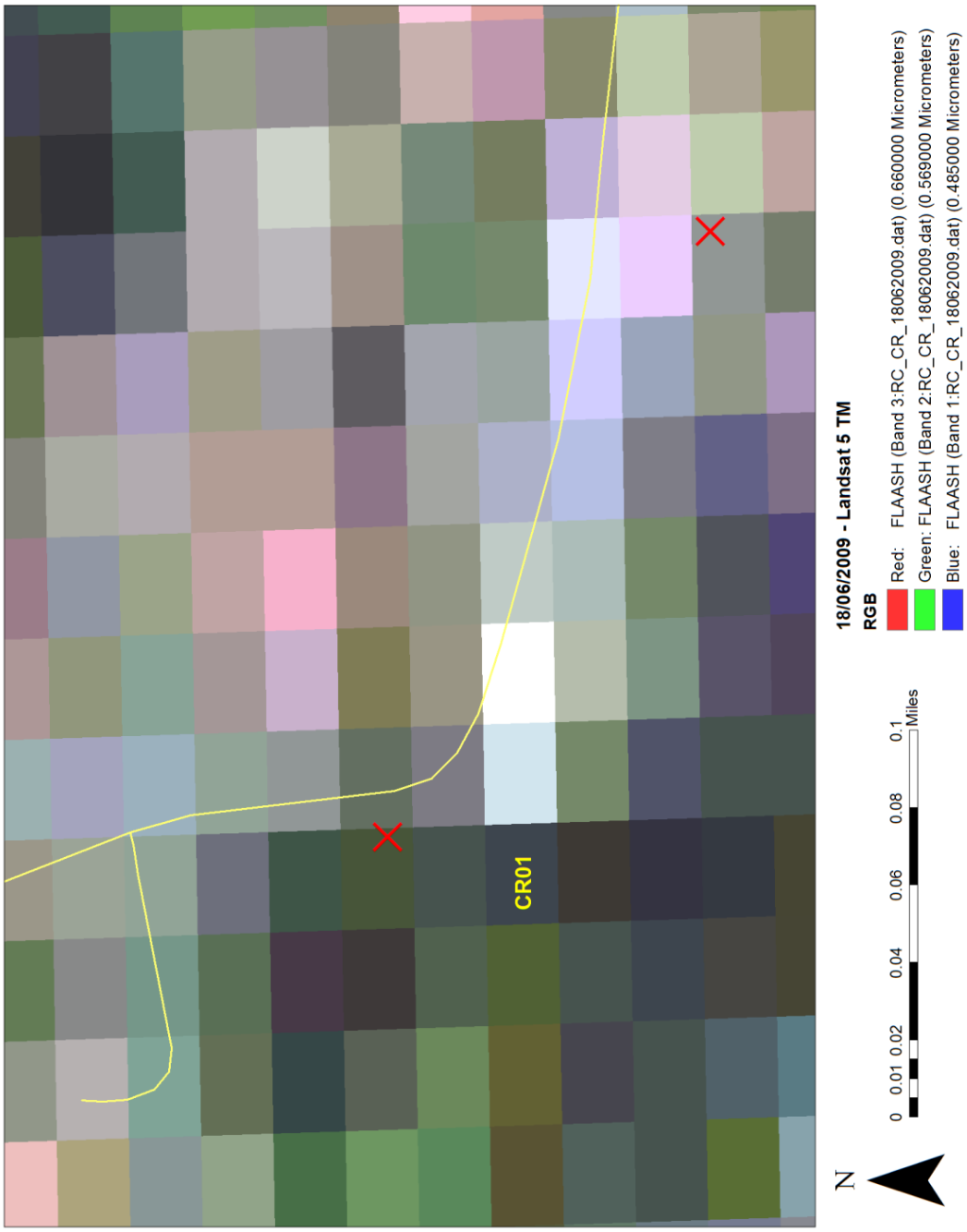

Figure 4-130 - Landsat 5 TM FLAASH image for 18/06/2009 showing CR01 - CR13 is also represented by a red X.

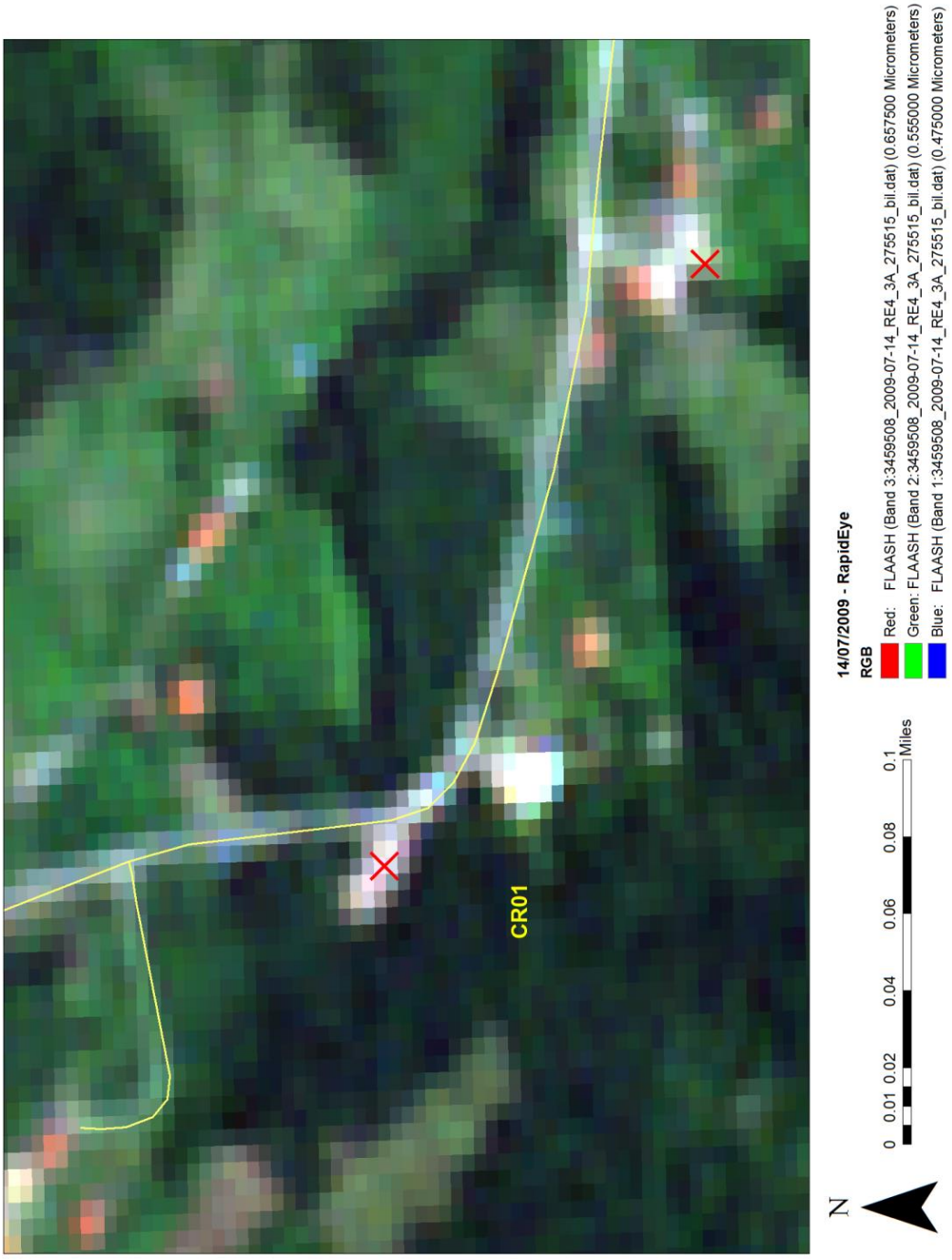

Figure 4-131 - RapidEye FLAASH image for 14/07/2009 showing CR01 - CR13 is also represented by a red X.

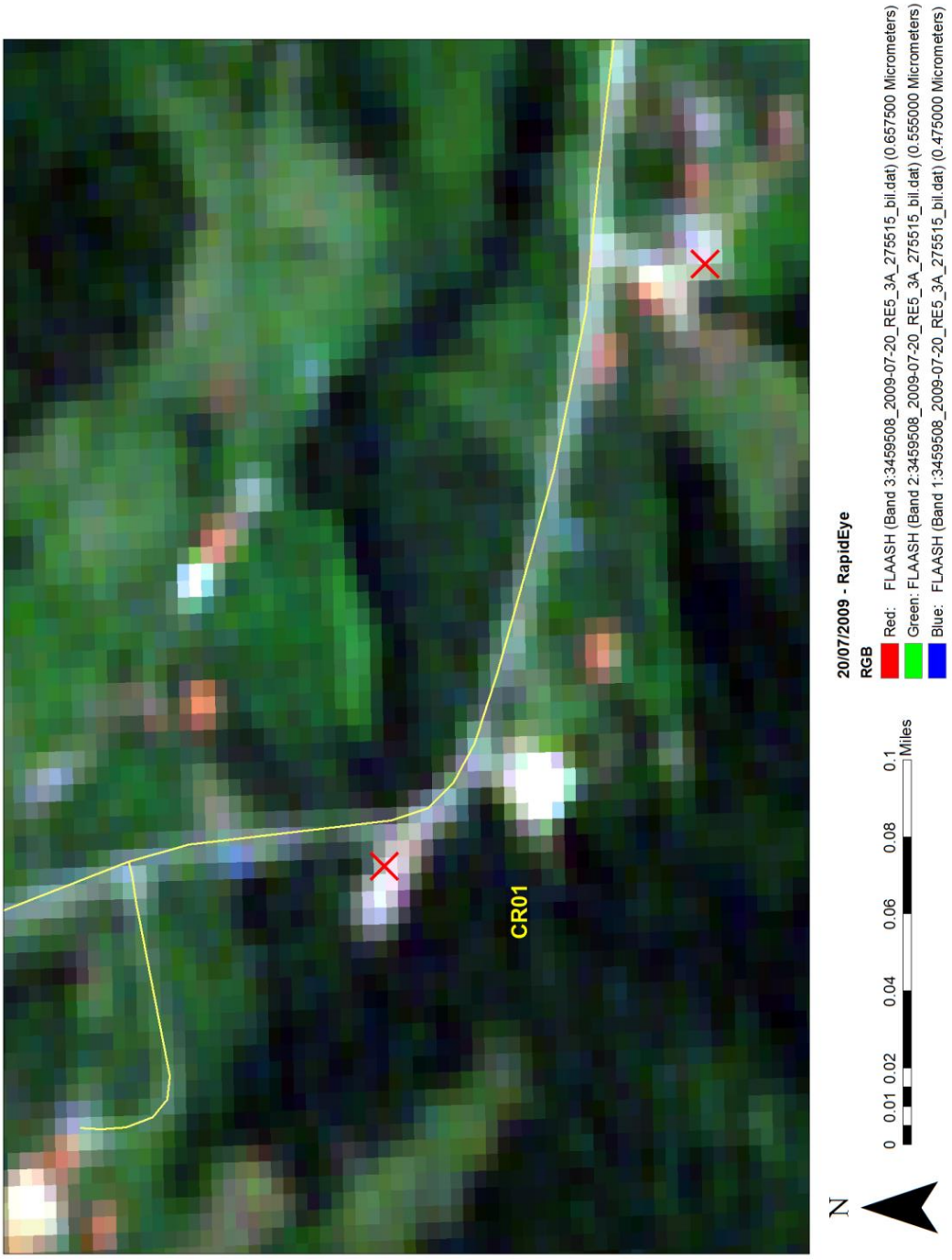

Figure 4-132 - RapidEye FLAASH image for 20/07/2009 showing CR01 - CR13 is also represented by a red X.

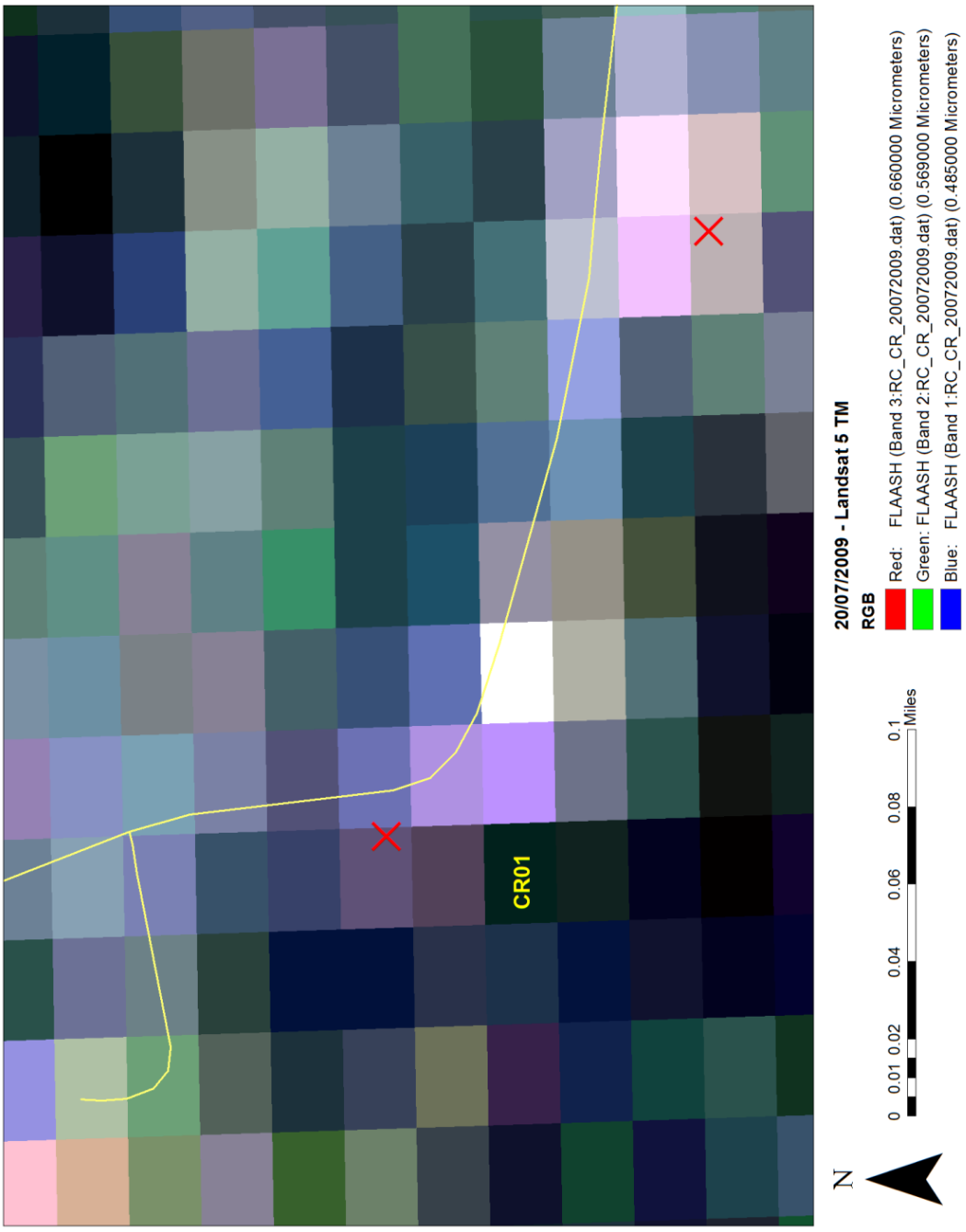

Figure 4-133 - Landsat 5 TM FLAASH image for 20/07/2009 showing CR01 - CR13 is also represented by a red X.

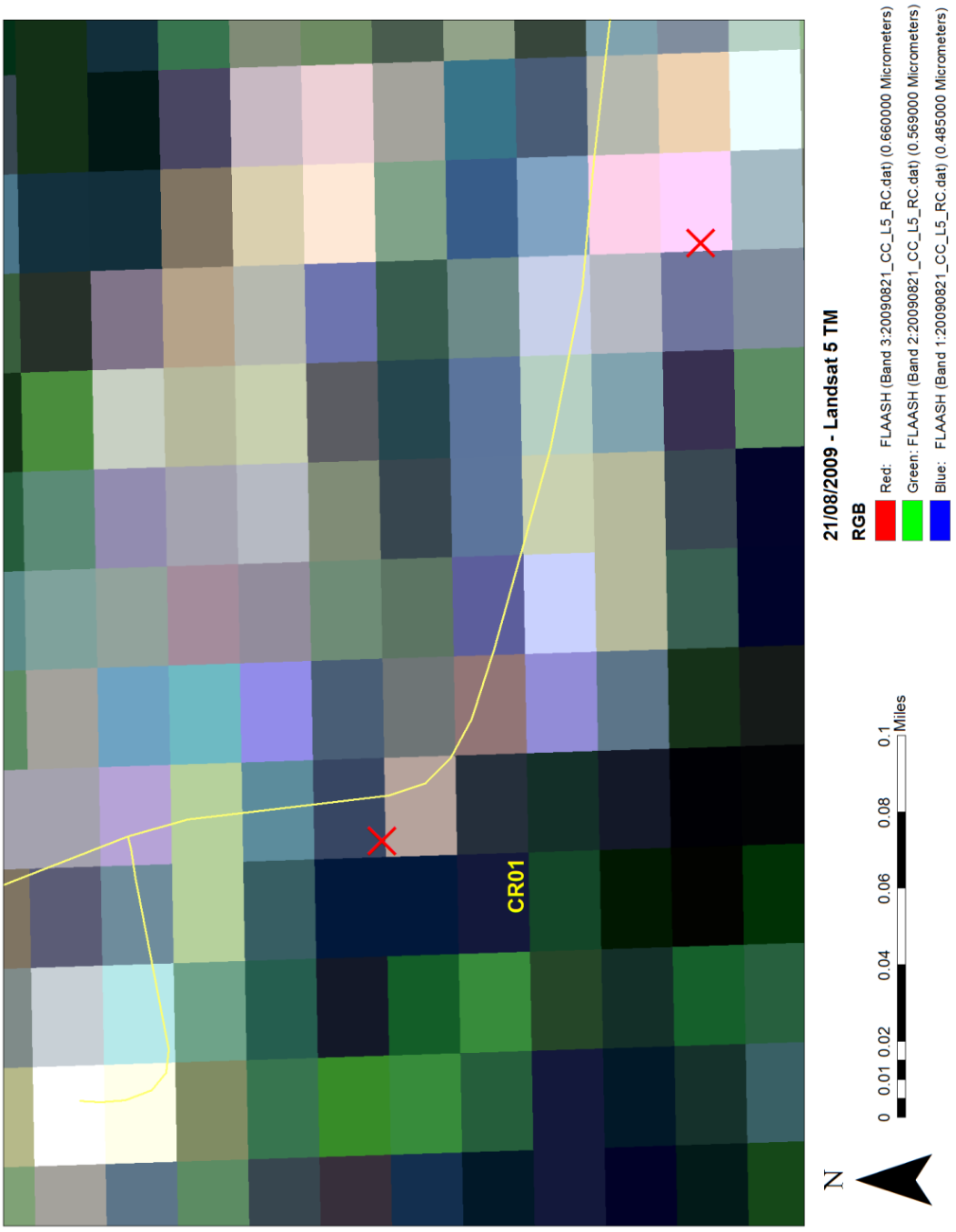

Figure 4-134 - Landsat 5 TM FLAASH image for 21/08/2009 showing CR01 - CR13 is also represented by a red X.

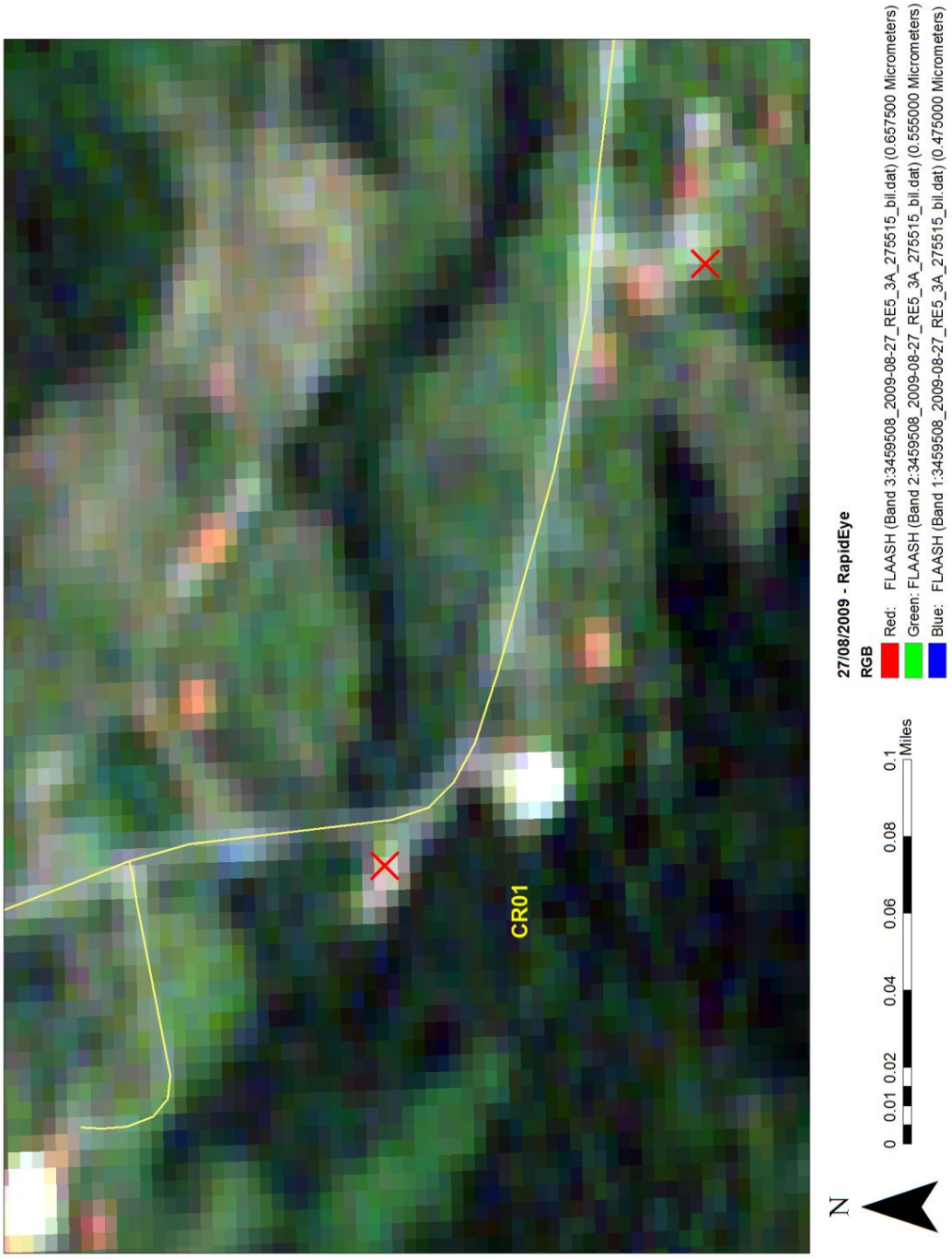

Figure 4-135 - RapidEye FLAASH image for 27/08/2009 showing CR01 – CR13 is also represented by a red X.

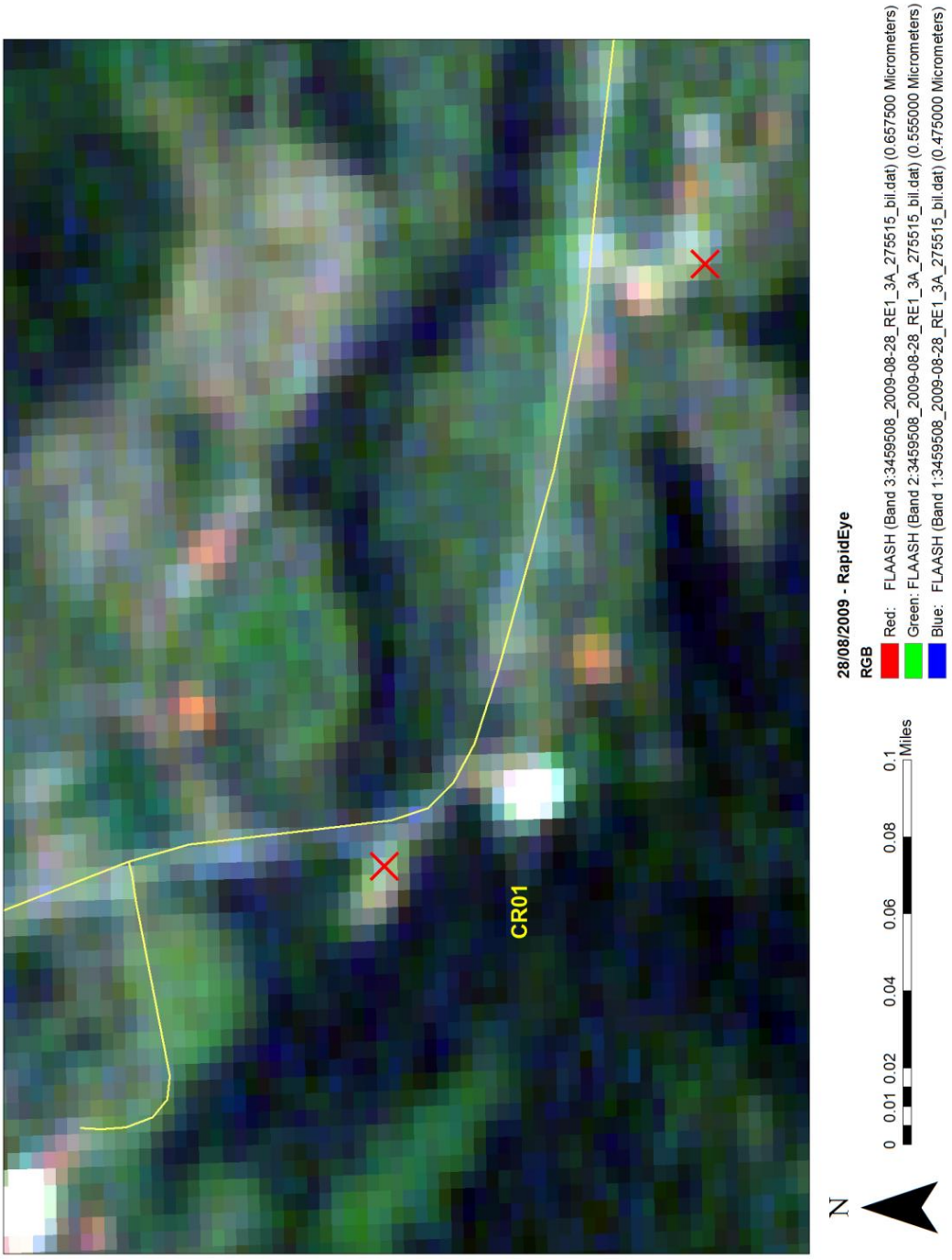

Figure 4-136 - RapidEye FLAASH image for 28/08/2009 showing CR01 - CR13 is also represented by a red X.

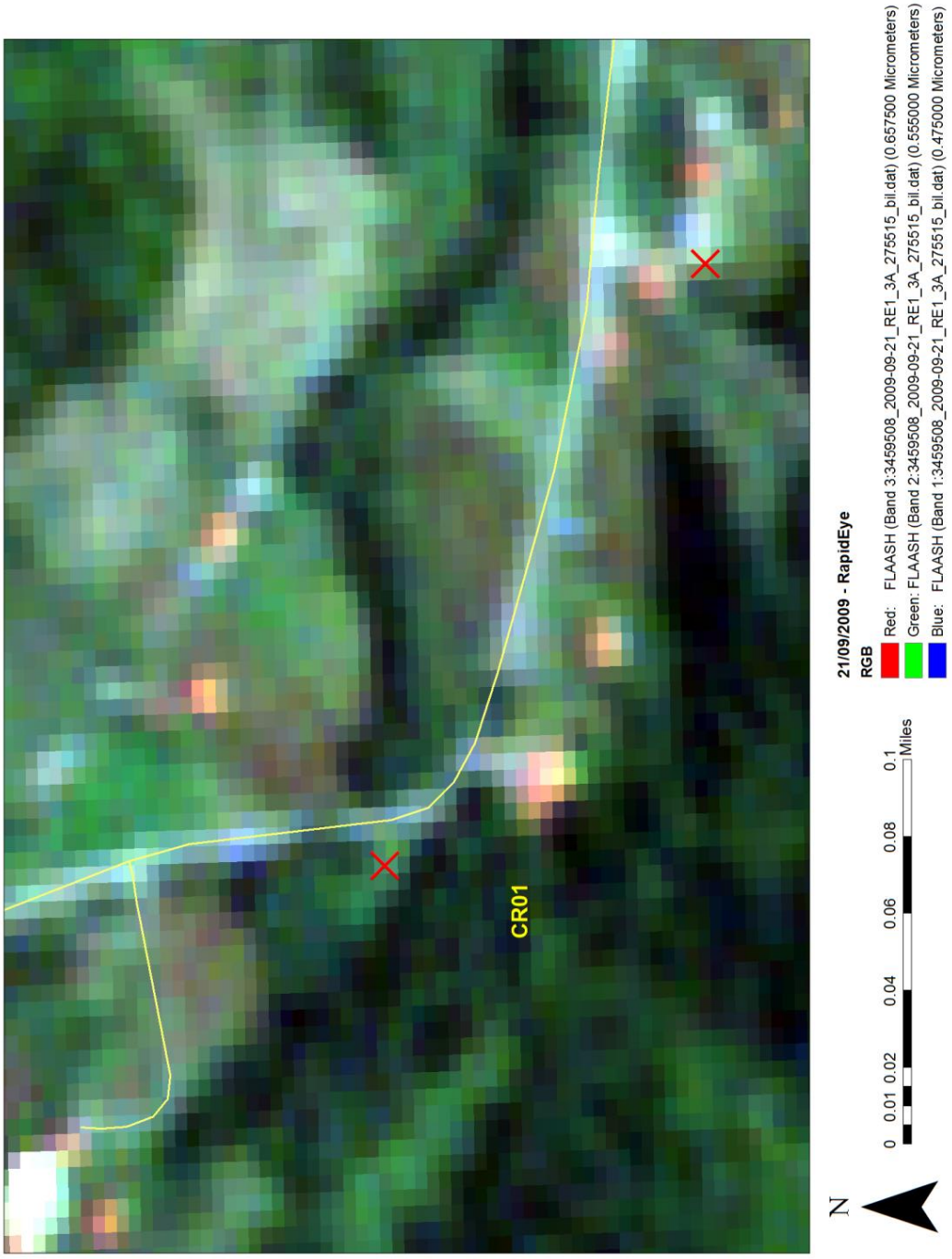

Figure 4-137 - RapidEye FLAASH image for 21/09/2009 showing CR01 - CR13 is also represented by a red X.

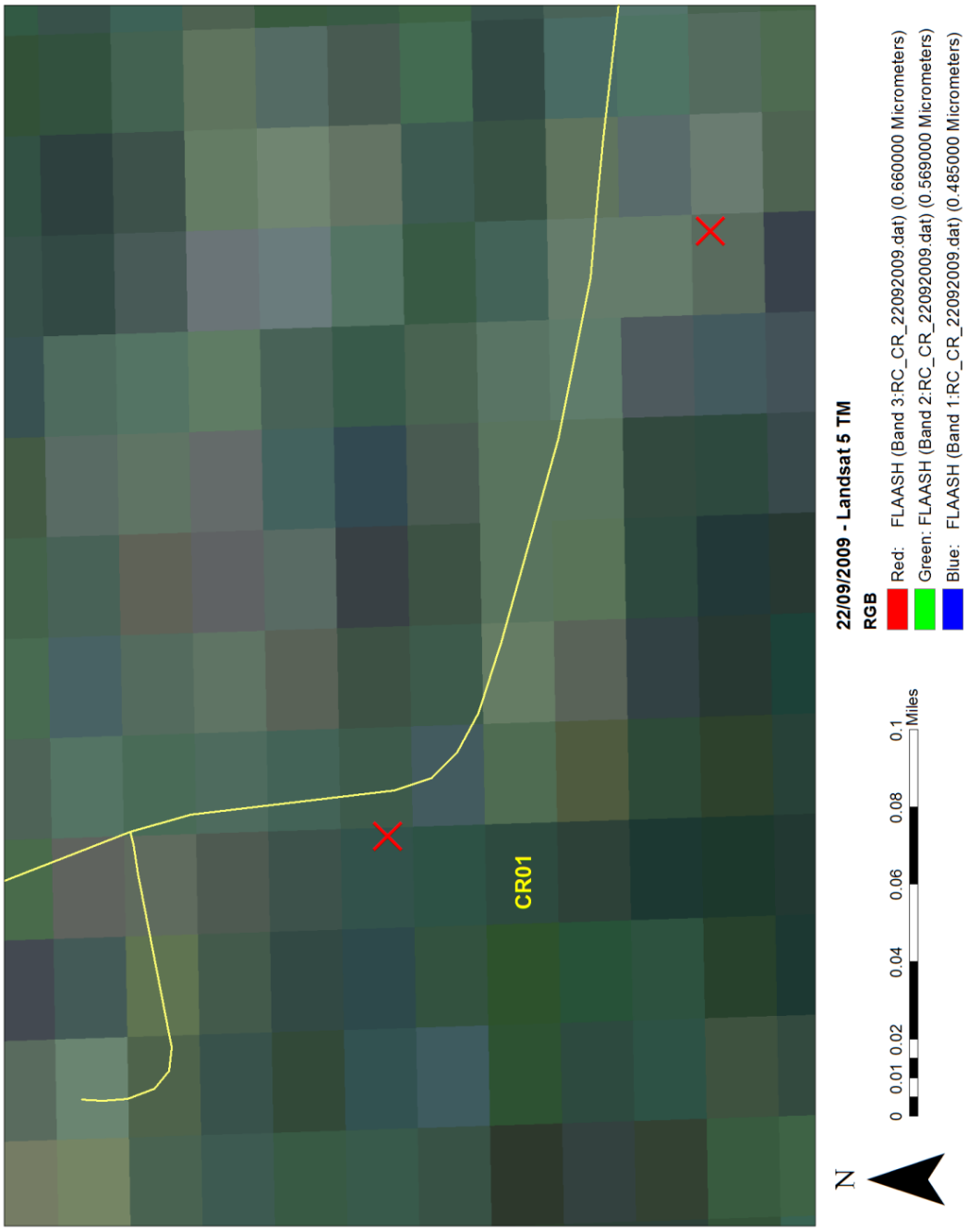

Figure 4-138 - Landsat 5 TM FLAASH image for 22/09/2009 showing CR01 - CR13 is also represented by a red X.

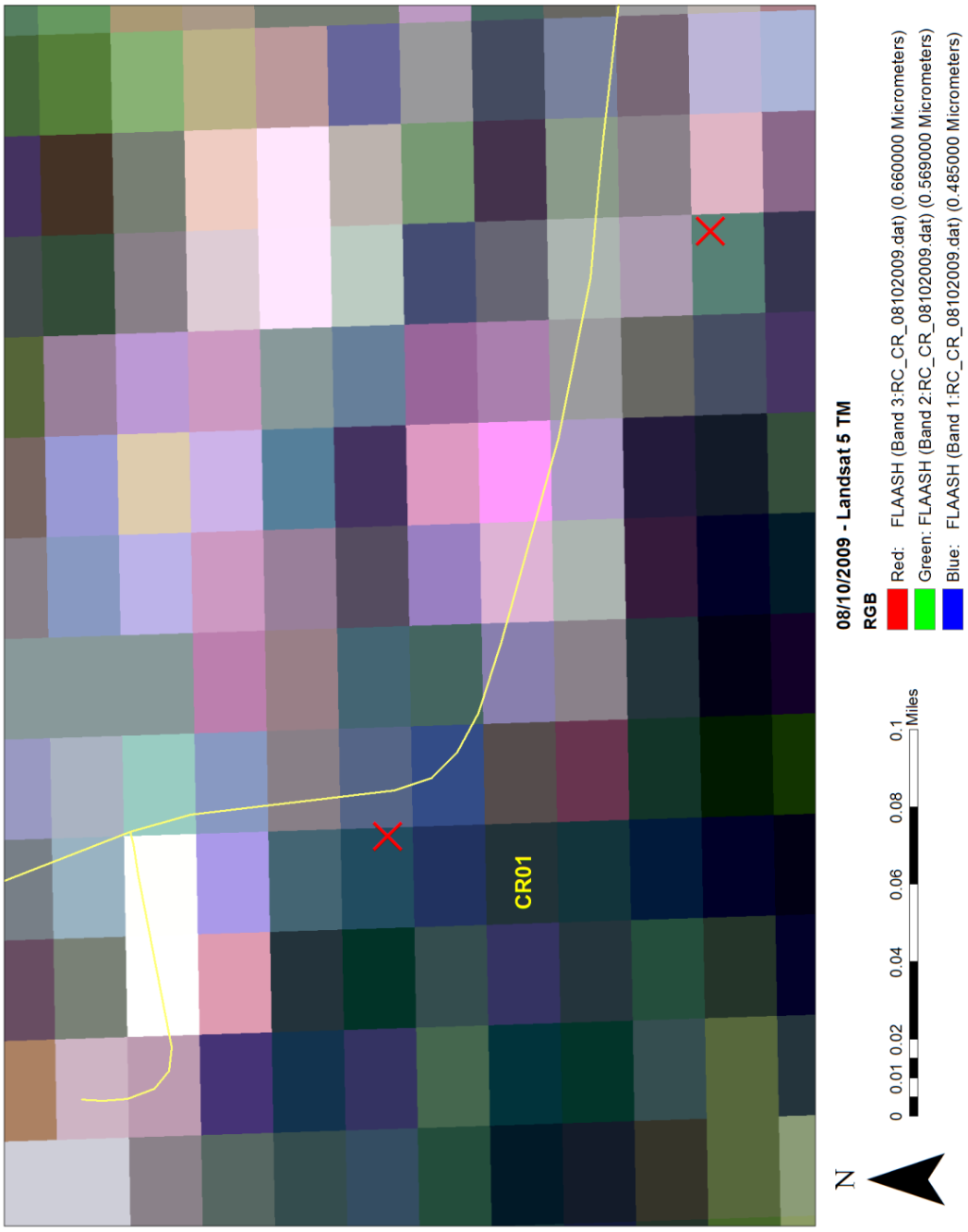

Figure 4-139 - Landsat 5 TM FLAASH image for 08/10/2009 showing CR01 - CR13 is also represented by a red X.

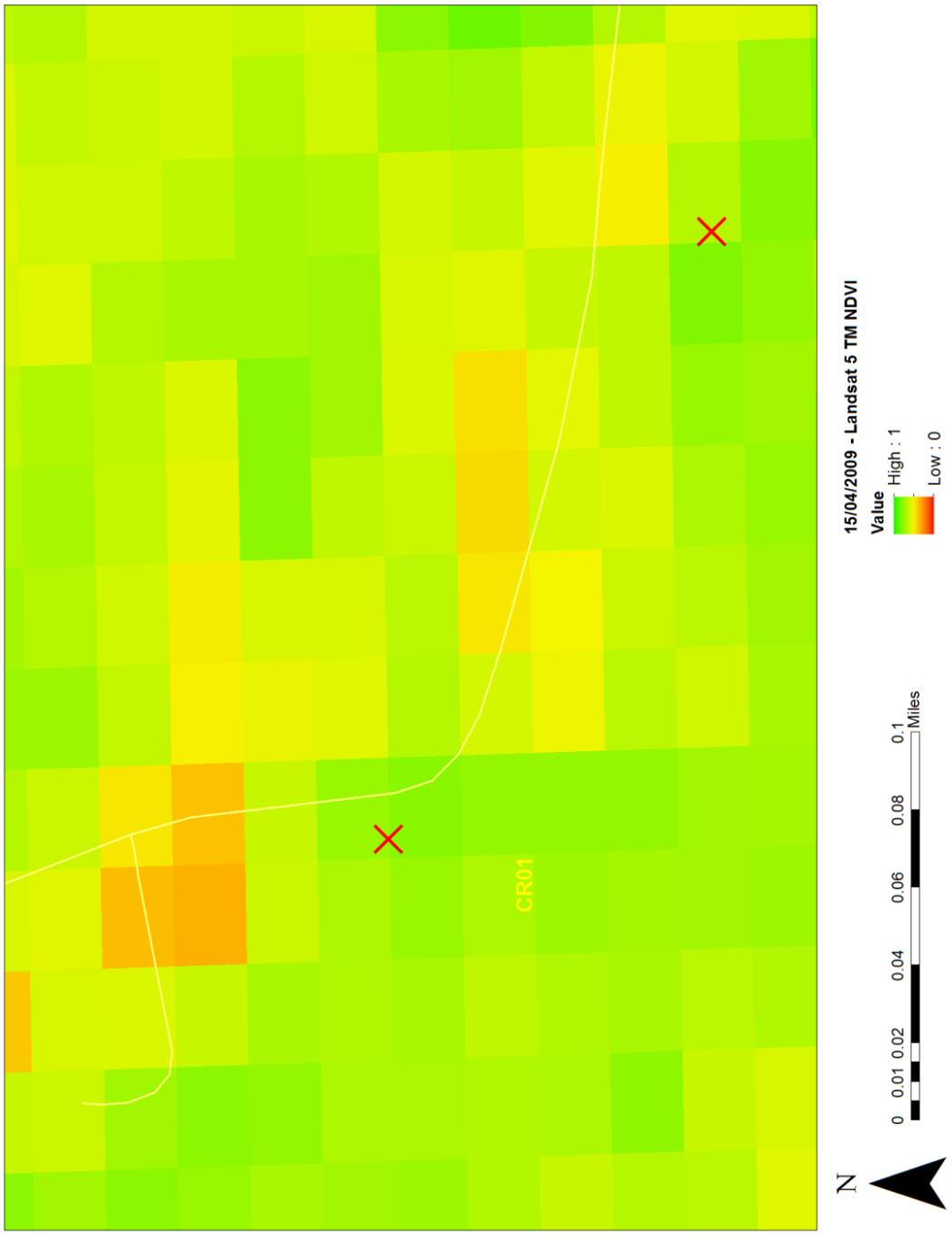

Figure 4-140 - Landsat 5 TM NDVI image for 15/04/2009 showing CR01 - CR13 is also represented by a red X.

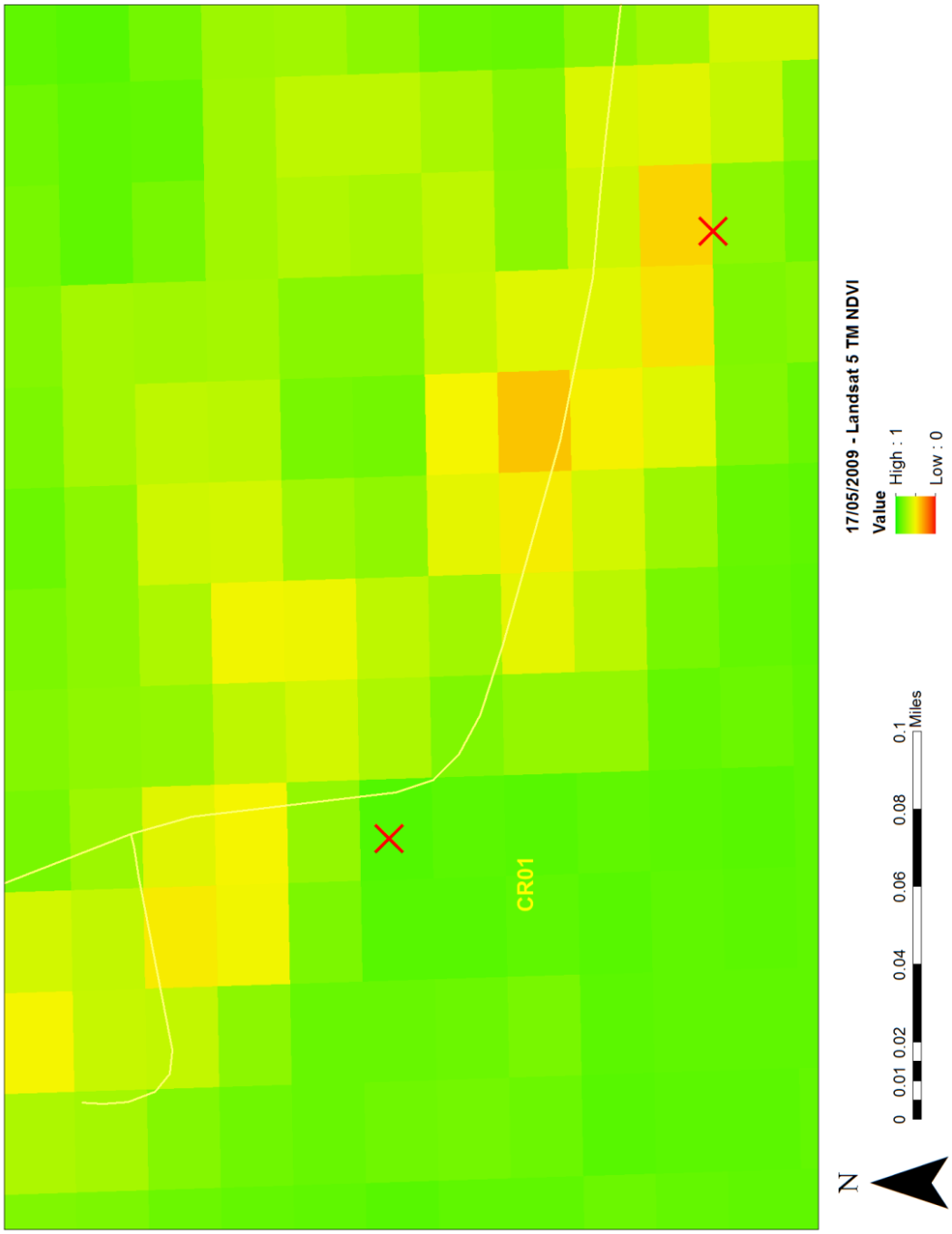

Figure 4-141 - Landsat 5 TM NDVI image for 17/05/2009 showing CR01 - CR13 is also represented by a red X.

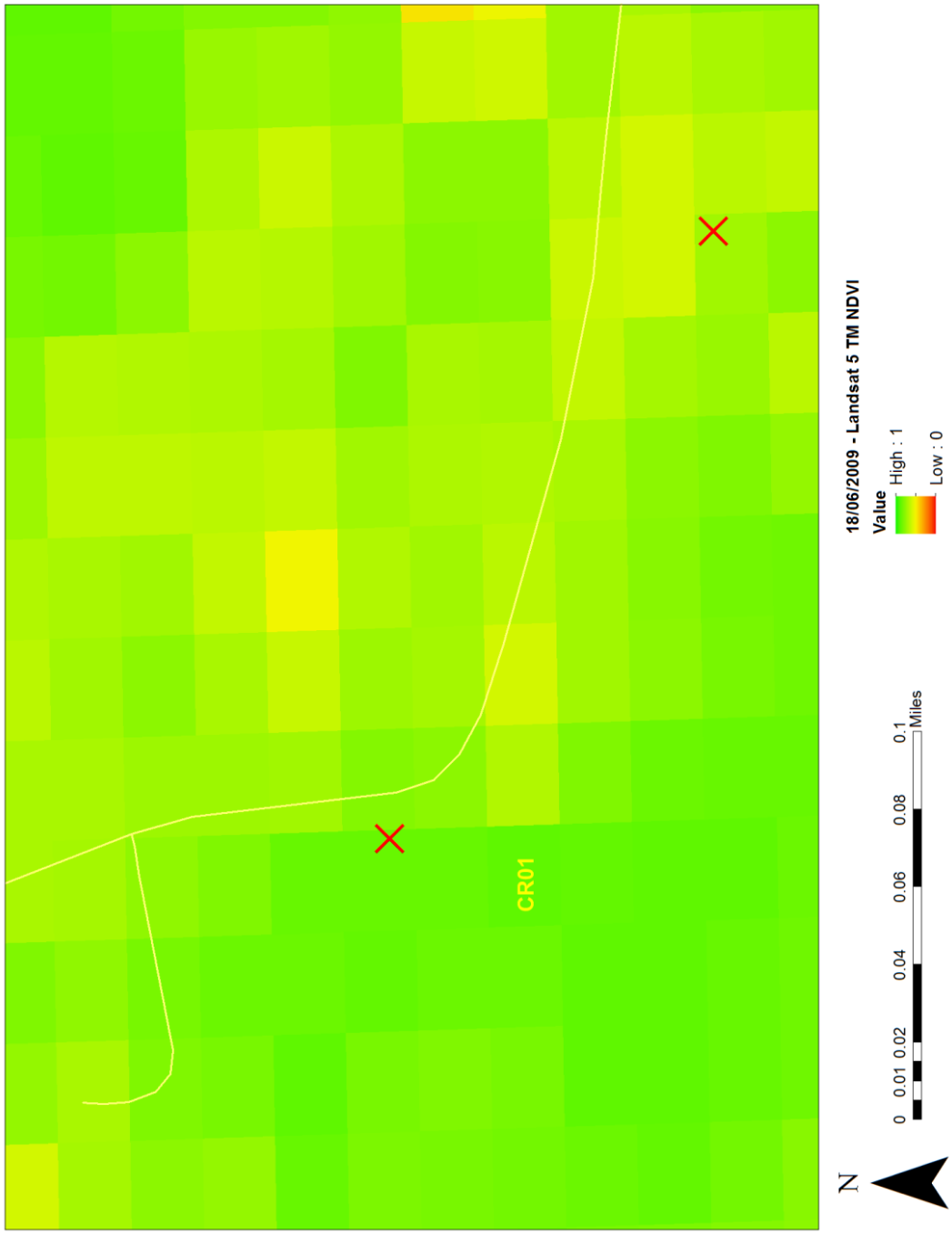

Figure 4-142 - Landsat 5 TM NDVI image for 18/06/2009 showing CR01 - CR13 is also represented by a red X.

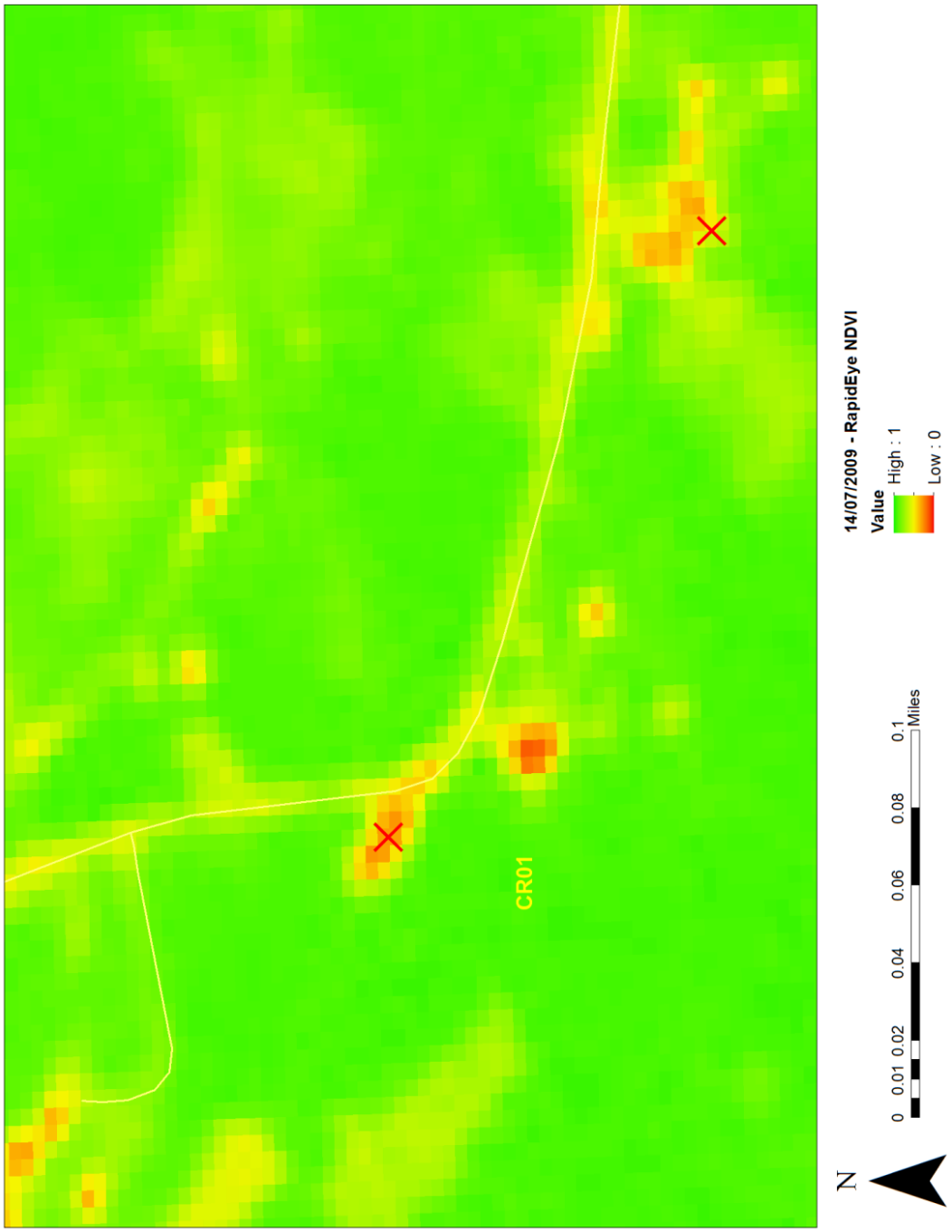

Figure 4-143 - RapidEye NDVI image for 14/07/2009 showing CR01 - CR13 is also represented by a red X.

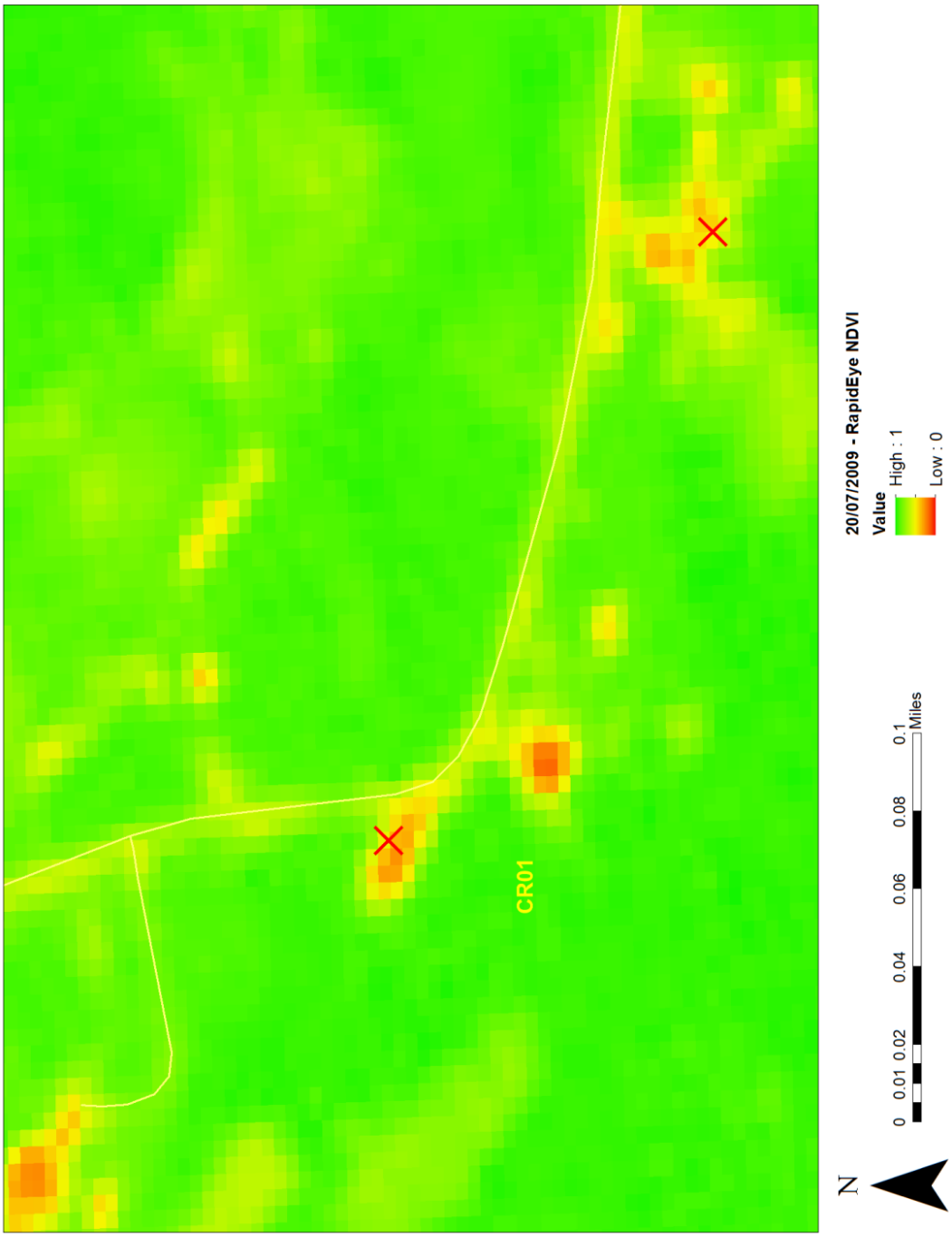

Figure 4-144 - RapidEye NDVI image for 20/07/2009 showing CR01 - CR13 is also represented by a red X.

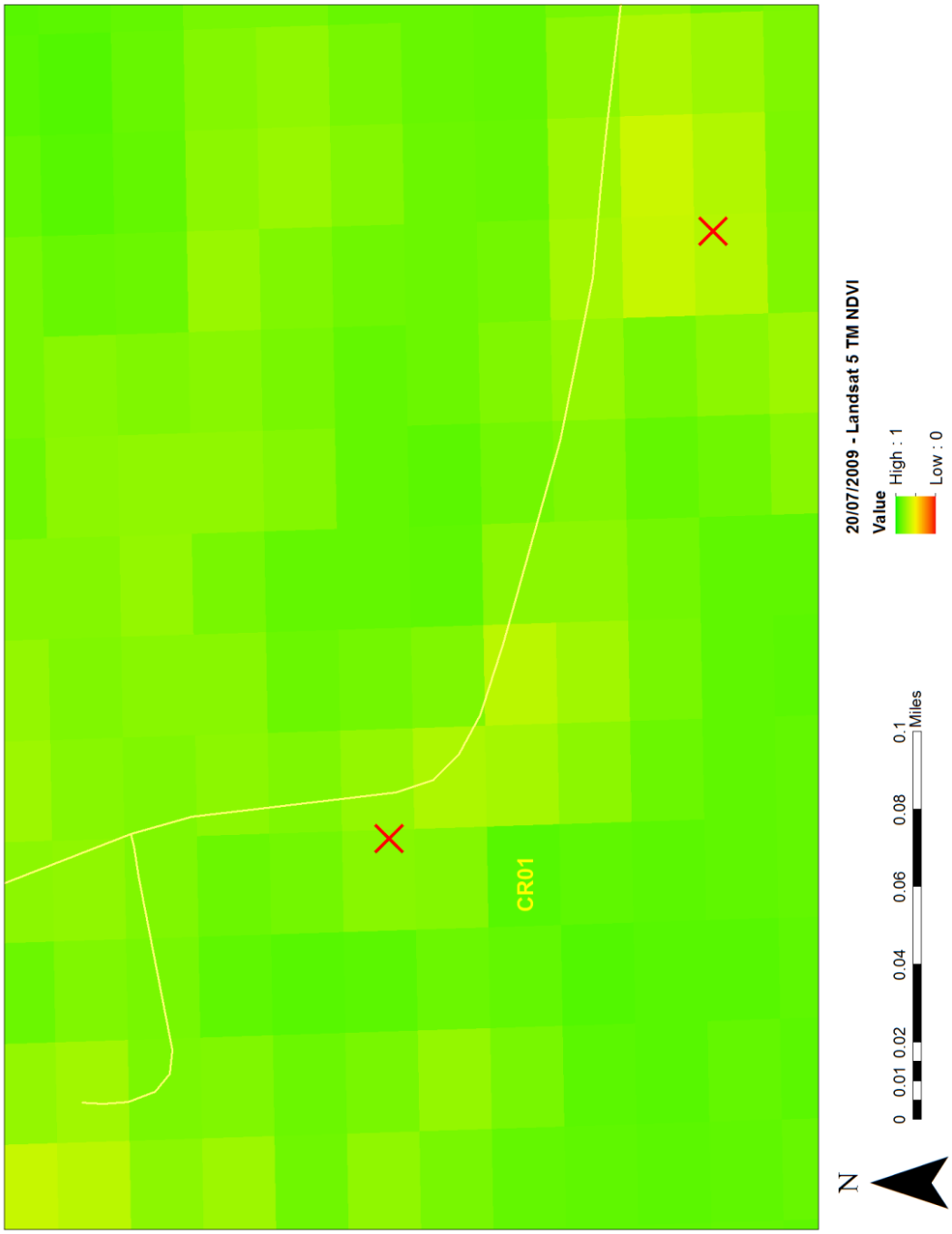

Figure 4-145 - Landsat 5 TM NDVI image for 20/07/2009 showing CR01 - CR13 is also represented by a red X.

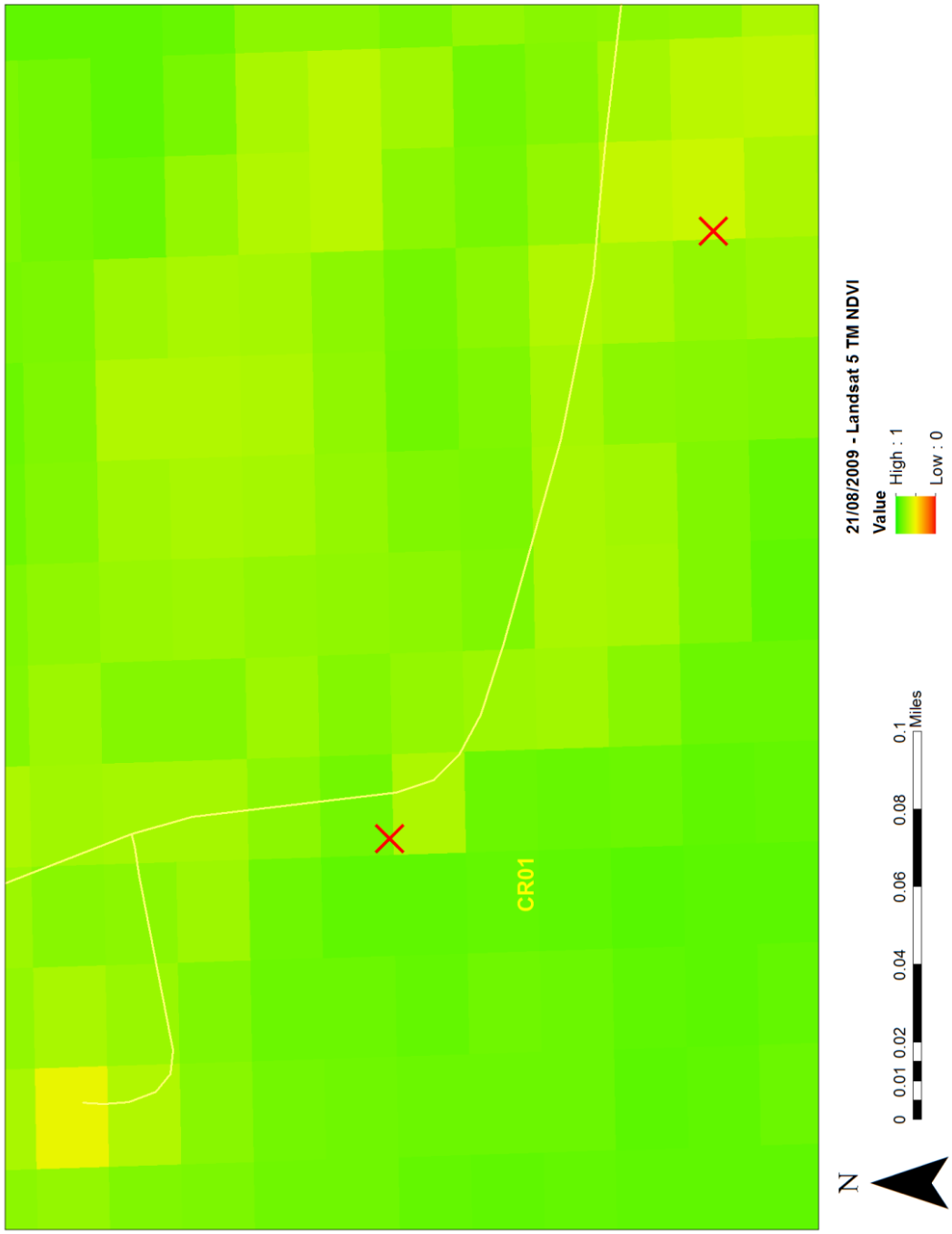

Figure 4-146 - Landsat 5 TM NDVI image for 21/08/2009 showing CR01 - CR13 is also represented by a red X.

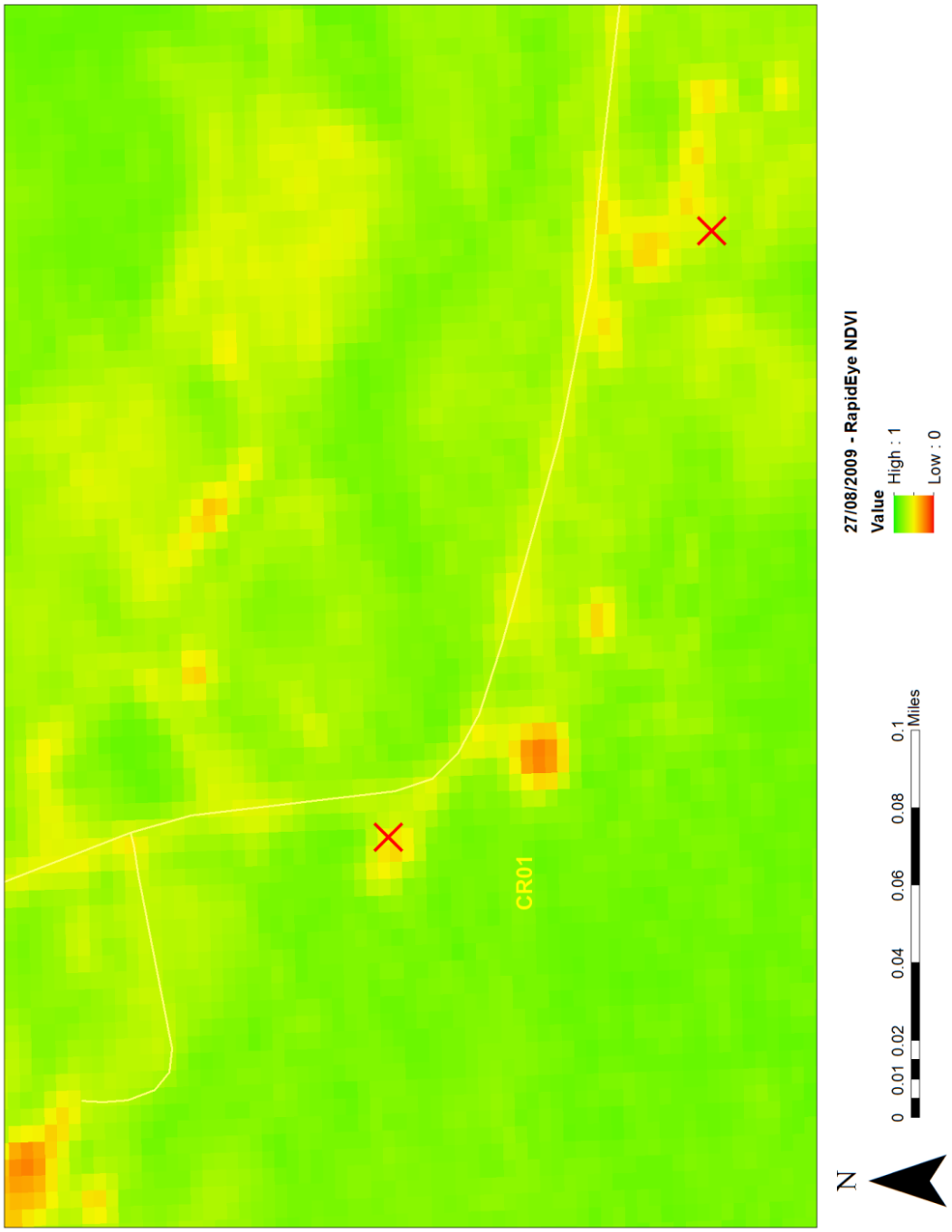

Figure 4-147 - RapidEye NDVI image for 27/08/2009 showing CR01 - CR13 is also represented by a red X.

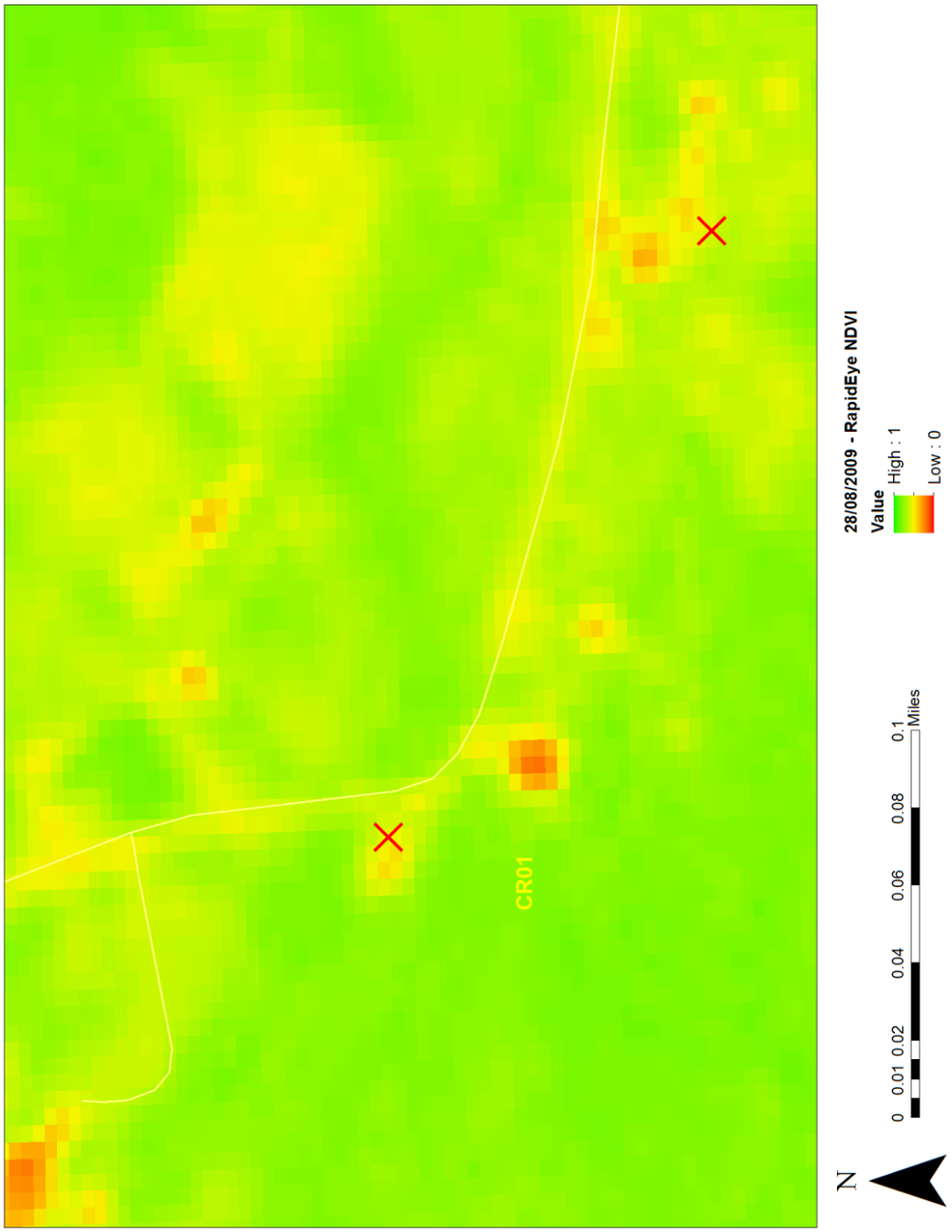

Figure 4-148 - RapidEye NDVI image for 28/08/2009 showing CR01 - CR13 is also represented by a red X.

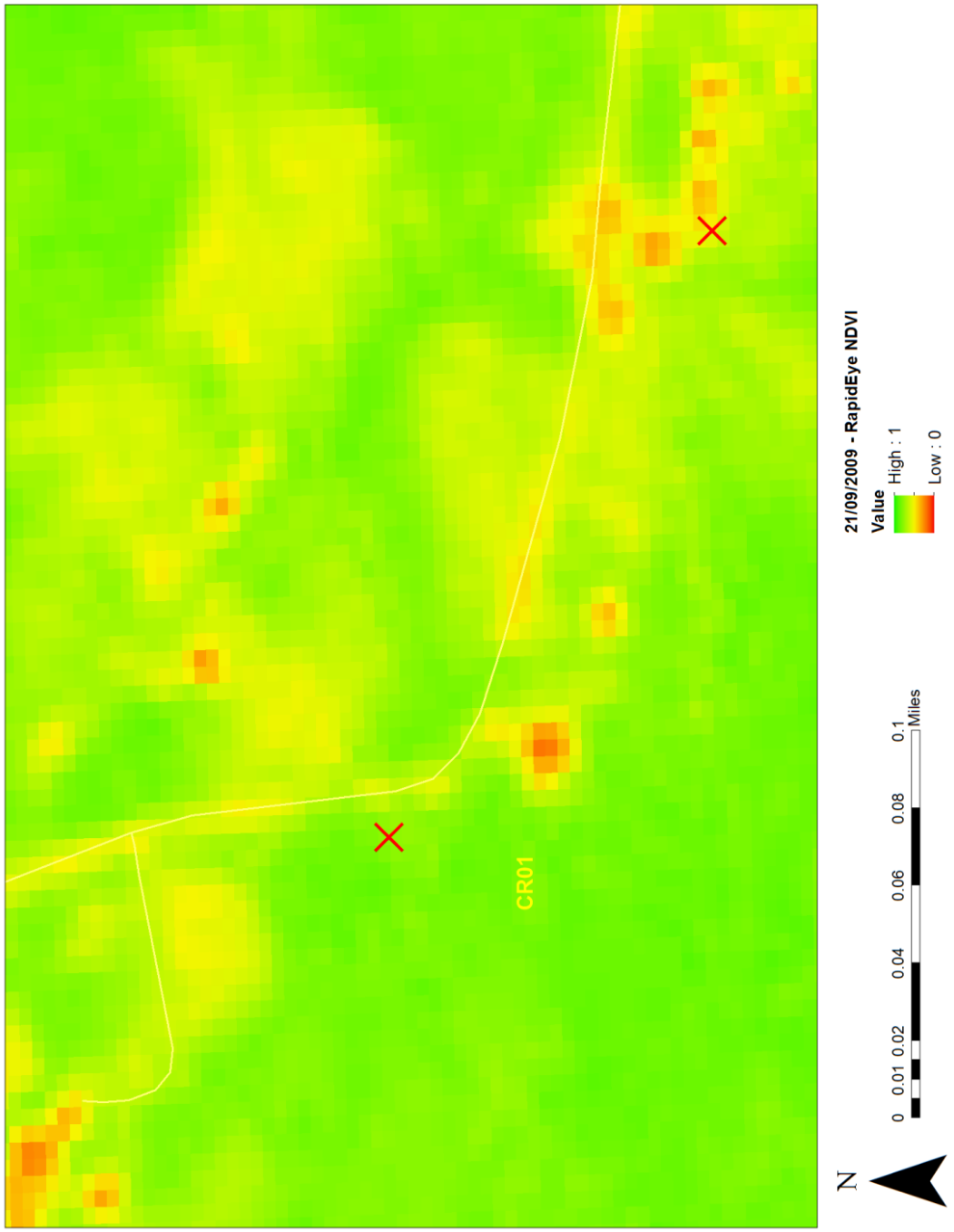

Figure 4-149 - RapidEye NDVI image for 21/09/2009 showing CR01 - CR13 is also represented by a red X.

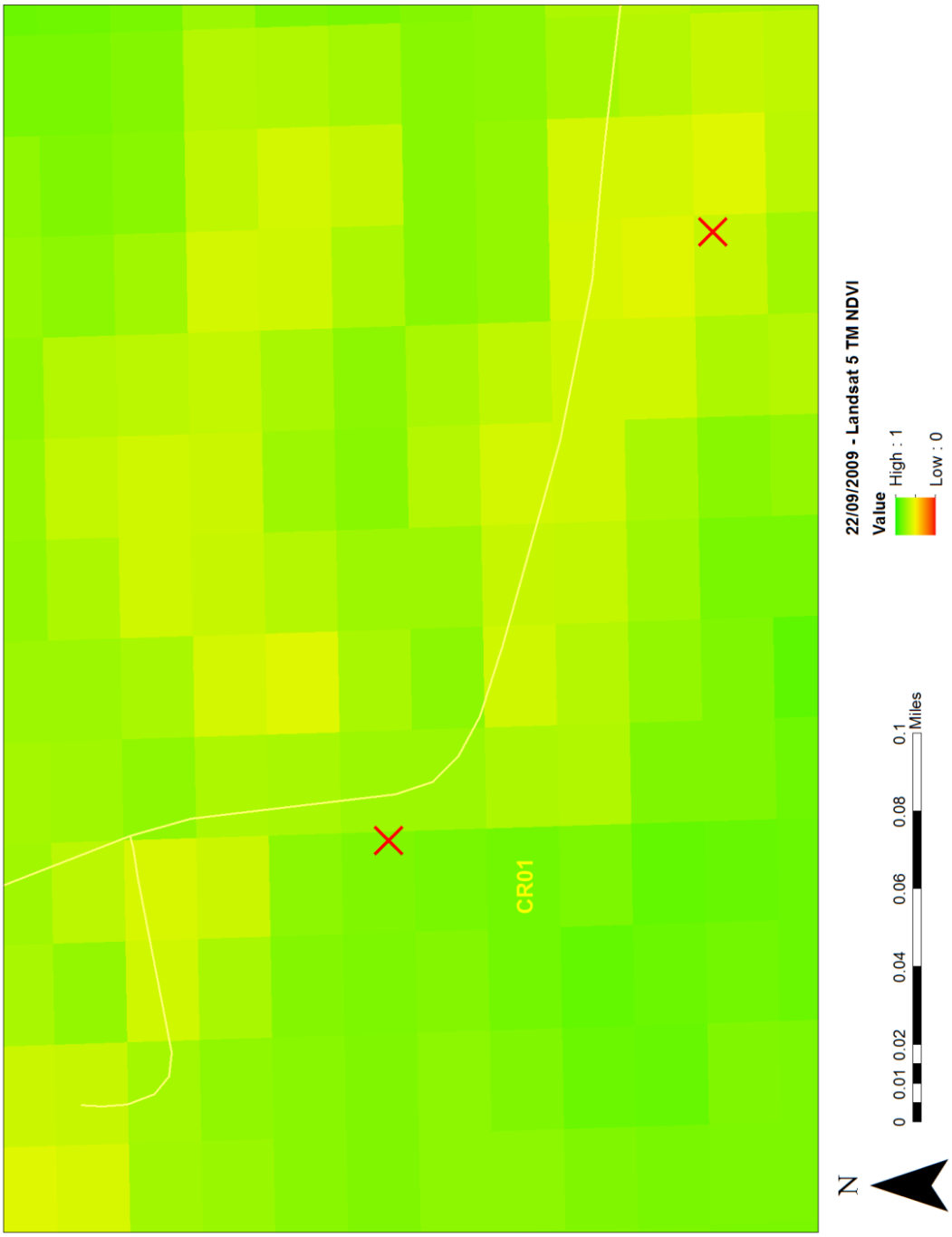

Figure 4-150 - Landsat 5 TM NDVI image for 22/09/2009 showing CR01 - CR13 is also represented by a red X.

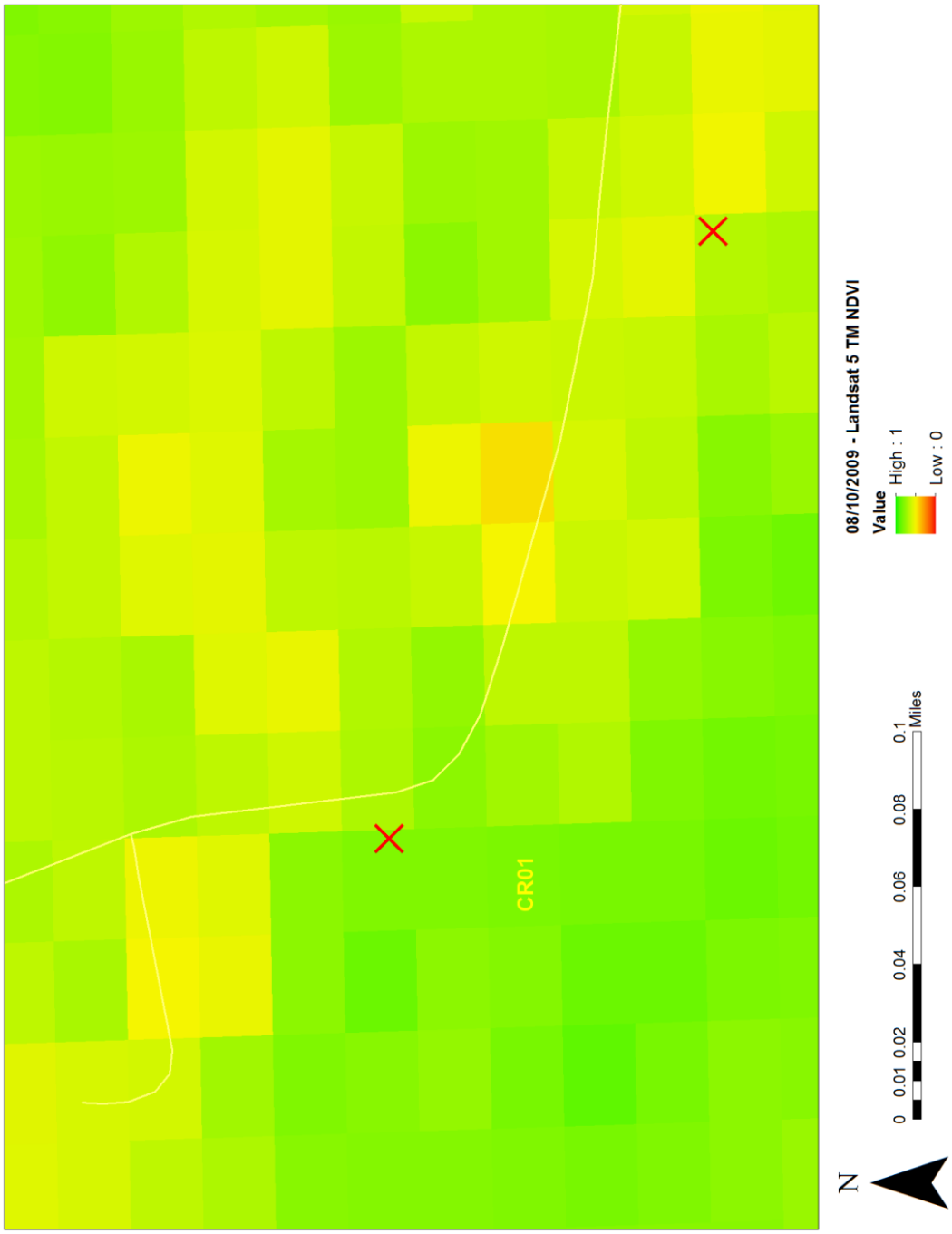

Figure 4-151 - Landsat 5 TM NDVI image for 08/10/2009 showing CR01 - CR13 is also represented by a red X.

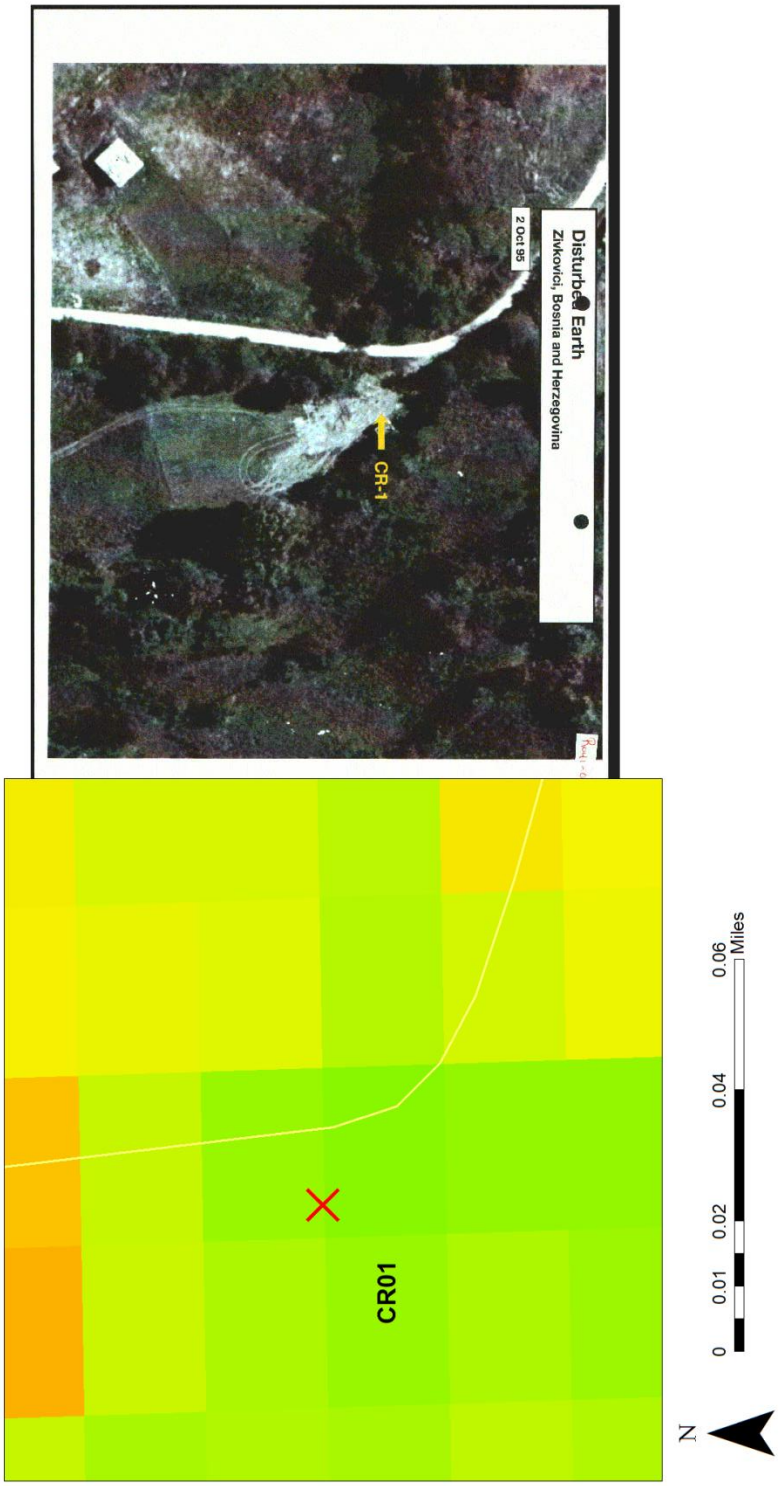

Figure 4-152 - Landsat 5 TM NDVI image (left) for 15/04/2009 showing CR01 compared with the aerial image (right) showing disturbed earth from 2 October 1995 (ICTY 2011c).

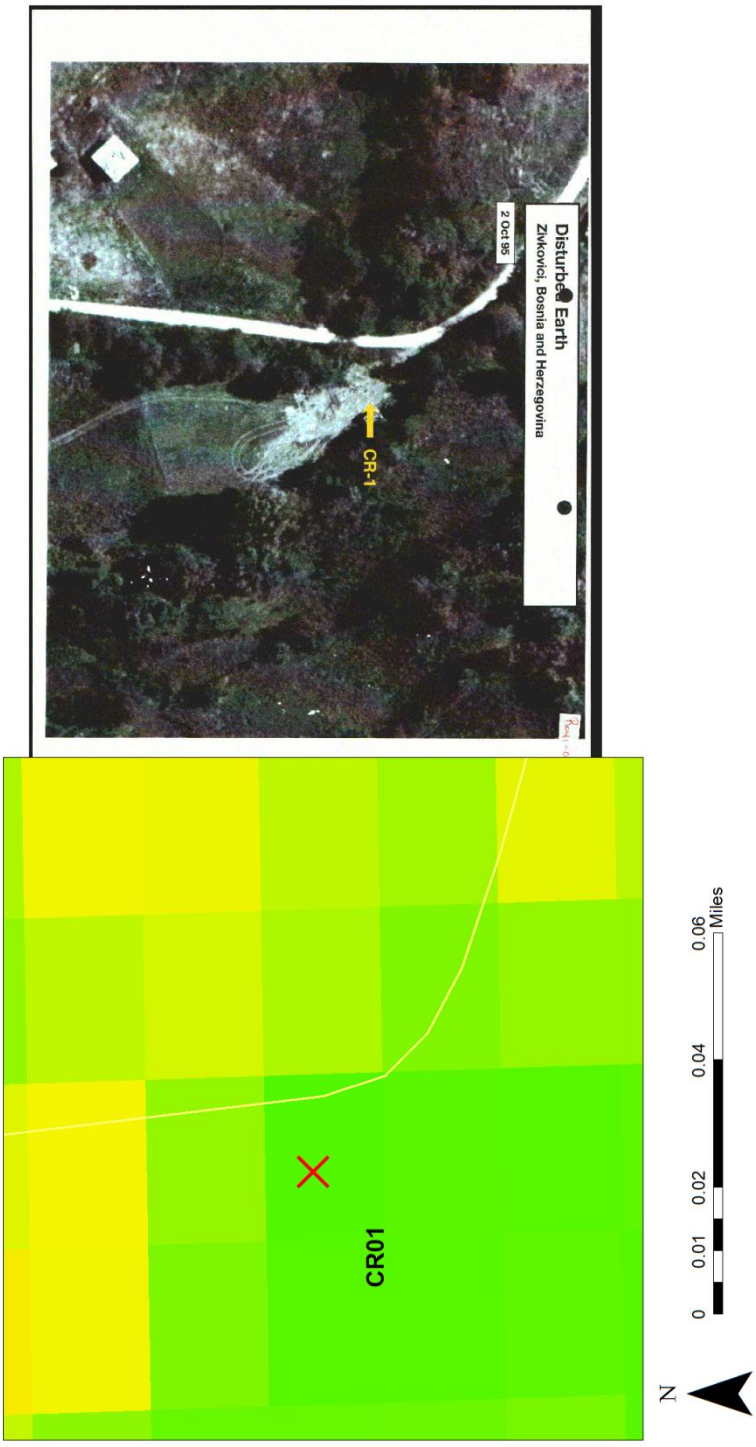

Figure 4-153 - Landsat 5 TM NDVI image (left) for 17/05/2009 showing CR01 compared with the aerial image (right) showing disturbed earth from 2 October 1995 (ICTY 2011c).

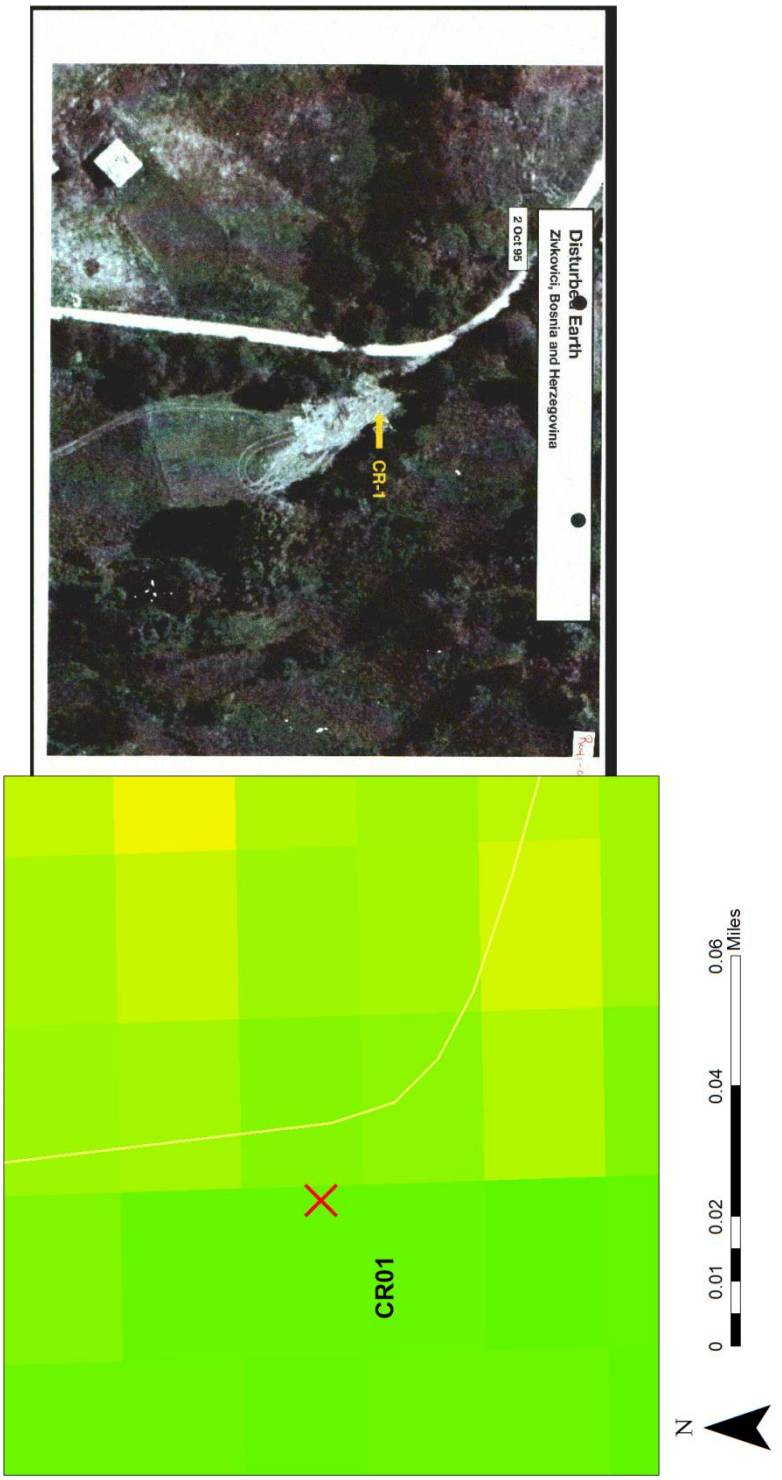

Figure 4-154 - Landsat 5 TM NDVI image (left) for 18/06/2009 showing CR01 compared with the aerial image (right) showing disturbed earth from 2 October 1995 (ICTY 2011c).

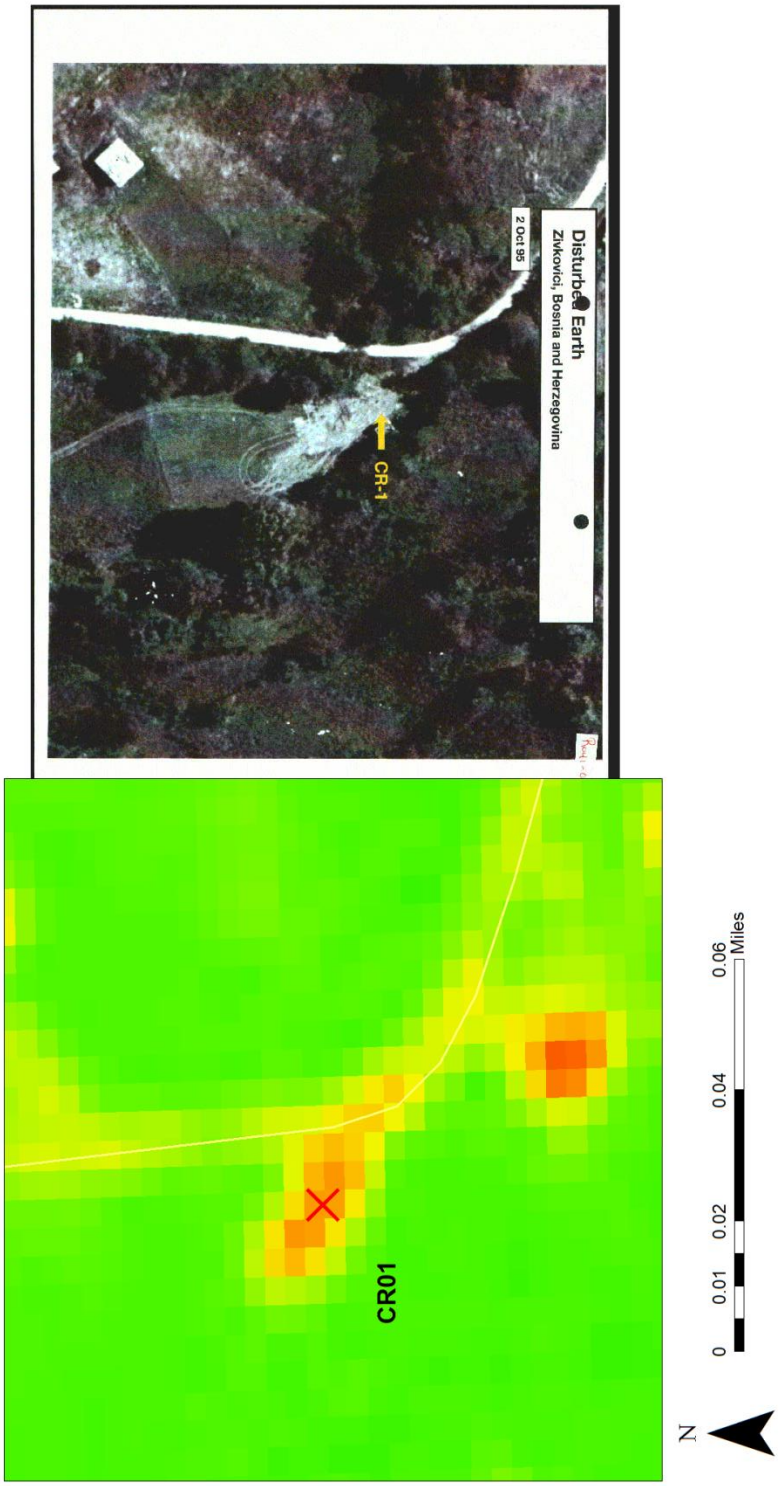

Figure 4-155 - RapidEye NDVI image (left) for 14/07/2009 showing CR01 compared with the aerial image (right) showing disturbed earth from 2 October 1995 (ICTY 2011c).

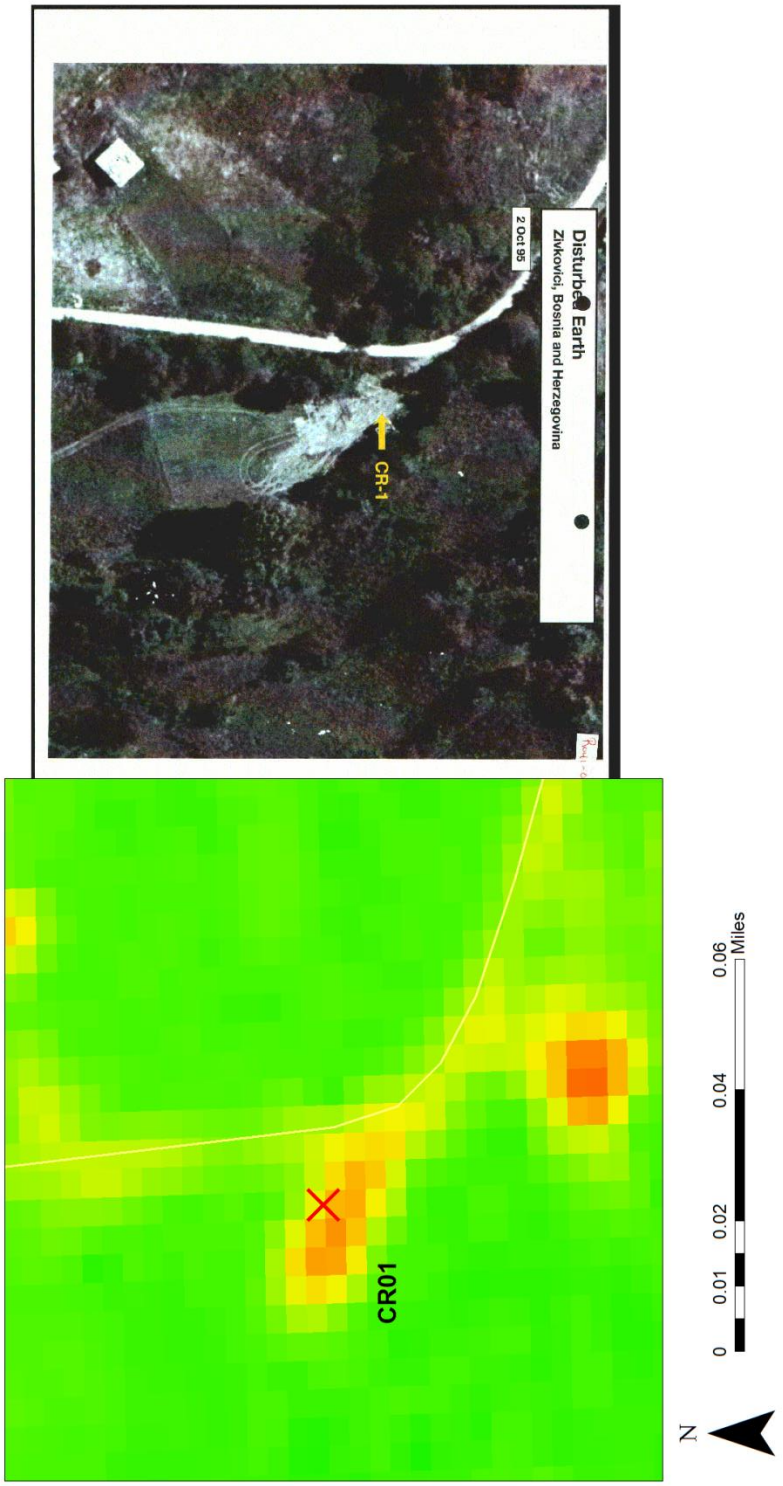

Figure 4-156 - RapidEye NDVI image (left) for 20/07/2009 showing CR01 compared with the aerial image (right) showing disturbed earth from 2 October 1995 (ICTY 2011c).

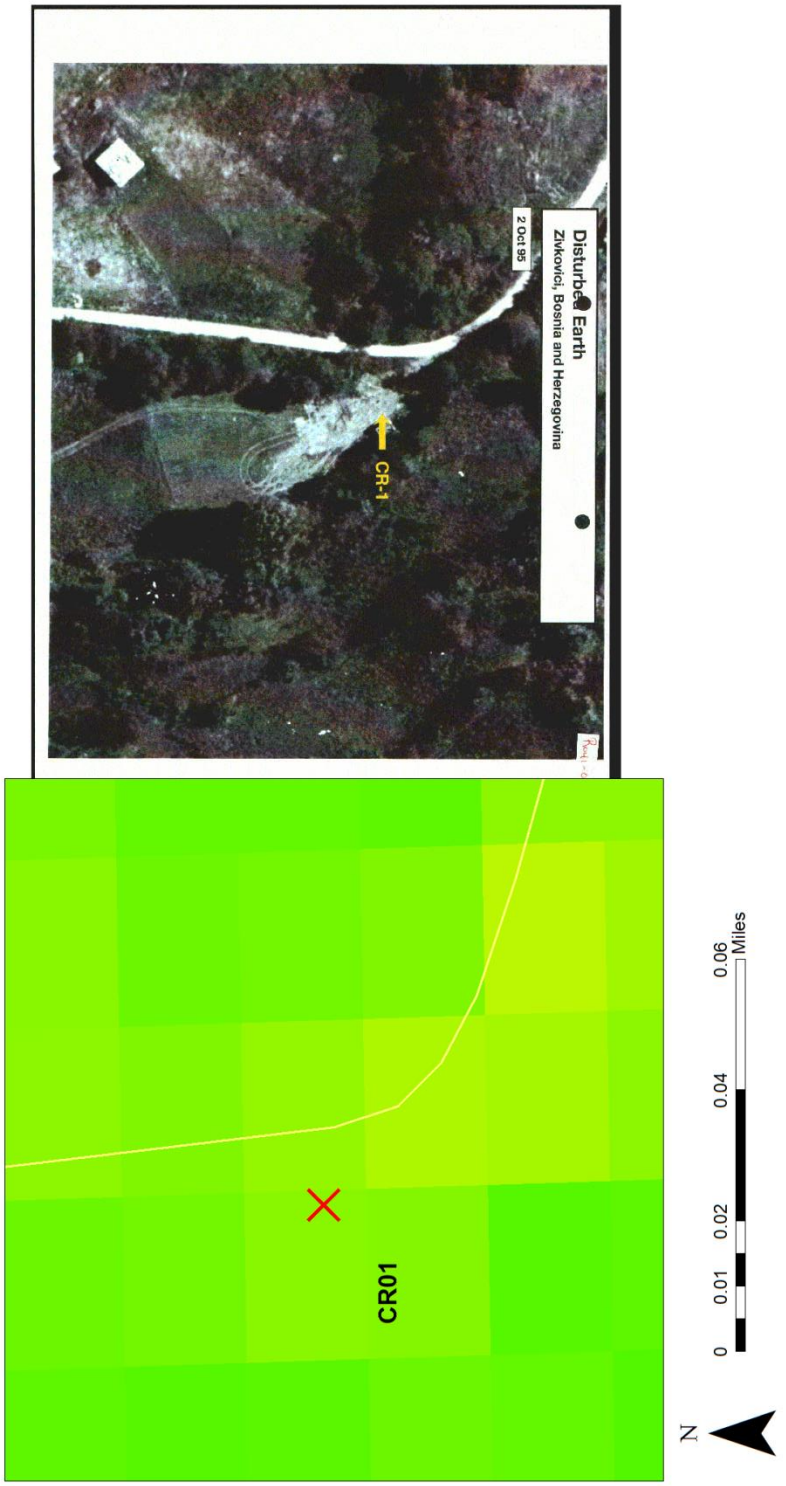

Figure 4-157 - Landsat 5 TM NDVI image (left) for 20/07/2009 showing CR01 compared with the aerial image (right) showing disturbed earth from 2 October 1995 (ICTY 2011c).

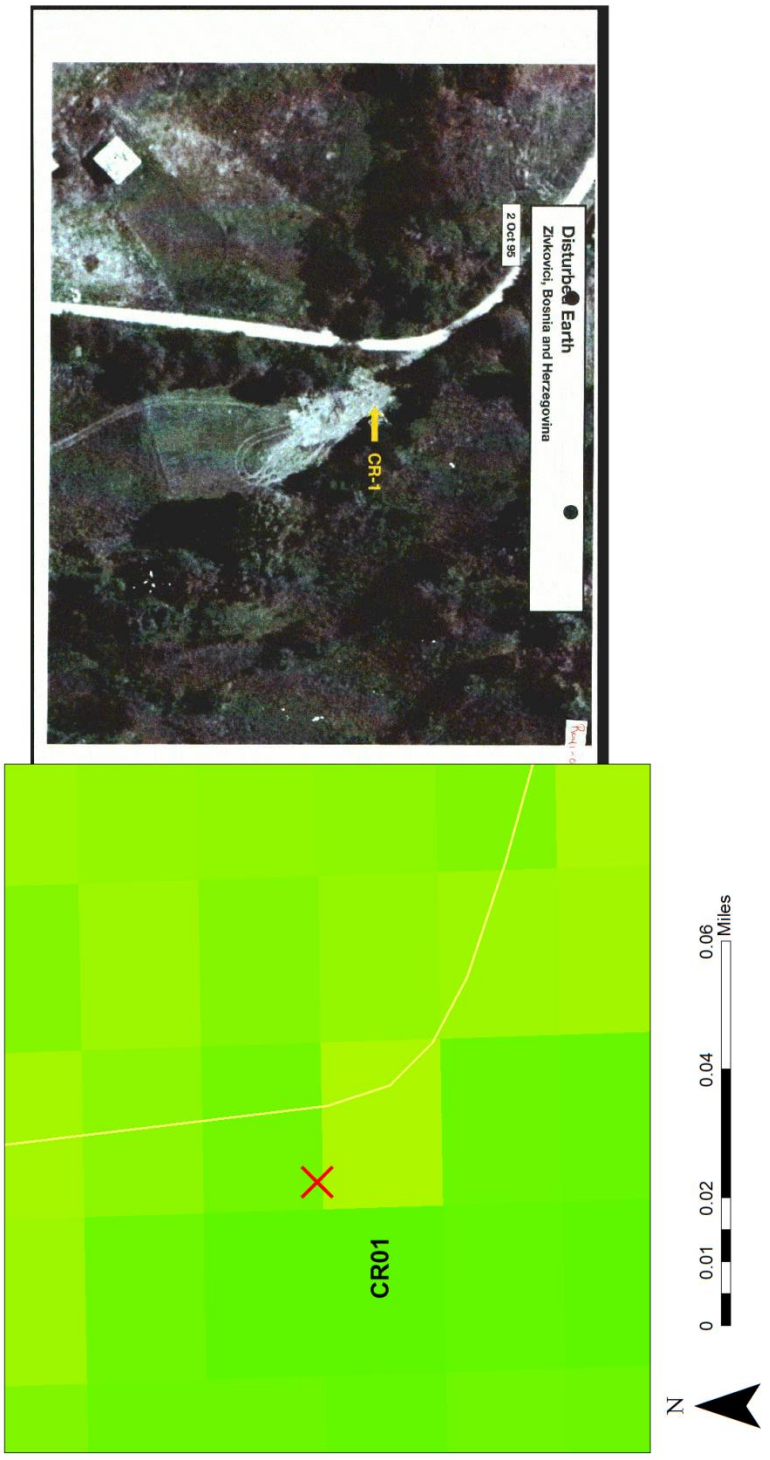

Figure 4-158 - Landsat 5 TM NDVI image (left) for 21/08/2009 showing CR01 compared with the aerial image (right) showing disturbed earth from 2 October 1995 (ICTY 2011c).

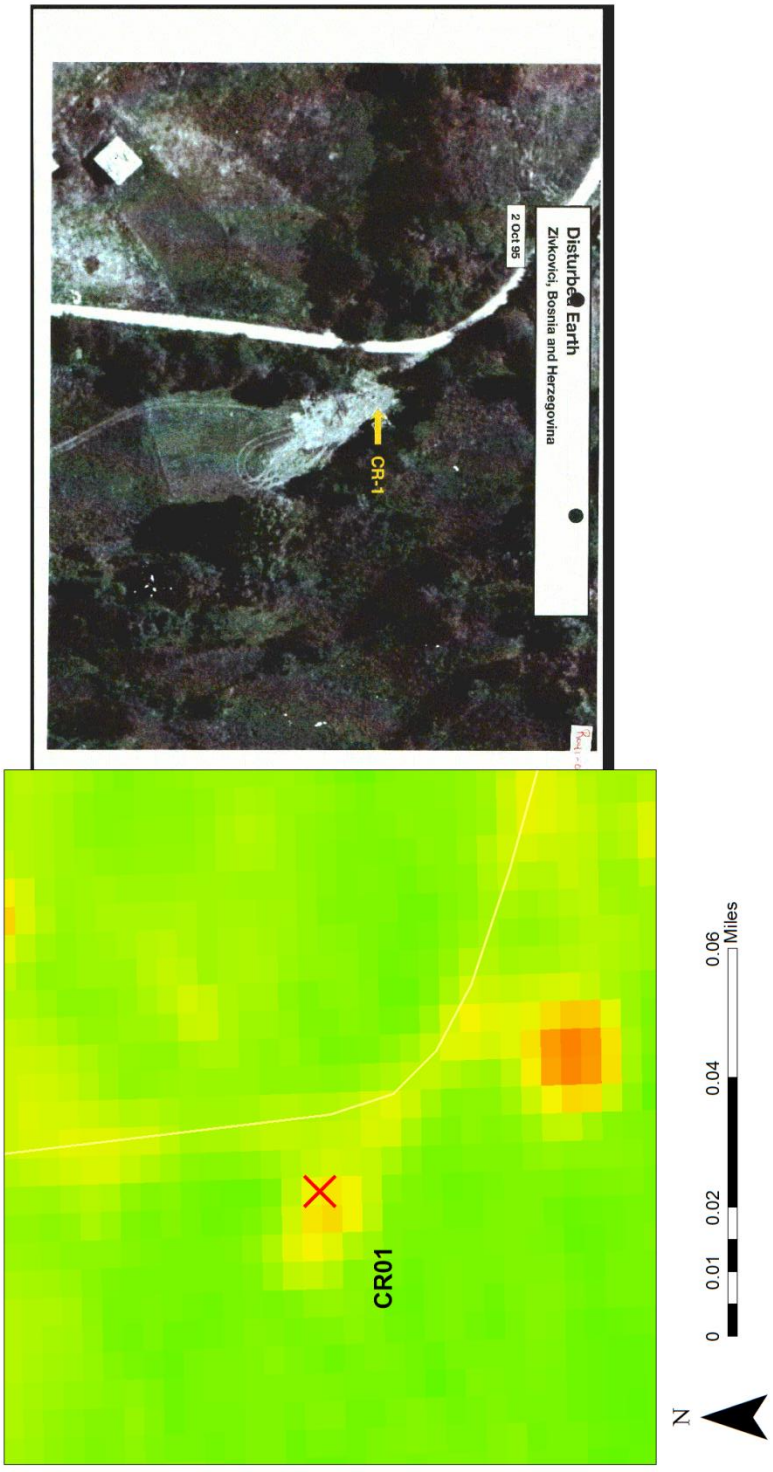

Figure 4-159 - RapidEye NDVI image (left) for 27/08/2009 showing CR01 compared with the aerial image (right) showing disturbed earth from 2 October 1995 (ICTY 2011c).

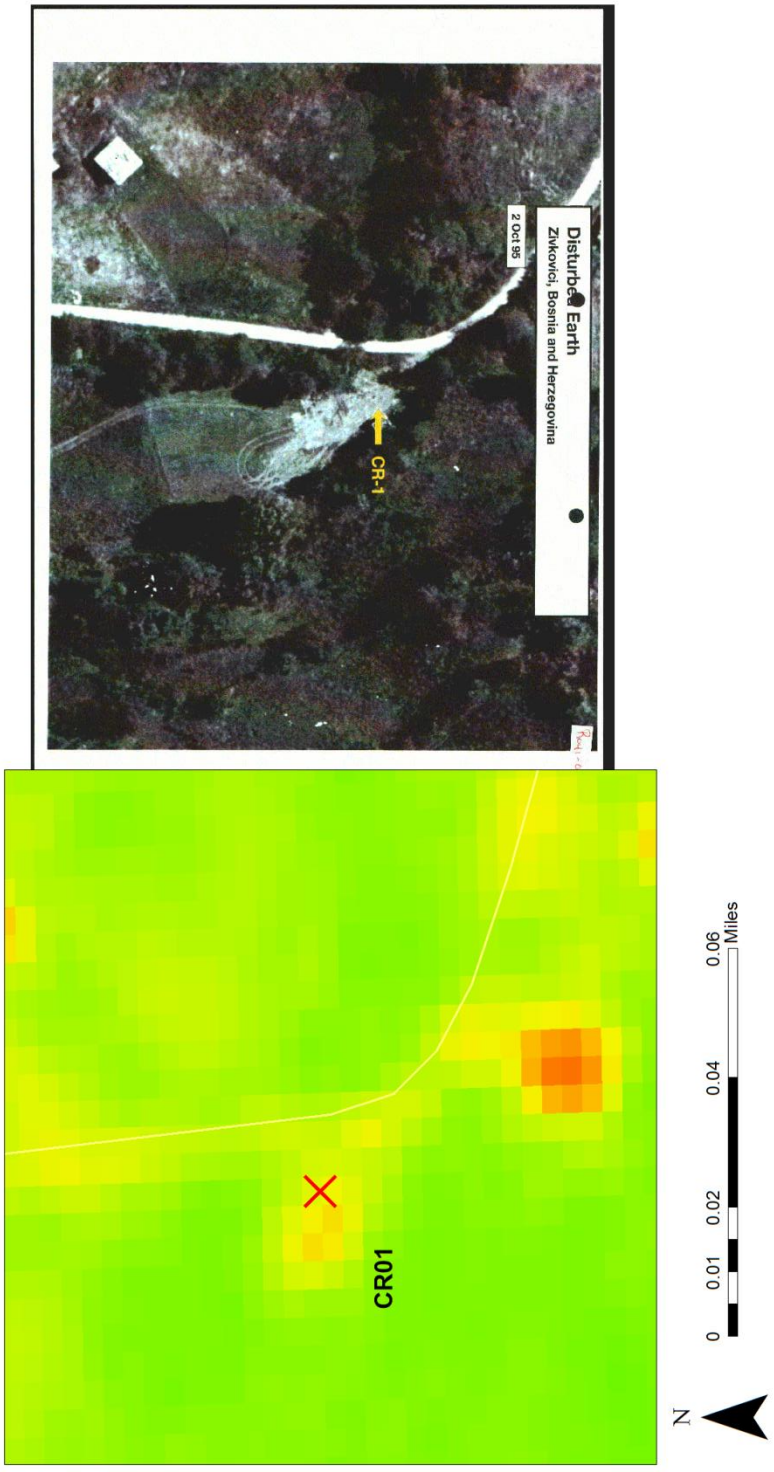

Figure 4-160 - RapidEye NDVI image (left) for 28/08/2009 showing CR01 compared with the aerial image (right) showing disturbed earth from 2 October 1995 (ICTY 2011c).

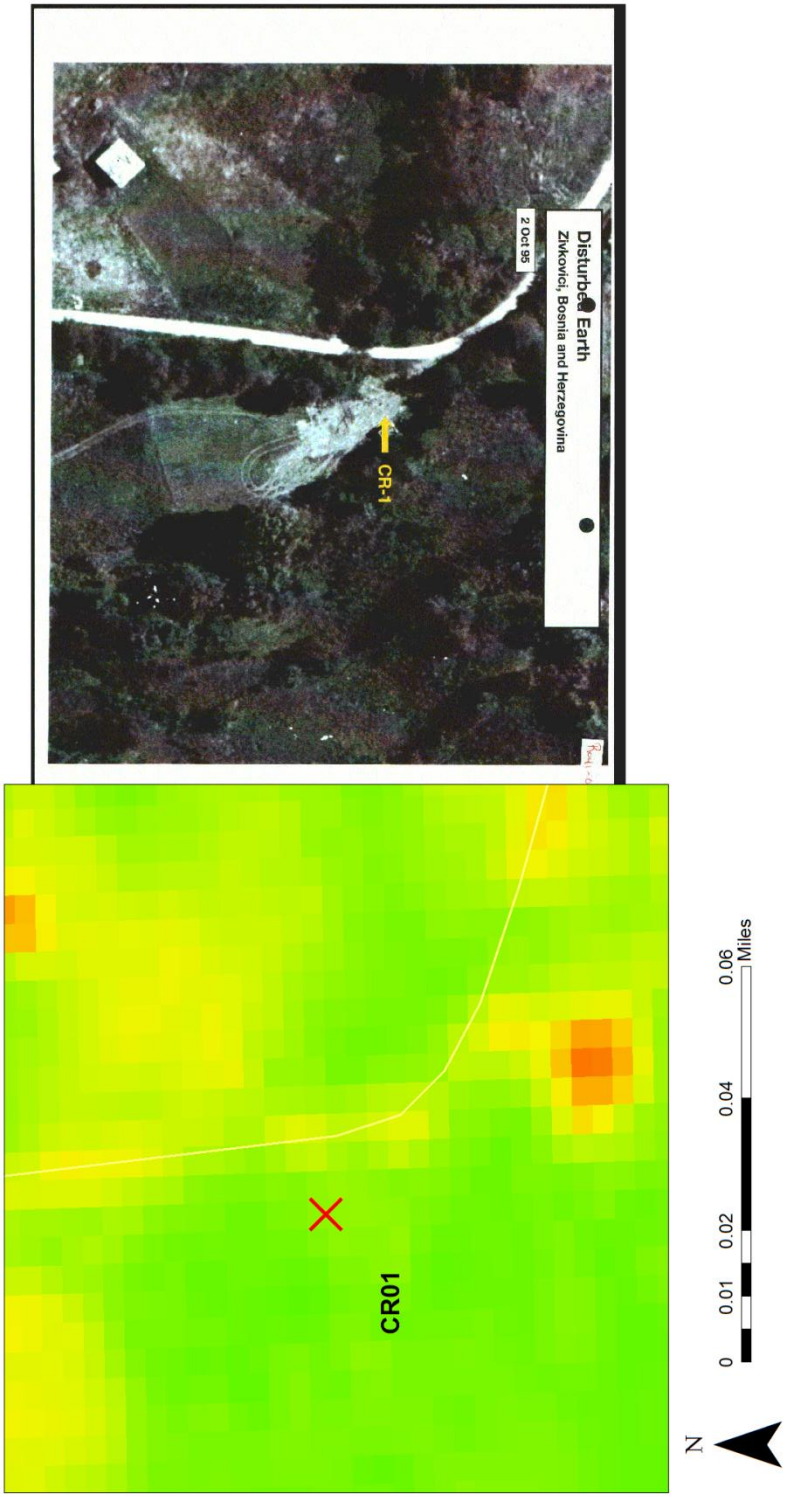

Figure 4-161 - RapidEye NDVI image (left) for 21/09/2009 showing CR01 compared with the aerial image (right) showing disturbed earth from 2 October 1995 (ICTY 2011c).

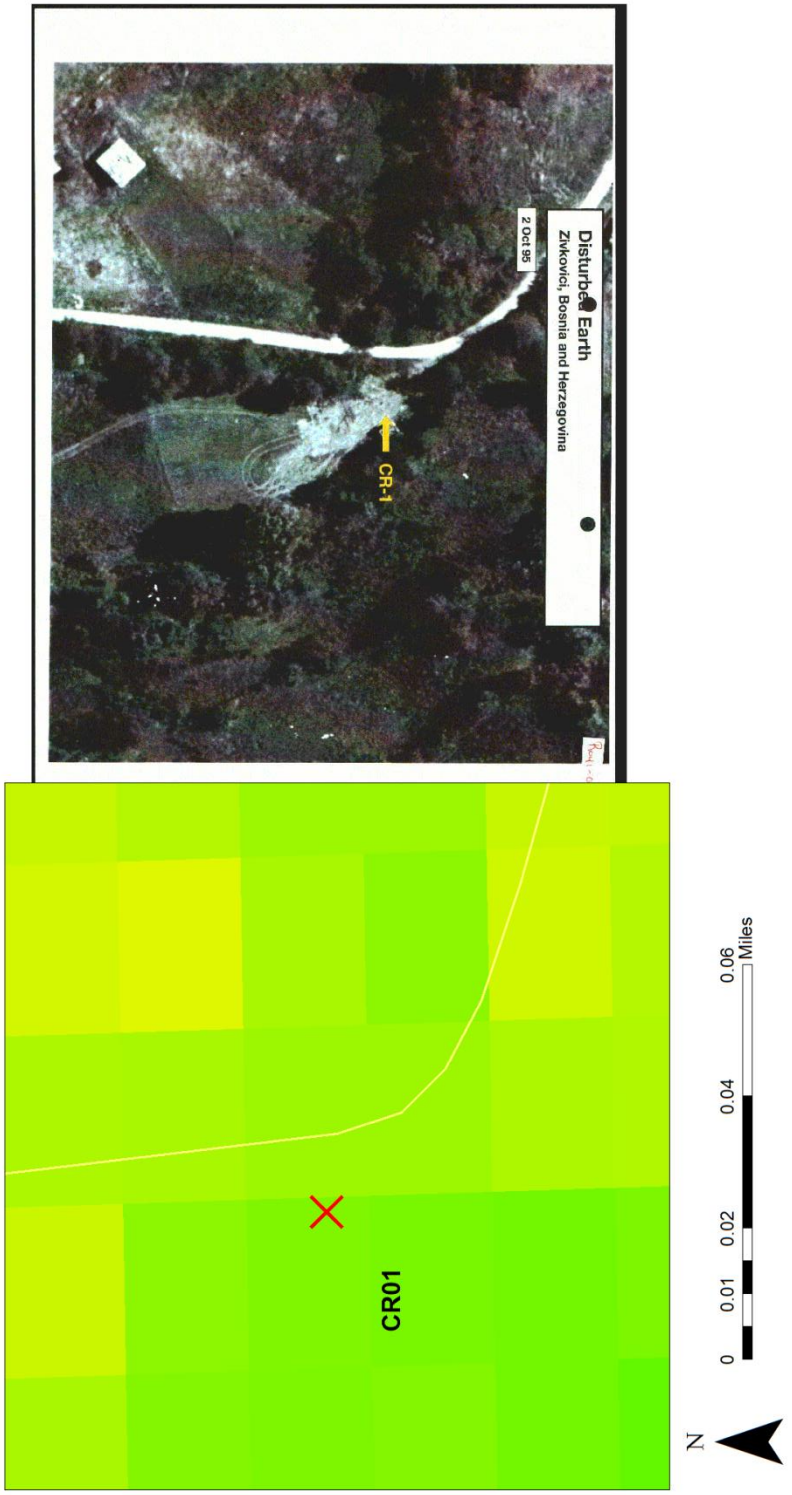

Figure 4-162 - Landsat 5 TM NDVI image (left) for 22/09/2009 showing CR01 compared with the aerial image (right) showing disturbed earth from 2 October 1995 (ICTY 2011c).

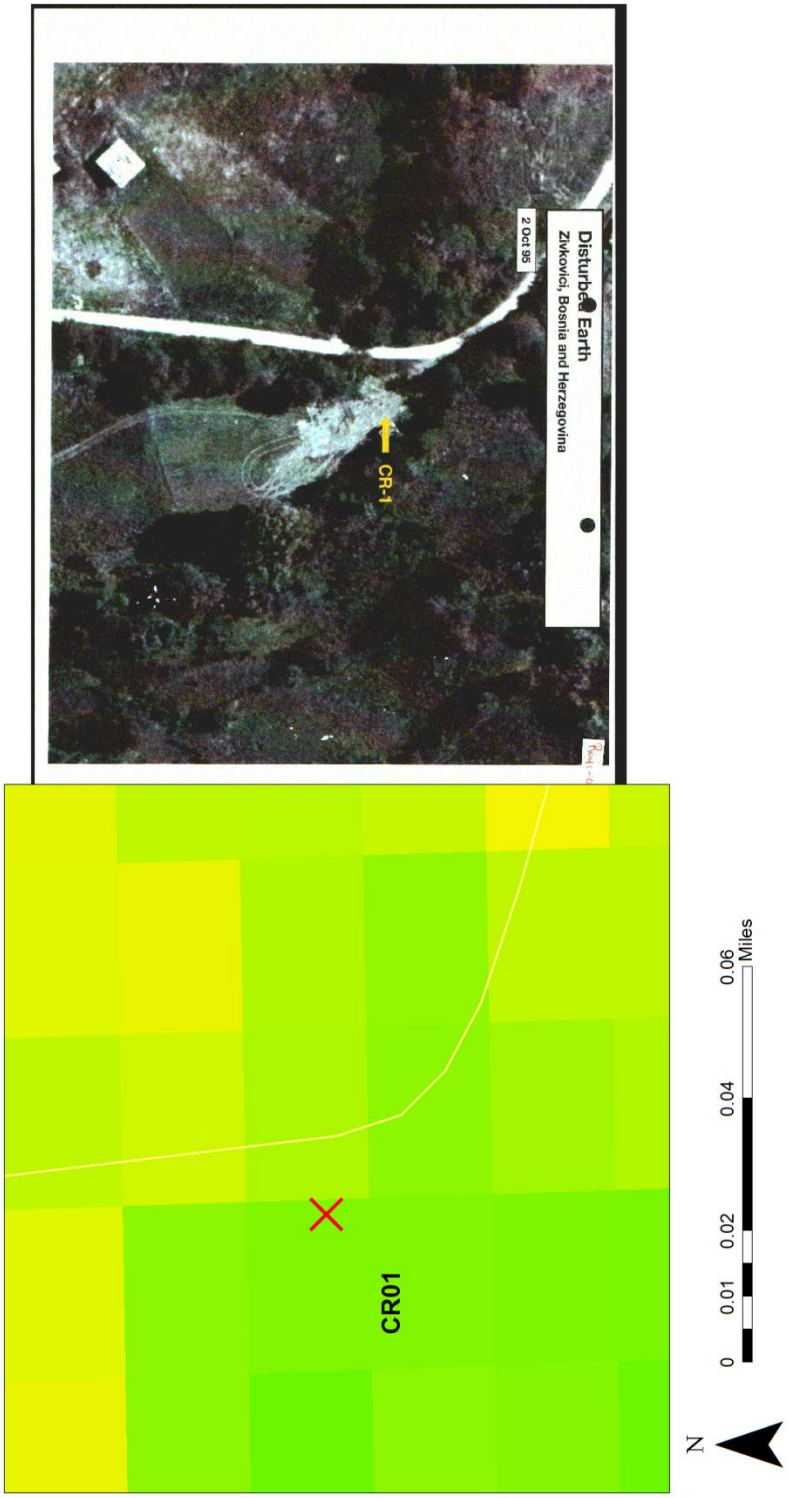

Figure 4-163 - Landsat 5 TM NDVI image (left) for 08/10/2009 showing CR01 compared with the aerial image (right) showing disturbed earth from 2 October 1995 (ICTY 2011c).